

# Stable isotope mass spectrometry and AMS dating applied to a multi-proxy climate record from the Bliden Lake, Denmark



ph.d. thesis by Jesper Olsen

University of Aarhus, Department of Physics and Astronomy  
AMS  $^{14}\text{C}$  Dating Centre, Ny Munkegade, bld 1520, DK-8000 Aarhus C



## Table of Contents

List of publications . . . . .	v
Preface. . . . .	vi
The Lake Bliden project. . . . .	vi
Participation in other projects . . . . .	vii
Outline of thesis. . . . .	ix
Acknowledgement . . . . .	ix
<b>Chapter 1: Stable isotope theory and notation</b>	
Introduction . . . . .	2
Isotopes . . . . .	2
Definitions and notation . . . . .	3
Isotopic fractionation . . . . .	4
Equilibrium fractionation . . . . .	5
Kinetic fractionation . . . . .	5
The fractionation factor. . . . .	5
Mass balance . . . . .	6
<b>Chapter 2: Stable isotope ratio mass spectrometry</b>	
Introduction . . . . .	8
CF-EA stable isotope calculations . . . . .	10
Calculating delta values of carbon and oxygen . . . . .	11
Calculating delta values of nitrogen . . . . .	14
Calibration of carbon and nitrogen isotope values . . . . .	15
Calculating delta values of sulphur . . . . .	16
Calibration of sulphur isotope values . . . . .	17
Calculating weight percentage values . . . . .	17
The CF-EA method . . . . .	18
Quality assurance results . . . . .	22
Carbon and nitrogen analysis. . . . .	23
Results of carbon and nitrogen blank samples. . . . .	23
Results of carbon and nitrogen stable isotope analysis. . . . .	25
Results of carbon and nitrogen weight percentage analysis. . . . .	26
Carbon and nitrogen analysis linearity . . . . .	31
Sulphur analysis . . . . .	34
Results of sulphur stable isotope analysis. . . . .	38
Results of sulphur weight percentage analysis . . . . .	38
Sulphur analysis linearity . . . . .	38
Discussion . . . . .	39
Stable isotopes of carbon and nitrogen . . . . .	40
Stable isotopes of sulphur . . . . .	41
Weight percentage values . . . . .	43
Conclusion . . . . .	43

<b>Chapter 3: Automated AMS sample preparation system</b>	
Introduction . . . . .	46
Method and design . . . . .	46
Results and Discussion . . . . .	52
Freeze procedure . . . . .	52
<sup>14</sup> C analysis – background and memory effects . . . . .	52
Stable isotope analysis . . . . .	56
Conclusion . . . . .	57
<b>Chapter 4: The Bliden Lake - site description, motivation and perspectives</b>	
Introduction . . . . .	60
The site . . . . .	60
Perspectives . . . . .	60
The modern Danish climate . . . . .	62
The Holocene environment in broad terms . . . . .	62
Possible sources of short-term Holocene climate oscillations . . . . .	63
Possible implications of relative sea-level changes . . . . .	66
The Mesolithic to Neolithic transition . . . . .	68
An attempt at dating the Mesolithic to Neolithic transition . . . . .	70
Aims of this work . . . . .	73
<b>Chapter 5: Interpreting lacustrine environments</b>	
Introduction . . . . .	76
Freshwater lakes . . . . .	76
Lacustrine organic matter . . . . .	79
The lacustrine carbon cycle . . . . .	79
Organic carbon isotopes ( $\delta^{13}\text{C}_{\text{ORG}}$ ) . . . . .	82
The lacustrine nitrogen cycle . . . . .	84
Nitrogen isotopes ( $\delta^{15}\text{N}_{\text{ORG}}$ ) . . . . .	84
The lacustrine sulphur cycle . . . . .	85
Sulphur isotopes ( $\delta^{34}\text{S}_{\text{ORG}}$ ) . . . . .	86
C/N and C/S ratios of organic matter . . . . .	87
The isotopic composition of calcium carbonate . . . . .	88
The $\delta^{13}\text{C}_{\text{carb}}$ of calcium carbonate . . . . .	88
The $\delta^{18}\text{O}_{\text{carb}}$ of calcium carbonate . . . . .	88
The covariance of $\delta^{13}\text{C}_{\text{carb}}$ and $\delta^{18}\text{O}_{\text{carb}}$ values . . . . .	90
Magnetic susceptibility . . . . .	91
Conceptual interpretation scheme . . . . .	91
<b>Chapter 6: Applied methods and results</b>	
Introduction . . . . .	94
Methods . . . . .	94
Geochemical methods . . . . .	94
Geochemical results of the Bliden Lake . . . . .	97
Diagenesis . . . . .	97
Estimating the $\delta^{18}\text{O}_{\text{w}}$ composition and the E/I ratio . . . . .	99
Radiocarbon dating . . . . .	100

## **Chapter 7: Facies, sedimentology and geochemistry**

Introduction . . . . .	104
Facies and terminology . . . . .	104
Facies associations . . . . .	104
High water (A) facies association . . . . .	104
Facies – sedimentology, geochemistry and interpretation . . . . .	106
Interpretation of facies association . . . . .	128
Shallow water (A) facies association . . . . .	129
Facies - sedimentology and geochemistry . . . . .	129
Interpretation of facies association . . . . .	133
Intermediate water facies association . . . . .	134
Facies – sedimentology, geochemistry and interpretation . . . . .	134
Interpretation of facies association . . . . .	138
Shallow water (B) facies association . . . . .	139
Facies – sedimentology, geochemistry and interpretation . . . . .	139
Interpretation of facies association . . . . .	143
High water (B) facies association . . . . .	143
Facies – sedimentology, geochemistry and interpretation . . . . .	143
Interpretation of facies association . . . . .	146

## **Chapter 8: Age Model of the Bliden Lake**

Introduction . . . . .	148
Age modelling . . . . .	149
Bayes' theorem and radiocarbon dating . . . . .	151
The age model of Blaauw and Christen . . . . .	151
Age models based on simulated data . . . . .	153
Chronology of the Bliden Lake . . . . .	156
Revisiting the sedimentology . . . . .	157
An age-to-depth model for Bliden Lake core . . . . .	158
Discussion . . . . .	162
Conclusion . . . . .	163

## **Chapter 9: Discussion**

Introduction . . . . .	166
General climatic trends of the Bliden Lake record . . . . .	166
Anthropological impacts and climatic changes . . . . .	169
Comparison with northern hemisphere climate events . . . . .	170
Possible indications of climatic forcing . . . . .	175
The Littorina transgressions . . . . .	177
Paleo-salinity . . . . .	178
Concurrent lake level changes in Bliden Lake and Tissø Lake . . . . .	179
The climate during the Mesolithic to Neolithic transition . . . . .	182
Conclusion . . . . .	183

<b>Chapter 10: Conclusion summary</b>	
Conclusions .....	186
Main conclusions on stable isotope analysis.....	186
Automation of <sup>14</sup> C sample preparation .....	187
Main conclusions on Bliden Lake climate history.....	187
The Littorina transgressions.....	188
The climate during the Mesolithic to Neolithic transition.....	188
<b>Appendix A: Age-to-depth model of Tissø Lake</b>	
The Site .....	192
Age-depth-model.....	192
Discussion .....	192
References.....	194

## List of publications

- Fischer, A., J. Olsen, M. Richards, J. Heinemeier, Á. E. Sveinbjörnsdóttir and P. Bennike (submitted for publication-a). "Coast-inland mobility and food composition in the Danish Mesolithic and Early Neolithic - evidence from stable isotope values of humans and dogs." Journal of Archaeological Science.
- Fischer, A., M. Richards, J. Olsen, D. Robinson, P. Bennike, L. Kubiak-Martens and J. Heinemeier (submitted for publication-b). "Reconstructing the Mesolithic Menu -food remains versus stable iso-topes in bones. A case study from the submerged settlement on the Argus Bank, Denmark." European Journal of Archaeology.
- Olsen, J., J. Heinemeier, K. G. Bahner, B. Graney and A. Pililips (submitted for publication). "Integrating Continuous Flow Mass Spectrometry with Automated CO<sub>2</sub> collection for AMS." Radiocarbon.
- Olsen, J., J. Heinemeier, P. Bennike, K. M. Hornstrup and H. Thrane (in preparation). "Characterisation and Blind Testing of the Method for Radiocarbon Dating of Cremated Bone." Radiocarbon.
- Olsen, J., I. Seierstad, B. Vinther, S. Johnsen and J. Heinemeier (2006). "Memory effect in deuterium analysis by continuous flow isotope ratio measurement." International Journal of Mass Spectrometry **254**(1-2): 44-52.
- Seierstad, I. K., S. J. Johnsen, B. M. Vinther and J. Olsen (in press). "The duration of the Bølling-Allerød (Greenland Interstadial 1) period in the GRIP ice core." Annals of Glaciology **42**.
- Vinther, B. M., H. B. Clausen, S. J. Johnsen, S. O. Rasmussen, K. K. Andersen, S. L. Buchardt, I. K. Seierstad, M.-L. Siggaard-Andersen, J. P. Steffensen, A. M. Svenson, J. Olsen and J. Heinemeier (2006). "A synchronized dating of three Greenland ice cores throughout the Holocene." Journal of Geophysical Research.
- Yde, J. C., N. T. Knudsen, N. K. Larsen, C. Kornborg, O. Bjørslev-Nielsen, J. Heinemeier and J. Olsen (in press). "The presence of thrust-block naled after a major surge event." Annals of Glaciology **42**.

## Preface

During my three years as a ph.d. student, I have been involved in a number of different projects all of which have been concerned with stable isotope analysis. In the following, I will give a brief overview of my work and the projects I have participated in. My aim is not to give a full description of each project but to focus on the subjects to which I have contributed. First, an introduction to this thesis is presented.

### The Lake Bliden project

Lacustrine environments are excellent archives for past climate changes. The application of stable isotope analysis and other geochemical parameters on freshwater lake deposits trace past environmental changes in and around the lake. This is exemplified by the high resolution paleoclimate investigation of the Bliden Lake, which is situated on Sjælland in eastern Denmark (see chapter 4). More than 8000 individual measurements of different geochemical parameters have been carried out and 18 samples have been AMS  $^{14}\text{C}$  dated.

The reasons for studying ancient climate changes are many. Presently, the debate on possible climate changes in the near future caused by human activities is ongoing and almost everybody from experts over politicians to ordinary people has their own opinion on possible future scenarios (see e.g. Manabe and Stouffer 1999; Danny Harvey 2000; Gerhard et al 2001; Ruddiman 2001; Lomborg 2003). One aspect of this debate has been the role played by natural causes such as solar irradiance, the Milankowitch theory, tectonic movements and anthropogenic causes like the increased release of  $\text{CO}_2$ , the ozone layer and water drainage (see e.g. Lowe and Walker 1997; Danny Harvey 2000; Gerhard et al 2001; Ruddiman 2001; Alley et al 2003; Ruddiman 2005; Broecker 2006). However, present natural and anthropogenic causes cannot be distinguished unless the natural variability of the climate in the past is well known. For this purpose, paleoclimate studies of the Holocene climate is of the utmost importance, not only because it is known that climate changes have occurred, but also because it is the period in the history of the earth that bears the greatest resemblance to present climate conditions. Furthermore, the Holocene climate archives are among the best preserved and thus therefore more suitable paleoclimate investigations. Information on ancient climates may also help in explaining the development of new human cultures and the expansion of these (see e.g. Roberts 2004). Hence, better knowledge of developments in ancient human history may be gained from climate research.

Modern measurement techniques are necessary tools for obtaining climate information from any deposit. Therefore, the first part of this thesis concerns the quality assurance of measurements made by stable isotope mass spectrometry in our laboratory (see chapter 2). The stable isotope ratio mass spectrometer has been in operation since 2003. Monitoring of the performance of the mass spectrometric measurements is essential to obtaining reliable results. The majority of the Bliden Lake results were obtained by stable isotope mass spectrometry analysis on carbon, oxygen, nitrogen and sulphur (see chapter 6). Routine sulphur isotope composition measurement techniques for large amounts of samples have been developed within the last decade. This technique has been applied to the Bliden Lake record. In general sulphur isotope studies are well known in marine environments but the approach has only been applied to lacustrine environments in few cases. The majority of these studies have been on sulphur pollution effects in recent deposits. Thus, sulphur isotopes are not commonly used for ancient lacustrine deposits.

The radiocarbon content has been measured on terrestrial samples found in the Bliden Lake core and is used to make a depth-to-age relation (see chapter 8). Chronology is essential for correlating with information obtained by other studies. A new method for obtaining a chronology of lake sediments on the basis of radiocarbon dating has been applied and will be presented

(Blaauw and Christen 2005). **The chemistry of and natural cycles in lacustrine environments** are briefly presented (see chapter 5) in order to obtain a paleoclimatic interpretation of the Bliden Lake record (see chapter 7). This climate information is applied to demonstrate possible climate changes during the introduction of agriculture in Denmark and to demonstrate the possible influence of relative sea level changes.

### **Participation in other projects**

My work began with the hand-over of a newly installed isotope ratio mass spectrometer with various types of inlet systems by GV Instruments in the summer of 2002. Despite the many pitfalls for an inexperienced operator of stable isotope mass spectrometers, the machine was up and running routine analysis within 6 months. This early work involved extensive testing, the development of quality assurance routines for data evaluation and database programming in order to keep track of the large amount of produced data. However, this work was very difficult and lengthy due to an inadequately equipped laboratory. Stable isotope mass spectrometers are able to measure per mill difference with very high precision but require a well defined temperature range of  $22 \pm 2$  °C in order to operate properly. By contrast, the room hosting the mass spectrometer on occasions displayed temperatures well above 28 °C with differences between day and night of the order of 8 °C to 10 °C, thus making stable isotope analysis impossible. Huge amounts of worthless results were produced due to this and it became apparent that the mass spectrometer could not be properly operated from June to August depending on weather conditions.

The performance and quality assurance parameters were presented on a poster at the ESIR (European Society for Isotope Research) workshop VII in Seggau, Austria 2004. Apart from this (see chapter 2), I have been training our laboratory technician in the routine operation of the mass spectrometer as well as Inger Seierstad and Bo Vinther (Department of Geophysics, University of Copenhagen) in analysing the isotope composition of small water samples from Greenland ice cores. Bo Vinther and Inger Seierstad managed to analyse in excess of 12 000 samples within 1.5 years with a precision exceeding their initial expectations.

Inger Seierstad has, among other things, used  $\delta D$  measurements to estimate the duration of the Bølling-Allerød period in the GRIP ice core (Seierstad et al in press) and Bo Vinther applied deuterium analysis to make an extended ice core chronology (Vinther et al 2006). Furthermore, I have carried out deuterium analysis in collaboration with Jacob Yde (Department of Earth Sciences, University of Aarhus) and the results have been published in 'Annals of Glaciology' (Yde et al in press). In connection with hydrogen isotope analysis, my primary objective has been to perform the initial performance tests of the system in order to ensure good reproducibility and long-term stability. This included verification of isotope  $\delta D$  values of the more than 20 water standards made available to us by Sigfus Johnsen (Department of Geophysics, University of Copenhagen) and Árný E. Sveinbjörnsdóttir (Science Institute, University of Iceland) relative to international standards. However, contrary to our expectations the hydrogen analysis on water samples showed significant intersample memory effects. The hydrogen isotope analysis on water samples was described by Morrison (Morrison et al 2001), who mentioned minor but insignificant intersample memory effects. Therefore a systematic investigation of the intersample memory effect was performed with the goal of reducing the intersample memory effect to a minimum. By a few technical improvements and by monitoring specific parameters, the memory effect was reduced from 6% to 1% (Olsen et al 2006).

As the mass spectrometer took up routine analysis the focus was moved from installing the mass spectrometer to scientific research projects. I have been involved in two major cooperative projects; one concerning radiocarbon dating of cremated bones with Karen Margrethe Horn-

strup (Holstebro Museum), Pia Bennike (Laboratory of Biological Anthropology, Institute of Forensic Medicine, University of Copenhagen), and Henrik Thrane (Department of Prehistoric Archaeology, University of Aarhus), the other concerning paleodietary interpretations of prehistoric human bones with special attention paid to the Mesolithic – Neolithic transition, with (among others) Anders Fischer (Kalundborg Regional Museum), Mike Richards (Department of Archaeological Sciences, University of Bradford) and Pia Bennike.

Until recently, cremated bones were not considered a suitable material for radiocarbon dating. The archaeological community is very pleased about the possibility of radiocarbon dating cremated bones, since the most common burial practise during the Danish Bronze Age was cremation. The cremation of human bones leaves no organic bone material, i.e. collagen, behind for  $^{14}\text{C}$  dating, which has left us with a deficit of  $^{14}\text{C}$  dating for a whole cultural epoch. The method for radiocarbon dating cremated bones was introduced by Lanting et al (Lanting et al 2001). **Theoretically, the method assumes that, exposed to the high temperatures of cremation, the bone structural carbonate fraction re-crystallises into larger and chemically more inert crystals, hence making removal of adsorbed carbonate possible. Verifying that this re-crystallisation has taken place is thus essential. Therefore we have introduced infrared spectroscopy (IR) as a method for characterising the degree of cremation. For this purpose, we were extremely lucky to have at our disposal a Late-Neolithic individual apparently caught in a fire and exhibiting the full spectrum from charred to fully “cremated” going from one end of a single bone (left radius) to the other (Fischer et al submitted for publication-a). This individual exhibited the high temperature re-crystallisation in a marked step in the IR parameters as well as in  $\delta^{13}\text{C}$  along the bone. As part of the project, we tested the method of Lanting et al (Lanting et al 2001) by blind dating 11 cremated or partly cremated prehistoric bones against either charcoal, pitch or a dendrochronological age (Olsen et al in preparation).**

Palaeodiet is the science of prehistoric dietary habits. Information on palaeodiet is not only of direct interest to the history of civilization, but has also become increasingly important for precise radiocarbon dating, since different food sources may have different apparent  $^{14}\text{C}$  ages. Thus, the marine biological environments show apparent  $^{14}\text{C}$  ages several hundreds of years too high because of the long residence time of carbon in the deep ocean and the slow mixing rate with surface sea waters. Hence humans whose diet relied heavily on marine resources will also display correspondingly high apparent  $^{14}\text{C}$  ages. Paleodietary investigations can reveal the amount of consumed seafood and thereby provide models for corrections of the measured radiocarbon ages. At the Middle Mesolithic settlement on the Argus Bank, which is now submerged to a depth of 4-6 metres, 2 km off the Danish coast, the  $\delta^{13}\text{C}$  and  $\delta^{15}\text{N}$  values of five humans and a dog bones has been measured (Fischer et al submitted for publication-b). From various sites, both inland and coastal but mainly within the Åmose area, the  $\delta^{13}\text{C}$  and  $\delta^{15}\text{N}$  values together with the  $^{14}\text{C}$  dates have been measured on 42 individual bone samples. In addition,  $\delta^{13}\text{C}$  and  $\delta^{15}\text{N}$  values were measured for an array of Stone Age food source animals (Fischer et al submitted for publication-a). The  $\delta^{13}\text{C}$  and  $\delta^{15}\text{N}$  values have been used to estimate the food composition of inland and coastal sites in Denmark during the Mesolithic – Neolithic transition. In order to establish a chronology of these data, the estimated food composition determined from the combined values of  $\delta^{13}\text{C}$  and  $\delta^{15}\text{N}$  have been used to make a modelled estimate of the reservoir age of each individual. The calculation of  $^{14}\text{C}$  reservoir ages for many of these individuals is complicated because they have consumed significant amounts of freshwater fish exhibiting a large range of  $^{14}\text{C}$  reservoir ages. Although these two projects have taken up a significant part of my time, I have unfortunately not been in a position to present them in this thesis pending their publication elsewhere. Therefore quotations like ‘Fischer et al submitted for pub-

lication' refer to work where I have made significant contributions. Some of the scientific problems from this part of my work are briefly mentioned in chapter 4.

As a ph.d. student, you will also be teaching and part of my teaching has been the development of experimental exercises for secondary school students in cooperation with Torbon Benoni (Egå Gymnasium). Two experimental programs have been developed, a paleodiet program (<http://www.phys.au.dk/tilbud/pages/ams/home.htm>) and a climate program (<http://www.phys.au.dk/tilbud/pages/ams/home.htm>). For the paleodietary program, the students had a lecture on mass spectrometry and the principles of prehistoric paleodietary interpretation. They then had to apply these principles on a sample from their own nails. The climate project is an interdisciplinary program between the Department of Physics and Astronomy and the Department of Earth Sciences (Marit-Solveig Seidenkrantz). The students were given two lectures, one on the global isotope water cycle and one on the Earth's general climate history. For the practical part, they looked at foraminifera and measured the deuterium content of a 'simulated' ice core sample, and then had to determine whether it was from a cold or warm period.

### **Outline of thesis**

Stable isotope analysis provides the 'red line' through my work and a very brief introductory chapter on fractionation theory and the common nomenclature used in stable isotope analysis is therefore presented in chapter 1. The application of isotope ratio mass spectrometry (*IRMS*) in terms of calculations, working principle and quality assurance and evaluation is presented in chapter 2, whereas chapter 3 focus on the development of combining stable isotope analysis with  $^{14}\text{C}$  sample  $\text{CO}_2$  trapping. Collective chapter 2 and 3 together with Olsen, Seierstad et al (2006) sum the work done to make the mass spectrometer run for routine analysis and furthermore provides details on the methods employed to obtain high quality isotope values of a variety of sample types (e.g. lake sediments, bones and water). Chapter 4 and onwards represents a detailed example of the application of stable isotope analysis in the field of paleolimnology and climate research. The general the perspective and aims of the investigation on Bliden Lake are discussed in chapter 4 (*as also briefly discussed in this preface, see above*). Chapter 5 presents a brief introduction to paleolimnology with focus on the interpretation of stable isotope in lacustrine environments and chapter 6 provides a description of the applied methods and their possible limitations. Chapter 7, 8 and 9 are the key chapters providing a sedimentological and geochemical interpretation of the Bliden Lake deposits (*chapter 7*) followed by the construction of a depth-to-age model based on  $^{14}\text{C}$  dated sample material from the lake (*chapter 8*). An attempt to combine the chronology and interpretation of the Bliden Lake is presented in chapter 9 in terms of relative sea level changes, climate changes and anthropogenic impacts. Furthermore a comparison with general northern hemisphere climate proxies is presented. Last chapter 10 provides a summary of the main achieved conclusion.

### **Acknowledgement**

I would like to thank the Carlsberg Foundation and Nanna Noe-Nygaard for funding a major part of my project. Also I would like to thank the Department of Physics and Astronomy and Jan Heinemeier at the AMS  $^{14}\text{C}$  Dating Centre for financial support to this project. Without their financial support this work could not have been carried out. I am very grateful to Nanna Noe-Nygaard for making the Bliden Lake core available to me and for many fruitful discussions. Anthony Ruter is thanked for letting me use his unpublished  $^{14}\text{C}$  data in Tissø Lake. These have been of great value for constructing an age-to-depth model for the upper part of Tissø Lake. Also I would like to thank Mikkel Ulfeldt Hede for helping me with the Geographical information system (*GIS*). Without his help I could not have presented the figures of the Bliden Lake. H.A.J

Meier, H van der Plicht, A. Aerts-Bijma and the staff at Center for Isotope Research, Groningen are thanked for fruitful discussions and for letting me have the anthracite background material – an invaluable sample for testing the  $^{14}\text{C}$  background level of the developed the  $^{14}\text{C}$  sample preparation device. Finally I would like to thank the staff at the AMS  $^{14}\text{C}$  Dating Centre Ann-Berith Jensen, Hanne Jakobsen, Helle Christensen and Vibeke Jensen for always having helped me when I got lost in the laboratory. As English is not my native language grammar and spelling can sometimes become very difficult and I am therefore extremely thankful to Morten Hjelm Hansen for correcting my manuscripts. Klaus Bahner is also thanked for the numerous good discussions we have had and for the support that he has given me during the period of writing as well as before.

The past four years have been a turbulent period in my life with both great pleasures and sorrows. I am very grateful to my wife Helen Nordahl Madsen and to my two sons Silas Nordahl Olsen and Julius Nordahl Olsen for accepting my many weeks and hours away from home, and for all the support they have given me through out the years. My mother Jytte Olsen is thanked for her help and her invaluable supportiveness. Thomas Olsen and Katrine Kastberg are thanked for looking after Silas and for their help during periods of busyness, especially for letting a work room to my availability. Also I would like to thank Søren Hartman Hede and Jesper Aron Kjær for providing me a place to stay during my numerous and long visits in Copenhagen. Last I would like to memory my father Sven Max Olsen who the fifth of November 2002 died of cancer. Often I have had his voice in my inner ear telling me to keep going on in periods of depression or despair. Words cannot tell how sad I am not being able to show him this work.



1

**Stable isotope theory  
and notation**

## Introduction

This section gives a brief introduction to isotopes and the fractionation theory. It is mainly based on the books of Clark and Fritz (1997) and Criss (1999). The reader is referred to these books for a more detailed description of the subjects discussed here. An introduction to the conventional notation used for stable isotopes is also given.

## Isotopes

The structure of the nucleus is defined by its number of protons ( $Z$ ), which defines the element, and the number of neutrons ( $N$ ), which defines the isotope of that element (see e.g. Hodgson *et al* 1997). The mass of a nucleus is approximately given by the sum of the masses of protons and neutrons ( $A=Z+N$ ). The notation of an element  $X$  is given by  ${}^A_ZX_N$ , but the shorter notation  ${}^AX$  will be used here.

Nuclei are held together by the short ranged attractive strong nuclear force. Stable nuclei have nearly similar numbers of protons and neutrons. As the number of protons increases, the number of neutrons becomes progressively greater. This because the electromagnetic force between protons makes nuclei rich in protons unstable (Hodgson *et al* 1997). To maximise their binding energy, protons and neutrons couple in pairs and nuclei with an even number of protons and neutrons have greater binding energy than odd-even, while the odd-even nuclei have greater binding energy than odd-odd (Hodgson *et al* 1997). This is also reflected in the natural abundances of isotopes, as is revealed by Table 1.1. Even-even isotopes are more abundant than odd-odd isotopes.

**Table 1.1: Natural abundances of H, C, N, O and S**

Reference: [www.webelements.com](http://www.webelements.com)

Isotope	Mass (amu)	Natural abundance (atom %)	$\pm$	Nuclear spin (I)	Z	N
${}^1\text{H}$	1.007	99.989%	0.001%	1/2	1	0
${}^2\text{H}$	2.014	0.012%	0.007%	1		1
		100.000%				
${}^{12}\text{C}$	12	98.93%	0.08%	0	6	6
${}^{13}\text{C}$	13.003	1.07%	0.08%	1/2		7
${}^{14}\text{C}$	14.003			0		8
		100.00%				
${}^{14}\text{N}$	14.003	99.63%	0.01%	1	7	7
${}^{15}\text{N}$	15.000	0.37%	0.01%	1/2		8
		100.00%				
${}^{16}\text{O}$	15.994	99.757%	0.02%	0	8	8
${}^{17}\text{O}$	16.999	0.038%	0.001%	5/2		9
${}^{18}\text{O}$	17.999	0.205%	0.01%	0		10
		100.00%				
${}^{32}\text{S}$	31.972	94.93%	0.31%	0	16	16
${}^{33}\text{S}$	32.971	0.76%	0.02%	3/2		17
${}^{34}\text{S}$	33.967	4.29%	0.28%	0		18
${}^{36}\text{S}$	35.967	0.02%	0.01%	3/2		19
		100.00%				

Some nuclei are radioactive and spontaneously decay to form other nuclei. Radioactive nuclei are either cosmogenic or radiogenic. The radiogenic nuclei are formed in stellar interiors or by supernova explosions and spread throughout the universe to be used in the formation of new stellar matter. They can thus in principle be used for dating meteorites or the age of the Earth provided that their mean half life is large enough. Cosmogenic radioactive isotopes, on the other hand, are relatively short-lived and their abundance on Earth can only be explained by continued formation by other processes, like for example the bombardment of the atmosphere by cosmic radiation. The  $^{14}\text{C}$  nucleus is formed in this way (see Table 1.1). As with radiogenic isotopes, the natural abundance of stable cosmogenic isotopes on Earth is the result of stellar processes.

### Definitions and notation

Stable isotopes are measured as the ratio between the two most abundant isotopes of a given element  $X$  and is given by

$$(1.1) \quad {}^A_Z R = \frac{{}^A_Z F}{{}^{A^*}_Z F},$$

where  $F$  is the concentration of isotope of element  $X$ . The term  ${}^A_Z F$  denotes the most abundant isotope. The measurement of absolute isotope ratios is not straightforward. However the absolute isotope ratios are not the most important to most investigations, which deal with isotope variations instead. Hence the isotope ratio of a sample is by convention always stated relative to a standard by the delta ( $\delta$ ) notation (Clark and Fritz 1997; Criss 1999) as

$$(1.2) \quad \delta^A X_{\text{sample/standard}} = \frac{{}^A R_{\text{sample}} - {}^A R_{\text{standard}}}{{}^A R_{\text{standard}}},$$

where  $R$  reflects the isotope ratio of element  $X$ .  $\delta$  values are dimensionless and are conventionally given per mil (‰). The internationally adopted reference materials are given in Table 1.2.

In order to re-express  $\delta$  values relative to other reference materials the following equation can be useful:

$$(1.3) \quad \delta^A X_{a/c} = \delta^A X_{a/b} + \delta^A X_{b/c} + \frac{\delta^A X_{a/b} \times \delta^A X_{b/c}}{1000},$$

**Table 1.2: Reference materials for stable isotopes**

The V denotes Vienna and symbolises that the original adopted material has been replaced. Compiled after Clark & Fritz (1997).

Element	$\delta\text{D}$	$\delta^{13}\text{C}$	$\delta^{15}\text{N}$	$\delta^{18}\text{O}$	$\delta^{34}\text{S}$
Standard	VSMOW <sup>1</sup>	VPDB <sup>2</sup>	AIR	VSMOW <sup>1</sup> VPDB <sup>2</sup>	VCDT <sup>3</sup>
Material	water	calcite	atmospheric air	water calcite	FeS

<sup>1</sup> Standard Mean Ocean Water. VSMOW is used exclusively for waters while carbonate  $\delta^{18}\text{O}$  values can be referred to using both VSMOW and VPDB. <sup>2</sup> Calcite from a fossil *Belemnitella americana* from the Cretaceous Pee Dee Formation in South Carolina. <sup>3</sup> Troilite phase (FeS) of the Cañon Diablo meteorite.

where the  $a$  may indicate a sample and  $b$  the work gas, for example.  $\delta_{a/b}$  is thus read as the delta value of a sample  $a$  given relative to the work gas or a standard  $b$  respectively. To reformulate a  $\delta_{b/a}$  value given relative to  $a$ , to a delta value relative to  $b$  ( $\delta_{a/b}$ ) the inverse formula can be used

$$(1.4) \quad \delta^A X_{a/b} = \left( \frac{1000}{\delta^A X_{b/a} - 1000} + 1 \right) \times 1000$$

Both formulas can be deduced from the definition of the  $\delta$  values equation (1.2). Equations (1.3) and (1.4) are used for converting  $\delta$  values stated relative to an internal standard to  $\delta$  values relative to an international reference material.

### Isotopic fractionation

Isotopic fractionation is a change in the isotopic abundance ratio caused by physical, chemical or biological processes. Chemical reactions depend on the electron structure of the molecules. Reaction rates are in general insensitive to atomic or molecular masses. However, the minor mass differences between molecular species of different isotopes results in slightly different reaction rates. For many processes this will result in mass dependent effects where the reaction

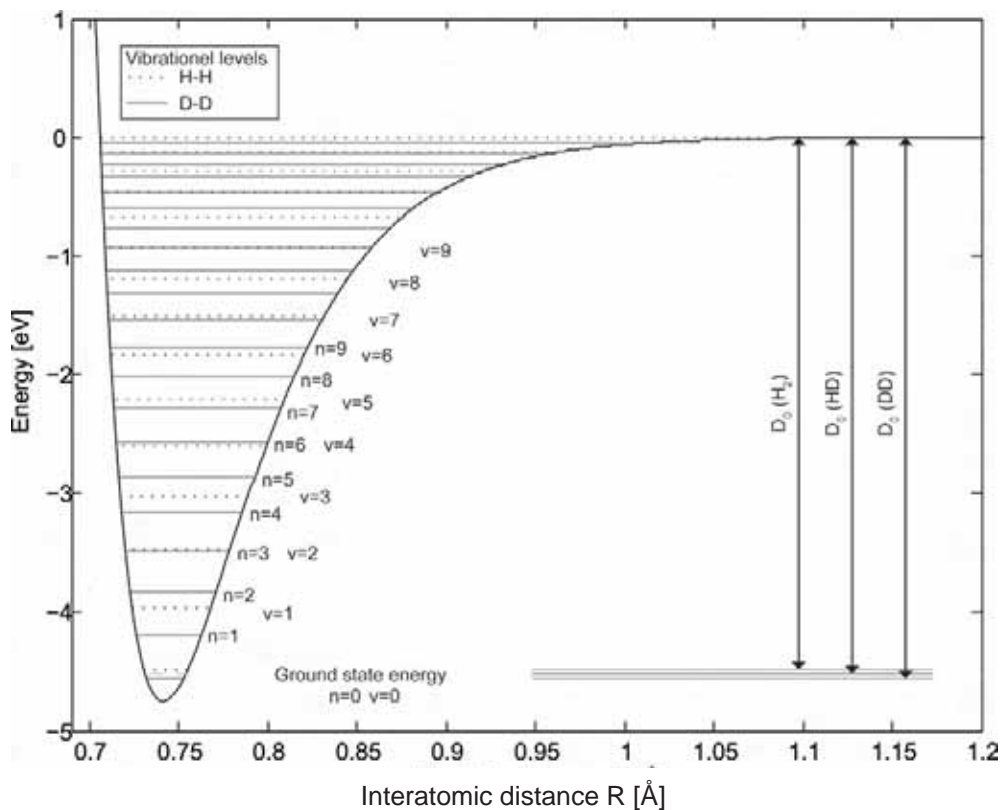


**Figure 1-1.** Shown is the potential energy for a bound state of the hydrogen molecule ( $H_2$ ) as a function of the interatomic distance  $R$ . The zero point energy of  $H_2$ , HD and  $D_2$  is shown. The dissociation  $D_0$  represent the energy required to move the atoms so far apart that they no longer interact that is the energy required the break them apart. As seen this energy  $D_0$  ( $D_2$ ) is greater for heavy isotope molecule of two deuterium atoms than the  $D_0$  ( $H_2$ ) for the two hydrogen atoms. The vibrational energy levels for  $H_2$  (dotted lines) and  $D_2$  (solid lines) are also shown and  $n$  denotes the vibrational energy level for  $D_2$  and  $v$  the vibrational energy level for  $H_2$ . The form of the potential energy is taken by the Morse potential (Bransden 1996; Criss 1999) with data from (Criss 1999). The vibrational frequencies are calculated by the harmonic approximation using the Morse potential (Bransden 1996) and with data from (Criss 1999).

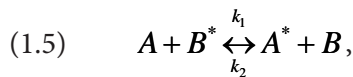
product will be isotopically enriched or depleted relative to the starting material. Lighter molecules will have higher probability of participating in chemical reactions as heavier molecules have stronger bonds (Clark and Fritz 1997; Criss 1999). This is illustrated by Figure 1-1. A distinction between two types of fractionation processes can be made 1) equilibrium and 2) kinetic fractionation.

### Equilibrium fractionation

Chemical equilibrium occurs when the forward and backward reaction rates of a chemical process are equal. In such a situation the isotope composition of reactant and product will remain constant though not similar. Both the equilibrium time and the equilibrium position is temperature dependent (Clark and Fritz 1997), in such a way that the fractionation diminishes at high temperatures and displays the largest difference between reactants and products at low temperatures (Criss 1999).

### Kinetic fractionation

Kinetic fractionation or non-equilibrium fractionation occurs by a sudden change in temperature or the addition or removal of reactants or products that will move the chemical reaction away from equilibrium. It may also be due to biological processes which in general are irreversible (Clark and Fritz 1997). Consider the generalised exchange reaction:



where A and B are two phases sharing a common element and A\* and B\* represent the trace element of these phases (Criss 1999). Thermodynamic equilibrium is characterised by the forward and reverse reaction rates being equal ( $k_1=k_2$ ). In this steady state, the major and trace elements of both sides of the reaction are constant. However, it is common that forward and reverse reaction rates are unequal ( $k_1 \neq k_2$ ), and hence the two phases are out of isotopic equilibrium and will tend to approach equilibrium conditions with the passing of time. An example of kinetic fractionation is the evaporation of water, which may be viewed in terms of transport rates of water molecules from the water to the vapour phase and from the vapour and back to the water phase. In this system equilibrium is only attained when no net evaporation occurs, i.e. at 100% humidity (Criss 1999).

### The fractionation factor

The fractionation factor  $\alpha$  expresses the magnitude of partitioning between two phases A and B and is defined as (Clark and Fritz 1997; Criss 1999)

$$(1.6) \quad \alpha_{A-B} = \frac{R_A}{R_B} = \frac{1000 + \delta_A}{1000 + \delta_B},$$

where R is the isotope ratio of phase A and B respectively. The last term states the fractionation factor in terms of  $\delta$  values for the phases A and B. The enrichment factor  $\epsilon$  gives the isotope ratio difference between the two phases A and B and is defined by the  $\delta$  notation as

$$(1.7) \quad \epsilon_{A-B} = \left( \frac{R_A}{R_B} - 1 \right) \times 1000 = (\alpha - 1) \times 1000.$$

The last term gives the enrichment factor  $\epsilon$  expressed by the fractionation factor  $\alpha$ . The enrichment factor may also be expressed in terms of  $\delta$  values

$$(1.8) \quad \epsilon_{A-B} = \frac{1 + \delta_A}{1 + \delta_B} - 1 \approx \delta_A - \delta_B.$$

### Mass balance

A multi-component system can be expressed as the sum of its constituent parts. For the isotope value of a system consisting of  $N$  parts this can be written as

$$(1.9) \quad \delta_{system} = \sum_{j=1}^N X_j \cdot \delta_j \quad \text{with} \quad \sum_{j=1}^N X_j = 1,$$

where  $j$  is the  $j$ 'th constituent and  $X_j$  the  $j$ 'th fraction of the whole system (Crisp 1999).

2

---

**Stable isotope ratio**

**mass spectrometry**

## Introduction

Isotope ratio mass spectrometer measurements of the light stable isotopes of hydrogen, nitrogen, carbon and sulphur is a powerful tool for a variety of research fields ranging from palaeodietary investigations to climate research in both the past and present (Noe-Nygaard 1988; Ghosh and Brand 2003; Harrison and Katzenberg 2003; Richards *et al* 2003; Filippi and Talbot 2005; Noe-Nygaard *et al* 2005). In the present case, the stable isotope technique will be employed to obtain paleoclimate information about the Bliden Lake Core by measuring the stable isotope of carbon, nitrogen, oxygen and sulphur using the continuous flow elemental analyser (CF-EA) method. This section provides a detailed account of how stable isotope values are calibrated and monitored at the AMS  $^{14}\text{C}$  Dating Centre. The focus is on the continuous flow method and the aim is to demonstrate how systematic analysis procedures may help in the long-term quality assurance of routine measurements.

Stable isotope analysis is carried out by isotope ratio mass spectrometers (IRMS) and IRMS measurements are cross-calibrated by the consensus values of certain materials, also known as international standards. The international standards are distributed in small amounts by the Analytical Quality Control Services, a sub department of the International Atomic Energy

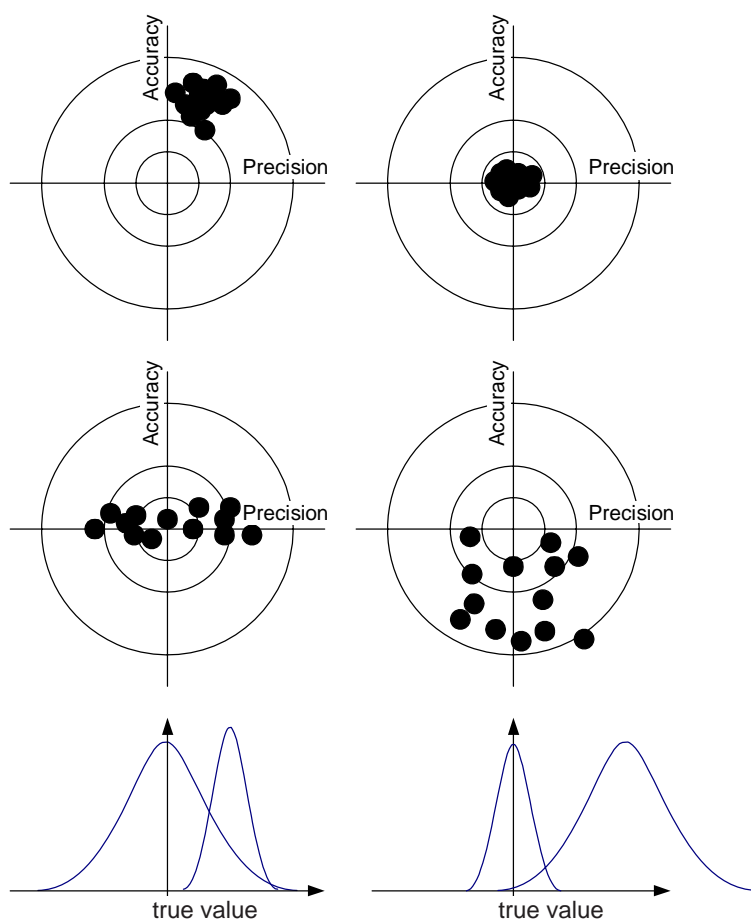


**Figure 2-1.** Graphical representation of precision and accuracy. **Upper right corner:** A very precise and accurate measurement. This is shown as a the normal distributed curve centered around the true value (*high accuracy*) and thin and high (*high precision*). **Upper left corner:** Precise but inaccurate measurement. This is shown as a narrow distribution with a mean value off from the true value. **Lower left corner:** A very accurate but imprecise measurement. This is shown as a broad distribution centered around the true value. **Lower right corner:** Inaccurate and imprecise measurement. This is shown as a broad and off set distribution. In real measurements however the true value is not known, but rather what is to be estimated. Hence the off set from the true value is not easily found, i.e. systematic errors may be hard to find.

**Table 2.1: Molecular species for IRMS analysis**

The natural abundances values are calculated by the values in Table 1.1

		Isotope	Mass (amu)	Natural abundance (atom %)			Isotope	Mass (amu)	Natural abundance (atom %)
H <sub>2</sub>	2	<sup>1</sup> H <sup>1</sup> H	2.015	99.977%	SO <sub>2</sub>	64	<sup>32</sup> S <sup>16</sup> O <sup>16</sup> O	63.961	94.4692008%
	3	<sup>1</sup> H <sup>2</sup> H	3.021	0.023%		65	<sup>33</sup> S <sup>16</sup> O <sup>16</sup> O	64.961	0.7563109%
	4	<sup>2</sup> H <sup>2</sup> H	4.028	0.0000013%			<sup>32</sup> S <sup>16</sup> O <sup>17</sup> O	64.966	0.0719715%
N <sub>2</sub>	28	<sup>14</sup> N <sup>14</sup> N	28.006	99.26535424%		66	<sup>34</sup> S <sup>16</sup> O <sup>16</sup> O	65.957	4.2691759%
	29	<sup>14</sup> N <sup>15</sup> N	29.003	0.73329152%			<sup>33</sup> S <sup>16</sup> O <sup>17</sup> O	65.965	0.0005762%
	30	<sup>15</sup> N <sup>15</sup> N	30.000	0.00135424%			<sup>32</sup> S <sup>16</sup> O <sup>18</sup> O	65.966	0.3882672%
CO <sub>2</sub>	44	<sup>12</sup> C <sup>16</sup> O <sup>16</sup> O	43.989	98.44978437%			<sup>32</sup> S <sup>17</sup> O <sup>17</sup> O	65.970	0.0000137%
	45	<sup>12</sup> C <sup>16</sup> O <sup>17</sup> O	44.994	0.0750041%		67	<sup>34</sup> S <sup>16</sup> O <sup>17</sup> O	66.961	0.0032525%
		<sup>13</sup> C <sup>16</sup> O <sup>16</sup> O	44.993	1.06480612%			<sup>33</sup> S <sup>16</sup> O <sup>18</sup> O	66.965	0.0031084%
	46	<sup>12</sup> C <sup>17</sup> O <sup>17</sup> O	45.998	0.00001429%			<sup>33</sup> S <sup>17</sup> O <sup>17</sup> O	66.969	0.0000001%
		<sup>13</sup> C <sup>16</sup> O <sup>17</sup> O	45.997	0.00081122%			<sup>32</sup> S <sup>17</sup> O <sup>18</sup> O	66.970	0.0001479%
		<sup>12</sup> C <sup>16</sup> O <sup>18</sup> O	45.994	0.40462736%		68	<sup>36</sup> S <sup>16</sup> O <sup>16</sup> O	67.956	0.0199029%
	47	<sup>12</sup> C <sup>17</sup> O <sup>18</sup> O	46.998	0.00015413%		<sup>34</sup> S <sup>16</sup> O <sup>18</sup> O	67.961	0.0175463%	
		<sup>13</sup> C <sup>16</sup> O <sup>17</sup> O	47.001	0.00000015%		<sup>34</sup> S <sup>17</sup> O <sup>17</sup> O	67.966	0.0000006%	
		<sup>13</sup> C <sup>16</sup> O <sup>18</sup> O	46.997	0.00437086%		<sup>33</sup> S <sup>17</sup> O <sup>18</sup> O	67.969	0.0000012%	
	48	<sup>12</sup> C <sup>18</sup> O <sup>18</sup> O	47.998	0.00041575%		<sup>32</sup> S <sup>18</sup> O <sup>18</sup> O	67.970	0.0003989%	
		<sup>13</sup> C <sup>17</sup> O <sup>18</sup> O	48.001	0.00000167%	69	<sup>36</sup> S <sup>16</sup> O <sup>17</sup> O	68.961	0.0000152%	
	49	<sup>13</sup> C <sup>18</sup> O <sup>18</sup> O	49.001	0.0000045%		<sup>34</sup> S <sup>17</sup> O <sup>18</sup> O	68.966	0.0000067%	
						<sup>33</sup> S <sup>18</sup> O <sup>18</sup> O	68.969	0.0000032%	
				70	<sup>36</sup> S <sup>16</sup> O <sup>18</sup> O	69.961	0.0000818%		
					<sup>36</sup> S <sup>17</sup> O <sup>17</sup> O	69.965	0.0000000%		
					<sup>34</sup> S <sup>18</sup> O <sup>18</sup> O	69.966	0.0000180%		
				71	<sup>36</sup> S <sup>17</sup> O <sup>18</sup> O	70.965	0.00000003%		
				72	<sup>36</sup> S <sup>18</sup> O <sup>18</sup> O	71.965	0.0000001%		

Agency (IAEA). New standards are accepted only after first being distributed and measured by a number of laboratories in a so called inter-comparison test (Allison *et al* 1993; Confiadini *et al* 1993; Stichler 1993; Coplen and Krouse 1998; Werner and Brand 2001) and by this approach the consensus values of the international reference materials are determined. However, these inter-comparison tests also reveal that there are large deviations between results from different laboratories and that these deviations cannot always be explained by large measurement uncertainties. Hence inter-comparison tests clearly show that IRMS measurements are very precise, but that a higher control of accuracy may be needed.

The term precision is used to describe the reproducibility of a measurement. It is commonly assumed to follow a given probability distribution, such as the normal probability distribution with a zero mean and a standard deviation  $\sigma$ . The standard deviation is a measure of the precision as seen by Figure 2-1. Accuracy, on the other hand, quantifies the systematic errors. In the simple picture of Figure 2-1, this is shown as an offset from what is denoted to be the true value of the measurement. Systematic errors are in many aspects much harder to find, but may in general be found by good calibration or by monitoring over long periods of time.

## CF-EA stable isotope calculations

Stable isotope analysis is carried out on molecular gases ( $H_2$ ,  $N_2$ ,  $CO_2$  and  $SO_2$ ) rather than on elemental atoms. Thus, to obtain the elemental isotope composition, corrections have to be applied. The correction scheme for the calculation of the isotope composition of carbon is shown in Figure 2-2, but the general correction pathway applies for  $N_2$  and  $SO_2$  as well. Table 2.1 displays the molecular species measured for hydrogen, carbon, nitrogen, oxygen and sulphur stable isotope analysis. First, the molecular delta values are calculated from integrated peak areas (see Figure 2-3 and 2-4 for peak spectrograms), which are then converted to elemental raw delta values. This step may include a correction for isobaric interference. The next two steps are optional: the first is the drift correction and the second the blank correction. Any linear trends are removed by the drift correction by linear fitting to the standard  $\delta^{13}C_{raw}$  values versus time, whereas the blank correction removes the contribution from the tin cups. The last step is to convert the elemental raw delta values to elemental delta values relative to the international standards as agreed by the IAEA (Allison *et al* 1993; Coplen 1996; Krouse and Coplen 1997; Coplen and Krouse 1998; Coplen *et al* 2002) by either a single point method or a linear method. In the case of the single point method, the elemental delta values are converted to an internationally agreed scale by the use of one internal standard. The linear method is employed for batches that include a variety of different standards. Here, the international elemental delta values are found by fitting the raw elemental delta values as a function of the international agreed value. The details for calculating the elemental delta values of nitrogen, carbon, oxygen and sulphur are given in the following sections.

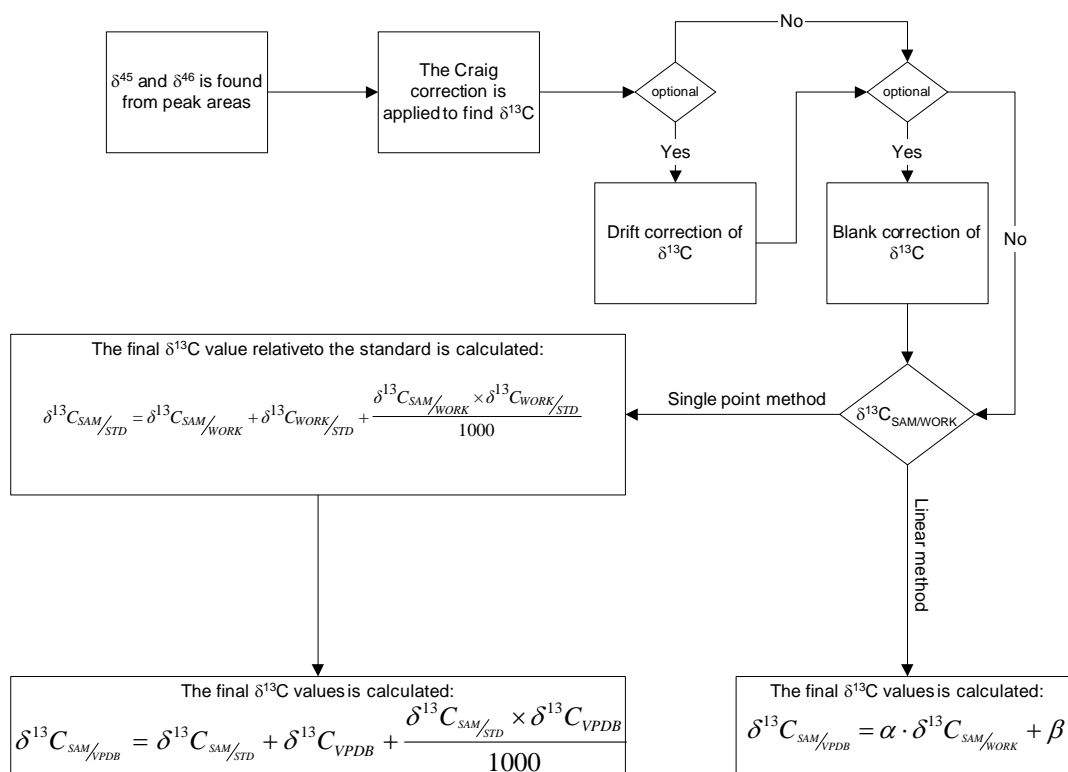
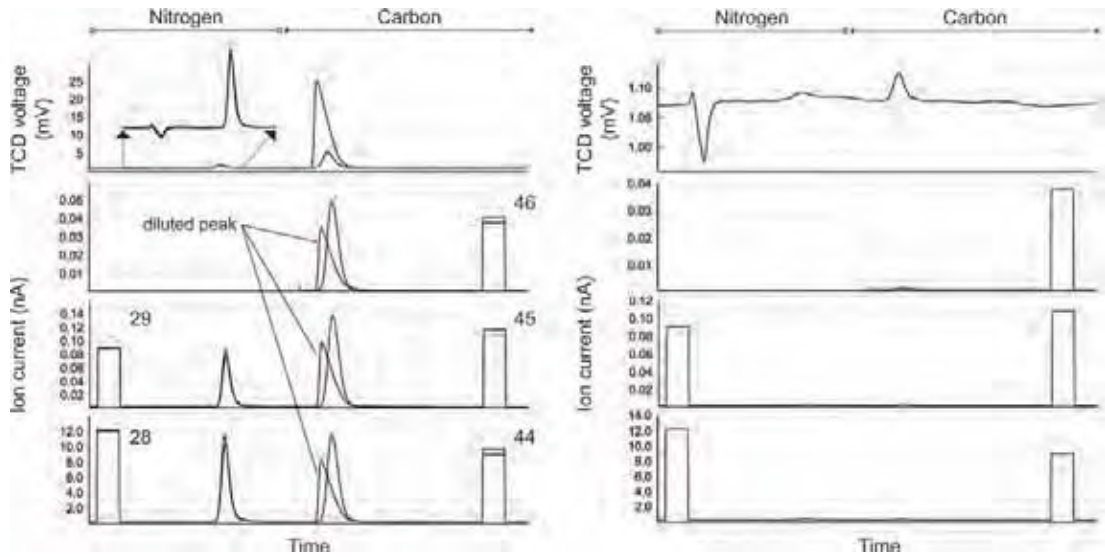
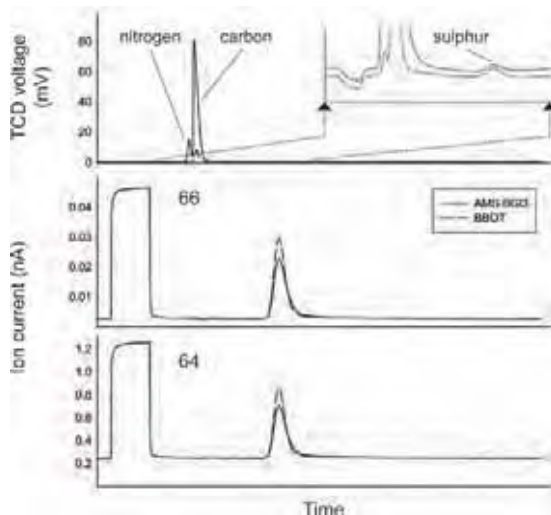


Figure 2-2. Flow diagram illustrating the sample processing.



**Figure 2-3.** Chromatograms for CF-EA carbon and nitrogen analysis. *Left:* The TCD voltage signal is shown in upper panel and the nitrogen peak is enlarged. In the lower panels the MS ion current for the major, minor 1 and minor 2 beams are shown. Note the difference between the diluted carbon peak for the TCD signal compared to the ion current signals. *Right:* Shown are the signals for a blank sample. Note that only the carbon blank signal is visible.



**Figure 2-4.** Chromatograms for CF-EA sulphur analysis. *Upper panel:* The TDC voltage signal. Both the carbon and nitrogen signal are displayed. The sulphur signal is near the detection limit, and is visible in the enlarged panel. Note that the nitrogen and carbon signal are poorly resolved. *Lower panels:* The ion currents for the mass 64 and 66 are shown.

### Calculating delta values of carbon and oxygen

Carbon is measured as carbondioxide and has 6 isobars as shown in Table 2.1. Mass spectrometers fitted with a triple collector system measures the masses of 44, 45 and 46 of  $\text{CO}_2$ . The fractional abundances of the different carbon dioxide masses are written as (Santrock *et al* 1985; Allison *et al* 1993)

$$\begin{aligned}
 {}^{44}\text{F} &= {}^{12}\text{F} \cdot {}^{16}\text{F} \cdot {}^{16}\text{F} \\
 (2.1) \quad {}^{45}\text{F} &= {}^{13}\text{F} \cdot {}^{16}\text{F} \cdot {}^{16}\text{F} + 2 \cdot {}^{12}\text{F} \cdot {}^{16}\text{F} \cdot {}^{17}\text{F} \\
 {}^{46}\text{F} &= {}^{12}\text{F} \cdot {}^{17}\text{F} \cdot {}^{17}\text{F} + 2 \cdot {}^{12}\text{F} \cdot {}^{16}\text{F} \cdot {}^{18}\text{F} + 2 \cdot {}^{13}\text{F} \cdot {}^{16}\text{F} \cdot {}^{17}\text{F}
 \end{aligned}$$

The corresponding results for the isotope ratios are

$$(2.2) \quad \begin{aligned} {}^{45}R &= \frac{{}^{45}F}{{}^{44}F} = {}^{13}R + 2 \cdot {}^{17}R \\ {}^{46}R &= \frac{{}^{46}F}{{}^{44}F} = 2 \cdot {}^{18}R + 2 \cdot {}^{13}R \cdot {}^{18}R + {}^{17}R^2 \end{aligned}$$

The goal of the correction algorithm is to obtain the carbon and oxygen isotope composition of a sample relative to the adapted international standard. The results are usually expressed through the  $\delta^{13}C$  and  $\delta^{18}O$  values, which are defined as

$$(2.3) \quad \delta^{13}C = \left( \frac{{}^{13}R_{sam}}{{}^{13}R_{std}} - 1 \right) \cdot 1000\text{‰}$$

and

$$(2.4) \quad \delta^{18}O = \left( \frac{{}^{18}R_{sam}}{{}^{18}R_{std}} - 1 \right) \cdot 1000\text{‰}$$

The indices *sam* and *std* refer to the isotope ratios of the sample and standard respectively. Combining the equations (2.2) and (2.3) yields

$$(2.5) \quad \delta^{13}C = \frac{{}^{45}R_{std} \cdot \delta^{45} - 2 \cdot {}^{17}R_{sam} + 2 \cdot {}^{17}R_{std}}{{}^{13}R_{std}}$$

The sample oxygen ratio  ${}^{17}R_{sam}$ , however, is not determined by the measurement and is thus unknown. It can be eliminated by assuming mass dependent fractionation in which case the  ${}^{17}R$  and  ${}^{18}R$  ratios are connected by (Craig 1957; Santrock *et al* 1985; Assonov and Brenninkmeijer 2003)

$$(2.6) \quad \frac{{}^{17}R_{sam}}{{}^{17}R_{std}} = \left[ \frac{{}^{18}R_{sam}}{{}^{18}R_{std}} \right]^\lambda$$

Setting  $\lambda=0.5$  yields

$$(2.7) \quad \frac{{}^{17}R_{sam}}{{}^{17}R_{std}} = \left[ \frac{{}^{18}R_{sam}}{{}^{18}R_{std}} \right]^{0.5} \approx 1 + \frac{\delta^{18}O}{2}$$

where the last term is obtained by a Taylor series expansion. This result can be used in (2.5) to eliminate the ratio  ${}^{17}R_{sam}$  thus giving

$$(2.8) \quad \delta^{13}C = \frac{{}^{45}R_{std}}{{}^{13}R_{std}} \delta^{45} - \frac{{}^{17}R_{std}}{{}^{13}R_{std}} \delta^{18}O = c_1 \cdot \delta^{45} - c_2 \cdot \delta^{18}O$$

A similar equation for  $\delta^{18}O$  can be written

$$(2.9) \quad \delta^{18}O = \frac{{}^{46}R_{std}}{2 \cdot {}^{18}R_{std}} \delta^{46} + \frac{{}^{13}R_{std} \cdot {}^{17}R_{std}}{{}^{18}R_{std}} \delta^{13}C = c_3 \cdot \delta^{46} + c_4 \cdot \delta^{13}C$$

**Table 2.2: Correction constants for carbon, oxygen and sulphur isotope analysis**

Publication	Standard	$^{13}\text{R}_{\text{std}}$	$^{17}\text{R}_{\text{std}}$	$^{18}\text{R}_{\text{std}}$	$^{33}\text{R}_{\text{std}}$	$^{34}\text{R}_{\text{std}}$	$c_1$	$c_2$	$c_3$	$c_4$	Comments
<i>Carbon correction constants</i>											
H. Craig 1957 two collector system	PDB	0.0112372 <sup>1</sup>	0.0007599	0.002079			1.0676	0.0676	1.0014	0.009	$\lambda=0.5$
Masslynx 4.0 values MS software							1.0676	0.0338	1.001	0.0021	
C.E. Allison et al 1993	PDB	0.0112372 <sup>1</sup>	0.00037995	0.002079 <sup>1</sup>			1.0676	0.0338	1.0021	0.0021	$\lambda=0.5$
C.E. Allison et al 1993	VPDB	0.0112372 <sup>1</sup>	0.00037886660	0.00206716068			1.0674	0.0337	1.0021	0.0021	$\lambda=0.5$ ; Used as correction constants.
C.E. Allison et al 1993	NBS 19	0.01125911254	0.00037844962	0.00206261293			1.0672	0.0336	1.0021	0.0021	$\lambda=0.5$
C.E. Allison et al 1993	VPDB CO <sub>2</sub>	0.0112372 <sup>1</sup>	0.00038080334	0.00208834908			1.0678	0.0339	1.0020	0.0021	$\lambda=0.5$
S.S. Assonov and Breninkmeijer 2003	VPDB CO <sub>2</sub>	0.0112372 <sup>1</sup>	0.00039511	0.00208834908 <sup>2</sup>			1.0703	0.0352	1.0020	0.0021	$\lambda=0.528$
C.E. Allison et al 1993	NBS 19 CO <sub>2</sub>	0.01125911254	0.00038038423	0.00208375471			1.0676	0.0338	1.0021	0.0021	$\lambda=0.5$
Santrock Abundances	VPDB	0.0112372 <sup>1</sup>	0.00041085	0.002079 <sup>1</sup>			1.0731	0.0366	1.0022	0.0022	$\lambda=0.516$
<i>Sulphur correction constants</i>											
Jensen and Nakai 1962	CDT	0.0112372 <sup>1</sup>	0.00038672 <sup>4</sup>	0.0020052 <sup>5</sup>	0.00789 <sup>3</sup>	0.0450045005	1.0892			0.0892	
Ding et al 2001	VCDT	0.0112372 <sup>1</sup>	0.00038672 <sup>4</sup>	0.0020052 <sup>5</sup>	0.0078772411	0.044162589	1.0909			0.0909	
Ding et al 1999	VCDT	0.0112372 <sup>1</sup>	0.00038672 <sup>4</sup>	0.0020052 <sup>5</sup>	0.0078795 <sup>1</sup>	0.0441520597 <sup>††</sup>	1.0909			0.0909	
Thode et al 1961	CDT	0.0112372 <sup>1</sup>	0.00038672 <sup>4</sup>	0.0020052 <sup>5</sup>	0.00789 <sup>3</sup>	0.044994 <sup>†</sup>	1.0892			0.0892	
Ding & Zhang 1989	CDT	0.0112372 <sup>1</sup>	0.00038672 <sup>4</sup>	0.0020052 <sup>5</sup>	0.00789 <sup>3</sup>	0.045035 <sup>†</sup>	1.0891			0.0891	
MacNamarra & Thode 1950	CDT				0.00789 <sup>†</sup>						

<sup>1</sup> H. Craig 1957; <sup>2</sup> C.E. Allison et al 1993; <sup>3</sup> MacNamarra & Thode 1950; <sup>4</sup> S.S. Assonov and Breninkmeijer 2003 (VSMOW); <sup>5</sup> VSMOW IAEA

<sup>†</sup> Values from Coleman 2004. <sup>††</sup> Values from Ding et al 2001.

Thus the sample carbon isotope composition  $\delta^{13}\text{C}$  depends on the sample oxygen isotope composition  $\delta^{18}\text{O}$  and vice versa. By combining the equations (2.8) and (2.9) the  $\delta^{13}\text{C}$  and  $\delta^{18}\text{O}$  values can be expressed as a function of the measured quantities  $\delta^{45}$  and  $\delta^{46}$

$$\delta^{13}\text{C} = \frac{c_1 \cdot \delta^{45} - c_2 \cdot c_3 \cdot \delta^{46}}{1 - c_2 \cdot c_4}$$

(2.10)

$$\delta^{18}\text{O} = \frac{c_3 \cdot \delta^{46} - c_1 \cdot c_5 \cdot \delta^{45}}{1 - c_2 \cdot c_4}$$

These equations are referred to as the Craig corrections, named after Harmon Craig (1957) who derived similar equations in 1957 for mass spectrometers fitted with two collectors (*further details can be found in (Verkouteren 2001), (Allison et al 1993) and (Santrock et al 1985)*). It should be noted that in the present context of EA-CF measurements on carbon dioxide only the  $\delta^{13}\text{C}$  value has practical significance, since the oxygen isotope composition will be a mixture of oxygen originating from the sample and oxygen added by the EA during combustion.

The correction constants used in equation (2.10) depend on the absolute isotope ratios  $^{13}\text{R}$ ,  $^{17}\text{R}$  and  $^{18}\text{R}$  of the used standard. For carbon, the PDB calcite material is used as the primary standard material, but since the original PDB material has been exhausted, the PDB scale has been fixed to the NBS 19 standard as VPDB. Determination of  $^{13}\text{R}$ ,  $^{17}\text{R}$  and  $^{18}\text{R}$  and the associated correction constants are shown in Table 2.2. The main difference in the values comes from establishing  $^{17}\text{R}$  from  $^{18}\text{R}$  by equation (2.6). The fractionation constant  $\lambda$  has been measured by Meijer and Li (1998) and by Santrock *et al* (1985). For  $\lambda$  values other than 0.5 the combination of equation (2.8) and (2.9) can not be solved analytically to obtain equation (2.10). Thus a numerical method must be adopted (Santrock *et al* 1985; Verkouteren 2001). The internationally recommended values are given in the IAEA TEC-DOC 825 by Allison *et al* (1993).

### Calculating delta values of nitrogen

Nitrogen is measured as molecular nitrogen with masses 28 and 29. The fractional abundances are given by

$$\begin{aligned} {}^{28}\text{F} &= {}^{14}\text{F} \quad {}^{14}\text{F} \\ {}^{29}\text{F} &= {}^{14}\text{F} \quad {}^{15}\text{F} \\ {}^{30}\text{F} &= {}^{15}\text{F} \quad {}^{15}\text{F} + {}^{14}\text{F} \quad {}^{16}\text{F} \end{aligned}$$

(2.11)

The last term for mass 30 stems from non-reduced NO and is of relevance only to CF-EA diagnostics. Hence the isotope ratio is simply given by the ratio of the relative abundances

$${}^{29}\text{R} = \frac{{}^{29}\text{F}}{{}^{28}\text{F}} = {}^{15}\text{R}$$

(2.12)

and the isotope composition is then given by the ratios

$$\delta^{15}\text{N} = \left( \frac{{}^{15}\text{R}_{sam}}{{}^{14}\text{R}_{std}} - 1 \right) \times 1000\text{‰}$$

(2.13)

The measured  $^{30}\text{F}_{\text{sample}}$  can be used to monitor the EA chemicals because it includes the molecule NO. When the reduction chemicals are exhausted, the contribution of NO to mass 30 increases. Hence, the relevant parameter to monitor is the amount of oxygen  $^{16}\text{F}_{\text{sample}}$  contributing to mass 30 ion current which can be found using equation (2.11) as

$$(2.14) \quad ^{16}\text{F}_{\text{sam}} = \frac{^{30}\text{F}_{\text{sam}} - ^{15}\text{F}_{\text{sam}}^2}{^{14}\text{F}_{\text{sam}}} .$$

This can be rewritten as

$$(2.15) \quad ^{16}\text{F}_{\text{sam}} = \frac{^{30}\text{F}_{\text{sam}}}{\left(^{28}\text{F}_{\text{sam}}\right)^{1/2}} - \frac{\left(^{29}\text{F}_{\text{sam}}\right)^2}{\left(^{28}\text{F}_{\text{sam}}\right)^{3/2}}$$

by eliminating  $^{14}\text{F}$  and  $^{15}\text{F}$  with the measured quantities  $^{28}\text{F}$  and  $^{29}\text{F}$ .

### Calibration of carbon and nitrogen isotope values

Prior to any calibration, the raw isotopes values have to be corrected for inter sample memory effects, time drifts and blank contributions. The blank contribution to sample delta values can be found by applying the mass balance equation (1.9), which yields (Fry *et al* 1992; Criss 1999; Werner and Brand 2001)

$$(2.16) \quad \begin{aligned} \delta^{13}\text{C}_{\text{meas}} \times A_{\text{meas}} &= \delta^{13}\text{C}_{\text{sample}} \times (A_{\text{meas}} - A_{\text{blank}}) + \delta^{13}\text{C}_{\text{blank}} \times A_{\text{blank}} \\ \Downarrow \\ \delta^{13}\text{C}_{\text{sample}} &= \frac{\delta^{13}\text{C}_{\text{meas}} \times A_{\text{meas}} - \delta^{13}\text{C}_{\text{blank}} \times A_{\text{blank}}}{A_{\text{meas}} - A_{\text{blank}}} . \end{aligned}$$

However, establishing reliable values of  $\delta^{13}\text{C}_{\text{blank}}$  and  $\delta^{15}\text{N}_{\text{blank}}$  can be a rather difficult task, especially for nitrogen. An alternative approach is to rearrange equation (2.16) and shift to nitrogen isotopes yields instead (Fry *et al* 1992):

$$(2.17) \quad \delta^{15}\text{N}_{\text{meas}} = \delta^{15}\text{N}_{\text{sam}} + \left(\delta^{15}\text{N}_{\text{blank}} - \delta^{15}\text{N}_{\text{sam}}\right) \frac{A_{\text{blank}}}{A_{\text{meas}}} .$$

Hence, when plotting the measured  $\delta^{15}\text{N}_{\text{meas}}$  values as a function of the inverse peak area, the y-intercept gives the  $\delta^{15}\text{N}_{\text{sample}}$  value of the sample, and the  $\delta^{15}\text{N}_{\text{blank}}$  of the sample can then be calculated from the slope if the blank area  $A_{\text{blank}}$  is known. Neither of these methods provide unique  $\delta^{15}\text{N}_{\text{blank}}$  values and the first approach is followed here (equation 2.16).

Two pathways can be followed, in order to calibrate sample with standards: either a one-point calibration (*scale factor 0*) or a linear normalisation (*scale factor not 0*). The one-point calibration is carried out by applying equation (1.3) twice. First, the  $\delta^{13}\text{C}_{\text{SAM/WG}}$  is converted to  $\delta^{13}\text{C}_{\text{SAM/WSTD}}$  and the latter is then converted to  $\delta^{13}\text{C}_{\text{SAM/VPDB}}$  (*WG denotes work gas, see also Figure 2-2*).

The linear normalisation is carried out by plotting  $\delta^{13}\text{C}_{\text{WSTD/WG}}$  versus  $\delta^{13}\text{C}_{\text{WSTD/VPDB}}$  which are then fitted with

$$(2.18) \quad \delta^{13}\text{C}_{\text{SAM/VPDB}} = \alpha \cdot \delta^{13}\text{C}_{\text{SAM/WG}} + \beta$$

to obtain a linear calibration relation.

### Calculating delta values of sulphur

Sulphur is measured as sulphur dioxide, thereby giving rise to isobaric interference of molecular ions of equal mass. Sulphur dioxide is a composite of 9 different masses ranging from the most abundant mass 64 up to mass 72 (see Table 2.1). For mass spectrometer isotope ratio analysis, only mass 64 and 66 are measured and their relative abundances and the isotope ratio of mass 66 are given by

$$(2.19) \quad {}^{64}F = {}^{32}F \cdot {}^{16}F \cdot {}^{16}F \\ {}^{66}F = {}^{34}F \cdot {}^{16}F \cdot {}^{16}F + 2 \cdot {}^{33}F \cdot {}^{16}F \cdot {}^{17}F + 2 \cdot {}^{32}F \cdot {}^{16}F \cdot {}^{18}F + {}^{32}F \cdot {}^{17}F \cdot {}^{17}F,$$

and

$$(2.20) \quad {}^{66}R = \frac{{}^{66}F}{{}^{64}F} = {}^{34}R + 2 \cdot {}^{33}R \cdot {}^{17}R + 2 \cdot {}^{18}R + {}^{17}R^2$$

This can be manipulated in a fashion similar to the Craig correction to give

$$(2.21) \quad 1 + \delta^{66} = \frac{\left(1 + \delta^{34}S\right) {}^{34}R_{std} + 2 \cdot \left(1 + \frac{\delta^{34}S}{2}\right) \cdot {}^{33}R_{std} \cdot \left(1 + \frac{\delta^{18}O}{2}\right) \cdot {}^{17}R_{std} + 2 \cdot {}^{18}R + \left(1 + \frac{\delta^{18}O}{2}\right)^2 \cdot {}^{17}R_{std}^2}{{}^{34}R_{std} + 2 \cdot {}^{33}R_{std} \cdot {}^{17}R_{std} + 2 \cdot {}^{18}R + {}^{17}R_{std}^2},$$

where equation (2.7) is used to eliminate  ${}^{17}R_{sam}$ . A similar manipulation for  ${}^{33}R_{sam}$  yields

$$(2.22) \quad \frac{{}^{33}R_{sam}}{{}^{33}R_{std}} = \left[ \frac{{}^{34}R_{sam}}{{}^{34}R_{std}} \right]^{0.5} \approx 1 + \frac{\delta^{34}S}{2}.$$

Rearranging equation (2.21) and neglecting all delta cross products gives

$$(2.23) \quad \delta^{34}S = \frac{{}^{34}R_{std} + 2 \cdot {}^{33}R_{std} \cdot {}^{17}R_{std} + 2 \cdot {}^{18}R_{std} + {}^{17}R_{std}^2}{{}^{34}R_{std} + {}^{33}R_{std} \cdot {}^{17}R_{std}} \times \delta^{66} + \frac{{}^{33}R_{std} \cdot {}^{17}R_{std} + 2 \cdot {}^{18}R_{std} + {}^{17}R_{std}^2}{{}^{34}R_{std} + {}^{33}R_{std} \cdot {}^{17}R_{std}} \times \delta^{18}O \\ = s_1 \cdot \delta^{66} + s_2 \cdot \delta^{18}O.$$

As for carbon, the  $\delta^{34}S$  values cannot be obtained without also measuring the  $\delta^{18}O$  content of the sample. The sulphur correction is, however, different compared to the Craig correction in two ways: only mass 64 and 66 are measured in CF-EA sulphur analysis, whereas for carbon the masses 44, 45 and 46 are measured simultaneously. For this reason, it is not possible to express  $\delta^{34}S$  as a function of measured quantities such as  $\delta^{65}$  and  $\delta^{66}$  in order to correct for the oxygen isotope composition. Assuming that mass 65 was measured, the sulphur correction would be inappropriate since the corresponding sulphur Craig correction is (Coleman 2004)

$$(2.24) \quad \delta^{34}\text{S} = 10.16 \cdot \delta^{66} - 18.23 \cdot \delta^{65} .$$

As revealed by equation (2.24), another approach to the correction of isobaric inferences in CF-EA sulphur analysis must be found (*further details on calculations can be found in (Coleman 2004)*).

The  $\delta^{18}\text{O}$  content of the sample is a composite of the possible oxygen from the sample itself and the isotopic composition of oxygen added during combustion (*tank oxygen*). The isotope oxygen composition after the flash combustion is given by the mass balance equation (1.1). If complete mixing of all oxygen during combustion is assumed (Criss 1999)

$$(2.25) \quad \delta^{18}\text{O}_{\text{combustion}} \times n_{\text{combustion}} = \delta^{18}\text{O}_{\text{sample}} \times n_{\text{sample}} + \delta^{18}\text{O}_{\text{tank}} \times n_{\text{tank}} .$$

The EA adds 25ml of oxygen during the sample insertion of which about 10ml are used for the combustion of the tin cup and the remaining 15ml for the sample combustion corresponding to  $\sim 0.62\text{mmol O}_2$ . The latter must be compared with typical oxygen bearing samples like for example  $\text{BaSO}_4$ . In the case of  $50\mu\text{g BaSO}_4$  about  $0.85\mu\text{mol}$  of oxygen is added by sample. Therefore the EA adds about 700 times more oxygen (*tank oxygen*) than the sample. Equation (2.25) shows that when the  $\delta^{18}\text{O}_{\text{tank}}$  and the  $\delta^{18}\text{O}_{\text{sample}}$  are equal and the amount of the tank oxygen is much larger than the oxygen concentration of the sample ( $n_{\text{tank}} \gg n_{\text{sample}}$ ), then the oxygen content of the combusted sample  $\delta^{18}\text{O}_{\text{combusted}}$  is almost equal to the tank oxygen  $\delta^{18}\text{O}_{\text{tank}}$ . Hence in most cases the term  $\delta^{18}\text{O}$  in the sulphur correction equation (2.23) can be assumed to be constant and will only depend on the difference between the oxygen isotope composition of the tank  $\delta^{18}\text{O}_{\text{tank}}$  and the reference gas  $\delta^{18}\text{O}_{\text{ref gas}}$  defined as  $\Delta^{18}\text{O}$ . The sulphur correction formula may thus be reformulated as (Grassineau *et al* 2001; Poulson 2005)

$$(2.26) \quad \delta^{34}\text{S} = s_1 \cdot \delta^{66} + \text{constant} .$$

The sulphur correction equation has now been reduced to a linear relation between  $\delta^{34}\text{S}$  and the measured  $\delta^{66}$ . For all CF-EA sulphur routine analysis the slope  $s_1$  is set to 1.089 and the intercept is found by fitting and using at least two standards. Poulson (2005) tested the assumption that  $\Delta^{18}\text{O}$  was constant during CF-EA analysis by measuring three different  $\text{BaSO}_4$  samples with similar  $\delta^{34}\text{S}$  values but with differing  $\delta^{18}\text{O}$  values ranging from 10‰ to 30‰, and found that the  $\Delta^{18}\text{O}$  variance was less than 2‰. The ratios  $^{33}\text{R}$  and  $^{34}\text{R}$  for sulphur reference materials can be found in Table 2.2 together with values of the associated correction constants  $s_1$  and  $s_2$  (equation (2.23)).

### Calibration of sulphur isotope values

Prior to calibration, the raw sulphur isotope values must be corrected for time drifts, i.e. a systematic change of the isotope values as a function of time. The CF-EA sulphur analysis displays no blank areas when running blank samples. Therefore, the blank correction is not applied for CF-EA sulphur analysis. After the drift correction, the sulphur isotope raw values are converted to VCDT by using at least two standards (*internal or international*) and using equation (2.26).

### Calculating weight percentage values

The elemental weight percentages can either be obtained from the EA TCD (*thermo chromatographic detector*) signal or by the integrated current signal from the mass spectrometer. The elemental weight percentages can be obtained either from the TCD signal or from the

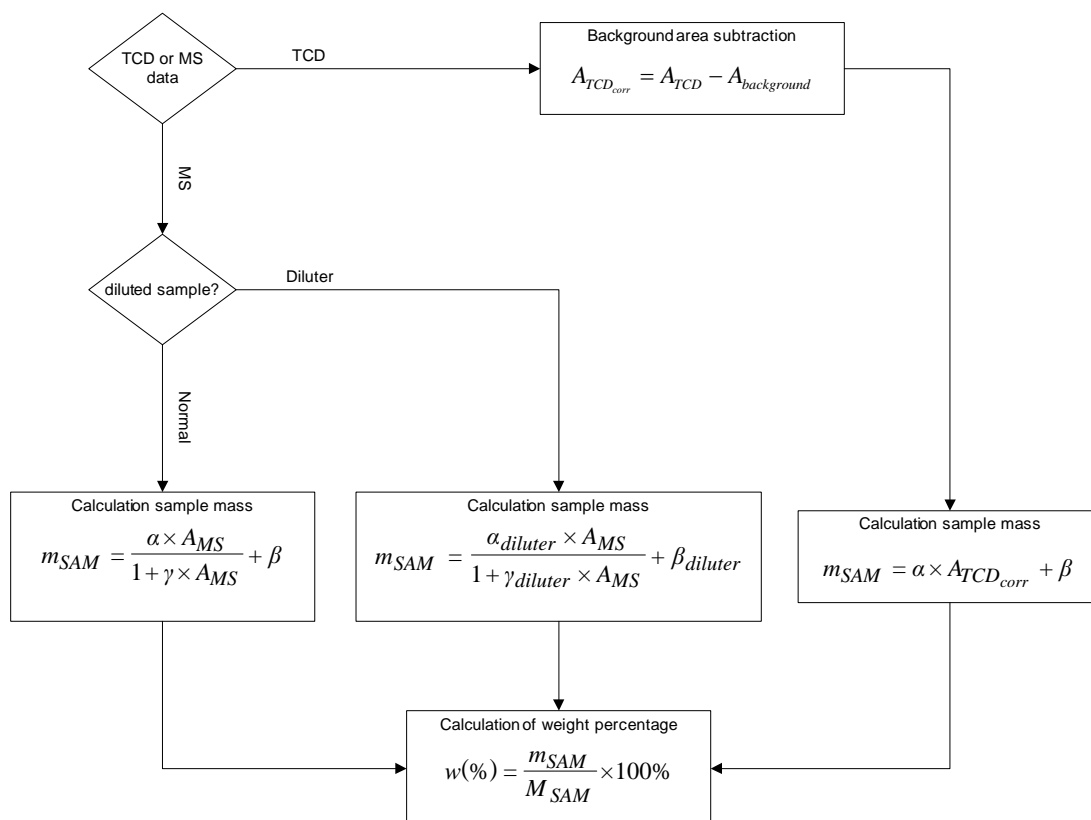


Figure 2-5. Flow diagram of the calculation algorithm for weight percentage values.

integrated mass spectrometer (MS) peak areas. In both cases a calibration is obtained by measuring samples with known weight percentage compositions. For all TCD samples the blank area has to be subtracted (see also Figure 2-5).

### The CF-EA method

Measured sample materials are often solids (*plant materials, lake sediments or bone collagen*) which need to be converted to gaseous samples prior to analysis. This can be done either off-line or on-line by an inlet preparation system. The continuous flow elemental analyser (CF-EA) (EuroVector 3024, see Figure 2-6) can convert solid samples to gaseous molecules and can be operated to give CO<sub>2</sub> and N<sub>2</sub> simultaneously and, with a different setup, SO<sub>2</sub>. Micrograms of sample material is wrapped in small tin cups and loaded into the sample tray.

Running in the carbon and nitrogen mode (Werner *et al* 1999) the CF-EA is fitted with a combustion tube and a reduction tube. The CF-EA entrance is kept at a constant helium pressure of 110kPa, resulting in a flow of approximately 110ml/min through the system. The combustion tube (*18mm/6mm quartz tube*) is filled to about half its full length with 2/3 chromium oxide (Cr<sub>2</sub>O<sub>3</sub>) in the upper part and 1/3 silvered cobalt oxide in the lower part. It is then heated to 1040°C. As the samples are dropped into the reactor tube, a pulse of oxygen is added and timed to meet the samples as they hit the reactor chemicals. The occurring flash combustion ensures complete oxidation of the samples. The chromium oxide adds additional oxygen if needed and the silvered cobalt oxide removes impurities such as sulphur. In the reduction reactor (*18mm/6mm quartz tube*), the formed nitrogen oxides are reduced to pure N<sub>2</sub> gas by copper kept at 650°C. To avoid isobaric interference, water is removed by a magnesium perchlorate water trap. The N<sub>2</sub> and CO<sub>2</sub> gases are then separated by a gas chromatographic column kept at 40°C (*3m*

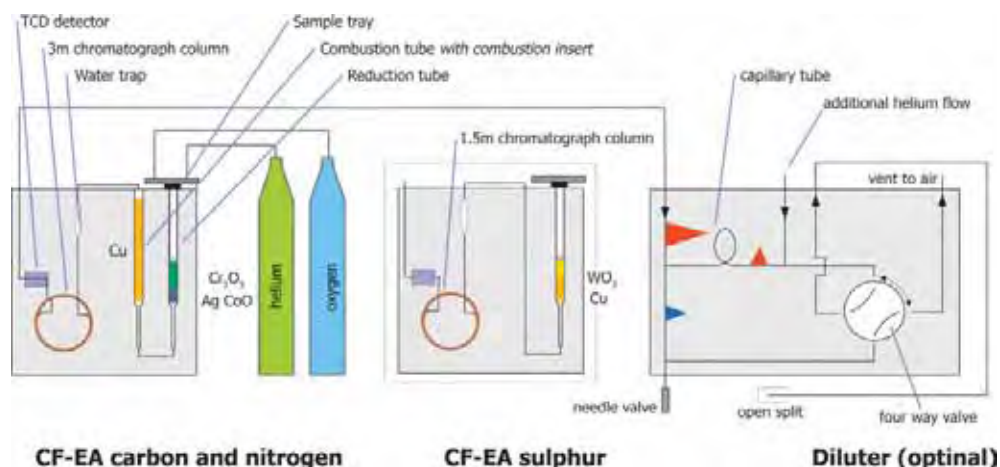


**Figure 2-6.** Schematic drawing of CF-EA inlet system. *Left:* Shown is CF-EA carbon and nitrogen setup (for details see text). *Middle:* Shown is CF-EA sulphur setup (for details see text). *Right:* Shown is the dilution box. When gaseous molecules produced in the EA enters the diluter box it may follow two main pathways to the mass spectrometer (MS). One pathway disables the capillary loop by switching the four way valves in a position such that the gas goes directly to the open split connection to the MS. The gas going through the capillary line is vented to air. The other pathway enables the capillary loop by switching the direction of the four way valve. Only a small fraction of the gaseous sample entering the diluter is going through the capillary loop due to its high flow resistance. Hence the sample gas following this pathway is reduced in size. To maintain constant He flow additional helium is added on this line. The amount of gas running through the capillary line is controlled by the adjustable needle valve.

stainless steel packed GC) and lead into the mass spectrometer via an open split (Platzner *et al* 1997). The reduction reactor will provide 120 to 200 samples as observed by the dark grey colour of the formed CuO. The combustion and water trap are routinely replaced for every 400 samples and no indication of exhaustion have been observed. The atomic carbon to nitrogen ratio is more than 3 for most sample materials and therefore an optional diluter system is inserted between the EA and the mass spectrometer (see Figure 2-6). Its function is to reduce the amount of carbon entering the mass spectrometer to avoid peak saturation of the collectors and at the same time to ensure that enough nitrogen is entering the mass spectrometer for analysis. The EA is also fitted with a thermochromatographic detector (TCD) for detection of the total sample amount. It is used for weight percentage determination and for diagnostic purposes.

In the sulphur mode (Kester *et al* 2001; Yun *et al* 2004), the CF-EA is fitted with a combined combustion and reduction tube (18mm/6mm quartz tube; see Figure 2-6). Wolfram oxide is used as an oxidative chemical and pure copper wire for the reduction of sulphates and sulphites to sulphur dioxide. The CF-EA entrance is kept at a constant helium pressure of 60kPa and a flow of approximately 100ml/min. Because most natural samples contain far more carbon and nitrogen than sulphur, the limiting factor for the durability of chemicals is the amount of copper added. The durability of the chemicals is about 100 to 120 samples per tube. During sulphur analysis the water trap is replaced for every 120 samples to avoid the formation of sulphuric acid, which can be a great hazard to the whole system. The formed  $\text{N}_2$ ,  $\text{CO}_2$  and  $\text{SO}_2$  gasses are separated by a 0.8m gas chromatographic column (PorapakQ) kept at 115°C (Morrison *et al* 1996).

To ensure stable long-term conditions for flash combustion in both modes, the combustion tube is fitted with a small glass tube insert closed at one end by silica wool to collect the ashes from the combusted samples. The glass insert has small side holes near the bottom to ensure a constant helium flow as they are filled with ash. The glass inserts are replaced for every 40 samples.

The IsoPrime mass spectrometer (GV Instruments) is coupled to a dual inlet used for reference pulse injections during CF-EA analysis (see Figure 2-7). Traditionally, the dual inlet is used for analysis of off-line prepared carbon dioxide samples. It is fitted with two bellows: one for refer-

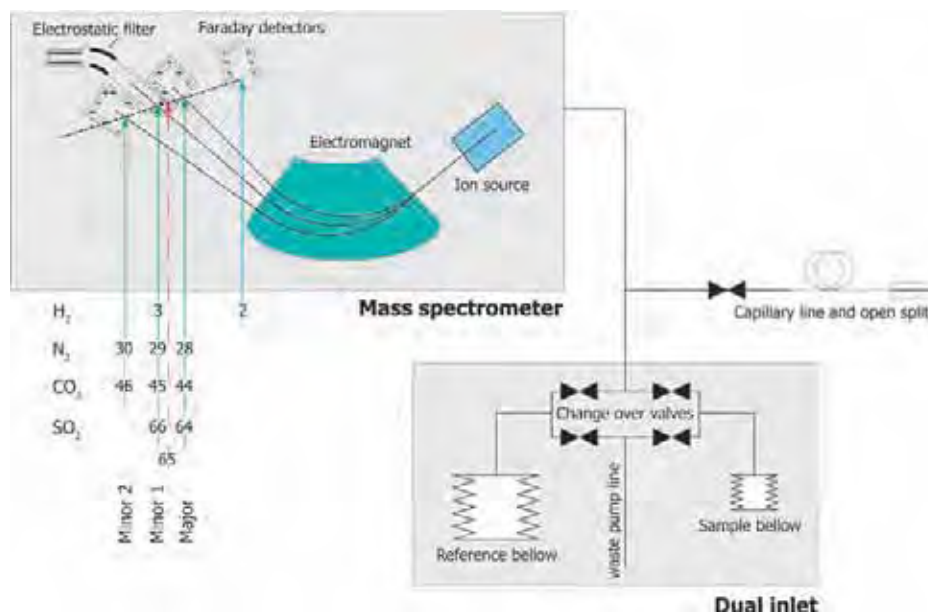


**Figure 2-7.** Schematic drawing of the mass spectrometer and the dual inlet system. The gaseous samples enter the mass spectrometer through the open split from EA inlet system. In the CF-EA mode the dual inlet operates as a reference gas injector (for details see text). The mass spectrometer is fitted with an electron impact ion source (see also Figure 2-8), an electromagnet and a Faraday detector system (for details see text). The approximate positions of the masses corresponding to gaseous samples of H<sub>2</sub>, N<sub>2</sub>, CO<sub>2</sub> and SO<sub>2</sub> are shown.

ence gas CO<sub>2</sub> and one for sample gas CO<sub>2</sub>. Two capillaries connect the bellows with the change-over valve block and are narrowed at their ends in order to reduce gas pressure to an appropriate level for the ion source (approx 10<sup>-6</sup> Torr). The dimensions of the capillaries are set in order to obtain a viscous gas flow which ensures that the mean free path length of the gaseous molecules is much smaller than the capillary dimensions. This is important in order to avoid back diffusion and isotopic fractionation of gas and sample reservoirs. The change-over valves ensure a continuous gas flow out of the dual inlet by letting the reference gas into the mass spectrometer and the sample gas into the waste line (*vacuum pump*) and *vice versa*. This ensures an equal flow rate and a steady gas flow through the capillaries of both gas reservoirs at all times (see e.g. Platzner *et al* 1997). During analysis, the two bellows are adjusted to give equal major beams (*mass 44*) in the mass spectrometer Faraday cups and the reference and sample gas pulses are then measured in turns. In the CF-EA carbon and nitrogen mode the change-over valves are only operated to give reference pulses of carbon and nitrogen, so that the 'reference gas' bellow is filled with N<sub>2</sub> and the 'sample bellow' with CO<sub>2</sub>. For CF-EA sulphur analysis only the 'reference bellow' is used and it is filled with SO<sub>2</sub> gas. In other words, in the CF-EA mode the otherwise sophisticated dual inlet only serves as a gas reservoir holding the reference gases needed for analysis.

The mass spectrometer consists of three main parts: an ion source, an electromagnet and a Faraday cup detection system (see Figures 2-7 & 2-8). The ion source ionizes the gaseous molecules by electron impact. The electrons are generated by a thorium-coated filament. A permanent magnet is fitted between the filament and the electron cup making the emitted electrons spiral, thus both guiding and increasing their pathways and thereby also the electron to molecule collision probability. The source housing is typically kept at around 3000 volts. This potential difference generates an acceleration force yielding an energy of approximately 3 keV. The extraction slits are set at a fixed percentage of the source potential (~80%). The upper part of the extraction slits is called the half-plate. It is kept at the extraction voltage and its voltage can be adjusted by

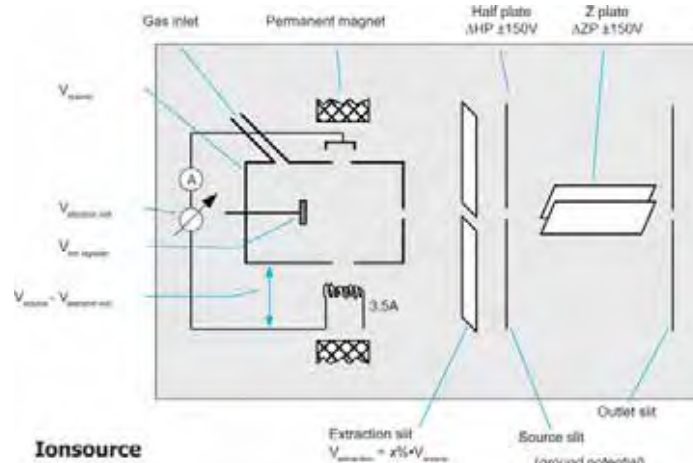


Figure 2-8. Schematic drawing of the ion source.

$\pm 150$  volts for vertical beam adjustments. Similarly, the voltage difference between the Z plates can be set to  $\pm 150$  volts for horizontal beam adjustments.

The electromagnet is used for the mass separation by momentum focusing. A moving charged particle or molecule entering an electromagnetic field will obey Lorentz' law (see e.g. Griffiths 1989):

$$(2.27) \quad \mathbf{F} = q \cdot \mathbf{v} \times \mathbf{B}.$$

Where  $q$  is the particle charge,  $\mathbf{v}$  its velocity,  $\mathbf{B}$  the magnetic field and  $\mathbf{F}$  is the resulting force. When the velocity  $\mathbf{v}$  and the magnetic field  $\mathbf{B}$  are perpendicular the resulting force  $\mathbf{F}$  will always be perpendicular to the plane spanned by  $\mathbf{v}$  and  $\mathbf{B}$ . Hence, the resulting motion of the particle will be circular. Inserting the centrifugal acceleration  $v^2/r$  and the particle mass  $m$  and taking the numerical value of the vector fields equation (2.27) yields

$$(2.28) \quad m \frac{v^2}{r} = qvB$$

$$\Downarrow$$

$$\frac{mv}{q} = rB = \text{constant}.$$

Thus for the beam to enter a collector the ratio of particle momentum ( $\mathbf{p}=m \cdot \mathbf{v}$ ) versus the particle charge  $q$  must equal the product of the deflection radius  $r$  and the magnetic field  $B$ . Particles diverging in mass will, on coming out of the ion source, have the same energy distributions and charge states but different momentums. Hence, the magnetic field will separate particles of different mass.

One of the collectors is fitted with an electrostatic filter used for hydrogen analysis of water samples (Merren 2000; Morrison *et al* 2001). The filter is mounted to avoid interference of scattered helium ions in the mass 3 detector during hydrogen analysis (see Figure 2-7). Particles passing through this particular electrostatic filter must follow a circular track and the conditions for passing can thus be found by setting the centrifugal force equal to the electrostatic force:

$$(2.29) \quad m \frac{v^2}{r} = qE.$$

Inserting the classical kinetic energy  $w$  ( $w=mv^2/2$ ) equation (2.29) yields:

$$(2.30) \quad w = \frac{qEr}{2} = \text{constant} .$$

Thus the electrostatic filter functions as an energy filter, because only particles with a kinetic energy equal to  $qEr/2$  will have free passage between the two parallel curvature plates. Taking the magnetic field and electrostatic filter in combination yields

$$(2.31) \quad v = \frac{r_{magnet}}{r_{electrostatic}} \times \frac{E}{B} .$$

Thus only particles with a velocity equal to the ratio of radius of the magnetic curvature  $r_{magnet}$  and the electrostatic curvature  $r_{electrostatic}$  multiplied by the ratio of the electric field  $E$  versus the magnetic field  $B$  will enter this collector. Together, they work as a velocity filter that disables the detection of scattered helium ions during hydrogen analysis, since they will have different velocities compared to the mass 3 hydrogen molecules.

### Quality assurance results

Important in stable isotope analysis is the identical treatment principle (Werner and Brand 2001), which states that standards and samples must receive the same treatment during analysis. Thus, for example, isotope results may not be reported against the internal work gas but should be reported relative to standards, having their analysis gas obtained in an identical way to the sample gas.

CF-EA carbon and nitrogen batch analysis		CF-EA sulphur batch analysis	
Autosampler position	Sample	Autosampler position	Sample
1	Internal standard	1	Internal Standard I
2	Internal standard	2	Internal Standard I
3	Blank	3	Internal Standard I
4	Internal standard	4	Internal Standard II
5 ... 12	Samples	5	Internal Standard II
13	Internal standard	6 ... 12	Samples
14	Blank	13	Performance standard
15	Blank	14 ... 24	Samples
16	Internal standard	25	Performance Standard
17	Internal standard	26 ... 31	Samples
18 ... 24	Samples	32	Internal Standard I
25	Performance standard	33	Internal Standard I
24 ... 31	Samples	34	Internal Standard II
32	Internal standard	35	Internal Standard II
32	Internal standard	36	Internal Standard II
33 ... 36	Samples	37 ... 40	Samples
37	Performance Standard		
38 ... 40	Samples		

**Figure 2-9.** CF-EA batch analysis setup for carbon, nitrogen and sulphur. **Left:** Pre-filled sample list for CF-EA carbon and nitrogen with fixed positions for one standard, one performance standard and samples. **Right:** Pre-filled sample list for CF-EA sulphur analysis with fixed positions for the two standards, one performance standard and samples.

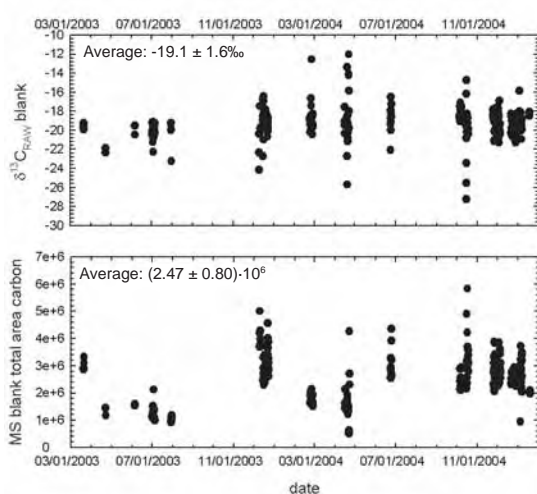


**Figure 2-10.** Time series of mass spectrometer carbon blank area and  $\delta^{13}\text{C}_{\text{blank}}$  values.

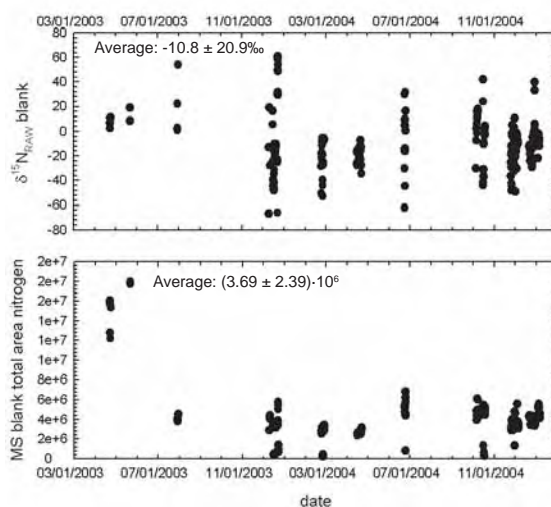


**Figure 2-11.** Time series of mass spectrometer nitrogen blank area and  $\delta^{15}\text{N}_{\text{blank}}$  values.

Monitoring the day-to-day analysis environment and long-term accuracy and precision are central aspects of stable isotope analysis. Therefore, a batch sample list contains a pre-filled mandatory fixed position for internal standards, performance standards and blanks as recommended by Werner *et al* (2001) for all routine CF-EA analysis (see Figure 2-9). The internal standards are used for isotope calibration to the internationally accepted scales (*VPDB*, *AIR* and *VCDT*) and also for correction of drift trends. The performance standards are used for quality assurance purposes only and are treated as unknown samples. They are chosen to resemble real samples as closely as possible. The data of available international standards and internal standards are shown in Table 2.3. Blank samples are measured for monitoring purposes and for blank corrections of standards and samples. All unknown samples are measured twice as an extended quality assurance, except for samples in connected sequences, like sedimentary samples. These are only measured once, as any out-liers can be found by plotting against depth, for example. The repeated sample measurement is, by rule of thumb, separated from the original by at least one intermediate batch run.

### Carbon and nitrogen analysis

In the following, a presentation of the standards and performance standards for the CF-EA carbon and nitrogen method is given. The covered period goes back to early 2003 and forward to the spring 2005. In total, 4500 combined carbon and nitrogen analyses were carried out and of these 37% were on standards. The mass and TCD spectrum for nitrogen and carbon is shown in Figure 2-3. Also shown is an example of a diluted carbon sample.

#### *Results of carbon and nitrogen blank samples*

Determining the contribution from blank samples is important to both isotope ratio analysis and weight percentage calculations. Figures 2-10 and 2-11 show the mass spectrometer area of blank samples together with their isotope  $\delta^{13}\text{C}_{\text{raw}}$  and  $\delta^{15}\text{N}_{\text{raw}}$  values. The carbon blank time series (Figure 2-10) shows constant behaviour for both the measured areas and isotope values. Blank areas and  $\delta^{13}\text{C}_{\text{blank}}$  values are found, by the normal distribution probability plot in Figure 2-12, to be  $2.47 \pm 0.80 \cdot 10^6$  and  $-19.1 \pm 1.6\text{‰}$  respectively. The nitrogen blank areas and  $\delta^{15}\text{N}$  values exhibit significantly larger scatter and, as revealed by the normal distribution probability

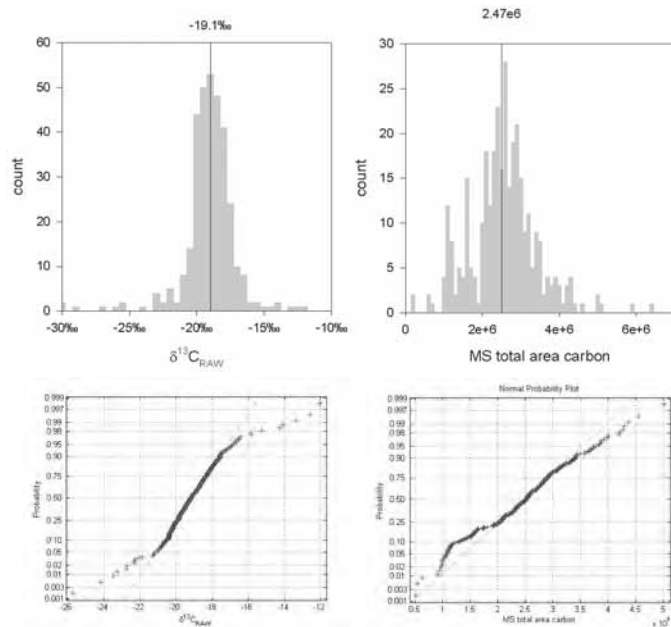


**Figure 2-12.** Estimation of the carbon mass spectrometer blank area and  $\delta^{13}\text{C}_{\text{blank}}$  value. In the upper panels histograms of all measured mass spectrometer carbon blank areas and  $\delta^{13}\text{C}_{\text{blank}}$  values are shown. In the lower panels normal probability plots are shown. The carbon blank area is estimated to be  $2.47 \cdot 10^6$  and the  $\delta^{13}\text{C}_{\text{blank}}$  value to be  $-19.1\text{‰}$ .

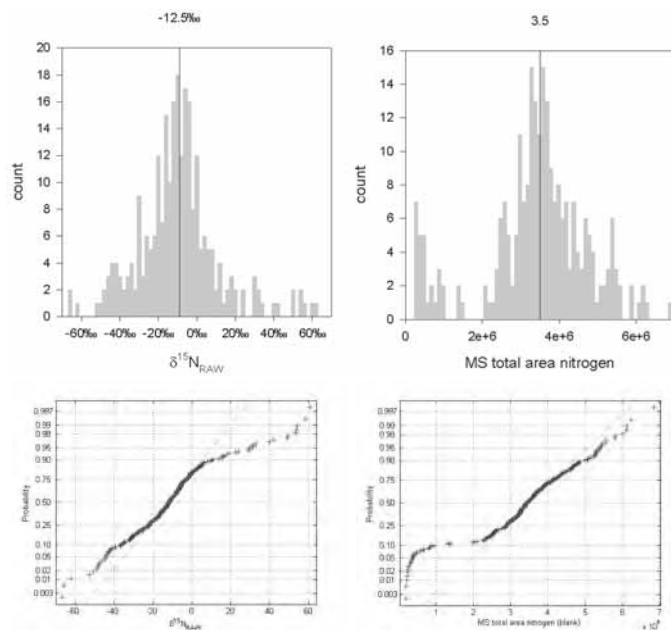


**Figure 2-13.** Estimation of the nitrogen mass spectrometer blank area and  $\delta^{15}\text{N}_{\text{blank}}$  value. In the upper panels histograms of all measured mass spectrometer nitrogen blank areas and  $\delta^{15}\text{N}_{\text{blank}}$  values are shown. In the lower panels normal probability plots are shown. The nitrogen blank area is estimated to be  $3.5 \cdot 10^5$  and the  $\delta^{15}\text{N}_{\text{blank}}$  value to be  $-12.5\text{‰}$ . The nitrogen blank data frequently displays extreme values as seen by both the histogram and the normal probability plot for both parameters.

**Table 2.3: IRMS standard materials**

The assigned values of the international standards are shown and can be found at IAEA (Details and reference to reports can be found at: <http://www.iaea.org/programmes/aqcs/pdf/catalogue.pdf>). Unless otherwise stated the values of the internal work and performance standards are average and standard deviation of all data. All weight percentage data are average and standard deviation where values greater than  $\pm 2\sigma$  have been removed unless otherwise stated. ( ) denote carbon or nitrogen weight percentage data from CF-EA sulphur analysis. All weight percentage values has been obtained by the CF-EA carbon and nitrogen method unless otherwise stated.

Standard	Material	$\delta^{13}\text{C}$	$\sigma$	$\delta^{15}\text{N}$	$\sigma$	$\delta^{34}\text{S}$	$\sigma$	Measured weight percentage		
		‰ VPDB		‰ AIR		‰ VCDT		carbon	nitrogen	sulphur
International standards								deviations $>\pm 2\sigma$ removed		
IAEA-C6	Sucrose	-10.80						43.8 $\pm$ 2.3%		
IAEA-C7	Oxalic Acid	-14.50						21.8 $\pm$ 3.7%		
IAEA-C8	Oxalic Acid	-18.30						20.4 $\pm$ 1.8%		
IAEA-N-1	Ammonium Sulfate			0.40				21.5 $\pm$ 0.6%		
IAEA-N-2	Ammonium Sulfate			20.30				19.8 $\pm$ 1.4%		
IAEA-NO-3	Potassium Nitrate			4.70				13.7 $\pm$ 0.4%		
IAEA-S-1	Silver Sulfide					-0.30				12.4 $\pm$ 0.5%
IAEA-S-2	Silver Sulfide					22.70	0.20			12.3 $\pm$ 0.6%
IAEA-S-3	Silver Sulfide					-32.30	0.20			12.9 $\pm$ 0.4%
NBS 123	Sphalerite					17.10				29.9 $\pm$ 3.7%
NBS 127	Seawater Sulfate					20.30				12.4 $\pm$ 0.9%
NIST OX-I	Oxalic Acid	-19.00						20.2 $\pm$ 0.6%		
NIST OX-II	Oxalic Acid	-17.80						22.3%		
USGS 40	L-Glutamic Acid	-26.60	0.10	-4.50	0.1			42.3 $\pm$ 2.1%	9.9 $\pm$ 1.0%	
USGS 41	L-Glutamic Acid	37.80	0.10	47.60	0.1			43.0 $\pm$ 2.1%	10.3 $\pm$ 0.9%	
Internal work and performance standards										
AMS BGD	Bone, Collagen	-16.1	0.3	11.6 11.4 <sup>o</sup>	0.7 1.5 <sup>o</sup>	14.0	0.9	42.3 $\pm$ 2.0% (42.8 $\pm$ 0.8%)	15.8 $\pm$ 0.4% (15.4 $\pm$ 0.3%)	0.32 $\pm$ 0.03%
Anthracite <sup>1</sup>	Charcoal									
Bbot <sup>2</sup>		-26.9	0.5			17.60 <sup>†</sup>	0.20	72.5% <sup>††</sup>	6.5% <sup>††</sup>	7.4% <sup>††</sup>
BWB II <sup>3</sup>	Bone, Collagen	-18.84 <sup>†</sup>	0.10	14.28 <sup>†</sup>	0.10			49.8 $\pm$ 1.5%	15.3 $\pm$ 0.3%	
CTH2ST51 <sup>3</sup>	Corn meal					1.9	0.3	(40.6 $\pm$ 2.2%)	(1.7 $\pm$ 0.3%)	0.12% <sup>††</sup>
GelA	Gelatine	-22.30 <sup>†</sup>	0.16	6.42 <sup>†</sup>	0.15	4.88 <sup>†</sup>	0.15	45.4 $\pm$ 1.2%	16.7 $\pm$ 0.8%	0.44 $\pm$ 0.03%
Urea <sup>2</sup>	Urea	-48.24		-0.19				20.00% <sup>††</sup>	46.65% <sup>††</sup>	

<sup>1</sup>Center for Isotope Research, Grönningen; <sup>2</sup> EuroVector, Milan, Italy; <sup>3</sup> GV Instruments, Manchester, UK <sup>†</sup>Values from Table 2.4 <sup>‡</sup> Values from Table 2.5 <sup>††</sup> Used as weight percentage standards. <sup>o</sup> All data used. Above deviations  $>\pm 2\sigma$  removed

plots (Figure 2-13), they do not follow normal distribution to the same extent as carbon and are thus difficult to interpret.

Figure 2-14 shows the blank TCD data; both carbon and nitrogen show constant values. Note, however, that nitrogen has a few high values compared to carbon.

#### Results of carbon and nitrogen stable isotope analysis

During normal routine analysis the BWB II and GelA internal working standards are used for calibration. To monitor long-term performance, the performance standards AMS BGD and BBOT are used. The AMS BGD standard is used for analysis where dilution of carbon was not employed, whereas the performance standard BBOT is used in connection with diluted carbon samples. The AMS BGD standard is extracted collagen (Brown *et al* 1988) from a whalebone

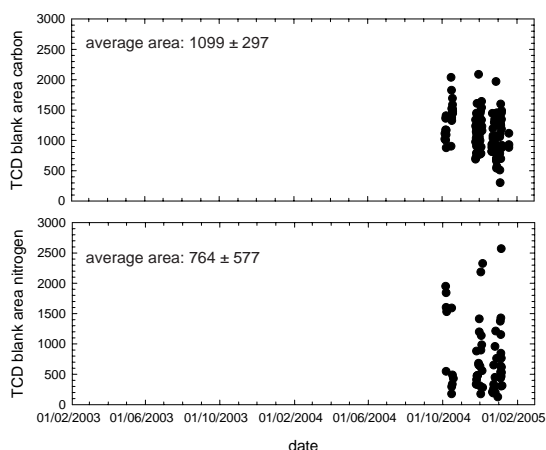


**Figure 2-14.** Time series of carbon (*upper*) and nitrogen (*lower*) TCD blank areas. Note that TCD measurements first started in autumn 2004.

and is prepared in small batches. Thus, apart from monitoring the performance of mass spectrometric analysis, the AMS BGD standard is also monitoring the stability of our collagen extraction method.

Figure 2-15 shows the  $\delta^{13}\text{C}_{\text{VPDB}}$  time series of the performance standards AMS BGD and BBOT together with the primary working standards, together with similar data for  $\delta^{15}\text{N}_{\text{AIR}}$ . The primary working standards BWB II and Gela displays the general measurement scatter. Periods with offset values or high scatter of the performance standards are periods of poor reproducibility and accuracy, and thus indicate a general analysis problem.

For the main purpose of calibrating the primary internal working standards, the international standards are also measured. Batches that include international standards are never one-point calibrated, but either follow along the sample processing as a pseudo performance standard (*i.e. they treated as normal samples*) or several are measured and the isotope calculations are done *via* equation (2.18). Figures 2-16 and 2-17 show the time series of international standards used as pseudo performance standards for carbon and nitrogen. The carbon series of international pseudo standards are in general within  $\pm 2\%$  difference from their assigned value (*denoted true value*), except for USGS 41, which deviates significantly from 0‰. The nitrogen data (*Figure 2-17*) shows periods of very high scatter indicating poor analysis conditions and the standards IAEA N1, USGS 40 and USGS 41 generally show significantly large deviations from 0‰.

The linear calibrations are normally carried out with three or more international standards. The measured differences from their assigned isotope values as a function of their assigned values may therefore carry information on general offsets from their true value, *i.e.* problems of storage or analysis or information on scale expansion, as seen by Figures 2-18 and 2-19.

Table 2.4 shows the calibration outcome of the BWB II and Gela internal standards together with the associated measurements on the performance standard AMS BGD.

#### *Results of carbon and nitrogen weight percentage analysis*

The weight percentage calibration plots for mass spectrometer total areas for carbon and nitrogen are shown in Figures 2-20A and 2-20B. The calibration plots for the TCD data are shown in Figures 2-20C and 2-20D. The right hand side of these graphs displays a sample weight histogram of all samples. Note that some TCD carbon sample data fall out of the range of the calibration line and should therefore be considered with caution. The different slopes of grouped data for both carbon and nitrogen (*Figures 2-20A and 2-20B*) reflect variable ion source settings during the different batch analyses. Figure 2-21 shows the weight percentage time series of the performance standards AMS BGD and Gela (*note that in contrast to the isotope analysis, Gela*

**Table 2.4:  $\delta^{13}\text{C}$  and  $\delta^{15}\text{N}$  calibration of the Internal standards BWB II and Gela**

The standards have been calibrated by the linear method by use of several international standards.

SLI <sup>†</sup>	$\delta^{13}\text{C}$				$\delta^{15}\text{N}$				$\delta^{13}\text{C}$				$\delta^{15}\text{N}$								
	$\sigma$	$\sigma$	$\sigma$	$\sigma$	dev	$R^2$	$\delta^{15}\text{N}$	$\sigma$	n	dev	$R^2$	$\delta^{13}\text{C}$	$\sigma$	$\sigma$	n	dev	$R^2$	$\delta^{15}\text{N}$	$\sigma$	n	
	%o VPDB				%o AIR				%o VPDB				%o AIR								
<i>BWB II, Collagen extracted from whale bone</i>																					
67							14.33	0.30	7	0.2	1.000										
68							14.89	0.30	8	2.0	0.9996										
70	-18.39	0.23	8	1.9	0.9947	14.66	0.35	6	1.1	0.9976	-15.96	0.87	2	12.30	0.09	2	12.30	0.09	2	12.30	0.09
72	*-18.56	0.07	8		0.9972	*15.46	0.18	7		0.9971	-15.98	0.01	2	12.32	0.02	2	12.32	0.02	2	12.32	0.02
89	-18.65	0.27	12	0.7	0.9960						-15.91	0.25	3								
159	-18.82	0.04	16	0.3	0.9994						-16.13	0.03	4								
160	-18.93	0.07	16	-1.4	0.9998						-16.29	0.13	4								
247	-18.98	0.15	2	-1.0	1.0000	14.07	0.21	2	-1.0	0.9998	-16.10	0.09	4	12.03	0.31	4	12.03	0.31	4	12.03	0.31
248	-19.14	0.28	4	-1.1	0.9999	14.55	0.39	4	0.7	0.9993	-16.27	0.10	4	11.86	0.67	4	11.86	0.67	4	11.86	0.67
Micromass <sup>†</sup>	-18.50	0.20 <sup>◊</sup>	-	1.7	-	14.06	0.20 <sup>◊</sup>	-	-1.1	-											
Mike Richards <sup>††</sup>	-18.71	0.20 <sup>◊</sup>	-	0.6	-	14.22	0.20 <sup>◊</sup>	-	-0.3	-											
	-18.84	0.06	$\chi^2_{\text{meas}}$	11.6		14.28	0.10	$\chi^2_{\text{meas}}$	8.1		-16.00	0.13	31.7	12.31	0.14	15.9					
			$\chi^2$	14.1					12.6												11.1
<i>Gela, Gelatine</i>																					
242	-22.34	0.30	10	-0.2	1.0000	6.28	0.27	8	-0.5	0.9994	-16.13	0.01	2	11.76	0.12	2	11.76	0.12	2	11.76	0.12
244	-22.27	0.20	15	0.1	1.0000	6.74	0.32	9	1.0	1.0000	-15.94	0.08	4	12.03	0.58	4	12.03	0.58	4	12.03	0.58
245	-22.30	0.25	16	0.0	0.9996	6.46	0.24	9	0.2	0.9988	-15.83	0.10	4	12.77	0.19	2	12.77	0.19	2	12.77	0.19
247	-22.31	0.13	16	-0.1	1.0000	6.29	0.36	12	-0.4	0.9998	-16.10	0.09	4	12.03	0.31	4	12.03	0.31	4	12.03	0.31
248	-22.53	0.22	16	-1.0	0.9999	6.26	0.40	12	-0.4	0.9993	-16.27	0.10	4	11.86	0.67	4	11.86	0.67	4	11.86	0.67
260	-22.39	0.14	8	-0.7	1.0000						-15.98	0.05	2								
286	-22.23	0.11	8	0.6	1.0000						-16.02	0.05	2								
287	-22.29	0.08	8	0.1	1.0000						-15.99	0.03	2								
294	-22.21	0.11	8	0.7	1.0000						-16.01	0.03	2								
310	-22.32	0.08	8	-0.2	1.0000						-16.06	0.07	2								
	-22.30	0.06	$\chi^2_{\text{meas}}$	2.6		6.42	0.14	$\chi^2_{\text{meas}}$	1.6		-16.10	0.02	54.1	12.04	0.19	20.6					
			$\chi^2$	16.9					9.5												9.5

Dev  $\sigma$  denotes the deviation from the mean value given in units of the standard deviation.  $R^2$  denotes regression coefficient for the linear fit.  $\chi^2_{\text{meas}}$  is measured  $\chi^2$  values and  $\chi^2$  represents the theoretical value. For the data to be normal distributed  $\chi^2_{\text{meas}} \leq \chi^2$ . <sup>†</sup> Sample List ID \* Disregarded measurement <sup>††</sup> Now GV Instruments <sup>†††</sup> Mike Richards, Department of Archaeological Science, Bradford <sup>◊</sup> Measurement uncertainty not given by submitter.

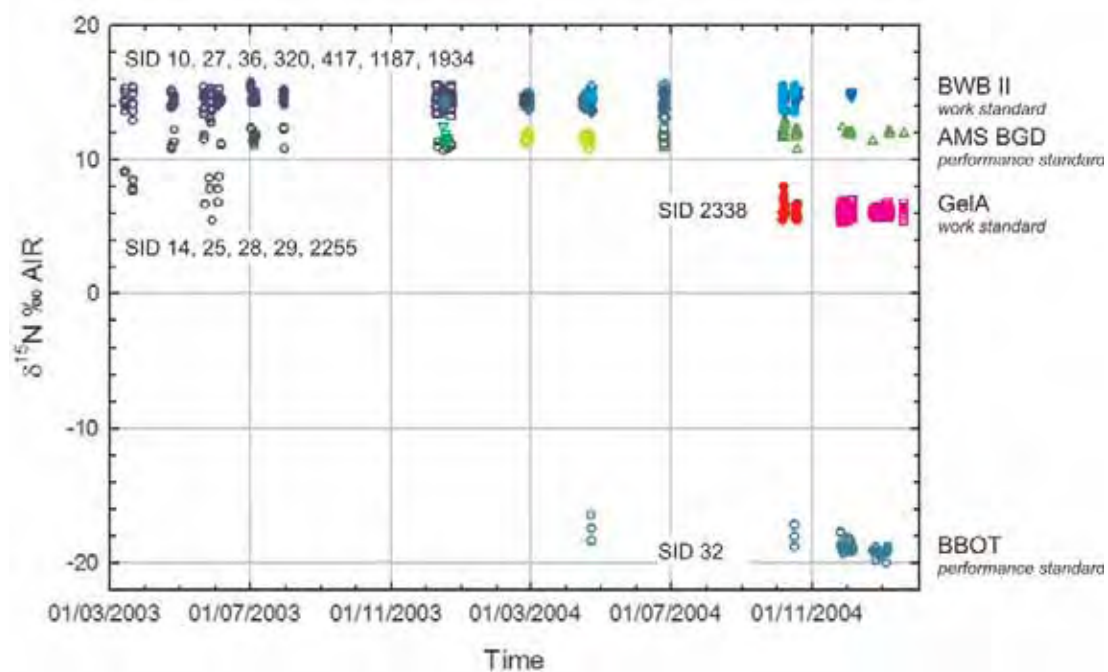
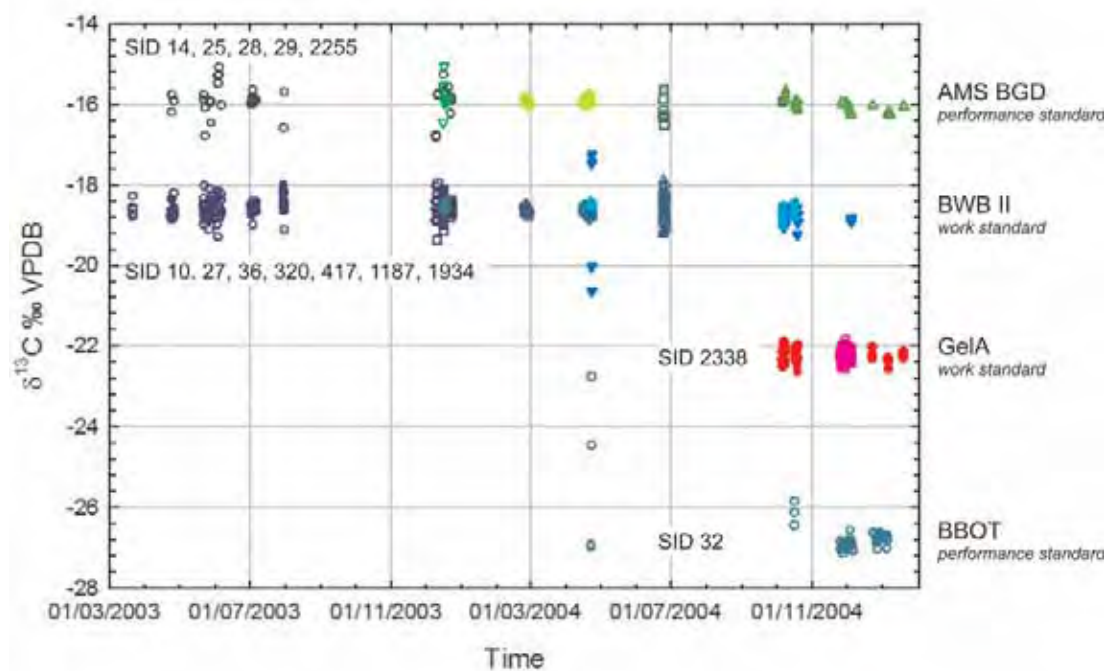


**Figure 2-15.** *Upper part:*  $\delta^{13}\text{C}$  performance standards and working standards as a function of time. *Lower part:*  $\delta^{15}\text{N}$  performance standards and working standards as a function of time. Open symbols denote measured values, whereas filled symbols are calibrated values. Each standard is marked with a colour code and each sample ID (SID) is marked by different symbols.

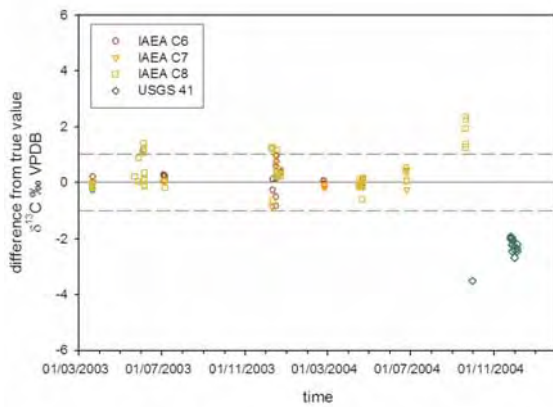


**Figure 2-16.**  $\delta^{13}\text{C}$  values of measured international standards not used for calibration. The difference between the measured and assigned values (*true*) is shown as a function of time. Note the very large deviation of USGS 41. The vertical lines are placed at  $\pm 1\%$ .

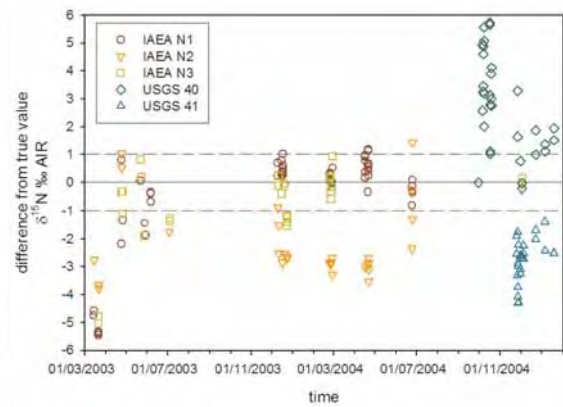


**Figure 2-17.**  $\delta^{15}\text{N}$  values of measured international standards not used for calibration. The difference between the measured and assigned values (*true*) is shown as a function of time. The international standards IAEA-N-1 and USGS 40 and USGS 41 all show large deviations from 0‰. The vertical lines are placed at  $\pm 1\%$ .

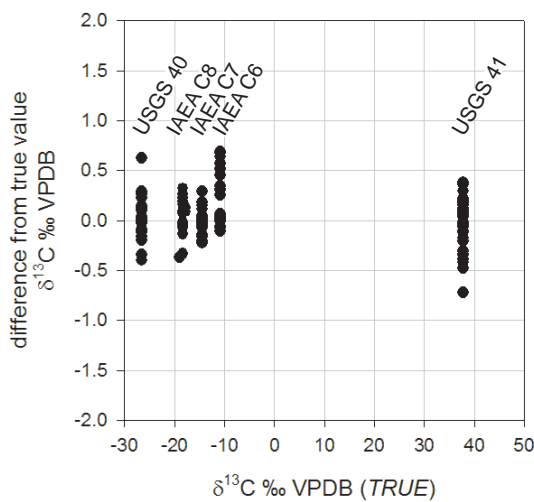


**Figure 2-18.**  $\delta^{13}\text{C}_{\text{VPDB}}$  values of international standards used for calibration. The difference between the measured and assigned values (*true*) is shown as a function of the true  $\delta^{13}\text{C}$ .

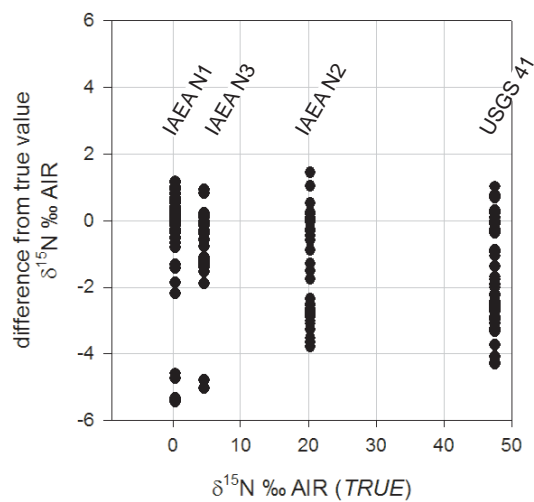


**Figure 2-19.**  $\delta^{15}\text{N}_{\text{AIR}}$  values of international standards used for calibration. The difference between the measured and assigned values (*true*) is shown as a function of the true  $\delta^{15}\text{N}$ . Note the large deviations towards more negative values for enriched samples, which could indicate scale problems.

is used as a weight percentage performance standard) for carbon and nitrogen. Figures 2-22 and 2-23 show the measured weight percentage of the used calibration standards as a function of their elemental weight.

Figure 2-24 displays the TCD carbon area versus the mass spectrometer total area for diluted and non-diluted samples. The average dilution factor is calculated to be 6.5.

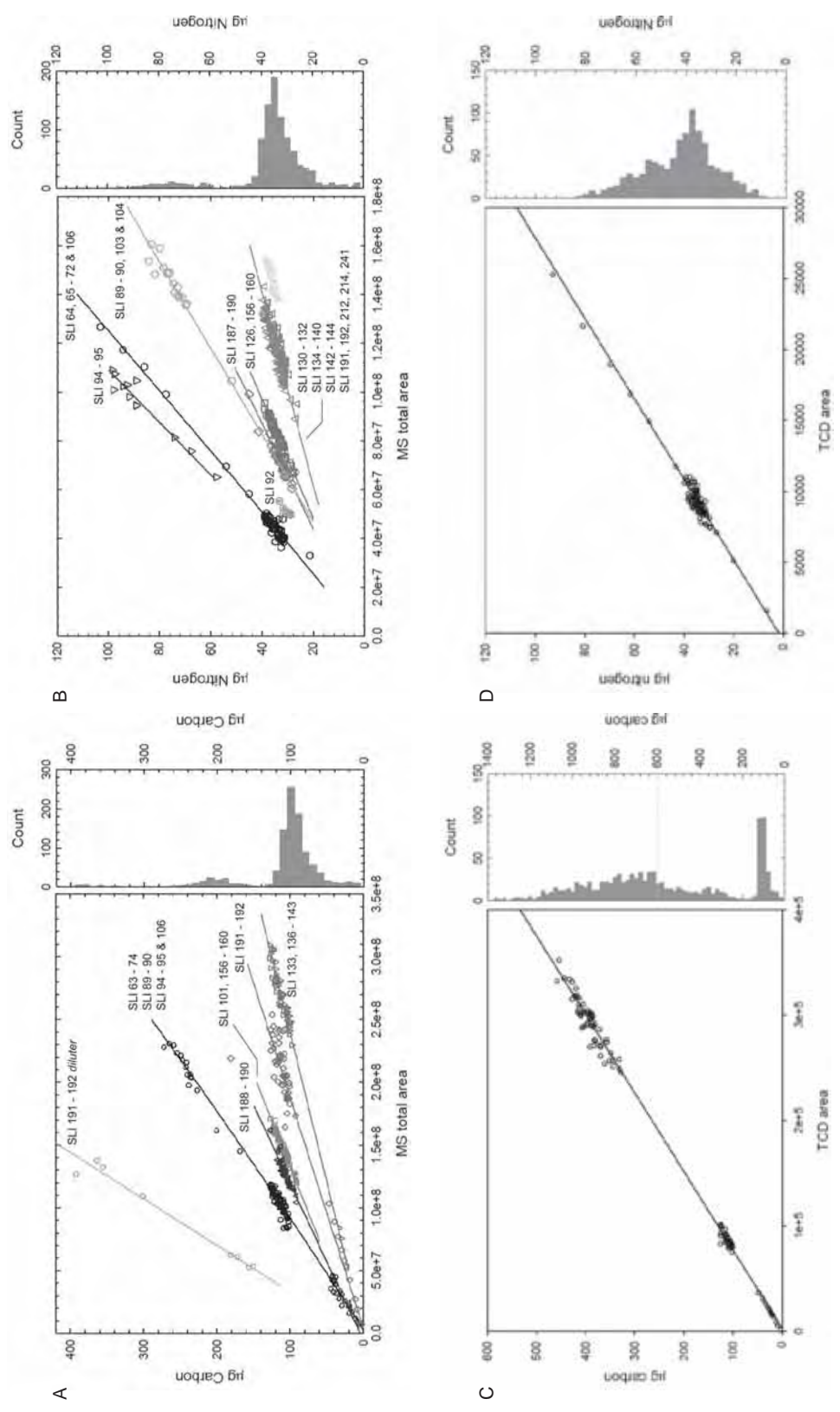
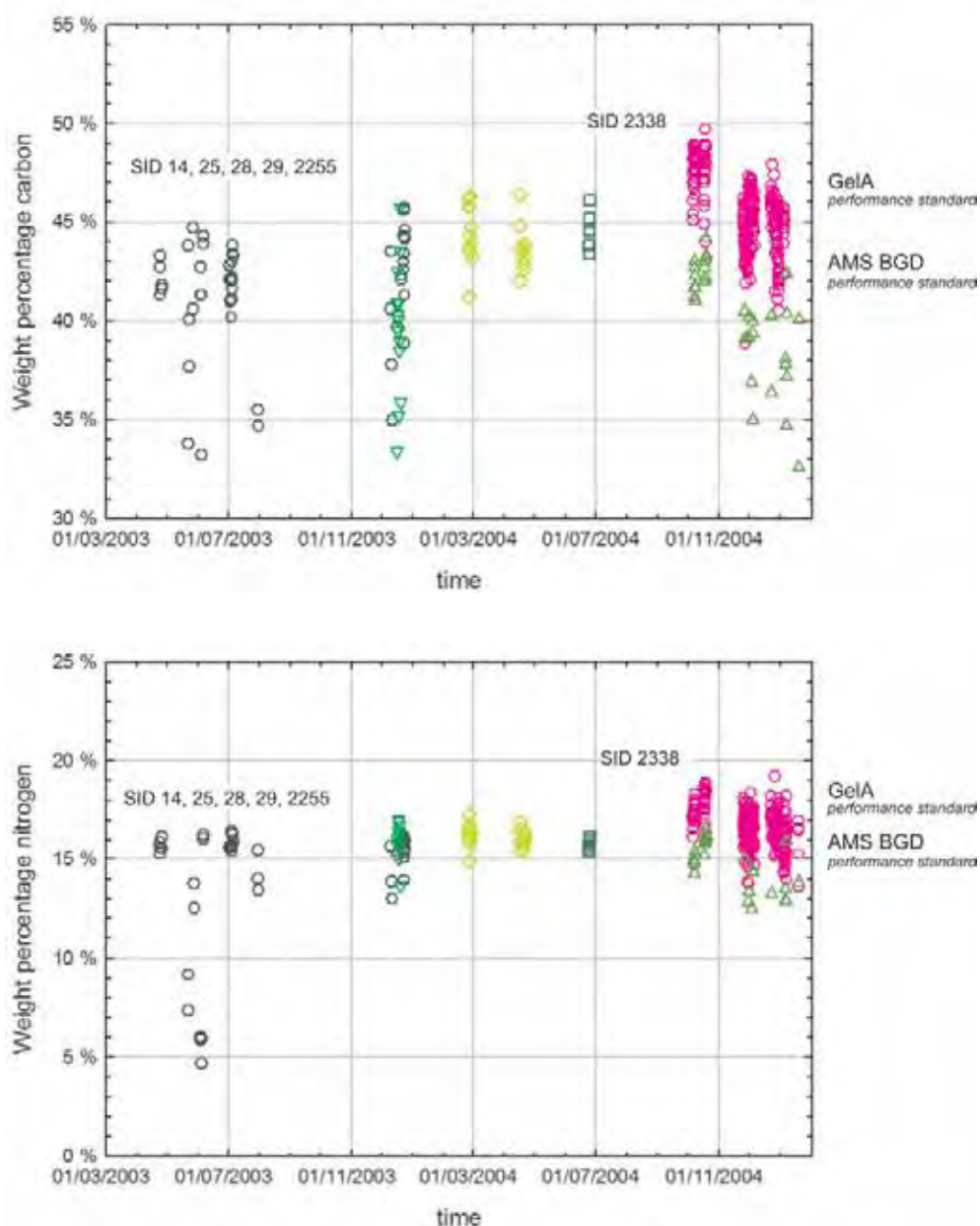


Figure 2-20. Calibration curves for weight percentage calculations. The calibration curves are based on BBOT, BWB II and Urea standards. Each calibration line is calculated on grouped sample list ID (SLI) values. A: Calibration plot for the calculation of weight percentage of carbon by use of the total mass spectrometer peak area. Displayed is also a histogram showing the mass distribution in µgC for all samples measured within the range of the calibration. B: Similar calibration plot for the calculation of weight percentage of nitrogen. C & D: Similar calibration plot for the calculation of weight percentage of carbon and nitrogen by use of the TCD area.



**Figure 2-21.** *Upper part:* Weight percentage carbon performance standards as a function of time. *Lower part:* Weight percentage nitrogen performance standards as a function of time. Each standard are marked with a colour code and each sample ID (SID) are marked by different symbols.

### Carbon and nitrogen analysis linearity

In the majority of cases, the unknown elemental weight percentage values of samples is a complicating factor in CF-EA analysis, since peak areas are expected to vary heavily. This demands high ion source linearity over a large range. The system linearity is high if the observed  $\delta^{13}\text{C}$  and  $\delta^{15}\text{N}$  values are constant as a function of sample mass. System linearity is tested by ranging the sample masses from the detection limit and up to the maximum mass limit. To verify system linearity, three unknown samples have been picked (SID 740, 803 and 915) and weighted in different amounts. The resulting  $\delta^{13}\text{C}_{\text{VPDB}}$ ,  $\delta^{15}\text{N}_{\text{AIR}}$  and elemental weight percentages are plotted against their elemental weights for carbon and nitrogen as shown in Figure 2-25 and 2-26. It

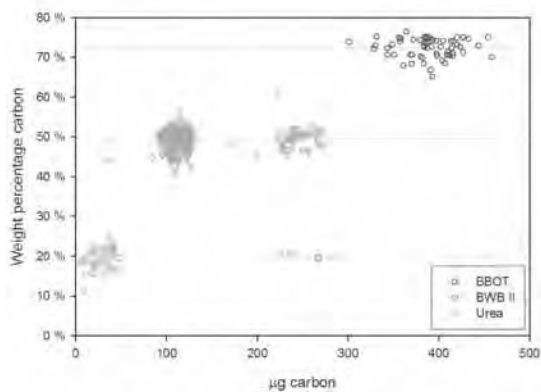


**Figure 2-22.** Weight percentage carbon calibration standards as function of  $\mu\text{gC}$ .

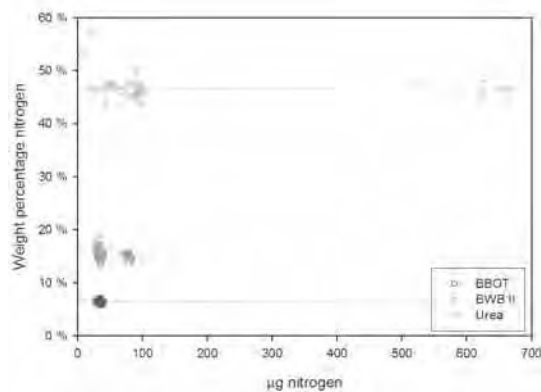


**Figure 2-23.** Weight percentage nitrogen calibration standards as function of  $\mu\text{gN}$ .

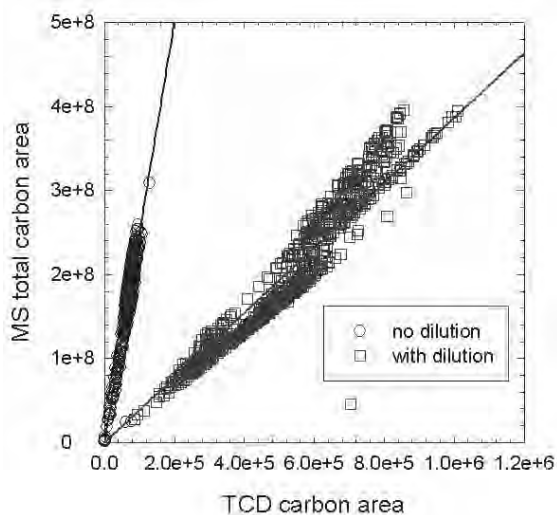


**Figure 2-24.** Shown is the TCD area of carbon diluted samples and non-diluted samples versus their mass spectrometer (MS) total area. The TCD area is a measure of the total carbon in the sample and is independent of dilution. The MS areas are measured after dilution. The data therefore falls in two groups a diluted and a non-diluted. By fitting a straight line to each data group and taking the ratio of the two slopes the mean dilution factor can be estimated. The average dilution factor for the diluted samples illustrated here is 6.5.

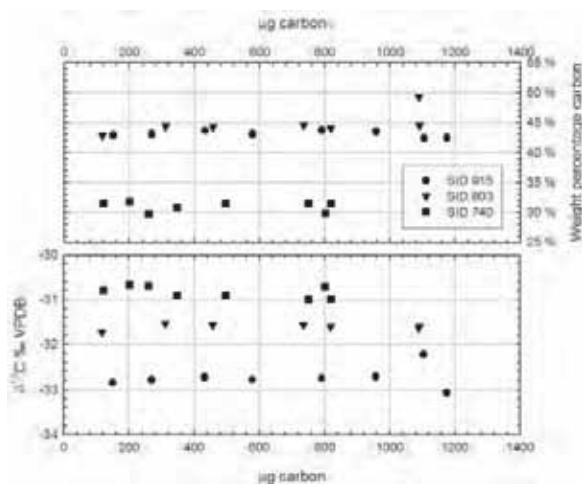


**Figure 2-25.** Linearity test of  $\delta^{13}\text{C}$  and weight percentage carbon. All shown samples are diluted, hence the carbon weight scale is expanded with approximately 6.5 (the dilution factor) relative to non-diluted samples.

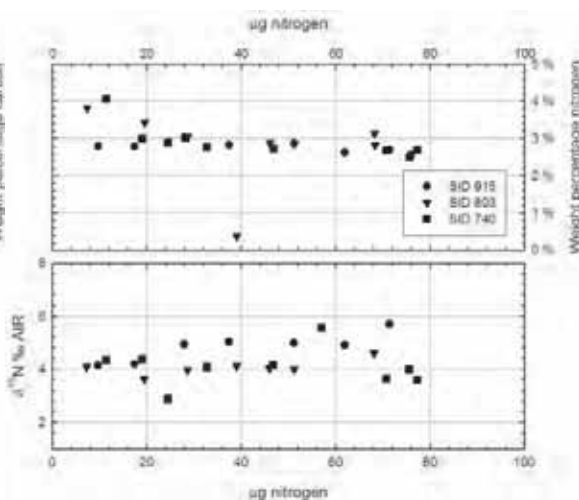


**Figure 2-26.** Linearity test of  $\delta^{15}\text{N}$  and weight percentage nitrogen. Note that for small amounts of nitrogen weight percentage values are slightly higher.

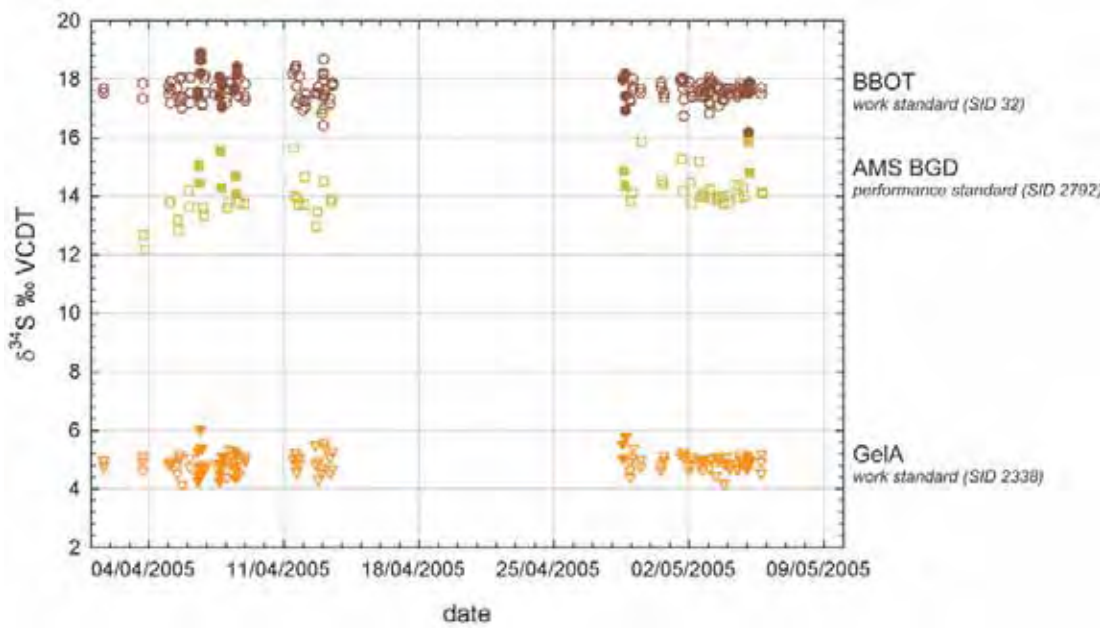


**Figure 2-27.** Sulphur performance standards and working standards as a function of time. Open symbols denotes measured values, whereas filled denote calibrated values. SID denotes sample ID.

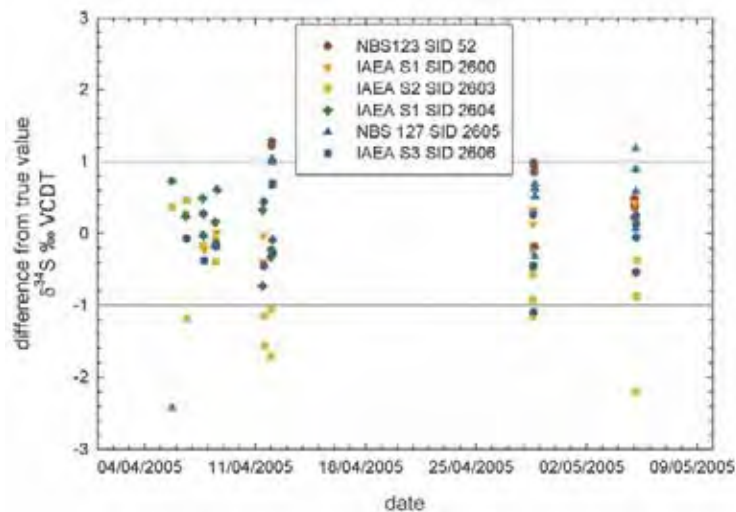


**Figure 2-28.** Sulphur analysis of international standards. All standards are used for linear calibration of the internal standards BBOt and GelA. SID denotes the sample ID.

can be observed that the carbon linearity ranges from 15 $\mu$ gC to 170  $\mu$ gC, whereas the nitrogen linearity ranges from 8 $\mu$ gN to 75 $\mu$ gN.

### Sulphur analysis

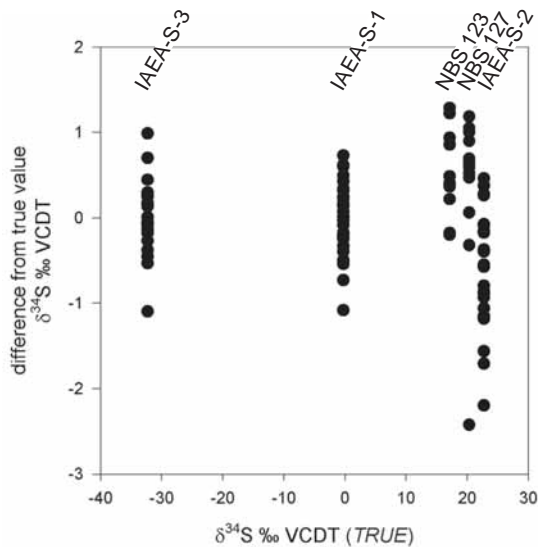
The sulphur data covers the period from February 2005 to May 2005. In total, 2005 samples were analysed of which 46% were standards. The vast majority of samples were sediment samples from the Bliden lake core B1. The mass and TCD spectra for sulphur are shown in Figure 2-4. The sulphur background is well below the detection limit, thus blank corrections are not necessary for CF-EA sulphur analysis. Both nitrogen and carbon show clear peaks in the TCD signal. The nitrogen and carbon weight percentages can therefore in principle also be determined by CF-EA sulphur analysis.

**Table 2.5:  $\delta^{34}\text{S}$  calibration of the internal standards BBOT and GelA**

The standards have been calibrated by the linear method by use of several international standards.

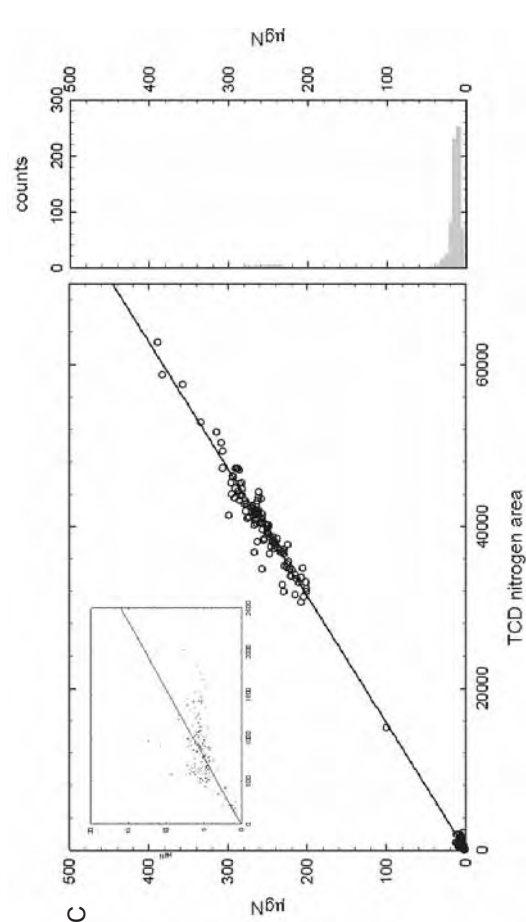
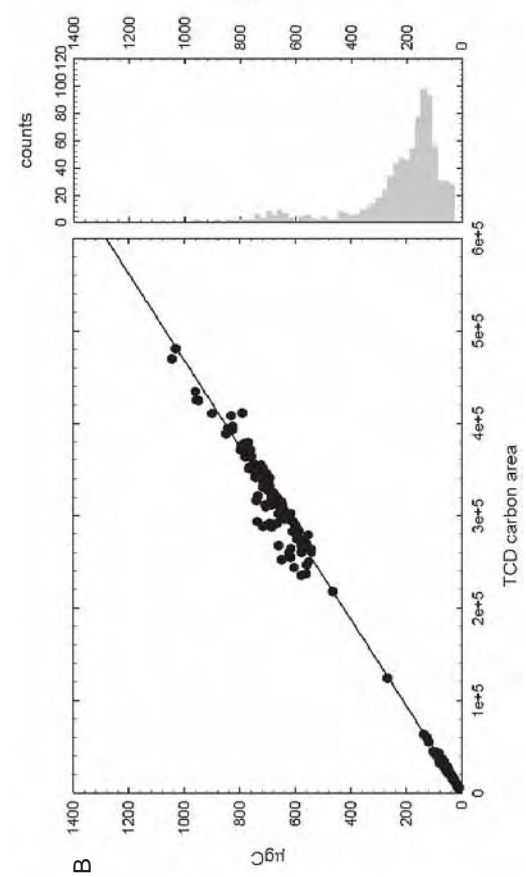
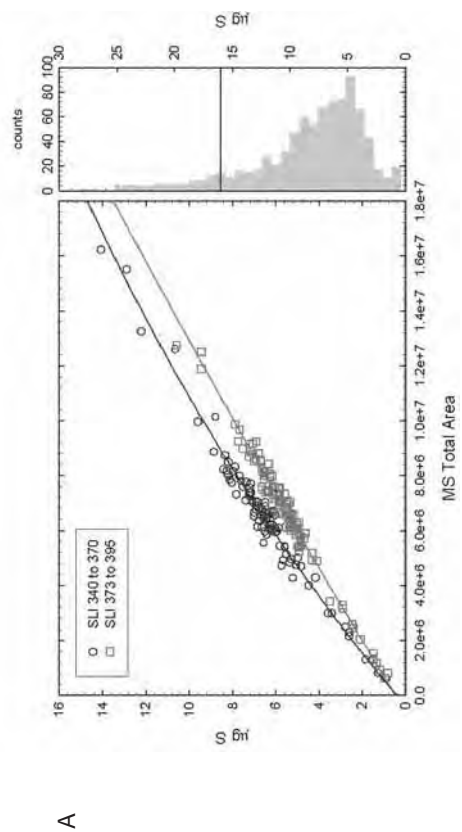
SLI	$\delta^{34}\text{S}$ ‰ VCDT	$\sigma$	n	dev $\sigma$	$\delta^{34}\text{S}$ ‰ VCDT	$\sigma$	n	dev $\sigma$	$R^2$	$\delta^{34}\text{S}$ ‰ VCDT	$\sigma$	n	dev $\sigma$	Calibration based on:
	<i>GelA, Gelatine</i>				<i>BBOT</i>					<i>AMS BGD, Collagen</i>				
340	4.65	0.19	6	-1.2	17.27	0.27	3	-1.2	0.9993	*12.28	0.27	3		IAEA-S-1, IAEA-S-2, IAEA-S-3 & NBS 123
355	4.90	0.62	8	0.0	18.14	0.65	5	0.8	0.9943	14.74	0.41	2	0.2	IAEA-S-1, IAEA-S-2 & IAEA-S-3
358	4.72	0.32	5	-0.5	17.64	0.42	5	0.1	0.9986	14.91	0.89	2	0.3	IAEA-S-1, IAEA-S-2 & IAEA-S-3
360	4.85	0.39	5	-0.1	18.04	0.40	5	1.1	0.9984	14.38	0.42	2	-0.7	IAEA-S-1, IAEA-S-2 & IAEA-S-3
373	5.54	0.34	4	1.9	17.70	0.52	5	0.2	0.9968	14.61	0.35	2	-0.2	IAEA-S-1, IAEA-S-2, IAEA-S-3, NBS 123 & NBS 127
387	4.97	0.18	5	0.5	17.48	0.55	8	-0.2	0.9983	15.34	0.76	2	0.9	IAEA-S-1, IAEA-S-2, IAEA-S-3, NBS 123 & NBS 127
	4.88	0.15	$\chi^2_{\text{meas}}$	5.8	17.60	0.20	$\chi^2_{\text{meas}}$	3.5		14.66	0.23	$\chi^2_{\text{meas}}$	1.4	
			$\chi^2$	11.1			$\chi^2$	11.1				$\chi^2$	9.5	

SLI denotes sample list ID. Dev  $\sigma$  denotes the deviation from the mean value given in units of the standard deviation.  $R^2$  denotes regression coefficient for the linear fit.  $\chi^2_{\text{meas}}$  is measured  $\chi^2$  values and  $\chi^2$  represents the theoretical value. For the data to be normal distributed  $\chi^2_{\text{meas}} \leq \chi^2$ .



**Figure 2-29.**  $\delta^{34}\text{S}_{\text{VCDT}}$  values of international standards used for calibration. Shown is the difference between the measured value and the assigned values (*denoted true*) as a function the assigned  $\delta^{34}\text{S}_{\text{VCDT}}$ .

**Figure 2-30.** A: Calibration plot for calculation of weight percentage sulphur by use of the total mass spectrometer peak area. Displayed is also a histogram showing the mass distribution in  $\mu\text{gS}$  for all measured samples. Note that a few samples fall out of the calibration range. The calibration is based on BBOT standards. B: Calibration plot for calculation of weight percentage of carbon by use of the TCD area for CF-EA sulphur analysis. The calibration is based on BBOT and Gela standards. C: Calibration plot for calculation of weight percentage of nitrogen by use of the TCD area for CF-EA sulphur analysis. The calibration is based on BBOT and Gela standards. The enlarged panel shows the data up to  $20\mu\text{gN}$ . Each calibration line in plot A, B and C are grouped by sample list ID (SLI) values.



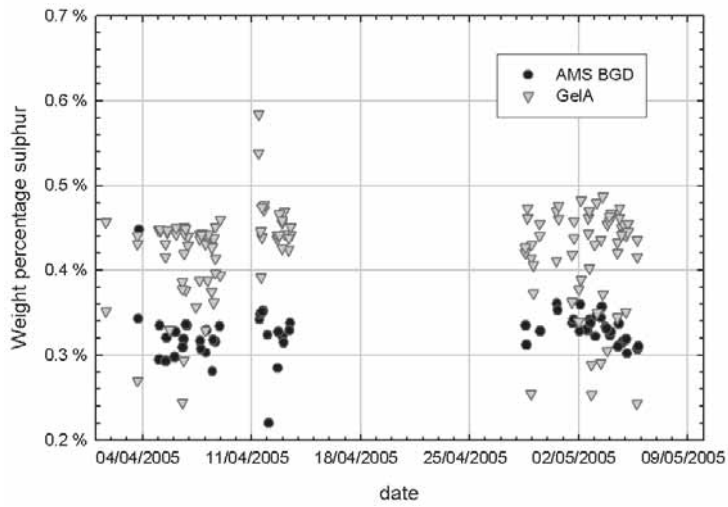


**Figure 2-31.** Weight percentage of sulphur performance standards as a function of time.

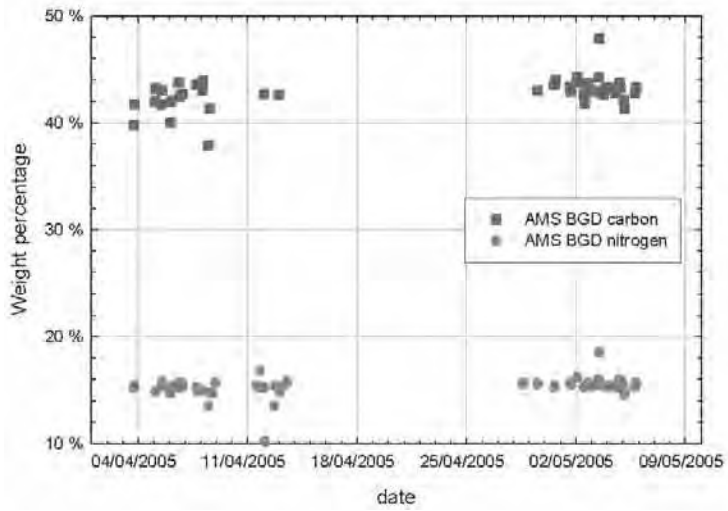


**Figure 2-32.** Weight percentage of carbon and nitrogen performance standards as a function of time for CF-EA sulphur analysis

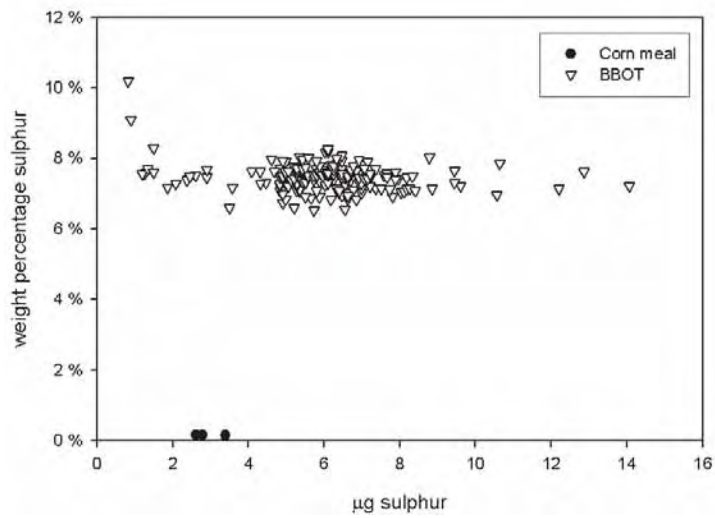


**Figure 2-33.** Sulphur weight percentage calibration standards as function of µgS

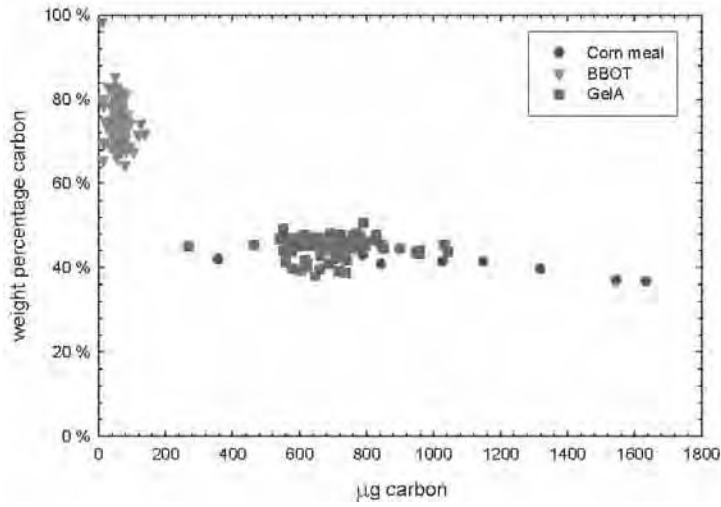


Figure 2-34. Carbon weight percentage calibration standards as function of  $\mu\text{gC}$

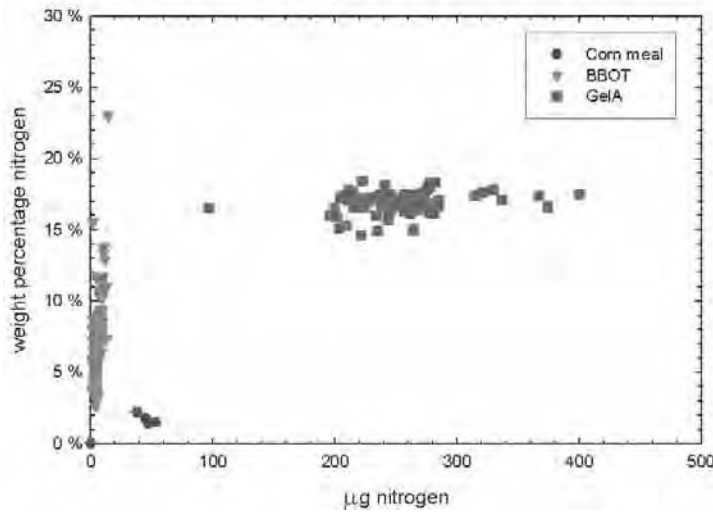


Figure 2-35. Weight percentage nitrogen calibration standards as function of  $\mu\text{gN}$ .

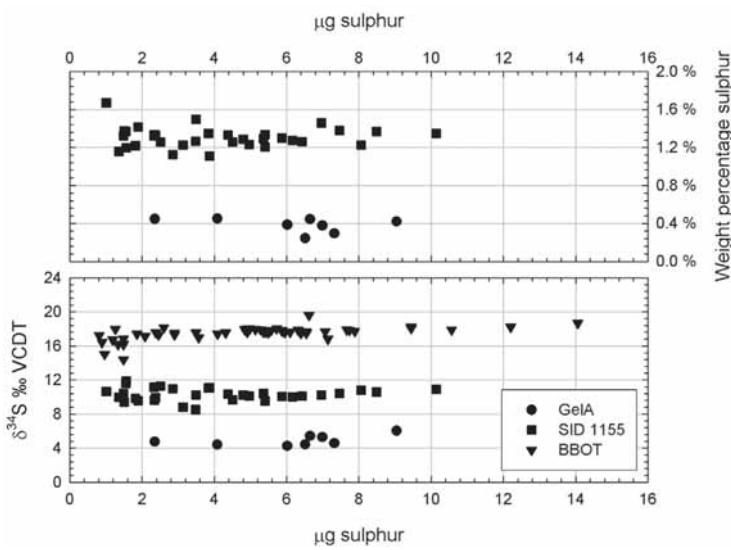
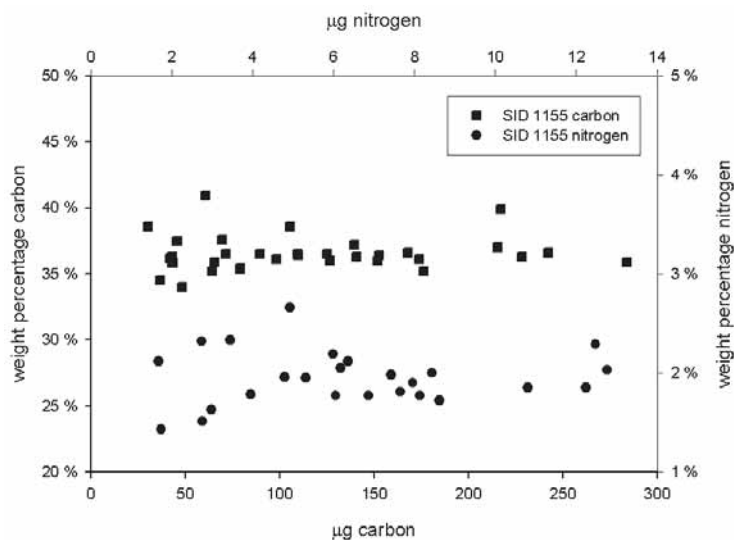


Figure 2-37. Linearity test of sample SID 1155, GelA and BBOT. Note that BBOT and GelA are used for calibration sulphur isotope data. However the data displayed here are only used to test the mass spectrometer linearity. *Upper panel:* Shown is the weight percentage of GelA and SID 1155 in the range from  $1\mu\text{gS}$  to  $10\mu\text{gS}$ . *Upper panel:* Shown is the  $\delta^{34}\text{S}$  values for SID 1155, BBOT and GelA in the range from  $1\mu\text{gS}$  to  $14\mu\text{gS}$ .



**Figure 2-38.** Linearity test of sample SID 1155 of weight percentage carbon and nitrogen.

#### Results of sulphur stable isotope analysis

During routine CF-EA sulphur analysis the BBOT and Gela are used as the internal calibration standards. The AMS BGD standard is used as performance standard. The  $\delta^{34}\text{S}_{\text{VCDT}}$  time series for AMS BGD, BBOT and Gela are shown in Figure 2-27. The internal calibration standards BBOT and Gela reflect the general measurement scatter (*precision*), whereas the performance standard AMS BGD reflects the general analysis accuracy.

All international standards that have been analysed are used for calibration of the internal calibration standards BBOT and Gela, but also for quality assurance. Figure 2-28 shows the  $\delta^{34}\text{S}_{\text{VCDT}}$  time series plot for all international standards used for calibration and Figure 2-29 shows the difference between the measured and assigned  $\delta^{34}\text{S}_{\text{VCDT}}$  values as a function of the assigned  $\delta^{34}\text{S}_{\text{VCDT}}$  value. Table 2.5 shows the calibration outcome of the BBOT and Gela internal standards together with the associated measurements on the performance standard AMS BGD.

#### Results of sulphur weight percentage analysis

The weight percentage calibration plot for the mass spectrometer total area of sulphur is shown in Figure 2-30A. The weight percentage calibration plots for TCD data of carbon and nitrogen are shown in Figure 2-30B and 2-30C. Figure 2-31 shows the sulphur weight percentage time series for the performance standard AMS BGD and Gela (*note that Gela is used as a sulphur weight percentage performance standard*). The Gela sulphur weight percentage data exhibit large scatter relative to AMS BGD. The carbon and nitrogen weight percentage time series of the performance standard AMS BGD for CF-EA sulphur analysis are shown in Figure 2-32. Figure 2-33, 2-34 and 2-35 show weight percentage standards plotted versus their elemental weight.

#### Sulphur analysis linearity

The CF-EA sulphur analysis linearity was tested using samples with SID 1155. This sample was analysed at different times during sulphur analysis with weights ranging from 1 $\mu\text{gS}$  to 14 $\mu\text{gS}$ . The outcome of the measurements is shown in Figure 2-37 for  $\delta^{34}\text{S}_{\text{VCDT}}$  and weight percentage of sulphur. The weight percentages of carbon and nitrogen are shown in Figure 2-38.

## Discussion

Proper  $\delta^{13}\text{C}$ ,  $\delta^{15}\text{N}$  and  $\delta^{34}\text{S}$  values in CF-EA analysis require good combustion of the samples. Incomplete combustion may ultimately lead to fractionation, and thus cause unacceptable precision levels and inaccurate measurements. The CF-EA flash combustion is a complicated function that depends on many parameters, such as helium pressure, chemicals, temperature as well as timing, magnitude and duration of the added oxygen peak. The helium pressure is a function of the chemical packing and more specifically the flow resistance of the GC column. It is therefore a fixed parameter. Combustion parameters like temperature and the properties of the oxygen peak are adjustable parameters, which can be optimised to achieve better results. The setting of these parameters may be sample specific. Collagen samples, which can be considered as small concentrated organic samples without impurities, are more combustible than sedimentary samples containing non-organic materials. Tests have shown that collagen samples are combusted by a short oxygen pulse whereas bigger lake sediment samples need a longer oxygen pulse for perfect combustion for equal amounts of oxygen.

Inspired by the Centre for Isotope Research in Gröningen, The Netherlands, a small glass insert was developed. It consists of a small tube that opens at both ends and fits into the reactor tubes. It is closed by quartz wool in one end and is equipped with small side holes. Its main function is to collect sample ashes from the combusted samples, thereby avoiding sample ash build-up in the reactor tube. This might otherwise result in incomplete combustion, as the temperature is lower away from the centre of the reaction furnace. By frequent replacement of this insert the reactor chemicals will last longer and samples are combusted at similar temperatures. Further, it also prevents blocking of the reactor tube. The great disadvantage of the insert is that upon replacement the helium stream has to be switched off and the EA has to be opened while still hot. This can, of course, result in damage to the chemicals as atmospheric air is let into the system. Especially the reduction copper chemicals are in danger of being corrupted if the EA is open for long periods of time. However, daily routine analysis has shown that this constitutes only a limited problem.

Most reports on CF-EA sulphur analysis argue the need for using combustion additives to improve the combustion of sulphur-bearing samples (Glesemann *et al* 1994; Kester *et al* 2001; Fry *et al* 2002; Yun *et al* 2004; Poulson 2005). The most widely used combustion additive is vanadium pentoxide ( $\text{V}_2\text{O}_5$ ).  $\text{V}_2\text{O}_5$  is a poisonous material hazardous to the environment and should be avoided if possible. The initial tests on CF-EA sulphur analysis at this laboratory were performed on standards with and without  $\text{V}_2\text{O}_5$ . The subsequent comparison showed no evidence of improved combustion by using  $\text{V}_2\text{O}_5$ . Neither the peak chromatogram nor precision and accuracy were improved, as also shown by (Morrison *et al* 1996). Thus the stable isotope analysis presented here was performed without using  $\text{V}_2\text{O}_5$  as a combustion additive.

The samples, reference materials and international standards should to a large extent be treated identically to avoid disproportional fractionation between samples and standards during pre-treatment methods or EA combustion. This is known as the identical treatment (IT) principle (Werner and Brand 2001). However, as revealed by Table 2.3 most international standard materials are very different from the sample materials commonly analysed. As the calibration of internal work standards is always carried out using international standards this may be a considerable problem. For the majority of cases differences in pre-treatment methods are not considered to be of significant relevance. More-over, the combustion of different materials requires different settings for oxygen amounts and the duration of oxygen pulses and this may compromise the IT principle. This is because the oxygen amount and the duration of the oxygen pulses are fixed parameters during multi-sample batch analysis. The international standards for CF-EA nitrogen and sulphur analysis consist mainly of inorganic materials and thus differ

largely from the mostly organic samples commonly analysed and, more importantly, from the organic materials used as internal standards. Hence, international reference materials that resemble commonly analysed samples are urgently needed. This also emphasises the importance of making cross-measurements between laboratories in order to check isotope values of the internal applied reference materials.

### Stable isotopes of carbon and nitrogen

Both carbon and nitrogen show a blank contribution by combustion of tin cups (see Figure 2-3). However, as illustrated by Figure 2-10, 2-11, 2-12 and 2-13 the exact amount and the isotope values of the blank samples are difficult to estimate. This, of course, weakens the confidence in the isotope blank correction by either equation (2.16) or (2.17). Due to the very low abundances of carbon and nitrogen, blank measurements are close to the detection limit of the system. Therefore, they can be expected to show higher scatter. As seen by the histograms in Figure 2-12 and 2-13 both carbon and nitrogen has many extreme values outside of the otherwise normally distributed values. The reasons for these extreme values are poorly understood. However the ultimate tests of the utility of the deduced blank values are the linearity tests displayed in Figure 2-25 and 2-26. Both the carbon and the nitrogen isotope values show linearity over a large range. For carbon linearity is demonstrated down to  $15\mu\text{gC}$  and for nitrogen the linearity is down to  $10\mu\text{gN}$ , thus indicating that the deduced blank values of carbon and nitrogen are sufficiently accurate. Note, however, that the isotope linearity for nitrogen displays some scattered values which may be caused by incorrect nitrogen blank values.

The performance standards of Figure 2-15 are used for quality assurance of the carbon and nitrogen stable isotope analysis. The isotope values of the AMS BGD and BBOT are used to illustrate periods of poor reproducibility. These are easily distinguishable by offset values and high scatter. This can also be seen in Table 2.3. By removing nitrogen isotope values that devi-

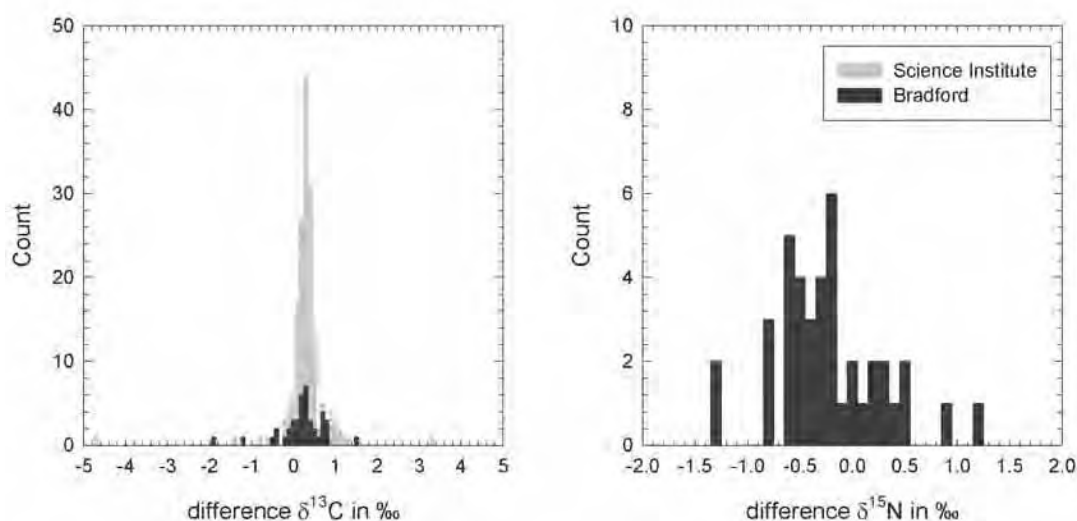


**Figure 2-39.** Comparison of  $\delta^{13}\text{C}$  (left) and  $\delta^{15}\text{N}$  (right) values measured at the Science Institute, Iceland and Department of Archaeology, Bradford (Fischer *et al.* in prep-a). Shown are the isotope values of the other laboratory minus the isotope values from this laboratory. The  $\delta^{13}\text{C}$  difference between the Science Institute and Aarhus is  $0.2\pm 0.6\text{‰}$  ( $n=174$ ) and the  $\delta^{13}\text{C}$  difference between Bradford and Aarhus is  $0.2\pm 0.4\text{‰}$  ( $n=31$ ). For  $\delta^{15}\text{N}$  the difference between Bradford and Aarhus is  $-0.2\pm 0.4\text{‰}$ . The  $\delta^{13}\text{C}$  values from the Science Institute are measured on  $\text{CO}_2$  samples prepared in Aarhus and have been measured by the dual inlet method and the Bradford isotope values are measured by the CF-EA carbon and nitrogen method.

ate more than  $2\sigma$  from the mean value, the standard deviation of all measurements of the AMS BGD standard is reduced from 1.7‰ to 0.7‰. For the carbon isotope the standard deviation of samples of AMS BGD and BBOT is 0.3‰ and 0.5‰ respectively. However, since only reproducibility problems can be observed by the use of performance standards, problems with accuracy are not detectable to the same extent. Periods with offset values can be observed through the performance standards but a general offset in isotope values caused by inaccurate values of the internal standards is not easily deduced.

To estimate the general accuracy of the isotope measurements, a total of 205 samples have been measured elsewhere. The  $\delta^{13}\text{C}$  value of 174 samples have been measured by the Science Institute, Iceland and the combined  $\delta^{13}\text{C}$  and  $\delta^{15}\text{N}$  values of 31 samples have been measured by Mike Richards at the Department of Archaeological Science, Bradford (Fischer *et al* submitted for publication-a). A comparison of the measured samples is shown in Figure 2-39 and indicates that the  $\delta^{13}\text{C}$  values from this laboratory display a mean offset in the order of 0.2‰. The offset in  $\delta^{15}\text{N}$  values is -0.2‰. These  $\delta^{13}\text{C}$  and  $\delta^{15}\text{N}$  offset values are similar to the isotope values obtained on the BWB II standard by Micromass and Mike Richards (*see Table 2.4*). Thus the accuracy is around  $\pm 0.2\text{‰}$  for both  $\delta^{13}\text{C}$  and  $\delta^{15}\text{N}$  measurements. Further, these are also reflected by Figure 2-16 (carbon international standards used as pseudo performance standards) and to a lesser extent by Figure 2-17 (*nitrogen international standards used as a pseudo performance standard*). Figure 2-16 shows that the international carbon standards in the majority of cases fall within  $\pm 1\text{‰}$ . The values for the international standards of nitrogen paint a different picture, since many of the standards display  $\delta^{15}\text{N}$  values which are a few per mil lower than their assigned values. Especially the IAEA-N1, USGS 40 and USGS 41 show large deviations. Note that the  $\delta^{13}\text{C}$  value of USGS 41 deviates by 2‰. This could indicate an analysis problem for these standards resulting in poor accuracy. However, since no samples in the comparisons with the Science Institute or the Bradford laboratory show a similar tendency, this indicates a combustion problem in these samples, as previously noted.

### **Stable isotopes of sulphur**

The sulphur isotope performance standard AMS BGD shown in Figure 2-27 provides a picture of the general CF-EA sulphur isotope analysis. Clearly, early measurements display a significantly larger scatter than the later. The precision of the sulphur analysis is found to be 0.5‰, as shown by Table 2.5. This is greater than the precision found for both carbon and nitrogen isotope analysis. The precision is comparable to that observed in other studies (Glesemann *et al* 1994; Yun *et al* 2004), but lower than the standard deviation reported by GV Instruments (Morrison 1996).

CF-EA sulphur analysis is complicated by many factors. The carbon to sulphur ratio is generally very high, i.e. the sulphur weight percentage content of the samples is very low. This means that the required sample sizes are very large, typically 550µg total weight. For the Bliden lake core samples, the total weight ranged from 130µg and up to 3400µg with an average sulphur weight percentage of 1.6%. This should be seen in relation to the total average weight of the standards, which are 81µg for BBOT, 1300µg for GelA and 1800µg for the AMS BGD. The international standards contain no carbon and have very high sulphur weight percentages. The total weight for IAEA-S-1, IAEA-S-2, IAEA-S-3 and NBS 127 is as little as 60µg, and the average weight of the NBS 123 standard is even lower at 20µg. Both samples and standards resulted in mass 64 peak heights between 0.8 to 1.0nA. These dissimilarities result in different usage of both the supplied tank oxygen and the oxygen coming from  $\text{WO}_3$  in the CF-EA combustion tube. In addition, the oxygen content of the samples varied greatly (Yun *et al* 2005). This, then, is clearly a violation of the IT principle (Werner and Brand 2001) and may explain the observed scatter. It

also indicates that the method pointed out by Poulson (2005) is inadequate and does not correct for the sample oxygen content to mass 66 sufficiently well. However, it should be noted that the measured samples display constant  $\delta^{34}\text{S}$  values over a large sulphur weight range, as shown by Figure 2-37.

The oxygen effect on accuracy is not easily estimable. For the CF-EA sulphur analysis no comparisons with other laboratories have been made. Yun *et al* (2005) report differences between off-line and on-line prepared  $\text{SO}_2$  samples to be as high as 2.9‰ which they suggest originate in differences in sample oxygen isotope composition. Thus, the sample accuracy may be as low as 3‰. The accuracy of the international standards is nevertheless most likely to be within  $\pm 1\%$ , as illustrated by Figure 2-28 and 2-29.

Coleman (2004) and Fry *et al* (2002) point out that sulphur analysis on gaseous  $\text{SO}_2$  and  $\text{SO}$  (mass 48, 49 and 50) from the same sample may resolve the isobaric oxygen problem in CF-EA

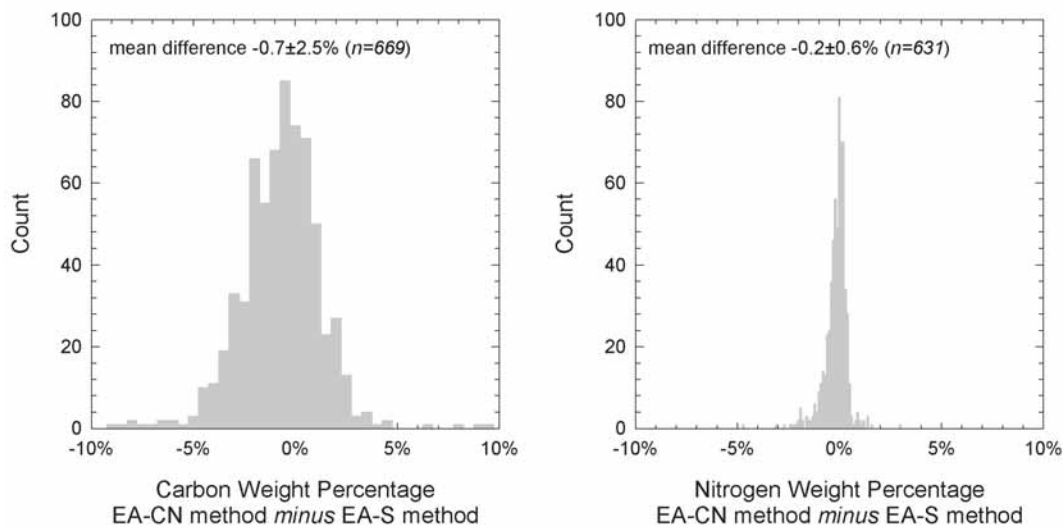


**Figure 2-40.** Shown is the difference between weight percentage values obtained by the CF-EA carbon and nitrogen method versus values determined by the CF-EA sulphur method. **Right panel:** Histogram of differences in carbon weight percentage values **Left panel:** Histogram of differences in nitrogen weight percentage values.

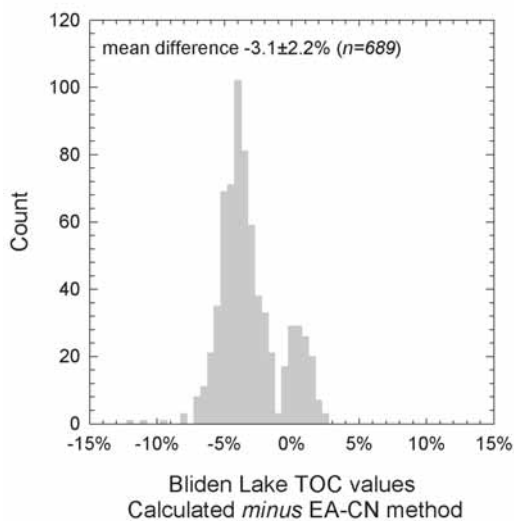


**Figure 2-41.** Shown are the total organic content (TOC) values from the Bliden lake core B1 and the carbon weight percentage values obtained by the CF-EA carbon and nitrogen method. The TOC values are calculated by equation (6.2). The weight percentage values by the CF-EA carbon and nitrogen method has been converted to TOC values by equation (6.4). Note that the correlation coefficient of these data is  $\rho=0.88$ .

sulphur analysis.  $\text{SO}^+$  is formed in the ion source nearly as efficiently as  $\text{SO}_2$ , hence sulphur CF-EA analysis can also be performed on SO (Fry *et al* 2002; Baubllys *et al* 2004). By splitting the produced  $\text{SO}_2^+$  in the EA into two capillary lines and using a valve to chose one line from the other, Fry *et al* (2002) demonstrated a modified CF-EA sulphur system for simultaneous measurement on SO and  $\text{SO}_2$ . To minimise the effect of the sample oxygen composition, the  $\text{WO}_3$  of the combined reaction and reduction furnace is skipped and an oxygen buffer reactor is added. The oxygen buffer reactor consists of  $\text{SiO}_2$  chips heated to 890°C. As the samples pass through this reactor, their oxygen isotope composition is balanced by exchange with  $\text{SiO}_2$  chips, thus minimising the variance of the  $\text{SO}_2$  oxygen composition (Fry *et al* 2002). This modified CF-EA system is a significant improvement on CF-EA sulphur analysis and should be adopted in the future.

### Weight percentage values

Carbon and nitrogen weight percentage values of the Bliden lake core B1 have been determined by the CF-EA carbon and nitrogen method and by the TCD data from CF-EA sulphur analysis. The two methods are compared in Figure 2-40. As illustrated, the two methods produce similar results. Note that both the carbon and nitrogen weight percentage signals are highly correlated with a correlation coefficient  $\rho=0.96$  for the carbon weight percentages values and  $\rho=0.69$  for nitrogen weight percentage values. This confirms the adequacy of both methods. However, note that many of the CF-EA sulphur method samples were cancelled due to a too small nitrogen peaks or because the carbon peaks were so large that the nitrogen peaks could not be resolved. For nitrogen amounts below 20 $\mu\text{gN}$ , the CF-EA sulphur method for nitrogen weight percentages is not appropriate, as shown by Figures 2-30C and 2-35.

The total organic content (TOC) of the Bliden core samples were obtained by Metalyt 90S measurements (*see section 6*). Figure 2-41 compares the Metalyt 90S measurements with the weight percentage carbon values of the CF-EA carbon and nitrogen method. The weight percentage values have been converted to TOC values by equation (6.2) or (6.4). As seen, the difference between the two methods is for the majority of samples a few percent. The mean difference is given at  $-3.1\pm 2.2\%$ . However, the correlation between the two TOC signals is  $\rho=0.88$ . The discrepancy between these two signals is not sufficiently understood, but the high correlation value suggests that the CF-EA carbon and nitrogen and the Metalyt 90S values are similar within 3.1% and display similar trends. Thus, the overall accuracy of the carbon weight percentage values is around 3%.

The weight percentage linearity of carbon, nitrogen and sulphur is illustrated in Figures 2-25, 2-26, 2-37 and 2-38. The carbon weight percentage linearity of CF-EA carbon and nitrogen method is excellent (*Figure 2-25*), whereas the nitrogen weight percentage linearity displays a tendency for small offsets for lower weights. For the CF-EA sulphur method (*Figure 2-38*) both carbon and nitrogen weight percentages show minor offsets for low weights. Note that in contrast to *Figure 2-35* the linearity (*Figure 2-38*) suggests that nitrogen weights as low as 5 $\mu\text{gN}$  can be measured without problems. The sulphur weight percentage in *Figure 2-37* displays excellent linearity between 2 and 10 $\mu\text{gS}$ .

### Conclusion

The quality assurance programme has been demonstrated by the performance plots of  $\delta^{13}\text{C}$ ,  $\delta^{15}\text{N}$  and  $\delta^{34}\text{S}$  values in Figures 2-15 and 2-27. The performance standards in these plots mimic real samples as closely as possible. They are placed in each analysis batch of samples and thus periods of poor reproducibility can easily be observed. The typical precision for  $\delta^{13}\text{C}$  values is

0.2‰ and for  $\delta^{15}\text{N}$  values a precision of 0.3‰ have been observed. The  $\delta^{34}\text{S}$  precision is found to be 0.5‰.

A complicating factor in CF-EA isotope analysis is the unknown contents of carbon, nitrogen and sulphur in the samples to be analysed. This demands high system linearity over a large range thus requiring that samples with diverting mass spectrometer peak heights of carbon, nitrogen and sulphur all yield accurate  $\delta^{13}\text{C}$ ,  $\delta^{15}\text{N}$  and  $\delta^{34}\text{S}$  values. The system linearity is demonstrated in Figures 2-25, 2-26 and 2-37 showing high linearity spanning a large range of elemental weight values. The  $\delta^{13}\text{C}$  linearity ranges from 15 $\mu\text{gC}$  to 170 $\mu\text{gC}$  and the  $\delta^{15}\text{N}$  linearity ranges from 8 $\mu\text{gN}$  to 75 $\mu\text{gN}$ . The  $\delta^{34}\text{S}$  linearity ranges from 2 $\mu\text{gS}$  to 14 $\mu\text{gS}$ .

The accuracy of the CF-EA carbon and nitrogen system has been estimated by comparing samples with the Science Institute on Iceland and the Department of Archaeological Science in Bradford and has been found to  $\pm 0.2\text{‰}$  for  $\delta^{13}\text{C}$  and  $\delta^{15}\text{N}$  measurements (*see Figure 2-39*). The accuracy of the CF-EA sulphur isotope analysis may be compromised by the interference of the sample oxygen isotope composition of the analysed  $\text{SO}_2$  molecules. Worst-case estimates are as high as  $\pm 3\text{‰}$  for samples and approximately  $\pm 1\text{‰}$  for international standards (*see Figures 2-28 and 2-29*).

# 3

---

## **Automated AMS sample preparation system**

## Introduction

This chapter presents the development of an automated CO<sub>2</sub> collection device for radiocarbon samples. Radiocarbon measurements by accelerator mass spectrometry (AMS) of organic samples require combustion to obtain CO<sub>2</sub> for graphitization and for  $\delta^{13}\text{C}$  determination by stable isotope mass spectrometry. Commonly, samples for radiocarbon analysis are after pre-treatment procedures combusted off-line in sealed evacuated tubes containing CuO. Afterwards the produced CO<sub>2</sub> is manually transferred to the graphitization system and a small aliquot is stored for stable isotope  $\delta^{13}\text{C}$  analysis.  $\delta^{13}\text{C}$  measurements are mandatory for  $^{14}\text{C}$  measurements in order to correct for fractionation (Stuiver and Polach 1977; McNichol *et al* 2001). A simplifying step is therefore to combine the combustion in a continuous flow elemental analyzer (CF-EA) stable isotope ratio mass spectrometry (IRMS) with cryogenic trapping of CO<sub>2</sub> for AMS graphite targets. Automated or semi-automated trapping devices for CO<sub>2</sub> coupled to elemental analysis continuous flow isotope mass spectrometers have previously been published (Bronk Ramsey and Humm 2000; Aerts-Bijma *et al* 2001; Hatte *et al* 2003). However, a fully automated system integrated into the mass spectrometer equipment and software has not yet been reported. Furthermore, the combination of CF-EA analysis and CO<sub>2</sub> trapping additionally provides determination of  $\delta^{15}\text{N}$ . Many studies require the measurement of both  $\delta^{13}\text{C}$  and  $\delta^{15}\text{N}$  as it is the case for paleodietary studies (Leach *et al* 2001; Ambrose and Krigbaum 2003; Richter and Noe-Nygaard 2003; Newsome *et al* 2004; Noe-Nygaard *et al* 2005; Fischer *et al* submitted for publication-a; Fischer *et al* submitted for publication-b), but also for plant material used in climate or ecological research (Ghosh and Brand 2003; Filippi and Talbot 2005; Kohn and Law 2006; Talbot *et al* 2006).

## Method and design

Previous designs of automated sample preparation of AMS samples suffered either of being semi-automatic or from being very large and are in general disconnected from the mass spectrometer software commonly controlling the CF-EA sample combustion sequence (Bronk Ramsey and Humm 2000; Aerts-Bijma *et al* 2001; Hatte *et al* 2003). Hence a demand in designing the automated AMS sample preparation system was that it should be fully integrated and compatible with the IRMS equipment. Furthermore it should be simple, easily operated and straightforward to set up. The last point is especially important as the IRMS is capable of connecting to a variety of inlet systems, i.e. CF-EA carbon and nitrogen, CF-EA sulphur, CF-EA hydrogen and dual inlet analysis (see e.g. Werner and Brand 2001).

For routine  $\delta^{13}\text{C}$  and  $\delta^{18}\text{O}$  analysis on off-line prepared CO<sub>2</sub> samples a Gilson robot 220XL with its 50 sample manifold bed is operated to transfer the CO<sub>2</sub> samples from spring loaded sample vials to the dual inlet for stable isotope analysis. To the existing Gilson robot arm a 90 degree rotated U extension arm holding a dewar is added, see Figure 3-1. The dewar is positioned directly below the needle and is placed on a threaded spindle which is driven by a motor drive in order to move the dewar vertically. A slide is fixed to the bottom of the U formed extension, to which a vertical holder is placed. The vertical holder is attached to the end of the existing Gilson robot arm. The slide and a wheel placed on the vertical holder allows the Gilson to make movements in the  $x$  and  $y$  direction without adding extra weight to the existing Gilson robot arm. The extension robot arm is constructed in aluminium and is made as light and rigid as possible (see Figure 3-2). The extension arm is readily removed from the Gilson robot at the assembly points (Figure 3-1).

The integrated systems consist of a modified continuous flow elemental analyser (CF-EA) (*EuroVector 3024*) producing gaseous N<sub>2</sub> and CO<sub>2</sub> of solid samples wrapped in tin cups (Aerts-Bijma *et al* 2001), a modified Gilson 220XL for cryogenic CO<sub>2</sub> trapping and isotope ratio mass

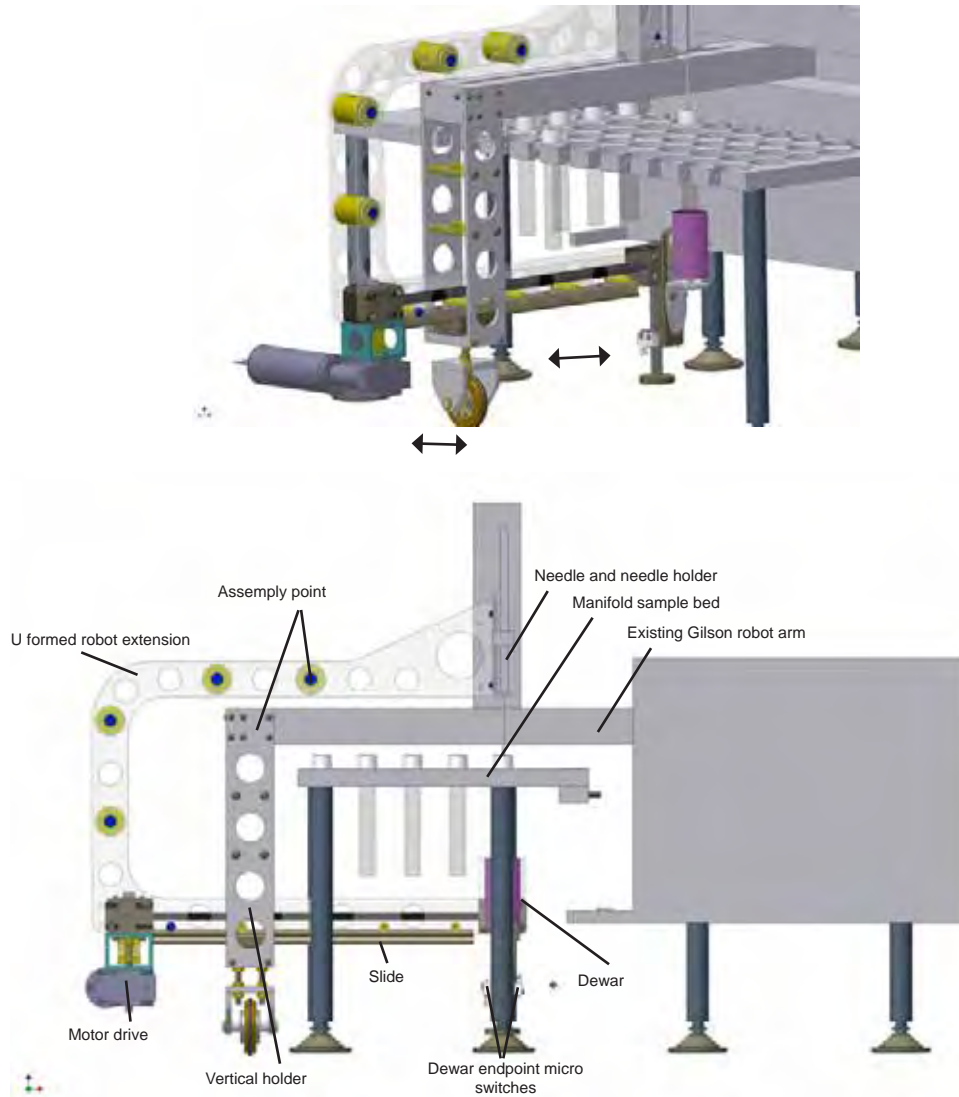


**Figure 3-1:** Design of the robot extension arm and the modified Gilson 220XL (CAD drawing by Henrik Bechthold, Department of Physics and Astronomy (construction), University of Aarhus).

spectrometer (IRMS) (*GV Instruments IsoPrime*) for stable isotope analysis of  $\delta^{13}\text{C}$  and  $\delta^{15}\text{N}$  (Werner and Brand 2001) as illustrated in Figure 3-3. The system is under complete control of the IRMS computer. The CF-EA is modified after Aerts-Bijma *et al* (2001). However, in contrast to Aerts-Bijma *et al* (2001) an adjustable needle valve has been added to IRMS-line of the modified CF-EA to dilute the carrier helium flow in order to reduce the amount of sample entering the IRMS detectors. The stable isotopes are converted to the VPDB scale for  $\delta^{13}\text{C}$  values and the AIR scale for  $\delta^{15}\text{N}$  values (Craig 1957; Allison *et al* 1993; Werner and Brand 2001).

The produced  $\text{CO}_2$  by the CF-EA system is transferred to septum sealed sample vials via a double carriageway needle (*Figure 3-4*) maintaining a continuous carrier flow at all times. A small vial insert containing a second septum (*Figure 3-5*) has been developed to ensure that the  $\text{CO}_2$  is transferred to cold region at the bottom of the vial for cryogenic trapping. The injection needle first penetrates the vial septum sealing to atmosphere and only the needle tip penetrates the vial insert septum while the gas outlet stays between the septa. The dewar is made of stainless steel and its side wall and bottom is isolated by 5mm PTFE. A stain-

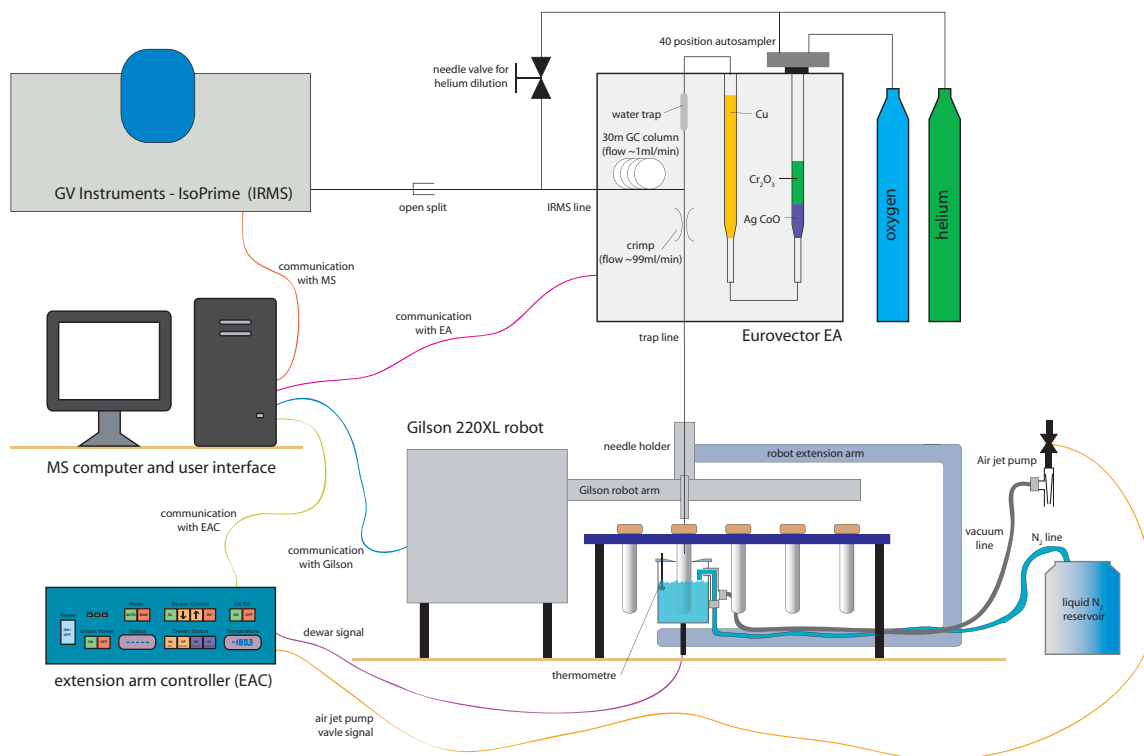


**Figure 3-2:** Schematics of the EA AMS automated sample preparation system.

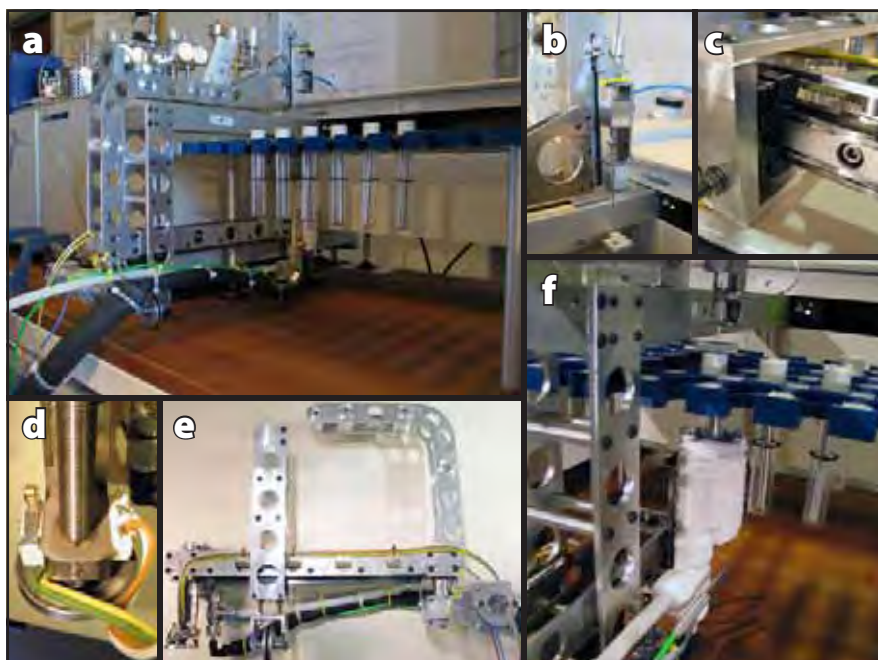


**Figure 3.3:** a) The U formed extension arm mounted on the Gilson robot. b) Needle and needle holder. c) Horizontal slider. d) Dewar spinnel and microswitches. e) The U formed extension arm. f) Trapping a sample with the modified Gilson robot.

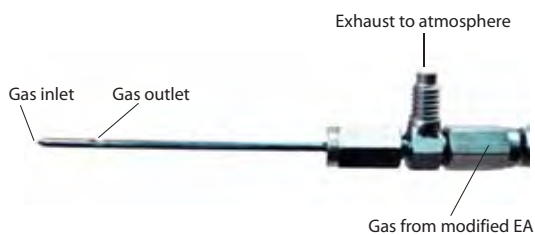


Figure 3-4: The dual carriageway needle.

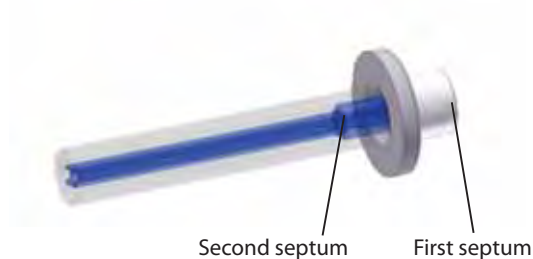


Figure 3-5: Illustration of the vial and vial insert.

less steal disc with a hole matching the diameter of the sample vials is placed at the top of dewar. The disc hole is sleeved to provide vial guidance. When the dewar is at its upward position the dewar interior is a closed system into which liquid nitrogen is transferred by an air jet pump producing vacuum (Figure 3-3). Both the dewar position and the air jet pump is controlled by an additional extension arm controller (EAC).

The main function of the extension arm controller (EAC) is to control the dewar motor drive (*dewar position*) and the liquid nitrogen filling by measuring the dewar temperature and controlling the air jet pump valve (Figure 3-3) as well as to provide a communication interface to the IRMS software. The dewar position is controlled by two microswitches DL and DH. The EAC may be operated remotely by the IRMS software or manually for adjustments and testing. The communication with the IRMS software (Figure 3-6) is provided by 4 Boolean signals VA, VP, HC and VI. VA and VP activate the liquid nitrogen filling and the dewar position respectively. HC and VI report the status of the dewar position and temperature.

The IRMS software script ensures that prior to the CF-EA sample drop the vial is fully flushed with helium and the dewar is raised to its upper position and cooled. Before letting the Gilson move to the sample position the status of the dewar position and N<sub>2</sub> filling is checked. Thus, if and only if the dewar is at its lower position and the nitrogen filling is off, then the Gilson goes to the sample vial and injects the needle and flushes the vial with carrier helium. Then the IRMS requests the EAC to raise the dewar. When the dewar is in its upper position the liquid nitrogen filling is initiated. When the EAC signals the IRMS software that the dewar has reached an appropriate temperature the sample is dropped into CF-EA combustion tube. After the trap time has passed the IRMS commands the EAC to terminate the liquid nitrogen filling and to lower the dewar. When the dewar is at its lower position the Gilson withdraws the needle and returns to its home position; ready for the next sample (see Figure 3-7).

The liquid nitrogen fill procedure is activated by setting VA true (*set by IRMS*). The dewar temperature is read and compared to a upper threshold (-160°C, *the maximum dewar temperature allowed*) and to a lower threshold temperature (-180°C). If the temperature is higher than the upper threshold then liquid nitrogen is pumped into the dewar, whereas

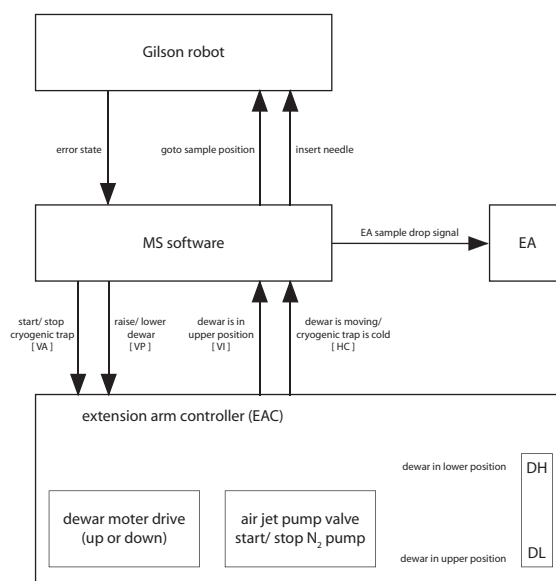
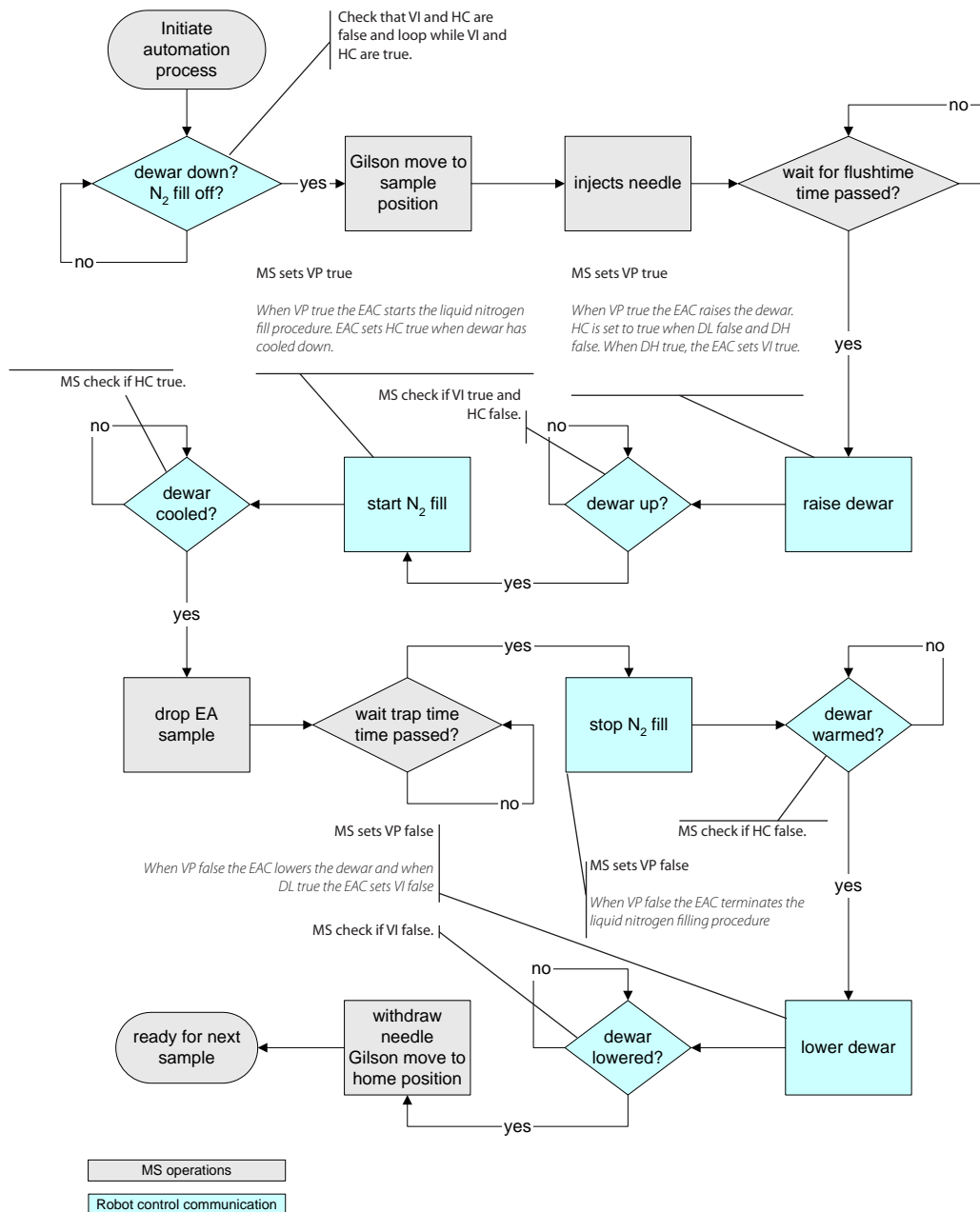


Figure 3-6: Schematic of IRMS communication pathways



**Figure 3-7:** Flow diagram of the MS software script for sample handling and cryogenic trapping of EA produced CO<sub>2</sub>. The read back signals (*VI* and *HC*) ensures that the mass spectrometer commands are executed, and hence to abort in case of malfunctioning or an error state in the robot controller. Furthermore, the read back signal of the dewar position also work as a flag to the mass spectrometer software to avoid movements of the robot during the trap procedure. Any movement of the robot arm while the dewar is up or the when cryogenic trap is on can cause damage to the system. The read back of the cryogenic trap status is used as a trigger for dropping the sample into CF-EA combustion furnace to ensure that the cryogenic trap has the proper temperature conditions for CO<sub>2</sub> trapping.

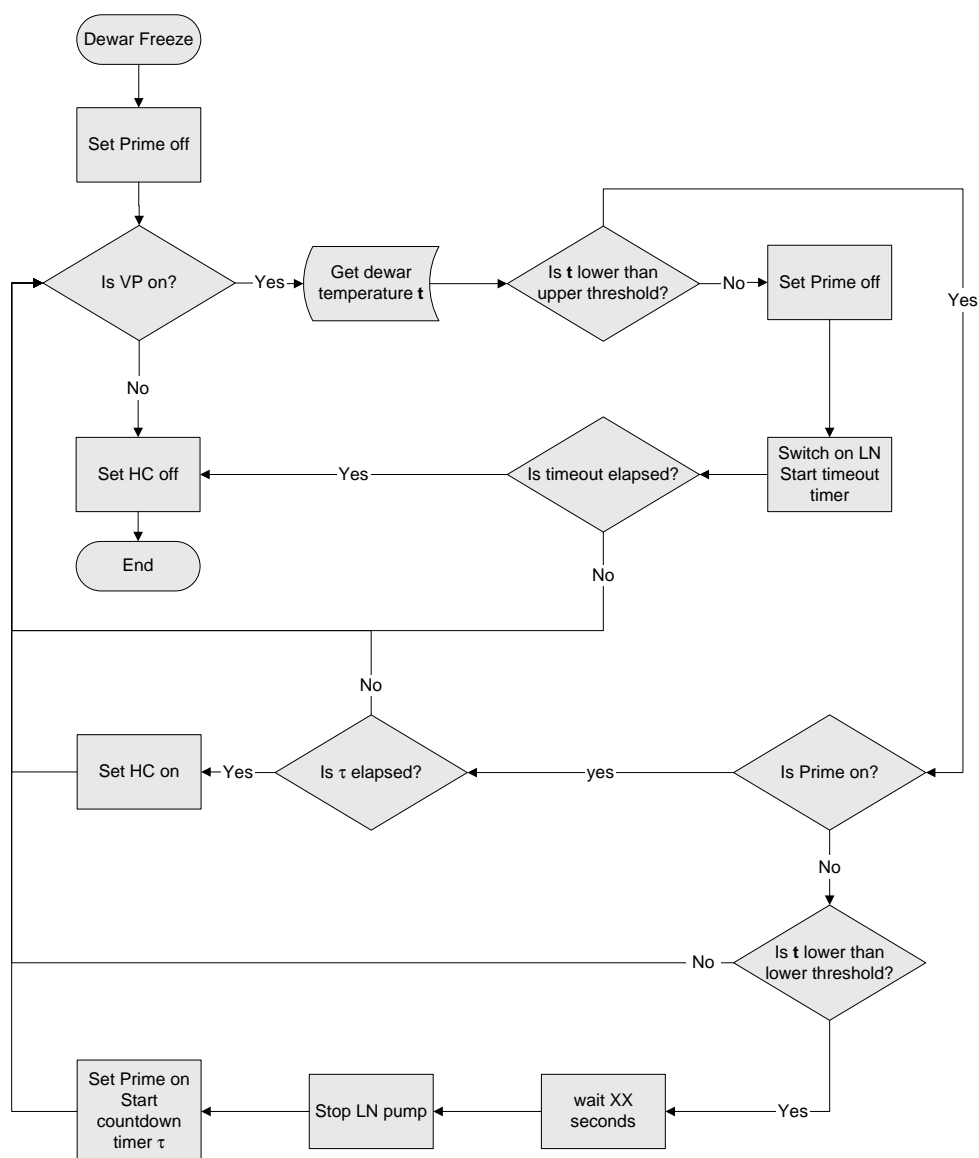


Figure 3-8: Flow diagram of the cryogenic trap procedure.

if it is lower than the lower threshold temperature then the liquid nitrogen pumping is switched off. A timeout timer ensures that during malfunctioning the air jet pump is stopped if the dewar is not cooled below the upper threshold temperature within 360 seconds and a countdown timer ensures that HC is set to true if and only if the dewar has been below the upper threshold temperature for more than 20 seconds in order to ensure that the dewar is cold prior to the sample EA sample drop (see Figure 3-8).

During analysis and CO<sub>2</sub> trapping error handling is performed solely by the IRMS software through the Gilson robot error state and HC and VI (Figure 3-6). Furthermore the Gilson main power is controlled by the EAC in order to avoid returning power to the Gilson after electric power failures which potentially could damage the Gilson robot or the robot extension if the dewar is at the upper position. The Gilson always returns to its home position when power is switched on. The EAC commands are accessible from the IRMS user interface and further enable the user to set the needle vertical position, the vial flush time and the cryogenic trap time together with all other commonly available parameters of IRMS CF-EA analysis.

## Results and Discussion

The freeze procedure, the AMS  $^{14}\text{C}$  background level and the stable isotope analysis have been investigated and are discussed below.

### Freeze procedure

For successful cryogenic trapping of the produced  $\text{CO}_2$  gas it is essential that the vial bottom temperature is below the  $\text{CO}_2$  freezing point during the entire trapping time. Optimal parameters of the trapping procedure have been found by an iterative process of trial and error while monitoring the temperature of both the dewar and the vial. Figure 3-9 displays the final outcome of the trap procedure parameters. For the first ca. 60 seconds the vial and dewar drops rapidly in temperature to about  $-180^\circ\text{C}$  where it stabilises. If the temperature stays below  $-160^\circ\text{C}$  for a minimum of 20 seconds then the sample is dropped into the EA combustion furnace ensuring that the setting the sample drop signal from the EAC to IRMS software (HC) is independent of the time used to cool the dewar. The temperature is then maintained below  $-160^\circ\text{C}$  by sequentially pumping liquid nitrogen into the dewar. However, even though the dewar temperature fluctuates by approximately  $20^\circ\text{C}$  to  $30^\circ\text{C}$  the vial temperature is fairly constant and, more important, it is maintained below the  $\text{CO}_2$  freezing point all the time.

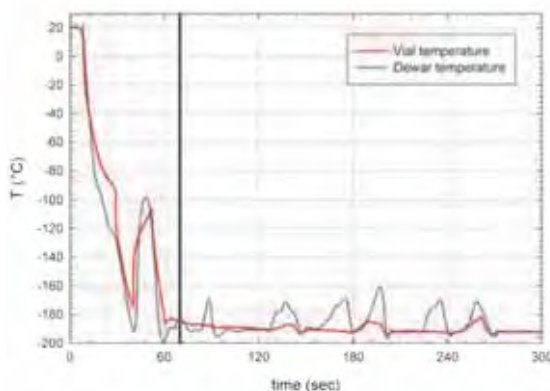


**Figure 3-9:** Monitored vial and dewar temperature. The solid vertical line represents the setting of the EA sample drop signal (HC) by the EAC.

### $^{14}\text{C}$ analysis – background and memory effects

A batch of 19 samples in total of radiocarbon standards was analyzed with the CF-EA-AMS sample preparation device (*Table 3.1 and Figure 3-10*) for determination of a possible  $^{14}\text{C}$  intersample memory effect. 2 samples failed both stable isotope analysis and  $\text{CO}_2$  trapping and further 1 sample failed  $\text{CO}_2$  trapping but was successfully analyzed for  $\delta^{13}\text{C}$ . These samples failed due to malfunctioning of the injection needle. During analysis small pieces of septum rubber are stuck within the needle inlet cylinder thus partially blocking the helium flow. Hence, for successful  $\text{CO}_2$  trapping and stable isotope analysis the needle was cleaned for every second sample.

The  $^{14}\text{C}$  analysis is among other things sensitive to the  $^{14}\text{C}$  background level, i.e. the  $^{14}\text{C}$  activity of dead  $^{14}\text{C}$  materials, and to memory effects caused by the CF-EA system (Aerts-Bijma *et al* 2001; Olsen *et al* in preparation). Aerts-Bijma *et al* (2001) demonstrated that the position of the T-split for dividing the gas flow to the IRMS and the trapping device is crucial in order to minimize memory effects. Likewise the CF-EA chemicals may also lead to memory effects by bypassing the GC column. Intersample memory effects were not detected (*Figure 3-10*) as also reported by Aerts-Bijma *et al* (2001) on their modified CF-EA trapping system. The  $^{14}\text{C}$  background level of anthracite samples are slightly increased for small samples (*Figure 3-11*) indicating addition of a minor amount of contaminating carbon of higher  $^{14}\text{C}$  activity during the sample processing, i.e. either during CF-EA combustion and trapping or by the subsequent graphitization procedure. The size effect of the analyzed NIST OX-I samples (*Figure 3-12*) does on the other hand not give a simple picture. The observed variability is not

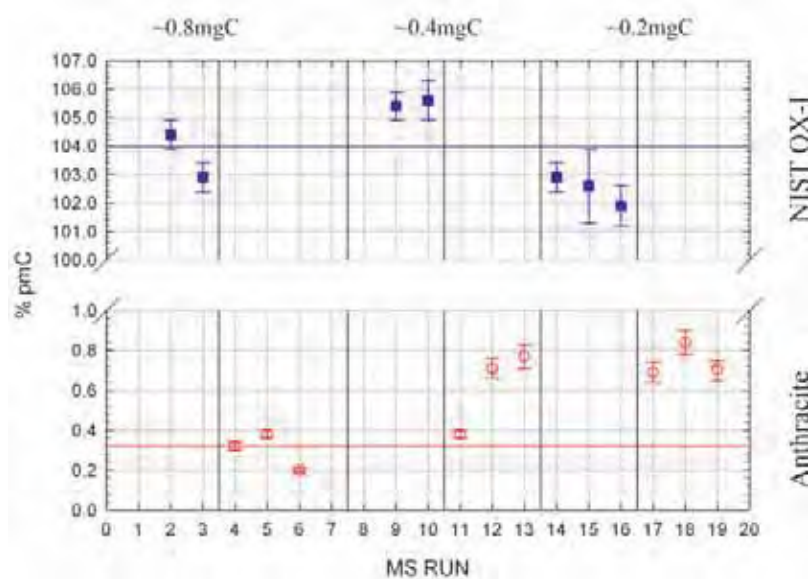


**Figure 3-10:** pmC values of alternating NIST OX-I and Anthracite samples as a function of MS run number. The upper solid line represents the NIST OX-I pmC value of 103.98% and the lower solid line represents the anthracite 0.8mgC pmC value of  $0.31 \pm 0.01\%$ .

understood at presents and shows no systematic dependence on sample size.

The  $^{14}\text{C}$  background level of the anthracite sample can be determined from the three 0.8mgC samples to a pmC value of  $0.31 \pm 0.01\%$  which is only slightly higher than Icelandic double spar with a pmC value of 0.20% normally used for monitoring the  $^{14}\text{C}$  background level for AMS radiocarbon analysis. However, it has been reported that the tin cups used for CF-EA combustion may significantly contribute a carbon contaminant thereby increasing the  $^{14}\text{C}$  background level for CF-EA processed AMS samples (Bronk Ramsey and Humm 2000). A test measurement of the  $^{14}\text{C}$  content of the CF-EA tin cups was therefore carried out by processing anthracite by normal off-line combustion in three different runs with none, one and five tin cups added, respectively. The radiocarbon results are shown in Table 3.2 illustrating that the anthracite samples processed without the addition of tin cups is in excellent agreement with the 0.8mgC CF-EA-AMS processed anthracite samples in Table 3.1. However the anthracite processed with 5 tin cups added show slightly higher pmC values indicating the CF-EA tin cups are

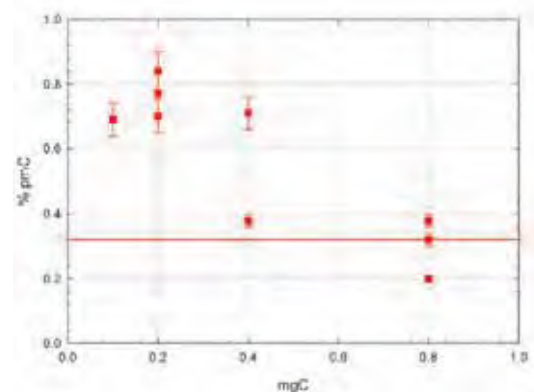


**Figure 3-11:** Size effect of analysed anthracite samples. The solid line represents the anthracite 0.8mgC pmC value of  $0.31 \pm 0.01\%$ .

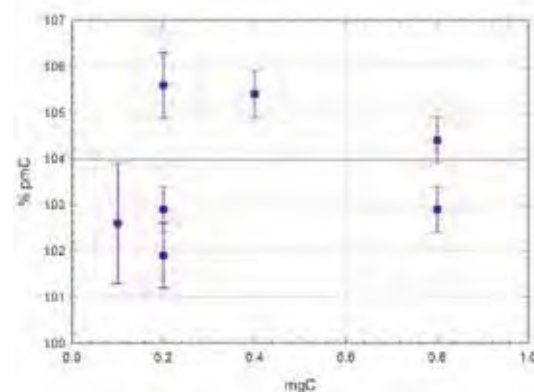


**Figure 3-12:** Size effect of analysed NIST OX-I samples. The solid line represents the NIST OX-I pmC value of 103.98%.

**Table 3.1: AMS trap device batch (Radiocarbon standards)**

	SID	Cathode	Sample Name	Mass $\mu\text{g}$	$\delta^{13}\text{C}$ $\text{‰ VPDB}$	Trapping efficiency	size $\text{mgC}$	%pmC
1	16		NIST OX-I	5941		n/a		
2	16	18018	NIST OX-I	5731	-19.1	83.8%	0.8	104.4 $\pm$ 0.5
3	16	18019	NIST OX-I	5627	-19.0	80.9%	0.8	102.9 $\pm$ 0.5
4	2953	18020	Anthracite	1258	-23.2	72.0%	0.8	0.32 $\pm$ 0.02
5	2953	18021	Anthracite	1261	-23.1	75.1%	0.8	0.38 $\pm$ 0.02
6	2953	18022	Anthracite	1347	-23.2	83.6%	0.8	0.20 $\pm$ 0.01
7	2792		AMS BGD	3037	-16.0	n/a		
8	16		NIST OX-I	2882		n/a		
9	16	18024	NIST OX-I	2826	-19.1	76.1%	0.4	105.4 $\pm$ 0.5
10	16	18195	NIST OX-I	2803	-19.0	74.9%	0.2	105.6 $\pm$ 0.7
11	2953	18023	Anthracite	616	-23.2	73.5%	0.4	0.38 $\pm$ 0.02
12	2953	18196	Anthracite	603	-23.1	71.6%	0.4	0.71 $\pm$ 0.05
13	2953	18197	Anthracite	470	-23.1	53.8%	0.2	0.77 $\pm$ 0.06
14	16	18025	NIST OX-I	1379	-18.9	83.4%	0.2	102.9 $\pm$ 0.5
15	16	18198	NIST OX-I	1693	-19.0	38.4%	0.1	102.6 $\pm$ 1.3
16	16	18199	NIST OX-I	1552	-19.0	64.4%	0.2	101.9 $\pm$ 0.7
17	2953	18026	Anthracite	282	-23.0	63.5%	0.1	0.69 $\pm$ 0.05
18	2953	18200	Anthracite	366	-23.0	63.3%	0.2	0.84 $\pm$ 0.06
19	2953	18201	Anthracite	345	-23.1	73.2%	0.2	0.70 $\pm$ 0.05
			Anthracite		-23.1 $\pm$ 0.08 $\text{‰}$	Average of anthracite of 0.8mgC 0.31 $\pm$ 0.01 % pmC		
			NIST OX-I		-19.0 $\pm$ 0.08 $\text{‰}$			

The pmC values are not corrected of background level. The stable isotope  $\delta^{13}\text{C}$  values are normalised by using the NIST OX-I samples with an assigned  $\delta^{13}\text{C}$  value of -19.0 $\text{‰}$ .

**Table 3.2:  $^{14}\text{C}/^{13}\text{C}$  content of tin cups**

anthracite			anthracite (1x tin cup)			anthracite (5x tin cup)		
Chatode	% pmC	dev $\sigma$	Chatode	% pmC	dev $\sigma$	Chatode	% pmC	dev $\sigma$
			17991	0.19 $\pm$ 0.02	-4.9	17992	0.35 $\pm$ 0.03	-2.7
18086	0.35 $\pm$ 0.02	2.0	18087	0.40 $\pm$ 0.02	5.5	18088	0.43 $\pm$ 0.02	-0.5
18191	0.29 $\pm$ 0.01	-1.8	18192	0.28 $\pm$ 0.01	-0.9	18193	0.47 $\pm$ 0.02	1.9
	0.32 $\pm$ 0.01	7.2<3.8		0.30 $\pm$ 0.01	54.3<6.0		0.44 $\pm$ 0.01	11.4<6.0

**Table 3.3: Off-line  $\text{CO}_2$  trap tests**

Test	Sample weight	mgC	Trapped mgC	Trap %
1	1648	1195	1147	96%
2	1952	1416	1352	96%
3	1608	1166	1147	98%
4	1615	1171	1156	99%

**Table 3.4: AMS trap device batch (stable isotopes)**

SID	Sample Name	Mass	Carbon %			$\delta^{13}\text{C}$ ‰ VPDB			Nitrogen %			$\delta^{15}\text{N}$ ‰ AIR		
		$\mu\text{g}$	true	meas	dev	true	meas	dev	true	meas	dev	true	meas	dev
2338	GelA	2487		41.3%	4.3%		-22.1	-0.2		16.0%	1.0%		6.0	0.4
2338	GelA	2341	45.6%	47.6%	-2.0%	-22.3	-22.2	-0.1	17.0%	18.3%	-1.4%	6.4	5.9	0.5
2338	GelA	2567		44.6%	1.0%		-22.3	-0.0		17.2%	-0.2%		5.9	0.6
2345	IAEA N1	4163							21.6%	21.2%	0.4%	0.4	1.2	-0.8
3	IAEA C6	2355	44.1%	42.4%	1.7%	-10.8	-10.7	-0.1						
2341	IAEA N2	4532							20.4%	21.2%	-0.8%	20.3	20.6	-0.3
373	IAEA C7	6188		28.0%		-14.5	-14.6	0.1						
3599	IAEA N3	2478							13.9%	14.1%	-0.3%	4.7	5.0	-0.3
374	IAEA C8	5454	19.9%	21.5%	-1.6%	-18.3	-18.4	0.1						
2792	AMS BGD	2945	40.9%	42.7%	-1.8%	-16.0	-16.4	0.4	15.0%	16.0%	-1.0%	11.7	11.8	-0.0
2345	IAEA N1	3731							21.6%	21.2%	0.4%	0.4	1.2	-0.8
3	IAEA C6	2732	44.1%	41.9%	2.2%	-10.8	-10.7	-0.1						
2341	IAEA N2	4039							20.4%	18.8%	1.6%	20.3	20.5	-0.2
373	IAEA C7	6001		27.4%		-14.5	-14.6	0.1						
3599	IAEA N3	3067							13.9%	12.2%	1.6%	4.7	4.7	0.0
374	IAEA C8	4943	19.9%			-18.3								
2792	AMS BGD	2749	40.9%	41.9%	-1.0%	-16.0	-16.3	0.4	15.0%	15.7%	-0.7%	11.7	11.8	-0.1
2345	IAEA N1	3693							21.6%	20.6%	1.0%	0.4	1.2	-0.8
3	IAEA C6	2537	44.1%	41.4%	2.7%	-10.8	-10.8	-0.0						
2341	IAEA N2	3707							20.4%	20.7%	-0.3%	20.3	20.6	-0.3
373	IAEA C7	5932	17.5%			-14.5								
3599	IAEA N3	2499							13.9%	11.7%	2.1%	4.7	5.0	-0.3
374	IAEA C8	5529	19.9%	20.1%	-0.3%	-18.3	-18.5	0.2						
2338	GelA	2555		44.9%	0.7%		-22.3	0.0		17.4%	-0.4%		5.8	0.6
2338	GelA	2471	45.6%	46.1%	-0.5%	-22.3	-22.3	0.0	17.0%	17.8%	-0.8%	6.4	5.7	0.7
2338	GelA	2248		43.3%	2.2%		-22.3	0.0		16.8%	0.2%		5.7	0.7
	Average				0.6%			0.1			0.1%			-0.0
	Standard deviation				2.0%			0.2			1.0%			0.5

contributing by a pmC value of approximately  $0.024 \pm 0.003\%$ . Commonly the CF-EA tin cups are thoroughly cleaned prior the CF-EA combustion of radiocarbon samples (Bronk Ramsey and Humm 2000); a procedure which is not adopted here. However, for very small samples or very old radiocarbon samples a tin cup cleaning procedure may successfully be adopted. Aerts-Bijma *et al* (2001) reported a background level of the anthracite sample of  $0.24 \pm 0.05\%$  pmC and hence slightly lower than the anthracite value found here.

As may be observed from Table 3.1 the trapping efficiency is heavily varying. Maximum trapping efficiency values are about 84% and values as low as 38% are in some instances approached. The trap efficiency was measured off-line during initial tests to ensure that the trap efficiency of the final system was high. The off-line measurements were performed manually by suspending the vial in a large dewar filled with liquid nitrogen and setting in the injection needle by hand prior to the CF-EA sample drop. The measured trap efficiency of these off-line tests was determined to about 97% (*see Table 3.3*) and was verified prior to the batch analysis. Consequently,

**Table 3.5: Anthracite stable isotope analysis**

EA-CF AMS	EA-CF	Dual inlet
-23.1 ± 0.1‰	-23.2 ± 0.2‰	-23.1 ± 0.2‰

**Table 3.6:  $\delta^{13}\text{C}$  values of Anthracite on the same gas by both the EA-AMS and DI method.**

SID	Cathode	Sample name	$\delta^{13}\text{C}$ ‰ VPDB		
			EA AMS	DI on trapped gas	dev
2953	18020	anthracite	-23.2	-23.3	0.1
2953	18021	anthracite	-23.1	-23.1	0.0
2953	18022	anthracite	-23.2	-23.3	0.1

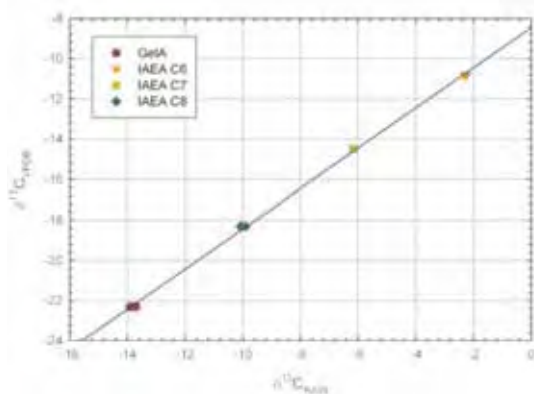


**Figure 3-13:** Raw  $\delta^{13}\text{C}$  (measured relative to machine working gas) as function of assigned (true)  $\delta^{13}\text{C}$  value.

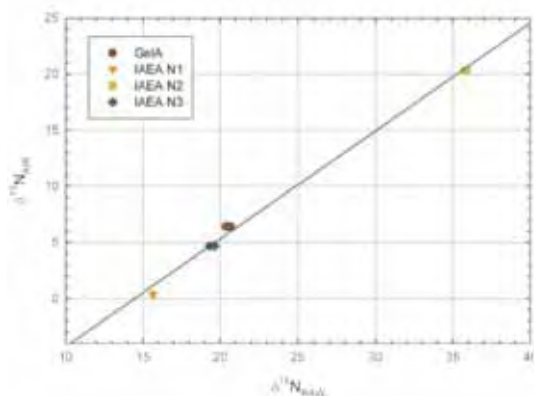


**Figure 3-14:** Raw  $\delta^{15}\text{N}$  (measured relative to machine working gas) as function of assigned (true)  $\delta^{15}\text{N}$  value.

the lower trap efficiencies observed during the batch analysis are ascribed to injection-needle malfunction.

The injection needle malfunction will in the future be solved by providing the injection needle with a side hole placed just above the needle tip to prevent pieces of septa blocking the needle. Furthermore, an improved needle holder is set into production enabling fine adjustments of the needle in the  $x$  and  $y$  plane of the manifold bed to ensure that the needle perfectly penetrates the centre of both septa.

### Stable isotope analysis

A batch of 25 stable isotope standards was analyzed to determine the precision and accuracy of the CF-EA AMS sample preparation device (Table 3.4 and Figure 3-13 & 3-14). The observed precision and accuracy is  $0.1 \pm 0.2$ ‰ and  $0.1$ ‰, respectively, for  $\delta^{13}\text{C}$  analysis and  $0.0 \pm 0.5$ ‰ and  $0.1$ ‰ for  $\delta^{15}\text{N}$  analysis. Hence, the elemental composition of carbon and nitrogen and the stable isotope analysis of  $\delta^{13}\text{C}$  and  $\delta^{15}\text{N}$  perfectly match the result expected for normal CF-EA analysis (Werner and Brand 2001). Likewise, the AMS BGD sample of Table 3.1 having a measured  $\delta^{13}\text{C}$  value of  $-16.0$ ‰ is in agreement with the assigned  $\delta^{13}\text{C}$  value of  $-16.1$ ‰ (internal  $\delta^{13}\text{C}$  and  $^{14}\text{C}$  standard). The anthracite standard has also been measured by both the normal CF-EA method and by the DI method (Table 3.5). Compared with the CF-EA-AMS analysis (Table 3.1) the three methods display excellent mutual agreement.

The  $\delta^{13}\text{C}$  values of the three 0.8mgC anthracite samples (Table 3.1; Cathode 18020, 18021 & 18022) were also determined on the cryogenically trapped  $\text{CO}_2$  fraction (Table 3.6). The deviation between the  $\delta^{13}\text{C}$  values determined by the CF-EA-AMS and the DI method on the same  $\text{CO}_2$  gas all mutually agree indicating that isotopic fractionation during the splitting of the produced  $\text{CO}_2$  gas does not occur.

## Conclusion

A CF-EA-AMS sample preparation system combined with stable isotope analysis of  $\delta^{13}\text{C}$  and  $\delta^{15}\text{N}$  have been designed and successfully tested. The system is based on a modified CF-EA and Gilson 222XL robot enabling cryogenic trapping of  $\text{CO}_2$ . The system is under full IRMS control and is able to handle various safety issues. A user interface is incorporated into the IRMS software enabling the user easy and simple access to method parameters. Furthermore, the system is flexible, and shifting between DI applications and CF-EA-AMS applications of Gilson robot is straightforward.

The  $^{14}\text{C}$  background is demonstrated to be at an acceptable level with a PmC value of  $0.0029 \pm 0.0013$ . Likewise the  $^{14}\text{C}$  measurements indicate that the contaminant carbon added during either CF-EA combustion or trapping or during the graphitization step is of intermediate  $^{14}\text{C}$  activity. The stable isotope analysis of  $\delta^{13}\text{C}$  and  $\delta^{15}\text{N}$  has been found to be in excellent agreement with the expected precision and accuracy of normal CF-EA isotope analysis. However, the sample analysis also revealed that the design of the needle and needle holder are to be improved before routine samples can be analyzed.



# 4

---

## **The Bliden Lake**

**site description, motivation  
and perspectives**

## Introduction

In this section a brief history of the geological development of the Bliden Lake area and core drilling site is presented. The sediments of the Bliden Lake offer an opportunity to investigate past climates as well as the marginal propagation of marine sea level changes; the so-called Littorina transgressions. For this purpose, a short introduction to past Danish relative sea level changes is presented. Furthermore, it has been suggested that the onset of the Neolithic in Denmark, Sweden, Ireland and Britain may have been triggered by a climate change and thus a paleoclimate investigation of the Bliden Lake may potentially provide further evidence. This section provides a short overview of the climate history and an introduction to Neolithic culture, however, for a detailed presentation of these issues the reader is referred to the substantial literature within this field (see e.g. Lowe and Walker 1997; Gerhard *et al* 2001; Jensen 2001; Ruddiman 2001; Roberts 2004).

## The site

The Bliden Lake is located on the Danish island Sjælland (see *Figure 4-1*) probably created by a dead ice block left behind from the retreating ice sheet around 10.000 years ago. The Sjælland tills were formed during the Weichselian glacial period. During the latest glacial maximum, which occurred in the period 23 to 21 kyr BP, the ice sheet covered most of Scandinavia with the main stationary ice line running from south to north through the middle of Jylland (Houmark-Nielsen and Kjær 2003). After the deglaciation period (21-19 kyr BP), the Baltic ice stream advanced westward and terminated in Jylland in the period 18 to 17 kyr BP. The Baltic glacier then retreated to a position southwest and east of Fyn and was later followed by the Bælthav readvance of the glaciers in the valleys of Lille Bælt and Store Bælt (Houmark-Nielsen and Kjær 2003). Around 17 to 16 kyr BP this ice sheet retreated and followed the borders of the Swedish west coast. These advances and retreats of ice sheets and glaciers formed the tills of northwest Sjælland (Noe-Nygaard 1995). The final retreat of the Bælthav ice sheet left behind blocks of dead ice in a steppe landscape dominated by grass and herbs (Houmark-Nielsen and Kjær 2003) and the Bliden and Tissø lakes were most likely formed by one of these dead ice blocks (*Figure 4-1*).

The Bliden Lake is positioned southeast of Tissø Lake (*Figure 4-1 & 4.2*) and has an oblong shape which runs parallel to the Tissø Lake shoreline. Its length is 330 meters and it is 165 meters wide and covers an approximate area of 0.0428 km<sup>2</sup>. The distance between Bliden Lake and Tissø Lake is around 250 meters and separated by a moraine ridge. The present water level of Bliden Lake is 2.5 meters above normal sea level, and the only outlet is placed in the southward end of the lake, and runs through a small valley into Tissø Lake (see *Figure 4-2*). At present no modern limnological data on the Bliden Lake exists, nor is its morphology known. The lack of modern hydrological knowledge of the Bliden Lake naturally restricts the interpretations of the Bliden Lake core. However, due to the small size it is likely a shallow lake with probable depth of about 2 to 8 metres. The drainage system of the lake is presumably very small and restricted to the tills to the east and northeast as may be indicated by the numerous minor brook inlets (see *Figure 4-2*). It is therefore most likely that the Bliden Lake is mainly fed by ground-water inflow.

## Perspectives

Lacustrine environments are ecosystems that respond quickly to global and regional environmental changes. Therefore, they are excellent archives of past climates. However they are not just able to record ancient climate history, but may also track major environmental changes caused by human activities, such as for example the introduction of arable farming.

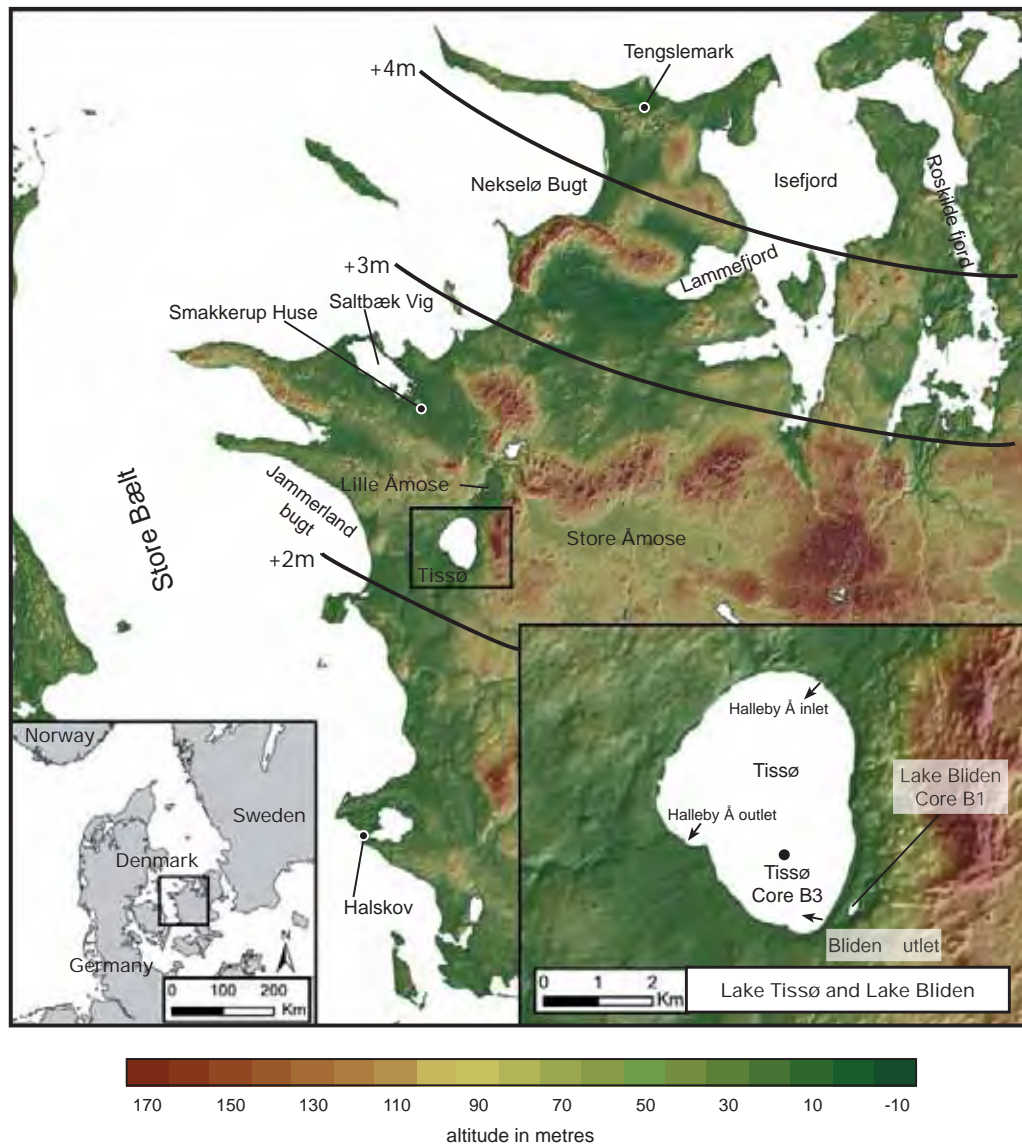


**Figure 4-1.** A contour map of the north eastern part of Sjælland. The isobase lines reflects the total land rebound since the time of the last ice age are shown as solid lines (Mertz 1924). In the lower right corner the Bliden Lake and the Tissø Lake are shown. The position of the Tissø core B3 and the Halleby Å inlet and outlet are indicated. (The map was produced with help from Mikkel Ulfeldt-Hede, Department of Geology, University of Copenhagen. GIS G15-03)



**Figure 4-2:** Left: Map showing the Bliden Lake area. Right: Map showing the Bliden Lake northern inlet and southern outlet to the Tissø Lake.

### The modern Danish climate

Denmark has a typical coastal climate with mild and humid weather in winter and cool and changeable weather in summer. The mean temperatures do not vary greatly between summer and winter (see Figure 4-3, Laursen *et al* 1999) and due to the heat transfer from the Gulf Stream the Danish climate is relatively warm compared to other geographical regions on the same latitude (*Hudson Bay in Canada and Siberia in Russia*) (Lowe and Walker 1997). The heat transfer may locally warm annual mean temperatures by up to 10°C and it is likely that Scandinavia, Great Britain, Ireland, The Netherlands and Belgium is warmed by several degrees with the greatest effect in the winter (Rahmstorf 2000). The weather is strongly influenced by the proximity to the sea and to the European continent and thus the weather changes according to the prevailing wind direction (Laursen *et al* 1999). The predominant wind direction is westerly and frequently easterly, while southern and northern wind directions are infrequent. The westerly wind direction brings in low pressure frontal systems, resulting in windy and rainy weather (Laursen *et al* 1999). In contrast, an eastern or southern wind direction yields continental weather conditions, viz. very cold during winter and warm during summer. However, southern wind directions are commonly associated with more moist air and often result in fog (Laursen *et al* 1999).

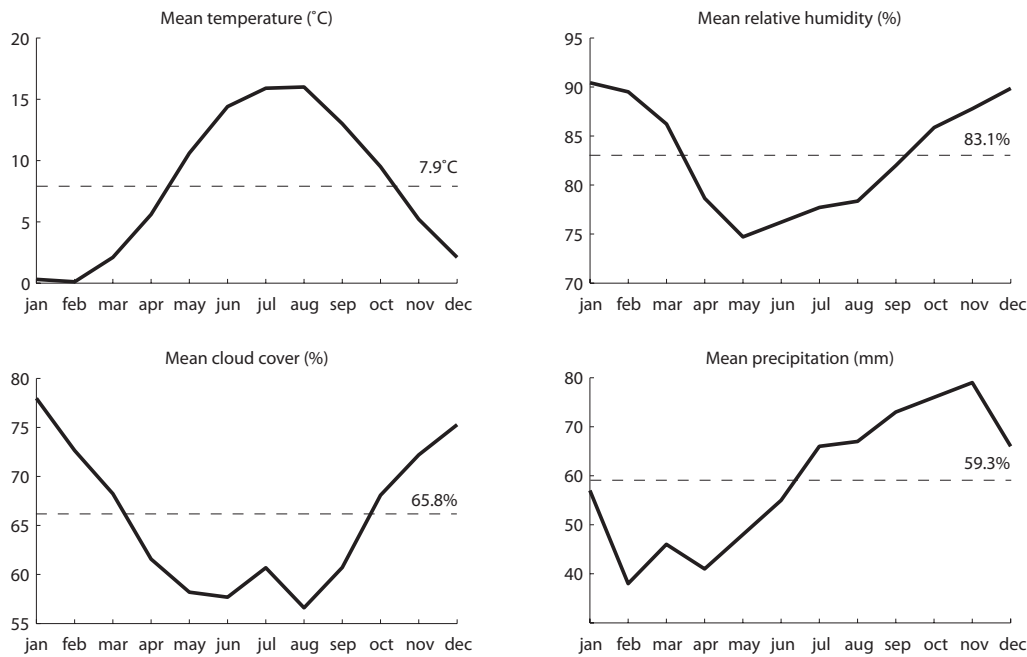


Figure 4-3. Shown are the modern monthly mean temperature, mean relatively humidity, mean cloud cover and mean precipitation of Denmark covering the period 1961-90. Source: Danish Meteorological Institute (Frich *et al* 1997; Laursen *et al* 1999).

### The Holocene environment in broad terms

The deglaciation 11.000 years ago resulted in an increase of mean annual temperatures with about 17°C (Johnsen *et al* 2001) concurrent with an increase in the atmospheric CO<sub>2</sub> levels from 190 ppm to 280 ppm and a doubling of atmospheric methane levels (Lowe and Walker 1997; Bluemle *et al* 2001; Ruddiman 2001). The Scandinavian climate experienced a long term optimum warm period from about 7800 cal BP with the onset of a cooler climatic trend from about 5100 cal BP, mainly due to orbital forcing mechanisms (*Milankovitch theory, see e.g. (Lowe and Walker 1997; Petersen 2003)*) resulting in changes in northern hemisphere summer insolation (see Figure 4-7, Pekarek 2001; Ruddiman 2001). From borehole temperature measure-

ments in the GRIP and Dye 3 ice cores, it has been shown that the temperatures of the period from 8000 to 5000 years ago were 2.5°C warmer than present followed by decreased temperatures in the period from 5000 to 2000 years ago with minimum temperatures 0.5°C colder than present (Dahl-Jensen 1998), which is confirmed by pollen based temperature reconstructions (Magny 2004; Seppä *et al* 2005). Superimposed on these general trends are short-term centurial to millennial fluctuations (Pekarek 2001; Ruddiman 2001) such as the medieval warm period, reported to be 1°C warmer than present, and the little ice age, about 0.7°C colder than present (Dahl-Jensen 1998; Moberg *et al* 2005).

Likewise, the deglaciation resulted in major changes to land vegetation. In the glacial climate of the northern hemisphere prior to 11000 cal BP the deciduous forest was positioned southward towards the equator and at the end of the Pleistocene the European continent was predominately an open landscape with tundra and steppe vegetation (Ruddiman 2001; Roberts 2004). Between 11000 and 9000 cal BP, the open landscape was replaced by the northward spreading of tree species as a consequence of the warmer climate and the retreat of the continental ice sheet. Birch and pine were the first trees to appear followed by deciduous trees such as hazel and elm, and later on the oak, lime, alder and ash arrived. Thus by 9000 cal BP the steppe and tundra vegetation was replaced by boreal forest landscape covering almost all available land (Iversen 1967; Ruddiman 2001; Roberts 2004). The effects of the climate deterioration from 5500 cal BP on vegetation are often disguised by human disturbances. For example, the northward spread of beech may have been caused by climate cooling as well as by the forest clearances of the bronze and iron age populations creating gaps in the forest (Roberts 2004). The climate deterioration is revealed in Denmark by an increase in sphagnum from about 5000 cal BP, probably suggesting the onset of a wetter climate (Iversen 1967).

#### *Possible sources of short-term Holocene climate oscillations*

In general, the oscillations between glacial and inter-glacial climate conditions at least during the last 800,000 years are explained by the Milankovitch theory (Lowe and Walker 1997; Ruddiman 2001). However, ice core records such as GRIP and GISP2 (O'Brian *et al* 1995; Stuiver *et al* 1995; Johnsen *et al* 2001; Vinther *et al* 2006; Seierstad *et al* in press) show evidence of high frequency climatic oscillations during the last 120 kyr and typically reflect abrupt changes in oxygen isotope values during which temperatures fluctuated about 5°C to 8°C (Lowe and Walker 1997). These relatively short-lived Dansgaard-Oeschger events cannot be explained by the Milankovitch theory and rather appear to reflect ice sheet fluctuations, oceanographic changes and atmospheric circulation variations (Lowe and Walker 1997; Hall *et al* 2004). Presently, there is a growing body of evidence that these short-lived periodic events have persisted into the Holocene epoch as for instance the 8200 cal BP and 2800 cal BP cold periods (see e.g. Geel *et al* 1996; von Grafenstein 1998; Dergachev *et al* 2004; Veski *et al* 2004; Hammarlund *et al* 2005) together with the perhaps more well-known 'little ice age' (Matthews and Briffa 2005; Gil *et al* 2006). Moreover, Bond *et al* (Bond *et al* 1997; Bond *et al* 2001) have demonstrated *ca.* 1500 year cycles of ice rafted debris in marine cores of the north Atlantic, which are attributed

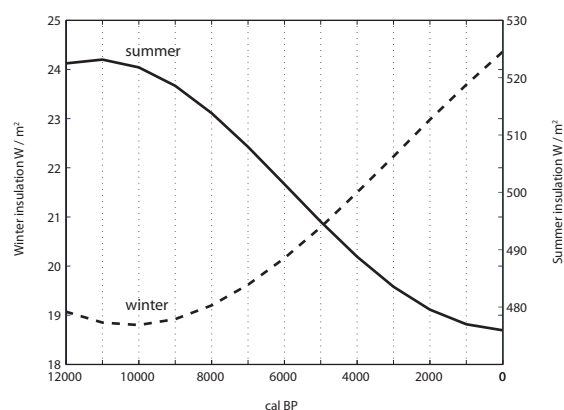


**Figure 4-4:** Shown is the summer and winter insolation at 60°N during the past 12,000 years (Berger and Loutre 1991).

to changes in the north Atlantic deep water formation and probably forced by changes in solar activity (Bond *et al* 2001).

The ocean circulation system appears to function as a conveyor belt, transporting warm waters northward in the Atlantic where it cools and sink to form the southwards moving deepwater mass denoted the North Atlantic Deep-Water (NADW). Changes in NADW and thus in the northeast transfer of heat from the Gulf Stream to Western Europe may have major consequences for regional and hemispheric climates (Lowe and Walker 1997). The NADW formation is very sensitive to the amount of freshwater entering the North Atlantic (Rahmstorf 2000) and it has been proposed that the NADW formation has occasionally been switched off completely, and thus been proposed as an explanation for the cold Younger Dryas period (Manabe and Stouffer 1999) and as an underlying mechanism for the *ca.* 1500 year periodicity in the Greenland ice cores which pervades the Holocene (see e.g. Bond *et al* 1997; Marchitto *et al* 1998; Bond *et al* 2001; Alley *et al* 2003; Oppo *et al* 2003; Nederbragt and Thurow 2005).

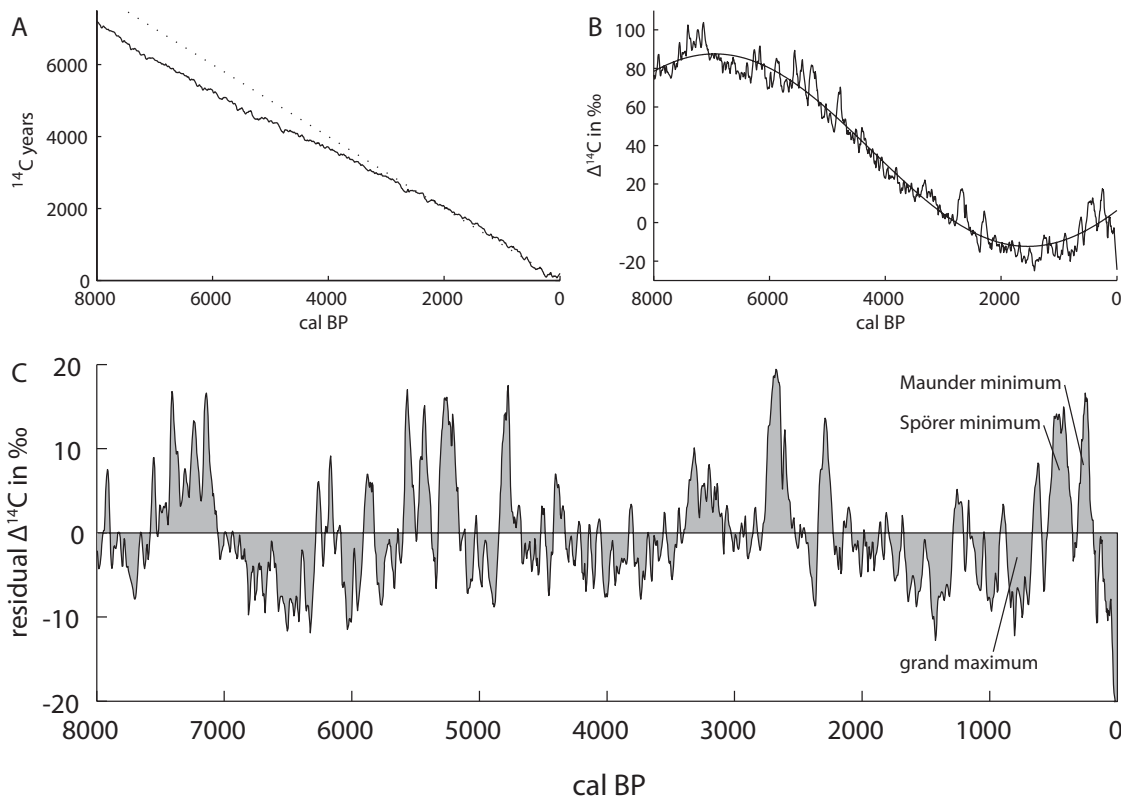


**Figure 4-5. Panel A:** Shown is the radiocarbon calibration curve for past 8000 years (Reimer *et al.* 2004b, a). The solid line represents a constant atmospheric production rate of  $^{14}\text{C}$  and is denoted  $^{14}\text{C}_{\text{ref}}$  i.e. the  $^{14}\text{C}$  reference activity at time  $t$ ; whereas the measured  $^{14}\text{C}$  activity at time  $t$  is denoted inventory  $^{14}\text{C}$  activity ( $^{14}\text{C}_{\text{inv}}$ ) (Sonnnett and Finney 1990). **Panel B:** Shown is the  $\Delta^{14}\text{C}$  signal of the past 8000 years (Reimer *et al.* 2004b, a). The  $\Delta^{14}\text{C}$  is defined by  $\Delta^{14}\text{C} = (^{14}\text{C}_{\text{ref}} - ^{14}\text{C}_{\text{inv}}) / ^{14}\text{C}_{\text{inv}}$  (Sonnnett *et al.* 1990). The solid line represent a least square fit of the period, amplitude and phase of a sinusoid and is attributed to modulations of the incident cosmic ray flux at the top of the atmosphere by changes in the geomagnetic field (Eddy 1976; Sonnnett and Finney 1990). **Panel C:** Shown is the residual  $\Delta^{14}\text{C}$  signal obtained by subtracting the fitted sinusoid from the  $\Delta^{14}\text{C}$  signal of panel B. For the Holocene period this signal is mainly reflecting changes in the  $^{14}\text{C}$  production in the upper atmosphere. Shown is also two periods of pronounced higher atmospheric  $^{14}\text{C}$  activity corresponding to the Spörer and Maunder sunspot minima. The Spörer and Maunder sunspot minima are periods in the sunspot record of very few or none visual observed sunspots indicating a very low solar activity. These sunspot minima occurs simultaneously with the little ice age (Eddy 1976). The period denoted grand maximum is a period of a higher than normal number of sunspots. In the residual  $\Delta^{14}\text{C}$  this is a period of decreased atmospheric  $^{14}\text{C}$  production and corresponds in the historical record to the period named the Medieval warm period (Eddy 1976).

Bond *et al* (2001) indicated that solar activity changes may explain changes in the NADW formation and moreover are likely to explain some of the observed Holocene cold periods (see e.g. Eddy *et al* 1990; Geel *et al* 1996; Thejll and Lassen 2000; Björck *et al* 2001; Pekarek 2001; Braun *et al* 2005; Turney *et al* 2005). Furthermore, it has been suggested that the solar irradiance may account for 20 to 25% of 20<sup>th</sup> century warming (Keller 2004) and thus the sun may also account for a significant amount of the climate variations observed during the Holocene. However, the solar irradiance has been estimated to vary as little as 0.24% throughout the Holocene, corresponding to a temperature change of around 0.1°C which is too small to explain the observed climatic changes in the Holocene. Hence some amplification mechanism must be at play (Eddy *et al* 1990; Keller 2004; Mauquoy *et al* 2004). Two indirect mechanisms that may amplify the role of the sun further have been proposed (Bard *et al* 2000; Keller 2004): One is changes in the sun's ultra violet radiation causing changes in the stratospheric ozone production (see e.g. Keller 2004; Mauquoy *et al* 2004) and another is changes in the solar winds, which affect cloud formation (Friis-Christensen and Lassen 1991; Lassen and Friis-Christensen 1995; Svensmark 1998; Marsh and Svensmark 2000a; Marsh and Svensmark 2000b; Kristjansson *et al* 2004). These processes are presently being studied extensively and thus at this point they may only be offered as potential explanations or mechanisms of Holocene climate variability.

Radiocarbon is a cosmogenic isotope continuously produced in the upper atmosphere by cosmic radiation. Hence, changes in the cosmic radiation cause changes in the production of the <sup>14</sup>C nuclei. During the sun's combustion of hydrogen it expels particles into space, known as solar wind. The solar wind generates a magnetic field and this magnetic field is a function of solar activity. The magnetic fields deflect charged particles, the solar wind acts as shield, decreasing the amount of cosmic radiation on Earth during periods of high solar activity and increasing it during low solar activity. Therefore the production of <sup>14</sup>C is modulated by solar activity (Eddy 1976; Berger and Sonett 1990; Sonnett and Finney 1990; Bard *et al* 1997; Bard *et al* 2000). In general, however, variations of the <sup>14</sup>C production may have been caused by variations in the ocean uptake of CO<sub>2</sub>, by modulation of the incident cosmic ray flux by the geomagnetic field or by modulation of the cosmic ray flux by changes in solar activity (Sonnett and Finney 1990; Dergachev *et al* 2004). Removing the effects of Earth's magnetic field yields the residual  $\Delta^{14}\text{C}$  signal, which potentially reflects changes in solar activity (see Figure 4-5 and Usoskin and Kromer 2005). Furthermore, the atmospheric <sup>14</sup>C activity is dependent on the total carbon budget on Earth. During glacial periods, atmospheric CO<sub>2</sub> concentrations are significantly lowered and at the termination of the last ice age the CO<sub>2</sub> concentrations increased from 180ppm to 280ppm resulting in significant changes to the <sup>14</sup>C to <sup>12</sup>C ratio of atmospheric CO<sub>2</sub> (Oeschger and Beer 1990). However, the <sup>10</sup>Be and <sup>14</sup>C signals show similar trends during the last 10000 years. Thus, variations in  $\Delta^{14}\text{C}$  during the Holocene probably reflect changes in <sup>14</sup>C production and may thus serve as a proxy for solar activity changes (Oeschger and Beer 1990). Moreover, solar activity displays a cyclic behaviour (Solanki *et al* 2000) as demonstrated by spectral analysis of sunspot numbers and reflected in the <sup>14</sup>C and <sup>10</sup>Be proxies with periodicities of 10 to 11 years, 22 years, 50 to 80 years, 90 to 140 years, 170 to 260 years, *ca.* 360, *ca.* 420, *ca.* 500 years, *ca.* 570, *ca.* 700 years, *ca.* 960 years and *ca.* 2300 years (Berger and Sonett 1990; Reid 2000; Ogurtsov *et al* 2001; Ogurtsov *et al* 2002; Vasiliev and Dergachev 2002; Dergachev 2004). Hence, if solar activity is the driving force behind climate changes, these cyclicities should be observable in climate records.

Furthermore, other climate oscillations, such as the North Atlantic Oscillation (NAO), are also known to have a great impact on the European climate. The NAO is defined as a pressure gradient between the high pressure cell of the Azores and the low pressure cell north of Iceland causing the predominantly westerly wind patterns over north and western Europe and Scandi-

navia (Visbeck *et al* 2001; Wanner *et al* 2001). The NAO mainly affects winter temperatures and precipitation. A high pressure gradient between Iceland and the Azores increases the strength of the westerlies and is denoted NAO<sup>+</sup>. A weakened low pressure cell north of Iceland and less pronounced high pressure cell over the Azores results in a weakened pressure gradient and therefore decreases the strength of the westerlies and is denoted NAO<sup>-</sup>. The NAO<sup>+</sup> phase is associated with increased precipitation and above average temperatures for Scotland and south-western Norway. By contrast, the NAO<sup>-</sup> phase causes high amounts of precipitation over the Mediterranean region and the Black sea (Wanner *et al* 2001). The NAO<sup>-</sup> phase results in temperatures below average in northern Europe and Scandinavia.

A NAO period of 65 to 70 years has been identified in northern hemisphere temperatures (Schlesinger and Ramankutty 1994), and spectral analysis on stalagmite from the Uamh an Tair cave (North West Scotland) provides evidence of oscillations with a period of between 50 to 70 years (Proctor *et al* 2002). These findings are also confirmed by studies on ice cores (Fischer and Mieding 2005). The NAO has been studied extensively within the last 10 years (Visbeck *et al* 2001), but progress is, however, hindered by the limited gathering of instrumental data since the mid 19<sup>th</sup> century. An adequate natural NAO proxy that reaches far back in time is yet to be found. However, recent work using ice core winter  $\delta^{18}\text{O}$  data has proven very useful and can potentially be extended further back in time (Vinther *et al* 2003; Fischer and Mieding 2005).

#### *Possible implications of relative sea-level changes*

The Baltic and Scandinavian regions underwent dramatic geological transformations during the last deglaciation period. The retreating ice sheet and minor readvances formed the Scandinavian landscape (Noe-Nygaard 1995; Houmark-Nielsen and Kjær 2003; Kjær *et al* 2003). The Baltic Sea underwent significant changes from periods as a dammed glacier freshwater lake to the present day sea caused by a complex interplay of isostatic uplift, readvances and retreats of ice sheets (Björck 1995a), but also by the general eustatic sea level rise caused by the worldwide melting of ice sheets (Fairbanks 1989; Chappell and Polach 1991; Bard *et al* 1996). The volume of water stored in ice sheets during the last glacial maximum lowered the eustatic sea level by 120 metres relative to present sea levels (Fairbanks 1989; Peltier 2002; Peltier and Fairbanks In Press, Corrected Proof). Between 9500 to 9000 <sup>14</sup>C years ago BP the Ancylus Lake was formed (Björck 1995b). The coast lines of Kattegat were at that time situated north of the Storebælt and the North Sea coast lines were situated west of England (Noe-Nygaard 1995; Noe-Nygaard and Hede 2006). Sweden and Denmark was land-bridged through the Øresund strait. Earlier, the Baltic Ice Lake had been connected to Kattegat through the central part of Sweden. This connection was closed due to isostatic uplift and initiated the formation of the Ancylus Lake (Björck 1995b). The water level of the Ancylus Lake rose and exceeded the threshold at Darss Sill situated between Lolland (*Denmark*) and Fehmarn (*Germany*) resulting in the formation of the Dana River running through the valley of Storebælt (Björck 1995b).

Storebælt was transgressed by the sea during the early Atlantic. The very rapid sea level rise occurring after 7600 cal BP over a period of 600 years took place at a rate that may have approached 5 metres per 100 years (Christensen 1995; Noe-Nygaard 1995; Noe-Nygaard *et al* 1998). The eustatic sea level rise of the period was 2 metres per 100 years (melt water pulse 1B Fairbanks 1989). This transgression resulted in the establishment of a marine connection between the Ancylus Lake and Kattegat. The Littorina Sea was formed and the main contour of the present Sjælland was established. This fast eustatic sea level rise was driven by the melting of the North American ice sheet. The increasing sea level lifted the ice sheets on the continental shelf from the sea floor causing an increased rate of iceberg formation. The subsequent melting of these icebergs resulted in increased sea levels (see e.g. Lowe and Walker 1997; Ruddiman 2001; Coe

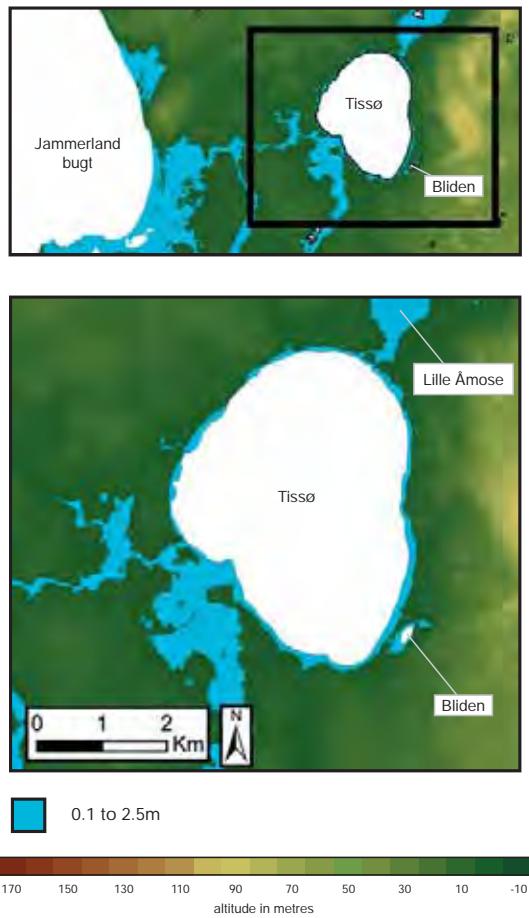


**Figure 4-6.** Map showing the Tissø region where the 0.1 to 2.5 meter contours are blue coloured. (The map was produced with help from Mikkel Ulfeldt-Hede, Department of Geology, University of Copenhagen. GIS G15-03)

2003). In the Sjælland region, the relative sea level changes were caused by a complex interplay of climate fluctuations, isostatic rebound and eustatic sea level rises and resulted in successive regression and transgression phase replacements of the marine shore lines known as the Littorina transgression (Iversen 1937; Noe-Nygaard 1995; Christensen and Andreasen 1999; Christensen 2001; Hede 2003; Richter and Noe-Nygaard 2003; Noe-Nygaard and Hede 2006).

From Smakkerup Huse (Hede 2003, see Figure 4-1) and Halskov (Christensen and Andreasen 1999, see Figure 4-1) two periods of high relative sea levels have been identified. The high relative sea level reported from Halskov are from the periods between 6750 cal BP to 5950 cal BP and again between 5650 cal BP to 5400 cal BP (Christensen and Andreasen 1999), whereas the Smakkerup Huse site reveals high relative sea level from 7010 cal BP to 6250 and again from 5850 cal BP to 5500 cal BP (Hede 2003). Likewise, a good correlation between the water level changes in the Åmose basin and the marine shoreline displacements has been reported by Noe-Nygaard (1995; Noe-Nygaard *et al* 2003). Furthermore recent work from Tengslemark reveals high relative sea levels in the periods from 7500 cal BP to 7150 cal BP, from 6470 cal BP to 6300 cal BP, from 6080 cal BP to 5815 cal BP, from 5350 cal BP to 5730 cal BP and from 4700 cal BP to 4000 cal BP (pers. com. Noe-Nygaard). Due

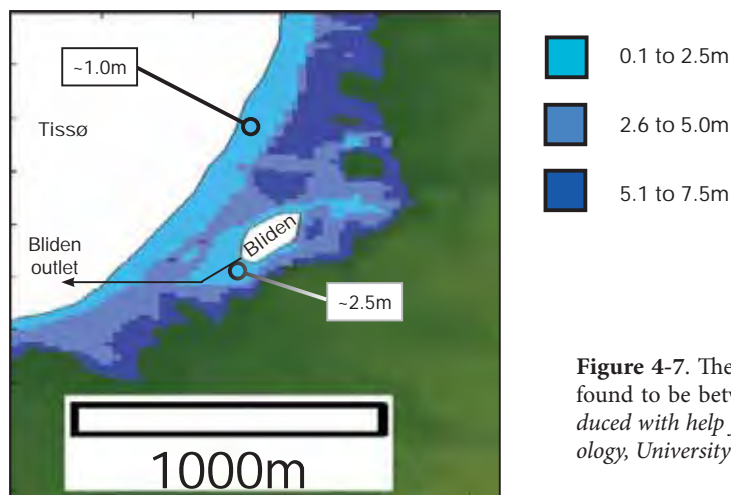


**Figure 4-7.** The threshold between Tissø and Bliden can be found to be between 1.1 and 2.5 meters. (The map was produced with help from Mikkel Ulfeldt-Hede, Department of Geology, University of Copenhagen. GIS G15-03).

to the low threshold between the Jammalund bugt and the Tissø Lake, the water levels of both the Tissø and Bliden Lakes may plausibly have changed in concord with the *Littorina* transgressions. In Tissø Lake the intrusion of brackish or saline marine water is probable (Noe-Nygaard and Hede 2006) whereas for Bliden Lake level changes in concord with relative sea level changes were most likely caused by changes in groundwater levels (see Figure 4-6 & 4-7). Furthermore, sub-boreal relative sea level changes has also been reported (see e.g. Christensen 1981, 1995; Christensen 2001; Clemmensen 2001)

### **The Mesolithic to Neolithic transition**

One of the greatest worldwide changes in ancient cultural history was the adoption of agriculture. It developed in the Middle East along with the onset of the present inter-glacial climate about 11,000 years ago (see e.g. Jensen 2001; Roberts 2004). The introduction of agriculture made it possible to feed more people and to live together in larger villages and to limit periods of famine. These small scale societies were predecessors for the development of civilisation as we know it. From about 7000 BC, agriculture started to spread across the Mediterranean region and over the Balkans to northern Europe (Jensen 2001). Agriculture was introduced in Northern France, the Netherlands, North Germany and Poland in the period between 5900 BC to 5400 BC (Jensen 2001; Bonsall *et al* 2002). However, it was not widely adopted in Southern Scandinavia, on the British Isle or in Ireland until 4100 BC to 3800 BC (Tauber 1981; Noe-Nygaard 1988; Jensen 2001; Bonsall *et al* 2002; Fischer 2002; Schulting and Richards 2002b; Richards *et al* 2003; Richter and Noe-Nygaard 2003; Rowley-Conwy 2004; Noe-Nygaard *et al* 2005).

The onset of the Danish Neolithic is characterised by the initial introduction of agriculture. Paleodietary evidence from human and dog bones indicate a rapid shift from a Mesolithic diet consisting mainly of fish to a Neolithic diet consisting mainly of terrestrial resources (see Figure 4-3, Tauber 1981; Noe-Nygaard 1988; Schulting and Richards 2002b; Richards *et al* 2003; Richter and Noe-Nygaard 2003; Fischer *et al* submitted for publication-a; Fischer *et al* submitted for publication-b).

The combined values of  $\delta^{13}\text{C}$  and  $\delta^{15}\text{N}$  of bone collagen are commonly used for paleodietary studies (see e.g. DeNiro and Epstein 1978, 1981; Schoeninger and DeNiro 1984; DeNiro 1985, 1987; Lidén 1995; Ambrose and Krigbaum 2003; Erikson 2003; Richter and Noe-Nygaard 2003; Noe-Nygaard *et al* 2005; Fischer *et al* submitted for publication-a; Fischer *et al* submitted for publication-b). A measurement of the isotope composition of collagen mainly reflects the protein fraction of the diet (Ambrose and Norr 1993; Schwarcz 2000) and in general the  $\delta^{13}\text{C}$  values are useful for distinguishing between diet protein coming either from terrestrial or from marine resources. Terrestrial diet protein in human bones has  $\delta^{13}\text{C}$  values around -21‰ whereas values ranging between -10‰ to -12‰ are derived from marine protein. The  $\delta^{13}\text{C}$  values between these end values reflect a partial use of both terrestrial and marine resources (Little and Little 1997; Arneborg *et al* 2002). The nitrogen isotope composition of bone collagen depends on the trophic level of the consumer since each level in the food chain is associated with a fractionation of approximately +3‰ (Minagawa and Wada 1984; Bocherens and Drucker 2003). Thus herbivores have significantly lower  $\delta^{15}\text{N}$  values than carnivores. Because the aquatic food chain is longer than the terrestrial, marine mammals have higher  $\delta^{15}\text{N}$  values than terrestrial carnivores (Schoeninger and DeNiro 1984; Schoeninger 1989). It is therefore possible to distinguish aquatic protein diets from terrestrial protein diets (Cook *et al* 2001).

Figure 4-8 illustrates a reproduction of Taubers plot (1981) but presently extended to include both  $\delta^{13}\text{C}$  and  $\delta^{15}\text{N}$  values of humans and dogs exclusively taken from Danish sites. The presented data are mainly from (Fischer *et al* submitted for publication-a) and the majority of the  $\delta^{13}\text{C}$  and  $\delta^{15}\text{N}$  data were obtained by the author (see also the preface section). The  $\delta^{13}\text{C}$  values

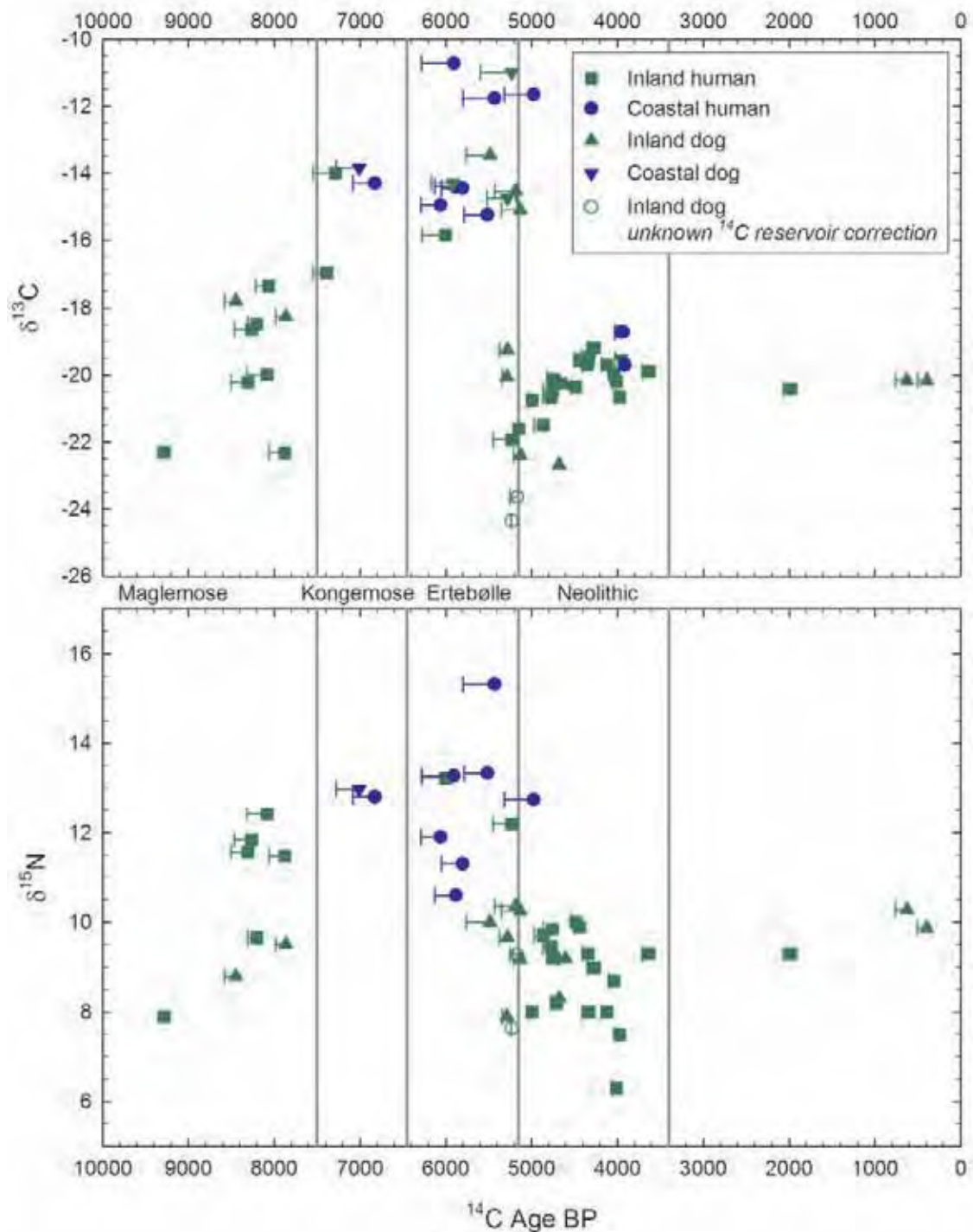


**Figure 4-8. Upper panel:** Shown are the collagen  $\delta^{13}\text{C}$  values of human and dog samples as a function of time in  $^{14}\text{C}$  years. **Lower panel:** Shown are the collagen  $\delta^{15}\text{N}$  values of human and dog sample as a function of time in  $^{14}\text{C}$  years (the cultural periods Maglemose, Kongemose and Ertebølle are all Mesolithic sub-periods).

The samples have been divided into inland and coastal sites as displayed by the green and blue colour code respectively. The  $^{14}\text{C}$  reservoir correction has been calculated by the combined use of  $\delta^{13}\text{C}$  and  $\delta^{15}\text{N}$  values (for details see Fischer *et al.* submitted for publication-a). The magnitude of the  $^{14}\text{C}$  reservoir correction is shown by the bars to the left of the data point. Note the simultaneous drop in both  $\delta^{13}\text{C}$  and  $\delta^{15}\text{N}$  values. This is taken as evidence of transition from a hunter-gather culture and over to the adoption of agriculture. This figure is an illustration taken from Fischer *et al.* (submitted for publication-a) (with supplementary data from Noe-Nygaard 1988; Richards and Koch 2001; Richards *et al.* 2003)

shift from values around -11‰ to values around -20‰ simultaneously, with a shift in  $\delta^{15}\text{N}$  values from about 14‰ to 9‰. The combined  $\delta^{13}\text{C}$  and  $\delta^{15}\text{N}$  values in the late Mesolithic are interpreted as indicating a diet largely derived from marine food resources, whereas the low combined  $\delta^{13}\text{C}$  and  $\delta^{15}\text{N}$  values are seen as indicating a terrestrial diet based mainly on vertebrates. The terrestrial diet could perhaps even be domesticated cattle but red deer and roe deer may also contribute. Thus Figure 4-8 illustrates a major diet transition and is taken as evidence for the introduction of agriculture (Tauber 1981; Noe-Nygaard 1988; Fischer *et al* submitted for publication-a). There is an ongoing discussion on how rapidly this transition actually occurred and to which degree the present data set of humans and dogs can adequately provide evidence for a rapid transition (see e.g. Hedges 2003; Milner *et al* 2003; Rowley-Conwy 2004). Nevertheless, there is no doubt that the transition did occur.

After farming was introduced in the northern parts of Europe another thousand years would pass before agriculture was introduced to the British Isles, Ireland and Southern Scandinavia. In these regions it was introduced more or less simultaneously. This may seem mysterious and the underlying causes are subject to intense discussions. Some claim that the Neolithic was brought about by socioeconomic factors and may have been a result of social dynamics and trade relations (Jensen 2001). **The agricultural products were highly desired in the competition for status** (Jensen 2001) and this acted as a kind of driving force. Others claim that the introduction of agriculture was a result of migration from the south (Skak-Nielsen 2003; Rowley-Conwy 2004; Skak-Nielsen 2004).

However, Bonsall *et al* (2002) **claim that no satisfactory explanation for the adoption of Neolithic farming, nor its simultaneity, exists.** They suggest that this simultaneity cannot be coincidental, but rather must be a response to a climate change favourable to the introduction of agriculture. Similarly, Noe-Nygaard and Hede (2006) **argue that the reclaimed coastal areas, due to a relative sea level change resulting in a regression, provided an ideal biotope for grass and salt marsh vegetation providing open land areas for grazing by domestic cattle.** Furthermore, the Mesolithic to Neolithic transitions occur almost simultaneously with the elm decline, observed as a dramatic decline of elm pollen in numerous North European pollen diagrams around 3900 BC (Rasmussen *et al* 2002; Roberts 2004; Rasmussen 2005). **The decline of the elm tree created openings in the dense forest covering land areas during the Atlantic period, which were useable for domestic cattle and agriculture as well as providing favourable conditions for grass, herbs and bushes to grow** (Rasmussen *et al* 2002; Roberts 2004; Noe-Nygaard and Hede 2006). Some have argued that the elm decline was caused by the invading agriculture, but the decline is most likely to have been caused by the elm disease (Rasmussen *et al* 2002; Roberts 2004; Rasmussen 2005). Hence it seems very likely that Neolithic culture was not only brought about by social and cultural causes but it may also be induced by changes in the natural environments, e.g. through significant climate changes.

#### *An attempt at dating the Mesolithic to Neolithic transition*

Two cultural events are interesting with respect to the adoption of agriculture in Denmark: the initial introduction of agriculture, i.e. the Mesolithic to Neolithic transition and the landnám event. The word landnám means taking inhabited land into possession by the clearing of woodland by burning (Jensen 2001; Roberts 2004). **The major landnám period occurred in Denmark around 3500 BC (Jensen 2001). In Dallund lake (Denmark) the first indications of arable farming occurred around 3460 BC as indicated by cereal grains (Rasmussen 2005). Both events are likely to have been recorded in natural archives such as lake sediments. Especially the landnám event, characterised by its massive slash and burn of forests, is very likely to have resulted in increased amounts of erosional material reaching lake sediments. Similarly, the onset of the Neo-**

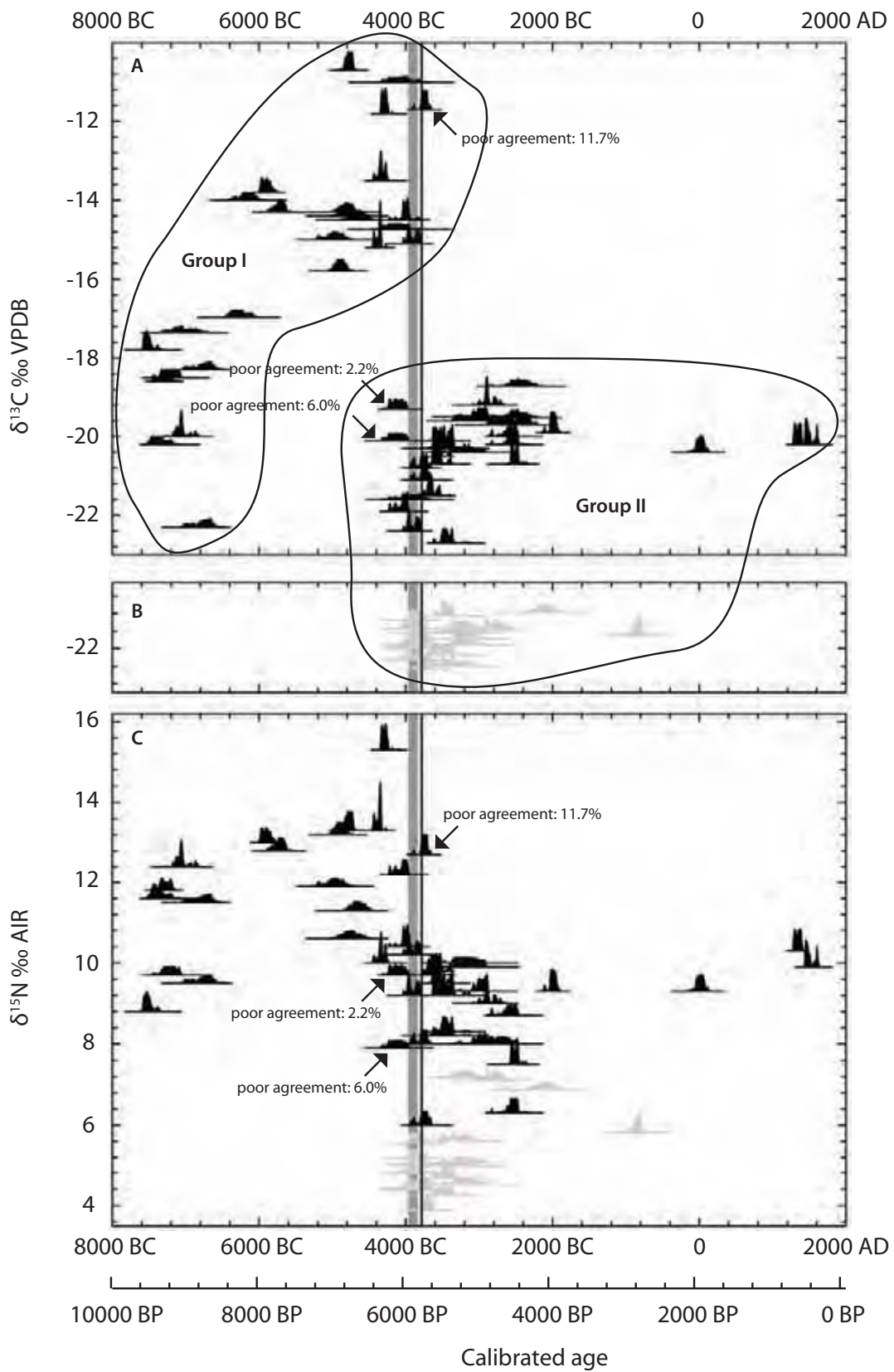


**Figure 4-9.** Shown are the calibrated age distributions of the human and dog samples displayed in Figure 4-8 as a function of their  $\delta^{13}\text{C}$  and  $\delta^{15}\text{N}$  values (panel A & C, Noe-Nygaard 1988; Richards and Kock 2001; Richards et al 2003; Fischer et al submitted for publication-a). In panel B the age distributions as a function of the  $\delta^{13}\text{C}$  values of the domestic cattle presented in Noe-Nygaard *et al* (2005) is presented (*the  $\delta^{15}\text{N}$  values of the domestic cattle is displayed in panel C*).

lithic period is likely to have been recorded but to a much lesser degree than the landnám event. Thus it is a great challenge to differentiate these anthropogenic effects from naturally occurring changes and it would therefore be very beneficial to have a good age control in particular of the Mesolithic to Neolithic transition.

The compelling amount of data (e.g. *Figure 4-8*) that points to a dietary shift as one of the cultural characteristics of the Mesolithic to Neolithic transition may provide a basis for dating the transition. Yet in order to use the presented data set as a basis for dating, two assumptions must be fulfilled: 1) the data must be representative of the transitional period and 2) in order to model the data, a sharp transition must be assumed to constrain the data. The first assumption may be questioned because there seems to be a bias in coastal sites represented in the pre-transition period relative to the post-transition period. Hence it may be argued that the lack of a Neolithic marine diet is simply due to the lack of represented marine sites in the Neolithic period. However, recent studies reveal coastal Neolithic sites with a predominately terrestrial diet (Noe-Nygaard 1988; Richards and Kock 2001; Schulting and Richards 2002a) **thus suggesting a general shift in diet for the Neolithic period.** The latter assumption may also be questioned, as it seems rather unlikely that agriculture was adopted 'overnight'. It seems more likely that the two cultural periods co-existed during a transitional phase, and a more interesting question would then be: how long was this transitional phase? This question is hardly answerable given the presented data (*Figure 4-8 & 4-9*). In addition, Rowley-Conwy (2004) **argues for a very rapid transition (*the substitution phase*)** taking place within a century or two, which lends further support to the model. Despite these difficulties, a tentative time estimate of the Mesolithic to Neolithic transition may be given by grouping the samples with a highly marine diet in one group (*group I; Figure 4-9*) and samples with a high terrestrial diet component in another (*group II; Figure 4-9*). In the group II data (*Figure 4-9*), the domestic cattle samples of Noe-Nygaard *et al* (2005) **are added. The resulting transition date range is then modelled (*OxCal 3.10 (Buck et al 1996; Ramsey 1998; Ramsey 2001)*)** to have occurred between 3950 BC and 3850 BC (*with 95.4% confidence, grey shaded area in Figure 4-9*). Notably, only 3 of the 84 samples used yield poor agreement with the model assumption of a stepwise transition. This, of course, may suggest that a stepwise transition is a poor assumption and that the adoption of the Neolithic culture occurred over a period of time. Furthermore, it must be emphasised that this model strongly depends on the correctness of the reservoir correction of the very marine samples (Fischer *et al* submitted for publication-a), **which may be very uncertain considering the large time-span and site diversity of the samples.**

Yet another way of estimating the age of the Mesolithic to Neolithic transition is by using the <sup>14</sup>C dates of domestic cattle samples (Noe-Nygaard *et al* 2005) **provided that they represent domestication as opposed to wild living**Noe-Nygaard and Hede (2005) **argues, on the basis of the isotope composition of bone remains from domestic cattle and aurochs, that the domestic cattle appeared ready domesticated and that they likely have been feed by grass as also convincingly advocated by Rowley-Conwy (2004). Hence, the first cattle samples may be taken as evidence of the appearance of Neolithic culture.** The age distribution of the earliest domesticated cattle from Noe-Nygaard *et al* (2005) **yields that domesticated cattle appeared in Denmark no later than 3790 BC (*solid black line in Figure 4-9*).** Other reports on the date of early domesticated cattle in Denmark suggest *ca.* 3850 BC (Richards *et al* 2003). Hence, the transition to the Neolithic culture is most likely to have occurred in the range from 3950 BC to 3850 BC and no later than 3790 BC.

### **Aims of this work**

Lake deposits have proven excellent archives for paleoclimate investigations and a high-resolution paleoclimate investigation of the Bliden Lake core B1 will be presented. In particular, the stable isotopes of carbon and nitrogen are used to provide information concerning climate changes. The stable isotopes of organic sulphur material, commonly used in marine environments and to study anthropogenic pollution in lacustrine environments, will be used as a paleoclimate indicator to interpret the lacustrine environments of ancient times. Examples of research using sulphur isotopes as paleoclimate indicators in lacustrine environments are very few. Lakes are highly sensitive to variations in temperature and lakes respond rapidly to both regional and global climate changes. Thus lakes may provide detailed knowledge about climate changes in general. In particular, information on a possible climate change at the onset of the Neolithic is provided. However, the climate of ancient times can only emerge from the analysed lake deposits if the mechanisms and processes resulting in the sedimentation of material are well understood. Therefore, a brief introduction to the carbon, nitrogen and sulphur cycles in lacustrine environments will be presented with the emphasis on stable isotopes. The outcome of the paleoclimate investigation will be used to identify possible climate changes during the Mesolithic to Neolithic transition and, if possible, to detect the marginal effects Littorina transgression on inland lakes as well as arriving at a climate interpretation in general. Furthermore, a chronology of the Bliden Lake record is essential for a comparison with climate events found elsewhere. Since simultaneous events occurring at different locations on Earth most likely have a common cause, the identification of these events is of the utmost importance. For this purpose, chronology is an essential parameter for correlating different climate archives. Thus, in order to make an adequate climate investigation a depth to age model has to be made.



# 5

---

## **Interpreting lacustrine environments**

## Introduction

This chapter is an introduction to limnological chemistry and the carbon, nitrogen and sulphur cycles in lakes. Knowledge of both the chemistry and the flow of particulate and dissolved organic and inorganic species is essential to the interpretation of the analysed geochemical parameters and therefore to the attainment of climate information from lacustrine lakes in general, and from the Bliden Lake core in particular. Lakes respond quickly to natural and anthropogenic environmental changes and are therefore great archives of past environmental changes (see e.g. Wolfe *et al* 1999; Hammarlund *et al* 2005; McFadden *et al* 2005; Rasmussen and Anderson 2005; Rasmussen and Bradshaw 2005; Seppä *et al* 2005; Talbot *et al* 2006). However, the sediments reflect the materials, which have survived possible post-depositional alterations and may therefore reveal limited information only. Stable isotopes are very useful tools in obtaining climate information and identifying the sources of organic material. Therefore, a detailed description of the behaviour of the stable isotopes of carbon, nitrogen and sulphur is provided. For comprehensive text books on limnology, lake ecology and stable isotopes in lake environments the reader is referred to Reading (1996), Last and Smol (2001), Cohen (2003) and O'Sullivan and Reynolds (2004).

## Freshwater lakes

Lakes are found in a variety of geological settings, such as volcano crater lakes, rift zones (e.g. lake Baikal, Asia) or glacially shaped lakes formed by retreating ice sheets (see e.g. Reading 1996; Cohen 2003; O'Sullivan and Reynolds 2004). Hence, they are not easily classifiable, but may generally be distinguished by their nutrition contents and vertical mixing regimes. Oligotrophic lakes are normally forest lakes or found in sandy and nutritionally poor environments, whereas eutrophic lakes are most common in moraine landscapes with highly nutritional soils that deliver nitrates and phosphates. This distinction is also reflected in the pH values of lakes, so that lakes with a pH value higher than 7 are eutrophic whereas lakes with pH values lower than 7 are oligotrophic (Abrahamsen 1994).

The physical and chemical dynamics of lakes are mainly determined by evaporation, by the difference in the inflow to outflow ratio and by differences in water densities, which are functions of temperature. The greatest source of heat is solar irradiance and loss of heat is the result

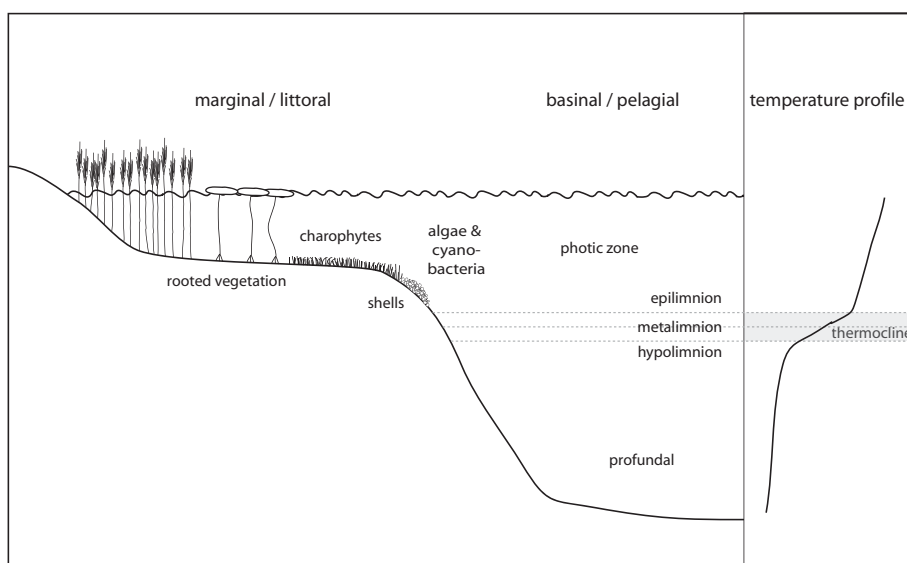


Figure 5-1. Lake zones, terminology and definitions of the lake environment (Modified after (Platt and Wright 1991)).

of thermal radiation from the lake surface. The water column temperature profile is created in response to the penetration of solar radiation which decays exponentially with depth and is a function of water transparency (Cohen 2003). The solar heating of surface water may prevent turbulent vertical mixing of the water column due to the density differences, which results in stratification of the lake. In thermally stratified lakes an upper warm layer, the epilimnion, overlays a cooler and denser layer, the hypolimnion. The mixing zone is termed the metalimnion and the zone where temperature decreases most rapidly with depth is defined as the thermocline (see Figure 5-1, Talbot and Allen 1996; Cohen 2003).

Lake waters tend to be stratified either seasonally (*dimictic*) or permanently (*meromictic*). Stratification inhibits mixing of gases, solutes and nutrients across the thermocline resulting in chemical stratification, which may impact the geochemical and fossil archives of the sediment (Cohen 2003). The presence or absence and duration of stratification are recorded in the sediments because vertical remixing redistributes oxygen to the hypolimnion and thus provides conditions for benthic organisms, which in turn can bioturbate sediments (Cohen 2003). The epilimnion is normally well supplied with oxygen and nutrients. Hence, most of the autochthonous primary production takes place here. On the contrary, the hypolimnion can become completely stagnant and depleted in oxygen and nutrients, thus limiting benthic life and thereby resulting in good preservation of epilimnion organic material (Einsele 2000). Optimal preservation of sedimentary organic material is essential to paleoclimate investigations. However, in temperate regions a permanent anoxic hypolimnion cannot be developed. During the summer, warm surface water will overlay cooler and dense benthic waters leading to stratification. In the winter, surface water will cool and become dense leading to mixing between epilimnion and hypolimnion water masses. In spring, surface water heats and vertical mixing occurs again, since water has the highest density around 4°C (Talbot and Allen 1996; Einsele 2000; Cohen 2003). Hence, most temperate lakes are dimictic.

Lacustrine organic matter originates from a complex mixture of lipids, carbohydrates, proteins and other organic compounds produced by organisms that have lived in or around the lake. Thus, lake organic matter is either allochthonously or autochthonously derived, where allochthonous matter originates outside the lake basin in the catchments area and the atmosphere. Allochthonous matter consists mostly of organic and inorganic nutrients and enters the lake in dissolved, colloidal or suspended form, either in stream water or by groundwater. To a lesser extent, allochthonous matter may also be of biogenic origin, such as particulate fragments of leaves, seeds, twigs, fruits and pollen dissolved in streams or precipitated directly on the surface of the lake (O'Sullivan 2004). In contrast, autochthonous matter originates solely from the lake itself and consists of plants and algae together with chemical, precipitated and biologically derived  $\text{CaCO}_3$  (O'Sullivan 2004).

Lakes can be divided into regions that are penetrated by sufficient light for photosynthesis to occur (*the photic zone, see Figure 5-1*) (Cohen 2003). The benthic environment that exists within the photic zone is named the littoral zone. The distribution of aquatic macrophytes is essentially littoral, whereas the profundal zone is typically outside the range in which rooted photoautotrophs are able to function (Pokorný and Kvet 2004). At intermediate depth, where photosynthesis occurs exclusively by benthic algae and cyanobacteria, is denoted the sub-littoral zone. Hence the littoral zone is restricted to the region where large submerged plants are

**Figure 5-2.** A schematic layout of the flow of inorganic and organic species and their interactions. The interactions of the carbon, nitrogen and sulphur cycles with organic matter produced in the lake ultimately define the isotope composition of sedimentary organic matter. The fractionation factor  $\epsilon$  between selected species is given (*see chapter 1 for a definition of  $\epsilon$* ) together with the likely isotope composition range. This figure is compiled from the following references (Jørgensen 1983; Krumbein and Swart 1983; Stoddard 1994; Urban 1994; Meyers and Teranes 2001; Talbot 2001).

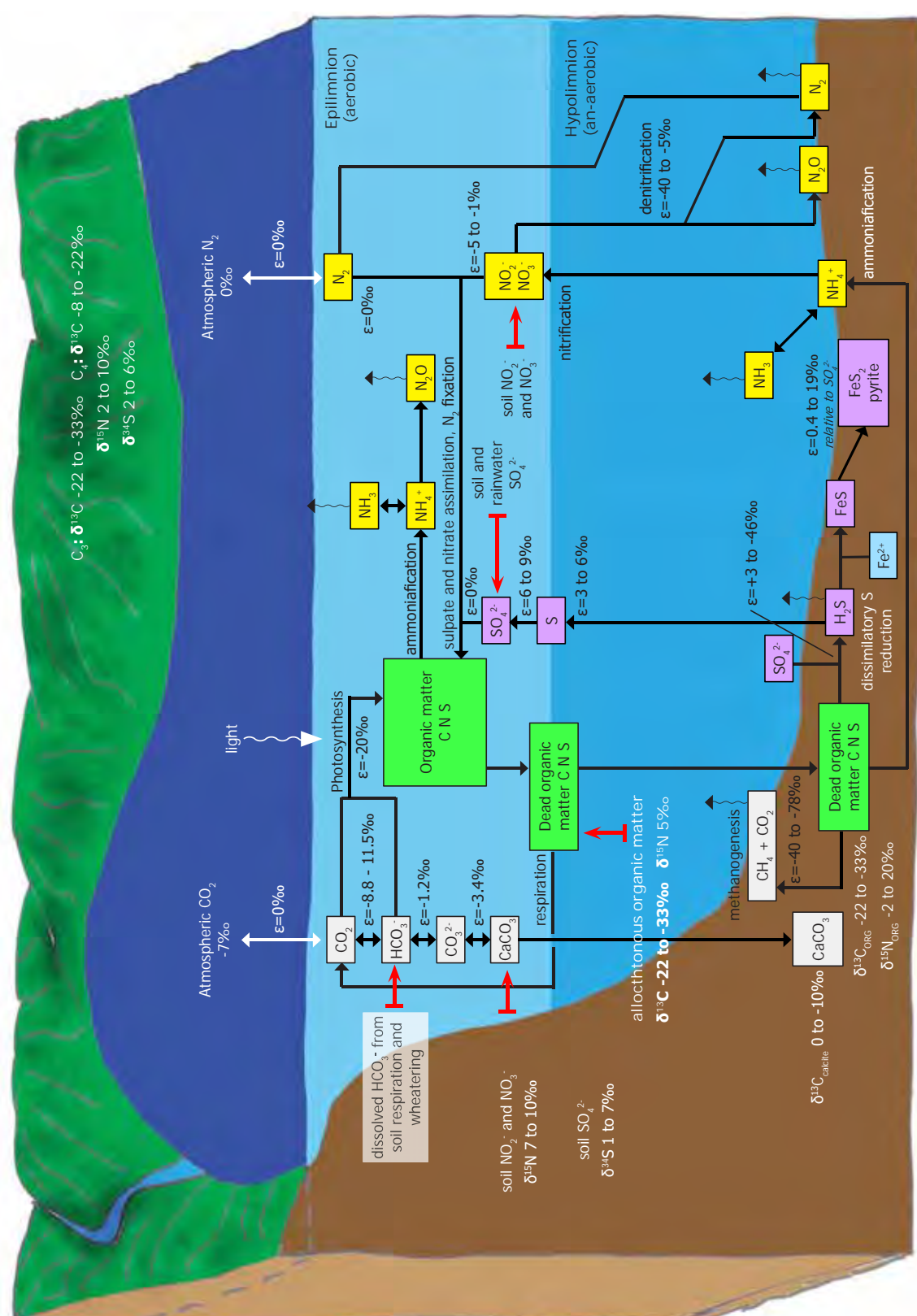


Figure 5-2

found (Figure 5-1, Cohen 2003). Shells and molluscs commonly accumulate after death in the shell accumulation zone at 5 to 10 metres depth, whereas their fragments originate from lower waters where they are destroyed by wave activity (Figure 5-1, Berg 1950).

Most temperate lakes are hydrological open systems, with sufficient inflow and outflow from rivers or groundwater leading to a more or less stable depositional system (Einsele 2000). In contrast, hydrological closed lakes are lakes with no in- or out-flow. The hydrological equilibrium in such lakes is a balance between inflow and evaporation. For hydrological open lakes, the water level is in general a balance between inflow and outflow, either river or groundwater, and evaporation. The water level may fluctuate with the relative sea level as this may influence the groundwater level. The average water residence time of a lake is a complex function of morphology, evaporation, wind fetch, and the inflow to outflow ratio. The mean water residence time of a lake controls the concentrations and accumulative capacity of all substances entering the lake (Einsele 2000). Thus the mean water residence time may have a pronounced effect on the organic productivity of the lake.

### **Lacustrine organic matter**

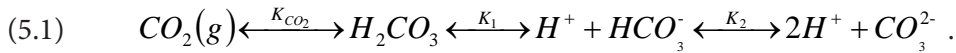
In freshwater lakes most deposits consist of detritus, defined as either particulate or dissolved dead organic material, where far the largest part is of autochthonous origin and a much lesser part of allochthonous origin. The primary decomposers of detritus are saprobe microorganisms like mushrooms and bacteria (Abrahamsen 1994). Organic matter can be differentiated into two distinctive groups, namely vascular plants containing large proportions of fibrous tissues (*grass, shrubs and trees on land and macrophytes*) and non-vascular plants with little or no carbon-rich cellulose or lignin (*phytoplankton*) (Meyers and Teranes 2001). In general, organic matter derived from these two groups retains its source distinctions (Meyers and Lallier-Vergés 1999), and the total organic carbon (TOC) content together with total organic nitrogen (TON) content is an integrate measure of allochthonous and autochthonous origin. Thus, the TOC content reflects the primary bio-production and its degradation together with allochthonously derived organic material (Meyers and Teranes 2001; Routh *et al* 2004). The allochthonous organic matter may enter the lake either as dissolved organic matter or as particulate organic matter. The largest carbon reservoir in lakes consists of dissolved organic matter, whereas in the sediments the dominant source is the particulate organic fraction (Dean 1999). In most lakes, the flux of allochthonous organic matter is much less than the flux of autochthonous particulate organic matter into the sediment (Cohen 2003). However, several factors affect the proportions of allochthonous particulate and organic matter that ends up in the sediment. In shallow lakes the proportion of allochthonous particulate organic matter may be high in contrast to very deep lakes, where it may vanish due to dissolution in the epilimnion (Cohen 2003). In general the TON values correlate with the TOC values, whereas the ratio of TOC to TON (*C/N ratio*) may fluctuate significantly.

### **The lacustrine carbon cycle**

The global carbon cycle is extensively studied due to its importance to life (Krumbein and Swart 1983; Schlesinger 1997; Coddéris 2001). Living organisms metabolise carbon into their body tissue from a variety of carbon reservoirs. In the terrestrial biosphere, carbon is incorporated from carbon dioxide into plant tissue via photosynthesis and then transferred to higher trophic animals. Whereas terrestrial plants utilise gaseous  $\text{CO}_2(\text{g})$  directly from the atmosphere, aquatic plants utilise carbon either as dissolved  $\text{CO}_2(\text{aq})$  or as bicarbonate ( $\text{HCO}_3^-$ ). The bicarbonate ion is formed by dissolution of atmospheric  $\text{CO}_2$  and from carbon dioxide evolving from

various processes such as respiration and the decomposition of dead organic matter from various sources. A schematic overview of the lacustrine carbon cycle is shown in Figure 5-2.

The relative concentration of dissolved  $\text{CO}_2$  and bicarbonate is determined by the chemical equilibrium reaction (Clark and Fritz 1997)



Where  $K_{\text{CO}_2}$ ,  $K_1$  and  $K_2$  are the chemical equilibrium constants (see Table 5.1). The relative concentrations of  $\text{CO}_2$ ,  $\text{HCO}_3^-$  and  $\text{CO}_3^{2-}$  are a function of the pH values and are shown in Figure 5-3. The sum of these concentrations is denoted dissolved inorganic carbon (DIC). In temperate lakes, pH values normally range from 6 to 9 and are buffered by the bicarbonate system (Talbot and Allen 1996; Einsele 2000). At this pH range the dissolved  $\text{CO}_2(aq)$  is a minor constituent (less than 50%) relative to  $\text{HCO}_3^-$  (see Figure 5-3). Hence, the availability of dissolved  $\text{CO}_2$  for

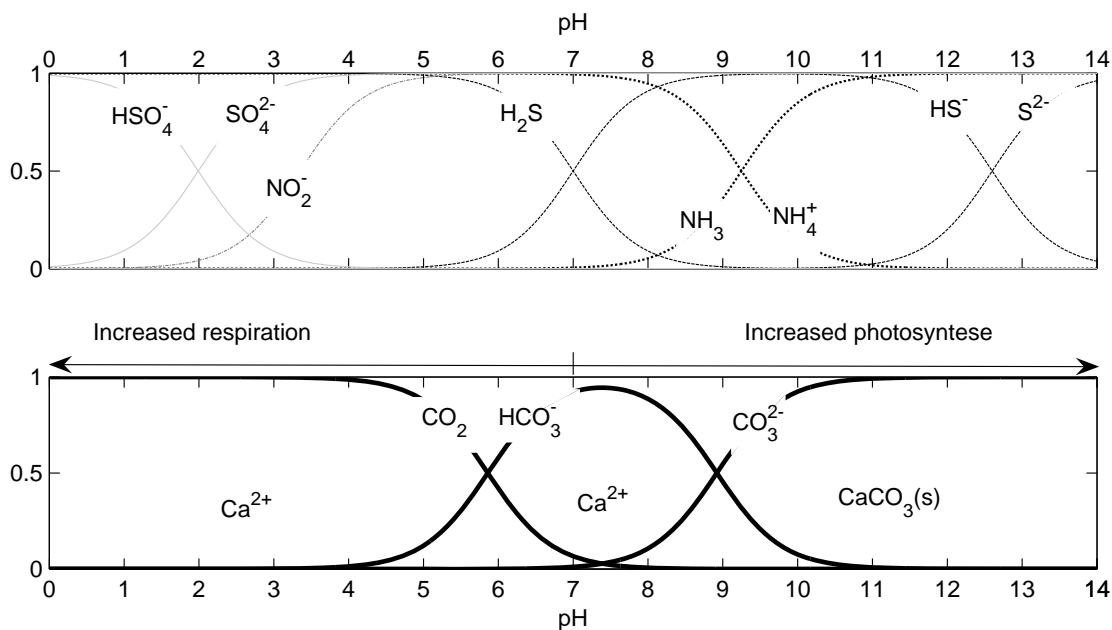


**Figure 5-3. Upper panel:** Bjerrum diagrams for the dissolved  $\text{H}_2\text{SO}_4$ ,  $\text{HNO}_2$ ,  $\text{H}_2\text{S}$  and  $\text{NH}_3$ . **Lower panel:** Shown are the relative concentrations of the carbonate equilibrium system as a function of pH. Lakes commonly have pH values around 8; at this pH value the concentration of  $\text{CO}_2$  is low. Therefore many aquatic plant are specialised in using  $\text{HCO}_3^-$  as their primarily carbon source for photosynthesis. As the lake's primary production increases the  $\text{CO}_2$  concentration is lowered and the pH is increasing. The decomposition of dead organic matter releases  $\text{CO}_2$  and hence decreases the pH value. The used  $\text{pK}_s$  values are given in Table 5.1.

**Table 5.1. Chemical Equilibrium Constants**

Equilibrium system	$\text{pK}_s$ values (25°C)	Reference
$\text{H}_2\text{CO}_3 \leftrightarrow \text{HCO}_3^- + \text{H}^+ \leftrightarrow \text{CO}_3^{2-} + 2\text{H}^+$ (5.1)	$\text{pK}_{\text{CO}_2} = -1.47$ , $\text{pK}_1 = -6.35$ , $\text{pK}_2 = -10.33$	Clark and Fritz (1997)
$\text{CaCO}_3 \leftrightarrow \text{Ca}^{2+} + \text{CO}_3^{2-}$ (5.3)	$\text{pK}_{\text{CaCO}_3} = 8.48$	Clark and Fritz (1997)
$\text{HNO}_2 \leftrightarrow \text{NO}_2^- + \text{H}^+$	$\text{pK}_1 = 3.35$	Andersen et al (1995)
$\text{NH}_3 + \text{H}^+ \leftrightarrow \text{NH}_4^+$	$\text{pK}_1 = 9.75$	Andersen et al (1995)
$\text{H}_2\text{S} \leftrightarrow \text{HS}^- \leftrightarrow \text{S}^{2-}$ (5.7)	$\text{pK}_1 = 6.96$ , $\text{pK}_2 = 12.90$	Andersen et al (1995)
$\text{H}_2\text{SO}_4 \leftrightarrow \text{HSO}_4^- + \text{H}^+ \leftrightarrow \text{SO}_4^{2-} + 2\text{H}^+$	$\text{pK}_1 = -3.0$ , $\text{pK}_2 = 1.99$	Andersen et al (1995)

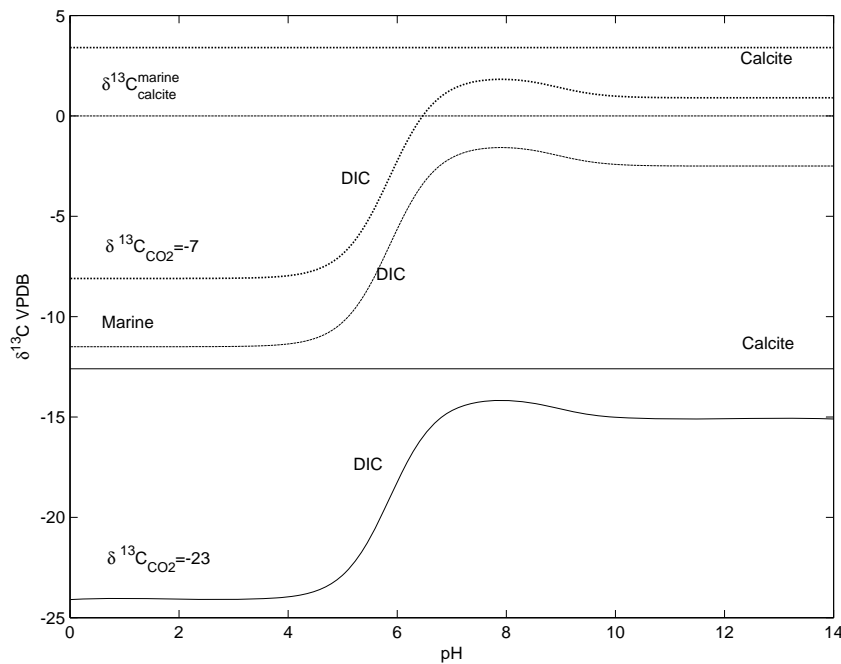
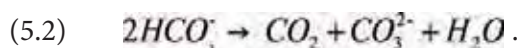


**Figure 5-4.** The DIC  $\delta^{13}\text{C}$  isotope values in equilibrium with marine calcite (0‰), atmospheric  $\text{CO}_2$  (-7‰) or soil  $\text{CO}_2$  (-23‰) is shown. The DIC is defined as the sum of concentrations of  $\text{CO}_2$ ,  $\text{HCO}_3^-$  and  $\text{CO}_3^{2-}$  (see Figure 5-3). The  $\delta^{13}\text{C}$  value is calculated by using the enrichment factors given in Figure 5-2. The DIC isotope composition is not only a function of pH but also strongly mirrors the isotope composition of its origin. Modified after Clark and Fritz (1997).

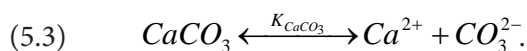
photosynthetic uptake is limited in comparison with the terrestrial biosphere. High primary productivity further diminishes  $\text{CO}_2$  availability and thus enhances plant or algal utilisation of  $\text{HCO}_3^-$  by photosynthesis (Meyers and Lallier-Vergés 1999).

Most algae and many plants contain the *anhydrase* enzyme which allows them to derive  $\text{CO}_2$  from dissolved  $\text{HCO}_3^-$  (Smith and Walker 1980; Thompson and Ferris 1990; Laws *et al* 1995). Two examples are the Chara (*charaphytes*) green algae and Phacotus green algae, in which extracellular anhydrase catalyse the transformation of  $\text{HCO}_3^-$  to  $\text{CO}_2$  and  $\text{OH}^-$  (Figure 5-3) by the following reaction (Abrahamsen 1994)



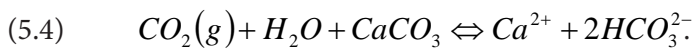
The liberated  $\text{CO}_2$  is then consumed by photosynthesis which in turn displaces the chemical equilibrium (eq. (5.1)) due to the increased concentration of the carbonate ion. Hence high concentrations of  $\text{CO}_3^{2-}$  may locally lead to higher alkalinity. By this pathway, local pH values can reach values as high as 11 near plants (Abrahamsen 1994).

The solubility of  $\text{CaCO}_3$  is a function of the carbonate concentration (Clark and Fritz 1997) and is written as



Hence the increased carbonate ion concentration that follows from high primary productivity by utilisation of  $\text{HCO}_3^-$  promotes  $\text{CaCO}_3$  precipitation on surface waters and macrophytes (Pokorný and Kvet 2004), i.e. the so-called biogenically induced  $\text{CaCO}_3$ . Lake waters are often supersaturated with  $\text{CaCO}_3$  and massive precipitation may not occur until a triggering mechanism develops and phytoplankton blooms may provide nucleating surfaces (Dean 2002; Cohen

2003). Biogenically induced calcium carbonate can sometimes be observed as a small thin calcareous surface layer on plants and stones during spring and summer. However, in very productive lakes the dissolved  $\text{HCO}_3^-$  is readily consumed and  $\text{HCO}_3^-$  may then be released by dissolution of  $\text{CaCO}_3$  together with  $\text{OH}^-$ . As a result, limewater is formed ( $\text{Ca}(\text{OH})_2$ ) (Abrahamsen 1994). Likewise, increasing primary productivity may not simply result in increased  $\text{CaCO}_3$  precipitation because increased organic productivity also results in increased decomposition and respiration producing  $\text{CO}_2$  (Dean 1999; Cohen 2003). In turn  $\text{CO}_2$  dissolves the precipitated  $\text{CaCO}_3$ . Thus, lakes with high decomposition rates release  $\text{CO}_2$  (*respired  $\text{CO}_2$* ), displacing pH towards lower values enhancing calcium carbonate dissolution according to the equilibrium reaction (Clark and Fritz 1997)



This equilibrium reaction is the connecting pathway between organic and inorganic components of carbonate isotopes. The calcium ion mainly stems from weathering.

The bulk calcium carbonate (*measured as weight percentage*) originates both from allochthonous and autochthonous sources. The bulk  $\text{CaCO}_3$  content is divided into different fractions: the allogenic fraction, the authigenic fraction and the endogenic fraction. The allogenic fraction consists of  $\text{CaCO}_3$  originating from out-washed calcium carbonate from the surrounding tills in the catchments area or from the dissolution of  $\text{CaCO}_3$  by respired soil carbon dioxide and transported to the lake by water inflow (Dean 1981; Ito 2001; O'Sullivan 2004). The authigenic and endogenic fractions are both produced autochthonously. The endogenic fraction is produced in the sediment (O'Sullivan 2004), whereas the authigenic  $\text{CaCO}_3$  fraction is produced by chemical precipitation and flocculation within the water column. Most authigenic matter enters the lake in solution via stream or groundwater and is thus ultimately allochthonous in origin. The authigenic fraction may also be biogenically derived (O'Sullivan 2004) either as shells and molluscs or induced by photosynthetic activity. The authigenic fraction is typically formed in thermodynamic equilibrium with lake water in the epilimnion, due to photosynthetic uptake of dissolved  $\text{CO}_2$  or due to evaporation of water and evasion of  $\text{CO}_2$  (Dean 1981). Variations in  $\text{CaCO}_3$  content can be a result of variable production of  $\text{CaCO}_3$ , variable dilution of  $\text{CaCO}_3$  by other components and variable dissolution of  $\text{CaCO}_3$  or of a combination of these factors (Dean 2002).

### Organic carbon isotopes ( $\delta^{13}\text{C}_{\text{ORG}}$ )

The isotopes of carbon are crucial in assessing organic matter sources, for the reconstruction of past productivity rates, and for identifying changes in the availability of nutrients in the surface waters (Dean 1999; Schwab and Dean 2002; Filippi and Talbot 2005; Hammarlund *et al* 2005; Jessen *et al* 2005; Talbot *et al* 2006).

Phytoplankton ( $C_3$  algae) produces organic matter 20‰ lighter than the carbon ratio of its DIC source, being either  $\text{CO}_2$  or  $\text{HCO}_3^-$  (see Figure 5-2, Craig 1954; Pardue 1976; Wong 1978; O'Leary 1988; Lamb *et al* 2006). The production of algal organic matter thus removes  $^{12}\text{C}$  from surface waters. This in turn enriches the surface aquifer in  $^{13}\text{C}$ , thus leading to high DIC carbon isotope values. A continued photosynthetic uptake from a progressively heavy isotope DIC pool then subsequently leads to isotopic heavy organic material. Thus increased autochthonous organic production can be observed as increased  $\delta^{13}\text{C}_{\text{ORG}}$  values and often in concord with increased  $\delta^{13}\text{C}_{\text{carb}}$  values (Wolfe *et al* 1999; Muzuka *et al* 2004; Talbot *et al* 2006). The  $\delta^{13}\text{C}_{\text{carb}}$  values traces the isotope composition of the DIC according to equation (5.1) and (5.3). This effect can be further intensified when the concentration of  $\text{CO}_2$  becomes low and utilisation of dissolved

$\text{HCO}_3^-$  becomes important. Dissolved  $\text{HCO}_3^-$  (1‰) is isotopically heavier than dissolved  $\text{CO}_2$  (-7‰) and photosynthetic utilisation of  $\text{HCO}_3^-$  may yield very elevated  $\delta^{13}\text{C}_{\text{ORG}}$  values. However, intensified use of  $\text{HCO}_3^-$  as the primary carbon source can also be initiated by changes towards higher pH, i.e. increased alkalinity (Routh *et al* 2004). Decreasing productivity of organic material yields decreasing DIC isotopic composition values as less  $^{12}\text{C}$  is removed by photosynthetic uptake. As the DIC isotope values become lighter the  $\delta^{13}\text{C}_{\text{ORG}}$  values also becomes lighter. Increased or decreased productivity therefore yields a respective increase or decrease in  $\delta^{13}\text{C}_{\text{ORG}}$  of organic matter. However, this is only the case for situations with a steady DIC supply with constant carbon isotope composition. Delivery of isotopically depleted soil DIC with  $\delta^{13}\text{C}_{\text{CO}_2}$  values around -12‰ by inflowing water can, on the other hand, lower the  $\delta^{13}\text{C}_{\text{ORG}}$  values of lacustrine organic matter significantly (see Figure 5-4, Meyers and Teranes 2001; Routh *et al* 2004). When the concentrations of nutrients are limited to the autochthonous organic production, then the  $\delta^{13}\text{C}_{\text{ORG}}$  values will mirror changes of the isotopic composition of the inflowing DIC. Furthermore, changes in pH, temperature, nutrient limitations and growth rate will also affect the  $\delta^{13}\text{C}_{\text{ORG}}$  of phytoplankton (Meyers *et al.* 2001). Note that because little or no fractionation occurs when atmospheric  $\text{CO}_2$  is dissolved in water, the terrestrial vascular and lacustrine non-vascular  $\text{C}_3$  plants are isotopically indistinguishable when using atmospheric  $\text{CO}_2$  as their primary carbon source (Meyers *et al.* 2001).

Increased autochthonous productivity is linked to an increased supply of nutrients. A wet climate will increase the amount of allochthonous nutrients provided by the lake surroundings, whereas a dry climate will decrease the supply of allochthonously derived nutrients. An increased supply of nutrients can also be caused by vertical mixing of the water column supplying the epilimnion with decomposed material from the hypolimnion as well as supplying the otherwise anoxic hypolimnion with oxygen increasing the decomposition rate of organic material. Vertical mixing is related to temperature and can be caused by shifts from climate conditions favouring a permanently stratified lake to a temperate climate allowing for annual vertical mixing. Hence, vertical mixing may occur when going from a warmer to a colder climate. Vertical mixing can also be caused by decreasing water levels, which lowers the thermocline. This may be caused by a shift from a wetter to a drier climate.

The equilibrium isotope fractionations are temperature dependent. Hence the isotope fractionations between the different inorganic carbon species shown in Figure 5-4 are only valid for 25°C; at other temperatures the fractionations will be slightly different. For example, the  $\delta^{13}\text{C}$  value of  $\text{CO}_2$  in equilibrium with  $\text{HCO}_3^-$  has a  $\delta^{13}\text{C}$  of -9.2‰ at 0°C and is increased to -6.8‰ at 30°C. The solubility of  $\text{CO}_2$  is also temperature dependent. The solubility increases with decreasing temperatures resulting in decreased fractionation with increasing temperature (Håkansson 1985). Combining both of these temperature dependent effects results in increasing  $\delta^{13}\text{C}_{\text{ORG}}$  values with increasing temperature and *vice versa* (Håkansson 1985). Furthermore, fractionation during photosynthesis varies as a function of  $\text{CO}_2(\text{aq})$  concentrations and phytoplankton growth rate, with larger fractionation at high  $\text{CO}_2(\text{aq})$  concentrations (Laws *et al* 1995; Meyers 1997).

The decomposition of organic material in the sediments can also be accompanied by the process of methanogenesis, where organic material is decomposed to  $\text{CO}_2$  and  $\text{CH}_4$ . Methanogenesis is mediated by anaerobe bacteria and it is associated with large fractionations. Methane produced by methanogenesis has  $\delta^{13}\text{C}$  values ranging between -50 to -65‰. Thus, the remaining organic material in the sediment is enriched during this process and the possible oxidation of the  $^{12}\text{C}$  depleted  $\text{CH}_4$  may yield strongly depleted isotope values of newly produced organic matter (Schlesinger 1997).

### The lacustrine nitrogen cycle

Ammonium ( $NH_4^+$ ), nitrate ( $NO_3^-$ ) and nitrite ( $NO_2^-$ ) are important components of the dissolved inorganic nitrogen (DIN) pool, as they represent the principal nutrient sources of nitrogen available for primary production (see Figure 5-2). The relative DIN concentration as a function of pH is shown in Figure 5-3.

Ammonia and nitrate assimilation are the two principal processes by which nitrogen is obtained during primary production. Nitrite provides an additional but subsidiary dissolved nitrogen source. The dissolution of atmospheric  $N_2$  gas makes dissolved  $N_2(aq)$  available for nitrogen fixation plants and may well represent the largest aquatic nitrogen reservoir. The process of nitrogen fixation is metabolically expensive, due to the large amount of energy required to break the triple bonds in the  $N_2$  molecule, and is therefore confined to specialised bacteria like diazotrophs, blue-green algae and cyanobacteria (Talbot 2001; Padisák 2004). However, nitrogen fixing cyanobacteria may be dominant in eutrophicated systems (Geel *et al*) due to the competitive advantage of nitrogen fixing where dissolved inorganic nitrogen is in short supply.

Recycling of organically bound nitrogen occurs by the process of ammonification, where organic nitrogen is bacterially reduced to  $NH_3$  or  $NH_4^+$  and requires anoxic conditions. Ammonia may be re-oxidised to nitrate or nitrite by aerobic bacteria (*nitrification*) (Talbot 2001). The reverse process of denitrification of  $NO_3^-$  to  $N_2O$  and  $N_2$  is catalysed by anoxic or dysoxic bacteria and usually takes place within the sediment and this process is thus limited by diffusive supply of nitrate (Stoddard 1994; Talbot 2001). Denitrification can be of major importance to the nitrogen cycle of a lake, and may result in significant losses of nitrogen. Globally, denitrification and return of  $N_2$  must be the main process responsible for maintaining a balanced nitrogen cycle. Loss of nitrogen can also occur through ammonia volatilisation (Talbot 2001). This process is strongly pH dependent. As revealed by Figure 5-3, a sharp rise in ammonia content is found at a pH value of 8.5. Therefore alkaline lakes may experience significant losses of nitrogen in the form of ammonia.

### Nitrogen isotopes ( $\delta^{15}N_{ORG}$ )

Nitrogen isotopes are useful for identifying changes in the past availability of nitrogen to the aquatic primary producers and organic productivity (Meyers and Teranes 2001; Talbot 2001; Watanabe *et al* 2004; McFadden *et al* 2005). The biochemical processes involved in transforming dissolved ammonium, nitrate and nitrite into organic matter involves discrimination against the heavy nitrogen isotope  $^{15}N$  (see Figure 5-2). The fractionation during nitrogen assimilation by phytoplankton can be as large as -4‰ to -5‰ if nitrogen is in excess (O'Reilly *et al* 2002). One exception to this scheme is nitrogen fixation by cyanobacteria, which involves little or no fractionation, thus leading to  $\delta^{15}N$  values around -1 to 1‰. Atmospheric  $N_2$  is the most common nitrogen source for terrestrial plants. In contrast, for lacustrine environments the most common nitrogen source used by algae is dissolved  $NO_3^-$  supplied to the lake from the surrounding areas. The  $\delta^{15}N$  value of  $NO_3^-$  is typically heavier than the isotopic composition of atmospheric nitrogen  $N_2$ . Atmospheric nitrogen has  $\delta^{15}N$  values around 0‰, whereas the expected  $\delta^{15}N$  values of nitrate range from 7‰ to 10‰ (Meyers and Lallier-Vergés 1999). This difference is preserved in plankton with  $\delta^{15}N$  values around 8‰ and terrestrial  $C_3$  plants with  $\delta^{15}N$  values of approximately 1‰ (Meyers and Lallier-Vergés 1999).

In a limited nitrogen system, continued preferential uptake of light nitrogen of organic matter progressively enriches the remaining DIN pool with  $^{15}N$ . Thus, algal utilisation of the DIN pool increases the  $\delta^{15}N_{DIN}$  values of nitrate and the drawdown of the DIN reservoir results in higher  $\delta^{15}N$  values in algal organic matter (Routh *et al* 2004). As nitrate is removed from surface waters by organic material, its  $\delta^{15}N_{DIN}$  value increases and creates a corresponding increase in

the  $\delta^{15}\text{N}_{\text{ORG}}$  value of organic matter produced from the remaining supply (Meyers and Teranes 2001). Hence increased organic productivity leads to increasing  $\delta^{15}\text{N}_{\text{ORG}}$  values and *vice versa*. Increased organic productivity is linked to an increased supply of nutrients, and thus most likely in wetter climates, whereas decreased productivity most likely is linked to drier climates. However, as phosphorus commonly limits primary productions in lakes, a depleted concentration of phosphorus will result in low organic productivity. Consequently, as the only minor amounts of the available nitrogen is consumed by organic production the isotope composition of the DIN reservoir remains at constant values, i.e.  $\delta^{15}\text{N}$  of organic algae matter will reflect unchanging  $\delta^{15}\text{N}$  values in this case (Meyers and Teranes 2001).

The process of denitrification in anoxic basins will considerably enrich residual nitrogen in  $^{15}\text{N}$  and thus also cause an increase in  $\delta^{15}\text{N}_{\text{ORG}}$  values. Abundant increases in nitrogen fixing cyanobacteria would decrease the  $\delta^{15}\text{N}_{\text{ORG}}$  values of organic matter (Meyers and Teranes 2001), whereas addition of heterotrophic organic matter will increase the  $\delta^{15}\text{N}_{\text{ORG}}$  values of organic matter, as  $\delta^{15}\text{N}$  increases 3-4‰ per trophic level (Minagawa and Wada 1984; Meyers and Teranes 2001; O'Reilly *et al* 2002).

### The lacustrine sulphur cycle

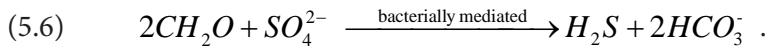
Like carbon and nitrogen, the sulphur cycle is affected by both organic and inorganic chemical reactions. Sulphur is found naturally in a variety of oxidation states (*from -2 to +6*). Thus the sulphur cycle is very complex and driven by many oxidation and reduction reactions. Sulphur is essential to life, especially as building blocks in the formation of proteins.

The supply of sulphur to freshwater lakes is mainly atmospheric  $\text{SO}_4^{2-}$  dissolved in rain droplets and gaseous  $\text{SO}_2$ , together with allochthonous terrestrial dissolved  $\text{SO}_4^{2-}$  and organically bound sulphur. In temperate regions, the export of terrestrially derived sulphur is in balance with atmospheric inputs, such that lake  $\text{SO}_4^{2-}$  concentrations are directly related to the rate of atmospheric deposition (Howarth *et al* 1992). In the water column, the plant uptake of  $\text{SO}_4^{2-}$  is followed by assimilatory reduction into the amino acids cysteine, methionine and cystine, the main constituents of protein (Losher 1989; Howarth *et al* 1992; Schlesinger 1997). The assimilated sulphate is reduced to sulphide for incorporation into the organic sulphur compounds within the cells (Canfield 2001). The various organically bound sulphur compounds may be recycled within the water column or accumulate in the sediments. In common lacustrine environments, sulphur does not restrict organic productivity (Urban 1994) and sulphur concentrations are therefore not greatly affected by organic productivity. Hence, in the absence of changes in the major nutrient supply such as phosphorus and nitrogen, alterations in  $\text{SO}_4^{2-}$  concentrations are not likely to lead to fluctuations in algal sulphur biota or sedimentation, because the nutrient requirement for sulphur is unaltered.

Sulphur compounds reaching lacustrine sediments are dissolved  $\text{SO}_4^{2-}$  and organic bound sulphur (Losher 1989). In aerobic sediments the organically bound sulphur is readily reduced to sulphur, which is then re-oxidised and thereby released back into the water column. However, a high supply rate of organic matter will rapidly cause anaerobic conditions to develop. In anaerobic sediments the dissolved  $\text{SO}_4^{2-}$  and the organically bound sulphur compounds are dissimilatorily reduced to  $\text{H}_2\text{S}$  (Jørgensen 1983; Losher 1989; Urban 1994). The dissimilatory reduction reaction requires the catalytic mediation of bacteria and does not occur spontaneously (Chambers and Trudinger 1978). In cases where other oxidising agents are present, these bacteria yield more energy by using  $\text{O}_2$ , nitrate, manganese or iron as electron donors. Thus thermodynamics predict that sulphur reduction only occurs when the concentration of other electron donors is very low (Urban 1994). These microbial processes are also denoted secondary organic productivity, since new organic matter is produced, and it may serve as a sink for oxidised or reduced

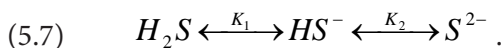
sulphur compounds (Loshner 1989). The produced hydrogen sulphide may then react further to form metal sulphides and ultimately pyrite (Butler *et al* 2004), or escape to the atmosphere. In the oxic epilimnion, H<sub>2</sub>S is either re-oxidised chemically or by chemoautotrophic or photoautotrophic bacteria to S<sup>0</sup>, S<sub>x</sub><sup>2-</sup> or SO<sub>4</sub><sup>2-</sup> (Howarth *et al* 1992). Up to 90% of the produced hydrogen sulphide may be re-oxidised with SO<sub>4</sub><sup>2-</sup> as the end product (Canfield 2001; Bottrell and Newton 2006).

The metabolism of the dissimilatory sulphur reducing bacteria can be expressed by (Berner 1984; Berner and Raiswell 1984; Loshner 1989)



In lake sediments the concentration of SO<sub>4</sub><sup>2-</sup> is very low and diffusion of SO<sub>4</sub><sup>2-</sup> may thus be limited. Bacterial sulphate reduction is therefore of less significance in lacustrine lakes (Jørgensen 1983; Loshner 1989). This is a fundamental difference to marine sediments, where sulphate reduction is of major importance. In marine environments the limiting factor for sulphur reduction is the low supply of organic matter, whereas freshwater lakes under normal circumstances have a high influx of organic matter. Thus in lacustrine environments the limiting factor is the supply of SO<sub>4</sub><sup>2-</sup>. The concentration of SO<sub>4</sub><sup>2-</sup> can be as much as two orders of magnitude lower compared to that of the ocean (Berner 1984; Nriagu and Soon 1985; Loshner 1989). Hence, most dissolved sulphate is reduced within the upper few centimetres of the sediment. In marine environments with a high concentration of reduced iron, the end product of dissimilatory sulphate reduction is commonly the formation of pyrite. By contrast, lacustrine environments have low concentrations of reactive reduced iron (Fe<sup>2+</sup>) and the formation of pyrite may therefore be limited (Loshner 1989). Furthermore, many lakes in temperate regions are dimictic and therefore pyrite is readily oxidised to Fe<sup>2+</sup> ions and dissolved SO<sub>4</sub><sup>2-</sup> (Urban 1994). Thus, the oxidation of the bottom during lake turnover may remove any produced pyrite (Jørgensen 1983; Urban 1994; Schippers and Jørgensen 2002; Bottrell and Newton 2006).

The fraction of escapable hydrogen sulphide is largely controlled by the lake pH values as the formation of H<sub>2</sub>S establishes the equilibrium equation (*see also Figure 5-4*)



Thus in an acidic environment most of the produced H<sub>2</sub>S remains as dissolved H<sub>2</sub>S, whereas at high alkalinity it is found as dissolved sulphide. Large concentrations of dissolved hydrogen sulphide are toxic to biota and it should be noted that even at normal lake pH, a minor fraction of H<sub>2</sub>S is present.

Both the processes of dissimilated sulphate reduction and methanogenesis are anaerobic and therefore competitive. However, the dissimilate sulphate reduction is more efficient than methanogenesis, and methanogenesis only occurs if the dissimilate sulphate reduction does not occur (Schlesinger 1997).

### Sulphur isotopes (δ<sup>34</sup>S<sub>ORG</sub>)

The sulphur isotopes are used to identify the source of sulphur and much attention has been given to the dissimilate sulphate reduction and the formation of pyrite in marine environments (Jørgensen 1977; Berner 1984; Jørgensen 1990; Canfield 2000; Schippers and Jørgensen 2002). The sulphate isotope composition in the ocean is surprisingly uniform and has a value of 20‰ (Thode *et al* 1961; Rees *et al* 1978; Petersen and Howarth 1987; Strauss 1999; Strauss 2003; Bottrell and Newton 2006). Continental vegetation has sulphur isotope values δ<sup>34</sup>S ranging from 2

to 6‰, whereas the dissolved sulphate of continental precipitation ranges from 1 to 7‰ (Petersen and Howarth 1987). The sulphur isotope composition  $\delta^{34}\text{S}$  values in lacustrine sediments depend primarily upon the aqueous sulphate in lake water derived from atmospheric or lithospheric sources (Mayer and Schwark 1999). Thus, lacustrine organic  $\delta^{34}\text{S}$  values are normally to be found in the range between the isotopic composition of  $\text{SO}_4^{2-}$  and that of pyrite (Urban 1994).

The fractionations associated with the assimilatory sulphate reduction are small and range from 0.9 to 2.8‰ for green algae and around 1.5‰ for higher plants (Trust and Fry 1992; Canfield 2001). Thus, the  $\delta^{34}\text{S}$  values of organic compounds generally reflect the aqueous sulphate. Reduced sulphur compounds such as sulphides or pyrite can be significantly depleted. The fractionation of dissimilate sulphate reduction is reported to be in the range between +3‰ and -46‰ (Habicht and Canfield 1997), and even values as low as -72‰ have been reported (Wortmann *et al* 2001; Brunner and Bernasconi 2005). The pyrite formed in lake sediments by sulphate reduction show depletions of 0.4 to 18.8‰ relative to sulphate isotopic composition (Urban *et al* 1999). Fractionations of the dissimilate sulphate reduction are known to be dependent on the sulphate concentration. High concentrations preferentially favour  $^{32}\text{S}$  in the formation of monosulphides and pyrite, in contrast to low concentrations where the sulphur isotope fractionation is lower (Mayer and Schwark 1999). However, if all sediment sulphate is reduced, little or no fractionation is expected (Nriagu *et al.* 1985). Elemental sulphur and sulphate formed by oxidation of  $\text{H}_2\text{S}$  by the chemoautotroph bacteria *Thiobacillus concretivorus* are enriched in  $^{32}\text{S}$  by 3-6‰ and 6-9‰ relative to the initial  $\text{H}_2\text{S}$  (Chambers and Trudinger 1978).

Low  $\delta^{34}\text{S}$  values of organic material may be attributed to times of great eutrophication (Urban *et al* 1999). The assimilatory uptake by primary production is associated with only a very small fractionation and the depletion in the heavy sulphur isotope is generally attributed to isotopic fractionation during dissimilatory sulphate reduction (Jedrysek and Skrzypek 2005). Hence this observation may be explained by microbial incorporation of reduced sulphur into the organic material.

### **C/N and C/S ratios of organic matter**

Lake sediments may contain organic matter from several sources, such as aquatic plants, terrestrial plants, algae and soil humus. The nitrogen content of these different species differs significantly. Non-vascular plants like phytoplankton has C:N values between 4 and 10, whereas vascular plants have C:N values greater than 20 (Meyers 1997; Meyers and Lallier-Vergés 1999; Meyers and Teranes 2001). However, under limited nitrogen conditions algae growth may have C:N values as high as 20. Most sediments have C:N ratios that are much higher due to a high content of terrestrial plants, which contain cellulose and lignin both of which are poor in nitrogen. The average C:N ratio for terrestrial biomass is around 160, whereas soil C:N values are reported to be about 15. Lacustrine C:N ratios of organic material are thus useful in distinguishing aquatic from terrestrial derived sources (Meyers and Teranes 2001; Lamb *et al* 2006). Note that C:N values are expected to vary at different points in the lake, and in general decreasing C:N values can be expected with increasing distances to the shore (Meyers and Teranes 2001). High organic production that yields dysoxia or anoxia may elevate C:N values due to microbial degradation via denitrification preferentially utilising nitrogen rich compounds and leaving nitrogen poor organic matter intact (Meyers 2006). Furthermore, constant C:N ratios may occur during periods of increased organic productivity in contrast to low productivity periods that tend to display variable C:N values (Routh *et al* 2004).

The average sulphur content of living matter is approximately 1 wt%. Plant material has values of 0.5 wt%, whereas animals have values of 4 wt% (Loshier 1989). The C:S values of lacustrine al-

gae range from 16 to 30, whereas C:S values for soil organic matter are higher and range between 60 and 120 (Bernier 1984; Nriagu and Soon 1985). Common marine C:S values are reported to be around 8 (Bernier and Raiswell 1984; Morse and Bernier 1995).

The low sulphate concentration of lacustrine environments cause sulphate to be rapidly and totally reduced within the first few centimetres of the sediments, leaving behind little pyrite and preserving much of the organic matter which causes low C:S values (Bernier 1984; Nriagu and Soon 1985). Freshwaters conditions lead to a lack of correlation between pyrite sulphur versus organic material and correspondingly high C:S<sub>pyrite</sub> ratios. Hence, C:S<sub>pyrite</sub> may serve as paloesalinity indicator (Bernier 1984). However, as pointed out by Losher and Kelts (1989), the measured quantity for lacustrine sediments is commonly total sulphur weight percentage. Thus the method of Bernier and Raiswell (1984) cannot be universally applied to lacustrine environments where only the total sulphur weight percentage (*TS*) is available. However, strong density stratification may affect the C:S values due to bacterial sulphate reduction and incorporation of sulphide into the sediments thus lowering the C:S ratio (Routh *et al* 2004).

### **The isotopic composition of calcium carbonate**

The  $\delta^{18}\text{O}_{\text{carb}}$  and  $\delta^{13}\text{C}_{\text{carb}}$  values of calcium carbonate reflect the source from which it is precipitated. The  $\delta^{13}\text{C}_{\text{carb}}$  values of lacustrine carbonates are primarily a function of the isotope composition of the DIC (*see Figure 5-4*) and the  $\delta^{18}\text{O}_{\text{carb}}$  values primarily reflect the  $\delta^{18}\text{O}$  values of the paleo-water. Furthermore, both the  $\delta^{13}\text{C}_{\text{carb}}$  and  $\delta^{18}\text{O}_{\text{carb}}$  values may be controlled by the hydrological balance of the lake and by vapour exchange with the atmosphere (Talbot 1990; Li and Ku 1997; Dean 1999; Mayer and Schwark 1999; Schwalb and Dean 2002; Hammarlund *et al* 2003; Kirby *et al* 2004; Hammarlund *et al* 2005).

### **The $\delta^{13}\text{C}_{\text{carb}}$ of calcium carbonate**

The  $\delta^{13}\text{C}_{\text{carb}}$  values of lacustrine sediments are primarily a mixture of the isotopic composition of the inflowing DIC and a function of the primary production within the lake. Furthermore, changes in the hydrological balance and evaporation effects are also traced by  $\delta^{13}\text{C}_{\text{carb}}$  values, but only to a minor extent. In isotopic equilibrium with atmospheric  $\text{CO}_2$  at -7‰, the  $\delta^{13}\text{C}_{\text{carb}}$  values are around +1 to 2‰ (*see Figure 5-4*). This, however, is rarely the case and in most cases the isotope composition of the inflowing DIC is depleted, reflecting its terrestrial origin. The decomposition of organic material in soils generates large amounts of  $\text{CO}_2$  which produces acidic soils when  $\text{CO}_2$  is dissolved by rainwater. This carbonic acid then dissolves the till calcium carbonate resulting in inflowing  $\delta^{13}\text{C}$  values of around -5‰.

The autochthonous primary biogenic production preferentially removes the light carbon dioxide; progressively enriching the remaining DIC pool and resulting in increased  $\delta^{13}\text{C}_{\text{carb}}$  values. Hence, biogenically induced autochthonous calcium carbonate will display enriched  $\delta^{13}\text{C}_{\text{carb}}$  values. If high primary productivity results in an enriched DIC pool, depleted organic  $\delta^{13}\text{C}_{\text{ORG}}$  values will be followed by successively enriched calcium carbonate  $\delta^{13}\text{C}_{\text{carb}}$  values (Dean 2002).

The isotopic composition of the DIC may change seasonally because of annual mixing, resulting in an increase of the respired  $\text{CO}_2$  from decomposed organic material which is depleted in  $^{13}\text{C}$ . Seasonal changes of the isotope composition of the DIC can also be a result of the extraction of  $^{12}\text{C}$  during high photosynthetic organic productivity in the spring or by the evasion of  $\text{CO}_2$  gas during warm summers (Ito 2001).

### **The $\delta^{18}\text{O}_{\text{carb}}$ of calcium carbonate**

The isotopic composition of lake water traces the hydrological lake balance which is given by the sum of water inflow minus the sum of water outflow. The lake water oxygen isotope com-

position is controlled by the combined isotopic composition of input waters and by evaporative enrichment (Anderson *et al* 2001; Schwab 2002; Seppä *et al* 2005). The  $\delta^{18}\text{O}_{\text{carb}}$  values of authigenic precipitated  $\text{CaCO}_3$  depend on the isotopic composition of the water from where it precipitates and the ambient water temperature (Eicher and Siegenthaler 1976; Seppä *et al* 2005). Hence the  $\delta^{18}\text{O}_{\text{carb}}$  values are a combined function of the lake water isotope composition ( $\delta^{18}\text{O}_W$ ) and the temperature dependent fractionation ( $\alpha_{A-B}$ ) during precipitation. The isotopic composition of carbonate may be used to estimate the paleo-isotope composition of the lake water:

$$(5.8) \quad \delta^{18}\text{O}_W = \delta^{18}\text{O}_{\text{carb}} + \varepsilon_{A-B},$$

where  $\varepsilon_{A-B}$  is the enrichment factor between the oxygen isotope composition of the carbonate mineral and water. The precipitated  $\text{CaCO}_3$  is enriched in  $^{18}\text{O}$  relative to the isotopic composition of lake water and empirically the fractionation factor follows the equation:

$$(5.9) \quad \varepsilon_{A-B} \approx 1000 \ln \alpha_{A-B} = C_1 + C_2 \frac{10^6}{T^2},$$

where the constants  $C_1$  and  $C_2$  are material dependent (*see Table 5.2*) and the temperature  $T$  is given in Kelvin ( $K$ ) (*see e.g. Friedman and O'Neil 1977; Clark and Fritz 1997; Criss 1999*). However, this approach for estimating the  $\delta^{18}\text{O}_W$  composition may only be safely applied if the carbonate is formed in equilibrium with the water and if the paleo-temperature of the ambient water is known; which is commonly not the case. Furthermore, one carbonate mineral component is commonly selected for calculations due to the different fractionation factors of disparate carbonate minerals. Moreover, bulk carbonate analysis is at risk of including out-washed allochthonous particulate  $\text{CaCO}_3$ , which may significantly obscure the oxygen isotope precipitation signal and only the authigenically or biogenically induced  $\text{CaCO}_3$  formed in thermodynamic equilibrium with lake water (*low concentration magnesium in calcium carbonate*) may be used for paleotemperature determinations (Ito 2001). However, a high fraction of allochthonous  $\text{CaCO}_3$  may be observed as high  $\delta^{13}\text{C}_{\text{carb}}$  and  $\delta^{18}\text{O}_{\text{carb}}$  values (Hammarlund and Buchardt 1996). The  $\delta^{18}\text{O}_{\text{carb}}$  values of the surrounding tills are in the range from 0‰ to -4‰ (Kolstrup and Buchardt 1982; Hammarlund and Buchardt 1996; Noe-Nygaard and Heiberg 2001), whereas the  $\delta^{13}\text{C}_{\text{carb}}$  values of the Cretaceous and Danian rocks of Lolland have been reported to be around 1‰ with a  $\text{CaCO}_3$  content of approximately 30 wt% (Kolstrup and Buchardt 1982; Noe-Nygaard and Heiberg 2001). Hence, a very high fraction of allochthonous  $\text{CaCO}_3$  may result in the  $\delta^{13}\text{C}_{\text{carb}}$  and  $\delta^{18}\text{O}_{\text{carb}}$  values approaching that of the till  $\text{CaCO}_3$  isotopic composition.

The  $\delta^{18}\text{O}_W$  composition is modulated by the isotopic composition of precipitation ( $\delta^{18}\text{O}_p$ ) by the combined effect of direct precipitation, surface run-off and groundwater from inflowing water. From modern observations, a relation between the  $\delta^{18}\text{O}_p$  composition and annual temperatures has been established (Dansgaard 1964, eq (5.10a) ; Rozanski *et al* 1992, eq (5.10b)):

$$(5.10a) \quad \delta^{18}\text{O}_p = 0.695 T_{\text{annual}} - 13.6\text{‰},$$

**Table 5.2: Material dependent constants for equation 5.9**

Phase B: water

Phase A	$C_1$	$C_2$	Range (K)	$\alpha$ (298K)	Reference
Calcite	-2.91	2.78	273-773	1.0288	O'Neil <i>et al</i> 1969
Dolomite	-1.52	3.20	573-783	1.0351	Northrop and Clayton 1966

$$(5.10b) \quad \delta^{18}O_p = (0.59 \pm 0.08) T_{annual} - 14.24\text{‰} .$$

The oxygen isotopic composition of surface run-off is likely to resemble that of local precipitation, whereas the oxygen isotopic composition of inflowing groundwater may be significantly altered due to evaporative effects. Moreover, the lake water  $\delta^{18}O_w$  composition is strongly modulated by evaporation and changes in the hydrological balance. Thus, the  $\delta^{18}O_w$  composition of lake water is rarely identical to that of the contemporaneous meteoric precipitation (Ito 2001; Leng and Marshall 2004). Exceptions to this are short time residence lakes in humid environments.

The evaporation to inflow ratio ( $E/I$ ), which reflects the combined effect of net evaporation and water inflow (*groundwater or surface run-off*) may be usefully employed to determine relative lake levels. Relatively lower lake levels during dry climate periods favour the evaporation of water from the lake basin ( $E/I > 1$ ) preferentially removing  $^{16}O$  and consequently enriching the precipitated  $CaCO_3$  in  $^{18}O$ . By contrast, relatively high lake levels are characterised by less evaporation and a higher water inflow ( $E/I < 1$ ) lowering the  $\delta^{18}O_{carb}$  values of the precipitated  $CaCO_3$  (Kirby *et al* 2004). Seasonal variations in  $\delta^{18}O_w$  from precipitation should be minimal when compared to the annual effect of evaporation (Kirby *et al* 2004). Therefore, the  $\delta^{18}O_{carb}$  data predominantly reflect changes in the  $E/I$  ratio (*evaporation to inflow ratio*) with  $\delta^{18}O$  of precipitation as a secondary effect (Schwalb 2002; Kirby *et al* 2004; Hammarlund *et al* 2005; Seppä *et al* 2005).

### The covariance of $\delta^{13}C_{carb}$ and $\delta^{18}O_{carb}$ values

Cross-plots of  $\delta^{18}O_{carb}$  versus  $\delta^{13}C_{carb}$  may help to distinguish hydrological open systems from hydrological closed systems (Talbot 1990; Li and Ku 1997). A strong covariance between  $\delta^{13}C_{carb}$  and  $\delta^{18}O_{carb}$  exists for hydrological closed systems due to effects caused by the hydrological balance of the lake or by vapour exchange with atmospheric moisture and are mainly results of longer water residence times for hydrological closed lakes.

When the water level in a hydrological closed lake is raised, the  $\delta^{13}C_{carb}$  and  $\delta^{18}O_{carb}$  values will reflect this change if there is a difference in the isotopic composition of the  $\delta^{13}C$  and  $\delta^{18}O$  values of the inflowing water relative to the lake  $\delta^{13}C$  and  $\delta^{18}O$  values. Generally, the isotopic composition of the discharged water is depleted leading to depletion of  $\delta^{13}C_{carb}$  and  $\delta^{18}O_{carb}$  values. This effect is expected to be smaller for the  $\delta^{13}C_{carb}$  values than for the  $\delta^{18}O_{carb}$  values (Li and Ku 1997). If inflow is high and evaporation is low, the lake water  $\delta^{18}O_{carb}$  is expected to be similar to that of precipitation. This is most likely to be the case in wet climates (Mayer and Schwark 1999).

A rapid water volume reduction caused by increased evaporation will elevate the  $\delta^{18}O_{carb}$  values as the light  $^{16}O$  isotope preferentially escapes. If the decrease in water volume is caused by a combination of increased evaporation and reduced inflow, then the  $\delta^{13}C_{carb}$  values also increases due to photosynthetic removal of light carbon and also because strong evaporation increases the partial pressure of carbon dioxide  $p_{CO_2}$  resulting in loss of  $CO_2$ . Thus, decreasing water levels will increase  $\delta^{13}C_{carb}$  and  $\delta^{18}O_{carb}$  values (Li and Ku 1997; Mayer and Schwark 1999; Dean and Schwalb 2000). This is most likely for dry periods. A decreasing water level may also lead to increased organic productivity, as the thermocline is lowered. This consequently leads to vertical mixing and thus increased supply of nutrients. At a steady state water level, the  $\delta^{13}C$  and  $\delta^{18}O$  tend to be uncorrelated (Li and Ku 1997).

## Magnetic susceptibility

Magnetic susceptibility of bulk samples is a measure of the concentration of ferromagnetic minerals, and of these mainly magnetite (Sandgren *et al* 1990). Minerals are normally found in clay and silt, transported to the lake by outwash from the lake catchments area. Thus, magnetic susceptibility is a proxy for the degree of erosion and outwash of mineralogical material from the catchments area (Sandgren *et al* 1990 ; McFadden *et al* 2005). Mainly two processes may result in changing the allochthonous input: either the amount of outwashed material from the lake surroundings is changing due to changes in rainfall or deforestation, or the SUS values are changing due to increases or decreases in the lake water level. Transgressions commonly yield an increase in the SUS values, since more allochthonous material is eroded into the lake, whereas regressions may also yield somewhat higher SUS values from erosion in the littoral zone, thus adding mainly reworked limnic material to the deposit. However, the SUS values also vary as a function of distance from the lake shore. A greater distance to the lake shore yields decreased and somewhat dampened SUS values compared to shorter distances to the lake shore where the original SUS signal is more likely to be fully preserved (McFadden *et al* 2005). However, wet climates with heavy rainfall thereby increase the outwash of mineralogical materials. Hence an increase in magnetic susceptibility can be interpreted as going from a warmer and dryer climate to a wetter and colder, and *vice versa*.

## Conceptual interpretation scheme

A simplistic conceptual interpretation scheme modified after Hammarlund (2003) is proposed and shown in Figure 5-5. The  $\delta^{18}\text{O}_{\text{carb}}$  values are to a large extent coupled to the hydrology of the drainage basin (Kirby *et al* 2004; Hammarlund *et al* 2005) through the E/I ratio. A large E/I ratio causes  $\delta^{18}\text{O}_{\text{carb}}$  values to increase, whereas a small E/I ratio causes them to decrease (Talbot 1990; Li and Ku 1997). In chapter 4 it was hypothesised that the Bliden Lake is mainly ground-water fed and the  $\delta^{18}\text{O}_{\text{carb}}$  values are therefore likely to reflect changes in the E/I ratio. However, the lack of a modern analogy to the Bliden Lake hydrology, for example through  $\delta^{18}\text{O}$  and  $\delta\text{D}$  isotope water measurements, weakens this assumption. Present  $\delta^{18}\text{O}$  and  $\delta\text{D}$  water data from the lake would have revealed important information on the water residence time, the effect of local precipitation as well as the extent of evaporative effects.

Fluctuations in lake water inflow are most likely coupled to changes in nutrient supply and hence also to organic productivity (Meyers 1997; Talbot *et al* 2006). The  $\delta^{13}\text{C}_{\text{ORG}}$ ,  $\delta^{15}\text{N}_{\text{ORG}}$  and  $\delta^{34}\text{S}_{\text{ORG}}$  values are linked to organic productivity, yielding increasing values during periods with increased nutrient supply and *vice versa* (Wolfe *et al* 1999; McFadden *et al* 2005; Talbot *et al*

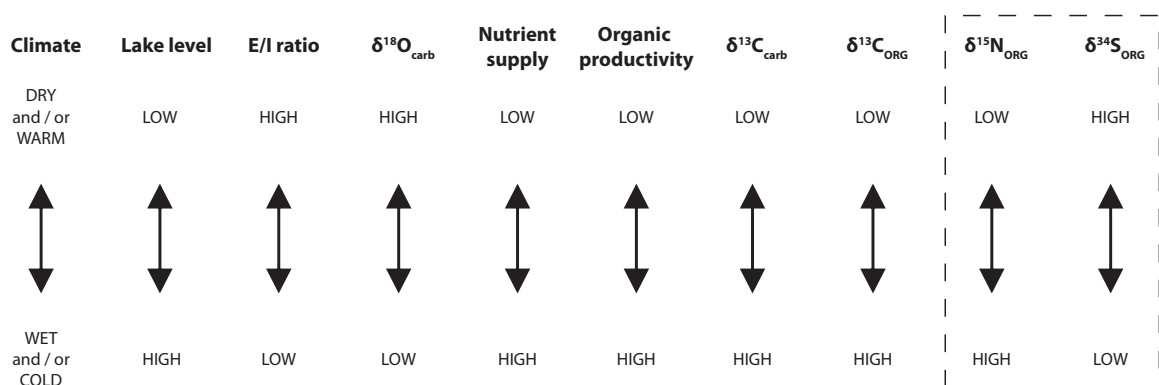


Figure 5-5. Illustrated is a conceptual scheme for the interpretation of the Bliden Lake geochemical data.

2006). However, a correlation between the  $\delta^{15}\text{N}_{\text{ORG}}$  and  $\delta^{34}\text{S}_{\text{ORG}}$  values may be coupled to the development of prolonged periods of anoxia (Watanabe *et al* 2004), yielding increased  $\delta^{15}\text{N}_{\text{ORG}}$  values due to ammonia volatilisation or denitrification and decreased  $\delta^{34}\text{S}_{\text{ORG}}$  values due to bacterial sulphate reduction.

# 6

---

**Applied methods and results**

## Introduction

The Bliden drill core consists of 14 one meter sections with 10 cm overlap taken with a Russian corer by Nanna Noe-Nygaard and her team in March 1996. The one meter cores with diameters of 7.5 cm were wrapped in plastic and stored at 4°C in a dark freeze room. The core was cut into two; one half was used for geochemical samples and stable isotope analysis taken with 2 cm intervals, the other was saved for screening and future analysis (*e.g. pollen*). Each sample was freeze dried and crushed prior to any analysis in order to obtain a homogenous sample material. Large fragments of shells and organic microfossil material (*all identified microfossil terrestrial organic material were <sup>14</sup>C dated, see chapter 8 and below*) were removed prior to freeze drying. However many fragments were too small for complete removal and may potentially obscure the interpretation of the results. The upper and lower part of the core has been screened for additional <sup>14</sup>C dateable material. In following the terminology and methods employed are briefly described and discussed (*see also chapter 5 for further details*).

## Methods

*Magnetic susceptibility (SUS)*: The magnetic susceptibility was measured on freeze dried samples by a Geofyzica Brno KLY-2 Kappabridge and corrected for the magnetic susceptibility value of the sample container. The weight of the sample material was determined to calculate mass specific magnetic susceptibility values given as  $\mu\text{m}^3/\text{g}$ .

## Geochemical methods

*Calcium carbonate content*: The  $\text{CaCO}_3$  content has been found by titration and is given as the percentage of total dry sample weight. Around 0.5g of sample material is added to a glass container with 200 ml of distilled water and 25 ml of 0.5N HCl. The sample was boiled for 30 minutes for removal of dissolved carbon dioxide. After cooling the remaining acid was found by adding NaOH (0.5N) to neutral pH. The weight percent carbonate was then found by

$$(6.1) \quad \text{CaCO}_3 \text{ wt\%} = \frac{(V_{\text{HCl}} \cdot N_{\text{HCl}} - V_{\text{NaOH}} \cdot N_{\text{NaOH}}) \times M_{\text{CaCO}_3}}{20 \cdot w_{\text{sample}}} .$$

Where  $V_{\text{HCl}}$  and  $V_{\text{NaOH}}$  is the added volume of HCl and NaOH,  $N_{\text{HCl}}$  and  $N_{\text{NaOH}}$  their molar concentrations,  $M_{\text{CaCO}_3}$  is the molar weight of calcium carbonate and  $w_{\text{sample}}$  the weight of the sample. The  $\text{CaCO}_3$  content reflect an integrate measure of open water precipitation of  $\text{CaCO}_3$  and detrital carbonate from the drainage basin (McFadden *et al* 2005).

*Total carbon, sulphur and organic content*: The total carbon (TC) and total sulphur (TS) content is determined by burning of 100 mg of dry sample material in ceramic vessels at 1250°C in a Metalyt 90S, where  $\text{CO}_2$  and  $\text{SO}_2$  is detected by their infrared absorbance. The total carbon is a composite of both organic and inorganic carbon, by the use of the carbonate content the total organic carbon fraction TOC can be found as

$$(6.2) \quad \text{TOC wt\%} = \text{TC wt\%} - \text{CaCO}_3 \text{ wt\%} \times \frac{12}{100} .$$

According to Meyers *et al* (Meyers and Teranes 2001) there are two fundamentally ways of obtaining TOC values; indirectly and directly. Indirect means that the TOC values are calculated, whereas by the direct method they are measured directly by removal of  $\text{CaCO}_3$  prior to analysis. In this study the direct method is applied and the indirect values have been used for a consistency check of the directly obtained values (*see also the discussion on weight percentage in chapter 2*).

By using the  $\text{CaCO}_3$  and TOC weight percent values, the mineralogical content has been found by

$$(6.3) \quad \text{Mineralogical wt\%} = 100\% - \text{CaCO}_3 \text{ wt\%} - 2.5 \times \text{TOC wt\%} .$$

The sulphur weight percentage of the sediments has been found to be too small for reliable TS measurements by the Metalyt 90S. Therefore the TS values presented here are obtained by stable isotope analysis as described in chapter 2 and below.

*$\delta^{13}\text{C}$  and  $\delta^{15}\text{N}$  of organic matter:* All carbonate is removed from samples prior to analysis by addition of 10% HCl and subsequently heated to the boiling point. The residual sample material is washed to pH 7 and dried in an oven at 80°C. Between 1.5 and 2.7 mg of dry pre-treated sample material is wrapped in 5x9mm tin cups for combustion in a EuroVector elemental analyser coupled to GV-Instruments IsoPrime stable isotope mass spectrometer (EA-IRMS, see chapter 2 for a detailed description).

The EA is equipped with a thermo chromatograph detector (TCD) measuring the signal of total carbon and nitrogen, from which the TOC and total organic nitrogen (TON) can be found. The measured  $C_{\text{org}}$  signal can be converted to TOC values by taking into account the reduced weight by removal of  $\text{CaCO}_3$  during pre-treatment. Hence, the measured TOC values are calculated by

$$(6.4) \quad \text{TOC wt\%} = \frac{M_{\text{sample}} \times C_{\text{org}}}{M_{\text{sample}} / (1 - \text{CaCO}_3 \text{ wt\%})} = C_{\text{org}} \times (1 - \text{CaCO}_3 \text{ wt\%}) .$$

In a similar fashion the total organic nitrogen TON can be found by

$$(6.5) \quad \text{TON wt\%} = N_{\text{org}} \times (1 - \text{CaCO}_3 \text{ wt\%}) .$$

The TOC and TON values are an integrate measure of the both allochthonous and autochthonous organic matter minus decay (Dean 1999; Meyers and Lallier-Vergés 1999).

*$\delta^{13}\text{C}$  and  $\delta^{18}\text{O}$  of inorganic matter ( $\text{CaCO}_3$ ):* The  $\delta^{13}\text{C}$  and  $\delta^{18}\text{O}$  values of carbonate have been measured by a GV-Instruments IsoPrime stable isotope mass spectrometer coupled to a multiflow inlet device and were performed by Bjørn Buchardt (*Geological Institute, University of Copenhagen*). Between 500 and 600  $\mu\text{g}$  of sample  $\text{CaCO}_3$  has been put into small septum sealed vials. The sample vials are heated to 70°C and flushed with helium for 10 minutes prior to acid injection. De-hydrated phosphoric acid ( $\text{H}_3\text{PO}_4$ ) is then manually injected with a syringe and  $\text{CO}_2$  is liberated. The samples are left to react with phosphoric acid for 3 hours and the produced  $\text{CO}_2$  is then transferred into the mass spectrometer by pressurising the sample vial with helium to just above atmospheric pressure. This overpressure expands the sample gas into the sample loop (*a small capillary column*) and after stabilising for 5 seconds the sample is transferred via an open split into the mass spectrometer by a continues helium flow where the mass to charge ratio ( $m/z$ ) 44, 45 and 46 of  $\text{CO}_2$  are measured simultaneously by the triple collector system. The  $\delta^{13}\text{C}$  and  $\delta^{18}\text{O}$  values are then obtained via the Craig correction formula (*equation 2.10, chapter 2*).

The  $\text{CaCO}_3$  content and the  $\delta^{13}\text{C}_{\text{carb}}$  and  $\delta^{18}\text{O}_{\text{carb}}$  values are an integrate measure of the total bulk  $\text{CaCO}_3$  fraction and hence their values reflect different origins both allochthonous and autochthonous. However as fragments and whole shells were removed prior to crushing and freeze drying the bulk sample will reflect only the particulate  $\text{CaCO}_3$  content. The  $\text{CaCO}_3$  con-

tent may originate from biogenic activity either as shells or from chemical precipitation due to increasing temperature or photosynthetic activity (*the authigenic fraction*). The authigenic fraction may furthermore originate from CaCO<sub>3</sub> produced in streams or elsewhere, and is thus not necessarily originating from the lake itself. Likewise the CaCO<sub>3</sub> content may originate from minerals or as crystalline particles from the surrounding catchments area (*the allogenic fraction*). However only the authigenic CaCO<sub>3</sub> fraction is formed in thermodynamic equilibrium with the water from which they precipitated. Even the authigenic fraction may show considerable offset from thermodynamic equilibrium if ostracods or gastropods are analysed due to the vital effect (Schwalb 2002). This naturally set some restrictions of the possible interpretations which may be gained from  $\delta^{13}\text{C}_{\text{carb}}$  and  $\delta^{18}\text{O}_{\text{carb}}$  isotope composition. Furthermore stable isotope analysis of ostracode samples may have revealed important difference between the isotopic composition of bottom waters and surface waters (Schwalb and Dean 1998, 2002). Commonly the  $\delta^{13}\text{C}$  values of ostracode and bulk samples are remarkably similar whereas the  $\delta^{18}\text{O}$  values display a constant value offset but often similar trends (Schwalb and Dean 1998, 2002).

Methods such as X-ray diffraction are able to resolve the mineralogical structure of the deposited CaCO<sub>3</sub> and thus information on the origin and amounts of the CaCO<sub>3</sub> may be gained by using this method (see e.g. Ito 2001; Dean 2002). However such methods have not been employed in this study.

*$\delta^{34}\text{S}$  of bulk samples:* All carbonate is removed from the sample prior to analysis by addition of 10% HCl and subsequently heated until boiling. The residual sample is washed to pH 7 and dried in an oven at 80°C. Between 1.5 and 2.7 mg of dry pre-treated sample material is wrapped in 5x9mm tin cups for combustion in a EuroVector elemental analyser coupled to GV-Instruments IsoPrime stable isotope ratio mass spectrometer (EA-IRMS) (*see chapter 2 for details*).

From the measured sulphur weight percentages  $S_{\text{ORG}}$  the total sulphur content (TS) can be found by

$$(6.6) \quad TS \text{ wt\%} = S_{\text{org}} \times (1 - \text{CaCO}_3 \text{ wt\%}) .$$

Where CaCO<sub>3</sub> wt% is the calcium carbonate weight percentage. Note that the calculated TS values only will represent total sulphur content if the pre-treatment with HCl has not removed sulphur from the samples.

*Atomic ratios of TOC, TON and TS:* All stated ratios are *atomic ratios* as they reflect the chemical stoichiometry. The atomic ratios of TOC versus TON and TOC versus TS where calculated by

$$(6.7) \quad \begin{aligned} C/N \text{ (atom)} &= \frac{TOC \text{ wt\%}}{TON \text{ wt\%}} \times \frac{14}{12} \\ C/S \text{ (atom)} &= \frac{TOC \text{ wt\%}}{TS \text{ wt\%}} \times \frac{34}{12} . \end{aligned}$$

Values of C:N are determined by the direct method, i.e. after removal of CaCO<sub>3</sub>, may be biased because the nitrogen fraction may consist of both inorganic and organic nitrogen (Talbot 2001). Normally the sedimentary inorganic nitrogen concentrations are small, and this should only be problematic for low TOC sediment samples (Meyers and Teranes 2001).

## Geochemical results of the Bliden Lake

The geochemical parameters have all been measured in random order and periods or samples displaying discrepancies have all been checked for consistency. For the stable isotopes of bulk  $\text{CaCO}_3$  ( $\delta^{13}\text{C}_{\text{carb}}$  and  $\delta^{18}\text{O}_{\text{carb}}$ ) only every fourth sample has been measured (*in total 160 samples*). A data table of all measured geochemical parameters can be found at [www.phys.au.dk/~jespero](http://www.phys.au.dk/~jespero). Average values have been used for core overlap sections.

In the majority of cases the measurement uncertainty of the geochemical parameters is unknown. Knowledge of these measurement uncertainties is essential for data interpretation and uncertainty estimates or noise levels are therefore highly needed. However, estimating the noise level of the geochemical parameters is not straight forward due to the nature of the ‘time’ signal containing discontinuities and long term trends. The method of wavelet denoising has been applied to estimate the general noise level of each parameter. The wavelet method has the advantage over other methods like autocorrelation periodograms and time series analysis (Brandt 1999) that it is able to resolve discontinuities (Mallat 1999; Misiti *et al* 2004). A Daubechies level 5 (*db5*) wavelet has been used to decompose the signal into 5 approximation and detail sections. The noise level is then removed by cutting off high amplitude peaks in each detail section assuming white noise. The approximation and detail sections are then summed to give the denoised signal and the noise level is estimated by the standard deviation of the residual signal between the original and denoised signal. By assuming white noise the residual signal must follow a Gaussian normal distribution with zero mean and a standard deviation corresponding to the measurement uncertainty. Further the residual signal should display no correlation by either an autocorrelation or a Fourier power spectrum. For all uncertainty estimates stated, residual signals were checked for cyclic behaviour and they were shown to follow a Gaussian normal distribution. The estimated uncertainties are shown in Table 6.1.

**Table 6.1. Estimated uncertainty of Geochemical Parameters**

Uncertainty estimation and signal de-noising by using discrete wavelets (db5 level 5) and assuming white noise

Method:	estimated $1\sigma$
Magnetic susceptibility	1.5 $\mu\text{m}^3/\text{g}$
TC	0.33 wt%
TS	0.07 wt%
TOC	0.87 wt%
TON	0.11 wt%
$\text{CaCO}_3$	1.3 wt%
$\delta^{13}\text{C}_{\text{ORG}}$	0.16 ‰
$\delta^{15}\text{N}_{\text{ORG}}$	0.39 ‰
$\delta^{34}\text{S}_{\text{ORG}}$	0.64 ‰
$\delta^{13}\text{C}_{\text{carb}}$	0.25 ‰
$\delta^{18}\text{O}_{\text{carb}}$	0.12 ‰
<i>Calculated parameters:</i>	
Mineralogical content	1.1 wt%
C:N ratio	1.4
C:S ratio	4.0

## Diagenesis

Diagenesis is the post-depositional conversion of sedimentary constitutions into a new product by chemical or mineralogical reactions which may complicate the interpretation of the geochemical data because the observed sediment may not necessarily be similar to the contemporaneous sediments that was deposited. As organic material accumulate on the lake bottom it slowly decomposes with  $\text{CO}_2$  being the ultimate end product. Some organic compounds

decompose more rapidly than others and nitrogen bearing components of organic material is known to decompose very rapidly (Talbot and Johannessen 1992). Also sulphur bearing organic compounds like proteins or amino acids is labile compounds which are rapidly re-mineralised in the sediments. Since chemical or bacterial reactions commonly are accompanied by isotopic fractionation significant alteration of the original isotope signal can be expected (Talbot and Johannessen 1992). The post-depositional decomposition of nitrogen bearing materials like proteins or amino acids will consequently result in preferential loss of organic nitrogen. Loss of organic nitrogen relative to organic carbon can be observed as decreasing weight percentage values of nitrogen ( $TON\ wt\%$ ) and as increasing C:N values. Also the C:N ratios may provide systematically offsets if positive ammonium ions are adsorbed onto the negatively charged surface and interlayers of clay minerals resulting in a high inorganic nitrogen content of some sediments (Talbot 2001). The presence of inorganic nitrogen may also influence the  $\delta^{15}N_{ORG}$  values. A straight line fit of the Bliden Lake TOC and TON data yields a TON intercept of 0.01 wt% ( $\rho=0.86$ ;  $r^2=0.74$ , see also Figure 7-5A) suggesting that inorganic nitrogen is not present in the sediments. Hence the C:N and  $\delta^{15}N_{ORG}$  values are therefore more likely to reflect real source differences of organic matter (Talbot 2001).

Diagenetic effects may also be observed when diagenetically produced  $CO_2$ ,  $CH_4$ ,  $NO_3$ ,  $NH_3$  or  $H_2S$  is released into the water column and becomes available for assimilation by phytoplankton and bacteria. As these diagenetically produced species are accompanied by large isotopic fractionation the recycling of these species will cause extreme isotope values of autochthonous organic matter (Talbot and Livingstone 1989). An increased concentration of  $CO_2$  due to diagenetic processes leads to lower pH values (see Figure 5-3). Thus high rates of post-depositional decomposition of organic material may lead to total or partial removal of  $CaCO_3$  (Dean 1999). Early diagenetic transformations of sulphur may occur by either inorganic processes or microbial oxidation of organic matter. If the organic flux to the sediments is higher than the diffusive supplies of oxygen then the oxygen concentration is rapidly depleted (Loshier 1989). Theoretically, sulphate reduction only occurs after all Manganese (Mn) and Iron (Fe) is consumed because the Gibbs free energy for reduction of organic material is larger when Mn and Fe are used as electron donors instead of sulphur (Loshier 1989). However, this contradicts the findings of Loshier (1989) which suggests that more energy is gained by sulphate reduction via microbial bacteria. Thus the driving force for diagenetic transformations of organic sulphur may be anaerobe microbial bacteria.

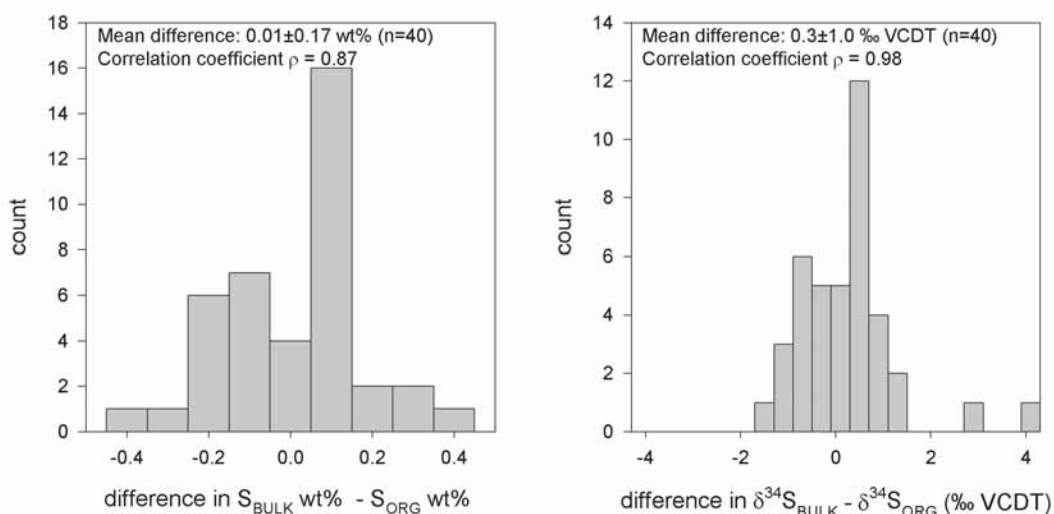


Figure 6-1. Shown is the sulphur weight percentage and  $\delta^{34}S$  difference between bulk and acidified samples.

The main sulphur compounds in the deposits are most likely either found as pyrite ( $\text{FeS}_2$ ), dissolved  $\text{SO}_4^{2-}$  or organic bound sulphur. The Bliden Lake core B1 was drilled in 1996 and stored in a cooling room at  $4^\circ\text{C}$ . Each 1 meter core was wrapped in plastic. Pyrite is rapidly oxidised when exposed to atmospheric air. Therefore it is believed that the possible produced pyrite in the sediments has with time been oxidised by the diffusive supply of atmospheric oxygen to sulphate ( $\text{SO}_4^{2-}$ ). To avoid this possible diagenetic produced  $\text{SO}_4^{2-}$  and to avoid too large amounts of carbon during stable isotope sulphur measurements, the acidified samples were used for analysis. To identify the difference of sulphur weight percentage content and isotope  $\delta^{34}\text{S}$  values 40 bulk samples were measured from the upper and middle part of the core. The differences between bulk and organic samples are shown in Figure 6-1. Both the differences in weight percentage and  $\delta^{34}\text{S}$  values show high correlation coefficients at 0.87 and 0.98 respectively. Their mean difference is  $0.01 \pm 0.17$  wt% sulphur and  $0.3 \pm 1.0$ ‰ for the  $\delta^{34}\text{S}$  values. Thus these sporadic data indicate that most of the sulphur is bound in the sedimentary organic material and that the content of sulphate and pyrite in the sediments is of minor concentrations.

### Estimating the $\delta^{18}\text{O}_w$ composition and the E/I ratio

The lake water oxygen isotope composition ( $\delta^{18}\text{O}_w$ ) can accurately be calculated from information on the paleo-temperature of the lake water (see equation (5.8) and (5.9)), which on the other hand is hardly ever obtained. However the ambient lake water  $\delta^{18}\text{O}_w$  composition may tentatively be derived from annual paleo-temperatures on assuming approximately equal long term changes in annual atmospheric temperature and ambient lake water temperature (Seppä *et al* 2005). Seppä *et al* (2005) provides an annual paleo-temperature ( $T_{\text{ann}}$ ) based on a pollen diagram from Lake Flarken (southern Sweden), hence assuming that the atmospheric paleo-temperature of southern Sweden resembles that of eastern Denmark the  $T_{\text{ann}}$  curve may be employed for estimating the  $\delta^{18}\text{O}_w$  composition of the Bliden Lake using an enrichment factor temperature sensitivity ( $\partial\alpha_{A-B}/\partial T$  see eq. (5.6)) of  $-0.25$ ‰/°C (Craig 1965) to the temporal deviations from modern temperature conditions (average modern temperature  $7.9^\circ\text{C}$ , 1960-90 (Laurson *et al* 1999)) as derived from the  $T_{\text{ann}}$  curve (Seppä *et al* 2005).

This approach for estimating the  $\delta^{18}\text{O}_w$  composition however, critically depends on the presumption of authigenic precipitated  $\text{CaCO}_3$  in equilibrium with the ambient lake water, which may be strongly uncertain for the bulk sample of the Bliden Lake core even though both the  $\delta^{13}\text{C}_{\text{carb}}$  and  $\delta^{18}\text{O}_{\text{carb}}$  data and sedimentological observations point towards mainly a biogenic derived  $\text{CaCO}_3$  content (for details see chapter 7). Moreover the absence of modern hydrological and sedimentological data prevents the inferred  $\delta^{18}\text{O}_w$  composition (see Figure 6-2) of being anchored to the VSMOW scale. Thus the scale of the  $\delta^{18}\text{O}_w$  curve is denoted 'floating'.

The water inflow to the Bliden Lake may potentially resemble the oxygen isotope composition of the precipitation ( $\delta^{18}\text{O}_p$ ) which can be estimated by applying the modern regression equation from European observations (see equation (5.10b), Rozanski *et al* 1992) together with the  $T_{\text{ann}}$  data (see Figure 6-2). However the Bliden Lake is most likely feed by groundwater discharge which potentially may be enriched in  $^{18}\text{O}$  due to evaporation along its pathway. On the other hand the oxygen isotope composition of the discharging groundwater ultimately derive from precipitation and thus probably resemble the long term trends of  $\delta^{18}\text{O}_p$ . Again modern hydrological data may have been greatly beneficial by providing data on ground and lake water isotopic composition and the general water residence time of the lake. Assuming that the water inflow of the Bliden Lake resembles the long term trends of the estimated  $\delta^{18}\text{O}_p$  data may provide an approximate estimation of the E/I ratio by the temporal changing separation between the  $\delta^{18}\text{O}_p$  and  $\delta^{18}\text{O}_w$  curves (see Figure 6-2 and Seppä *et al* 2005). Conditional on the assumptions employed for the estimation of the  $\delta^{18}\text{O}_p$  and  $\delta^{18}\text{O}_w$  curves, it may be revealed that hydrologi-

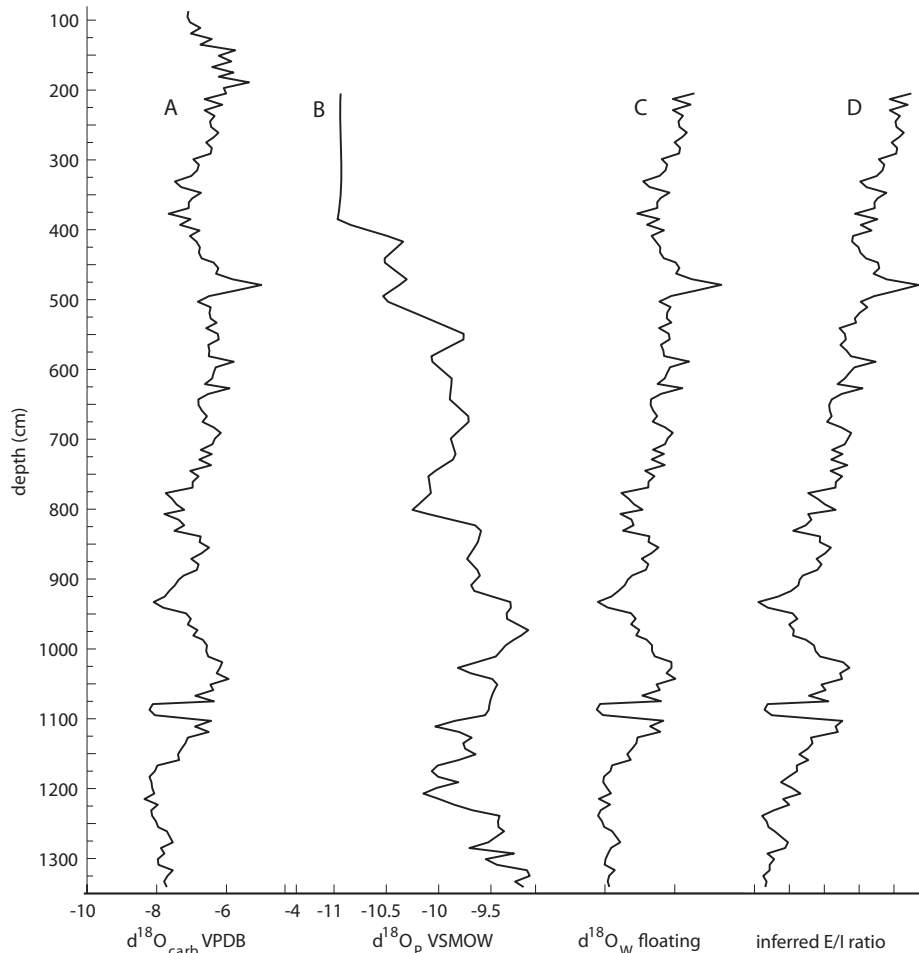


**Figure 6-2:** Panel A displays the  $\delta^{18}\text{O}_{\text{carb}}$  values of the Bliden Lake record. Panel B displays the isotopic composition of the precipitation ( $\delta^{18}\text{O}_p$ ) based on the  $T_{\text{ann}}$  presented by Seppä *et al* (2005). Panel C displays the estimated paleo-water isotopic composition of the Bliden Lake. The temperature dependent fractionation between water and  $\text{CaCO}_3$  is based on  $T_{\text{ann}}$  (Seppä *et al*. 2005). Panel D display the separation between  $\delta^{18}\text{O}_p$  and  $\delta^{18}\text{O}_w$  and represents a tentative estimate of the E/I ratio of the Bliden Lake. The  $T_{\text{ann}}$  curve has been converted to the Bliden depth scale by employing the age-to-depth model presented in chapter 8 by interpolation between nearest neighbours.

cal changes are the most important variation in the Bliden Lake  $\delta^{18}\text{O}_{\text{carb}}$  data (Kirby *et al* 2004; Hammarlund *et al* 2005; Seppä *et al* 2005).

### Radiocarbon dating

A chronology for the Bliden Lake record is essential for correlating with information obtained by other studies and the radiocarbon content on mostly terrestrial samples has been measured and used to make a depth-to-age relation (*see chapter 8*). The nomenclature used for age quoting are ‘cal BP’ for ‘calendar years before present (BP)’. By convention the year 1950 is set to zero, thus BP translates to ‘before 1950 AD’. Ages with the suffix ‘AD’ or ‘BC’ are calendar years ‘anno domini (AD)’ and ‘before Christ (BC)’. Note that due to variations in  $^{14}\text{C}$  production during past times, common calendar years are not similar to  $^{14}\text{C}$  years, a distinguishing which is maintained by quoting  $^{14}\text{C}$  years as ‘ $^{14}\text{C}$  years BP’, where again BP is before 1950 AD.

In total 18 individual samples have been dated, and are presented in Table 6.2. Some of the samples have been lumped to single AMS graphite targets for a single  $^{14}\text{C}$  age determination to ensure enough material for high precision (*see Table 6.2 for details*).

**Table 6.2: Radiocarbon dated samples from the Bliden core B1**

See Figure 8-6 for an age to depth plot of the calibrated  $^{14}\text{C}$  data.

#	AAR	Sample	depth (cm)	Material	Total weight (mg) / prep yield	$\delta^{13}\text{C}$ † ‰ VPDB	$^{14}\text{C}$ age BP	Reservoir age	Calibrated age BP	
									1 $\sigma$ interval	2 $\sigma$ interval
1	9743	B1 K1 1.48-1.50	149	hornbl aquatic	16.4 / 43.3%	-18.05	559 ± 36		635 to 600 (34.2%) 560 to 530 (34.0%)	650 to 580 (50.1%) 570 to 510 (45.3%)
2	9744	B1 K1 1.50-1.52	151	Twig	0.9 / 58.9%	(-25)	275 ± 65		460 to 280 (63.0%) 170 to 150 (5.2%)	550 to 100 (91.1%) 50 to -51 (4.3%)
3	9745	B1 K1 1.52-1.54	153	Leaf	2.7 / 66.7%	-21.96	469 ± 37		535 to 500 (68.2%)	550 to 465 (95.4%)
4	9060	B1 K2 1.80-1.82	181	Leaf	1.6 / 59.8%	(-25)	585 ± 60		650 to 580 (47.3%) 570 to 530 (20.9%)	670 to 520 (95.4%)
5	9062	B1 K3 3.18-3.20	319	Leaf	3.0 /	-30.37	753 ± 44		725 to 665 (68.2%)	770 to 650 (93.7%) 590 to 560 (1.7%)
6	9063	B1 K3 3.18-3.20	319	Insect	1.1 / 49.5%	(-26)	1100 ± 400		1400 to 650 (68.2%)	1950 to 250 (95.4%)
7	9746	B1 K5 4.92-4.94 B1 K5 4.94-4.96	494	Leaf Leaf	1.2 / 69.2%	-27.48	1790 ± 110		1860 to 1850 (1.2%) 1830 to 1560 (67.0%)	2000 to 1400 (95.4%)
8	9747	B1 K6 5.44-5.46	545	Seed	5.9 / 59.3%	-19.49	2167 ± 44		2310 to 2230 (34.9%) 2190 to 2110 (32.4%) 2080 to 2070 (0.9%)	2330 to 2040 (95.4%)
9	9748	B1 K6 5.70-5.72 B1 K6 5.72-5.74	572	Seed (star) Seed (myotis)	1.7 / 94.1%	-25.82	2170 ± 39		2310 to 2230 (36.7%) 2190 to 2110 (31.5%)	2320 to 2050 (95.4%)
10	9065	B1 K6 6.14-6.16	615	Seed	11.1 / 55.5%	-17.46	2580 ± 44		2760 to 2700 (52.1%) 2640 to 2610 (10.1%) 2590 to 2540 (5.9%)	2780 to 2680 (59.0%) 2640 to 2610 (12.4%) 2600 to 2490 (24.0%)
11	9067	B1 K8 8.02-8.04	803	Shell	22.6 / 46.9%	-9.23	4545 ± 55	1175 ± 57†	3970 to 3940 (7.3%) 3930 to 3820 (53.8%) 3790 to 3770 (4.4%) 3750 to 3730 (2.7%)	3990 to 3700 (95.4%)
12	9070	B1 K9 8.60-8.62	861	Twig	117.3 / 70.8%	-27.64	3570 ± 50		4570 to 4420 (68.2%)	4810 to 4760 (7.0%)
13	9071	B1 K11 9.88-9.90	989	Leaf	10.1 / 50.2%	-26.62	4035 ± 50		4700 to 4670 (1.9%) 5930 to 5880 (26.1%) 5830 to 5750 (42.1%)	4650 to 4410 (86.5%) 5990 to 5970 (2.1%) 5950 to 5730 (93.3%)
14	9072	B1 K13 11.72-11.74	1173	Twig	9.3 / 35.3%	-28.63	5115 ± 50		6740 to 6560 (68.2%)	6800 to 6480 (95.4%)
14	9749	B1 K14 13.44-13.46	1345	Leaf	2.0 / 60.0%	-27.48	5845 ± 65		6780 to 6760 (3.2%) 6750 to 6640 (65.0%)	6850 to 6810 (2.4%) 6800 to 6550 (93.0%)
15	9750	B1 K14 13.44-13.46	1345	Leaf	11.5 / 59.1%	-26.10	5880 ± 50			

† The calendar year of level 8.03m is found by the age to depth model to 3618 years BP. From the calibration curve (IntCal04 Reimer et al 2004b) this corresponds to 3370±14  $^{14}\text{C}$  years BP. The reservoir age is then calculated as the 4545 ± 55 minus 3370±14  $^{14}\text{C}$  years BP.  $\delta^{13}\text{C}$  values in ( ) are estimated values.

Samples for radiocarbon dating were pre-treated by the acid-alkali-acid (AAA) method prior to conversion to CO<sub>2</sub> by burning in sealed evacuated ampoules with CuO. The AAA method is as follows: 1M HCl (80°C 24hrs) followed 1M NaOH (80°C one to several days) and lastly 1M HCl (Thomsen 1990). The produced carbon dioxide is then converted to graphite targets and measured in the EN Tandem accelerator at Aarhus University, AMS <sup>14</sup>C Dating Centre, Department of Physics and Astronomy.

The shell sample (AAR-9067) is affected by the <sup>14</sup>C reservoir effect. The δ<sup>13</sup>C value of the shell has been determined to be -9.23‰ which is considerable lower than the isotope value δ<sup>13</sup>C<sub>carb</sub> of -5‰ of the contemporaneous bulk CaCO<sub>3</sub> in the Bliden Lake (see Figure 7-2 & Table 6.2). Eight leaf samples and three twigs have been measured. Two of these sample (twig AAR-9744 & leaf AAR-9060) were very small, thus their δ<sup>13</sup>C values could not be determined and was estimated to be -25‰; the common value of terrestrial organic C<sub>3</sub> material (O’Leary 1988). The remaining leaves and twigs have been measured and their δ<sup>13</sup>C values span from -30.37 to -26.1‰. However, note that the leaf sample AAR-9745 has much higher δ<sup>13</sup>C value at -21.96‰, i.e. 3‰ higher than the estimated value of -25‰ for AAR-9060 both coming from an approximately similar depth. The four dated seed samples range in δ<sup>13</sup>C from -25.82 to -17.46‰. One fraction from an insect has also been dated; its δ<sup>13</sup>C has been estimated to -26‰. Calibrated dates have been obtained by using OxCalc 3.10 (Ramsey 1995, 2001). The 1σ and 2σ calibrated age intervals are shown in Table 6.2.

# 7

---

## **Facies, sedimentology and geochemistry**

## **Introduction**

The Bliden Lake record represents a complete and continuous submerged deposit of the Late Holocene. In this chapter the Bliden Lake stratigraphy is presented together with an interpretation of the sedimentological observations and geochemical parameters. A survey of common interpretation pathways from geochemical parameters are presented in chapter 5 and are applied to interpret the Bliden Lake deposit. For further details please confront chapter 5 and references herein.

## **Facies and terminology**

The term facies is used of a body of rocks with specified characteristics (Reading 1989). In this context a facies is a group of sediments differing from other sediments by virtue of their visual appearance such as colour, grain size and macroscopic and microscopic organic content (Noe-Nygaard 1995).

The term gyttja is defined as a mud-like homogeneous non-plastic deposit with grain size less than 0.1 mm. Gyttja contains no macroscopic structure but may contain macrofossils or littoral microscopic remains of plant or animals. (Noe-Nygaard 1995; Cohen 2003). Detritus is defined as fragments of terrestrial plants of varying size. The terms gyttja and detritus are often combined indicating that the deposit may contain some proportion of organic material of terrestrial origin such as herbs or trees (Noe-Nygaard 1995). The term drifted is used of material derived from the high energy environment of the beach zone down to a depth of about 1.5 meters in contrast to fine detritus gyttja which is commonly deposited in a low energy environment at greater depths from suspension and hence below the wave base (Noe-Nygaard 1995). In total 28 facies have been identified and the Bliden Lake sediment and lithological core log are presented in Figure 7-1.

## **Facies associations**

Facies associations are groups of succeeding facies that occur together and are considered to be genetically or environmentally related (Reading 1989). The 28 facies of the Bliden Lake core has been grouped into five facies associations by virtue of their common characteristics. For convenience the facies associations are named after their interpretation; a high water (A & B) facies association, a shallow water (A & B) facies association, and an intermediate water facies association. A description and interpretation of each of the facies associations and their related facies and geochemical parameters will be given in the following. Figure 7-2 displays the lithological log and the geochemical data as function of depth. Scatter plots of selected geochemical parameters grouped after their facies and facies associations are displayed in Figure 7-3 to 7-9. Furthermore a survey of the geochemical data and physical properties of the facies and facies association are presented in Table 7.1 and 7.2. A discussion of the interpretation of the geochemical parameters and physical properties is presented in chapter 5 which solidifies the basis for several of the following facies interpretations.

### **High water (A) facies association**

This facies association consists of 12 facies spanning the lower half of the Bliden Lake core from 1350 cm to 639 cm. The deposit is 710 cm thick and consists of fine to medium grained detritus gyttja mostly containing autochtoneous organic material and subsidiary amounts of allochthonous organic material. All transitions between facies are gradual and weakly defined.

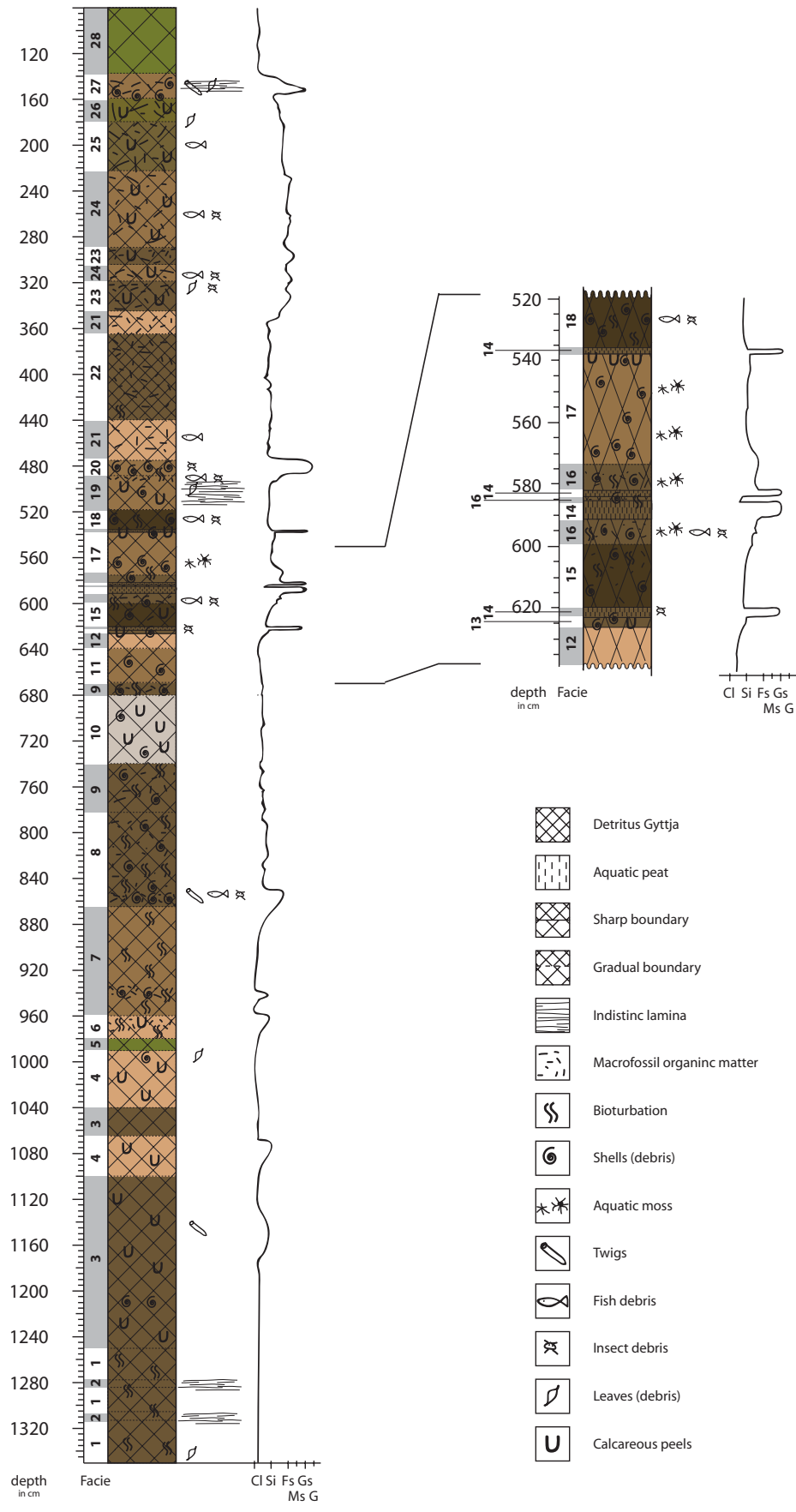


Figure 7-1. Lithological log of the Bliden Lake core B1.

### *Facies – sedimentology, geochemistry and interpretation*

*Facies 1 (1250 cm to 1278 cm, 1284 cm to 1306 cm and 1313 cm to 1350 cm):* A dark brown medium grained detritus gyttja of about 1 metre thick. This facies occurs in three depth intervals: i) 1350 cm to 1313 cm, ii) 1306 cm to 1284 cm and iii) 1278 cm to 1250 cm. The sediment is bioturbated and contains minor amounts of microscopic fragments of leafs and other organic debris of terrestrial origin. This unit is displayed in 7-10.

*Geochemistry and physical properties:* i) The SUS values are slightly decreasing with a minor peak occurring between 1330 cm and 1313 cm. The mineralogical content is constant up to a depth of 1328 cm where after it increases towards 1313 cm. The CaCO<sub>3</sub> is slightly decreasing and increases from 1320 cm. The  $\delta^{13}\text{C}_{\text{carb}}$ ,  $\delta^{18}\text{O}_{\text{carb}}$  values and the TS content are constant. The TOC and TON values are slowly decreasing. The C:N and C:S values are slowly decreasing. The  $\delta^{13}\text{C}_{\text{ORG}}$  values are constant and display a peak from 1330 cm. The  $\delta^{15}\text{N}_{\text{ORG}}$  values are decreasing up to 1330 cm and then increasing. The  $\delta^{34}\text{S}_{\text{ORG}}$  values are decreasing. See Table 7.1 and Figure 7-2.

ii) The SUS values are increasing and the mineralogical content is decreasing. The CaCO<sub>3</sub> content is decreasing up 1300 cm and then slowly increasing. The  $\delta^{13}\text{C}_{\text{carb}}$  values are increasing whereas the  $\delta^{18}\text{O}_{\text{carb}}$  values are constant. The TS values are constant and the TOC and TON values are increasing. The  $\delta^{13}\text{C}_{\text{ORG}}$  values are steeply increasing followed by constant values from 1300 cm, whereas the  $\delta^{15}\text{N}_{\text{ORG}}$  values are decreasing. The  $\delta^{34}\text{S}_{\text{ORG}}$  values are increasing. See Table 7.1 and Figure 7-2.

iii) The SUS values are constant the mineralogical content values are slowly increasing. The CaCO<sub>3</sub> content is decreasing and the  $\delta^{13}\text{C}_{\text{carb}}$  values are increasing. The  $\delta^{18}\text{O}_{\text{carb}}$  values are decreasing. The TS values are increasing up to 1260 cm, followed by constant and lower values. The TOC and TON values are increasing. The  $\delta^{13}\text{C}_{\text{ORG}}$  values are increasing whereas the  $\delta^{15}\text{N}_{\text{ORG}}$  values are slowly increasing. The  $\delta^{34}\text{S}_{\text{ORG}}$  values are decreasing. See Table 7.1 and Figure 7-2.

*Interpretation:* The medium grain size and uniformity of this facies indicates that the sediment is deposited from suspension. The low amounts of macrofossil organic material of both aquatic and terrestrial origin in addition to the microscopic fragmentary organic debris observed of this deposit indicates that this deposit is most likely deposited in the upper profundal zone (See Figure 5-1). The C:N values with an average of 21 and the C:S values of 73 (See Table 7.1) indicate a high content of autochthonous organic matter with likely some portion of allochthonous organic matter in accordance with the sedimentological observations. The low SUS values and low mineralogical content (*less than 20 wt%*) suggest minor amounts of allochthonous eroded material.

*Depth interval i):* The decreasing SUS values indicate a decreasing amount of allochthonous material into the lake. The constant  $\delta^{13}\text{C}_{\text{ORG}}$  values and the decreasing  $\delta^{15}\text{N}_{\text{ORG}}$  values may together with the decreasing TOC and TON values suggest a decreasing organic productivity (Routh *et al* 2004; Filippi and Talbot 2005; McFadden *et al* 2005; Talbot *et al* 2006). The very high CaCO<sub>3</sub> content is most likely bioinduced which may be supported by the mutual correlations of the CaCO<sub>3</sub>, TOC and TON values for the interval from 1350 cm to approximately 1320 cm. Their decreasing values suggest a decreasing content of autochthonous organic productivity for this period and thus a decreased amount of bioinduced CaCO<sub>3</sub> (Dean 1999; Schwab 2002; McFadden *et al* 2005). The decreasing  $\delta^{34}\text{S}_{\text{ORG}}$  values may likely reflect sulphate reducing bacteria preferentially incorporation of light sulphur into their cell structure. In turn this may suggest the development of an increasing anoxic hypolimnion (Watanabe *et al* 2004; Jedrysek and Skrzypek 2005; Eimers *et al* 2006). Likewise the steepest decrease in the  $\delta^{34}\text{S}_{\text{ORG}}$  values is concurrent with increasing  $\delta^{15}\text{N}_{\text{ORG}}$  values from 1330 cm and may likely arise due to increased ammonia volatilisation or denitrification (Talbot *et al* 2006). However the increasing  $\delta^{15}\text{N}_{\text{ORG}}$  values may be due to a limited DIN source (Routh *et al* 2004; Ogrinc *et al* 2005). Hence this depth interval is most likely characterised by a general decreasing influx of nutrients. A decreased nutrient supply is likely to indicate a decreasing water inflow. If this is correct, a warmer and drier climate may potentially yield increased periods of stratification and development of hypolimnion anoxia.

*Depth interval ii)* The increasing SUS values between 1306 cm and 1284 cm probably represent an increase in allochthonous material. The increasing TOC and TON values are likely reflecting an increasing organic productivity as may likely be supported by the increasing  $\delta^{13}\text{C}_{\text{ORG}}$  and



**Table 7.1. Geochemical data physical properties of facies 1 to 28**

A summary of the geochemical data is given as a mean value and minimum and maximum values in parentheses.

Facies	Depth Interval (cm)	Mag. Sus.	Mineralogical content	CaCO <sub>3</sub> (wt%)	$\delta^{13}\text{C}_{\text{carb}}$ (‰)	$\delta^{18}\text{O}_{\text{carb}}$ (‰)	TS wt%	TOC wt%	TON wt%	C:N	C:S	$\delta^{13}\text{C}_{\text{org}}$ (‰)	$\delta^{15}\text{N}_{\text{org}}$ (‰)	$\delta^{34}\text{S}_{\text{org}}$ (‰)
Highwater B	28	59.9 (48.4 - 66.0)	29.4 (26.0 - 32.9)	48.7 (43.2 - 54.3)	-3.4 (-4.3 to -2.6)	-6.9 (-7.0 to -6.7)	0.9 (0.5 - 1.1)	8.0 (6.8 - 9.2)	0.5 (0.4 - 0.6)	19.7 (17.2 - 22.2)	26.3 (23.9 - 32.6)	-29.0 (-30.0 to -25.7)	9.0 (5.7 - 10.7)	-1.9 (-3.1 to 0.0)
	27	72.6 (44.4 - 95.0)	36.3 (25.7 - 44.8)	38.9 (30.0 - 50.1)	-3.0 (-3.6 to -1.9)	-6.3 (-6.5 to -6.2)	1.2 (0.9 - 1.4)	9.7 (9.3 - 10.0)	0.7 (0.6 - 0.7)	16.6 (16.4 - 17.1)	22.6 (20.2 - 24.0)	-29.4 (-30.3 to -28.0)	7.8 (7.1 - 10.0)	-2.8 (-4.3 to -0.8)
	26	130.1 (101.3 - 156.5)	48.4 (44.4 - 50.8)	24.5 (21.1 - 29.1)	0.5 (-0.1 to 1.1)	-6.0 (-6.0 to -6.0)	1.4 (1.2 - 1.6)	10.2 (10.1 - 10.5)	0.7 (0.5 - 1.0)	16.9 (13.0 - 19.5)	19.8 (17.5 - 26.1)	-29.0 (-30.1 to -26.8)	4.8 (1.3 - 8.3)	2.2 (0.1 to 3.9)
Shallow water B	25	154.4 (131.9 - 195.1)	41.8 (36.8 - 48.8)	27.0 (20.2 - 31.0)	1.6 (1.1 to 2.0)	-6.0 (-6.1 to -5.9)	0.6 (0.4 - 1.1)	12.1 (9.1 - 13.9)	0.8 (0.5 - 1.9)	18.4 (17.5 - 18.8)	59.4 (30.0 - 71.3)	-29.0 (-30.0 to -26.7)	4.0 (1.4 - 6.1)	11.5 (5.3 to 13.1)
	24	160.6 (117.3 - 203.9)	37.6 (30.5 - 41.7)	26.4 (20.7 - 33.8)	0.7 (-0.6 to 1.8)	-6.4 (-6.7 to -6.2)	0.5 (0.5 - 0.6)	14.0 (12.5 - 15.6)	0.9 (0.7 - 1.1)	18.7 (17.1 - 22.4)	74.0 (64.1 - 124.5)	-29.8 (-30.6 to -26.6)	4.1 (3.1 - 5.1)	11.5 (10.1 to 13.5)
	23	160.1 (143.6 - 170.3)	43.2 (42.4 - 43.7)	20.3 (19.2 - 23.5)	-0.1 (-0.4 to 0.3)	-6.8 (-6.9 to -6.8)	0.4 (0.3 - 0.6)	14.9 (13.3 - 15.7)	0.9 (0.7 - 1.1)	18.8 (18.2 - 19.8)	103.3 (64.1 - 179.5)	-30.5 (-30.6 to -30.1)	4.5 (4.4 - 4.7)	12.0 (11.5 to 12.2)
24	150.6 (141.9 - 158.7)	39.2 (34.8 - 42.3)	27.4 (25.7 - 27.9)	1.1 (0.9 to 1.2)	-7.0 (-7.0 to -6.9)	0.5 (0.4 - 0.7)	12.2 (11.7 - 13.0)	0.8 (0.7 - 0.9)	18.3 (18.2 - 18.4)	66.3 (57.8 - 74.2)	-29.7 (-30.0 to -29.6)	4.6 (4.3 - 4.8)	11.0 (10.9 to 11.3)	
23	115.3 (92.4 - 134.9)	31.9 (23.2 - 34.7)	28.3 (26.4 - 30.9)	1.4 (1.4 to 1.5)	-7.0 (-7.0 to -7.0)	0.8 (0.6 - 1.0)	15.5 (13.9 - 19.1)	1.0 (0.9 - 1.3)	18.3 (18.3 - 18.3)	57.7 (46.5 - 67.0)	-29.7 (-30.1 to -29.5)	3.8 (2.6 - 4.5)	12.0 (11.2 to 12.7)	

Table 7.1 continued

Facies	Depth Interval (cm)	Mag. Sus.	Mineralogical content	CaCO <sub>3</sub> (wt%)	$\delta^{13}\text{C}_{\text{carb}}$ (‰)	$\delta^{18}\text{O}_{\text{carb}}$ (‰)	TS wt%	TOC wt%	TON wt%	C:N	C:S	$\delta^{13}\text{C}_{\text{org}}$ (‰)	$\delta^{15}\text{N}_{\text{org}}$ (‰)	$\delta^{34}\text{S}_{\text{org}}$ (‰)	
	21	345 to 365	38.1 (20.6 - 85.0)	15.0 (12.7 - 16.3)	35.4 (32.3 - 37.9)	1.2 (1.0 to 1.6)	-7.1 (-7.1 to -7.0)	1.1 (1.0 - 1.2)	23.7 (21.0 - 26.2)	1.4 (1.1 - 1.6)	18.4 (18.4 - 18.4)	59.9 (57.8 - 63.5)	-29.9 (-30.2 to -29.7)	2.7 (2.2 - 3.2)	13.8 (12.8 to 15.0)
	22	365 to 440	34.4 (22.1 - 43.2)	16.3 (14.7 - 19.7)	32.9 (28.8 - 39.4)	-1.1 (-2.5 to 0.1)	-7.0 (-7.2 to -6.6)	1.1 (0.9 - 1.3)	25.7 (21.0 - 28.7)	1.7 (1.3 - 1.8)	17.9 (17.2 - 19.0)	68.6 (62.4 - 76.0)	-30.3 (-30.9 to -30.1)	2.6 (1.9 - 3.4)	13.4 (12.5 to 14.3)
Intermediate water	21	440 to 475	71.3 (50.1 - 92.6)	21.4 (16.5 - 26.1)	43.9 (40.2 - 47.0)	-2.7 (-2.8 to -2.7)	-6.2 (-6.5 to -5.6)	0.7 (0.7 - 0.8)	16.9 (14.8 - 20.4)	1.1 (1.0 - 1.2)	17.5 (16.3 - 18.7)	64.1 (54.5 - 67.8)	-31.0 (-31.4 to -30.8)	4.0 (3.4 - 4.7)	11.0 (10.0 to 12.3)
	20	475 to 487	83.7 (70.8 - 98.4)	19.2 (17.8 - 20.9)	50.4 (42.7 - 57.8)	-2.6 (-2.6 to -2.6)	-5.7 (-6.1 to -5.4)	0.9 (0.8 - 1.0)	15.5 (14.6 - 17.4)	1.2 (1.1 - 1.3)	16.0 (15.9 - 16.2)	51.5 (50.8 - 53.1)	-30.5 (-30.7 to -30.2)	4.1 (3.9 - 4.5)	11.5 (11.4 to 11.7)
	19	487 to 518	78.6 (72.4 - 82.5)	23.8 (19.4 - 32.4)	39.9 (35.0 - 44.7)	-2.2 (-2.5 to -1.9)	-6.5 (-6.6 to -6.4)	0.8 (0.7 - 1.0)	17.3 (15.5 - 19.3)	1.3 (1.2 - 1.4)	15.9 (15.9 - 16.0)	60.1 (52.3 - 63.9)	-31.2 (-31.5 to -30.9)	3.9 (3.8 - 4.0)	12.3 (11.8 to 12.7)
	18	518 to 536	67.6 (64.6 - 73.4)	21.1 (20.4 - 22.1)	33.3 (31.1 - 35.0)	-1.2 (-1.5 to -1.1)	-6.3 (-6.4 to -6.3)	1.0 (0.8 - 1.1)	22.0 (20.8 - 23.5)	1.5 (1.5 - 1.7)	15.5 (15.2 - 15.8)	61.7 (60.3 - 62.6)	-30.8 (-31.1 to -30.5)	3.9 (3.8 - 3.9)	11.8 (11.5 to 12.0)
	14	536 to 538	64.3 (64.3 - 64.3)	20.2 (20.2 - 20.2)	30.8 (30.8 - 30.8)	n/a	n/a	1.1 (1.1 - 1.1)	21.4 (21.4 - 21.4)	1.6 (1.6 - 1.6)	15.0 (15.0 - 15.0)	60.1 (60.1 - 60.1)	-31.3 (-31.3 to -31.3)	3.9 (3.9 - 3.9)	11.4 (11.4 to 11.4)
	17	538 to 576	81.1 (43.2 - 123.3)	19.0 (13.0 - 25.4)	43.8 (32.3 - 61.3)	-1.9 (-2.2 to -1.3)	-6.6 (-6.6 to -6.4)	0.8 (0.6 - 1.1)	17.6 (11.8 - 21.9)	1.5 (0.9 - 2.3)	14.8 (12.1 - 18.5)	60.2 (54.3 - 70.9)	-30.5 (-31.5 to -29.3)	4.2 (2.7 - 5.7)	11.5 (10.8 to 12.3)
	16	576 to 584	62.7 (58.3 - 68.4)	25.2 (21.8 - 28.6)	39.2 (37.3 - 41.6)	n/a	n/a	0.7 (0.6 - 0.8)	17.0 (16.6 - 17.2)	1.4 (1.3 - 1.5)	15.5 (15.2 - 15.7)	70.0 (62.8 - 75.1)	-28.1 (-28.7 to -27.8)	2.6 (2.5 - 2.8)	11.4 (11.2 to 11.7)
Shallow water A	14	584 to 586	58.8 (58.8 - 58.8)	22.8 (22.8 - 22.8)	43.0 (43.0 - 43.0)	n/a	n/a	0.7 (0.7 - 0.7)	16.9 (16.9 - 16.9)	1.1 (1.1 - 1.1)	15.9 (15.9 - 15.9)	62.3 (62.3 - 62.3)	-28.5 (-28.5 to -28.5)	3.1 (3.1 - 3.1)	11.1 (11.1 to 11.1)
	16	586 to 588	35.4 (35.4 - 35.4)	30.5 (30.5 - 30.5)	39.6 (39.6 - 39.6)	n/a	n/a	0.9 (0.9 - 0.9)	16.8 (16.8 - 16.8)	1.1 (1.1 - 1.1)	16.1 (16.1 - 16.1)	51.7 (51.7 - 51.7)	-29.6 (-29.6 to -29.6)	3.1 (3.1 - 3.1)	10.9 (10.9 to 10.9)
	14	588 to 592	47.3 (42.5 - 52.1)	22.0 (18.9 - 25.0)	44.0 (42.9 - 45.0)	n/a	n/a	0.9 (0.9 - 0.9)	16.3 (16.1 - 16.5)	1.1 (1.1 - 1.2)	16.1 (16.1 - 16.1)	47.6 (47.0 - 48.1)	-29.4 (-30.0 to -28.8)	2.8 (2.6 - 3.0)	10.6 (10.6 to 10.7)
	16	592 to 600	51.1 (46.4 - 61.0)	22.4 (20.7 - 24.3)	41.2 (36.9 - 45.2)	n/a	n/a	0.9 (0.8 - 0.9)	15.4 (15.2 - 15.7)	1.2 (1.1 - 1.3)	16.4 (16.1 - 16.8)	52.4 (50.9 - 53.7)	-28.6 (-29.6 to -27.9)	2.4 (2.2 - 2.7)	10.2 (10.0 to 10.4)
	15	600 to 620	65.1 (48.8 - 75.6)	23.3 (19.4 - 25.6)	39.3 (34.6 - 43.9)	-1.7 (-2.0 to -1.3)	-6.3 (-6.3 to -6.3)	1.0 (0.8 - 1.1)	18.6 (16.2 - 20.5)	1.2 (0.8 - 1.5)	18.0 (14.8 - 22.6)	56.3 (54.2 - 58.1)	-29.4 (-29.8 to -28.9)	4.0 (3.1 - 4.8)	9.7 (8.1 to 11.1)
	14	620 to 623	37.6 (34.3 - 40.9)	17.0 (16.3 - 17.7)	42.2 (38.0 - 46.3)	n/a	n/a	1.2 (1.2 - 1.2)	20.1 (18.7 - 21.5)	1.2 (1.2 - 1.2)	19.1 (19.0 - 19.1)	52.3 (52.0 - 52.6)	-31.9 (-32.3 to -31.5)	4.9 (4.9 - 5.0)	9.4 (9.3 to 9.5)
	13	623 to 626	31.7 (31.7 - 31.7)	15.6 (15.6 - 15.6)	51.6 (51.6 - 51.6)	n/a	n/a	0.7 (0.7 - 0.7)	17.0 (17.0 - 17.0)	1.2 (1.2 - 1.2)	19.2 (19.2 - 19.2)	53.2 (53.2 - 53.2)	-31.2 (-31.2 to -31.2)	5.0 (5.0 - 5.0)	9.2 (9.2 to 9.2)

Table 7.1 continued

Facies	Depth Interval (cm)	Mag. Sus.	Mineralogical content	CaCO <sub>3</sub> (wt%)	$\delta^{13}\text{C}_{\text{carb}}$ (‰)	$\delta^{18}\text{O}_{\text{carb}}$ (‰)	TS wt%	TOC wt%	TON wt%	C:N	C:S	$\delta^{13}\text{C}_{\text{org}}$ (‰)	$\delta^{15}\text{N}_{\text{org}}$ (‰)	$\delta^{34}\text{S}_{\text{org}}$ (‰)
12	626 to 639	36.3 (27.6 - 42.6)	15.6 (14.1 - 16.4)	45.2 (40.9 - 50.1)	-5.0 (-5.3 to -4.6)	-6.3 (-6.3 to -6.3)	1.0 (0.5 - 1.1)	20.1 (18.2 - 21.3)	1.2 (1.2 - 1.2)	19.5 (19.3 - 19.6)	64.4 (50.2 - 124.2)	-30.6 (-30.9 to -30.3)	5.0 (4.8 - 5.0)	9.4 (9.2 to 9.8)
11	639 to 668	12.2 (5.3 - 24.4)	8.8 (4.9 - 12.6)	54.3 (52.5 - 55.5)	-4.6 (-5.2 to -3.9)	-6.3 (-6.4 to -6.3)	1.0 (0.8 - 1.1)	20.4 (18.0 - 23.1)	1.3 (1.2 - 1.4)	18.9 (17.7 - 19.5)	59.2 (51.8 - 62.8)	-31.7 (-32.1 to -31.2)	4.4 (4.3 - 4.7)	9.5 (8.7 to 10.1)
9	668 to 680	11.2 (7.2 - 14.3)	5.8 (4.0 - 7.0)	53.6 (51.6 - 57.8)	n/a	n/a	1.1 (0.9 - 1.1)	22.6 (19.9 - 23.7)	1.5 (1.3 - 1.7)	16.9 (16.3 - 17.5)	58.1 (56.5 - 59.3)	-32.2 (-32.3 to -32.1)	4.3 (4.2 - 4.3)	8.8 (8.7 to 9.2)
10	680 to 740	10.3 (6.8 - 15.1)	7.7 (6.0 - 12.3)	59.7 (51.9 - 65.5)	-5.5 (-6.0 to -5.1)	-6.6 (-6.8 to -6.4)	0.9 (0.8 - 1.1)	17.5 (14.5 - 19.9)	1.3 (1.1 - 1.4)	16.5 (15.2 - 17.9)	52.2 (51.3 - 55.7)	-32.0 (-32.3 to -31.8)	4.1 (3.2 - 4.6)	10.1 (8.1 to 12.1)
9	740 to 772	18.2 (10.6 - 24.9)	15.0 (13.1 - 22.6)	43.2 (39.0 - 50.2)	-5.7 (-5.9 to -5.4)	-7.1 (-7.3 to -6.9)	1.2 (1.0 - 1.4)	20.9 (18.7 - 23.4)	1.3 (1.2 - 1.4)	18.1 (18.0 - 18.3)	51.2 (49.4 - 55.0)	-31.4 (-32.1 to -31.0)	3.6 (2.9 - 4.0)	8.9 (8.1 to 10.7)
8	772 to 865	12. (6.7 - 17.7)	13.5 (8.1 - 17.0)	40.6 (33.9 - 51.9)	-5.3 (-5.6 to -5.0)	-7.2 (-7.5 to -6.7)	1.0 (0.8 - 1.2)	22.3 (18.9 - 25.8)	1.4 (1.1 - 1.5)	19.3 (18.4 - 19.6)	64.9 (55.6 - 75.7)	-31.8 (-32.4 to -31.0)	3.5 (1.8 - 5.3)	10.0 (6.9 to 11.7)
7	865 to 960	14.9 (7.0 - 32.1)	13.4 (6.7 - 20.9)	47.2 (39.7 - 52.8)	-5.2 (-5.7 to -3.6)	-7.3 (-7.6 to -6.8)	0.8 (0.7 - 1.0)	19.8 (17.6 - 23.7)	1.1 (1.0 - 1.3)	20.7 (18.9 - 23.6)	68.3 (55.2 - 87.1)	-31.6 (-32.4 to -31.0)	5.0 (4.1 - 5.8)	9.5 (7.5 to 11.1)
6	960 to 980	6.7 (6.4 - 7.1)	9.0 (7.5 - 10.1)	54.6 (52.5 - 56.3)	-5.9 (-6.2 to -5.5)	-7.2 (-7.2 to -7.1)	0.8 (0.8 - 0.8)	19.1 (17.1 - 20.8)	1.2 (1.1 - 1.3)	19.3 (18.9 - 19.5)	68.9 (62.5 - 76.9)	-32.7 (-32.7 to -32.6)	5.1 (4.9 - 5.3)	7.2 (6.5 to 8.2)
5	980 to 990	6.7 (6.1 - 7.1)	10.1 (10.1 - 10.2)	56.1 (55.1 - 56.6)	-5.4 (-5.8 to -5.1)	-6.9 (-7.0 to -6.9)	0.8 (0.8 - 0.8)	16.6 (16.4 - 16.8)	1.0 (1.0 - 1.0)	18.4 (18.3 - 18.7)	57.9 (55.7 - 60.6)	-33.0 (-33.1 to -32.8)	5.1 (4.9 - 5.3)	6.6 (6.5 to 6.7)
4	990 to 1040	7.2 (4.4 - 12.2)	10.6 (9.5 - 11.9)	57.2 (52.3 - 61.4)	-5.6 (-6.1 to -5.4)	-6.6 (-6.8 to -6.3)	0.9 (0.9 - 1.0)	16.8 (15.9 - 18.8)	1.1 (1.0 - 1.2)	18.5 (18.3 - 18.6)	52.0 (50.3 - 54.9)	-32.5 (-32.9 to -31.9)	5.8 (5.4 - 6.1)	6.6 (5.5 to 7.5)
3	1040 to 1065	14.6 (12.5 - 17.7)	10.0 (9.5 - 11.1)	51.9 (49.9 - 54.7)	-5.3 (-5.4 to -5.3)	-6.2 (-6.2 to -6.1)	1.2 (1.0 - 1.4)	20.4 (19.5 - 21.0)	1.3 (1.2 - 1.3)	18.6 (18.5 - 18.9)	48.3 (42.1 - 52.0)	-33.0 (-33.8 to -32.3)	4.8 (4.2 - 5.3)	7.1 (6.3 to 7.5)
4	1065 to 1100	31.7 (20.8 - 40.7)	13.0 (10.7 - 14.3)	52.9 (48.6 - 55.0)	-5.1 (-5.2 to -5.0)	-7.4 (-8.2 to -6.5)	0.9 (0.6 - 1.3)	18.3 (17.0 - 20.1)	1.0 (0.9 - 1.3)	21.4 (19.1 - 22.8)	65.8 (41.9 - 83.7)	-31.9 (-32.9 to -31.6)	3.1 (2.5 - 4.1)	9.6 (4.9 to 13.0)
3	1100 to 1250	33.6 (22.5 - 58.8)	13.6 (10.4 - 16.7)	52.7 (43.7 - 60.2)	-5.5 (-6.0 to -5.2)	-7.5 (-8.1 to -6.6)	0.7 (0.6 - 1.3)	17.6 (15.3 - 19.3)	1.0 (0.9 - 1.1)	21.2 (19.9 - 21.8)	71.1 (45.1 - 88.3)	-31.9 (-32.6 to -31.2)	3.8 (3.0 - 5.1)	8.5 (1.2 to 13.2)
1	1250 to 1278	50.3 (47.4 - 52.7)	15.6 (14.9 - 16.4)	49.5 (45.2 - 53.4)	-5.5 (-5.5 to -5.5)	-8.1 (-8.1 to -8.0)	0.7 (0.5 - 1.1)	16.6 (15.0 - 19.0)	1.0 (0.8 - 1.1)	20.7 (20.4 - 21.0)	75.5 (46.3 - 84.0)	-31.7 (-31.9 to -31.6)	2.8 (2.8 - 2.9)	11.2 (10.6 to 11.6)
2	1278 to 1284	56.1 (55.0 - 56.7)	14.9 (14.8 - 14.9)	51.2 (50.4 - 52.1)	n/a	n/a	0.7 (0.6 - 0.7)	15.9 (15.3 - 16.2)	1.0 (0.9 - 1.0)	20.3 (20.3 - 20.3)	69.8 (63.0 - 77.1)	-32.0 (-32.0 to -32.0)	2.8 (2.8 - 2.9)	11.1 (10.9 to 11.3)
1	1284 to 1306	41.9 (31.5 - 54.7)	16.1 (15.0 - 17.0)	49.8 (48.4 - 53.3)	-5.5 (-5.6 to -5.5)	-7.9 (-8.0 to -7.9)	0.6 (0.6 - 0.7)	17.8 (14.6 - 26.6)	1.0 (0.8 - 1.3)	20.2 (20.2 - 20.3)	76.3 (64.6 - 106.6)	-32.1 (-32.5 to -32.0)	3.0 (2.9 - 3.2)	10.3 (9.5 to 10.8)
2	1306 to 1313	30.2 (29.7 - 31.0)	17.0 (16.9 - 17.0)	52.2 (50.1 - 53.7)	n/a	N/a	0.7 (0.7 - 0.7)	15.7 (15.3 - 16.1)	1.0 (1.0 - 1.0)	20.4 (20.3 - 20.4)	63.5 (61.1 - 66.0)	-32.4 (-32.5 to -32.2)	3.3 (3.2 - 3.4)	8.6 (8.0 to 9.2)
1	1313 to 1350	41.0 (30.0 - 65.0)	14.8 (13.7 - 16.8)	48.2 (46.6 - 49.2)	-5.6 (-5.6 to -5.6)	-7.8 (-7.8 to -7.8)	0.8 (0.7 - 0.8)	18.3 (16.0 - 25.9)	1.0 (1.0 - 1.0)	20.6 (20.4 - 20.8)	68.0 (59.4 - 81.6)	-31.8 (-32.0 to -31.5)	3.0 (2.6 - 3.4)	9.8 (7.5 to 11.8)

High water A

$\delta^{13}\text{C}_{\text{carb}}$  values (Dean 1981; Wolfe *et al* 1999; Dean 2002; McFadden *et al* 2005; Talbot *et al* 2006). The decreasing  $\delta^{15}\text{N}_{\text{ORG}}$  in concord with the increasing  $\delta^{34}\text{S}_{\text{ORG}}$  values may indicate less anoxic conditions (Watanabe *et al* 2004). However the lower  $\delta^{15}\text{N}_{\text{ORG}}$  values may also indicate an increased amount of algal organic matter (Muzuka *et al* 2004), likewise a relatively abundant supply of nitrogen favours maximum  $^{15}\text{N}$  discrimination yielding low  $\delta^{15}\text{N}_{\text{ORG}}$  values (Routh *et al* 2004; Talbot *et al* 2006). The increased organic productivity is probably a result of an increased inflow of nutrients as suggested by the increasing SUS values. Therefore the minor decrease in the  $\text{CaCO}_3$  may be due to volumetric changes in the fractions of the TOC, TON and  $\text{CaCO}_3$  content. However the lower  $\text{CaCO}_3$  in combination with the increasing TOC values may alternatively be explained by increased primary productivity resulting in increased decomposition of dead organic matter consuming all available oxygen resulting in elevated concentrations of  $\text{CO}_2$  in the hypolimnion. The consequently lower pH values in the hypolimnion results in dissolution of the biogenic induced  $\text{CaCO}_3$  (Dean 1999). The C:N values are low and indicates a high fraction of autochthonous organic matter. The slowly decreasing  $\delta^{18}\text{O}_{\text{carb}}$  values may likely indicate a slightly lower E/I ratio (Kirby *et al* 2004; Hammarlund *et al* 2005). A lower E/I ratio is most likely due to an increased water inflow and thereby increased nutrient supply.

*Depth interval iii)* The constant SUS values are likely to reflect a relatively constant amount of allochthonous eroded material whereas the increasing mineralogical content may indicate an increasing amount of allochthonous eroded material. The elevated and very slowly increasing C:N and C:S values suggests a slightly increasing amount of allochthonous organic matter (Meyers and Teranes 2001; Meyers 2006), which together with the constant and somewhat elevated SUS values are likely to indicate an increasing proximity to the littoral zone or an increasing influx of allochthonous material. The decreasing  $\text{CaCO}_3$  content may be due to volumetric changes in other parameters whereas the increasing  $\delta^{13}\text{C}_{\text{ORG}}$ ,  $\delta^{13}\text{C}_{\text{carb}}$  and  $\delta^{15}\text{N}_{\text{ORG}}$  values are most likely to indicate an increasing organic productivity in concord with the increasing TOC values (Wolfe *et al* 1999; McFadden *et al* 2005; Talbot *et al* 2006). An increasing organic productivity is likely a consequence of increasing nutrient supply which is in accordance with the decreasing E/I ratio (Kirby *et al* 2004; Hammarlund *et al* 2005) as a probably result of increased water inflow as viewed by the decreasing  $\delta^{18}\text{O}_{\text{carb}}$  values.

*Facies 2 (1313 cm to 1306 cm and 1284 cm to 1278 cm):* A dark brown medium grained detritus gyttja with indistinct calcareous lamina. This facies occurs in two depth intervals: i) 1313 cm to 1306 cm and ii) 1284 cm to 1278 cm. This unit is deposited in beds of a thickness up to 7 cm. A SMEAR slide revealed microscopic amounts of organic material of terrestrial origin in the lamina dark bands. The lighter bands are fine grained calcareous particles. This deposit is illustrated in 7-11.

*Geochemistry and physical properties:* The SUS values are i) 30 and ii) 56. The mineralogical content values are i) 17 wt% and ii) 15 wt%. The  $\text{CaCO}_3$  content is increasing whereas the TS, TOC and TON values are decreasing. The C:N ratio is constant and the C:S values are slowly increasing. The  $\delta^{13}\text{C}_{\text{ORG}}$  values are i) decreasing and ii) increasing. The  $\delta^{15}\text{N}_{\text{ORG}}$  values are decreasing and the  $\delta^{34}\text{S}_{\text{ORG}}$  values are increasing. See Table 7.1 and Figure 7-2 for details.

*Interpretation:* The fine grain size of the calcareous material indicates a low energy deposits and thus formation in deep water. The deposit is thus likely formed from suspension in the profundal zone (*see Figure 5-1*). Increased influx of terrestrial organic matter, warmer lake temperatures, increased water depth, prolonged ice free period or increased shelter (*reduced fetch*) may all lead to more stable summer stratification (Wolfe *et al* 1999). The indistinct lamina are likely indicating succeeding deposits of summer bio-induced calcium carbonate and winter decomposed organic material from the lake environment. The microscopic amounts of terrestrial organic debris suggest a reduced proximity to the littoral zone. This may have been caused by a lake level still stand or by a transgression flooding the lake shores. The geochemical data of this facies are few and furthermore this facies is interspersed in between facies 1. The

geochemical parameters all display a continuation of trends observed for the facies below. The interpretation of this facies is therefore made in relation to the deduced interpretation of facies 1. The development of an anoxic hypolimnion at 1313 cm prior to facies 2 is supportive of the formation of lamination as bioturbation is not likely to occur during heavy anoxic conditions limiting the spread of bottom scavengers. Thus the termination of the lower depth interval i) probably marks the onset of the flooding the lake shore area. In contrast the upper part ii) probably reflects a continuation of increased water inflow.

*Facies 3 (1250 cm to 1100 cm and 1065 cm to 1040 cm):* A fine grained humified dark brown detritus gyttja of thickness of up to 1.5 metres. This facies occurs in two depths intervals i) 1250 cm to 1100 cm and ii) 1065 cm to 1040 cm. Scattered and unsystematic calcareous coating fragments from the near shore marginal vegetation or stones are observed. Microscopic fragments of terrestrial organic material. Minor shell fragments of juvenile gastropods are found at 1210 cm lumped in thin patches up to 2 cm wide. For the upper section (1040 cm to 1065 cm) no calcareous crusts are observed and the vast majority of organic material is of limnic origin. Microscopically high amounts of charcoal were found and smaller fraction of terrestrial organic material. This deposit is illustrated in Figure 7-12.

*Geochemistry):* i) The SUS values and mineralogical content are decreasing with a superimposed peak between 1191 cm and 1139 cm with maximum values occurring around 1160 cm. The  $\text{CaCO}_3$  content is increasing from 45 wt% to 60 wt%. The  $\delta^{13}\text{C}_{\text{carb}}$  values are constant up to 1170 cm where they steeply increase. From 1150 cm the  $\delta^{13}\text{C}_{\text{carb}}$  values decreases and then increases again from 1130 cm. The  $\delta^{18}\text{O}_{\text{carb}}$  values are increasing. The TS values are constant up to 1160 cm where after they increase. The TOC values are constant up to 1200 cm and decreases up to 1160 cm from where they again are constant. The TON values are slowly decreasing. The C:N values are constant up to 1160 cm and decreases. The C:S and  $\delta^{34}\text{S}_{\text{ORG}}$  values are constant up to 1160 cm and then decreases until 1150 cm from where they are again constant. The  $\delta^{13}\text{C}_{\text{ORG}}$  values are decreasing with a peak occurring between 1191 cm and 1139 cm. The maximum  $\delta^{13}\text{C}_{\text{ORG}}$  peak values occurs around 1160 cm. The  $\delta^{15}\text{N}_{\text{ORG}}$  values are constant up to 1160 cm, from where they are increasing. See Table 7.1 and Figure 7-2 for details.

ii) The SUS values are decreasing and the mineralogical content show constant to slightly increasing values. The  $\text{CaCO}_3$  show a rapid decrease. The  $\delta^{13}\text{C}_{\text{carb}}$  and  $\delta^{18}\text{O}_{\text{carb}}$  values are slowly decreasing. The TS values are decreasing and the TOC and TON values display a peak with maximum values occurring around 1053 cm. The C:N ratio is constant at 19 and the C:S ratio at 49. The  $\delta^{13}\text{C}_{\text{ORG}}$  values are decreases and approaches -34‰. At 1050 cm a rapid increase followed by constant  $\delta^{13}\text{C}_{\text{ORG}}$  values is observed. The  $\delta^{15}\text{N}_{\text{ORG}}$  values are increasing. The  $\delta^{34}\text{S}_{\text{ORG}}$  values are decreasing from 7.5‰ to 6.3‰. See Table 7.1 and Figure 7-2 for details.

*Interpretation:* The fine grain size of this deposit suggests a suspension deposit in a low energy environment, which is supported by the uniformity of this facies. The small and scattered amounts of macrofossil organic material, molluscs and shells suggest that this deposit is most likely formed in the upper profundal zone or sub-littoral zone (see Figure 5-1). The C:N mean value of 20 and the C:S mean value of 68 (see Table 7.1) indicate a mixed origin of the organic matter likely with a majority of autochthonous organic matter (Meyers and Teranes 2001; Meyers 2006). The general decreasing SUS values and mineralogical content are likely related to a decreasing amount of allochthonous eroded material.

*Depth interval i):* The decreasing TOC, TON and  $\delta^{13}\text{C}_{\text{ORG}}$  values are probably related to a decreasing organic productivity (McFadden *et al* 2005; Talbot *et al* 2006). The slightly elevated and constant C:N and C:S values up to 1175 cm most probably are related to a somewhat higher fraction of allochthonous organic matter succeeded by a high autochthonous organic matter content for the upper part. The slowly decreasing TOC and TON values may represent volumetric changes due to a slightly increasing  $\text{CaCO}_3$  content. The scattered and unsystematic calcareous grain distribution is most likely small accumulations of bioinduced carbonate washed out from the lake shore. The calcareous peels may likely have been transported by wave or current action and then deposited in deeper waters. However the lumped juvenile gastropods may also be due to out washed material caused by wave activity in the vegetation zone.

Note that the minor peak in both the SUS values and the mineralogical occurring around 1160 cm is likely to be related to a minor increase in allochthonous eroded material as also in-

indicated by the minor increase in the  $\delta^{13}\text{C}_{\text{ORG}}$  and  $\delta^{13}\text{C}_{\text{carb}}$  values during the period of elevated SUS value. This minor event seems to have a great impact on the lake hydrology as observed by the increasing TS,  $\delta^{15}\text{N}_{\text{ORG}}$ , and  $\delta^{18}\text{O}_{\text{carb}}$  values, furthermore the  $\delta^{34}\text{S}_{\text{ORG}}$  values rapidly decrease to a lower level together with somewhat lower C:N and C:S values. The combined elevated  $\delta^{15}\text{N}_{\text{ORG}}$  and TS values and lower  $\delta^{34}\text{S}_{\text{ORG}}$  values may indicate sulphate reduction bacteria and ammonia volatilisation or denitrification which further may suggest the development of prolonged periods of hypolimnion anoxia (Watanabe *et al* 2004; Eimers *et al* 2006). The increasing  $\delta^{18}\text{O}_{\text{carb}}$  values may indicate an increasing E/I ratio (Kirby *et al* 2004; Hammarlund *et al* 2005) possibly due to increased evaporation or a decreased water inflow. This combined with the development of prolonged periods of anoxia most likely is related to a decreased water inflow and perhaps a somewhat warmer climate. A warmer climate may also have resulted in an increased chemical precipitation of  $\text{CaCO}_3$  which potentially may explain the increasing  $\text{CaCO}_3$  content despite the decreasing organic productivity.

*Depth interval ii):* The increasing  $\delta^{13}\text{C}_{\text{ORG}}$ ,  $\delta^{15}\text{N}_{\text{ORG}}$  and TOC values are likely indicating an increased organic productivity due to an increased inflow of nutrients (McFadden *et al* 2005; Talbot *et al* 2006). However the decreasing  $\delta^{34}\text{S}_{\text{ORG}}$  values and increasing  $\delta^{15}\text{N}_{\text{ORG}}$  values may in combination also suggest the formation of somewhat increased anoxic conditions (Watanabe *et al* 2004; Eimers *et al* 2006). The very low  $\delta^{13}\text{C}_{\text{ORG}}$  values may be due to increased methanogenesis as suggested by the anoxic bottom conditions (Teranes and Bernasconi 2005). However abundant  $\text{CO}_2$  production from decomposing organic matter produced a very low DIC and a high partial  $\text{CO}_2$  pressure which favours large kinetic fractionation during photosynthesis yielding low  $\delta^{13}\text{C}_{\text{ORG}}$  values (Talbot *et al* 2006). In turn the very low  $\delta^{13}\text{C}_{\text{ORG}}$  values may derive from the addition of light DIC from decomposed terrestrial organic material (Dean 1999; Wolfe *et al* 1999). The constant  $\delta^{18}\text{O}_{\text{carb}}$  values may suggest an unchanging E/I ratio (Kirby *et al* 2004; Hammarlund *et al* 2005).

*Facies 4 (1100 cm to 1065 cm and 1040 cm to 990 cm):* A fine grained light brown calcareous gyttja deposited in beds of around 50 cm in thickness. This facies occurs in two depth intervals: i) 1100 cm to 1065 cm and ii) 1040 cm to 990 cm. This unit is a homogeneous deposit with a gradual grain coarsening and colour lightning upwards. Microscopically an increasing amount of small calcareous grains and frequently small fragments of terrestrial organic material have been observed. At the depth of 992 cm a mollusc shell assembly of broken shells with diameters around 1 cm was found.

*Geochemistry and physical properties:* i) The SUS values are increasing with a fall at 1080 cm and the mineralogical content shows a broad peak between 1100 cm and 1080 cm. The  $\text{CaCO}_3$  content are increasing and the  $\delta^{13}\text{C}_{\text{carb}}$  values are constant. The  $\delta^{18}\text{O}_{\text{carb}}$  values display a decreasing trend up to 1080 cm and then increasing values. The TS values slowly decrease until 1082 cm, here after they are increasing. The TOC and TON values are elevated up to 1192 cm, then follows a rapid fall. From 1080 cm the TOC and TON values are increasing. The C:N values are slowly decreasing up to 1092 cm, then follows an interval between 1094 cm to 1080 cm with very elevated values. From 1080 cm an abrupt fall is observed followed by decreasing C:N values. The C:S values are elevated between 1100 cm and 1080 cm, here after the C:S values decrease. The  $\delta^{13}\text{C}_{\text{ORG}}$  values are constant with a rapid fall at 1070 cm. The  $\delta^{15}\text{N}_{\text{ORG}}$  values are increasing and the  $\delta^{34}\text{S}_{\text{ORG}}$  values display high values up to 1080 cm and then decreasing values. See Table 7.1 and Figure 7-2.

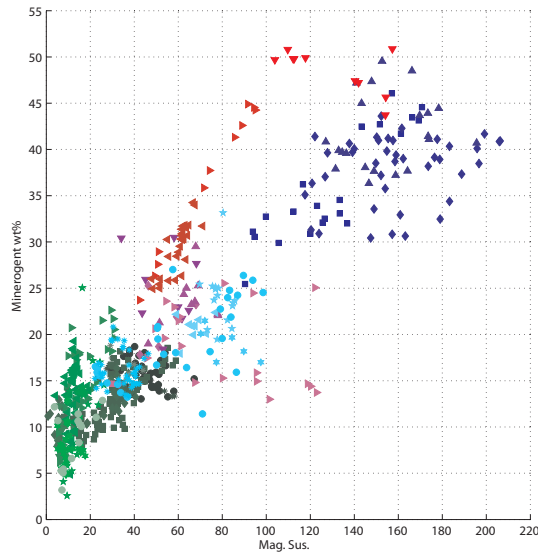


**Figure 7-3:** Magnetic susceptibility versus mineralogical content (for legend see opposite page).

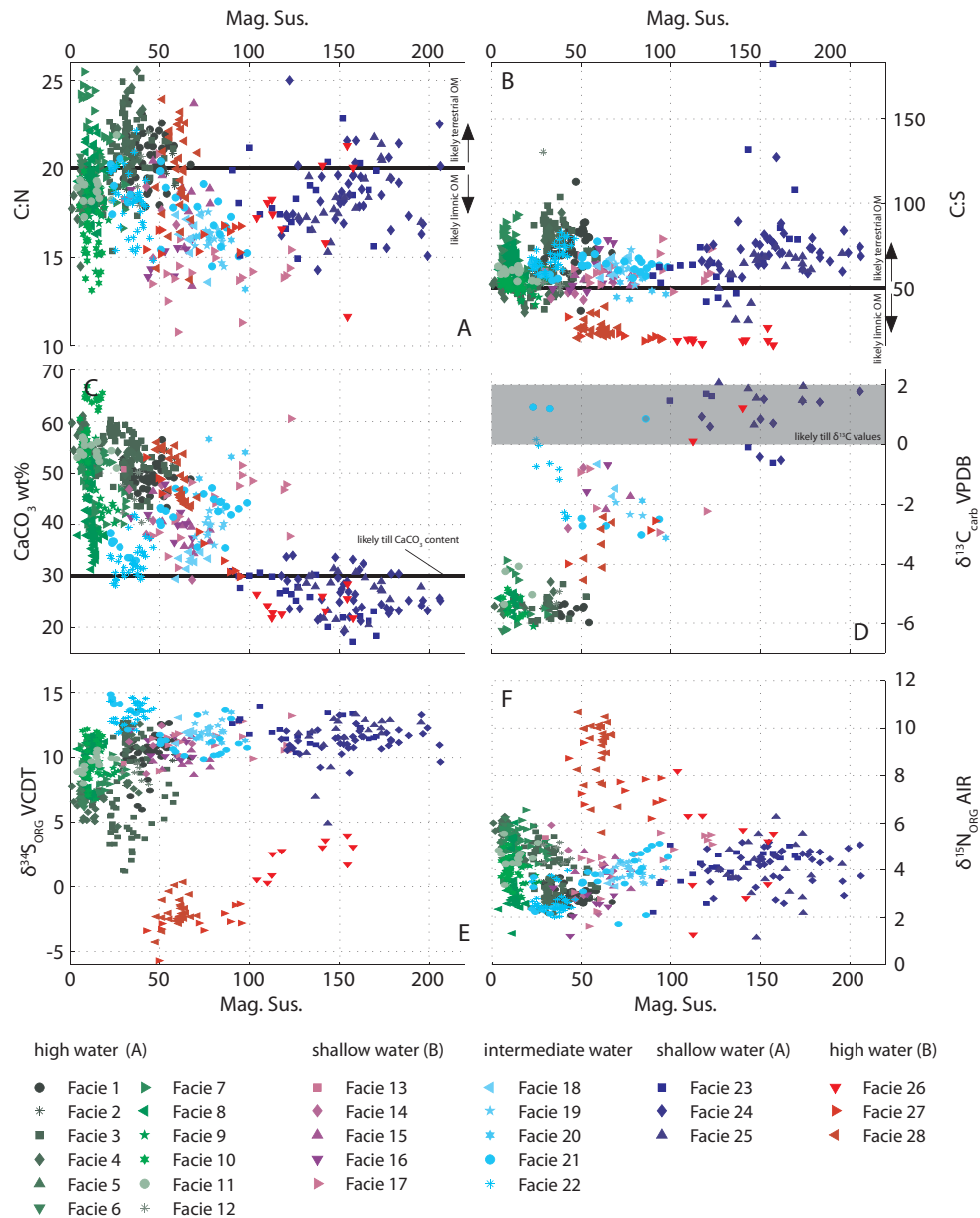


**Figure 7-4:** Scatter plots of magnetic susceptibility versus A) C:N (values above solid line are likely derived from terrestrial sources), B) C:S (values above solid line are likely derived from terrestrial sources), C)  $\text{CaCO}_3$  (solid line represent till  $\text{CaCO}_3$  content), D)  $\delta^{13}\text{C}_{\text{carb}}$  (grey shaded area represent likely till  $\delta^{13}\text{C}_{\text{carb}}$  values), E)  $\delta^{34}\text{S}_{\text{ORG}}$  and F)  $\delta^{15}\text{N}_{\text{ORG}}$ .

ii) The SUS values and the mineralogical content are decreasing. The  $\text{CaCO}_3$  is increasing up to 1020 cm from where the  $\text{CaCO}_3$  content is constant. The  $\delta^{13}\text{C}_{\text{carb}}$  values are constant and the  $\delta^{18}\text{O}_{\text{carb}}$  values are slowly decreasing. The TS values are slowly decreasing. The TOC and TON values are steeply decreasing until 1026 cm from where they slowly increase. The C:N and C:S ratio is constant. The  $\delta^{13}\text{C}_{\text{ORG}}$  values are decreasing and the  $\delta^{15}\text{N}_{\text{ORG}}$  and  $\delta^{34}\text{S}_{\text{ORG}}$  values are increasing. See Table 7.1 and Figure 7-2.

*Interpretation:* The homogeneity and fine grain size suggest a suspension deposit in a low energy environment below wave base. The calcareous grains are probably biogenically induced by limnic organic productivity, but may also be out washed calcium carbonate grains from surrounding tills. The increasing amount of microscopic organic material indicates an increased proximity to the littoral zone suggesting that this unit is most likely deposited in the upper profundal zone (see Figure 5-1). The increased SUS values of depth interval i) are likely to indicate a higher amount of allochthonous eroded material whereas the lower values of the upper

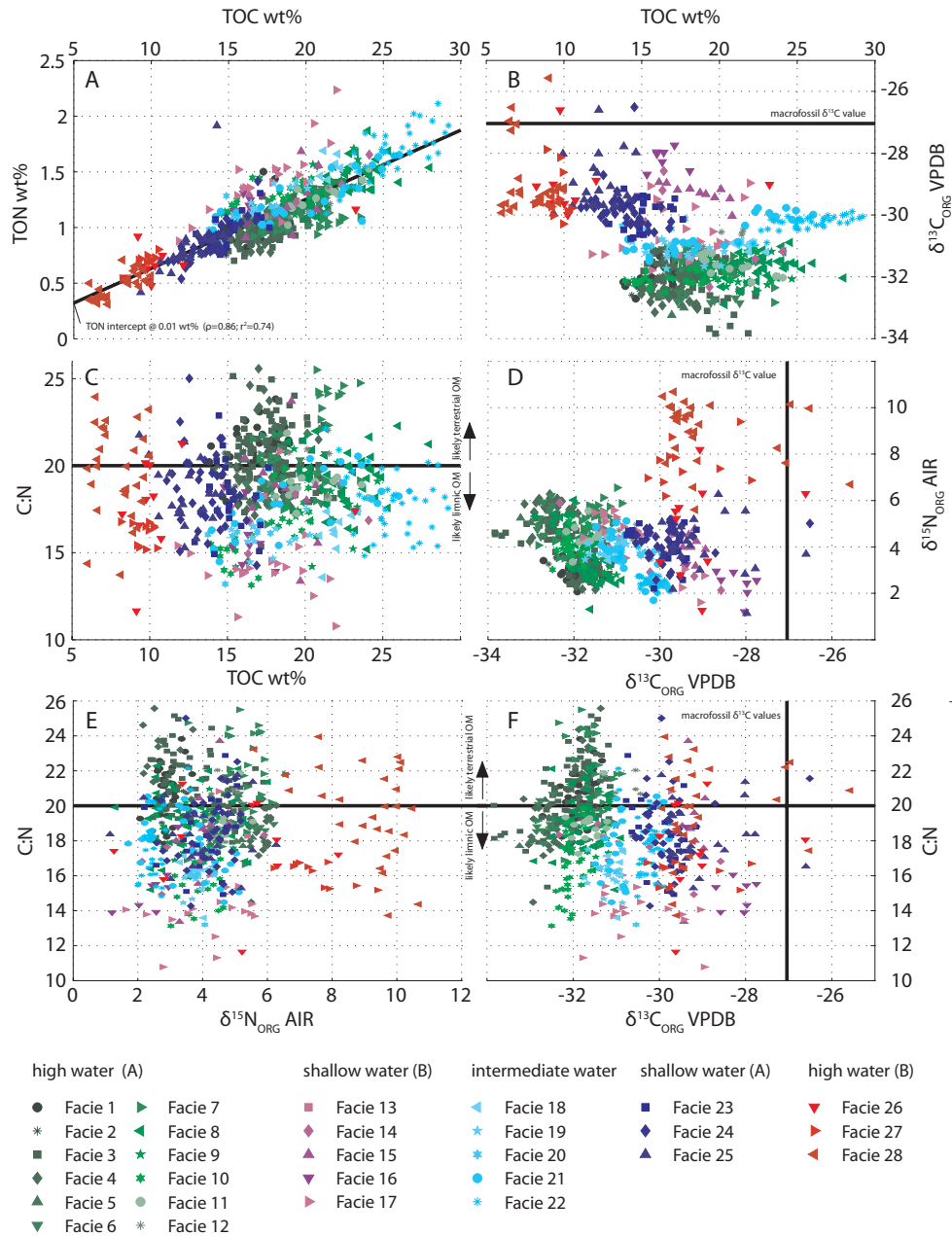


**Figure 7-5:** Scatter plots **A)** TOC versus TON. **B)** TOC versus  $\delta^{13}\text{C}_{\text{ORG}}$  (solid line represents average value of terrestrial macrophyte samples see Table 6.2), **C)** TOC versus C:N (values above solid line are likely derived from terrestrial sources), **D)**  $\delta^{13}\text{C}_{\text{ORG}}$  versus  $\delta^{15}\text{N}_{\text{ORG}}$ , **E)**  $\delta^{15}\text{N}_{\text{ORG}}$  versus C:N and **F)**  $\delta^{13}\text{C}_{\text{ORG}}$  versus C:N.

depth interval ii) indicate a reduced amount of allochthonous eroded material. Likewise this is reflected in the increased C:N and C:S values of the lower depth interval i) indicating an elevated fraction of allochthonous organic matter in contrast to the upper interval indicating a high autochthonous organic matter content (Meyers 1997; Meyers and Teranes 2001; Meyers 2006). Due to these markedly differences the interpretation has been divided according to the depth intervals i) and ii).

*Depth interval i)* The high  $\text{CaCO}_3$  content may indicate a considerable fraction of autochthonous precipitated  $\text{CaCO}_3$  as suggested by the generally increasing TOC and TON values. This may be supported by the elevated  $\delta^{13}\text{C}_{\text{ORG}}$  values (-32.0‰, an increase of about 1‰ relatively to facies 3 below) and the increasing  $\delta^{15}\text{N}_{\text{ORG}}$  values may indicate an increasing organic productivity

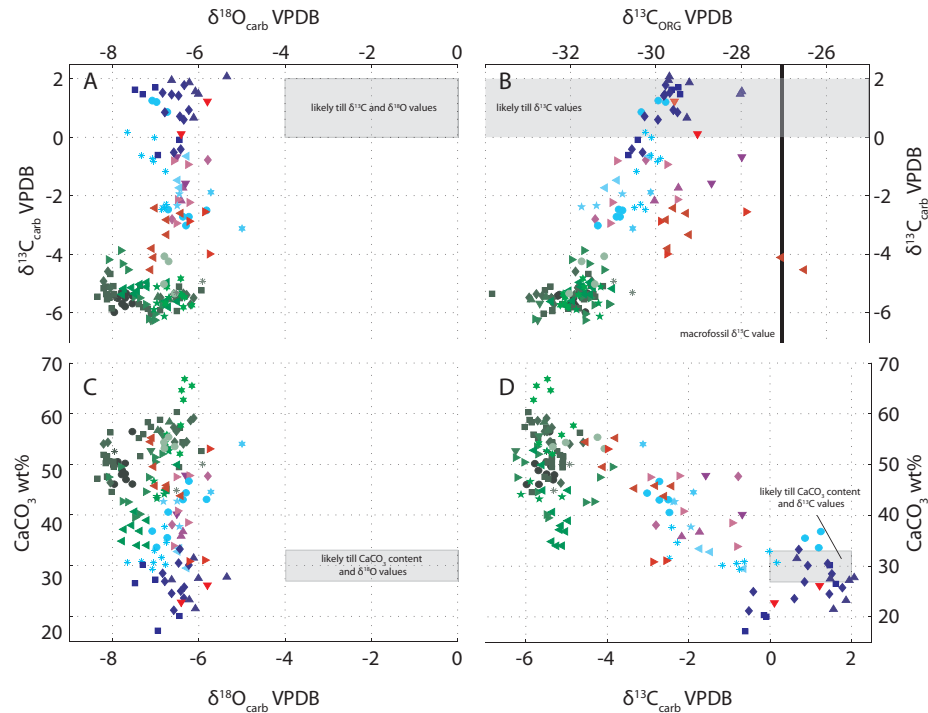


**Figure 7-6:** Scatter plots of **A)**  $\delta^{18}\text{O}_{\text{carb}}$  versus  $\delta^{13}\text{C}_{\text{carb}}$  (grey shaded area represent likely till  $\delta^{13}\text{C}_{\text{carb}}$  and  $\delta^{18}\text{O}_{\text{carb}}$  values), **B)**  $\delta^{13}\text{C}_{\text{ORG}}$  (solid line represents average value of terrestrial macrophyte samples see Table 6.2) versus  $\delta^{13}\text{C}_{\text{carb}}$ , **C)**  $\delta^{18}\text{O}_{\text{carb}}$  versus  $\text{CaCO}_3$  (gray shaded area represent the till  $\text{CaCO}_3$  content and  $\delta^{13}\text{C}_{\text{carb}}$  value) and **D)**  $\delta^{13}\text{C}_{\text{carb}}$  versus  $\text{CaCO}_3$  (gray shaded area represent the till  $\text{CaCO}_3$  content and  $\delta^{18}\text{O}_{\text{carb}}$  value) (legend on opposite page).

(McFadden *et al* 2005; Talbot *et al* 2006). However, the constant and higher  $\delta^{13}\text{C}_{\text{ORG}}$  values may suggest an increase in allochthonous organic matter as observed by the higher  $\delta^{13}\text{C}_{\text{ORG}}$  values of macrofossil organic material (see Figure 7-2, Hammarlund 1993; Lamb *et al* 2006). Towards the end of this interval the  $\delta^{34}\text{S}_{\text{ORG}}$  falls and the  $\delta^{15}\text{N}_{\text{ORG}}$  rises probably indicating the development of anoxic bottom conditions (Watanabe *et al* 2004) and perhaps a deepening of the lake. On the other hand the  $\delta^{34}\text{S}_{\text{ORG}}$  values around 12.5‰ for lower part of this interval concurs with elevated C:S values and may likely reflect a higher  $\delta^{34}\text{S}_{\text{ORG}}$  values of particulate allochthonous organic matter. Thus this period is most likely reflecting an increased or increasing organic productivity and consequently an increased influx of nutrients. This may be supported by the abruptly lower  $\delta^{18}\text{O}_{\text{carb}}$  values most probably indicating a low E/I ratio as a result of increased water inflow.

*Depth interval ii)* The very high  $\text{CaCO}_3$  content is most likely biogenic induced due to organic productivity in the photic zone. The decreasing TOC, TON and  $\delta^{13}\text{C}_{\text{ORG}}$  values most likely indicate a falling organic productivity and hence probably a decreasing nutrient supply (McFadden *et al* 2005; Talbot *et al* 2006). The somewhat lower  $\delta^{34}\text{S}_{\text{ORG}}$  values and higher  $\delta^{15}\text{N}_{\text{ORG}}$  values are likely to reflect anoxic hypolimnion conditions (Watanabe *et al* 2004). The slowly decreasing and elevated  $\delta^{18}\text{O}_{\text{carb}}$  values may suggest minor changes in the E/I ratio (Kirby *et al* 2004; Hammarlund *et al* 2005) and perhaps a somewhat higher inflow relative to evaporation.

*Facies 5 (990 cm to 980 cm):* A very fine grained homogenous massive olive brown algal gyttje with microscopic amounts of very fine grained terrestrial organic material. This unit is about 10 cm in thickness. Fragment remains of insects were observed. This deposit is illustrated in Figure 7-13.

*Geochemistry and physical properties:* The SUS values are increasing and the mineralogical content is constant. The  $\text{CaCO}_3$  content is slowly increasing. The TOC and TON values are constant whereas the TS values are very slowly decreasing. The C:N and C:S values are constant. The  $\delta^{13}\text{C}_{\text{ORG}}$  values are increasing and the  $\delta^{15}\text{N}_{\text{ORG}}$  and  $\delta^{34}\text{S}_{\text{ORG}}$  values are decreasing. See Table 7.1 and Figure 7-2 for details.

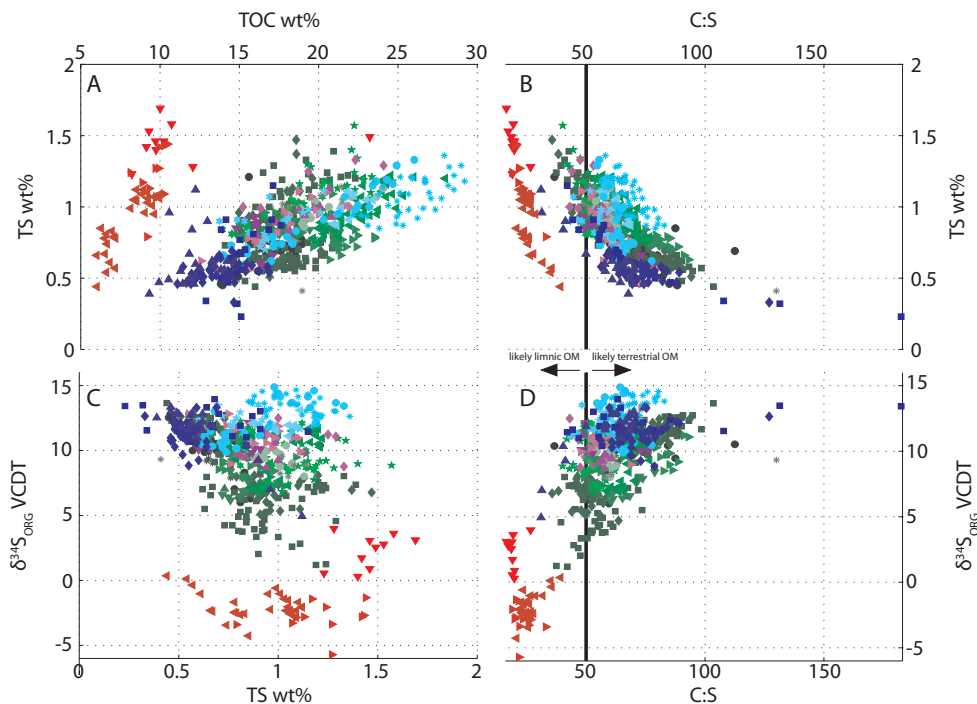


**Figure 7-7:** Scatter plots of **A)** TOC versus TS, **B)** C:S (values above solid line are likely derived from terrestrial sources) versus TS, **C)** TS versus  $\delta^{34}\text{S}_{\text{ORG}}$  and **D)** C:S versus  $\delta^{34}\text{S}_{\text{ORG}}$  (For legend see opposite page).

*Interpretation:* This unit is most likely deposited from suspension in a low energy environment below wave base. The low SUS values and very low mineralogical content is indicating a minor amount of allochthonous eroded material and perhaps an increased distance to the lake shore. The very fine grained and microscopic terrestrial organic matter and algal organic matter suggests that this unit is deposited in the profundal zone or the upper profundal zone (see Figure 5-1). The low and constant C:S and C:N values confirms the autochthonous origin of this deposit. However both the C:N and C:S values are compatible with a minor fraction of allochthonous organic matter (Meyers and Teranes 2001; Lamb *et al* 2006; Meyers 2006). The decreasing TOC, TON and TS values are most likely indicating a decreasing organic productivity perhaps due to a decreased influx of nutrients. This may be supported by the decreasing  $\delta^{15}\text{N}_{\text{ORG}}$  values (McFadden *et al* 2005; Talbot *et al* 2006). In contrast, the increasing  $\delta^{13}\text{C}_{\text{ORG}}$ ,  $\delta^{13}\text{C}_{\text{carb}}$  and  $\text{CaCO}_3$  values may indicate a slowly increasing organic production (Dean 1999; Schwalb 2002; McFadden *et al* 2005) and thereby an increased nutrient influx, which may also be supported by the decreasing  $\delta^{18}\text{O}_{\text{carb}}$  values. The decreasing  $\delta^{18}\text{O}_{\text{carb}}$  values are likely to indicate a decreased E/I ratio (Kirby *et al* 2004; Hammarlund *et al* 2005) most likely related to a higher water inflow as may also be suggested by the increasing SUS values.

*Facies 6 (980 cm to 960 cm):* This deposit consists of a light brown fine grained detritus gyttja. The unit is very homogenous and is slightly and gradually coarsening upwards. It has a thickness of 20 cm. The colour is gradually browning upwards. The deposit is rich in microscopic calcareous particles and is bioturbided. Very scattered small fragments of terrestrial and aquatic organic material of 2x2 mm in size were observed together with microscopic amounts of mainly aquatic organic material.

*Geochemistry and physical properties:* The SUS values are constant whereas the mineralogical content is slowly decreasing. The  $\text{CaCO}_3$  content and the TS values are decreasing. The TOC and TON values are increasing. The C:N values are constant whereas the C:S values are increasing. The  $\delta^{13}\text{C}_{\text{ORG}}$  and  $\delta^{15}\text{N}_{\text{ORG}}$  values are constant whereas the  $\delta^{34}\text{S}_{\text{ORG}}$  values are increasing. See Table 7.1 and Figure 7-2 for details.

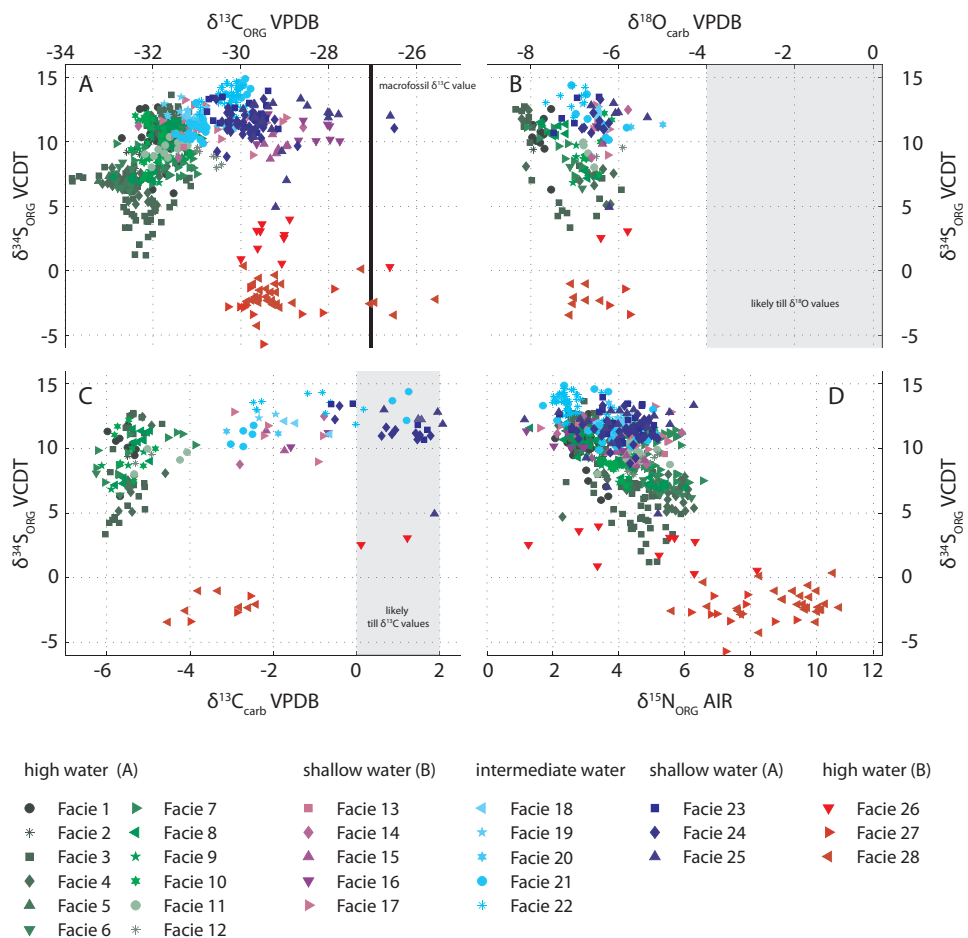


**Figure 7-8:** Scatter plots of A)  $\delta^{13}\text{C}_{\text{ORG}}$  (solid line represents average value of terrestrial macrophyte samples see Table 6.2) versus  $\delta^{34}\text{S}_{\text{ORG}}$ , B)  $\delta^{18}\text{O}_{\text{carb}}$  (gray shaded area represent the till  $\delta^{18}\text{O}_{\text{carb}}$  value) versus  $\delta^{34}\text{S}_{\text{ORG}}$ , C)  $\delta^{34}\text{S}_{\text{ORG}}$  versus  $\delta^{13}\text{C}_{\text{carb}}$  (gray shaded area represent the till  $\delta^{13}\text{C}_{\text{carb}}$  value) and D)  $\delta^{15}\text{N}_{\text{ORG}}$  versus  $\delta^{34}\text{S}_{\text{ORG}}$ .

*Interpretation:* This unit is most likely deposited in a low energy environment below wave base from suspension as suggested by the fine grain size. The low SUS values and mineralogical content indicates a minor fraction of allochthonous eroded material. This unit is likely deposited in the upper profundal zone in closer proximity to the vegetation zone (Figure 5-1) as suggested by the minor amounts of terrestrial and major component of microscopic aquatic material. The C: N values suggest a mixture of allochthonous and autochthonous organic matter whereas the increasing C:S values indicate an increasing fraction of allochthonous organic material in accordance with the sedimentological interpretation (Lamb *et al* 2006; Meyers 2006). The somewhat increased amount of allochthonous organic material may indicate a slightly increased run off from the catchments area. The constant  $\delta^{13}\text{C}_{\text{ORG}}$  and  $\delta^{15}\text{N}_{\text{ORG}}$  values most likely reflect a constant autochthonous organic productivity. In contrast the increasing TOC and TON values may most likely indicate an increasing organic productivity. Less anoxic conditions may be interpreted from the increasing  $\delta^{34}\text{S}_{\text{ORG}}$  values indicative of less bacterial sulphate reduction (Watanabe *et al* 2004; Eimers *et al* 2006). The calcareous material is possibly bio-induced by algal growth or limnic organic productivity. The increasing TOC values and the higher fraction of allochthonous organic matter may indicate an increasing nutrient inflow and hence perhaps a wetter climate which may be further supported by the decreasing  $\delta^{18}\text{O}_{\text{carb}}$  values most likely indicating a decreasing E/I ratio (Kirby *et al* 2004; Hammarlund *et al* 2005) due to an increased water inflow.

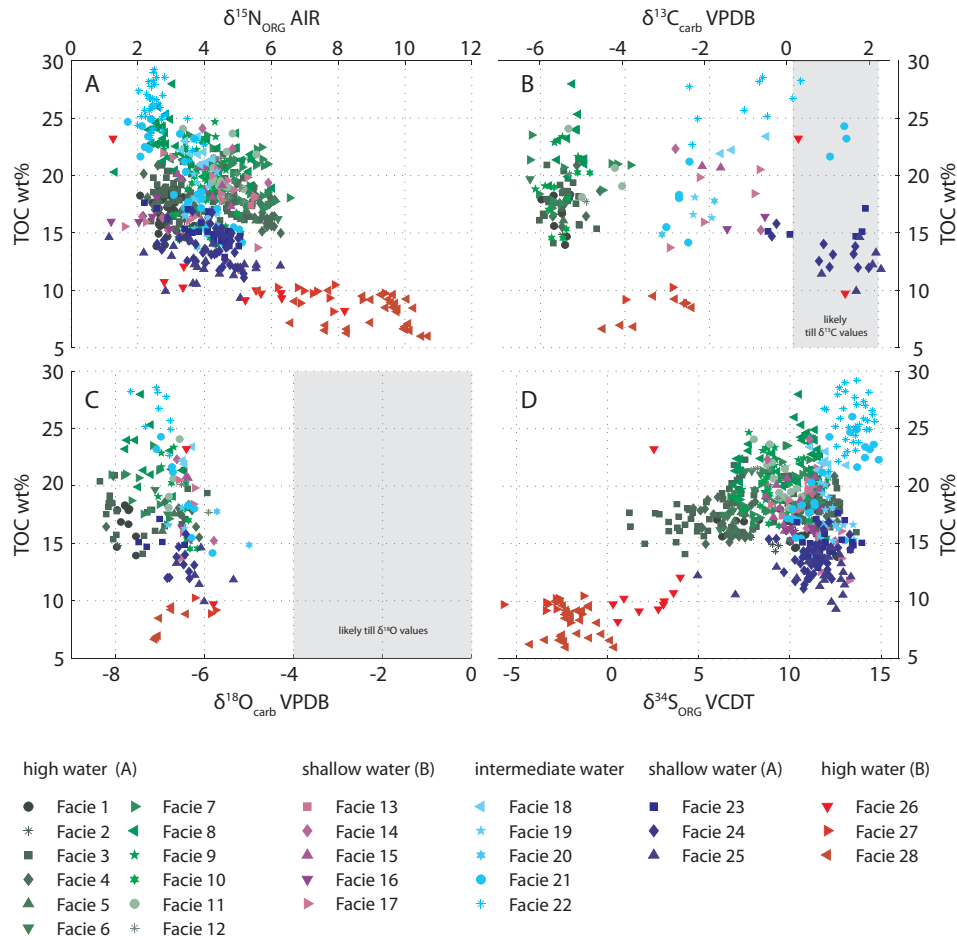


**Figure 7-9:** Scatter plots of **A)**  $\delta^{15}\text{N}_{\text{ORG}}$  versus TOC, **B)**  $\delta^{13}\text{C}_{\text{carb}}$  (gray shaded area represent the till  $\delta^{13}\text{C}_{\text{carb}}$  value) versus TOC, **C)**  $\delta^{18}\text{O}_{\text{carb}}$  (gray shaded area represent the till  $\delta^{18}\text{O}_{\text{carb}}$  value) versus TOC and **D)**  $\delta^{34}\text{S}_{\text{ORG}}$  versus TOC.

*Facies 7 (960 cm to 865 cm):* This unit consists of a fine grained brown detritus gyttja which is very homogeneous and has a thickness of about 95 cm. An increasing content of silt particles upwards to the middle followed by a decrease in the silt fraction is observed. Small and infrequent scattered calcareous peels are observed. The bottom part displays visible tracks from bottom scavengers. At the level from 940 cm to 942 cm macrofossil fragment of aquatic plants and a few very scattered fragments of gastropods are observed. Microscopically there is a high content of very small fragments of terrestrial organic material, and also few and small shell fragments together with amounts of fine aquatic organic material. This deposit is shown in Figure 7-14.

*Geochemistry and physical properties:* The SUS values are slowly increasing up to 906 cm, then follows steeply increasing SUS values. From 897 cm the SUS values are decreasing. The mineralogical content is increasing up to 897 cm followed by decreasing values. The  $\text{CaCO}_3$  content decreases until 910 cm, and then follows increasing values. The  $\delta^{13}\text{C}_{\text{carb}}$  values are low until 945 cm, then follows an abrupt increased succeeded by decreasing values. The  $\delta^{18}\text{O}_{\text{carb}}$  values decreases until 933 cm, and then increasing  $\delta^{18}\text{O}_{\text{carb}}$  values are observed. The TS values are increasing and the TOC values decreases until 900 cm from where they are constant. The TON values decreases until 940 cm and then increases up to 900 cm from they are again decreasing. The C:N values are elevated between 950 and 915 cm and the C:S values are constant up to 920 cm from where they are decreasing. The  $\delta^{13}\text{C}_{\text{ORG}}$  values are increasing up to 890 cm from where they are decreasing. The  $\delta^{15}\text{N}_{\text{ORG}}$  values are increasing up 940 from where they decrease. From 910 the  $\delta^{15}\text{N}_{\text{ORG}}$  values are again decreasing. The  $\delta^{34}\text{S}_{\text{ORG}}$  value increases up to 915 cm from they decrease. See Table 7.1 and Figure 7-2 for further details.

*Interpretation:* This deposit is likely formed in a low energy environment below wave base from suspension. The increasing SUS values and mineralogical content suggest an upwards increasing amount of allochthonous eroded material up to a depth of 895 cm. The decreasing SUS

values and mineralogical content from 895 cm suggests a decreasing amount of allochthonous eroded material. This is in agreement with sedimentological observation of increasing silt content upwards for the lower part and a decreasing content for the upper part. This unit is most likely deposit in the profundal zone or upper profundal zone (see Figure 5-1) due to the finely and scattered amounts of organic material and the fine grained size. This may be supported by the infrequent findings of small shell fragments. The microscopic amount of terrestrial material may confirm a deep water deposit. The C:N values indicate two periods of elevated an allochthonous organic matter content which is concurrent with somewhat elevated  $\delta^{15}\text{N}_{\text{ORG}}$  values indicative of allochthonous organic matter (Muzuka *et al* 2004). The first of these elevated C:N periods is very pronounced in both C:N and  $\delta^{15}\text{N}_{\text{ORG}}$  values and is furthermore concurrent with elevated  $\delta^{13}\text{C}_{\text{carb}}$  values. The elevated  $\delta^{13}\text{C}_{\text{carb}}$  values may result from particulate allochthonous  $\text{CaCO}_3$ . (Kolstrup and Buchardt 1982; Noe-Nygaard and Heiberg 2001). However the  $\text{CaCO}_3$  content and the  $\delta^{18}\text{O}_{\text{carb}}$  values are decreasing in disapproval of the latter interpretation (Kolstrup and Buchardt 1982; Hammarlund and Buchardt 1996; Noe-Nygaard and Heiberg 2001). The C:S values indicate a decreasing amount of allochthonous organic matter (Routh *et al* 2004). The decreasing TOC values may indicate decreasing organic matter productivity and hence likely a decreasing nutrient influx. This is further supported by the concordant trend in the  $\text{CaCO}_3$  content which indicates further that the  $\text{CaCO}_3$  is likely bioinduced. The negative correlation between the TOC and  $\delta^{13}\text{C}_{\text{ORG}}$  values ( $\rho=-0.68$ , see Figure 7-5B) may suggest increased utilisation of bicarbonate during periods with low organic productivity (Muzuka *et al* 2004) further suggesting a low nutrient influx. The negative correlation between the TOC and SUS values ( $\rho=-0.69$ ) may suggest dilution of the TOC signal due to increased amounts of allochthonous mineral matter in accordance with the increased C:S and C:N values. Hence it is likely that the TOC values may increase during the interval with increased mineralogical content. From 895 cm the SUS and  $\delta^{13}\text{C}_{\text{ORG}}$  values decreases and the TOC values and  $\text{CaCO}_3$  content increases thus displaying an opposite trend likely to indicate the onset of a shallowing of the lake, i.e. less eroded allochthonous material. The decreasing  $\delta^{18}\text{O}_{\text{carb}}$  values are likely indicating a decreasing E/I ratio (Kirby *et al* 2004; Hammarlund *et al* 2005) up to 933 cm which is most likely reflecting an increased water inflow. This may be supported by the increased C:N values during this interval. From about 930 cm the C:N values drops dramatically and the increasing  $\delta^{18}\text{O}_{\text{carb}}$  values are likely to indicate a decreased water inflow in accordance with a decreasing nutrient supply and organic productivity.

*Facies 8 (865 cm to 772 cm):* Dark brown finely grained detritus gyttja of 93 cm in thickness. This unit is homogeneous and bioturbed with scattered burrows from bottom scavengers and very scattered clusters of debris of gastropods. The unit contains macrofossil debris of small aquatic roots. Macrofossil terrestrial organic material was not observed. A microscopic content of terrestrial organic material and aquatic organic matter was observed. This deposit is shown in Figure 7-15A & B. At 860 cm in an interval of 1 cm to 2 cm a large concentration of terrestrial debris, such as twigs, insect remains (*ketin shield 1.5 cm long*) and debris of shell fragments was observed (*mayfly, twigs both bark and wood*). This interval is illustrated by Figure 7-15B.

*Geochemistry and physical properties:* The SUS values are constant and the mineralogical content slowly increases. The  $\text{CaCO}_3$  decreases until 800 cm, and then slowly increases. The  $\delta^{13}\text{C}_{\text{carb}}$  values are slowly increasing and the  $\delta^{18}\text{O}_{\text{carb}}$  values are decreasing. The TS values are constant up to 818 cm from where they are increasing. The TOC and TON values are increasing. The C:N values are constant whereas the C:S values are increasing up to 820 cm and then decreases. The  $\delta^{13}\text{C}_{\text{ORG}}$  values decreases until 850 cm and then increases. The  $\delta^{15}\text{N}_{\text{ORG}}$  values are decreasing. The  $\delta^{34}\text{S}_{\text{ORG}}$  values are increasing up to 800 cm from where they are constant. See Table 7.1 and Figure 7-2 for details.

*Interpretation:* This sediment deposited in a low energy environment below wave base from suspension as suggested by fine grain size and homogeneity. The high concentration of macrofossil debris observed at the 860 cm event could possibly reflect a storm event or sudden

dramatic transgression or regression. However, the thickness of 1 cm to 2 cm indicates that this event is not likely to be caused by stormy weather. On the other hand the 860 cm event is very confined in space and may therefore not be resolved by the geochemical sampling. Hence it is not likely to show up in the geochemical data. The 860 cm event may likely represent a correlative surface of forced regression.

The unit is likely deposited in the upper profundal zone or shell zone in close proximity to vegetation zone (*see Figure 5-1*) as indicated by the scattered content of aquatic roots, the scattered and fragmented gastropods and the microscopic content of terrestrial organic matter. The C:N values indicates a mixed origin of allochthonous and autochthonous organic matter whereas the C:S values indicate an increased amount of allochthonous organic matter upwards to 824 cm followed by a decreasing amount (Routh *et al* 2004; Meyers 2006). The increasing  $\delta^{13}\text{C}_{\text{ORG}}$ ,  $\delta^{13}\text{C}_{\text{carb}}$  and TOC values may indicate an increased organic productivity. The decreasing  $\delta^{15}\text{N}_{\text{ORG}}$  values may indicate a higher fraction of algal organic matter (Muzuka *et al* 2004). On the other hand, increased organic productivity may result in increased authigenic precipitation of  $\text{CaCO}_3$  in contrast to the observed steadily decreasing  $\text{CaCO}_3$  values. However the decreasing  $\text{CaCO}_3$  content may be the result of increased decomposition of organic matter producing  $\text{CO}_2$  and consequently decreasing the pH value in the hypolimnion. The increased hypolimnic acidity may then have caused  $\text{CaCO}_3$  dissolution (Dean 1999). Alternatively the  $\text{CaCO}_3$  decrease is due to dilution by other components. The increasing  $\delta^{34}\text{S}_{\text{ORG}}$  values suggest that the hypolimnion becomes oxidised and thus the more depleted  $\delta^{15}\text{N}_{\text{ORG}}$  values may be a result of less ammonia volatilisation (Talbot 2001; Talbot *et al* 2006). The development of more oxic bottom conditions is supported by the bioturbidity of this unit. The decreasing  $\delta^{18}\text{O}_{\text{carb}}$  values likely indicates a decreased E/I ratio (Kirby *et al* 2004; Hammarlund *et al* 2005) which probably reflects an increased water inflow during this period and thereby an increased nutrient influx in accordance with the increasing TOC,  $\delta^{13}\text{C}_{\text{ORG}}$  and  $\delta^{13}\text{C}_{\text{carb}}$  values.

*Facies 9 (772 cm to 740 cm and 680 cm to 668 cm):* A dark brown fine grained detritus gyttja. This facies occurs in two depths intervals: i) 772 cm to 740 cm and ii) 680 cm to 668 cm. The unit has a thickness of about 20 cm, it is homogeneous and bioturbed with scattered burrows from bottom scavengers and very scattered clusters of gastropod debris. Macrofossil debris of small aquatic roots is observed together with infrequent remains of terrestrial organic material. The unit contains a modest microscopic content of terrestrial organic material and aquatic organic matter.

*Geochemistry and physical properties:* i) The SUS values display a peak with maximum values around 760 cm whereas the mineralogical content is constant. The  $\text{CaCO}_3$  content and the  $\delta^{18}\text{O}_{\text{carb}}$  values are increasing and the  $\delta^{13}\text{C}_{\text{carb}}$  values are very slowly decreasing. The TS values display a peak whereas the TOC and TON values are decreasing. The C:N values are constant whereas the C:S values are decreasing. The  $\delta^{13}\text{C}_{\text{ORG}}$  and  $\delta^{34}\text{S}_{\text{ORG}}$  values are decreasing and the  $\delta^{15}\text{N}_{\text{ORG}}$  values are increasing. See Table 7.1 and Figure 7-2.

ii) The SUS values, the mineralogical and the  $\text{CaCO}_3$  content is decreasing. The TS and TOC values are increasing and the TON values are constant. The C:N values are increasing and the C:S values are constant. The  $\delta^{13}\text{C}_{\text{ORG}}$  and  $\delta^{15}\text{N}_{\text{ORG}}$  values are slowly increasing whereas the  $\delta^{34}\text{S}_{\text{ORG}}$  are slowly decreasing. See Table 7.1 and Figure 7-2.

*Interpretation:* This sediment is deposited from suspension in a low energy environment below the wave base as indicated by the fine grain size and the sediment homogeneity. The low SUS values and mineralogical content indicates small amount of allochthonous eroded material. The high content of microscopic organic matter with the observation of scattered and infrequent macrofossil debris of both terrestrial and aquatic organic matter probably indicate that this unit is deposited in the upper profundal zone (*see Figure 5-1*). The low C:N and C:S suggest a high fraction of autochthonous organic matter (Meyers and Teranes 2001; Meyers 2006). In general the geochemical parameters display different tendencies for the two depth intervals and the interpretation has therefore been divided.

*Depth interval i)* The upper interval is characterised by a peak in the SUS values indicating increased amounts of allochthonous eroded material. The decreasing  $\delta^{13}\text{C}_{\text{ORG}}$  values TOC and TON content suggest a decreased organic productivity and likely a reduced flux of nutrients (McFadden *et al* 2005; Talbot *et al* 2006). The decreasing  $\delta^{34}\text{S}_{\text{ORG}}$  values and co-occurring increasing  $\delta^{15}\text{N}_{\text{ORG}}$  values may indicate increased bacterial sulphate reduction and ammonia volatilisation and therefore probably the development of anoxic hypolimnion conditions (Watanabe *et al* 2004; Eimers *et al* 2006). However the increasing  $\delta^{15}\text{N}_{\text{ORG}}$  values may also be related to a limited DIN reservoir (Wolfe *et al* 1999; Routh *et al* 2004). The increased  $\delta^{18}\text{O}_{\text{carb}}$  values may indicate an increased E/I ratio (Kirby *et al* 2004; Hammarlund *et al* 2005) which is likely related to less inflow in accordance with the decreased nutrient supply. The increasing  $\text{CaCO}_3$  content may be caused by the reduced content of other components or due to increased temperatures or evaporation yielding higher precipitation of  $\text{CaCO}_3$  (Dean 1999; Schwalb 2002).

*Depth interval ii)* The decreasing SUS values and mineralogical content suggest a decreasing amount of allochthonous eroded material which may indicate a somewhat increased distance to the lake shore. The C:N and C:S values indicate a high fraction of autochthonous organic matter (Routh *et al* 2004; Meyers 2006). The increasing  $\delta^{13}\text{C}_{\text{ORG}}$ ,  $\delta^{13}\text{C}_{\text{carb}}$  and TOC values are likely to suggest an increasing organic productivity (Schwalb 2002; Talbot *et al* 2006). The decreasing  $\delta^{34}\text{S}_{\text{ORG}}$  values may suggest increased bacterial reduction of sulphur and therefore suggest the development of increased anoxia in the hypolimnion. The increasing  $\delta^{15}\text{N}_{\text{ORG}}$  values may be due to anoxia and ammonia volatilisation (Talbot 2001; Talbot *et al* 2006). The slightly decrease in the  $\text{CaCO}_3$  content is probably caused by dilution by other components and the very high  $\text{CaCO}_3$  content is most likely biogenic induced. The  $\delta^{18}\text{O}_{\text{carb}}$  values are elevated, however this period marks the onset of a decreasing trend of the  $\delta^{18}\text{O}_{\text{carb}}$  values which may likely suggest a decreasing E/I ratio (Kirby *et al* 2004; Hammarlund *et al* 2005) most likely reflecting increased inflow and perhaps a lower water evaporation rate. In accordance with the increasing organic productivity probably related to a higher nutrient inflow.

*Facies 10 (740 cm to 680 cm):* A very fine grained light grey massive detritus gyttja with a thickness of 60 cm. The unit is homogeneous with few scattered shell fragments. The macroscopic content of terrestrial organic material is very low. Microscopically fine grained calcareous particles, fragments of insects and gastropods are observed. The deposit has a high content of microscopic organic material, with a majority of aquatic origin.

*Geochemistry and physical properties:* The SUS values are constant until 710 cm and then increasing. The mineralogical content is decreasing until 720 cm and then increasing. The  $\text{CaCO}_3$  content is increasing. The  $\delta^{13}\text{C}_{\text{carb}}$  values are increasing up to 720 cm and then decreasing. The  $\delta^{18}\text{O}_{\text{carb}}$  values are slowly increasing. The TS values are decreasing until 700 cm and then constant. The TOC and TON values decreasing up to 690 cm and then they increase. The C:N values are decreasing up to 700 cm and then display constant values. The C:S values are very slowly increasing. The  $\delta^{13}\text{C}_{\text{ORG}}$  values are increasing up to 710 cm and then decrease. The  $\delta^{15}\text{N}_{\text{ORG}}$  values are in general increasing, but display very fluctuating values. The  $\delta^{34}\text{S}_{\text{ORG}}$  values are increasing up to 690 cm and then they decrease. See Table 7.1 and Figure 7-2.

*Interpretation:* This unit is deposited from suspension in a low energy environment below wave base as suggested by the fine grain size and homogeneity of the sediment. The constant and low SUS values suggest a very small amount of eroded allochthonous material whereas the increasing SUS values from 700 cm suggest an increasing amount of allochthonous eroded material. The constant C:S values are likely to indicate a high content of autochthonous organic matter, likewise the decreasing C:N values probably indicate an increasing amount of autochthonous organic matter in the sediment in accordance with the sedimentological observations (Routh *et al* 2004; Meyers 2006). The unit is probably deposited in closer proximity to the vegetation zone in deep water below wave base (see Figure 5-1). The very high  $\text{CaCO}_3$  content approaching 66 wt% (see Table 7.1) show a weak correlation to the SUS values ( $\rho=0.53$ , see Figure 7-4C) and a negative correlation to the TOC values ( $\rho=-0.62$ ) indicating that the  $\text{CaCO}_3$  is allochthonous in origin. However the very high  $\text{CaCO}_3$  content is most likely bioinduced as also supported by low

$\delta^{18}\text{O}_{\text{carb}}$  and  $\delta^{13}\text{C}_{\text{carb}}$  values and as furthermore supported by the very low mineralogical content and SUS values. The somewhat low organic content ranging between 14 wt% and 20 wt% (see Table 7.1) may indicate a reduced organic productivity and consequently a reduced influx of nutrients as may also be suggested by the decreasing amount of allochthonous organic matter. The decreasing tendency of both the  $\delta^{13}\text{C}_{\text{ORG}}$  and  $\delta^{15}\text{N}_{\text{ORG}}$  values may further support a decreasing organic productivity (Wolfe *et al* 1999; McFadden *et al* 2005; Talbot *et al* 2006) whereas the increasing TOC,  $\delta^{13}\text{C}_{\text{ORG}}$  and  $\delta^{15}\text{N}_{\text{ORG}}$  from 698 cm and onwards may suggest an increasing organic productivity. The increasing  $\delta^{34}\text{S}_{\text{ORG}}$  values suggest that the hypolimnion becomes progressively more oxygenated during this interval. This is supported by the decreasing  $\delta^{15}\text{N}_{\text{ORG}}$



**Figure 7-10:** (to the right). Facies 1, at depth 1267 cm (core diameter 7.5 cm).



**Figure 7-11:** (below). Facies 2. A) From 1275 cm to 1286 cm. B) From 1304 cm to 1315 cm.

**Figure 7-12.** Facies 3, at depth 1056 cm.

**Figure 7-13.** Facies 5, at depth 985 cm.

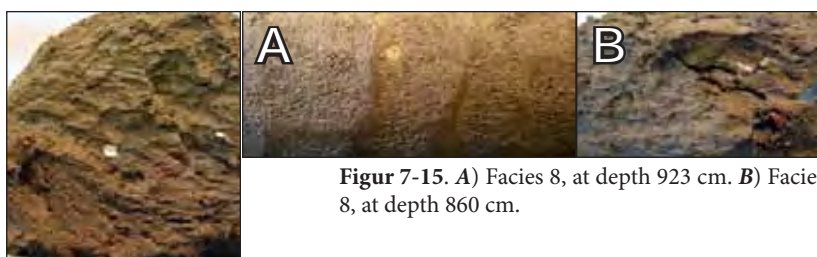


**Figure 7-14.** Facies 7, at depth 940 cm.



**Figur 7-15.** A) Facies 8, at depth 923 cm. B) Facies 8, at depth 860 cm.



**Figure 7-16.** Facies 11, depth from 646 cm to 661 cm.

values up to 698 cm probably indicating less ammonia volatilisation or a higher content of algal matter (Talbot 2001; Muzuka *et al* 2004; Talbot *et al* 2006). From 690 cm the  $\delta^{34}\text{S}_{\text{ORG}}$  values decrease which may indicate an increase in bacterial sulphate reduction and hence more anoxic conditions (Watanabe *et al* 2004; Eimers *et al* 2006). Hence the increasing TOC and  $\delta^{13}\text{C}_{\text{ORG}}$  values from about 690 cm may be due to increased preservation of organic matter due to an anoxic bottom environment. Thus the general decreasing TOC and  $\delta^{13}\text{C}_{\text{ORG}}$  values are most likely related to a decreasing nutrient supply and consequently most probably by a decreased water inflow. The increasing  $\delta^{18}\text{O}_{\text{carb}}$  values are probable to indicate an increased E/I ratio (Kirby *et al* 2004; Hammarlund *et al* 2005) and likely to support a reduced water inflow.

*Facies 11 (639 cm to 668 cm):* A fine grained brown detritus gyttja with a thickness of 30 cm. The colour is gradually changing from light brown to brown upwards. This unit is homogeneous with no visible organic remains. A very scattered content of gastropods fragments and in some instances even whole shells was observed. A microscopic content of very fine organic debris of terrestrial and aquatic origin were observed, with the aquatic organic material compositing the majority of the organic material. This deposit is shown in Figure 7-16.

*Geochemistry and physical properties:* The SUS values and the mineralogical content are slowly increasing. The  $\text{CaCO}_3$  content and the  $\delta^{13}\text{C}_{\text{carb}}$  values are constant. The  $\delta^{18}\text{O}_{\text{carb}}$  values are slowly decreasing. The TS, TOC and TON values are decreasing. The C:N and C:S values are constant. The  $\delta^{13}\text{C}_{\text{ORG}}$ ,  $\delta^{15}\text{N}_{\text{ORG}}$  and  $\delta^{34}\text{S}_{\text{ORG}}$  values are slowly increasing. See Table 7.1 and Figure 7-2.

*Interpretation:* This unit is deposited in a low energy environment below the wave base from suspension in deep water as indicated by the homogeneity and fine grain size. The lack of macroscopic plant remains may together with the high microscopic content of organic material suggests a closer proximity to the vegetation zone and deposition in the upper profundal zone (see Figure 5-1). The gradual coarsening upwards probably indicate an increased amount or allochthonous eroded material as supported by the steadily increasing mineralogical content and SUS values.

The increasing trend of the  $\delta^{13}\text{C}_{\text{ORG}}$  values and the decreasing TOC and TON content seems to contrast one another, but may be caused by increased utilisation of bicarbonate due to a limited concentration of dissolved  $\text{CO}_2$  (Muzuka *et al* 2004). However, the slowly increasing  $\delta^{13}\text{C}_{\text{ORG}}$  and  $\delta^{13}\text{C}_{\text{carb}}$  values are most likely indicating an increasing organic productivity (McFadden *et al* 2005; Talbot *et al* 2006), and the decreasing TOC and TON values may likely be a result of dilution by the increasing mineralogical content. Furthermore the increasing  $\delta^{15}\text{N}_{\text{ORG}}$  values may likely indicate increasing organic productivity (Talbot *et al* 2006), but they may alternatively result from a drawdown of DIN reservoir (Routh *et al* 2004). The C:N values indicate a mixed origin of allochthonous and autochthonous organic matter in the sediments with a higher fraction of autochthonous organic matter. The C:S values are indicative of autochthonous organic matter. This may find further support in the decreasing  $\delta^{18}\text{O}_{\text{carb}}$  values indicating a decreasing E/I ratio (Kirby *et al* 2004; Hammarlund *et al* 2005) probably indicating increased water inflow or a lower evaporation rate.

*Facies 12 (639 cm to 626 cm):* A fine grained to medium grained brown massive algal gyttja with a thickness of 13 cm. The unit shows a gradual coarsening upwards. Scattered peels of calcareous particles were observed.

*Geochemistry and physical properties:* The SUS values are increasing and the mineralogical content display constant values. The  $\text{CaCO}_3$  content increases. The  $\delta^{13}\text{C}_{\text{carb}}$  values are constant and the  $\delta^{18}\text{O}_{\text{carb}}$  values are decreasing. The TS, TOC and TON values are constant. The TOC values decreases from 630 cm. The C:N and C:S values are constant. The  $\delta^{13}\text{C}_{\text{ORG}}$  and  $\delta^{15}\text{N}_{\text{ORG}}$  values are constant. The  $\delta^{34}\text{S}_{\text{ORG}}$  values are slowly decreasing. See Table 7.1 and Figure 7-2.

*Interpretation:* The medium grain size suggests that this unit is deposited in a low energy environment below the wave base from suspension. The high content of algal organic matter and slightly coarser grain size suggest that the sediment is deposited in shallower waters probably in the upper profundal zone or perhaps in the sub-littoral zone (see Figure 5-1). The gradual coars-

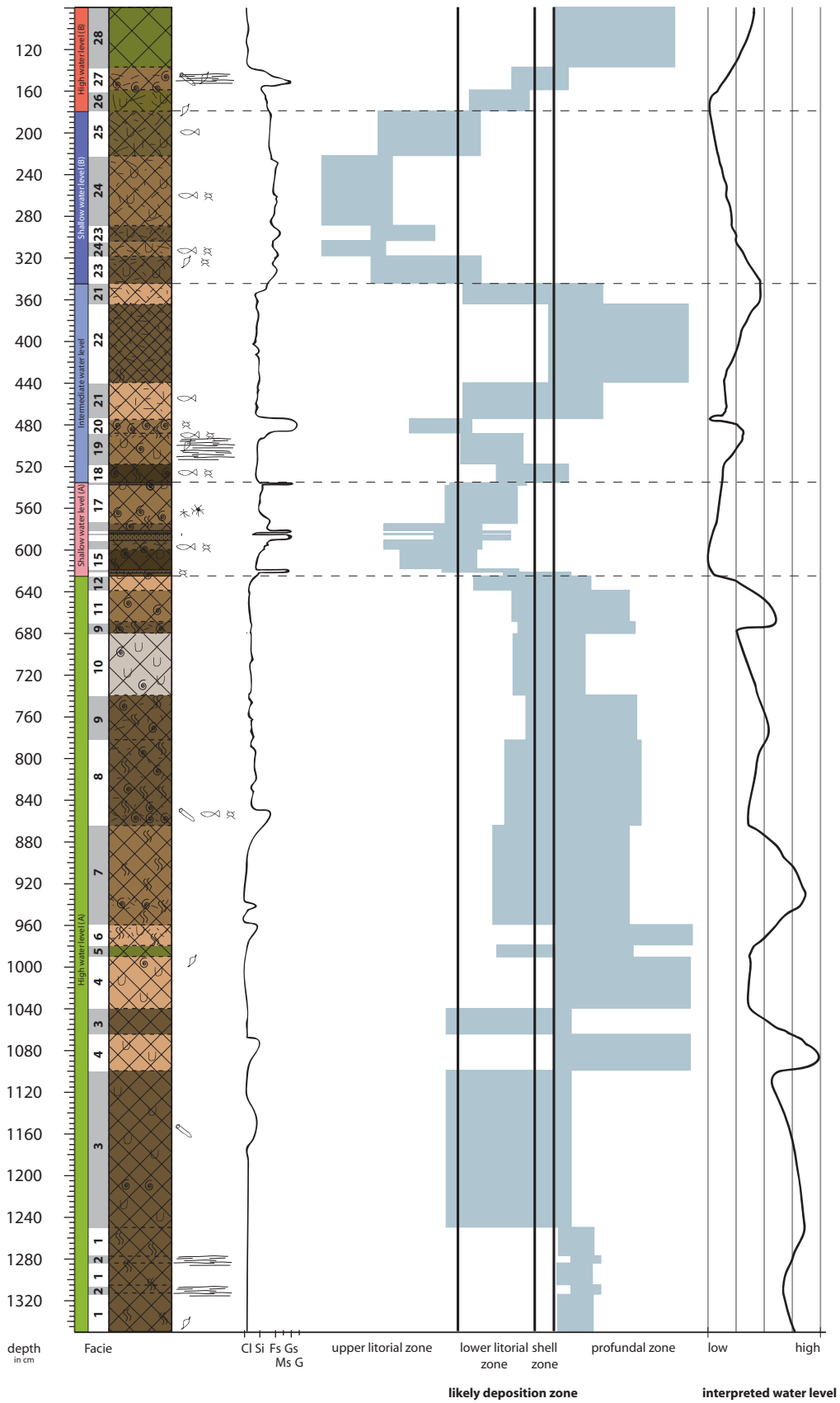


**Figure 7-17:** Presented is the most likely facies deposition zone (see also Figure 5-1) and an inferred water depth curve of the Bliden Lake.

**Table 7.2. Average geochemical data facies associations**

A summary of the geochemical data is given as a mean value, standard deviation and minimum and maximum values in parentheses. 1: High water A, 2: Shallow water A, 3: Intermediate water, 4: Shallow water B and 5: High water B.

fac. Ass.	Depth interval (cm)	Mag. Sus.	Mineralogical content	CaCO <sub>3</sub> (wt%)	$\delta^{13}\text{C}_{\text{carb}}$ (‰ VPDB)	$\delta^{18}\text{O}_{\text{carb}}$ (‰ VPDB)	TS wt%	TOC wt%	TON wt%	C:N	C:S	$\delta^{13}\text{C}_{\text{ORG}}$ (‰ VPDB)	$\delta^{15}\text{N}_{\text{ORG}}$ (‰ AIR)	$\delta^{34}\text{S}_{\text{ORG}}$ (‰ VCDT)
5	80 - 180	77 ± 31 (42 - 157)	34.7 ± 8.7 (23.7 - 50.9)	41.7 ± 11.1 (21.8 - 55.9)	-2.6 ± 1.7 (-4.5 to 1.2)	-6.5 ± 0.5 (-7.1 to -5.8)	1.1 ± 0.3 (0.4 - 1.7)	9.0 ± 2.5 (6.0 - 23.2)	0.6 ± 0.2 (0.3 - 1.2)	18 ± 3 (12 - 24)	24 ± 5 (16 - 39)	-29.1 ± 1.0 (-30.3 to -25.6)	7.9 ± 2.2 (1.3 to 10.7)	-1.3 ± 2.1 (-5.7 to 4.0)
4	180 - 345	149 ± 28 (90 - 206)	37.2 ± 4.6 (25.5 - 46.1)	26.2 ± 4.0 (17.2 - 34.1)	0.8 ± 0.9 (-0.6 to 1.8)	-6.7 ± 0.4 (-7.5 to -6.2)	0.6 ± 0.2 (0.2 - 1.2)	14.2 ± 1.5 (11.1 - 17.6)	0.9 ± 0.2 (0.5 - 1.4)	19 ± 2 (14 - 25)	73 ± 21 (42 - 182)	-29.9 ± 0.6 (-30.8 to -26.5)	4.2 ± 0.7 (2.2 to 5.2)	11.6 ± 1.0 (8.8 to 14.0)
3	345 - 536	55 ± 23 (22 - 99)	19.0 ± 4.0 (11.4 - 33.2)	37.5 ± 6.1 (28.2 - 56.6)	-1.4 ± 1.3 (-3.1 to 1.3)	-6.6 ± 0.5 (-7.7 to -5.0)	1.0 ± 0.2 (0.6 - 1.4)	21.5 ± 4.4 (13.8 - 29.2)	1.4 ± 0.3 (0.9 - 2.1)	17 ± 2 (13 - 22)	64 ± 8 (43 - 83)	-30.6 ± 0.5 (-31.7 to -29.8)	3.3 ± 0.9 (1.7 to 5.1)	12.5 ± 1.2 (9.9 to 14.9)
2	536 - 626	67 ± 24 (30 - 123)	21.2 ± 4.7 (13.0 - 30.5)	42.2 ± 5.9 (29.3 - 60.5)	-1.8 ± 0.8 (-2.9 to -0.7)	-6.4 ± 0.2 (-6.6 to -5.8)	0.9 ± 0.2 (0.5 - 1.3)	17.6 ± 2.6 (11.8 - 24.1)	1.3 ± 0.3 (0.9 - 2.2)	16 ± 3 (11 - 24)	58 ± 9 (43 - 79)	-29.8 ± 1.2 (-32.3 to -27.8)	3.8 ± 1.2 (1.2 to 5.9)	10.8 ± 1.2 (8.7 to 13.3)
1	626 - 1350	22 ± 14 (1 - 67)	12.6 ± 3.7 (2.6 - 25.0)	50.4 ± 6.8 (31.4 - 66.8)	-5.4 ± 0.5 (-6.3 to -3.9)	-7.2 ± 0.7 (-8.4 to -5.9)	0.9 ± 0.2 (0.4 - 1.6)	18.9 ± 2.5 (13.8 - 28.0)	1.1 ± 0.2 (0.7 - 1.9)	20 ± 2 (13 - 26)	64 ± 14 (36 - 130)	-31.9 ± 0.5 (-33.8 to -30.4)	4.1 ± 1.1 (1.3 to 6.6)	9.1 ± 2.3 (1.2 to 13.7)
All data	80 - 1350	51 ± 47 (1 - 206)	19.2 ± 10.6 (2.6 - 50.9)	44.1 ± 10.8 (17.2 - 66.8)	-3.5 ± 2.5 (-6.3 to 2.1)	-6.9 ± 0.7 (-8.4 to -5.0)	0.9 ± 0.2 (0.2 - 1.7)	17.8 ± 4.4 (6.0 - 29.2)	1.1 ± 0.3 (0.3 - 2.2)	61 ± 17 (16 - 182)	1.1 ± 0.3 (0.3 - 2.2)	-31.1 ± 1.3 (-33.8 to -25.6)	4.2 ± 1.6 (1.1 to 10.7)	9.2 ± 3.9 (-5.7 to 14.9)

ening upwards indicates an increased amount of allochthonous eroded material as supported by the slightly higher SUS values. The slightly elevated  $\delta^{13}\text{C}_{\text{ORG}}$  and  $\delta^{15}\text{N}_{\text{ORG}}$  values and lower TOC and TON values may indicate increased utilisation of the DIC and nutrient pool (Wolfe *et al* 1999; McFadden *et al* 2005; Talbot *et al* 2006). This is supported by somewhat higher  $\delta^{13}\text{C}_{\text{carb}}$  values. The C:N values suggests a higher fraction of allochthonous organic matter, which together with the high SUS values is likely to suggest a closer proximity to the littoral zone.

#### *Interpretation of facies association*

The fine to medium grain size and homogeneity of this facies association indicates deposition from suspension in a low energy environment probably below wave base. The facies of this facies association are likely deposited in upper profundal and sub-littoral zone to the profundal zone as indicated by the general lack of macrofossil material and other sedimentological observations. This is further supported by the low C:N and C:S ratios having mean values of 20 and 64 (*see Table 7.2*) respectively which indicate a mixture of organic matter of allochthonous and autochthonous origin with a bias towards a higher fraction of autochthonous derived organic matter (Meyers and Teranes 2001; Routh *et al* 2004; Meyers 2006). Furthermore the C:N values and the TOC content are completely uncorrelated indicating that a high TOC content is not accompanied by a high fraction of allochthonous organic matter in general (*Figure 7-5C*). The sediments may broadly be characterised as derived from a pelagical lake system with a scattered vegetation of submerged macrophytes. All transitions between facies are weakly defined and gradually indicating a continuous unit without erosional sections or hiatus (Reading 1989). The likely deposition zones are shown in the lower part of *Figure 7-17*. From 1250 cm to 1100 cm the inferred water level most likely display a general high level with minor fluctuations. The period from 1100 cm to 1065 cm display a significant increase in the water level as viewed from both an increasing nutrient content and lower  $\delta^{18}\text{O}_{\text{carb}}$  values. From 1065 cm to 930 cm the water level is most likely decreasing as inferred from a reducing nutrient inflow and decreasing  $\delta^{18}\text{O}_{\text{carb}}$  values. A short period of increasing water level is observed between 930 cm to 900 cm as evident from an increasing organic productivity and decreasing  $\delta^{18}\text{O}_{\text{carb}}$  values. From 900 cm and upwards to 626 cm the water level is generally decreasing imposed by minor fluctuations.

The scatter plots of the geochemical data (*Figure 7-3 to 7-9*) illustrates that the geochemical data of this facies association falls in groups significantly different from the remaining data; exceptions are the C:N and C:S values. Very large difference are the very low SUS values and mineralogical content with average values of 22 wt% and 13 wt% respectively (*see Table 7.2, average of all data are SUS: 51 and mineralogical content: 21 wt%*). This is interpreted as a very small content of allochthonous eroded material which may reflect a relatively large distance to lake shore. The very low  $\delta^{13}\text{C}_{\text{carb}}$  values are likely to indicate a DIC pool mainly derived from decomposing allochthonous organic matter producing  $\text{CO}_2$  very depleted in  $^{13}\text{C}$  (Wolfe *et al* 1999), and the constancy of the  $\delta^{13}\text{C}_{\text{carb}}$  values are likely to indicate a relatively high and constant influx of nutrients during this period as is also suggested by the general high TOC and TON values and further; as indicated by the high microscopic amounts of limnic organic matter. Likewise the low  $\delta^{13}\text{C}_{\text{ORG}}$  values (*less than -30‰, see Table 7.2*) are most probably derived from photosynthetic carbon assimilation from a light DIC pool (Wolfe *et al* 1999; McFadden *et al* 2005; Talbot *et al* 2006).

The  $\text{CaCO}_3$  content is an integrate measure of all carbonate in the lake and the high content may be caused by fragments of shells or allochthonous particulate  $\text{CaCO}_3$  from the catchments area. However, as only few shell fragments were observed in this facies association this is not likely to have caused the high  $\text{CaCO}_3$  content. Furthermore, the lack of a correlation between the SUS values and the  $\text{CaCO}_3$  content ( $\rho=-0.07$ , *see Figure 7-4C*) suggests that the  $\text{CaCO}_3$  content

is mainly precipitated due to photosynthetic activity. Moreover the very high  $\text{CaCO}_3$  content (ranging from 31 wt% to 67 wt%, see Table 7.2) is most likely induced by photosynthetic activity as also suggested by the frequent observations of  $\text{CaCO}_3$  encrustations. However the negative correlation ( $\rho=-0.66$ ) between the  $\text{CaCO}_3$  and TOC content does not at first hand favour this interpretation. Dean (1999) pointed out that common feature of profundal deposit in hard water lakes is a decreasing  $\text{CaCO}_3$  content with increasing TOC values as a result of decomposition of organic matter in the sediment yielding increased concentrations of  $\text{CO}_2$ . A high  $\text{CO}_2$  concentration lowers the pH values and consequently results in the dissolution of  $\text{CaCO}_3$  (Dean 1999; Schwalb 2002).

The  $\delta^{13}\text{C}_{\text{ORG}}$  isotope values show a weak tendency of higher  $\delta^{13}\text{C}_{\text{ORG}}$  values with increasing TOC content (Figure 7-5B) probably reflecting changes in the primary organic productivity (Wolfe *et al* 1999; McFadden *et al* 2005; Talbot *et al* 2006) which is further supported by the weak positive correlation between the  $\delta^{13}\text{C}_{\text{ORG}}$  and  $\delta^{13}\text{C}_{\text{carb}}$  values (Figure 7-6B).

The negative correlation between the  $\delta^{13}\text{C}_{\text{ORG}}$  and  $\delta^{15}\text{N}_{\text{ORG}}$  values (Figure 7-5D) indicates that the changes in the  $\delta^{15}\text{N}_{\text{ORG}}$  values are probably caused by other factors than primary productivity changes. The  $\delta^{34}\text{S}_{\text{ORG}}$  values are weakly correlated with the  $\delta^{15}\text{N}_{\text{ORG}}$  values ( $\rho=-0.58$ , see Figure 7-7D) suggesting that the nitrogen and sulphur cycles seem to be very closely connected. The anaerobic processes of ammonification and denitrification both heavily discriminate against  $^{15}\text{N}$  resulting in enrichment of the DIN reservoir and consequently also of subsequent produced organic matter (Wolfe *et al* 1999; Talbot *et al* 2006). Ammonification and denitrification may both or singly have resulted in high  $\delta^{15}\text{N}_{\text{ORG}}$  values during periods where an anoxic hypolimnion has been development. Further the very low or lower  $\delta^{34}\text{S}_{\text{ORG}}$  values may be a result of assimilate sulphate reduction by bacteria resulting in the production of very depleted hydrogen sulphide which upon re-oxidation in the epilimnion may produce organic matter with low  $\delta^{34}\text{S}_{\text{ORG}}$  values even though most of the produced hydrogen sulphide is likely to escape (Eimers *et al* 2006). Furthermore a correlation between the  $\delta^{34}\text{S}_{\text{ORG}}$  values, the TS content ( $\rho=0.57$ , see Figure 7-7D) and C:S ratio ( $\rho=0.75$ , see Figure 7-7B) is observed and suggests that low  $\delta^{34}\text{S}_{\text{ORG}}$  values and a high TS content are mainly associated with autochthonous organic matter (Eimers *et al* 2006). Hence the low  $\delta^{34}\text{S}_{\text{ORG}}$  values associated with high  $\delta^{15}\text{N}_{\text{ORG}}$  are mutually supportive and most likely indicating anoxic epilimnion conditions as also reported from Lake Baikal (Watanabe *et al* 2004).

### Shallow water (A) facies association

This facies association is represented by 5 facies and is found between 639 cm to 536 cm. The association is 103 cm thick and consists of a fine to coarse grained detritus gyttja containing primarily autochthonous organic matter and subsidiary various amounts of allochthonous organic matter. The facies included in the association contain a various amount of organic macrofossil of mainly limnic origin. The majority of the transitions between facies are gradual and indistinct; however a few are more sharply defined.

#### *Facies - sedimentology and geochemistry*

*Facies 13 (626 cm to 623 cm):* A fine to medium grained dark brown shell rich detritus gyttja of 2 cm to 3 cm in thickness. A very high content of fragmented gastropod debris, whole shells and juvenile shells was observed. Calcareous peels from plant stems and stones are also found some with clear imprints of plant remains. The unit is displayed in Figure 7-18.

*Geochemistry and physical properties:* The depth interval of this facies is so short that it only contains one measurement, for details see Table 7.1 and Figure 7-2.

*Interpretation:* This unit is low energy suspension deposit as indicated by the fine grain size. It is most likely deposited in the shell accumulation or sub-littoral zones (see Figure 5-1). The slightly increased SUS values and mineralogical content relative to facies 12 below may suggest a decreased distance to the lake shore. Thus compared to the facies below this is most likely to represent a regression of the lake. The C:N value of 18 and the C:S value of 60 (Figure 7-2 and Table 7.1) indicates a high autochthonous fraction of organic matter (Meyers and Lallier-Vergés 1999; Meyers and Teranes 2001). The calcareous peels most likely originate from near shore environment where it precipitates on stones or around plant stems as indicated by the finding of plant imprints on the peels due to increased temperature or a decrease in dissolved CO<sub>2</sub>. The termination of facies 13 marks the onset of a considerable increase in the SUS values, mineralogical content,  $\delta^{13}\text{C}_{\text{ORG}}$  and  $\delta^{13}\text{C}_{\text{carb}}$  values, probably the result of a significant change in the water level and in the catchments hydrology possibly inflicted by a climate change (see Figure 7-1).

*Facies 14 (623 cm to 620 cm, 592 cm to 588 cm, 586 cm to 584 cm and 538 cm 536 cm):* A charaphyte gyttja with small amounts of detritus. This unit is 2 cm to 4 cm in thickness and it consists of densely packed stalks. This facies occurs in numerous small depth intervals: i) 623 cm to 620 cm, ii) 592 cm to 588 cm, iii) 586 cm to 584 cm and iv) 538 cm 536 cm. The deposit is clustered in entangled planar units. The charaphytes are monospecific and of autochthonous origin. Insect remains were observed. The charaphytes are enclosed in fine to medium grained gyttja and is illustrated in Figure 7-19.

*Geochemistry and physical properties:* For a summary of the average values of the geochemical data see Table 7.1 and Figure 7-2.

*Interpretation:* This sediment is deposited in the submerged vegetation zone in close proximity to land perhaps in the littoral or sub-littoral zones (see Figure 5-1). The lack of macrofossils and shells suggests that the gyttja in this unit is deposited from suspension in a low energy environment below wave base. The low C:N (average 17) and C:S (average 50) values indicates that the organic matter of this unit is mainly of autochthonous origin (Meyers and Lallier-Vergés 1999; Meyers and Teranes 2001). The observation of charaphytes indicate that the water has most probable been very clear and translucent with a depth of about 5 metres. The high CaCO<sub>3</sub> content ranging between 29 wt% to 50 wt% is likely to be chemical precipitated and bioinduced (see Figure 7-2 and Table 7-1).

*Facies 15 (620 cm to 600 cm):* A very dark brown medium to coarse grained detritus gyttja containing a minor portion of silt. The unit is 20 cm thick. The sediment contains high scattered amounts of gastropod debris both fragments and whole shells. The unit is bioturbated with scattered visible tracks from bottom scavengers, some of which are 2 cm in diameter. A content of scattered calcareous peels encrustations are present. Macrofossil organic material is frequent and is mostly of aquatic origin. The sediment contains minor fragments of aquatic plant roots. Towards the upper part of the deposit aquatic mosses such as *Amblystegium* are frequently observed, and they are especially concentrated around 604 cm. Microscopically amounts of calcareous algal, horsetail (*Equisetales*) stems, fish scales and plant seeds are observed. This unit is illustrated in Figure 7-20A & B.

*Geochemistry and physical properties:* The SUS values and the mineralogical content are increasing. The CaCO<sub>3</sub> content display a peak between 620 cm and 614 cm with maximum occurring values around 617 cm. From 614 cm the CaCO<sub>3</sub> content is slowly increasing. The  $\delta^{13}\text{C}_{\text{carb}}$  values are increasing and the  $\delta^{18}\text{O}_{\text{carb}}$  values are constant. The TS values are increasing up to 605 cm and then decreasing. The TOC values are very slowly increasing, whereas the TON values are noisy by display a very slowly decreasing trend. The C:N values are noisy, but display a slowly decreasing trend. The C:S values are constant. The  $\delta^{13}\text{C}_{\text{ORG}}$  values are constant and the  $\delta^{15}\text{N}_{\text{ORG}}$  values are decreasing. The  $\delta^{34}\text{S}_{\text{ORG}}$  values are constant to very slowly increasing. See Table 7.1 and Figure 7-2 for details.

*Interpretation:* The uniform and medium to coarse grained sediment suggests that it is deposited from suspension in near shore waters. The high amounts of gastropods and macrofossil aquatic organic matter indicate the sediment is deposited near or in the vegetation zone or the

upper shell accumulation zone (see Figure 5-1) as further indicated by the scattered amounts of aquatic roots and the microscopic amounts of horsetail stems, fish scales and plant seeds. This interpretation is in accordance with the low and decreasing C:N values (average 19) indicating an increasingly higher fraction of autochthonous organic matter and the low C:S values (average 57) (Table 7.1) indicating organic matter of mostly autochthonous origin (Meyers and Lallier-Vergés 1999; Meyers and Teranes 2001). The increasing SUS values and mineralogical content may suggest a closer proximity to the lake shore and therefore likely represents a lower water depth.

The elevated TOC values and increasing TON and TS values may likely indicate an increase in the organic productivity. This may be in accordance with the weakly increasing CaCO<sub>3</sub> content which is presumably biogenically induced. The somewhat higher  $\delta^{13}\text{C}_{\text{ORG}}$  (ranging from -30.0‰ to -28.9‰, see Table 7.1) values concurs with higher  $\delta^{13}\text{C}_{\text{carb}}$  relative to the lower lying facies 14 and is likely indicating an increased organic productivity (Hammarlund and Keen 1994; Schwalb and Dean 2002; McFadden *et al* 2005). The weakly decreasing  $\delta^{15}\text{N}_{\text{ORG}}$  values may indicate a decreasing organic productivity or the higher content of algal organic matter (Wolfe *et al* 1999; Muzuka *et al* 2004; Talbot *et al* 2006). The high negative correlation between the  $\delta^{34}\text{S}_{\text{ORG}}$  values and the C:N values ( $\rho=-0.84$ ) suggest that the  $\delta^{34}\text{S}_{\text{ORG}}$  values reflects the organic source material, such that a higher fraction of allochthonous organic material yields lower  $\delta^{34}\text{S}_{\text{ORG}}$  values and *vice versa*. The  $\delta^{18}\text{O}_{\text{carb}}$  values are constant and are likely to reflect an unchanging E/I ratio (Kirby *et al* 2004; Hammarlund *et al* 2005).

*Facies 16 (600 cm to 592 cm, 588 cm to 586 cm and 584 cm to 576 cm):* A dark brown medium grained detritus gyttja containing silt sized carbonate precipitates. The thickness of this deposit



Figure 7-18. Facies 13, at depth 626 cm. Figure 7-19 (to the left). Facies 14, at depth 624 cm.

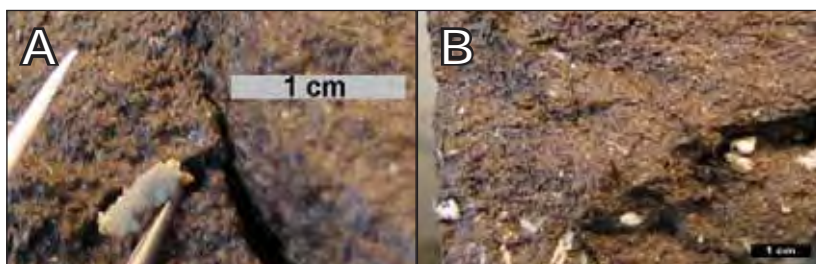


Figure 7-20. (below) A) Facies 15, at depth 600 cm. B) Facies 15, at depth 610



Figure 7-21. Facies 16, at depth 592

varies from 2 cm to 8 cm. This facies occurs in three depth intervals: i) 600 cm to 592 cm ii) 588 cm to 586 cm and iii) 584 cm to 576 cm (see Table 7.1 and Figure 7-2 for details). The deposit contains scattered amounts of ostracod valves primarily fragments and to lesser extent whole shells. The deposit is bioturbated and contains frequent scattered and planar orientated clusters of the aquatic moss *Amblystegium*. Macrofossil remains of scattered aquatic plant debris (an approximate size typically of 3x3 mm, but up to 7x7 mm) and dense small fragments of aquatic roots are observed. Scattered calcareous peels are observed and some with the preserved imprint of plant stems or leaves. Microscopic remains of fish scale, plant seeds and cocoons. The depth interval from 584 cm to 576 cm contains less distinct plant material. This sediment is shown in Figure 7-21.

*Geochemistry and physical properties:* i) The SUS values are decreasing and the mineralogical content display constant values. The CaCO<sub>3</sub> content is constant. The TS and TOC values are constant, and the TON values are increasing. The C:N values are decreasing and the C:S values are slowly decreasing. The  $\delta^{13}\text{C}_{\text{ORG}}$  and  $\delta^{34}\text{S}_{\text{ORG}}$  values are increasing and the  $\delta^{15}\text{N}_{\text{ORG}}$  values are decreasing.

ii) This depth interval consists of only one measurement point; see Table 7.1 for further details.

iii) The SUS values and the mineralogical content are increasing. The CaCO<sub>3</sub> content and the TS values are decreasing. The TOC and TON values are increasing. The C:N and C:S values are decreasing. The  $\delta^{13}\text{C}_{\text{ORG}}$  values are increasing, the  $\delta^{15}\text{N}_{\text{ORG}}$  values are constant and the  $\delta^{34}\text{S}_{\text{ORG}}$  values are increasing.

*Interpretation:* This sediment is likely deposited in quiet water below the wave base from suspension. It is probably deposited in the intermediate to lower littoral zone (see Figure 5-1). The low C:N values indicate a high fraction of autochthonous organic matter as also suggested by the high concentration of aquatic plant debris and the microscopic material of fish scale, plant seeds and cocoons. The microscopic material is probably trapped by the vegetation. The low C:S values of interval i) indicates a high fraction of autochthonous organic matter whereas the higher C:S values of interval ii) indicates an elevated fraction of allochthonous organic matter as may be confirmed by the upwards increasing SUS values and mineralogical content (Meyers 1997; Meyers and Teranes 2001). The slowly increasing TOC, TON and TS values of all depth intervals indicate an increasing primary organic production. The calcareous peels are likely biogenic induced as supported by their imprint of plant material and the constant CaCO<sub>3</sub> content may thus support a constant organic productivity.

*Depth interval i)* The increasing  $\delta^{13}\text{C}_{\text{ORG}}$  values (from -29.6‰ to -28.0‰) may suggest that an increasing amount of terrestrial organic matter have reached the lake (see macrophyte  $\delta^{13}\text{C}_{\text{ORG}}$  values in Figure 7-2), but may more likely represent an increasing organic productivity as may also be confirmed by the elevated  $\delta^{13}\text{C}_{\text{carb}}$  values. This is, however, contradicted by the decreasing  $\delta^{15}\text{N}_{\text{ORG}}$  values (from 4.1‰ to 1.2‰, see Table 7.1). The decreasing  $\delta^{15}\text{N}_{\text{ORG}}$  values may be a result of an increasing amount of nitrogen fixing bacteria assimilation atmospheric nitrogen and or due to a higher fraction of algal organic matter (Talbot 2001; Muzuka *et al* 2004; Talbot *et al* 2006). Commonly the  $\delta^{13}\text{C}_{\text{ORG}}$  values of terrestrial plant have values around -27‰ and  $\delta^{15}\text{N}_{\text{ORG}}$  values around 1‰ to 2‰ (Hammarlund 1993; Hammarlund and Keen 1994; Meyers 1997; Meyers and Teranes 2001; Talbot 2001; Muzuka *et al* 2004). However the low C:N and C:S values do not favour this interpretation. Likewise the increasing  $\delta^{34}\text{S}_{\text{ORG}}$  values in concord with decreasing  $\delta^{15}\text{N}_{\text{ORG}}$  values may indicate less anoxic conditions (Wolfe *et al* 1999; Watanabe *et al* 2004).

*Depth interval iii)* The decreasing  $\delta^{13}\text{C}_{\text{ORG}}$  values may indicate a relatively higher influx of light DIC from decomposing allochthonous organic matter. It may however also indicate a minor increase in the organic productivity (Wolfe *et al* 1999; McFadden *et al* 2005; Talbot *et al* 2006). The low  $\delta^{15}\text{N}_{\text{ORG}}$  may suggest a high content of algal organic matter in the deposit (Muzuka *et al* 2004). The less distinct plant material of the upper unit (584 cm to 576 cm) likely reflects a minor increase in the allochthonous organic matter. The decreasing  $\delta^{18}\text{O}_{\text{carb}}$  value of all depth intervals

may probably indicate a lower E/I ratio probably indicating an increased water inflow in accordance with an increasing nutrient supply (Kirby *et al* 2004; Hammarlund *et al* 2005).

*Facies 17 (576 cm to 538 cm):* A brown fine to medium grain detritus gyttja with a thickness of 34 cm. The deposit contains scattered amounts of gastropod debris primarily fragments and to a lesser extent whole shells. The shell density is highest in the lower part of the unit. The unit contains frequent unsystematic clusters of the aquatic moss *Amblystegium* in the intervals between 566 cm and 574 cm. Macrofossil remains of scattered aquatic plant debris (*typical of approximately 3x3 mm, but up to 7x7 mm*) and small fragments of aquatic roots of low density. Scattered calcareous peels encrustations are observed. At 540 cm a light brown band of about 1 cm with a high content of peels of calcareous material is observed.

*Geochemistry and physical properties:* The SUS values display a broad peak with maximum values occurring around 560 cm. The mineralogical content values are noisy but display a constant trend. The CaCO<sub>3</sub> content is decreasing, and the  $\delta^{13}\text{C}_{\text{carb}}$  and  $\delta^{18}\text{O}_{\text{carb}}$  values are decreasing and then increasing from 560 cm. The TS, TOC and TON values decreasing up to 562 cm then increasing. The C:N and C:S values are constant. The  $\delta^{13}\text{C}_{\text{ORG}}$  values are decreasing up to 570 cm and then increasing. The  $\delta^{15}\text{N}_{\text{ORG}}$  values are increasing up to 562 cm, and then decreasing. The  $\delta^{34}\text{S}_{\text{ORG}}$  values are decreasing. See Table 7.1 and Figure 7-2 for details.

*Interpretation:* This unit is deposited from suspension in a low energy environment below wave base as suggested by fine to medium grain size. The high content of gastropod debris and the macrofossil debris of mainly autochthonous organic matter suggests that the sediment is deposited in the sub-littoral zone. The very low C:N values (*average 14, Table 7.1 and Figure 7-2*) are related to a very high fraction of autochthonous organic matter in the deposit, similar with the decreasing C:S values up to 551 cm (Meyers 1997; Meyers and Teranes 2001). The higher shell density in the lower part of this unit may indicate deposition in closer proximity to shell accumulation zone (*see Figure 5-1*). The peak in the SUS values concurs with the increasing TOC, TON, TS,  $\delta^{13}\text{C}_{\text{ORG}}$  and  $\delta^{15}\text{N}_{\text{ORG}}$  values and may indicate a transgression period resulting in the deposition of a higher amount of allochthonous material which enhances an increasing organic productivity due to an increasing nutrient supply (Wolfe *et al* 1999; McFadden *et al* 2005; Talbot *et al* 2006). Alternatively the peak in the SUS values and the mineralogical content may suggest a period of increased precipitation or a more sparsely vegetated catchments area. However the decreasing  $\delta^{13}\text{C}_{\text{carb}}$  values may alternatively indicate an increased supply of light DIC from decomposed allochthonous organic matter (Hammarlund and Keen 1994; Schwalb and Dean 2002; McFadden *et al* 2005) and thus favour a higher nutrient influx indicating a transgressive period.

The scattered amounts of calcareous peels are likely precipitated in the warmer waters in the beach zone and by an increased organic productivity in the beach and upper coastal zone (McFadden *et al* 2005). The high content of calcareous peels observed at 540 cm is probably biogenic induced perhaps caused by increased autochthonous organic productivity or by minor raise in the lake water level resulting in increased outwash of biogenic calcareous material from the near shore environment. The  $\delta^{18}\text{O}_{\text{carb}}$  values are low probably reflecting a lower E/I ratio most probably related to an increased water inflow.

#### *Interpretation of facies association*

The fine to coarse grained detritus gyttja indicates deposition from suspension in a predominantly low energy environment. The primarily high content of autochthonous organic matter and subsidiary various amounts of allochthonous organic matter may suggest deposition in the vegetation zone. The indistinct and gradual transitions suggest a continuous record and lack of hiatus (Reading 1989) or a result of constant reshuffling of the material in the coastal zone or due to wave activity and bioturbation. The likely deposition zones are illustrated in Figure 7-17 and most likely represent a lower water depth during this period. The sediments are due to their

high content of macrofossil autochthonous organic matter content characterised by littoral to sub-littoral deposits, which is also reflected in their general elevated SUS values and mineralogical content suggesting closer proximity to land.

The littoral and upper telematic zone is the highest organic productive zone of a lake and the high content of autochthonous organic matter and nearly lack of allochthonous organic matter is thus a consequence of deposition in the vegetation zone. This is also reflected by the low C:N and C:S values generally indicating a high fraction of autochthonous organic matter (Meyers 1997; Meyers and Teranes 2001). The TOC and TON values are comparable to the values of other facies association but are however likely to be underestimated due to dilution from the high mineralogical content. Furthermore a higher decomposition rate of organic matter at lower water depth is susceptible of preventing organic matter to reach to bottom floor. The correlation between the  $\delta^{13}\text{C}_{\text{ORG}}$  values and the  $\delta^{13}\text{C}_{\text{carb}}$  values ( $\rho=0.70$ , see Figure 7-6B) suggests close link between organic productivity and the isotopic composition of the DIC pool (Hammalund and Keen 1994; Dean 1999; Wolfe *et al* 1999; Schwab 2002; McFadden *et al* 2005). Hence the  $\delta^{13}\text{C}_{\text{ORG}}$  values of the autochthonous organic matter almost completely reflect the carbon isotopic composition of the DIC pool indicating that productivity changes are the main factor controlling the isotopic composition of both the  $\delta^{13}\text{C}_{\text{ORG}}$  and the  $\delta^{13}\text{C}_{\text{carb}}$  values. This may indicate a somewhat limited concentration of available assimilatory carbon. The  $\delta^{15}\text{N}_{\text{ORG}}$  values are weakly negatively correlated with the  $\delta^{13}\text{C}_{\text{carb}}$  values ( $\rho=-0.61$ ) indicating that the low  $\delta^{15}\text{N}_{\text{ORG}}$  values concurs with high organic productivity suggesting a high content of algal organic matter (Muzuka *et al* 2004). This may also be illustrated by the strong negative correlation between the  $\delta^{13}\text{C}_{\text{ORG}}$  values and the  $\delta^{15}\text{N}_{\text{ORG}}$  values ( $\rho=-0.81$ , see Figure 7-5D). The  $\delta^{13}\text{C}_{\text{ORG}}$  values are most likely controlled by organic productivity changes and the high  $\delta^{15}\text{N}_{\text{ORG}}$  values occurring during low productivity periods may reflect a limited DIN pool (Routh *et al* 2004) whereas high productivity yields low  $\delta^{15}\text{N}_{\text{ORG}}$  values due to a high DIN concentration favouring maximum fractionation during nitrogen assimilation and hence low  $\delta^{15}\text{N}_{\text{ORG}}$  values (Wolfe *et al* 1999; Muzuka *et al* 2004; Watanabe *et al* 2004; McFadden *et al* 2005; Talbot *et al* 2006). The correlation between the  $\delta^{34}\text{S}_{\text{ORG}}$  values and the C:N values ( $\rho=-0.63$ ) suggests that the  $\delta^{34}\text{S}_{\text{ORG}}$  values are controlled by the fraction of allochthonous organic matter with a low  $\delta^{34}\text{S}$  values of the inflowing particulate allochthonous organic matter. The somewhat reduced influx of nutrient and the general lower lake level probably indicates a relatively warm and dry period.

### **Intermediate water facies association**

This facies association is represented by the 5 facies and is covering the depth range from 536 cm to 345 cm. The deposit is 191 cm thick and consists of fine to coarse grained detritus gyttja with mainly autochthonous organic matter content. Frequent and scattered amounts of mainly limnic macrofossil organic are observed. All transitions between facies are indistinct and weakly defined.

#### *Facies – sedimentology, geochemistry and interpretation*

*Facies 18 (536 cm to 518 cm):* A very dark brown fine grained detritus gyttja with a thickness of 3 cm to 18 cm. The deposit is homogeneous with very low density scattered amounts of gastropod debris fragments. The unit is bioturbided with scattered visible gravel tracks from bottom scavengers of 1 cm in diameter. The sediment has a low density of aquatic root and aquatic moss fragments. Microscopic high amounts of aquatic and terrestrial organic material, plant seeds, insect debris, and fish scale are observed. This sediment is illustrated in Figure 7-22.

*Geochemistry and physical properties:* The SUS values and the mineralogical content are increasing. The  $\text{CaCO}_3$  content is very slowly increasing and the  $\delta^{13}\text{C}_{\text{carb}}$  values are decreasing, whereas the  $\delta^{18}\text{O}_{\text{carb}}$  values are constant. The TS, TOC and

TON values are constant. The C:S and C:N values are slowly increasing. The  $\delta^{13}\text{C}_{\text{ORG}}$  and  $\delta^{15}\text{N}_{\text{ORG}}$  values are constant. The  $\delta^{34}\text{S}_{\text{ORG}}$  values slowly increasing. See Table 7.1 and Figure 7-2 for details.

*Interpretation:* This unit is a suspension deposit as suggested by the fine grain size and homogeneity. It most likely deposited in a low energy environment in calm waters. The findings of gastropod, allochthonous and autochthonous plant debris together with the low density of aquatic root fragments most likely reflect a closer proximity to the vegetation zone (see Figure 5-1). The slowly increasing C:N values (ranging from 13 to 17, see Table 7.1) and low C:S values suggest a high fraction of autochthonous organic matter (Routh *et al* 2004; Meyers 2006) and an upwards increasing amount of allochthonous organic matter as supported by the slowly increasing SUS values and mineralogical content. The constant  $\text{CaCO}_3$  content,  $\delta^{13}\text{C}_{\text{ORG}}$ ,  $\delta^{15}\text{N}_{\text{ORG}}$  and  $\delta^{34}\text{S}_{\text{ORG}}$  values may likely indicate a constant organic productivity (Wolfe *et al* 1999; McFadden *et al* 2005; Meyers 2006; Talbot *et al* 2006). The lower  $\delta^{13}\text{C}_{\text{ORG}}$  values and  $\delta^{13}\text{C}_{\text{carb}}$  values may indicate an increased inflow of light DIC from decomposed allochthonous organic matter (Wolfe *et al* 1999). The constant  $\delta^{18}\text{O}_{\text{carb}}$  values may likely reflect a stable E/I ratio (Kirby *et al* 2004; Hammarlund *et al* 2005) in accordance with a relatively constant nutrient supply.

*Facies 19 (518 cm to 487 cm):* A brown medium grained detritus gyttja with a thickness of 30 cm. The deposit is homogenous and is gradually changed towards light brown at the upper boundary. The deposit has frequent and scattered amounts of dense mats of aquatic mosses and contains fragments of calcareous peels. Indistinct and very weak lamina is observed especially around 508 cm. An increasing amount of macrofossil debris of both terrestrial and aquatic organic materials is observed towards the upper part of the deposit. Insects, leaf debris and peels of calcareous material together with infrequent and scattered amounts of ostracods were also observed in the upper part of the deposit. Towards the boundary a high content of bryozoa, winter lids and quartz sand, peels of calcareous material were observed together with a high amount of ostracod shells. The macrofossil content of the lower part of this deposit is very low. The microscopic content of aquatic organic matter is high for lower part, whereas microscopic terrestrial organic material is very infrequent. No visible tracks from bottom scavengers except just below the boundary to the upper facies. This unit is displayed in Figure 7-23.

*Geochemistry and physical properties:* The SUS values and the mineralogical content are increasing. The  $\text{CaCO}_3$  content is increasing and the  $\delta^{13}\text{C}_{\text{carb}}$  values are decreasing. The  $\delta^{18}\text{O}_{\text{carb}}$  values are slowly decreasing. The TS values decrease up to 507 cm and then increase. The TOC and TON values are decreasing up to 509 cm and then increasing. The C:N ratio is decreasing, whereas the C:S values are increasing up to 507 cm and then decreasing. The  $\delta^{13}\text{C}_{\text{ORG}}$  and  $\delta^{15}\text{N}_{\text{ORG}}$  values are constant, whereas the  $\delta^{34}\text{S}_{\text{ORG}}$  values are increasing up to 507 cm and then decreasing. See Table 7.1 and Figure 7-2 for details.

*Interpretation:* This unit is a suspension deposit as suggested by the medium grain size. It most likely deposited below the wave base in a low energy environment. The gradual colour change towards the top of this unit most likely reflects an increasing proximity to land. The C:N values are decreasing and indicate mainly the deposition of autochthonous organic matter (Lamb *et al* 2006; Meyers 2006). The increasing C:S values up to a depth of 509 cm may indicate an increasing fraction of allochthonous organic matter as supported by the observation of an upward increasing amount of macrofossil allochthonous terrestrial organic material (Routh *et al* 2004). The slowly increasing SUS values may indicate a somewhat decreased distance to the lake shore. Furthermore the observation of minor amounts of gastropod shell fragments suggests closer proximity to land upwards.

The increasing TOC values and  $\text{CaCO}_3$  content may indicate an increasing organic productivity in contrast to the constant  $\delta^{13}\text{C}_{\text{ORG}}$  and  $\delta^{15}\text{N}_{\text{ORG}}$  values suggesting an unchanging organic productivity (Wolfe *et al* 1999; Talbot *et al* 2006). However the slowly increasing  $\text{CaCO}_3$  content may probably also be a result of increasing summer temperature. The indistinct lamina concurs with maximum  $\delta^{34}\text{S}_{\text{ORG}}$  and C:S values and likely reflects increased stratification during this period and succeeding layers of summer precipitated  $\text{CaCO}_3$  and suspension fall out of



Figure 7-22. Facies 18, at depth 531 cm.

Figure 7-23. Facies 19, at depth 509 cm.



Figure 7-24. Facies 20, at depth 483

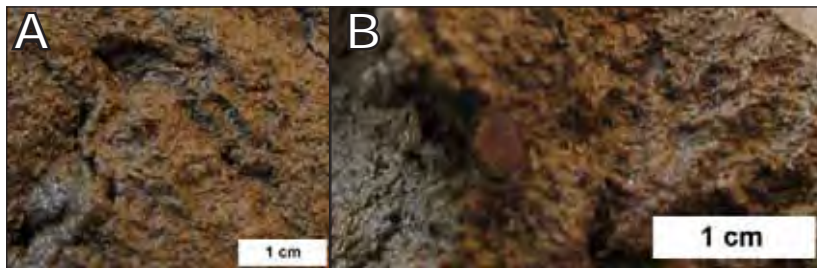


Figure 7-25. A) Facies 21. A) at depth 447 cm (fish scale). B) at depth 360



Figure 7-26. Facies 22, at depth 438

organic material during winters. Both prolonged ice cover and increased summer warmth may have resulted in development of increased stratification (Michelutti *et al* 2006). The decreasing  $\delta^{34}\text{S}_{\text{ORG}}$  may indicate the development of weak anoxic conditions due to increased stratification (Watanabe *et al* 2004). The somewhat increased  $\delta^{15}\text{N}_{\text{ORG}}$  values may indicate ammonia volatilisation (Talbot 2001). Furthermore the  $\delta^{18}\text{O}_{\text{carb}}$  values are very slowly decreasing and most likely suggest a decreasing E/I ratio (Kirby *et al* 2004; Hammarlund *et al* 2005) which probably reflects an increased inflow or decreased evaporation. An increased water inflow may support a slightly increased nutrient supply and hence a slightly increased organic productivity.

*Facies 20 (487 cm to 475 cm):* A brown medium to coarse grained shell detritus gyttja with a thickness of 12 cm. This unit consists of a dense layer of fragmented and whole *Bethynia* shells. From 482 cm to 484 cm a very intense *Bethynia* layer is observed containing many whole shells as well as freshwater mollusc debris (*bivalvia*, *Pisidium sp.*). Frequent and scattered amounts of winter lids and cadis fly larvae, waterlily seeds and insect debris was observed. This Facies is illustrated in Figure 7-24.

*Geochemistry and physical properties:* The SUS values are increasing and the mineralogical content display constant values. The  $\text{CaCO}_3$  content values display a peak with maximum values around 482 cm. The  $\delta^{13}\text{C}_{\text{carb}}$  values are constant and the  $\delta^{18}\text{O}_{\text{carb}}$  values are increasing. The TS, TOC and TON values are decreasing. The C:N and C:S values are slowly increasing. The  $\delta^{13}\text{C}_{\text{ORG}}$  values are decreasing and the  $\delta^{15}\text{N}_{\text{ORG}}$  values are increasing, whereas the  $\delta^{34}\text{S}_{\text{ORG}}$  values are constant. See Table 7.1 and Figure 7-2 for details.

*Interpretation:* This unit is most likely deposited from suspension as suggested by medium to coarse grain size and most likely deposited in the shell zone (see Figure 5-1) as indicated by the numerous amounts of *bethynia*. The increased SUS values and mineralogical content indicate an increased amount of allochthonous material which may likely indicate a decreased distance to the lake shore. The very low C:N and C:S values suggest a very high amount of autochthonous organic matter (Lamb *et al* 2006; Meyers 2006). The decreasing TS and TOC values and  $\delta^{13}\text{C}_{\text{ORG}}$  values are most likely suggesting a decreasing organic productivity and consequently a reduced nutrient supply (Talbot *et al* 2006). This may be further indicated by the increasing  $\delta^{15}\text{N}_{\text{ORG}}$  values due to a limited nitrogen supply (Routh *et al* 2004). The peak in the  $\text{CaCO}_3$  content is probably reflecting the high shell content of this unit that put the  $\delta^{13}\text{C}_{\text{carb}}$  and  $\delta^{18}\text{O}_{\text{carb}}$  values into doubt. On the other hand, elevated temperatures may have caused enhanced  $\text{CaCO}_3$  precipitation. However the increased  $\delta^{18}\text{O}_{\text{carb}}$  values may suggest an increased E/I ratio (Kirby *et al* 2004; Hammarlund *et al* 2005) probably indicating a reduced water influx in accordance with the decreasing TOC and  $\delta^{13}\text{C}_{\text{ORG}}$  values.

*Facies 21 (475 cm to 440 cm and 365 cm to 345 cm):* A light brown fine grained homogenous massive detritus gyttja of about 20 cm to 30 cm in thickness. This facies occurs in two depth intervals: i) 475 cm to 440 cm and ii) 365 cm to 345 cm. The unit contains minor amounts of silt. Infrequent and scattered amounts of macrofossil (1 mm to 2 mm in length) debris of mainly aquatic origin were observed in this unit. Microscopic amounts of mainly aquatic organic debris and very small amounts of terrestrial organic material were also observed. This unit is illustrated in Figure 7-25A & B.

*Geochemistry and physical properties:* See Table 7.1 and Figure 7-2 for details.

i) The SUS values and the mineralogical content are decreasing. The  $\text{CaCO}_3$  content is slowly decreasing and the  $\delta^{13}\text{C}_{\text{carb}}$  values are constant. The  $\delta^{18}\text{O}_{\text{carb}}$  values are decreasing. The TS, TOC, TON, C:N and C:S values are increasing. The  $\delta^{13}\text{C}_{\text{ORG}}$  values are constant and the  $\delta^{15}\text{N}_{\text{ORG}}$  values are decreasing. The  $\delta^{34}\text{S}_{\text{ORG}}$  values are decreasing up to 457 cm and then increases.

ii) The SUS values are increasing and the mineralogical content is constant. At 350 cm the SUS values and the mineralogical content increases dramatically. The  $\text{CaCO}_3$  content is slowly decreasing and the  $\delta^{13}\text{C}_{\text{carb}}$  and  $\delta^{18}\text{O}_{\text{carb}}$  values are constant. The TS values display a peak with maximum values around 350 cm. The TOC values are increasing. At 350 a rapid and dramatic decrease in the TOC values is observed. The TON values are increasing. The C:N values are constant and the C:S values are decreasing. The  $\delta^{13}\text{C}_{\text{ORG}}$  values are constant and decreases from 350 cm. The  $\delta^{15}\text{N}_{\text{ORG}}$  and  $\delta^{34}\text{S}_{\text{ORG}}$  values are decreasing.

*Interpretation:* The fine grain size and homogeneity of this unit indicates deposition from suspension in a low energy environment below wave base. The microscopic amounts of terrestrial and aquatic organic matter together with the low content and scattered content of macrofossil suggest that this sediment is probably deposited in the profundal zone or perhaps the sub-littoral zone. The C:S values around 60 (see Table 7.1) indicates a mixed origin of allochthonous and autochthonous organic matter probably with a somewhat higher fraction of autochthonous organic matter (Routh *et al* 2004). The increasing C:N values of the lower depth interval i) suggest an increasing amount of allochthonous organic matter upwards (Lamb *et al* 2006; Meyers 2006). The increasing TOC, TON and  $\delta^{13}\text{C}_{\text{ORG}}$  values of both intervals is likely related to an increasing organic productivity probably due to an increasing nutrient supply (Wolfe *et al* 1999; McFadden *et al* 2005; Talbot *et al* 2006). The decreasing  $\delta^{15}\text{N}_{\text{ORG}}$  values may indicate a high content of algal organic matter or an increased amount of nitrogen fixing algal matter (Talbot 2001; Filippi and Talbot 2005). This may be further supported by the decreasing  $\delta^{18}\text{O}_{\text{carb}}$  values probably reflecting a decreased E/I ratio (Kirby *et al* 2004; Hammarlund *et al* 2005) which is likely related to an increased water inflow. Likewise the low  $\delta^{13}\text{C}_{\text{carb}}$  values of depth interval i) may indicate a high influx of light DIC from decomposed allochthonous organic matter. The elevated plateau of the  $\text{CaCO}_3$  content and the increasing TOC values may suggest a slowly increasing organic productivity and an increased level of photosynthetic induced  $\text{CaCO}_3$  precipitation. On the other hand, the elevated  $\delta^{13}\text{C}_{\text{carb}}$  values of depth interval ii) may suggest an increased

amount of particulate allochthonous  $\text{CaCO}_3$  (Kolstrup and Buchardt 1982; Noe-Nygaard and Heiberg 2001). However, due to the low  $\delta^{18}\text{O}_{\text{carb}}$  values (Kolstrup and Buchardt 1982; Hammarlund and Buchardt 1996; Noe-Nygaard and Heiberg 2001) the higher  $\delta^{13}\text{C}_{\text{carb}}$  values are not likely caused by increased amounts of particulate allochthonous  $\text{CaCO}_3$  and the elevated  $\delta^{13}\text{C}_{\text{carb}}$  values may suggest a decreased flux of light DIC from decomposed organic matter and may yield the somewhat enriched  $\delta^{13}\text{C}_{\text{ORG}}$  values. The decreasing  $\delta^{34}\text{S}_{\text{ORG}}$  values may indicate bacterial sulphate reduction and the development of weak anoxia conditions (Watanabe *et al* 2004; Eimers *et al* 2006). However this contrasts the decreasing  $\delta^{15}\text{N}_{\text{ORG}}$  values indicating vanishing ammonia volatilisation. Hence the  $\delta^{34}\text{S}_{\text{ORG}}$  values may be related to differences in the ratio of allochthonous to autochthonous organic matter.

*Facies 22 (365 cm to 440 cm):* A dark brown fine to medium grained detritus gyttja. The unit is homogenous and contains only few macrofossil remains of about 1 mm to 2 mm in length. The microscopic organic content is mostly of aquatic origin, however a few debris fragments of terrestrial organic plant are observed. At 438 cm an 8 mm wide and 20 mm long gravel track from bottom scavengers containing ostracods and seed debris is found (*see Figure 7-26*).

*Geochemistry and physical properties:* The SUS values are decreasing and the mineralogical content is slowly increasing up to 387 cm and then display constant values. The  $\text{CaCO}_3$  content is decreasing and the  $\delta^{13}\text{C}_{\text{carb}}$  values are increasing and the  $\delta^{18}\text{O}_{\text{carb}}$  values are decreasing. The TS, TOC and TON values are increasing. The C:N values display a rapid decrease up to 430 cm followed by slowly increasing values. The C:S values are increasing up to 419 cm and then decreases. The  $\delta^{13}\text{C}_{\text{ORG}}$  values are increasing and the  $\delta^{15}\text{N}_{\text{ORG}}$  values are slowly decreasing up to 380 cm where they again increase. The  $\delta^{34}\text{S}_{\text{ORG}}$  values increases up to 420 cm and then they slowly decreases. See Table 7.1 and Figure 7-2 for details.

*Interpretation:* The fine to medium grain size and homogeneity of this sediment indicates deposition from suspension deposit in a low energy environment below wave base. The decreasing SUS values indicate a decreasing distance to the lake shore and probably an increasing water depth. The few macrofossil fragments and the numerous amounts of microscopic organic matter suggest that this unit is most likely deposited in the profundal zone (*see Figure 5-1*). The initial rapidly decreasing C:N values indicate an upward increase in the fraction of autochthonous organic matter (Lamb *et al* 2006; Meyers 2006) and the increasing TOC values may indicate an increased organic productivity. The strong correlation between the TOC values and the  $\delta^{13}\text{C}_{\text{ORG}}$  values ( $\rho=0.72$ , *see Figure 7-5B*) suggests that the  $\delta^{13}\text{C}_{\text{ORG}}$  values mimic the organic productivity. Hence the increasing  $\delta^{13}\text{C}_{\text{ORG}}$  and  $\delta^{13}\text{C}_{\text{carb}}$  values indicate an increasing organic productivity and thus an increasing influx of nutrients (Wolfe *et al* 1999; Talbot *et al* 2006). The increasing C:S values indicates an increased fraction of allochthonous organic matter supporting an increased nutrient supply (Routh *et al* 2004). The decreasing  $\delta^{15}\text{N}_{\text{ORG}}$  values may indicate an increased amount of algal organic matter (Muzuka *et al* 2004). The decreasing  $\delta^{18}\text{O}_{\text{carb}}$  values may suggest a decreasing E/I ratio (Kirby *et al* 2004; Hammarlund *et al* 2005) probably reflecting an increased water inflow in accordance with an increased nutrient supply.

#### *Interpretation of facies association*

The fine to coarse grained detritus gyttja indicates deposition by suspension in a low energy environment. The primarily high content of autochthonous organic matter and subsidiary various amounts of allochthonous organic matter suggests deposition in the sub-littoral zone to the upper profundal zone as also indicated by the high content of macrofossil organic matter. The high autochthonous organic matter content is confirmed by the low C:N (*average 19*, *see Table 7.2*) and C:S values (*average 73*, *see Table 7.2*) (Meyers and Teranes 2001; Routh *et al* 2004; Meyers 2006). The indistinct and gradual transitions suggest a continuous record and lack of hiatus (Reading 1989). The likely deposition zones are illustrated in Figure 7-17 and most likely represent a continued increase in the water depth during this period.

The TOC and TON values are ranging from 14 wt% to 29 wt% (see Table 7.2) and their general increasing values together with the general decreasing  $\delta^{18}\text{O}_{\text{carb}}$  values are most likely representing an increasing nutrient supply and water inflow to the lake (Kirby *et al* 2004; Hammarlund *et al* 2005; Talbot *et al* 2006). The high correlation between the TOC values and the  $\delta^{13}\text{C}_{\text{ORG}}$  values ( $\rho=0.71$ , see Figure 7-5B) suggests that the  $\delta^{13}\text{C}_{\text{ORG}}$  values are controlled by changes in organic productivity (Wolfe *et al* 1999; McFadden *et al* 2005; Talbot *et al* 2006) and is further supported by the correlation between the  $\delta^{13}\text{C}_{\text{ORG}}$  and  $\delta^{13}\text{C}_{\text{carb}}$  values ( $\rho=0.64$ , see Figure 7-6B). Hence the variations in the  $\delta^{13}\text{C}_{\text{carb}}$  values are most likely caused by organic productivity. The positive correlation between the  $\delta^{13}\text{C}_{\text{carb}}$  values and the  $\text{CaCO}_3$  content ( $\rho=0.66$ , see Figure 7-4C) may suggest that the  $\text{CaCO}_3$  content is partially derived from allochthonous sources. The negative correlation between the  $\text{CaCO}_3$  content and  $\delta^{13}\text{C}_{\text{carb}}$  values ( $\rho=-0.62$ , see Figure 7-6D) together with the negative correlation between the  $\delta^{13}\text{C}_{\text{carb}}$  and  $\delta^{18}\text{O}_{\text{carb}}$  values ( $\rho=-0.59$ , see Figure 7-6A) may however not support this, because a high allochthonous  $\text{CaCO}_3$  content is most likely to yield a positive correlation between the  $\delta^{13}\text{C}_{\text{carb}}$  and  $\delta^{18}\text{O}_{\text{carb}}$  values due to higher  $\text{CaCO}_3$  isotopic composition (Kolstrup and Buchardt 1982; Hammarlund and Buchardt 1996; Noe-Nygaard and Heiberg 2001). Hence the predominately component of the  $\text{CaCO}_3$  content is most likely bioinduced and the negative correlation between the TOC values and the  $\text{CaCO}_3$  content ( $\rho=-0.81$ ) is probably due to dissolution of  $\text{CaCO}_3$  due to a higher organic matter decomposition and thereby higher  $\text{CO}_2$  concentrations during periods with high organic productivity (Dean 1999).

The high negative correlation between the  $\delta^{13}\text{C}_{\text{ORG}}$  and  $\delta^{15}\text{N}_{\text{ORG}}$  values ( $\rho=-0.81$ , see Figure 7-5F) is likely reflecting an increased algal productivity during periods of high organic productivity (Muzuka *et al* 2004), but may also suggest a limited DIN pool during periods of low organic productivity (Routh *et al* 2004; Ogrinc *et al* 2005). Alternatively the negative correlation between the  $\delta^{15}\text{N}_{\text{ORG}}$  and  $\delta^{34}\text{S}_{\text{ORG}}$  values ( $\rho=-0.68$ , see Figure 7.8D) may indicate that higher  $\delta^{15}\text{N}_{\text{ORG}}$  values occur with low  $\delta^{34}\text{S}_{\text{ORG}}$  values indicating anoxic hypolimnion conditions and bacterial sulphate reduction (Watanabe *et al* 2004; Eimers *et al* 2006). Hence the high  $\delta^{15}\text{N}_{\text{ORG}}$  values may be due to denitrification or ammonia volatilisation (Talbot 2001).

### Shallow water (B) facies association

This facies association is represented by 3 facies and range from 345 cm to 180 cm. The deposit is 165 cm thick and consists of a medium grained detritus gyttja with mainly an autochthonous organic matter content and frequent macrofossil limnic organic material. This deposit contains minor portions of silt and clay material. All transitions between facies are indistinct and weakly defined.

#### *Facies – sedimentology, geochemistry and interpretation*

*Facies 23 (345 cm to 318 cm and 304 cm to 289 cm):* A dark brown medium grained plastic detritus gyttja with a thickness of about 25 cm. This facies occurs in two depths intervals: i) 345 cm to 318 cm and ii) 304 cm to 289 cm. This unit is homogeneous and has a very high and upwards increasing content of macrofossil aquatic organic material of sizes up to 3 mm times 10 mm. Infrequent and very low amounts and scattered macrofossil of terrestrial organic matter. Upwards increasing content of small root fragments of about 2 mm to 3 mm in length. A high content of whole and fragmented ostracods of size 1 mm to 2 mm was observed. The sediment contains silt particles and silt sized calcareous particles or peels. This unit has a high content of transparent insect wing debris and seeds. A very low content of microscopic fragmented shells was observed. This deposit is illustrated in Figure 7-27.

*Geochemistry and physical properties:* i) The SUS values and the mineralogical content are increasing. The  $\text{CaCO}_3$  content is decreasing and the  $\delta^{13}\text{C}_{\text{carb}}$  and  $\delta^{18}\text{O}_{\text{carb}}$  values are constant. The TS values are decreasing up to 330 cm and then increasing. The TOC and TON values are decreasing. The C:N and C:S ratio display constant values. The  $\delta^{13}\text{C}_{\text{ORG}}$  values rapidly

increases up to 340 cm succeeded by slowly decreasing values. The  $\delta^{15}\text{N}_{\text{ORG}}$  values rapidly increase up to 340 cm and are then slowly decreasing and the  $\delta^{34}\text{S}_{\text{ORG}}$  values are decreasing. See Table 7.1 and Figure 7-2 for details.

ii) The SUS values are slowly decreasing and the mineralogical content display constant values. The  $\text{CaCO}_3$  is decreasing and the  $\delta^{13}\text{C}_{\text{carb}}$  values display decreasing values, whereas the  $\delta^{18}\text{O}_{\text{carb}}$  values are increasing. The TS values are constant, but noisy. The TOC and TON values are slowly increasing. The C:N values are increasing and the C:S values are noisy, but display a constant value trend. The  $\delta^{13}\text{C}_{\text{ORG}}$  and  $\delta^{15}\text{N}_{\text{ORG}}$  values are decreasing, whereas the  $\delta^{34}\text{S}_{\text{ORG}}$  values are increasing. See Table 7.1 and Figure 7-2 for details.

*Interpretation:* The medium grain size and the homogeneity of this sediment suggest deposition from suspension in a low energy environment below the wave base. The numerous amounts of macrofossil aquatic and terrestrial organic matter, insect debris and ostracod fragments indicate deposition in the vegetation zone (see Figure 5-1). The low C:N and C:S values indicate a high fraction of autochthonous organic matter (Routh *et al* 2004; Lamb *et al* 2006; Meyers 2006). The plasticity and minor amount of silt may likely indicate increased amounts of wash material from the surrounding catchments area as indicated by the high SUS values and mineralogical content ( $\rho_{\text{SUS vs mineralogical}}=0.89$ , see Figure 7-3). Furthermore the SUS values are strongly negative correlated with the  $\text{CaCO}_3$  content ( $\rho=-0.85$ , see Figure 7-4C) suggesting that a high  $\text{CaCO}_3$  content is probably not related to particulate allochthonous  $\text{CaCO}_3$  eroded material. This is further supported by the negative correlation between the SUS values and the  $\delta^{13}\text{C}_{\text{carb}}$  values indicating that a high amount of allochthonous eroded material is associated with decreased  $\delta^{13}\text{C}_{\text{carb}}$  values in contrast to the stable isotope composition of the tills (Kolstrup and Buchardt 1982; Noe-Nygaard and Heiberg 2001). Hence the majority of the  $\text{CaCO}_3$  is most likely authigenic precipitated due to photosynthetic activity. The decreasing TOC values of depth interval i) may indicate a reduced organic productivity perhaps due to a reduced influx of nutrients, whereas the increasing TOC values of depth interval ii) may suggest an increasing organic productivity and thus probably an increasing nutrient supply. Therefore the two depth intervals are interpreted separately.

*Depth interval i)* The elevated and generally decreasing  $\delta^{13}\text{C}_{\text{ORG}}$  values may suggest an increased amount of allochthonous organic matter and a decreasing organic productivity. The latter is in accordance with the decreasing TOC values. The low C:N and C:S values indicate a high fraction of autochthonous organic matter (Routh *et al* 2004; Lamb *et al* 2006; Meyers 2006). The  $\delta^{13}\text{C}_{\text{carb}}$  values are very increased and approaches 1.7‰ indicating perhaps a decreased supply of light DIC from decomposed organic matter. However, more likely the  $\delta^{13}\text{C}_{\text{ORG}}$  values are related to the increased  $\delta^{13}\text{C}_{\text{carb}}$  values due to a high organic productivity. However this is in discrepancy with the decreasing TOC values, but elevated  $\delta^{13}\text{C}_{\text{ORG}}$  and  $\delta^{13}\text{C}_{\text{carb}}$  values may reflect the higher organic productivity in the littoral zone and perhaps the shallow water. The increasing  $\delta^{15}\text{N}_{\text{ORG}}$  and decreasing  $\delta^{34}\text{S}_{\text{ORG}}$  values may indicate increased bacterial sulphate reduction and ammonia volatilisation. Furthermore the high TS content may reflect preferential storage of sulphur in the organic material which may support bacterial sulphate reduction (Watanabe *et al* 2004; Eimers *et al* 2006). On the other hand the increasing  $\delta^{15}\text{N}_{\text{ORG}}$  values may probably also be related to a limited DIN pool (Routh *et al* 2004), and the decreasing  $\delta^{34}\text{S}_{\text{ORG}}$  values and elevated TS values may have an allochthonous origin as may be supported by the increased mineralogical content and SUS values. The increasing  $\delta^{18}\text{O}_{\text{carb}}$  values may indicate an increasing E/I ratio (Kirby *et al* 2004; Hammarlund *et al* 2005) probably related to a reduced water inflow as also suggested by the decreasing TOC and  $\delta^{13}\text{C}_{\text{ORG}}$  values.

*Depth interval ii)* The decreasing  $\delta^{13}\text{C}_{\text{ORG}}$  values and the slowly decreasing  $\delta^{15}\text{N}_{\text{ORG}}$  values are in contradiction with an increasing nutrient supply and are likely indicating a decreased organic productivity (Wolfe *et al* 1999; McFadden *et al* 2005; Talbot *et al* 2006). Thus the minor increase in the organic content is probably a result of a minor increase in the amount of allochthonous organic matter as also suggested by the somewhat higher C:N and C:S values (Routh *et al* 2004; Lamb *et al* 2006; Meyers 2006). The strong negative correlation between the SUS values and the  $\delta^{34}\text{S}_{\text{ORG}}$  values may indicate the addition of  $^{34}\text{S}$  depleted allochthonous material to the lake.

Likewise the increasing trend of the  $\delta^{18}\text{O}_{\text{carb}}$  values are probably related to an increased E/I ratio (Kirby *et al* 2004; Hammarlund *et al* 2005) and thus likely indicate a reduced water inflow.

*Facies 24 (318 cm to 304 cm and 289 cm to 222 cm):* A brown medium grained plastic and massive detritus gyttja with thickness up to about 30 cm. This facies occurs in two depths intervals: i) 318 cm to 304 cm and ii) 289 cm to 222 cm. The deposit has a high content of macrofossil organic material of aquatic origin and an infrequent and low content of macrofossil terrestrial organic matter. Microscopic amounts of aquatic and terrestrial organic matter, fish scale and seed is observed where the majority being of aquatic origin. The deposit contains numerous amounts of silt sized calcareous particles. The increasing amounts of macrofossil organic matter upward and a dense layer of macrofossil aquatic organic matter is located at the upper boundary at 222 cm (see Figure 7-28A & B). At 241 cm a well preserved leave of *phragmetis* was found (see Figure 7-28B).

*Geochemistry and physical properties:* i) The SUS values are constant and the mineralogical content is increasing. The  $\text{CaCO}_3$  and  $\delta^{13}\text{C}_{\text{carb}}$  values are decreasing, whereas the  $\delta^{18}\text{O}_{\text{carb}}$  values are slowly increasing. The TS, TOC, TON and C:N values are constant. The C:S values are slowly increasing. The  $\delta^{13}\text{C}_{\text{ORG}}$ ,  $\delta^{15}\text{N}_{\text{ORG}}$  and  $\delta^{34}\text{S}_{\text{ORG}}$  values are constant. See Table 7.1 and Figure 7-2 for details.

ii) The SUS values are increasing up to 270 cm and then abruptly fall to lower and re-increasing values. From 240 cm the SUS values are again decreasing. The mineralogical content is decreasing up to 249 cm succeeded by a peak with maximum values around 235 cm. The  $\text{CaCO}_3$  content is increasing up to 250 cm followed by a fall and constant values. The  $\delta^{13}\text{C}_{\text{carb}}$  and  $\delta^{18}\text{O}_{\text{carb}}$  values are increasing. The TS, TOC and TON values are constant. The C:N values are constant, but noisy and the C:S values are slowly decreasing. The  $\delta^{13}\text{C}_{\text{ORG}}$  values slowly increasing and the  $\delta^{15}\text{N}_{\text{ORG}}$  values are constant. The  $\delta^{34}\text{S}_{\text{ORG}}$  values are slowly increasing. See Table 7.1 and Figure 7-2 for details.

*Interpretation:* The medium grain size suggests deposition from suspension in a low energy environment below the wave base. The elevated SUS values and mineralogical content are likely related to a high amount of allochthonous eroded material as also suggested by the plasticity of the sediment. The numerous amounts of large macrofossil fragments of both terrestrial and aquatic origin suggest that this unit is deposited in the littoral zone. This is confirmed by C:N and C:S values indicating mixed organic matter content with a high fraction of autochthonous organic matter (Routh *et al* 2004; Lamb *et al* 2006; Meyers 2006). The well preserved character of the *phragmetis* fragment is likely to have been produced *in situ* which suggests that the water depth has not been greater than about 2 to 3 metres. The  $\text{CaCO}_3$  content of about 25 wt% (see Table 7.1) is likely bioinduced, but may derive from particulate allochthonous  $\text{CaCO}_3$  as may be suggested by the very high  $\delta^{13}\text{C}_{\text{carb}}$  values (Kolstrup and Buchardt 1982; Noe-Nygaard and Heiberg 2001). However the very low  $\delta^{18}\text{O}_{\text{carb}}$  values may indicate the contrary.

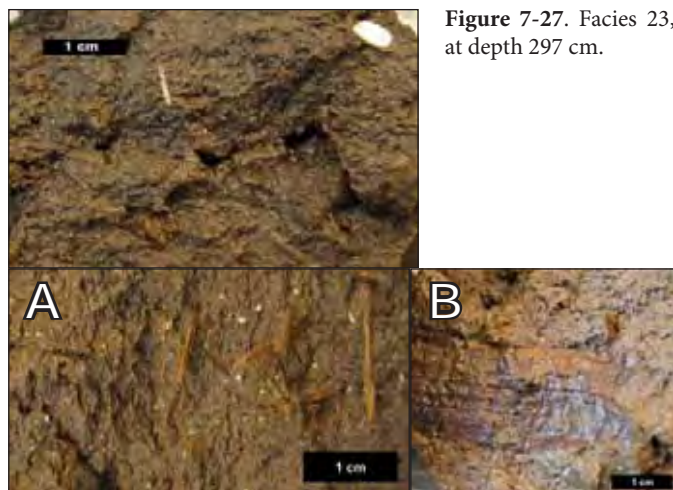


Figure 7-27. Facies 23, at depth 297 cm.

Figure 7-28. A) Facies 24, at depth 224 cm. B) Facies 24, at depth 241 cm.

*Depth interval i)* The decreasing TOC values, CaCO<sub>3</sub> content,  $\delta^{13}\text{C}_{\text{ORG}}$  and  $\delta^{13}\text{C}_{\text{carb}}$  values are probably indicating a decreasing organic productivity and is probably related to a decreased nutrient supply. The elevated  $\delta^{13}\text{C}_{\text{carb}}$  values may indicate a reduced inflow of light DIC from allochthonous decomposed organic matter. The somewhat elevated  $\delta^{18}\text{O}_{\text{carb}}$  values may indicate an increased amount of till CaCO<sub>3</sub> or a relatively elevated E/I ratio (Kirby *et al* 2004; Hammarlund *et al* 2005) perhaps related to a decreased water inflow as suggested by the decreasing organic productivity.

*Depth interval ii)* The constant TOC and TON values are probably suggesting an unchanging organic productivity. This may be supported by the somewhat elevated but constant  $\delta^{15}\text{N}_{\text{ORG}}$  values which likely are related to a limited DIN pool (Routh *et al* 2004). In contrast the increasing  $\delta^{13}\text{C}_{\text{ORG}}$  and  $\delta^{13}\text{C}_{\text{carb}}$  values may indicate an increasing organic productivity (Wolfe *et al* 1999; McFadden *et al* 2005; Talbot *et al* 2006). However the elevated  $\delta^{13}\text{C}_{\text{carb}}$  values may derive from a reduced inflow of light DIC from decomposing allochthonous organic matter or it may be related to an increased water residence time (Schwalb 2002; Schwalb and Dean 2002). Furthermore, during limited DIC conditions the isotopic composition of the produced organic matter mirrors the DIC isotopic composition because virtually all available DIC is consumed. Thus it is possible that the elevated  $\delta^{13}\text{C}_{\text{ORG}}$  values are a result of elevated  $\delta^{13}\text{C}_{\text{carb}}$  values. Otherwise the increasing  $\delta^{13}\text{C}_{\text{ORG}}$  values may suggest an increasing content of allochthonous organic matter. The increasing  $\delta^{18}\text{O}_{\text{carb}}$  values may indicate an increased E/I ratio (Kirby *et al* 2004; Hammarlund *et al* 2005) probably suggesting a somewhat reduced water inflow.

*Facies 25 (222 cm to 180 cm):* A brownish olive green medium grained plastic detritus gyttja with thickness of 42 cm. This unit has high clay content and a high content of macrofossil aquatic organic matter of up to 2 mm times 7 mm. The sediment has a very high microscopic content of aquatic organic material, fish scale and seed and a low microscopic content of terrestrial organic matter. Silt sized calcareous particles and quartz sand is also observed.

*Geochemistry and physical properties:* The SUS values are increasing up to 210 cm and then decreasing. The mineralogical content is increasing up to 194 cm and the decreasing. The CaCO<sub>3</sub> content is decreasing up to 190 cm followed by a rapid increase and then slowly decreasing values. The  $\delta^{13}\text{C}_{\text{carb}}$  values are constant and the  $\delta^{18}\text{O}_{\text{carb}}$  values are constant to very slowly increasing. The TS values are constant up to 190 cm and then increasing. The TOC values are constant up to 210 cm where a short period of decreased values is observed. From 200 cm the TOC values are slowly decreasing. The TON values are constant. The C:N and C:S values are decreasing. The  $\delta^{13}\text{C}_{\text{ORG}}$  and  $\delta^{15}\text{N}_{\text{ORG}}$  values are fluctuating but display a constant tendency. The  $\delta^{34}\text{S}_{\text{ORG}}$  values are constant up to 190 cm and then decreases. See Table 7.1 and Figure 7-2 for details.

*Interpretation:* The medium grain size gyttja suggest deposition from suspension in a low energy environment below the wave base. The elevated and decreasing SUS values indicate a high but decreasing allochthonous eroded content as also suggested by the sedimentological observation of high clay content. Likewise this is supported by the findings of quartz sand particles. The numerous amounts of aquatic macrofossil organic matter probably indicate deposition in the littoral zone (*see Figure 5-1*). The decreasing tendency of the C:N and C:S values further suggests a decreasing fraction of allochthonous organic matter (Routh *et al* 2004; Lamb *et al* 2006; Meyers 2006) as supported by the decreasing SUS values. The TOC and TON values are decreasing indicating a decreasing organic productivity and probably a decreasing nutrient supply. Likewise the increasing  $\delta^{13}\text{C}_{\text{carb}}$  values may suggest a decreased flux of light DIC from decomposed allochthonous organic matter (Dean 1999; Schwalb 2002; McFadden *et al* 2005). However the  $\delta^{13}\text{C}_{\text{carb}}$  values approaching 2‰ may likely indicate a high input of particulate CaCO<sub>3</sub> from the catchments tills (Kolstrup and Buchardt 1982; Noe-Nygaard and Heiberg 2001). On the other hand the low  $\delta^{18}\text{O}_{\text{carb}}$  values may not favour this interpretation (Kolstrup and Buchardt 1982; Hammarlund and Buchardt 1996; Noe-Nygaard and Heiberg 2001). Likewise the CaCO<sub>3</sub> content is decreasing in concord with the TOC values and probably indicating less bioinduced CaCO<sub>3</sub>. The constant and somewhat elevated  $\delta^{13}\text{C}_{\text{ORG}}$  and  $\delta^{15}\text{N}_{\text{ORG}}$  values may be related to allochthonous organic matter (Hammarlund 1993; Watanabe *et al* 2004). The increasing  $\delta^{18}\text{O}_{\text{carb}}$

values are likely to indicate an increasing E/I ratio (Kirby *et al* 2004; Hammarlund *et al* 2005) probably related to a decreasing water inflow in accordance with a reduced nutrient supply. Towards the upper part of this unit the  $\delta^{34}\text{S}_{\text{ORG}}$  values drops significantly towards lower values likely indicating the onset of bacterial sulphate reduction and suggesting the development of more anoxic conditions (Watanabe *et al* 2004; Eimers *et al* 2006).

#### *Interpretation of facies association*

The medium grained detritus gyttja indicates deposition from suspension in a low energy environment. The primarily high content of autochthonous organic matter and subsidiary various amounts of allochthonous organic matter suggests deposition in the littoral zone. The indistinct and gradual transitions suggest a continuous record and lack of hiatus (Reading 1989). The likely deposition zones are illustrated in Figure 7-17 and most likely represent a pronounced fall in the water depth.

All facies in this facies association display high clay content in concord with high SUS values and mineralogical content suggesting that considerable amounts of eroded allochthonous material have entered the lake. In contrast, both the low TOC (*less than 23 wt%*, see Table 7.2) and  $\text{CaCO}_3$  (*less than 34 wt%*, see Table 7.2) content suggest a low nutrient supply to the lake, even though the TOC and  $\text{CaCO}_3$  content may appear lower due to dilution by the very high mineralogical content (*higher than 26 wt% and up to 46 wt%*, see Table 7.2). Likewise the generally increasing  $\delta^{18}\text{O}_{\text{carb}}$  values are likely to indicate an increasing E/I ratio (Kirby *et al* 2004; Hammarlund *et al* 2005) probably reflecting a decreasing water inflow. The C:N ratios with an average of 19 and the C:S values with an average of 73 (see Table 7.2) both indicate a mixed composition of allochthonous and autochthonous organic matter dominated by autochthonous organic matter (Meyers and Teranes 2001; Routh *et al* 2004; Meyers 2006). The high correlation between the  $\delta^{13}\text{C}_{\text{ORG}}$  and  $\delta^{13}\text{C}_{\text{carb}}$  values ( $\rho=0.87$ , see Figure 7-6B) indicates that both organic isotope composition and the  $\delta^{13}\text{C}_{\text{carb}}$  values are mainly controlled by organic matter productivity (Wolfe *et al* 1999; McFadden *et al* 2005; Talbot *et al* 2006). Hence the generally increasing  $\delta^{13}\text{C}_{\text{ORG}}$  and  $\delta^{13}\text{C}_{\text{carb}}$  may likely indicate an upward increasing organic productivity perhaps reflecting an increased proximity to the littoral zone.

The high  $\delta^{13}\text{C}_{\text{carb}}$  values may on the other hand indicate a high amount of allochthonous particulate  $\text{CaCO}_3$ , but the low  $\delta^{18}\text{O}_{\text{carb}}$  values however do not support this (Kolstrup and Buchardt 1982; Hammarlund and Buchardt 1996; Noe-Nygaard and Heiberg 2001). Hence the  $\text{CaCO}_3$  content is probably predominately of autochthonous origin.

#### **High water (B) facies association**

This facies association is represented by 3 facies representing the upper 1 metre of the Bliden Lake core B1. The deposit consists of fine to coarse grained detritus gyttja with a low organic matter content of mainly autochthonous organic matter. Macrofossil organic material is only observed for the lower part of this deposit. All transitions are indistinct and weakly defined.

#### *Facies – sedimentology, geochemistry and interpretation*

*Facies 26 (180 cm to 159 cm):* A dark olive green brownish medium grained detritus gyttja with frequent macrofossil aquatic plant and root remains. The unit has a thickness of 21 cm. The sediment displays an upward grain coarsening towards the boundary to the overlying shell dominated detritus gyttja. Microscopically silt sized carbonate particles and fragments of terrestrial leaves and twigs were observed together with a high content of aquatic organic matter. A minor shell layer was found at 175 cm.

*Geochemistry and physical properties:* The SUS values are decreasing and the mineralogical content is slowly increasing. The  $\text{CaCO}_3$  values are constant and the  $\delta^{13}\text{C}_{\text{carb}}$  and  $\delta^{18}\text{O}_{\text{carb}}$  values are decreasing. The TS, TOC, TON, C:N and C:S values are constant. The  $\delta^{13}\text{C}_{\text{ORG}}$  values are constant and the  $\delta^{15}\text{N}_{\text{ORG}}$  values are increasing. The  $\delta^{34}\text{S}_{\text{ORG}}$  values are decreasing. See Table 7.1 and Figure 7-2 for details.

*Interpretation:* This medium grain size gyttja is probably deposited from suspension in a low energy environment below wave base. The very low C:S and C:N values of about 19 and 18 (see Table 7.1) respectively indicate a very high fraction of autochthonous organic matter (Routh *et al* 2004; Lamb *et al* 2006; Meyers 2006) in concord with the numerous fragments of terrestrial and limnic origin that indicate a near shore deposition regime probably in the littoral zone (see Figure 5-1). The shell layer at the upper part of this unit may indicate a gradual movement from the littoral zone towards the shell accumulation zone (see Figure 5-1), thus probably representing an increasing distance to the lake shore. The high mineralogical content of about 48 wt% (see Table 7.1) indicates that considerable amounts of out washed allochthonous material are present in the deposit. The decreasing but elevated SUS values suggests an upwards decreasing amount of allochthonous eroded material which may indicate decreased proximity to the lake shore.

The constant  $\delta^{13}\text{C}_{\text{ORG}}$  values and decreasing  $\delta^{13}\text{C}_{\text{carb}}$ , TOC and TON values may indicate an unchanging to slowly decreasing organic productivity. Thus if the high mineralogical content and elevated SUS values reflect a high flux of eroded material entering the lake then this suggests a poor nutrient content of the inflowing water. However the low TON and TOC content may be diluted by the very high mineralogical content and thus appear lower. On the other hand, the  $\text{CaCO}_3$  content may also support a low autochthonous organic productivity as consequently less biogenic induced  $\text{CaCO}_3$  is precipitated. The elevated  $\delta^{13}\text{C}_{\text{carb}}$  values (average 0.7‰, see Table 7.1) suggest either a less dense terrestrial vegetation and consequently a DIC pool containing less  $\text{CO}_2$  from decomposed terrestrial organic matter or a low nutrient supply to the lake resulting in an enriched  $^{13}\text{C}$  DIC pool. The latter is supported by the elevated  $\delta^{13}\text{C}_{\text{ORG}}$  values having a mean value of -29.1‰ (see Table 7.1). The elevated  $\delta^{13}\text{C}_{\text{ORG}}$  values are likely not related to a high fraction of allochthonous organic matter as seen by the low C:N and C:S values.

The steadily decreasing  $\delta^{34}\text{S}_{\text{ORG}}$  values approaching 0‰ (see Table 7.1) may reflect an increased usage of bacterially reduced hydrogen sulphide (Watanabe *et al* 2004; Eimers *et al* 2006) or alternatively an increased influx of depleted allochthonous sulphur bearing materials. The strong negative correlation between the  $\delta^{15}\text{N}_{\text{ORG}}$  values and the TOC content ( $\rho=-0.74$ , see Figure 7-9A) may suggest that  $\delta^{15}\text{N}_{\text{ORG}}$  periods of high productivity are caused by nitrogen fixing bacteria resulting in lower  $\delta^{15}\text{N}_{\text{ORG}}$  values and conversely that low productivity periods represent a limited DIN pool progressively enriching the DIN reservoir as  $^{14}\text{N}$  is preferentially removed (Routh *et al* 2004). The decreasing  $\delta^{18}\text{O}_{\text{carb}}$  values are likely to reflect the decreasing E/I ratio (Kirby *et al* 2004; Hammarlund *et al* 2005) probably related to an increased water inflow. Both interpretations may support a lake deepening and poorly terrestrial vegetation.

*Facies 27 (159cm to 138cm):* A medium to coarse grained shell gyttja containing increasingly fragments of shells gastropods up to a depth of 152 cm. The interval from 152 cm to 148 cm consists of an intense shell layer of mostly un-fragmented shells. The grain size is coarsening towards 152 cm and is followed by a trend towards finer grains size up to 138 cm. The transition towards the above fine grained detritus gyttja is indistinct. Indistinct lamina layers are observed in the interval between 148 cm to 138 cm of coarse grained gyttja and fragmented shell layers with an interlayer distance of approximately 3 mm to 5 mm. This unit is illustrated in 7-29.

*Geochemistry and physical properties:* The SUS values and the mineralogical content are decreasing. The  $\text{CaCO}_3$  content increases and the  $\delta^{13}\text{C}_{\text{carb}}$  and  $\delta^{18}\text{O}_{\text{carb}}$  values decrease. The TS, TOC and TON values are decreasing. The C:N and C:S values are slowly increasing. The  $\delta^{13}\text{C}_{\text{ORG}}$  and  $\delta^{15}\text{N}_{\text{ORG}}$  values are constant whereas the  $\delta^{34}\text{S}_{\text{ORG}}$  values are decreasing. See Table 7.1 and Figure 7-2 for details.

*Interpretation:* This unit is most likely deposited in near proximity to shell zone (see Figure 5-1) from suspension. The coarsening towards the shell bed may probably indicate an increased

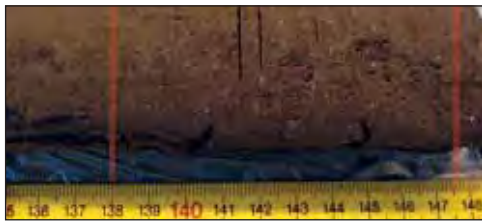


**Figure 7-29.** Facies 27, from 135 cm to 148 cm.

upward amount of eroded material. The well preserved shell bed probably indicates the onset of a transgression preserving the shells from wave energy as supported by the decreasing grain size upwards from the shell bed. The decreasing SUS values and mineralogical content indicate a decreasing amount of allochthonous material, which is perhaps likely to represent an increased distance to

lake shore. The laminas are likely representing spring to summer  $\text{CaCO}_3$  precipitation and the winter out fall of suspended organic material. The very low C:N (*average 16, see Table 7.1*) and C:S (*average 23, see Table 7.1*) values indicate that the organic matter is almost of autochthonous origin (Routh *et al* 2004; Lamb *et al* 2006; Meyers 2006).

The very low and constant TOC and TON values may suggest a low nutrient supply into the lake. The constant and elevated  $\delta^{13}\text{C}_{\text{ORG}}$  values (*average -29.4‰, see Table 7.1*) may suggest a low content of biogenic derived  $\text{CO}_2$  from decomposing terrestrial organic material indicating a more sparsely vegetation in the catchments area. This is further confirmed by the somewhat elevated  $\delta^{13}\text{C}_{\text{carb}}$  values (*average -3.1‰, see Table 7.1*). The decreasing  $\delta^{13}\text{C}_{\text{carb}}$  values may suggest a decreasing organic productivity in concord with the decreasing TOC and TON values (Dean 1999; Schwalb 2002; McFadden *et al* 2005; Talbot *et al* 2006). The increasing  $\text{CaCO}_3$  content from 150 cm suggests an increasing amount of biogenic precipitated  $\text{CaCO}_3$ . Due to the decreasing SUS values the increasing  $\text{CaCO}_3$  content is probably not reflecting an increased influx of particulate  $\text{CaCO}_3$ . The increasing  $\text{CaCO}_3$  content may be a result of the considerable reduction of mineralogical content from 45 wt% to 24 wt% (*see Table 7.1*). The increasing  $\delta^{15}\text{N}_{\text{ORG}}$  values and decreasing  $\delta^{34}\text{S}_{\text{ORG}}$  values may suggest the development of an anoxic hypolimnion (Watanabe *et al* 2004; Eimers *et al* 2006) as also suggested by the indistinct lamina observed between 148 cm to 138 cm. This is supportive of increased summer temperatures and deepening of the lake for the upper part of this unit. However prolonged periods of anoxic conditions may also be a result of prolonged winter ice cover (Michelutti *et al* 2006). The decreasing  $\delta^{18}\text{O}_{\text{carb}}$  values may likely indicate a decreasing E/I ratio (Kirby *et al* 2004; Hammarlund *et al* 2005) most probably related to an increased water inflow.

**Facies 28 (138 cm to 80 cm):** A massive very fine grained plastic olive green calcareous gyttja of a thickness of 58 cm. The unit is very homogeneous. No macrofossils and shells material present in this unit.

**Geochemistry and physical properties:** The SUS values and the mineralogical content are slowly decreasing. The  $\text{CaCO}_3$  content is slowly increasing and the  $\delta^{13}\text{C}_{\text{carb}}$  and  $\delta^{18}\text{O}_{\text{carb}}$  values are slowly decreasing. The TS, TOC and TON values are decreasing. The C:N and C:S values are increasing. The  $\delta^{13}\text{C}_{\text{ORG}}$ ,  $\delta^{15}\text{N}_{\text{ORG}}$  and  $\delta^{34}\text{S}_{\text{ORG}}$  values are constant, however the  $\delta^{34}\text{S}_{\text{ORG}}$  values increases from 90 cm.

**Interpretation:** The uniform fine grained and homogeneous plastic sediment is deposited from suspension. The lack of macrofossil organic matter suggests that this unit is deposited in deep water likely in the profundal zone (*see Figure 5-1*). The decreasing SUS values and mineralogical content suggest a decreasing amount of allochthonous eroded material, which is likely to represent an increased distance to the lake shore. The low TOC, TON and TS values may also suggest a very low organic productivity of the lake. The increasing C:N values suggest an increasing amount of allochthonous organic matter upward in concord with the increasing C:S values from a depth of 92 cm (Routh *et al* 2004; Lamb *et al* 2006; Meyers 2006). This may indicate an increase in precipitation as also suggested by a minor increase in the SUS values around 85 cm or it may suggest a transgression of the lake shore providing the lake with increased amounts of allochthonous organic matter. The elevated  $\delta^{15}\text{N}_{\text{ORG}}$  values and low  $\delta^{34}\text{S}_{\text{ORG}}$  values may suggest

anoxic hypolimnion conditions (Watanabe *et al* 2004; Eimers *et al* 2006). The decreasing  $\delta^{18}\text{O}_{\text{carb}}$  values are likely to indicate a decreasing E/I ratio (Kirby *et al* 2004; Hammarlund *et al* 2005) probably due to an increasing water inflow.

#### *Interpretation of facies association*

The fine to coarse grained detritus gyttja indicates deposition by suspension in a low energy environment. The very high content of autochthonous organic matter and nearly vanishing amount of allochthonous organic matter in the upper part suggests deposition from the sublittoral zone to profundal zone as also indicated by the absence of macrofossil organic matter. The high autochthonous organic matter content is supported by low C:N and C:S values (Meyers and Teranes 2001; Routh *et al* 2004; Meyers 2006). The indistinct and gradual transitions suggest a continuous record and lack of hiatus (Reading 1989). The likely deposition zones are illustrated in Figure 7-17 and most likely represent a continued increase in the water depth during this period.

The very high  $\delta^{15}\text{N}_{\text{ORG}}$  and very low  $\delta^{34}\text{S}_{\text{ORG}}$  values ( $\rho=-0.59$ , see Figure 7-8D) are likely indicating significant bacterial sulphate reduction and ammonia volatilisation or denitrification and thereby anoxic hypolimnion conditions (Talbot 2001; Watanabe *et al* 2004; Eimers *et al* 2006). The very high  $\text{CaCO}_3$  content is most likely bioinduced as also indicated by the low  $\delta^{13}\text{C}_{\text{carb}}$  (Dean 1999). The decreasing and very low TOC content may suggest a decreasing organic productivity. The high  $\delta^{13}\text{C}_{\text{ORG}}$  values are indicating a high allochthonous organic matter content (see Table 14C, Hammarlund 1993), which however is in conflict with the low C:N and C:S values. Moreover the decreasing organic productivity suggests a decreasing nutrient inflow and thereby a decreasing water inflow in discrepancy with the decreasing  $\delta^{18}\text{O}_{\text{carb}}$  values likely indicating a decreasing E/I ratio (Kirby *et al* 2004; Hammarlund *et al* 2005) and thus probably an increasing water inflow. Increased organic decomposition during this period may therefore likely be the case or the deposit may have been subject to post burial changes.

8

---

## **Age Model of the Bliden Lake**

## Introduction

In this section, a chronology of the Bliden Lake  $^{14}\text{C}$  data is presented by using a recently developed method (Blaauw and Christen 2005). Absolute chronology is essential to many scientific disciplines spanning from archaeology to multidisciplinary climate research projects. Precise age chronologies can be obtained from proxies displaying yearly markers such as growth rings in trees, i.e. dendrochronology and varves in sediments. Even the isotope composition of  $^{18}\text{O}$  to  $^{16}\text{O}$  and  $^2\text{H}$  to  $^1\text{H}$  in ice cores can be used for counting years, as fractionation depends on temperature and it is thus possible to differentiate between successive summers and winters (Johnsen *et al* 1999; Vinther *et al* 2006; Seierstad *et al* in press). However, counting years in ice cores is a very complex procedure, because the water molecules do not stay in fixed positions but diffuse, hence smearing the yearly isotope signal considerably (Johnsen *et al* 1999; Southon 2004). Materials containing radioactive atoms can also be used for dating purposes, providing the conditions under which they were formed are known. The most widely used methods are potassium argon ( $^{40}\text{K}/^{40}\text{Ar}$ ), uranium thorium ( $^{234}\text{U}/^{230}\text{Th}$ ,  $^{238}\text{U}/^{234}\text{Th}$ ) and  $^{14}\text{C}$  dating (see e.g. Geyh and Schleicher 1990). The applicable age span and precision of these methods depends highly on the half-life of the decaying atoms involved (Geyh and Schleicher 1990). However, for any of these methods single year precision is rarely achieved.

As regards the Holocene, the commonly adapted method is radiocarbon dating, discovered by Libby (1946). The radioactive  $^{14}\text{C}$  nuclei are continuously formed in the upper atmosphere by the interaction of cosmic rays with nitrogen atoms. Once formed, the  $^{14}\text{C}$  nuclei are converted to carbon dioxide and incorporated into plant tissue by photosynthesis. From plant tissue the  $^{14}\text{C}$  atoms are incorporated into the animal food chain, and via plant or animal metabolisms a constant exchange with the atmospheric carbon dioxide is maintained. Upon the death of the organism in question, the exchange halts and the incorporated  $^{14}\text{C}$  level starts to decrease due to radioactive decay (see e.g. van Strydonck *et al* 1998). Thus, by measuring the  $^{14}\text{C}$  content of a sample and knowing the  $^{14}\text{C}$  level of the carbon dioxide of the past atmosphere, the age of the sample can be determined (Bowmann 1990). However, the exchange of carbon between carbon reservoirs such as the atmosphere and the biosphere is associated with isotope fractionations, but an age correction can be established by measuring the  $^{13}\text{C}$  to  $^{12}\text{C}$  ratio of the sample.

In radiocarbon dating, a clear distinction between  $^{14}\text{C}$  years and calibrated years is necessary because the production of  $^{14}\text{C}$  in the atmosphere has fluctuated over time. A calibration curve between  $^{14}\text{C}$  years and calendar years has been established by measuring the  $^{14}\text{C}$  content of dendrochronologically dated oak and pine trees in North West Europe (see e.g. Bowmann 1990). A single  $^{14}\text{C}$  year will in some instances cover a broad range of calendar years and for other instances even a multitude of well-defined spans of calendar years. Extending this calibration curve back in time is an ongoing process (see e.g. van der Plicht 1998; Chiu *et al* 2005; Fairbanks *et al* 2005) and the latest internationally agreed curve is the IntCal04 curve going back to 25000 cal BP (Reimer *et al* 2004b). Radiocarbon is measured by conventional decay counting (see e.g. Bowmann 1990) or by accelerator mass spectroscopy (AMS) (see e.g. Tuniz *et al* 1998).

The marine and freshwater radiocarbon reservoirs differ from terrestrial environments for different reasons. These reservoirs are depleted in  $^{14}\text{C}$  relative to the atmosphere, thereby producing apparent  $^{14}\text{C}$  ages that are too old compared to terrestrial organisms. This age difference is called the reservoir age. Thus, marine organisms living in the upper, mixed layer of the open ocean in the North Atlantic appear to be about 400  $^{14}\text{C}$  years older than contemporaneous terrestrial organisms (Larsen *et al* 2002; Hughen *et al* 2004). Organisms that derive their carbon from freshwater and brackish environments can appear even older than their marine counterparts, because the dissolved carbon may contain admixtures of fossil carbon from the influx of groundwater from adjacent soil. The freshwater reservoir age is known to vary considerably

with time and location (Heier-Nielsen *et al* 1995; Lanting 1998). To avoid these effects, terrestrial materials are preferable for  $^{14}\text{C}$  dating.

The calendar age precision of the radiocarbon dating method is a composite of the uncertainty from the determination of the  $^{14}\text{C}$  content, uncertainties of the calibration curve and of the appearance of the calibration curve wiggles. The calendar age precision can be significantly improved by use of wiggle matching methods or by including stratigraphical knowledge in the framework of Bayesian statistics (Buck *et al* 1996; Goslar and Madry 1998; Ramsey 1998; Kilian *et al* 2000; Speranza *et al* 2000; Ramsey 2001; Buck *et al* 2003; Blockley *et al* 2004; Blaauw *et al* 2004; Mauquoy *et al* 2004; Blaauw and Christen 2005).

In this chapter, age-to-depth methods are discussed in general and a brief introduction to the formalism of Bayesian statistical methods are given. Lastly, a chronology of the Bliden Lake record is presented.

### Age modelling

Information on paleoclimate is mainly gained from proxy records of drilled ocean or lacustrine cores as well as ice cores. Different proxies trace different events and the information gained from a proxy can be dependent upon both global and local causal mechanisms. To obtain global paleoclimate information correlation between different cores is a necessity. Though correlation can be achieved by recognising event patterns in different cores, an absolute time scale is the best means to establish correlations between different locations or cores. Lacustrine and marine sediment chronologies are, in the majority of cases, derived from  $^{14}\text{C}$  measurements. However, the construction of depth-to-age relationships from calibrated  $^{14}\text{C}$  data is a technical and non-trivial problem as the calendar age probability distributions are often multi-modal.

Depth-to-age models can only be made based on calibrated  $^{14}\text{C}$  dates, since using the  $^{14}\text{C}$  dates directly will bypass the wiggles of the calibration curve (Bartlein *et al* 1995). Normally, depth-to-age models are established by the use of either linear or polynomial fitting (Andresen *et al* 2004) or linear (Brown *et al* 2002; Turcq *et al* 2002) or spline interpolation of the weighted averages of the probability distributions of the calibrated ages (Telford *et al* 2004a). The piecewise linear and spline interpolation has the disadvantage of going through every dated point of a dataset and thus resulting in a 'detailed' age-to-depth model not necessarily supported by the data. Further, it does not take into account that the measured  $^{14}\text{C}$  date is only an estimate of the true date, i.e. the noise from the  $^{14}\text{C}$  determination of the samples is forced into the model (Telford *et al* 2004a). Models based on linear polynomial fitting will bypass outlier dates. The linear fit may, however, be too much of a simplification and result in too narrow confidence intervals, whereas the polynomial fitting will result in an overestimation of details if applied to a small data set.

In most cases these models are based on estimates of the mean calendar age by a weighted average of the calibrated probability distribution (Telford *et al* 2004b; Heegaard *et al* 2005). These distributions are not Gaussian, but in many cases multi-modal and even non-uniform over large ranges. Hence, weighted averages are, in general, poor estimates of calibrated age means and these averages may even fall in a region of no probability. Telford *et al* (2004a) have reviewed and tested these age-to-depth models against a simulated data set and in general find that they all provide reasonable results if the age resolution is high. However, this requirement is rarely met.

Age modelling can be improved by incorporating stratigraphic knowledge into the model using Bayesian statistics. For most cores it is reasonable to assume that the sample age increases with increasing depth, and this can be used to impose constraints on the range of calibrated probability distributions. In order for Bayesian statistics to work properly, the age resolution should be high enough for the calibrated probability ranges to overlap. If the age resolution

becomes so high that the measured data resembles the calibration curve, very precise calibrated ages can be obtained by wiggle matching the data set (Goslar and Madry 1998; Speranza *et al* 2000; Blaauw *et al* 2004; Mauquoy *et al* 2004). For lacustrine sediments suitable terrestrial materials for  $^{14}\text{C}$  dating are sparse and thus these models are only of limited use.

Recently, Maarten Blaauw and José Andrés Christen (2005) have suggested a method for constructing age models within the framework of Bayesian statistics based on three simple assumptions:

1. The age model should be piecewise linear; equivalent to assuming that accumulation rates should be piecewise constant and that the calendar age of the sediments should become progressively older as the depth is increased
2. The core can be divided into sections where each section is piecewise linear
3. Hiatus may occur on transitions between two sections

Their approach for this model is based on peat cores, and it seems reasonable to assume linear piecewise accumulation for  $^{14}\text{C}$  data of samples taken from peat cores. Furthermore, hiatus may be a reasonable assumption for peat cores as it could be caused by forest fires or sudden water level rises flushing away peat material (Blaauw and Christen 2005). The question that needs to be answered is, however, whether these assumptions are also reasonable for freshwater sediments. If any of the assumptions are inappropriate, this model will not be suitable for freshwater sediments without modification.

A complex picture of variable accumulation rates and rapid transitions from one accumulation rate 'regime' to another may often stem from the interpretation of lacustrine deposits by employing sedimentological and geochemical evidence (*see e.g. chapter 7*). Therefore, assuming a division into sections of piecewise linearity seems reasonable. The resolution of geochemical analysis of freshwater cores is often high, whereas, in contrast, their age resolution is very low, generally speaking. The  $^{14}\text{C}$  content of organic aquatic material is affected by the reservoir effect and therefore not useful for age modelling. Hence,  $^{14}\text{C}$  data may result in a less detailed pattern than may otherwise be suggested by other evidence, i.e. sedimentological or geochemical. Peat cores normally contain enough material of terrestrial origin to convert  $^{14}\text{C}$  dates to calendar dates by the method of wiggle matching (Blaauw *et al* 2004). So the important difference lies not in assumptions but rather in age resolution. Hence, even though lithology or geochemical analysis gives beliefs of a large number of sections each with different accumulation rates, the age resolution may be too low to reflect this.

Hiatus seems a reasonable assumption for peat cores, but it might not occur in deep freshwater lake sediments. In most cases, cores taken from freshwater lakes display limnic sediments which are covered by water at all times. Hence, the sediments are protected by the water column and therefore not easily exposed to weathering. However, changes in the lake current pattern caused for example by increased wind intensity or storm draughts may remove considerable amounts of material. Brauer *et al* (2001) report hiatuses between 100 to 350 years for Lake Holzmaar and Meerfelder, Germany. As for peat cores, incomplete coring may result in missing sections and both cases should appear in either the sedimentology or geochemistry. Thus, by stating the suitable prior beliefs for the accumulation rate and hiatus for freshwater sediments, this model should be applicable for estimating age-to-depth relationships.

## Bayes' theorem and radiocarbon dating

The basic framework of Bayesian statistics is Bayes theorem, stating that the *a posteriori* probability is proportional to the likelihood multiplied by the *a priori* probability. Mathematically this is written as (Buck *et al* 1996; Rom 2000; Buck *et al* 2003):

$$(8.1) \quad p(\theta|y) \propto p(y|\theta) \times p(\theta),$$

where  $y$  denotes the measured entity (*a*  $^{14}\text{C}$  determination) and  $\theta$  the unknown parameter(s) (*the calendar years*).  $p(\theta|y)$  is the likelihood function, thus  $p$  indicates the probability of the observed data, given some values of the unknown parameters.  $p(\theta)$  is named the *a priori* probability or the belief (*probability*) attached to the unknown (*data*) prior to observation (Buck *et al* 1996). The *a posteriori* probability  $p(\theta|y)$  is thus the probability of  $\theta$  being true, given that  $y$  actually occurs, i.e.  $p(\theta|y)$  is the updated probability of  $\theta$  being true conditional on the observations  $y$ . Therefore in Bayesian statistics, current beliefs are updated in light of new information (Rom 2000).

Bayesian statistics is thus a tool for formalising prior beliefs and has for that reason been nicknamed subjective statistics; subjective in the sense that the *a posteriori* probability strongly depends on (*is proportional to*) the prior belief. However, stratigraphic information on the order of events at an archaeological site or the knowledge that the dates of a sediment core become older with increasing depths exists and the Bayesian statistics just offers a framework for formalising this. Putting it simply, data is interpreted prior to analysis in Bayesian statistics whereas the reverse is the case for a classical approach (Buck *et al* 1996).

The calibration of a  $^{14}\text{C}$  determination to calendar years may serve as an example of Bayesian statistics. The 5 year IntCal04 calibration curve (Hughen *et al* 2004; Reimer *et al* 2004b) is denoted  $\mu(\theta)$  and said to be piecewise linear. Hence, points falling between the measured calibration points (*knots*) on the calibration curve are estimated by linear interpolation. Any calendar date  $\theta$  can be translated into an expected  $^{14}\text{C}$  date by the piecewise linear calibration curve  $\mu(\theta)$ , as long as the calendar date is within the range of the calibration curve. A measured  $^{14}\text{C}$  date  $y$  attached with uncertainty  $\sigma$  has a normal distribution and the likelihood can thus be given as (Buck *et al* 1996; Rom 2000):

$$(8.2) \quad l(\theta, y) \propto \exp\left[-\frac{(y - \mu(\theta))^2}{2\sigma^2}\right] = \exp\left[-\frac{(y - a - b\theta)^2}{2\sigma^2}\right].$$

The constants  $a$  and  $b$  of the last term are the intercept and slope stemming from the interpolation between knots of the calibration curve. For a common  $^{14}\text{C}$  age calibration there is normally no additional information, which can be formulated into a prior probability. The *a priori* probability of the date is taken to be  $p(\theta)=1$  for the whole range of the calibration curve or in other words all dates are equally likely. This is a very weak prior probability and simply states that the age is expected to be somewhere on the calibration curve. Hence, the *a posteriori* probability  $p(\theta|y)$  is equal to the likelihood  $l(\theta, y)$  and may be evaluated numerically by Markov Chain Monte Carlo sampling (MCMC).

## The age model of Blaauw and Christen

Denoting a set of data with measured  $^{14}\text{C}$  ages as  $\mathbf{y}=(y_1, y_2 \dots y_m)$  and corresponding uncertainties  $\sigma$  taken at depths  $\mathbf{d}=(d_1, d_2 \dots d_m)$ , where  $d_1 > d_2 > \dots > d_m$  and  $m$  is the total number of

samples, the assumptions of Blaauw and Christen (2005) are mathematically formulated into the model  $G$  as:

$$(8.3) \quad G_M(d) = \theta_i + \alpha_i(d - c_{i-1}) \quad c_{i-1} < d \leq c_i ,$$

$M=(\theta, \alpha, c)$  are the model parameters, where the vector  $c=(c_1, c_2 \dots c_k)$  contains the depths of the break points between succeeding sections,  $\alpha$  contains the corresponding slopes  $\alpha=(\alpha_1, \alpha_2 \dots \alpha_k)$  and  $k$  denotes the number of sections.  $\theta$  are the calendar dates. The model has built-in constraints corresponding to the assumptions, such that the slope  $\alpha_i$  is always positive, i.e. the dates  $\theta_i$  increase with increasing depths. The date  $\theta_i$  is younger or equal at the transitions between two sections, where the condition 'is younger' allows for jumps (*hiatus*).

The  $^{14}\text{C}$  determinations  $y_j$  are assumed to be normally distributed and the model  $G_M(d_j)$  represents the calendar year of sample  $j$ . The likelihood is given as the product of the probability functions for all samples ( $j=1$  to  $m$ ) and is written as (Blaauw and Christen 2005):

$$(8.4) \quad l(M; y) = \prod_{j=1}^m \tau_j \{G_M(d_j)\}^{\frac{1}{2}} \exp\left[-\frac{1}{2} \tau_j \{G_M(d_j)\} (y_j - \mu\{G_M(d_j)\} - \delta_j \varphi_j)^2\right]$$

$$\text{with } \tau_j(\theta) = \frac{1}{\sigma_j^2 + \sigma^2(\theta)} .$$

$\mu$  represents the radiocarbon calibration curve and  $\tau\{\cdot\}$  is the combined variance of the  $^{14}\text{C}$  determination  $\sigma_j$  and the variance arising from the uncertainties in the calibration curve  $\sigma^2(\cdot)$  (Christen 1994; Buck *et al* 2003; Blaauw and Christen 2005). Outliers are defined as any  $^{14}\text{C}$  determinations that needs a shift  $\delta_j$  in order to be consistent with the remaining determinations (Christen 1994; Blaauw and Christen 2005).  $\varphi_j$  is a latent variable being 1 if  $y_j$  needs a shift  $\delta_j$  and otherwise 0, where a shift is interpreted as being an outlier (Christen 1994). Hence outliers are either 'real' outliers or  $^{14}\text{C}$  measurements that do not fit with the assumptions given by the model.

The *a priori* probability distribution for the shift  $\delta_j$  is given as (Blaauw and Christen 2005)

$$(8.5) , \quad \delta_j \propto \exp\left[-\frac{y_j}{4\sigma_j^2}\right] .$$

and the *a priori* probability  $p=P(\varphi_j=1)$  of the determination  $y_j$  being an outlier is set to 5%. The probability  $P(\varphi_j=1|y)$  is the *a posteriori* probability of sample  $j$  being an outlier and thus reflects the weight given to the determination  $y_j$  (Buck *et al* 2003). Hence,

$$(8.6) \quad F = 100 \frac{1}{m} \sum_{j=1}^m [1 - P(\varphi_j = 1|y)] .$$

is interpreted as adequacy of fit or the percentage of determinations that have actually been used in the inference (Blaauw and Christen 2005).

The prior distributions of the first sample date  $\theta_1 \sim U(L,E)$  are taken to be uniformly distributed within the range of the calibration curve. The prior distribution of the slope  $\alpha$  is taken as a gamma distribution with parameters  $c_\alpha$  and  $b_\alpha$ , where the mean *a priori* accumulation rate is given by  $\alpha_{mean} = c_\alpha \cdot b_\alpha$  with variance  $\alpha_\sigma = c_\alpha \cdot (b_\alpha)^2$ . The remaining prior dates are stated indirectly by using a gamma prior for hiatus with shape  $\alpha_H$  and rate  $\beta_H$  such that the hiatus is given by (Blaauw and Christen 2005)

$$(8.7) \quad J_i = \theta_{i+1} - (\theta_i + \alpha_i(c_i - c_{i-1})) \sim \frac{\alpha_H^{\beta_H}}{\Gamma(\alpha)} J_i^{\alpha_H - 1} \exp[-\beta_H J_i] .$$

Thus collecting all terms, the *a priori* probability distribution  $f(M)$  is written as (Blaauw and Christen, 2005)

$$(8.8) \quad f(M) = f(\theta_1) \prod_{i=1}^{k-1} f(J_i) \prod_{i=1}^k f(\alpha_i) f(c) \prod_{j=1}^m f(\delta_j) f(\phi_j) .$$

Finally, the *a posterior* distribution is given by Bayes theorem as:

$$(8.9). \quad f(M|y) \propto l(M; y) \times f(M) .$$

The *a posterior* probability distribution (8.9) is then estimated via a MCMC algorithm by the program Bpeat (Blaauw and Christen 2005).

### Age models based on simulated data

The Bpeat program was developed for peat cores where the age resolution is much higher (0.4 <sup>14</sup>C samples per cm for the peat core examined in (Blaauw and Christen 2005)) than for the lacustrine lakes (0.009 <sup>14</sup>C samples per cm in Bliden lake). In order to test the behaviour of the Bpeat program with data of much lower age resolutions, a number of tests were performed using simulated data. Each set of simulated data was constructed from a fixed age model starting at 500 cal years with an accumulation rate of 2 yr/cm down to a depth of 396 cm. From 396 to 1350 cm the accumulation was 5 yr/cm with no occurring hiatus. The depth data were randomly selected and the constructed calendar ages were converted to <sup>14</sup>C ages by the 'simulate' function of OxCalc 3.10 (Ramsey 1995; Ramsey *et al* 2001) and associated with random uncertainties sampled from a normal distribution with a mean of 50 and a standard deviation of 20 years. The simulated age data were chosen to mimic a simplified age-to-depth relation in Bliden records as closely as possible. The outcome of these simulated tests is displayed in Table 8.1 and Figure 8-1.

Initial test runs showed that the method was very sensitive to the setting of the prior probability distribution for the hiatus and, less markedly, to the prior distribution of the slope  $\alpha$ . Thus, the prior distributions have been changed to reflect the prior beliefs of the test model. The slope  $\alpha$  is set to a mean value of  $\alpha_m = 3.2$  yr/cm with a standard deviation of  $\alpha_\sigma = 2$  yr/cm, and the prior of the hiatus is changed to  $\alpha_H = 0.5$  (or 0.05) and the rate  $\beta_H = 0.005$ .

All test runs were first fitted using the assumption of one section only. This resulted in low  $F$  values and they were thus disregarded. Therefore in the proceeding fits two sections were assumed. For test III, the fit with 1 and 2 sections gave similar results, as seen in Table 8.1. For the remaining fits, the slopes  $\alpha_1$  and  $\alpha_2$  display very good agreement with the expected values whereas the break points  $c_i$  in general show offset values. This is also reflected in the large range of 95% confidence intervals for  $c_i$ . Attempts to improve the fits of test I to IV were made by changing the prior distributions and also by changing the MCMC algorithm settings. However, only test II-A and IV-A resulted in improvements. The hiatus of test II was reduced from 50 years to 10 years and the slope of section 1 ( $\alpha_1$ ) and the break point  $c_i$  of test IV improved their values and brought them closer to the expected. The improvement of test II-A was minor whereas the improvement of test IV was significant, as reflected by the fit adequacy values  $F$ .

Information on the spatial position of the break point can in some cases be available and used to fix the break point  $c_i$  at a defined value. A sensitivity test of fixing the break point  $c_i$  has been performed on the test data and is denoted with the subscripts F396, F376 and F416, where the

**Table 8.1: Age model fits on simulated  $^{14}\text{C}$  data**

Test run	Prior settings					Estimated parameters					Hiatus years	Comment
	sec.	$\alpha_m$ yr/cm	$\alpha_o$ yr/cm	$\epsilon$	$\alpha_H$ shape	$\beta_H$ rate	F	$\alpha_1$ yr/cm	$\alpha_2$ yr/cm	$c_1$ cm		
$^{14}\text{C}$ Samples = 12;												
I	2	3.2	2.2	8	0.5	0.005	98.83%	2.3 (1.5 - 2.9)	4.91 (4.73 - 5.13)	399 (375 - 625)	0	
I-F396	2	3.2	2.2	8	0.5	0.005	98.90%	2.2 (1.5 - 2.5)	4.90 (4.73 - 4.98)	fixed @ 396	0	
I-F376	2	3.2	2.2	8	0.5	0.005	98.64%	2.0 (1.3 - 2.3)	4.90 (4.73 - 4.98)	fixed @ 376	5	
I-F416	2	3.2	2.2	8	0.5	0.005	97.46%	2.32 (1.75 - 2.75)	0.5 (4.7 - 5.1)	fixed @ 416	30	
$^{14}\text{C}$ Samples = 12;												
II	2	3.2	2.2	8	0.5	0.005	99.39%	1.95 (1.75 - 2.25)	5.25 (4.95 - 5.35)	425 (355 - 475)	50	
II-A	2	3.2	2.2	8	0.05	0.005	99.27%	2.00 (1.65 - 2.25)	5.26 (4.93 - 5.33)	417 (355 - 455)	10	
II-F396	2	3.2	2.2	8	0.5	0.005	98.89%	1.89 (1.88 - 2.23)	5.18 (4.93 - 5.23)	fixed @ 396	0	
II-F376	2	3.2	2.2	8	0.5	0.005	99.11%	0.18 (1.65 - 2.05)	5.13 (4.91 - 5.17)	fixed @ 376	60	
II-F416	2	3.2	2.2	8	0.5	0.005	99.39%	1.96 (1.86 - 2.18)	5.29 (5.03 - 5.33)	fixed @ 416	0	
$^{14}\text{C}$ Samples = 12;												
III	1	3.2	2.2	8	0.5	0.005	74.68%	4.75				
III	2	3.2	2.2	8	0.5	0.005	78.79%	0.82 (0.35 - 1.55)	4.64 (4.61 - 4.73)	1245 (1233-1328)	450	
III-F396	2	3.2	2.2	8	0.5	0.005	98.44%	1.8 (0.9 - 2.1)	4.99 (4.95 - 5.05)	fixed @ 396	10	
III-F376	2	3.2	2.2	8	0.5	0.005	98.70%	1.5 (0.5 - 1.7)	4.99 (4.65 - 4.75)	fixed @ 376	0	
III-F416	2	3.2	2.2	8	0.5	0.005	98.31%	1.5 (0.9 - 3.9)	5.01 (4.95 - 5.05)	fixed @ 416	150	
$^{14}\text{C}$ Samples = 8;												
IV	2	3.2	2.2	8	0.5	0.005	97.28%	3.46 (1.75 - 4.25)	4.28 (1.75 - 5.3)	151 (325 - 825)	0	
IV-A	2	3.2	2.2	8	0.05	0.005	99.46%	1.7 (1.7 - 4.3)	4.87 (4.75 - 5.75)	321 (325 - 1175)	0	
IV-F396	2	3.2	2.2	8	0.5	0.005	98.59%	2.6 (1.7 - 3.7)	4.87 (4.45 - 5.05)	fixed @ 396	5	
IV-F376	2	3.2	2.2	8	0.5	0.005	98.45%	2.0 (1.5 - 3.7)	4.90 (4.45 - 5.05)	fixed @ 376	100	
IV-F416	2	3.2	2.2	8	0.5	0.005	98.69%	2.7 (1.9 - 3.9)	4.90 (4.45 - 5.05)	fixed @ 416	0	
$^{14}\text{C}$ Samples = 41;												
BIG-1	2	20	10	10	1	1/200	93.95%	2.27 (2.25 - 2.85)	4.9 (4.9 - 5.1)	678 (670 - 690)	730	T17: 100%
BIG-2	2	20	10	10	1	1/200	99.17%	2.02 (1.93 - 2.18)	4.99 (4.98 - 5.03)	400 (395 - 445)	0	T17 removed

MCMC setting for all runs: Long run 150000; Sample size 15000; store at each 3000. In (.) the 95% confidence interval is given.

number indicates the depth of the defined break point  $c_1$ . A break point fixed at the modelled break point ( $c_1=396$  cm) produced results that were in good agreement with expected values, whereas offset break points from 396 cm in many cases resulted in greater hiatus and more or less similar results for the slopes  $\alpha_1$  and  $\alpha_2$ .

In the test BIG, all samples of test I to IV were collected into one large sample in addition to a few extra samples and one obvious outlier sample (*T17*). The prior distributions were reset to the default values suggested by Blaauw and Christen (2005). In the initial analysis, the *a posteriori* outlier probability of sample T17 was found to be 100% and thus it should, in principle, not affect the fit. However, the results of this fit suggest a hiatus of 730 years and the break point  $c_1$  to be at 678 cm. The test BIG was also redone with different prior settings without improving the outcome. In the test BIG-1, the outlier T17 was removed and the resulting fit is in excellent agreement with the model. Hence, outliers may affect the final result and as a consequence should be removed.

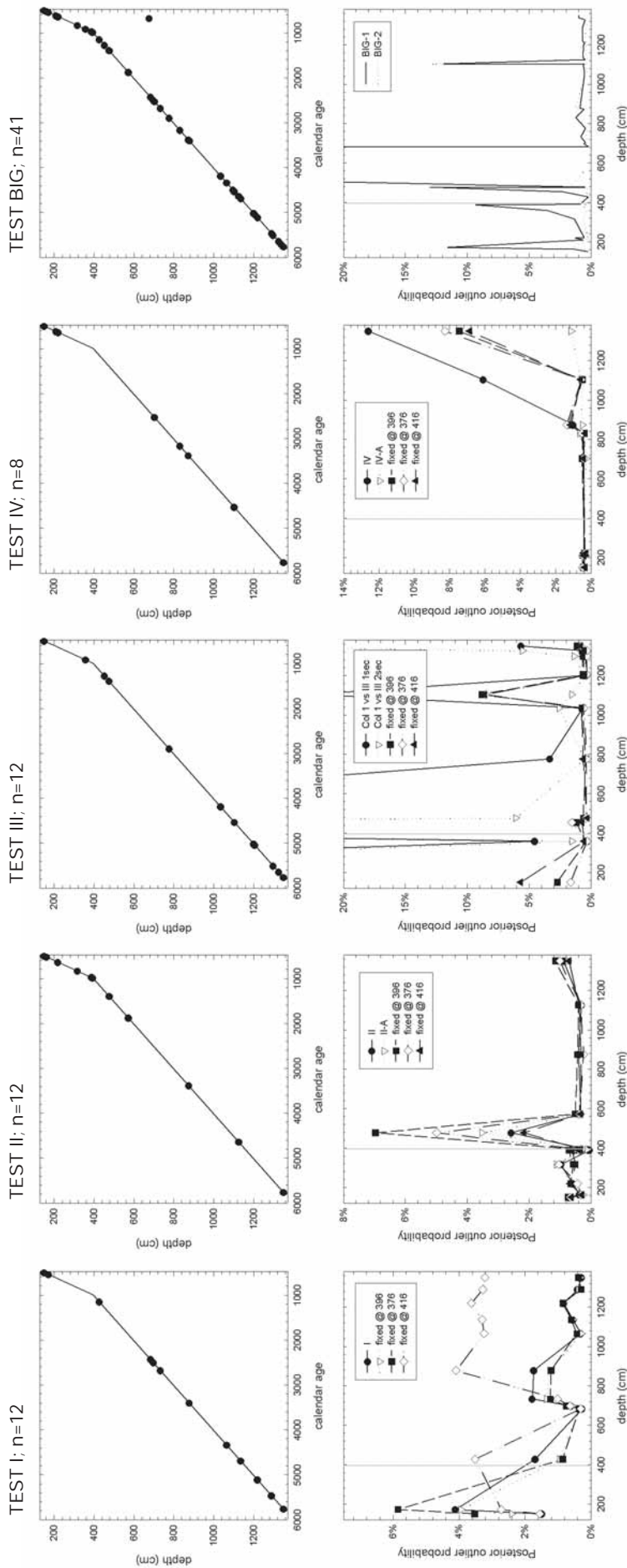


**Figure 8-1. Upper part:** Simulated age model. From 150 to 396 cm an accumulation rate of 2 yr/cm is used and from 396 to 1350 cm an accumulation rate of 5 yr/cm is used. The date points are randomly chosen, and the found calendar years are converted to  $^{14}\text{C}$  years by using OxCalc 3.10. **Lower part:** The *a posteriori* outlier probabilities of the simulated data points are shown for each Bpeat fit. For fit details see text and Table 8.1. The break point at 393 cm is shown by a solid grey line. The fits for the simulated data sets TEST I and TEST II show good agreement with the model. The fit TEST III however shows poor agreement

which is due to the only 2 data points in the section before the break point. This is also seen by the very high *a posteriori* outlier probabilities for this fit. Similar the TEST IV data set does not show perfect agreement with the model. The large gap with no data points set too few constraints to base the fit on. However changing the prior beliefs about the hiatus significantly improved the fit as seen by run IV-A. The last simulated dataset is compiled from all the test data with the addition of an outlier. This test shows that outliers may have a large effect upon the fit results if not removed prior to analysis.

## Chronology of the Bliden Lake

The Bliden  $^{14}\text{C}$  data (Table 6.2) has been fitted using the Bpeat 1.0 program (Blaauw and Christen 2005). The shell sample AAR-9065 has been excluded from all fits because it is influenced by the freshwater reservoir age. Depositional rates of freshwater lakes vary greatly and are dependent on the geological and hydrological settings of the lake surroundings. Reported values of accumulation rates range from 0.35 yr/cm to 50 yr/cm (0.35 to 3.3 yr/cm, Lake Geneva Switzerland (Loizeau et al 2003); 1 to 5 yr/cm, Sky Lake, Humphreys County, Mississippi (Davidson et al 2004); 10 to 50 yr/cm, Angissoq Island, lake N14, Greenland (Andresen et al 2004)) and 9 to 33 yr/cm (Hammarlund et al. 2003)). Therefore, the Bpeat parameters for the *a priori* accumulation rate probability distributions are not easily deducible. An initial fit assuming one section gave an accumulation rate  $\alpha$  of 5.5 yr/cm ( $F= 65.82\%$ ). This is in accordance with the reported values and the *a priori* slope values were chosen to be  $\alpha_m=3.2$  yr/cm with a standard deviation of  $\alpha_\sigma=2.2$  yr/cm. Based on the sedimentological evidence (see chapter 7 and Figure 7-1 and 7-2) hiatuses are not expected to occur in the Bliden core. Therefore the hiatus *a priori* probability distribution was chosen such that a hiatus is not likely to occur, i.e. the shape constant is chosen to  $\alpha_H=0.5$  and the rate constant to  $\beta_H=0.005$  (see Table 8.2 and Figure 8-2).

The fit B1 (see Table 8.2) of all  $^{14}\text{C}$  data with 2 sections gave a fit adequacy of 94.47% and an *a posteriori* outlier probability of AAR-9744 of 40% with a break point of 330 cm and a hiatus of 220 years. Both the high outlier probability of AAR-9744 and the large hiatus necessitates separate investigations into the consistency of the two sections. The Bpeat fit of the upper section (see SPLA & SPLB in Table 8.2, depth range from 149 cm to 181 cm) reported AAR-9744 as an outlier and as a result this sample is excluded from further analysis. The upper section was then extended to include samples AAR-9062 and AAR-9063 at 319 cm (SPLC Table 8.2) producing a fit adequacy  $F$  of 98.52% and a slope  $\alpha_1$  at 0.9 years per cm. The lower section from 494 cm to 1345 cm produced a fit adequacy  $F$  of 98.74% with a slope  $\alpha_2$  of 5.75. No outliers were detected.

**Table 8.2: Age model fits on the Bliden Lake core B1  $^{14}\text{C}$  data**

Bliden Core	Prior settings					Estimated parameters						Hiatus years	Comment
	sec.	$\alpha_m$ yr/cm	$\alpha_\sigma$ yr/cm	$\epsilon$	$\alpha_H$ shape	$\beta_H$ rate	$F$	$\alpha_1$ yr/cm	$\alpha_2$ yr/cm	$c_1$ cm			
B1	2	3.2	2.2	1	0.5	0.005	94.47%	1.0 (0.5 - 3.5)	5.71 (5.63 - 5.86)	330 (325 - 475)	220	All data; AAR-9744 40.03%	
SPL1A	1	3.2	2.2	1	0.5	0.005	82.12%	0.92 (0.25 - 5.52)				Depth range from 149 to 181cm; AAR-9743 32.99% & AAR-9744 35.19%	
SPL1B	1	3.2	2.2	1	0.5	0.005	97.64%	0.92 (0.25 - 3.75)				Depth range from 149 to 181cm; AAR-9744 excluded	
SPL1C	1	3.5	2.2	1	0.005	0.005	98.52%	0.9 (0.5 - 1.5)				Depth range from 149 to 319cm; AAR-9744 excluded	
SPL2	1	3.2	2.2	1	0.5	0.005	98.74%		5.75 (5.63 - 5.83)			Depth range from 494 to 1345cm;	
B2	2	3.5	2.2	1	0.05	0.005	96.77%	1.0 (0.5 - 3.7)	5.75 (5.63 - 5.88)	324 (325 - 475)	170	All data; AAR-9744 excluded; AAR-9062 25.33%	
B2A	2	3.5	2.2	1	0.05	0.005	96.31%	0.8 (0.5 - 4.1)	5.76 (5.40 - 5.83)	285 (225 - 625)	0	All data; AAR-9744 & AAR-9062 excluded	
B2fix	2	3.5	3.3	1	0.0005	0.0005	98.17%	1.0 (-)	5.74 (-)	Fixed @ 345	300	All data; AAR-9744 excluded	
B2Fix-1	2	3.5	3.3	1	0.0005	0.0005	98.28%	0.9 (-)	5.74 (-)	Fixed @ 345	300	All data; AAR-9744 excluded	

MCMC setting for all runs: Long run 150000; Sample size 15000; store at each 3000. In (.) the 95% confidence interval is given.

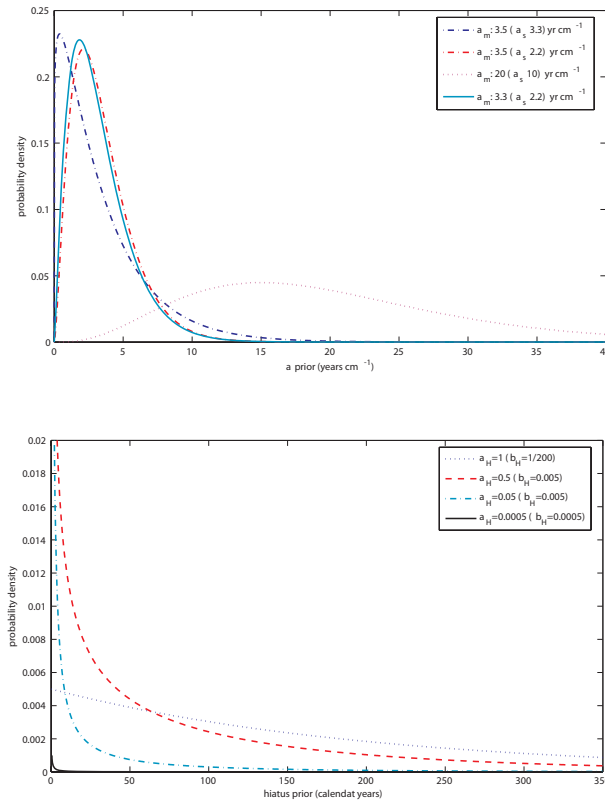


**Figure 8-2. Upper part:** Shown are the *a priori* values of the accumulation rate  $\alpha$  used for fitting the Bliden <sup>14</sup>C data by the Bpeat. **Lower part:** The *a priori* probability distribution of the hiatus is shown used for fitting the Bliden <sup>14</sup>C data. Note that the dotted line represents the Bpeat default values.

Collecting all data except AAR-9744 produced a fit adequacy  $F$  of 96.77% and an outlier probability of AAR-9062 of 25.33%. The hiatus was estimated to 170 years at a depth of 324 cm and the slopes  $\alpha_1$  and  $\alpha_2$  agreed with the former fits. A fit was performed excluding both AAR-9062 and AAR-9744 (see Table 8.2), since the hiatus of 170 years is unexpectedly large and AAR-9062 was suggested to be an outlier. The fit B2A gave a fit adequacy  $F$  of 96.31% and slope  $\alpha_1$  and  $\alpha_2$  similar to former findings. The hiatus is reduced to 0 years and the breakpoint is estimated to a depth of 285 cm.

### Revisiting the sedimentology

In summation, the <sup>14</sup>C dates of the upper (*fit SPL1C*) and lower (*fit SPL2*) sections yielded good linear fits to the data. However, combining the two sections yields an unexpectedly large hiatus (*fit B2*). Likewise, manipulating the *a priori* hiatus probability distribution and thereby forcing Bpeat to make a piecewise linear fit with a hiatus of zero years results in indications of numerous <sup>14</sup>C dates as probable outliers. At this point, the samples AAR-9744 and AAR-9062 are suggested as outliers.

The excluded twig sample AAR-9744 was too small to have its  $\delta^{13}\text{C}$  value determined and was estimated to be -25‰ (standard procedure at the AMS <sup>14</sup>C Dating Centre). Based on this, it may be reasonable to exclude this sample from the age model analysis. However, it should be considered that a 1‰ enrichment in  $\delta^{13}\text{C}$  only amounts to -8 <sup>14</sup>C years and thus a quite large  $\delta^{13}\text{C}$  correction has to be applied in order to shift the sample to be consistent with the remaining data. Alternatively, this sample may also have been reworked or it may be poorly preserved. Contrarily, there are no objective reasons for deeming sample AAR-9062 an outlier. In fit B2A,

it appears too young so it cannot be infiltrated by  $^{14}\text{C}$  depleted aquatic material. Hence, a possible reservoir effect can be excluded. Secondly, for the analysis of the upper section (*fit SPLA to SPLC*) ranging from 149 cm to 319 cm the sample AAR-9062 agreed excellently with other data. That AAR-9062 appears to be an outlier in this case seems therefore to be a result of the attempt to establish an age model with a 0 year hiatus. Consequently, fit B2A is most likely not representative of the Bliden Lake core.

The fit B2 suggests a hiatus of 170 years placed at a depth of 324 cm, which might be possible on sedimentological and geochemical grounds (*see Figure 7-1 and 7-2*). However, it seems more likely that the breakpoint should occur at 345 cm where a dramatic shift in geochemical parameters is observed (*especially magnetic susceptibility, mineralogical content, TOC and TON values, see Figure 7-2*). Likewise, the depth of 345 cm is the boundary between the facies association 'intermediate water' and 'shallow water B', indicating that a major sedimentological change is also occurring at this depth. Furthermore, the sedimentology does not show any signs of a sedimentological surface boundary in the deposit around the interval at depth 324 cm, as seen from Figure 8-3. A hiatus may develop due to erosion or fluvial processes caused by streams, for example, and are expected to develop a boundary surface in the deposit. By contrast, the deposit is homogenous showing no signs of boundary surface; in fact all surfaces in-between facies are indistinct and gradual for the facies association 'shallow water B' (*see chapter 7*).

Therefore, another fit series was performed with a fixed breakpoint at 345 cm inserted into the model. The resulting fit (*B2fix*) yielded a hiatus of 300 years, but displayed accumulation slopes similar to those of the original fit. Forcing Bpeat to an even smaller a priori hiatus probability yielded an almost similar fit, with a hiatus of 300 years (*B2fixh*) (*see Figure 8-4 and Figure 8-5*). Hence, Bpeat strongly suggests a quite large hiatus to occur at 345 cm. However as previously with the suggested breakpoint at 324 cm the deposit at 345 cm is very homogeneous with no observable surface boundary indicating that a hiatus is not likely to have occurred at this depth (*see Figure 8-6*).

### **An age-to-depth model for Bliden Lake core**

The fit adequacy  $F$  of the Bpeat fits with a fixed breakpoint at 345 cm are high, indicating that a breakpoint at 345 cm is in very good agreement with the  $^{14}\text{C}$  data. Furthermore, the accumulation rates  $\alpha_1$  and  $\alpha_2$  of the fits (*B2fix and B2fixh*) agree with the previous fits supporting the fit adequacy of B2fix and B2fixh. Likewise, the posterior outlier probability (*Figure 8-7*) is very low for both B2fix and B2fixh, even when compared to fit B2 where a fixed breakpoint is not assumed. It is therefore likely that the deposits in the depth range from 345 cm and upwards are represented by one accumulation rate  $\alpha_1$ , and that the interval from 345 cm and downwards is represented by another accumulation rate  $\alpha_2$ . Similarly, it is most probable that the breakpoint occurs at 345 cm. However, the depth range between 545 cm and 319 cm is only represented



**Figure 8-3:** The Bliden lake core between 316 cm and 334 cm. Note homogeneity of the deposit indicating that a hiatus in this depth interval is not likely.

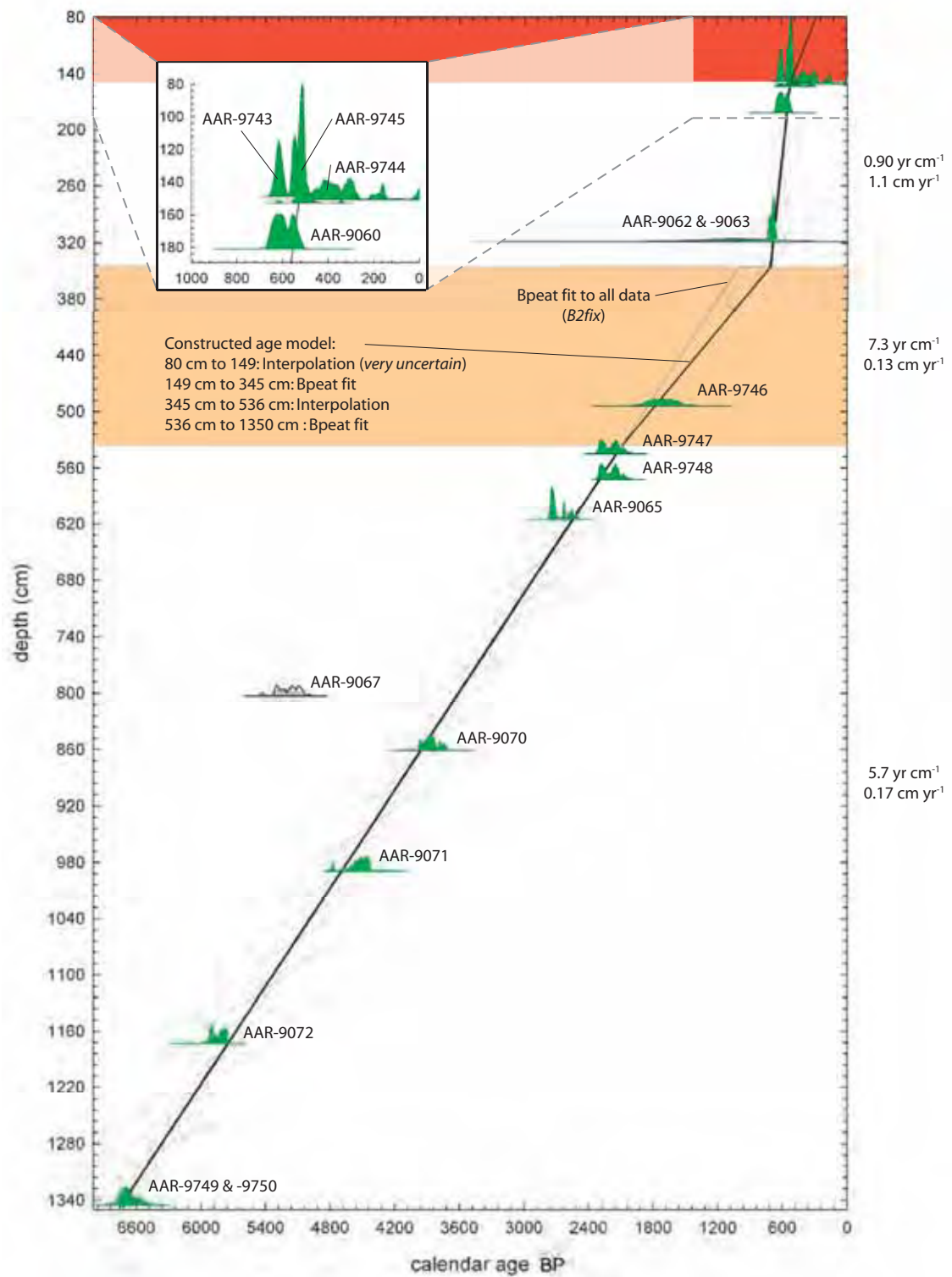


**Figure 8-4.** Shown by a grey solid line is the Bpeat 'B2fix' fit. The black the solid line represents the constructed age-to-depth based on the fit 'B2fix'. The calibrated age probability distributions of all <sup>14</sup>C dated samples from the Bliden core B1 are also displayed. The calibrated age probability distributions are found by OxCalc 3.10. The red color indicates a zone where no <sup>14</sup>C data exists. The light red zone indicates that the age model in this interval is interpolated between breakpoint at 536 cm and 345 cm. Shown to the right the estimated accumulation rate of each section.

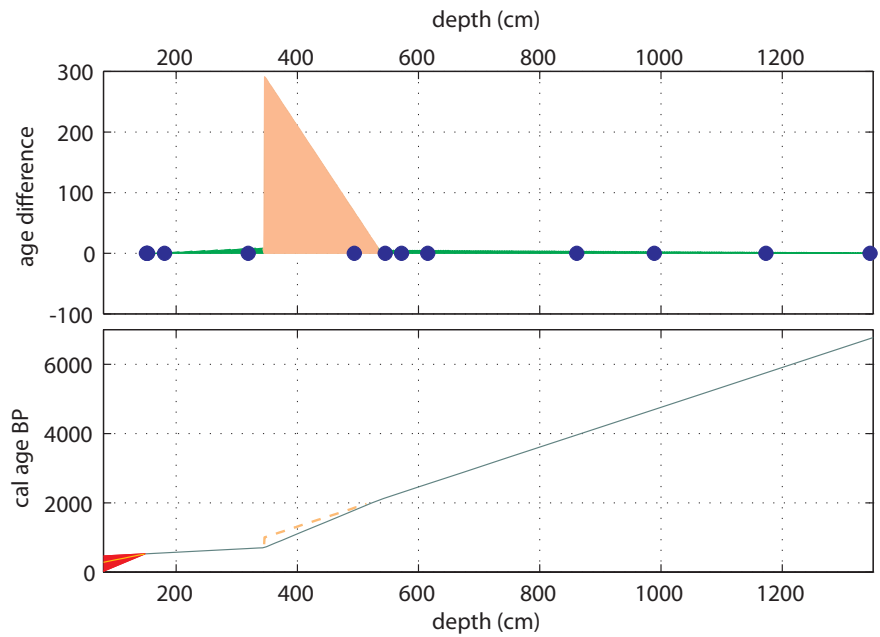


**Figure 8-5. Upper graph:** Shown is the age difference between the Bpeat fit 'B2fix' and the constructed age model versus depth. The  $^{14}\text{C}$  dates are shown by green dots. **Lower graph:** The age models as a function of depth. No  $^{14}\text{C}$  data exists for the red zone and thus the age model of this range is not to be taken at face value. The limits of the red zone is set by the maximum and minimum observed accumulation rates.



**Figure 8-6: Upper:** The depth interval from 336 cm to 357 cm. **Left:** The depth interval from 340 cm to 348 cm. **Right:** Cross section at 346 cm.

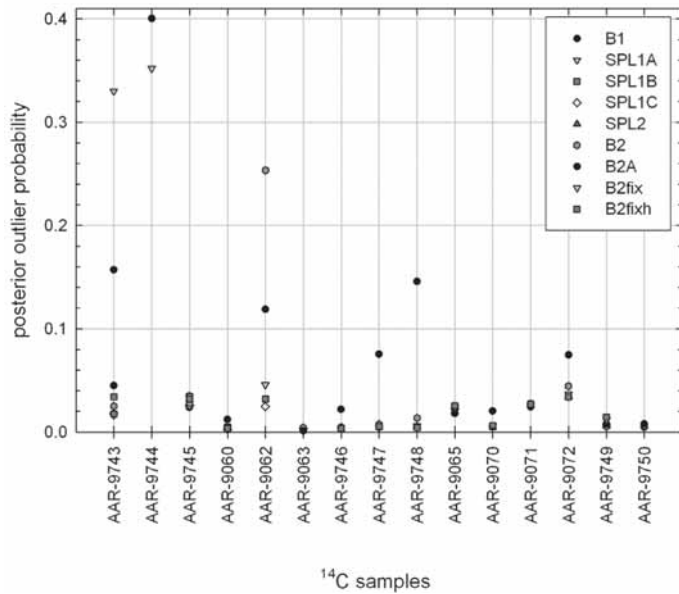


**Figure 8-7.** A posterior outlier probability of all fits to Bliden core B1. Note the high a posterior outlier probability of AAR-9062.

by one  $^{14}\text{C}$  date (AAR-9746) and thus by a poor age resolution. Moreover, this depth interval is more or less concurrent with the facies association ‘intermediate water’. Thus the sedimentology changes at 536 cm and may potentially have a different accumulation rate. Backed by only one  $^{14}\text{C}$  date, the Bpeat program is not able to track this hypothetical change in the accumulation rate for this depth range. However, assuming a breakpoint at 536 cm and again at 345 cm, with the condition of no hiatus, yields a new age-to-depth model for the Bliden Lake core (Figure 8-4 and Figure 8-5). Due to very broadly calibrated  $2\sigma$  age ranges of sample AAR-9746 (Table 6.2) there is statistically no significant difference between this constructed curve with a breakpoint added at 536 cm and the Bpeat fit B2fix (Figure 8-8). Hence, the two models are equally likely and the constructed curve with no hiatus is preferred, since no sedimentological evidence of hiatus exists for the Bliden Lake core. The accumulation rate for the depth interval between 536 cm and 345 cm is found to be  $7.3 \text{ yr cm}^{-1}$ . Even though this constructed age model may seem very *ad hoc*, it must be emphasized that the breakpoint cannot deliberately be placed lower than 545 cm. The  $^{14}\text{C}$  data in the range from 1345 cm and up to 545 cm are very consistent and constrained as shown by the various Bpeat fits. By contrast, there are no constraints on the breakpoint position in the depth range from 545 cm and up to 345 cm and any breakpoint depth therefore seems equally probable. However, the chosen breakpoint first of all represents a change in the sedimentology and secondly it is the most conservative approach possible, representing as it does the least possible change of the accumulation rate. These two factors combine to support the constructed age-to-depth model and it is believed to represent the most likely age-to-depth model of the Bliden Lake core B1.

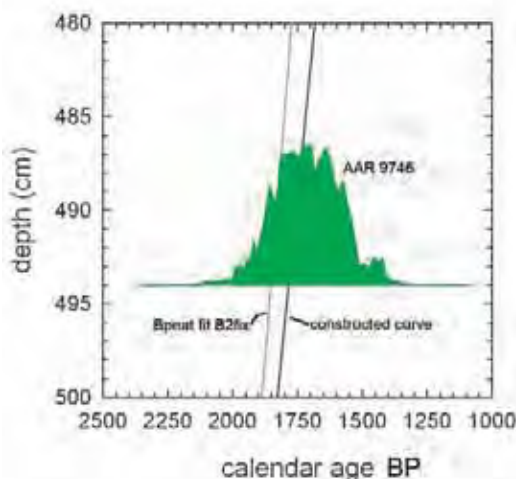


**Figure 8-8:** Shown is the calibrated probability distribution of the sample AAR-9746 at the depth 394 cm. The solid grey line represents the Bpeat fit ‘B2fix’, whereas the solid black line represents the construction age-to-depth model.

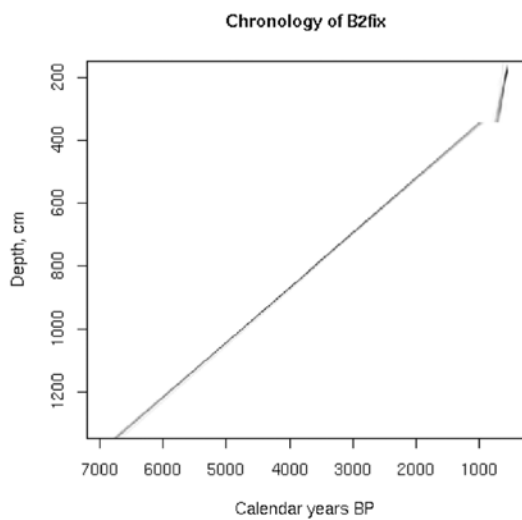
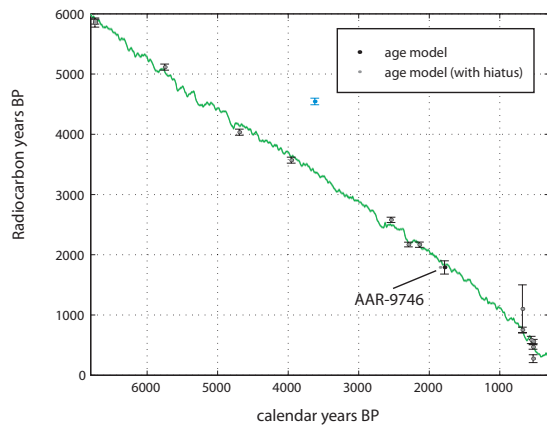


**Figure 8-9. Upper graph:** Shown is the fit B2fix and constructed age-to-depth model of the  $^{14}\text{C}$  data to the radiocarbon calibration curve (IntCal04 Reimer *et al.* 2004b). **Lower graph:** Shown is the age model of fit 'B2fix' for the Bliden  $^{14}\text{C}$  data. The grey scale indicate the probability given to each point and darker colors indicate high probability.

assumptions as possible. Considering the limited number of  $^{14}\text{C}$  dates for the Bliden core, it seems reasonable, at least with regard to a first approximation, to assume a constant sedimentation rate. Therefore, the piecewise linear model of Blaauw and Christen (2005) has been chosen to analyse Bliden core  $^{14}\text{C}$  data. However, due to the low number of  $^{14}\text{C}$  samples, the observed accumulation rates are likely to represent average accumulation rates and not the actual accumulation rate at a given depth, which may deviate from the average value.

One particular strength of Blaauw and Christen's (2005) depth-to-age model is that, unlike most other approaches, their model uses  $^{14}\text{C}$  ages as direct input parameters. Thus, the conversion to calendar ages is inherently part of the calculations, whereas for all other methods the multimodal probability distribution of the calibrated ages adds yet another layer of complexity. A disadvantage of the approach of Blaauw and Christen (2005) is the inherent belief in the existence of a hiatus, which need not necessarily be the case for all cores. As seen by equation (8.7) and (8.8), their algorithm for each MCMC run is driven by guessing the size of the hiatus. Thus, the hiatus assumption cannot be switched off and can only be scaled down by altering the *a priori* hiatus probability distribution. The analysis of the simulated test data revealed that

available for this section. However, assuming that the hypothetical point of 0 cm represents the present age (1950), a hypothetical and purely artificial depth-to-age model may be constructed with an accumulation rate of  $3.5 \text{ yr cm}^{-1}$  (see Figure 8-5). In fact, this accumulation is very close to the average value of the minimum and maximum accumulation rates. However, this part of the age-to-depth model is not backed up by any data whatsoever. It is merely shown for guidance and should not be taken at face value.

The fit of  $^{14}\text{C}$  data of the Bliden Lake core to the  $^{14}\text{C}$  calibration curve is shown in Figure 8-9 together with the maximum *a posteriori* probability for the Bpeat fit B2fix. Figure 8-4 illustrates the depth-to-age relations of both B2fix and the constructed age model together with the calibrated calendar age probability distributions obtained from OxCal (Ramsey 1995, 2001) by calibrating each sample date separately.

## Discussion

Age modelling by  $^{14}\text{C}$  dates can be very complex and may even produce artefacts (Gehrels *et al.* 2005). Great care must be taken in collecting suitable material for  $^{14}\text{C}$  dating and ensuring that the dated material cannot be compromised (Buck *et al.* 2003). Hence, suspicious material should in general be disregarded. Also, the model chosen to describe the data should be robust and contain as few

the final results were greatly dependent on the prior beliefs regarding the size of the hiatus. However, they also showed that setting the *a priori* hiatus probability distributions such that hiatuses were not likely to occur resulted in age-to-depth models with no hiatus. The simulated test results also revealed that outliers may significantly impact results and, on the other hand, that the off values of the accumulation rate *a priori* probability distribution did not lead to deviating results.

Given the age model, the reservoir age can be estimated by the shell sample (AAR-9067). The calendar age of level 803 cm is found by the age-to-depth model to be 3618 cal BP, which corresponds to  $3370 \pm 14$   $^{14}\text{C}$  years BP using the calibration curve (IntCal04, Reimer *et al* 2004b). Thus, the reservoir age of the shell sample AAR-9067 is calculated at  $1175 \pm 56$   $^{14}\text{C}$  years, in accordance with observations elsewhere (see e.g. Heier-Nielsen *et al* 1995; Geyh *et al* 1998).

## Conclusion

The program Bpeat (Blaauw and Christen 2005) has been applied to model the  $^{14}\text{C}$  samples of the Bliden core B1. Bpeat was developed to construct age models for peat cores where the age resolution is much higher than commonly observed for lacustrine cores. Therefore, Bpeat has been tested on simulated  $^{14}\text{C}$  data sets. These tests show that Bpeat can indeed be used for age modelling of lacustrine cores with lower age resolutions.

Using the method suggested by Blaauw and Christen (2005) results in an improved chronology for the Bliden record. The Bpeat analysis of the Bliden core  $^{14}\text{C}$  data indicated two sections, each with constant accumulation rate  $\alpha_1$  and  $\alpha_2$  with a breakpoint position fixed at 345 cm. The breakpoint position was estimated by using the sedimentology and geochemistry both of which exhibit dramatic changes at 345 cm. The Bpeat analysis furthermore suggested a hiatus of 300 years at the breakpoint position. However, since the sedimentology of the Bliden Lake core displays no evidence of hiatus, the suggested hiatus was eliminated by adding another breakpoint at 536 cm, which is the boundary surface between the facies associations 'shallow water A' and 'intermediate water'. The resultant constructed age-to-depth model shows good agreement with  $^{14}\text{C}$  dates and based on this the Bpeat fit and the constructed age-to-depth model seem equally likely. However, the constructed age-to-depth model is preferred, since it does not imply hiatus. Based on the depth-to-age model, the shell sample AAR-9067 yields an estimate of the freshwater  $^{14}\text{C}$  reservoir age of  $1175 \pm 56$   $^{14}\text{C}$  years.



9

---

## **Discussion**

## Introduction

The Bliden Lake is likely to reflect regional or local climate changes as well as global scale climate events. This chapter discusses the climate variability of the Bliden record in relation to regional and northern hemisphere climate by combining the sedimentological and geochemical interpretation of chapter 7 with the depth-to-age model derived in chapter 8. The literature on Holocene climate variability is substantial (see e.g. reviews by Kaufman *et al* 2004; Mayewski *et al* 2004; Versteegh 2005) and a fully and comprehensive comparison is therefore beyond the scope of this thesis. Here, a few examples of Holocene climate studies will be presented, showing the general trends of the period covered by the Bliden Lake. The generally accepted proxy records, such as ice rafted debris from North Atlantic marine cores (Bond *et al* 1997; Bond *et al* 2001), data from ice cores (O'Brian *et al* 1995; Johnsen *et al* 2001; Vinther *et al* 2006) and residual  $\Delta^{14}\text{C}$  (Reimer *et al* 2004b, a) are considered to be representative of northern hemisphere climate events, whereas the regional climate trends are presented as proxies from lakes in southern Sweden as well as German and Danish peat bogs (Aaby 1976; Barber *et al* 2004).

## General climatic trends of the Bliden Lake record

The main outcome of the sedimentological and geochemical investigations of the Bliden Lake is the inferred water level curve presented in Figure 7-17 and Figure 9-1. In this work, water depth is expressed with the qualitative terms 'low' and 'high', which are based exclusively on the sedimentological observations presented in chapter 7. However, past lake level fluctuations may be stratigraphically recorded in many ways and may not be easily and unambiguously determined from a single core (Digerfeldt 1988) and the employment of a single core from the Bliden Lake thus makes it difficult to univocally determine the exact water depth quantitatively. On the other hand, the relative water level changes are reflected by the multi-proxy approach of this work and are based on the interpretation of both sedimentological and geochemical evidence (*see chapter 7*).

Accordingly, the Bliden record may be divided into sections based on increasing or decreasing water levels by employing the inferred water level curve (*see Figure 9-1*) and in broad terms these inferred boundaries correspond to the generally accepted Holocene chronozones. The warm and humid Atlantic period terminates around 5800 cal BP to 5700 cal BP (Roberts 2004) and corresponds to the change from a high water level to a decreasing water level at 6250 cal BP in the Bliden Lake. However, for the period from 6250 cal BP to 5700 cal BP, the water level is still very high and only slightly in decline. Hence the latter date (*5700 cal BP*) is in excellent agreement with the termination of the Atlantic period and on this basis it could be argued that the Bliden Lake boundary should be moved from 6250 cal BP to 5700 cal BP. The Atlantic period is succeeded by the warm and dry sub-Boreal period (5700 cal BP to 2600 cal BP, Roberts 2004) and corresponds to the general decrease of water levels between 5700 cal BP and 2600 cal BP. Lastly is the cool and humid sub-Atlantic, representing the period from 2600 cal BP to the present (Roberts 2004), which corresponds to the increasing water levels from 2600 cal BP in the Bliden Lake.

The lower part, from ~6700 cal BP to 6250 cal BP, is characterised by a high water level with minor fluctuations, which may suggest a relatively wet climate. Between 6250 cal BP and 2600 cal BP the water level is generally decreasing, punctured however by three significant high water events from 5300 cal BP to 5150 cal BP, from 4600 cal BP to 4200 cal BP and from 2900 cal BP to 2600 cal BP. It is noteworthy that the rate at which water levels decrease during this period (*6250 cal BP to 2600 cal BP*) appears significantly lower at the onset and up to about 5700 cal BP, which may suggest that the relatively wet period from ~6700 cal BP to 6250 cal BP may be extended up to about 5700 cal BP.

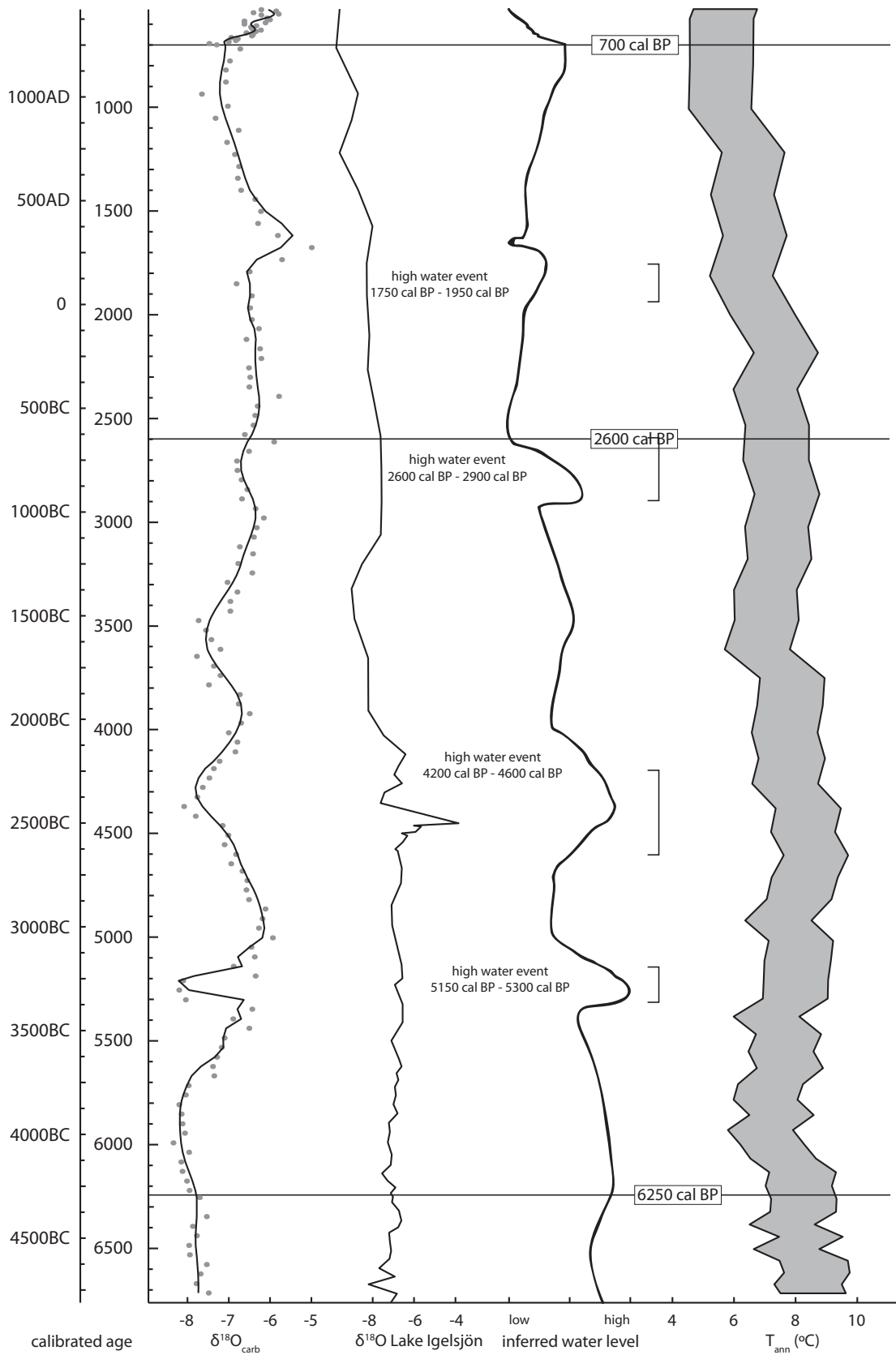


**Figure 9-1:** Shown is the  $\delta^{18}\text{O}_{\text{carb}}$  values together with the constructed Bliden Lake water level curve (see Figure 7-17). To the right the  $\delta^{18}\text{O}$  values from Lake Igelsjön (Jessen *et al* 2005; Hammarlund *et al* 2003) is shown together with the pollen based annual temperature curve by Seppä *et al* (2005). The horizontal lines indicate major breaks in the water level curve.

The study from Lake Igelsjön (*southern Sweden*) mainly reveals changes in effective humidity (*net change in precipitation and evaporation* (Hammarlund *et al* 2003)) due to its small size, no surface outflow and a hydrological regime dominated mainly by subsurface exchange of groundwater (Hammarlund *et al* 2003; Hammarlund *et al* 2005; Jessen *et al* 2005; Seppä *et al* 2005). Its location 200-300 km north east of the Bliden Lake makes it possible to compare Lake Igelsjön with the Bliden Lake, since the climatically induced changes of Lake Igelsjön are presumably similar to the ones experienced by Bliden Lake. Both lakes reveal uncorrelated  $\delta^{13}\text{C}_{\text{carb}}$  and  $\delta^{18}\text{O}_{\text{carb}}$  values, indicating that the isotopic composition of the  $\text{CaCO}_3$  is controlled mainly by hydrology rather than lake water temperature (Talbot 1990; Hammarlund *et al* 2003). However, the lack of verification of the likely biogenic origin of the  $\text{CaCO}_3$ , e.g. by X-ray diffraction analysis, in Bliden Lake renders the Bliden Lake  $\text{CaCO}_3$  susceptible to originating from allochthonous sources. Precautions against the interferences based on the  $\delta^{13}\text{C}_{\text{carb}}$  and  $\delta^{18}\text{O}_{\text{carb}}$  values from the Bliden Lake should therefore be taken.

Lake Igelsjön indicates that the period from 4950 to 4600 cal BP is characterised by low lake water levels and less effective precipitation (Jessen *et al* 2005) in accordance with the Bliden record (*see Figure 9-1*). However, in contrast to the Bliden Lake, Lake Igelsjön appears to indicate very stable effective humidity conditions prior to 4600 cal BP (Jessen *et al* 2005). The very high  $\delta^{18}\text{O}$  values which peak at 4450 cal BP in Lake Igelsjön (*see Figure 9-1*) are inferred as warm and/ or dry conditions (Jessen *et al* 2005), which is clearly in discord with the Bliden record. The Bliden Lake  $\delta^{18}\text{O}_{\text{carb}}$  values and inferred water level curve (*Figure 9-1*) indicate progressively wetter conditions from about 5000 cal BP to 4300 cal BP, and especially from 4700 cal BP to 4400 cal BP. However, Jessen *et al* (2005) report a substantial lake level rise between 4450 cal BP and 4350 cal BP, which coincides with a high water level event from 4200 cal BP to 4600 cal BP in Bliden Lake. Furthermore the increase in effective humidity from 4100 cal BP to 3800 cal BP (Jessen *et al* 2005) probably corresponds to the increasing water level in Bliden Lake with an onset at 3900 cal BP. Moreover, the halt in the trend towards cooler and/or wetter climate reported from 4350 cal BP to 4100 cal BP in Lake Igelsjön is also observed in the Bliden record (*see Figure 9-1*). The Bliden Lake may display increased effective precipitation from 3900 cal BP to about 3500 cal BP, which is also found in Lake Igelsjön (Jessen *et al* 2005). From 3500 cal BP to 2900 cal BP the lake level decreases slowly, most likely in accordance with the stable conditions of Lake Igelsjön in this period reported by Jessen *et al* (2005). Broadly speaking, Lake Igelsjön and the Bliden Lake are correlated. However, the dry period around 4450 cal BP in Lake Igelsjön and the significantly higher water level in Bliden Lake from 5300 cal BP to 5150 cal BP do not correlate. The reason for this discrepancy may perhaps reflect groundwater changes of the Bliden Lake aquifer related to relative sea level changes.

Between 2400 cal BP and 700 cal BP, the water level increases and appears with a relatively higher water level around 1800 cal BP, which probably reflects a minor wet period. The period from 1750 cal BP to 1950 cal BP appears wetter and the interval around 1650 appears very dry. From 700 cal BP to about 500 cal BP the water level decreases, possibly indicating more dry conditions. Above 500 cal BP is likely to represent the onset of wet climate conditions (*note that the age-to-depth model does not apply to ages younger than ca. 500 cal BP, see chapter 8*).

The sedimentation rates of the 'high water A' and 'Shallowwater A' facies associations are estimated to  $0.17 \text{ cm yr}^{-1}$  (*see chapter 8*). The sediments of the 'high water A' facies associations are mainly characterised as being very homogeneous and lacking macrofossil material, in contrast to the 'shallow water A' sediments which are very rich in mostly autochthonous macrofossil organic matter. Furthermore, the SUS values are significantly higher for the 'shallow water A' facies association. Hence, these differences, manifested by differences in water levels, may suggest the sedimentation rate of the 'shallow water A' facies association to be higher than the sedimenta-

tion rate of the 'high water A' facies association. In comparison, the sedimentation rate ( $0.13 \text{ cm yr}^{-1}$ ) of the 'intermediate water' facies association is only slightly lower than the estimated value of the 'high water A' and 'shallow water A' facies associations. On the other hand, relatively comparable sedimentation rates of these three facies associations could be expected, due to their relatively similar SUS values and mineralogical content (Figure 7-2 & 9-2), suggesting relatively similar catchments erosion rates. The sedimentation rate of  $1.1 \text{ cm yr}^{-1}$  (see chapter 8) of the 'shallow water B' facies association is markedly higher and the sediment is characterised by frequent observations of large macrofossil autochthonous organic matter and vegetation zone debris. Additionally, both the SUS values and mineralogical content of this facies association are significantly higher when compared to the sediments below and above, which is likely to indicate increased allochthonous erosion and thereby also an increased sedimentation rate. Even though the sedimentation rates may be expected to vary with lake level changes, seasonal ice cover and catchments erosion, the presented sedimentation rate estimates are in all probability average values which are likely to have fluctuated. These fluctuations cannot reasonably be expected to be captured by the depth-to-age model due the low age resolution of the core (see chapter 8).

### **Anthropological impacts and climatic changes**

In Denmark, the human impact on the landscape has been significant and probably on the rise since the Neolithic period. At present, the forest cover is ~12% whereas only 200 years ago it was as low as ~4% (Rasmussen 2005). Therefore, apparent climatic changes may be masked by anthropological impacts. However, Rasmussen, Bradshaw *et al*'s (Bradshaw *et al* 2005a; Bradshaw *et al* 2005b; Rasmussen 2005; Rasmussen and Bradshaw 2005) investigation of Dallund Sø (*Fyn, Denmark*) showed that a strong anthropogenic impact could not be observed before 1000 BC to 500 BC, where the landscape changed dramatically because of heavy forest clearance, resulting in a more open landscape dappled with forest zones (Rasmussen 2005). Prior to this, from 5000 BC to 3900 BC, the landscape around Dallund Lake was characterised by a closed forest (*deciduous tree pollen*  $\geq 95\%$ ) with localised openings around lakes and streams due to occasional flooding. The dense woodland landscape continuous beyond 3900 BC and the landnám period were identified to have occurred 3300 BC to 2800 BC and this period is characterised by forest clearance succeeded by woodland successions (Bradshaw *et al* 2005b; Rasmussen 2005). The first cereal grains appear around 3460 BC and indications of animal husbandry around 3320 BC (Rasmussen 2005).

The pattern from Dallund Lake may not be directly transferable to the Bliden Lake. However, the very low SUS values and mineralogical content up to the 'shallow water A' facies association (2600 cal BP, see Figure 9-2) probably suggest a minor catchments area erosion, which further is likely to indicate a minor anthropological impact and probably reflect a dense catchments area vegetation of deciduous forest (Rasmussen and Anderson 2005). From about 2800 cal BP, i.e. 200 years prior to the 'shallow water A' facies association, the SUS values and mineralogical content increase significantly (see Figure 9-2), suggesting increased catchments erosion, which may be a result of human activity. Thus, the higher SUS values and mineralogical content bear similarities with the deforestation interval in the Dallund Lake occurring 1000 BC to 500 BC (2950 cal BP to 2450 cal BP). The probable increase in anthropogenic impact on the Bliden Lake may be visualised by the archaeological discovery of a large Viking complex dated to have existed from the Iron to the late Viking (Jørgensen *et al* 2003). In addition, the onset of higher  $\delta^{13}\text{C}_{\text{carb}}$  values at 3000 cal BP to 2800 cal BP (Figure 9-2) may further support a major change in the catchments area vegetation, since the lower  $\delta^{13}\text{C}_{\text{carb}}$  values prior to this date may reflect dense vegetation in the catchments area providing the lake with a high concentration of  $^{12}\text{C}$  depleted

DIC from decomposing terrestrial organic matter. Furthermore, the high water level in the Dal-lund Lake until 3870 BC (Bradshaw *et al* 2005a) is in accordance with the inferred lake level of Bliden Lake, and the low lake level reported to start from 1000 BC to 500 BC (Bradshaw *et al* 2005a) is in concord with the 'shallow water A' facies association of the Bliden record (*see Figure 9-1 and 9-2*). Likewise, the constructed water level curve of the Bliden Lake is very similar to the lake level curve of Lake Bysjön in southern Sweden (Digerfeldt 1988) even though a direct comparison is impeded by the use of <sup>14</sup>C years for the Lake Bysjön water level curve. However, the high water level from 4600 cal BP to 4200 cal BP (*Figure 9-1*) does not seem to be observable in Lake Bysjön. Again, this may be caused by high groundwater related to a high relative sea level.

Magny (2004) compiled an impressive investigation of 26 mid-European lakes and identified 15 high water level episodes. The high water levels occurring between 6350 cal BP and 5900 cal BP, 5650 cal BP and 5200 cal BP, 2750 cal BP and 2350 cal BP, 1800 cal BP and 1700 cal BP and from 750 cal BP to 650 cal BP may all be identified in the Bliden Lake (*see Figure 9-1*). According to Magny (2004) the maximum water levels were reached in the period from 5300 cal BP to 5200 cal BP (*the 5650 to 5200 high level period*) which agrees excellently with the pronounced water level rise in the Bliden Lake (*Figure 9-1*). In addition, the shallow water level from 650 cal BP to 550 cal BP (Magny 2004) is clearly observed in the Bliden Lake (*Figure 9-1*). Furthermore, the high water level from 1300 cal BP to 1100 cal BP may also be identified in the Bliden Lake, but it is much less pronounced. In contrast, the high water levels occurring between 4850 cal BP and 4800 cal BP, 4150 cal BP and 3950 cal BP and from 3500 cal BP to 3100 cal BP (Magny 2004) are not clearly identifiable in the Bliden Lake. Interestingly, the high level between 4850 cal BP and 4800 cal BP is not identified in Lake Igelsjön either, whereas the 4150 cal BP to 3950 cal BP and 3500 cal BP to 3100 cal BP are observable in Lake Igelsjön (Jessen *et al* 2005).

Hence, it is most probable that the Bliden record reflects general climatic changes, possible groundwater changes and possible anthropogenic impacts; even though neither the Landnám period nor the Mesolithic to Neolithic transition appear traceable in the Bliden geochemical or sedimentological record (*see Figure 9-2*) according to generally decreasing SUS values, mineralogical content and C:N values from about the onset of the Neolithic period. By contrast, the late Bronze Age land clearance is clearly visible, as discussed above.

### **Comparison with northern hemisphere climate events**

Evidence of northern hemisphere warm and cold periods and of cyclic climate variability has been provided by numerous studies (*see e.g. Alley et al 2003; Davis et al 2003; Lamb et al 2004; Zaitseva et al 2004; Versteegh 2005; Wohlfarth et al 2006*). In the peat bogs Svanemose (*Denmark*) and Dosenmoor (*northern Germany*) wet shifts occurred at 3500 and 3350 cal BP (Barber *et al* 2004). Barber *et al* (2004) report that after 3500 cal BP the climate seems to have entered an unstable phase, which was cooler and possibly wetter with its climax around 2750 to 2600 cal BP. They report cooler and wetter periods to have occurred at 2250, 1950, 1750, 1400, and 1000 cal BP and wet shifts of special significance to have occurred in the Baltic region at 3500, 2700, 1950, 1400 and 650 cal BP (Barber *et al* 2004). Similarly, the investigation by Aaby (1976) indicated long-term cyclic climate variations of Danish raised bogs with a period of 260 years over the past 5500 years. Oppo *et al* (2003) report reduced NADW at 5000 cal BP and 2800 cal BP, and cold events at 5700, 4200, 2800, 1400 and 1000 cal BP from ice rafted debris (IRD) in the sub-polar North Atlantic Ocean have been reported (Bond *et al* 1997; Bond *et al* 2001). These cold events have been reconfirmed by studies of a lacustrine lake core in southern Greenland and a marine core from the Denmark straight between Iceland and Greenland (Andresen *et al* 2004). Concentrations of sea salt and terrestrial dust from the GISP2 ice core from Summit

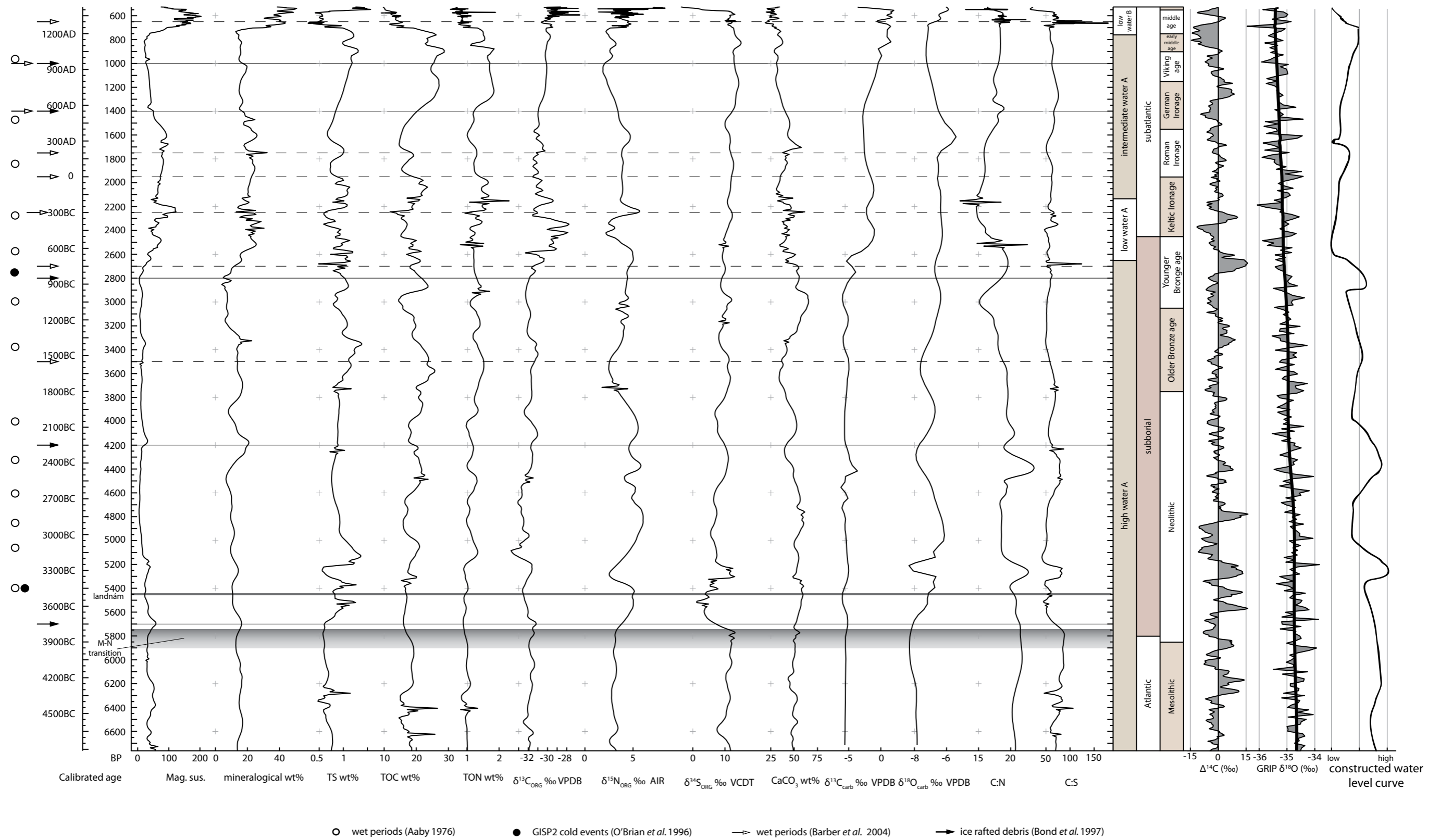


**Figure 9-2:** The Bliden Lake geochemical data as a function of calibrated age (*see also Figure 7-2*). The depth-to-age model is presented in chapter 8. Shown is also the NGRIP  $\delta^{18}\text{O}$  values (Johnsen *et al.* 2001; Vinther *et al.* 2006) and the residual  $\Delta^{14}\text{C}$  signal (Reimer *et al.* 2004b, a) together with the water level curve (*see Figure 7-17*).

(Greenland) showed cold periods between 0 to 600, 2400 to 3100, 5000 to 6100 and from 7800 to 8800 cal BP, with milder climates in the periods from 610 to 960, 1500 to 2700 and from 6300 to 7900 cal BP (O'Brian *et al* 1995). These climatic events are illustrated in Figure 9-2.

Due to the global character (*at least for the northern hemisphere*) of these events, they should be detectable in the Bliden record. However, the impact of northern hemisphere climatic events on Bliden Lake depends on numerous factors, like the strength of the climate event, the climate event time span and the sensitivity of the lake. Furthermore, as previously discussed, anthropogenic factors may significantly change or disguise possible climate events. Figure 9-2 also illustrates the denoised geochemical data of the Bliden Lake as a function of calibrated age together with the residual  $\Delta^{14}\text{C}$  curve (see Figure 4-5, Reimer *et al* 2004b, a) and the  $\delta^{18}\text{O}$  signal from the NGRIP ice core (Vinther *et al* 2006). The NGRIP ice core record shows a strong signal throughout the Holocene (Johnsen *et al* 2001) and is therefore chosen for comparison. Generally decreasing  $\delta^{18}\text{O}$  values corresponds to decreasing temperature and *vice versa* (Johnsen *et al* 2001) and hence the general trend of NGRIP  $\delta^{18}\text{O}$  data is very similar to the decreasing temperature trend revealed by the pollen based annual temperature curve (see Figure 9-1, Seppä *et al* 2005). Furthermore, the NGRIP  $\delta^{18}\text{O}$  values illustrate that ice cores capture the centennial-scale climate variability of the Holocene (Johnsen *et al* 2001).

The 5700 cal BP IRD cold event (Bond *et al* 1997; Bond *et al* 2001) does not appear clearly in the Bliden record (*Figure 9-1 & 9-2, see Figure 7-2 at 1164 cm*). The minor peaks in the SUS values and mineralogical content may, on the other hand, suggest increased catchments area erosion, which may result from increased precipitation. On the other hand, the date 5700 cal BP marks the onset of increased  $\delta^{15}\text{N}_{\text{ORG}}$  values and decreased  $\delta^{34}\text{S}_{\text{ORG}}$  values, very low C:S values and increased  $\delta^{18}\text{O}_{\text{carb}}$  values (*see facies 3 chapter 7*) and is interpreted as the onset of possibly a decreased water inflow to Bliden Lake. This signature is repeated during the IRD cold event at 4200 cal BP (Bond *et al* 2001) where again the Bliden Lake level decreases, the  $\delta^{15}\text{N}_{\text{ORG}}$  increases and the  $\delta^{34}\text{S}_{\text{ORG}}$  values decrease (*facies 7 at 903 cm, see chapter 7 & Figure 9-1 & 9-2*). This is in contrast to the general cooler and wetter conditions attributed to IRD events. However, it has been suggested that IRD events result in reduced NADW formation (Bond *et al* 2001). A reduction in NADW formation is most likely to result in a cooler climate in Western Europe (Manabe and Stouffer 1999), which may lead to drier conditions due to decreased evaporation of the cooler North Atlantic waters and reduced capacity of air to hold moisture under cooler conditions. The interval from 5800 cal BP to 5200 cal BP is reported to be especially dry, as indicated by Irish peat (Caseldine *et al* 2005), which may support the hypothesis of reduced precipitation during reduced NADW formation. Hence, the increased anoxic conditions inferred from the elevated  $\delta^{15}\text{N}_{\text{ORG}}$  values in combination with the decreased C:S and  $\delta^{34}\text{S}_{\text{ORG}}$  values may result from prolonged seasonal ice cover, while the decreasing water levels at 5700 cal BP and 4200 cal BP (*Figure 9-1*) may be caused by a decrease in effective precipitation. This is also in accordance with the Lake Igelsjön decreasing water level of this period (Jessen *et al* 2005). Furthermore, the reduced NADW at ~5000 cal BP (Oppo *et al* 2003) appears to coincide with shallow water levels (*facies 3 to 4 boundary at 1040 cm, see chapter 7 & Figure 9-1 & 9-2*) bearing a similar signature as above with increased  $\delta^{15}\text{N}_{\text{ORG}}$  values and decreased  $\delta^{34}\text{S}_{\text{ORG}}$  values and decreasing TOC and  $\delta^{13}\text{C}_{\text{ORG}}$  values together with elevated  $\delta^{18}\text{O}_{\text{carb}}$  values.

The increased IRD (Bond *et al* 1997; Bond *et al* 2001) and bog wet periods (Aaby 1976; Barber *et al* 2004) occurring around 1400 cal BP and 1000 cal BP are, by contrast, not observable in the Bliden Lake, whereas the 1800 cal BP event is. The peat bog wet period (Aaby 1976; Barber *et al* 2004) at 2200 cal BP shows up in the Bliden record as an increase in SUS values and mineralogical content, as well as in increased C:S values (*Figure 9-2*), which may indicate increased erosion

due to increased precipitation. Further, this assumed wet event is concurrent with a minor peak in  $\Delta^{14}\text{C}$  values.

The 'winter-like' conditions occurring between 6100 cal BP to 5000 cal BP and again from 3100 cal BP to 2800 cal BP, as inferred from the GISP2 ice core record (O'Brian *et al* 1995), seem to coincide with increased SUS values and mineralogical content (*Figure 9-1 & 9-1*). The latter period corresponds to the high water level period in the Bliden Lake, occurring 2900 cal BP to 2600 cal BP. Furthermore, this period concurred with elevated  $\Delta^{14}\text{C}$  values, increased IRD, reduced NADW formation, peat bog wet periods and a GISP2 cold event (*Figure 9-1 & 9-2*) (Aaby 1976; O'Brian *et al* 1995; Bond *et al* 2001; Oppo *et al* 2003; Barber *et al* 2004). Additionally, the high level period between 5150 cal BP and 5300 cal BP in the Bliden record (*Figure 9-1 & 9-2*) is concurrent with a  $\Delta^{14}\text{C}$  peak, a raised bog wet period (Aaby 1976) and a GISP2 cold event (O'Brian *et al* 1995) indicating a climate deterioration (*Figure 9-2*). Both the 5200 cal BP and the 2800 cal BP cold and/or wet event are recognised as global events (see e.g. Geel *et al* 1996; Mayewski *et al* 2004; Versteegh 2005). The 2800 cal BP event has been dated to occur between 2800 and 2710 cal BP by the archaeological 'terpen' period in the Netherlands (Geel *et al* 1996), and changes in solar activity have been suggested as the main cause for this climatic change (Bond *et al* 1997; Vos *et al* 1997; Bond *et al* 2001; Andresen *et al* 2004). Historically, low solar activity has been connected to colder climate conditions and for example the Maunder sunspot minimum occurring in the period from 305 to 235 cal BP indicates low solar activity and is associated with the 'little ice age' (Eddy 1976; Bard *et al* 2000). The Maunder sunspot minimum is also observed in the  $\Delta^{14}\text{C}$  data (*Figure 4-5*). It has been suggested that climate deteriorations occur during transitions from low to high  $\Delta^{14}\text{C}$  values (Geel *et al* 1996; Blaauw *et al* 2004b; Kuznetsova and Tsirulnik 2004; Mauquoy *et al* 2004), i.e. during periods of decreased solar activity. Significantly, there have been no massive freshwater releases or large area ice cover during the past 9000 years to explain changes in NADW, and hence the solar variability seems a plausible forcing mechanism despite its yet unknown operating mechanism (Kristjansson *et al* 2004; Mayewski *et al* 2004; Mendoza *et al* 2004; Palmer *et al* 2004; Ruzmaikin *et al* 2004).

Within historic time, two climate events, i.e. the medieval warm period (MWP) and the little ice age (LIA), have received much attention with regard to 20<sup>th</sup> century climate warming and natural climate variability (see e.g. Crowley and Lowery 2000) as they may serve as modern analogies of past climatic changes. The timing and intensity of these two events is still debated (see e.g. Crowley and Lowery 2000; Brazdil *et al* 2005; Matthews and Briffa 2005). It is, however, generally agreed that the MWP corresponds to the period from 1150 cal BP to 7-650 cal BP and the LIA from 6-550 cal BP to 100 cal BP (Matthews and Briffa 2005; Pederson *et al* 2005; Gil *et al* 2006). The MWP period is commonly said to be warm and dry in contrast to the LIA, which is cold and wet. The MWP period in the Bliden record covers the upper part of 'intermediate water' and almost the entire 'shallow water B' facies association, whereas the onset of the LIA corresponds approximately with the 'high water B' facies association (*see chapter 7*). Note that the depth-to-age model does not apply for the 'high water B' facies association (*see chapter 8*).

The general correlation between these global climate events and the Bliden Lake suggests that the Bliden Lake is sensitive to global climate changes. All Baltic region wet shifts of special significance, occurring ca. 3500, 2700, 1950, 1400 and 650 cal BP (Barber *et al* 2004), are identified in the Bliden Lake. However, the wet periods inferred from Danish and German bogs yield a high correlation from about 2800 cal BP and onwards, but this correlation almost vanishes in the period from 5200 cal BP to 2800 cal BP. The IRD events are excellently recorded by the Bliden Lake prior to 2800 cal BP, but hardly observable from 2800 cal BP and onwards. The sensitivity of the lake to different kinds of climate changes thus appears to vary. Bog wet periods suggest periods of increased rainfall (Blaauw *et al* 2004b). Presuming that the anthropogenic impact on

the Bliden Lake accelerated from about 2800 cal BP, possibly with heavy deforestation, then one possible explanation to this change in climate sensitivity may be that deforested land could be more susceptible to erosion compared to dense forest landscape. Thus the apparent change in climate sensitivity may be the result of an increased anthropogenic impact on the surrounding landscape and thereby also on the lake.

Lack of correlation with northern hemisphere climate events observed by other proxy records may, on the other hand, stem from dating uncertainties. Age models derived from marine and lacustrine sediments are commonly supported by an average of one  $^{14}\text{C}$  date per 2500 years (Kaufman *et al* 2004) and may thus be accompanied by significant uncertainties. Thus, even though the Bliden record age model is supported by *ca.* one  $^{14}\text{C}$  date per 500 years, uncertainties may still be quite large, as also revealed both by correlation to other records as well as the variability of 'events' not manifested in sedimentation rate changes. Moreover, inferences made from a single core may reflect local climate rather than regional or global climate. Hence, mismatches between northern hemisphere climate events and the Bliden Lake record may result from local factors, such as relative sea level changes. Despite these uncertainties, the general correlation observed between commonly accepted northern hemisphere climate events and changes in the Bliden Lake sedimentology and geochemistry may suggest that a common forcing mechanism is at play.

#### **Possible indications of climatic forcing**

The oxygen isotope composition of the lake water reflects changes in precipitation, water inflow and evaporation (*see discussion chapter 5 and 6*). Ultimately, the E/I ratio tracks changes to the lake water level and thereby also to effective humidity. Thus, periodic changes due to external forcing factors would probably show in the E/I ratio curve. In chapter 6 it was argued that most of the variance in the  $\delta^{18}\text{O}_{\text{carb}}$  values were likely to reflect changes in the E/I ratio, and the wavelet power spectrum (*Figure 9-3*) may therefore reveal possible periodicities in the Bliden Lake record. However, as has been pointed out, the bulk  $\text{CaCO}_3$  isotope measurements employed in this work carry the potential danger of being contaminated by allochthonous  $\text{CaCO}_3$ . Varying temporal mixtures of allochthonous  $\text{CaCO}_3$  will certainly yield erroneous results in the attempt to estimate possible periodicities and consequently the results presented in this section should be approached with caution. On the other hand, the amounts of allochthonous  $\text{CaCO}_3$  were discussed in some detail in chapter 7 and found likely to constitute only a minor fraction of the total  $\text{CaCO}_3$  content (*see e.g. Figure 7-4C & D, 7-6 and 9-6*). The wavelet analysis has been performed only on the lower part of the Bliden Lake core up to 536 cm (*~2100 cal BP; the first break point in the depth-to-age model, see chapter 8*) in order to obtain a section with as many samples as possible with equal time spacing.

The pollen-based temperature curve by Seppä *et al* (2005) was applied to the Bliden Lake data to derive an estimate of the paleo lake water isotope composition ( $\delta^{18}\text{O}_{\text{OW}}$ ) and these estimated  $\delta^{18}\text{O}_{\text{OW}}$  values were further used to estimate the E/I ratio by calculating the temporal difference between the inferred  $\delta^{18}\text{O}_{\text{precipitation}}$  values (Dansgaard 1961; Rozanski *et al* 1992) and the  $\delta^{18}\text{O}_{\text{OW}}$  values (*see section 6 for details*). *Figure 9-3* presents the wavelet power spectrum of the inferred  $\delta^{18}\text{O}_{\text{OW}}$  and  $\delta^{18}\text{O}_{\text{precipitation}}$  values. It must be emphasised that these latter curves are only tentatively derived and conclusions drawn by applying these curves should be drawn with caution. However, all three wavelet power spectra reveal a similar pattern, verifying that most of the observed variance is likely to originate from changes in the isotope composition of the lake water and probably reflects changes in the evaporation to inflow balance. The wavelet spectra suggest periodicities of mainly 210 years and about 425 years, both corresponding to the *ca.* 205 to 210 year and *ca.* 420 year solar cycles observed by spectral analysis of sunspot numbers and the so-

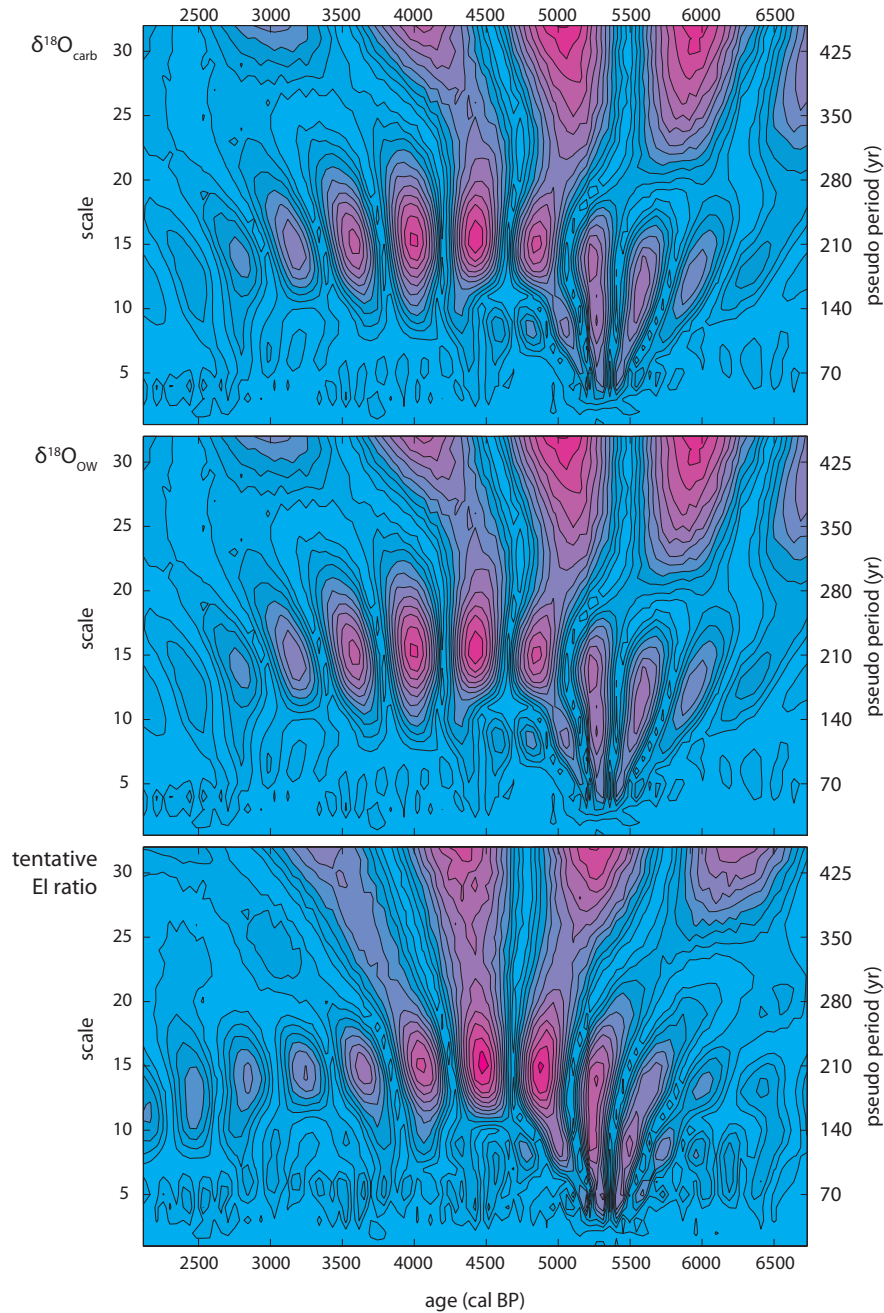


**Figure 9-3:** Shown is the absolute values of the wavelet coefficients using a morlet wavelet on the  $\delta^{18}\text{O}_{\text{carb}}$ , inferred  $\delta^{18}\text{O}_{\text{ow}}$  and inferred E/I values (see chapter 6) using a Morlet wavelet and by applying signal extension in order to avoid edge effects.

lar activity proxies  $^{14}\text{C}$  and  $^{10}\text{Be}$  (Ogurtsov *et al* 2002; Vasiliev and Dergachev 2002; Dergachev 2004), suggesting that changes in the water level may be attributed to changes in solar activity probably linked to changes in atmospheric and/ or oceanic circulation changes. The observed 210 year periodicity is very close to the 260 year periodicity observed by Aaby (1976) from raised peat bogs. Furthermore, the inferred E/I ratio wavelet power spectrum reveals a weakly defined periodicity of *ca.* 70 years, corresponding to the observed NAO periodicity. However, this periodicity is so weakly defined and is in fact below the classical Nyquist frequency of 82 years that it is most likely below the noise level. Interestingly, it seems that the observed periodicity is most pronounced in the period ranging from 5700 cal BP to about 3000 cal BP. As

Tissø Lake  
Core B3

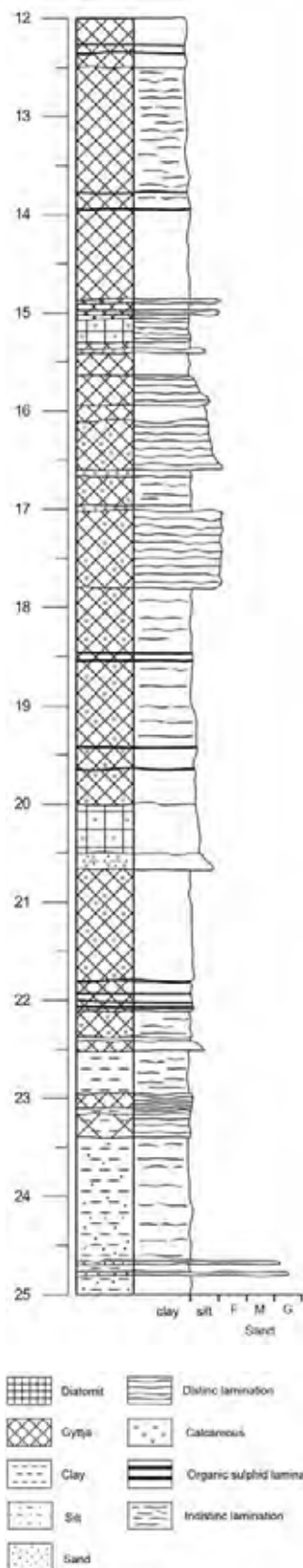


**Figure 9-4.** Lithological log of Tissø Lake (made by Nanna Noe-Nygaard & Mikkel Uldfeldt Hede, Geological Institute, University of Copenhagen).

argued above, in the period from about 3000 cal BP and onwards the catchments area is probably heavily influenced by human activity perhaps obscuring the climate signal. On the other hand, 5700 cal BP represents the termination of Holocene climatic optimum (see e.g. Kaufman *et al* 2004; Roberts 2004) and the transition from the Atlantic to the sub-Boreal period. Indeed, the period from 5700 cal BP to about 3000 cal BP represents a generally decreasing water level, however punctured by three high water level events and as indicated by other studies (see e.g. Barber *et al* 2004; Magny 2004; Magny and Haas 2004; Mayewski *et al* 2004) this period may represent a turbulent period in the Holocene climate history. On the other hand, this peculiarity may be the result of edge effects due to the wavelet analysis and may therefore be purely artificial.

### The Littorina transgressions

In Denmark the interplay of climate fluctuations, isostatic rebound and eustatic sea level rise resulted in succeeding regression and transgression phase replacements of the marine shore lines known as the Littorina transgression (see e.g. Iversen 1937; Noe-Nygaard 1995; Christensen and Andreasen 1999; Lambeck 1999; Christensen 2001; Hede 2003; Richter and Noe-Nygaard 2003). According to Noe-Nygaard *et al* (Noe-Nygaard *et al* 2003; Noe-Nygaard and Hede 2006) it appears likely that the Littorina sea transgressed the low land area between Tissø Lake and the sea, and thus that saline sea water may superficially have entered Tissø Lake. Furthermore, Noe-Nygaard (1995) observed increased groundwater levels in the Åmose basin (see map Figure 4-1) correlating with relative high sea levels. If this is correct, sea water may have entered the Bliden Lake either superficially or due to elevated groundwater levels. Hence, the adjacent position of Tissø Lake makes it very suitable for a comparison with Bliden Lake (Hansen 2003; Noe-Nygaard *et al* 2003) in order to detect the marginal propagation of the Atlantic and sub-

Boreal *Littorina* transgressions. The lithological log of Tissø Lake is presented in Figure 9-4 (see also appendix A).

### Paleo-salinity

One way of testing this is by employing the C:S ratios as a paleo-salinity indicator as seen in Figure 9-5 (Berner 1984; Berner and Raiswell 1984). As previously noted (see chapter 5), marine and lacustrine algae differ in their C:S ratios. The C:S values of lacustrine algae range from 16 to 30 (Nriagu and Soon 1985) whereas the common C:S values of marine algae are reported to be around 8 (Morse and Berner 1995).

The Tengslemark site (see map Figure 4-1) is a dried out ancient lagoon with alternating brackish and freshwater sediments identified by TS and TOC values and adequately dated (pers. com. Noe-Nygaard) as is also revealed by the slope of the Tengslemark TS and TOC values approaching the C:S values of marine algae (see Figure 9-5). The TS and TOC values of Tissø Lake cluster in three groups (Figure 9-5, see also the site description of Tissø Lake in Appendix A). One group displays combined TS and TOC values characteristic of lacustrine environments, whereas the other two groups display combined TS and TOC values indicating marine influence or elevated water salinity. These elevated TOC and TS values with C:S ratios appearing to reflect the presence of marine algae are dated to the period from 4700 cal BP to 2600 cal BP (see Figure 9-5). The increased periods of higher salinity may further be supported by the observation of brackish diatoms species concurring with the intervals of high TS and TOC values in Tissø Lake (Hansen 2003). Similarly, the high TOC versus TS values of the Bliden Lake might indicate elevated salinity and are dated to be older than 500 cal BP. Hence, the concurrent TS and TOC values of Bliden and Tissø Lake may suggest periods with high salinity; however, if these high salinity periods are caused by relative sea level changes, the high salinity periods must correlate between Bliden Lake and Tissø Lake or alternatively they may be identified in Tissø Lake but not in the Bliden Lake. In the latter case, the moraine ridge separating Tissø Lake from Bliden Lake probably serves as a marginal barrier preventing saline sea or brackish waters from entering the Bliden Lake. However, due to the adjacent position of the two lakes, saline waters caused

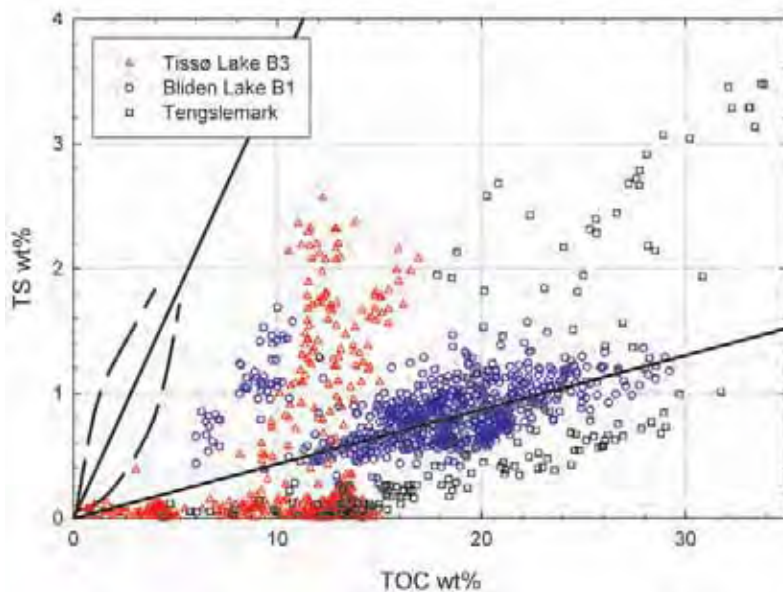


**Figure 9-5:** Illustrated is a scatter plot of TOC wt% versus TS wt% of the Bliden Lake, Tengslemark (pers. com. Noe-Nygaard, Fischer Mortensen and Christensen) and Tissø Lake (Hansen 2003; Noe-Nygaard et al 2003). The site locations are shown in Figure 4-1. The C:S values of marine and lacustrine algae are shown as solid lines and the oblong shape illustrated by the punctured lines denote the area in which most marine C:S values fall (Berner 1984).

by a transgressing sea should be concurrent with a lake level rise in the Bliden Lake induced by increasing groundwater levels. In summary, two scenarios may be applied to detect relative sea level changes by the combined use of Bliden Lake and Tissø Lake: 1) higher salinity is observed simultaneously in both lakes or 2) higher salinity is observed in Tissø Lake concurrent with an increasing or higher water level in Bliden Lake.

The first of these scenarios can be excluded because the periods of higher TS and TOC values in Bliden Lake and Tissø Lake are not concurrent. As mentioned above, the Bliden Lake deposits after 500 cal BP are more likely to reflect the onset of the little ice age, and the very high TS values (Figure 7-2) at the onset of this period may stem from a transgression of the lake shore resulting in increased amounts of sulphur and carbon from flooded decomposing lake shore vegetation (Talbot *et al* 2006). The high TS values are accompanied by very low C:S and  $\delta^{34}\text{S}_{\text{ORG}}$  values (see Figure 7-2) probably indicate heavy anoxic hypolimnion conditions (Watanabe *et al* 2004; Eimers *et al* 2006). Note that the high TS and TOC values in Tissø Lake may derive from similar anoxic conditions. Thus, it is not likely that saline or brackish waters influenced the Bliden Lake, which leaves only the second scenario as a likely possibility.

When employing the paleo-salinity method, the carbon to pyrite sulphur ratio ( $\text{C:S}_{\text{pyrite}}$ ) should be applied to distinguish between freshwater and marine sediments. The common pathway of  $\text{H}_2\text{S}$  produced by bacterial sulphate reduction in marine environments is the formation of pyrite. In contrast, pyrite is formed in lacustrine environments to a much lesser extent. Therefore the  $\text{C}_{\text{ORG}}:\text{S}_{\text{TOT}}$  ratio alone cannot be used as a paleo-salinity indicator and the  $\text{C}_{\text{ORG}}:\text{S}_{\text{pyrite}}$  ratio may be a much better indicator for paleo-salinity (Losher 1989). Even though pyrite formation following the sulphate reduction in marine environments (Berner 1984; Berner *et al.* 1984; Morse *et al.* 1995) may play a minor role in freshwater environments, it does however hold the key for the detection of paleo-salinity (Losher 1989; Losher *et al.* 1989), and thus also for an adequate detection of the Littorina transgression in lacustrine lakes. The TS values of the Bliden Lake represent the sulphur content of the organic material, in contrast to the data from both Tengslemark and Tissø Lake, which represents the total sulphur content. Hence, the TS data from Tengslemark and Tissø Lake may potentially include the sulphur content from pyrite, and may thus serve as a better paleo-salinity indicator than the TS data from the Bliden Lake.

### Concurrent lake level changes in Bliden Lake and Tissø Lake

Presumably, the hydrologies of the Bliden Lake and Tissø Lake are very different, because the catchments area of the Bliden Lake is rather small in comparison to Tissø Lake, which has a large catchments area of about 418 km<sup>2</sup> (Høy and Dahl 1993) covering the Åmose basin (see map Figure 4-1). This contrast is revealed by the isotopic composition of the bulk  $\text{CaCO}_3$  in each lake (see Figure 9-6). The high positive correlation between the  $\delta^{18}\text{O}_{\text{carb}}$  and  $\delta^{13}\text{C}_{\text{carb}}$  values of Tissø Lake may suggest hydrologically closed conditions (Talbot 1990; Li and Ku 1997) in contrast to the short water residence time of the lake of about 1.5 years (Hansen 2003). However, the isotopic composition of the lake water and DIC is not necessarily closely related to lake hydrology (Dean 2002). The covarying  $\delta^{13}\text{C}_{\text{carb}}$  and  $\delta^{18}\text{O}_{\text{carb}}$  values might therefore reflect the large water pathway through the Åmose bogs and lakes before entering the Tissø Lake possibly enriching the water in  $^{18}\text{O}$  due to evaporation and the DIC in  $^{13}\text{C}$  due to organic productivity along the flow path. Alternatively, the enriched  $\delta^{18}\text{O}_{\text{carb}}$  values may represent a transgressive phase of the lake increasing the surface area to volume ratio probably enhancing evaporative loss from the lake (Bright *et al* In Press, Corrected Proof). However, the linear trend of the  $\delta^{13}\text{C}_{\text{carb}}$  and  $\delta^{18}\text{O}_{\text{carb}}$  values appears to have an isotopic end-value similar to the isotopic composition of the surrounding tills (Kolstrup and Buchardt 1982; Hammarlund and Buchardt 1996; Noe-Nygaard and Heiberg 2001) and therefore the  $\delta^{13}\text{C}_{\text{carb}}$  and  $\delta^{18}\text{O}_{\text{carb}}$  values may reflect a varying mixture

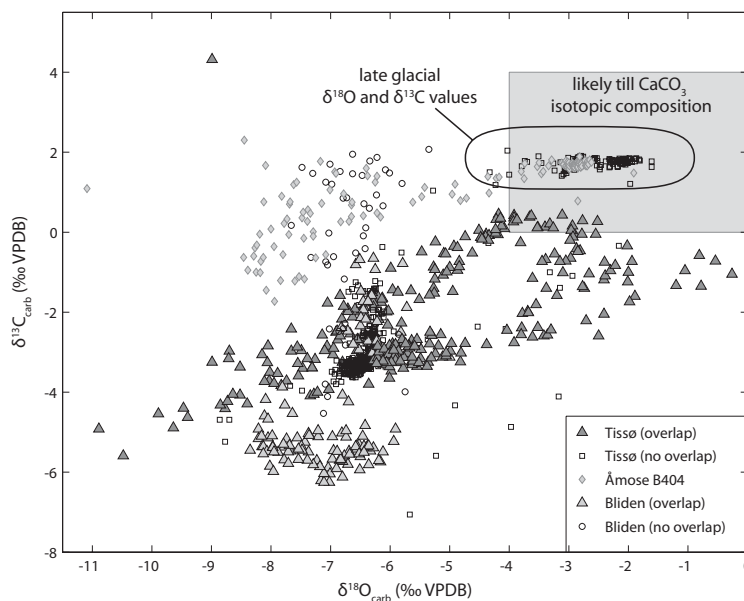


**Figure 9-6:** Scatter plot of  $\delta^{18}\text{O}_{\text{carb}}$  and  $\delta^{13}\text{C}_{\text{carb}}$  values of Bliden and Tissø Lake (Hansen 2003; Noe-Nygaard et al 2003). The data are grouped according mutual time overlap (see Figure 9-7). For comparison the  $\delta^{18}\text{O}_{\text{carb}}$  and  $\delta^{13}\text{C}_{\text{carb}}$  values from the Åmose core B404 are also shown (Noe-Nygaard 1995). The six samples displaying very low  $\delta^{13}\text{C}_{\text{carb}}$  values (range between -20‰ and -30‰) and  $\delta^{18}\text{O}_{\text{carb}}$  values (range between -15‰ and -20‰) and are not shown on this scatter plot.

of allochthonous detrital  $\text{CaCO}_3$ . Note that the combined  $\delta^{13}\text{C}_{\text{carb}}$  and  $\delta^{18}\text{O}_{\text{carb}}$  values of the late glacial sediments of Tissø Lake and Åmosen (B404, Noe-Nygaard 1995) are in excellent agreement with the till  $\text{CaCO}_3$  isotopic values. Furthermore, the lack of correlation between the Tissø Lake  $\delta^{13}\text{C}_{\text{ORG}}$  and  $\delta^{13}\text{C}_{\text{carb}}$  values may suggest that the isotopic composition of the DIC is mainly controlled by the inflowing water (Figure 9-7).

The SUS values of Bliden Lake and Tissø Lake are correlated except for dates older than approximately 5000 cal BP, but in contrast almost all other displayed geochemical parameters show uncorrelated values (Figure 9-7). The high correlation between the SUS values may suggest a good age correlation between the two cores. The Tissø Lake geochemical parameters show two major changes in the illustrated age range (Figure 9-7). The first occurs around 4900 cal BP and marks a change from constant values to more varying and elevated values (e.g. TS,  $\delta^{13}\text{C}_{\text{carb}}$  and  $\delta^{18}\text{O}_{\text{carb}}$ ) and is not observed in the Bliden Lake to a similar degree. The second is an abrupt change in most parameters at 2600 cal BP, concurrent with the increasing SUS values and  $\delta^{13}\text{C}_{\text{ORG}}$ ,  $\delta^{13}\text{C}_{\text{carb}}$  values in Bliden Lake. The date 2600 cal BP is associated with the onset of the 'shallow water A' facies association in Bliden Lake, which is a period characterised by a low but increasing water level (Figure 9-1). Notably, in the period from 2800 cal BP to 2600 cal BP both the Tissø Lake  $\delta^{13}\text{C}_{\text{carb}}$  and  $\delta^{18}\text{O}_{\text{carb}}$  values become very negative (see Figure 9-7). The  $\delta^{13}\text{C}_{\text{carb}}$  values approaching -29‰ may result from increased anoxic conditions producing very  $^{12}\text{C}$  depleted methane, which is oxidised in the epilimnion resulting in depleted DIC isotopic values (Teranes and Bernasconi 2005). The  $\delta^{18}\text{O}_{\text{carb}}$  values approaching -20‰ are, on the other hand, not fully understood. However, sea water has a rather uniform isotopic composition of 0‰ VSMOW which corresponds to about -30‰ VPDB (Clark and Fritz 1997). Hence, the very negative  $\delta^{18}\text{O}_{\text{carb}}$  values may be the result of intrusion by seawater. The development of anoxic hypolimnion conditions may be supported by the high TS values, which may indicate bacterial sulphate reduction (Watanabe *et al* 2004; Eimers *et al* 2006) for the entire period from 4900 cal BP to 2600 cal BP. Furthermore, increased anoxic conditions enhance the preservation of

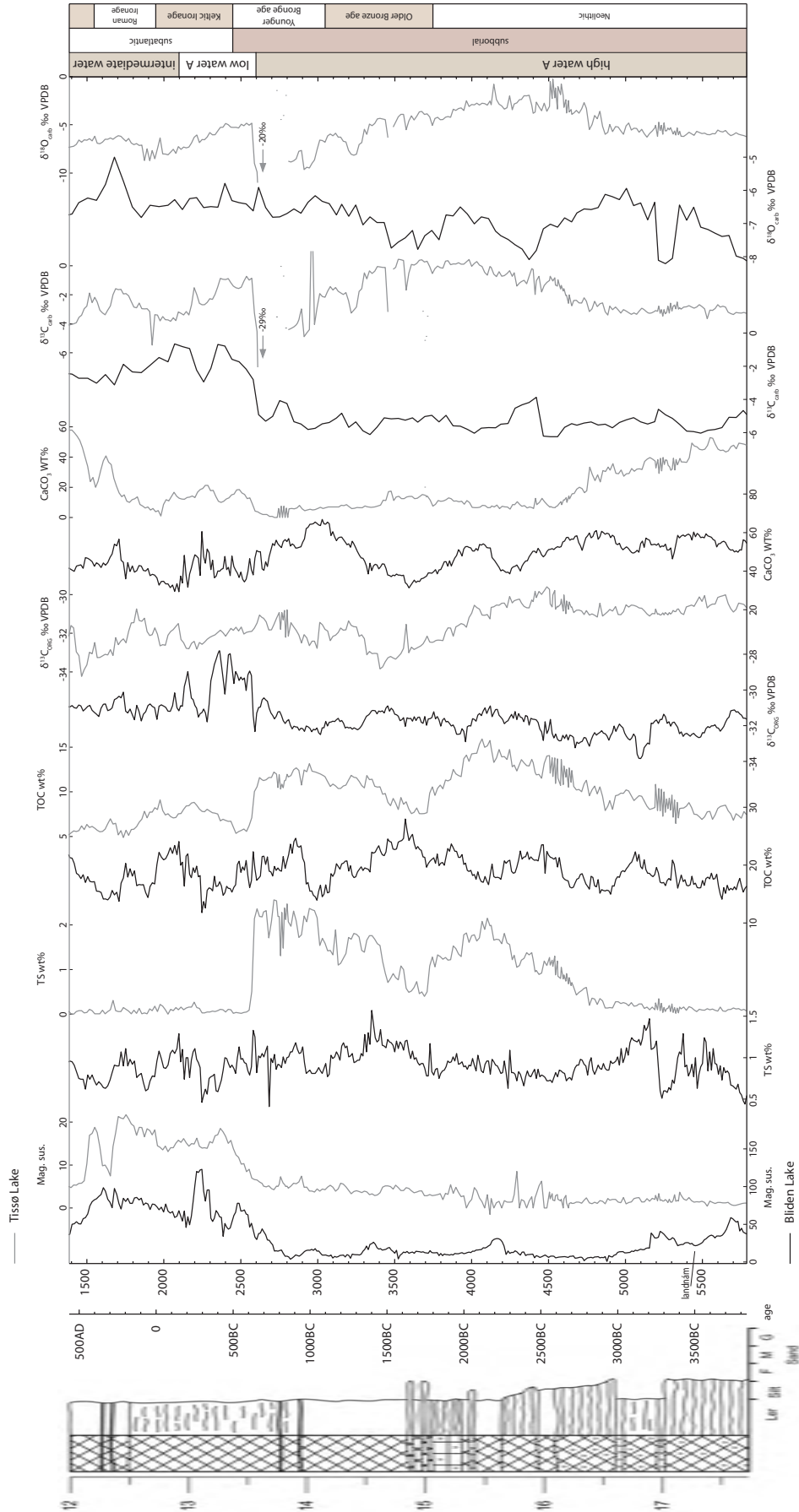


**Figure 9-7:** Comparison of the Bliden and Tissø Lake geochemical data. The Tissø Lake geochemical data have formerly been presented by Hansen (2003) and Noe-Nygaard et al (2003). The Bliden Lake age model is presented in appendix A. The graph covers the range from 1200 (range between -15‰ and -20‰) and are indicated by arrows. The Tissø Lake geochemical data have formerly been presented by Hansen (2003) and Noe-Nygaard et al (2003). samples display very low  $\delta^{13}C_{carb}$  values (range between -20‰ and -30‰) and  $\delta^{15}N_{carb}$  values (range between -15‰ and -20‰) and are indicated by arrows.

organic matter, which may explain the high correlation between the TS and TOC values during this period.

The TS and TOC peaks occurring between 4900 cal BP and 2600 cal BP has formerly been interpreted as resulting from the impact of two intense saltwater events, either as wash over or as saline groundwater (Hansen 2003; Noe-Nygaard *et al* 2003). Therefore the water level is most likely increasing from 4900 cal BP to 4100 cal BP and again from 3600 cal BP to 2800 cal BP, whereas it is probably decreasing from 4100 cal BP to 3600 cal BP (*Figure 9-7*). Thus, the high water levels observed in mid-European lakes from 4150 cal BP to 3950 cal BP and from 3500 cal BP to 3100 cal BP (Magny 2004) correspond relatively well with the high water level in Tissø Lake at 4100 cal BP and with the increasing water level in Tissø Lake from 3600 cal BP to 2800 cal BP. Furthermore, the water level in Tissø Lake is likely to have been high between 3000 cal BP and 2600 cal BP in agreement with high water level periods for mid-European lakes (Magny 2004). On the other hand, the high lake level of Tissø Lake displays a decent correlation with the high relative sea level observed at Tengslemark from 4700 cal BP to 4000 cal BP (pers. com. Noe-Nygaard) and, furthermore, is simultaneous with a high lake level in the Bliden Lake (*Figure 9-1*), thus fulfilling the criteria of scenario 2). Hence, the high lake levels of both Bliden Lake and Tissø Lake around 4900 cal BP to 4000 cal BP may be caused by a high relative sea level. The onset and peak of the lake level rise occurs later and before respectively in comparison with Tissø Lake, indicating the altitude difference between the two lakes as may also be observed from present-day topology. The increasing water level in Tissø Lake from 3600 cal BP to 2800 cal BP is not readily identifiable in Bliden Lake; however, the minor lake level rise peaking at 3500 cal BP to 3400 cal BP in Bliden Lake (*Figure 9-1*) may correspond to the increase in lake level in Tissø Lake. Thus, suggesting that these concurrent lake level changes may be associated with a high relative sea level. The correlation is weak, however, and may be due to other factors.

The younger Littorina transgression occurring about 6500 cal BP to 6300 cal BP at Tengslemark (pers. com. Noe-Nygaard) is hardly distinguishable from the climate induced generally higher lake levels of Lake Bysjön in southern Sweden and mid-European lake levels (Digerfeldt 1988; Magny 2004). However, it occurs simultaneously with an increasing lake level in Bliden Lake (see *Figure 9-1*) and a minor increase in the TS and TOC values in Tissø Lake (*not shown on graphs*) again indicating that this concurrent lake level rise in both lakes may be induced by a relative sea level change as well as a climatic one.

The lower TOC,  $\delta^{13}\text{C}_{\text{ORG}}$  and  $\text{CaCO}_3$  values after 2600 cal BP may suggest a decreasing organic productivity in the Tissø Lake (McFadden *et al* 2005; Talbot *et al* 2006), and thus probably reflects a reduced nutrient supply associated with a decreasing water inflow, which corresponds to the shallow water level period in Bliden Lake at this time. The abrupt change in the Tissø Lake at 2600 cal BP (see *Figure 9-7*), which is also indicated in the Bliden Lake (see *Figure 7-2 & 9-2*), may suggest a dramatic change in the land-to-sea connection in the Tissø Lake and Bliden Lake area. Perhaps the isostatic rebound resulted in a complete closing of the possible connection to the sea at this time.

### **The climate during the Mesolithic to Neolithic transition**

The Mesolithic to Neolithic transition in Denmark is estimated to have occurred between 5900 cal BP and 5800 cal BP and no later than 5740 cal BP (3950 BC to 3850 BC and no later than 3790 BC, see *chapter 4*). Furthermore, agriculture was adopted in Ireland, Britain and southern Sweden in the period from 6050 to 5750 cal BP and Bonsall *et al* (2002) claim that this similarity in time over such a large area cannot be purely incidental. Thus, the propagation of agriculture from France, Germany and Poland to the British Isles, Ireland and southern Scandinavia is

attributed to relatively dry and warm climate conditions from 6050 cal BP to 5150 cal BP preventing waterlogging of soil areas and thereby enhancing agricultural potential (Bonsall *et al* 2002).

The inferred Bliden Lake depth curve (*Figure 9-1*) indicates a period with decreasing water level from about 6250 cal BP which terminates at 5300 cal BP in accordance with the dryer conditions reported by Bonsall *et al* (2002). In contrast, evidence for a cold period about ~5700 cal BP (O'Brian *et al* 1995) is persuasive (*see discussion above*). This cold period may be supported by the NGRIP ice core  $\delta^{18}\text{O}$  values (Johnsen *et al* 2001; Vinther *et al* 2006) and by the temperature curve by Seppä *et al* (2005). Hence, not only did the decreasing rate of the eustatic sea level rise result in a rapid progradation of the coastline into shallow coastal waters creating new unforested land (Noe-Nygaard *et al* 2005), so too did probably decreasing lake levels. This new unforested land was readily immigrated by grass and herbs, forming a basis for grass-eating cattle (Noe-Nygaard *et al* 2005) and perhaps even creating land ready for cultivation. However, a causal link between climatic and cultural changes cannot be proven by paleolimnological investigations or by paleoclimate research in general (see e.g. Coombes and Barber 2005), i.e. the fact that a climatic change enhanced the possibility of land cultivation and grass eating cattle does not imply that the Neolithic culture was actually adopted by man. It may be conceivable that the adoption of the Neolithic culture and the simultaneous climatic change worked independently, even though it is a striking fact that the utilisation of marine resources was discontinued from the onset of the Neolithic, that the Neolithic was introduced over a large land area in very short course of time and lastly that these cultural changes occurred simultaneously with a climate change probably towards drier and cooler conditions.

## Conclusion

It has been demonstrated that the Bliden Lake record is decently well correlated with changes in effective humidity by comparing with Lake Igelsjön, southern Sweden (Hammarlund *et al* 2003; Hammarlund *et al* 2005; Jessen *et al* 2005; Seppä *et al* 2005). However, inferred stable climate conditions in terms of effective humidity prior to 4600 cal BP and the pronounced warm and/or dry period around 4450 cal BP did not correlate particularly well with conditions inferred from Lake Igelsjön (Jessen *et al* 2005). In addition, the Bliden Lake does not exhibit the decreasing water level of Lake Bysjön between 4600 cal BP and 4200 cal BP (Digerfeldt 1988). Similarly, some of the high water levels inferred from mid-European lakes (Magny 2004) are uncorrelated with the observed lake level change in the Bliden Lake as revealed by the constructed water level curve. Most pronounced are the high water level periods from 4850 cal BP to 4800 cal BP, from 4150 cal BP to 3950 cal BP and from 3500 cal BP to 3100 cal BP. The water level changes of Lake Igelsjön, Lake Bysjön and the mid-European lakes (Digerfeldt 1988; Hammarlund *et al* 2003; Magny 2004; Jessen *et al* 2005) are very likely to reveal changes in effective humidity, i.e. they may be applied to differentiate between wet and dry climate conditions of past mid- to northern Europe. Hence, uncorrelated lake level changes between Bliden Lake and these climate proxies may indicate that other factors are at play in Bliden Lake during these periods. These other factors may be anthropogenic effects, sea level changes or changes in climate sensibility.

The widely accepted northern hemisphere cold events occurring around 5200 cal BP and 2800 cal BP (see e.g. Geel *et al* 1996; Mauquoy *et al* 2004; Versteegh 2005) are both observed in the Bliden Lake. The 5200 cal BP cold event is illustrated by a dramatic decrease in the  $\delta^{18}\text{O}_{\text{carb}}$  values simultaneously with drastic changes in C:S, C:N,  $\delta^{34}\text{S}_{\text{ORG}}$ , and  $\delta^{15}\text{N}_{\text{ORG}}$  values, whereas the 2600 cal BP is less pronounced. The 5200 cal BP and 2600 cal BP events are associated with decreasing solar activity, suggesting a close link between solar activity and major climate changes, which is further indicated by the wavelet analysis of the  $\delta^{18}\text{O}_{\text{carb}}$  values of the Bliden Lake revealing pe-

riodicities of *ca.* 210 and 425 years. However, these observed periodicities may be artificial due to the employment of bulk  $\text{CaCO}_3$  analysis and the lack of verification of the mineralogy in the Bliden Lake. Hence, the  $\delta^{18}\text{O}_{\text{carb}}$  may have been contaminated with allochthonous  $\text{CaCO}_3$  from the surrounding tills. Momentarily disregarding this major weakness, the observed periodicities are in accordance with solar cycles as inferred from counts of sunspot numbers and  $^{14}\text{C}$  and  $^{10}\text{Be}$  proxies of solar activity (Ogurtsov *et al* 2002; Vasiliev and Dergachev 2002; Dergachev 2004). Furthermore, the Bliden Lake record may show weak evidence of prolonged seasonal ice cover during cold periods as revealed by increased anoxic conditions as indicated by elevated  $\delta^{15}\text{N}_{\text{ORG}}$  values and decreased  $\delta^{34}\text{S}_{\text{ORG}}$  values correlating with reduced NAWD formation (Bond *et al* 2001; Oppo *et al* 2003). The decreasing water level of the Bliden Lake during periods of reduced NAWD formation may further supply weak evidence for the association of dryer conditions with reduced NAWD formation at least in some instances.

The higher salinity and increasing lake water of Tissø Lake in the period between 4900 cal BP and 4000 cal BP combined with a simultaneous lake level rise in Bliden Lake is most likely induced by a relative sea level change. The high stand of this Littorina transgression is adequately dated, by employing the lake core from Tengslemark, to have occurred between 4700 cal BP and 4000 cal BP (pers. com. Noe-Nygaard). The succeeding high salinity period in Tissø Lake between 3600 cal BP and 2600 cal BP is, however, only weakly correlated with lake level changes in the Bliden Lake. Hence, the high water level at 3500 cal BP to 3400 cal BP in Bliden Lake may be induced by a high relative sea level. Furthermore, the high relative sea level observed in Tengslemark between 6500 cal BP and 6300 cal BP (pers. com. Noe-Nygaard) is concurrent with higher TS and TOC values in Tissø Lake and increasing water level in Bliden Lake, thus further indicating lake level changes induced by relative sea level changes. Notably, the high lake levels of mid-European lakes not confirmed by the Bliden Lake around 4800 cal BP, from 4150 cal BP to 3950 cal BP and between 3500 cal BP and 3100 cal BP may further suggest that during these periods relative sea level changes contributed to the observed lake level changes of Bliden Lake.

The decreasing water level from about 6250 cal BP, which terminates at 5300 cal BP, may suggest that not only did the decreasing rate of the eustatic sea level rise result in a rapid progradation of the coastline into shallow coastal waters creating new unforested land (Noe-Nygaard *et al* 2005) so too did decreasing lake levels. This new unforested land provided areas ready for cattle grazing and cultivation which may have enhanced the potential for adopting Neolithic culture.

# 10

---

**Conclusion summary**

## Conclusions

The application of isotope ratio mass spectrometry is widely employed within a diversity of different research fields such as geology, hydrology, climate research and archaeology. The quality assurance programme of the recently installed stable isotope mass spectrometer has been demonstrated and evaluated. It provides the basis on which high precision stable isotope values are obtained on numerous sample types spanning from lake sediments to human bones. As an example of one of these applications, a multi-proxy high-resolution paleoclimate investigation of the Bliden Lake has been presented with the main focus on the employment of stable isotope data. Furthermore, on the basis of radiocarbon dated samples, a chronology of the Bliden Lake record has been established using a recently developed method (Blaauw and Christen 2005). This method uses a Bayesian Statistics approach to establish a depth-to-age relation. With the help of simulated data, it has been shown that the method can also be applied cases with low age resolution. The interpretation of the sedimentological and geochemical data provided a climate history of the Bliden Lake of the past 6700 years. In particular the constructed water level curve of the Bliden Lake has been used to observe the marginal propagation of Atlantic and sub-Boreal relative sea level changes. Furthermore, the possible climate changes around the Mesolithic to Neolithic transition in Denmark were discussed.

### Main conclusions on stable isotope analysis

The central point in the quality assurance programme is the sample lists with mandatory prefixed positions for blank samples, standards and performance standards, where the performance standards are chosen to mimic real samples as closely as possible. This allows for easy and fast detection of problematic periods. The typical precision for  $\delta^{13}\text{C}$  and  $\delta^{15}\text{N}$  analysis is 0.2‰ and 0.3‰ respectively, and the typical  $\delta^{34}\text{S}$  precision is found to be 0.5‰. These numbers were confirmed by the error estimates of the geochemical parameters by denoising using a wavelet method (see chapter 6, Table 6.1). A complicating factor in CF-EA isotope analysis is the unknown content of carbon, nitrogen and sulphur in the samples to be analysed. This requires high system linearity over a wide mass range in terms of constant isotope values. If the system is linear, samples with different mass ratios of carbon, nitrogen and sulphur yield accurate isotope measurements of their respective  $\delta^{13}\text{C}$ ,  $\delta^{15}\text{N}$  and  $\delta^{34}\text{S}$  values. The  $\delta^{13}\text{C}$  linearity is observed to range from 15 $\mu\text{gC}$  to 170 $\mu\text{gC}$  and the  $\delta^{15}\text{N}$  linearity from 8 $\mu\text{gN}$  to 75 $\mu\text{gN}$ . The  $\delta^{34}\text{S}$  linearity is ranging from 2 $\mu\text{gS}$  to 14 $\mu\text{gS}$ . The accuracy of the CF-EA carbon and nitrogen system has been found by comparing sample isotope values with sample values obtained by equivalent methods at the Science Institute on Iceland and the Department of Archaeological Science in Bradford. For  $\delta^{13}\text{C}$  and  $\delta^{15}\text{N}$  measurements the mean difference between these samples has been found to be within  $\pm 0.2\text{‰}$ . The accuracy of the CF-EA sulphur isotope analysis may be compromised by the interference of the sample's sulphurdioxide isotopic oxygen composition. In the worst case it may be estimated to be as high as  $\pm 3\text{‰}$  for samples and approximately  $\pm 1\text{‰}$  for international standards.

The mass spectrometric analysis of carbon and nitrogen isotopes displays a performance similar to that observed in other studies. However improving the detection of blank samples and obtaining more precise isotope values of these will significantly improve the method, especially for small samples. Finding and if possible eliminating the sources of blank carbon and nitrogen will significantly improve this analysis method. The CF-EA sulphur method clearly needs improvements and elimination of the problems of oxygen correction. The suggested method where both  $\text{SO}_2$  and  $\text{SO}$  are measured simultaneously on the same sample will likely improve this method significantly. The presented accuracy estimate of the CF-EA sulphur method is unsatisfactory.

Furthermore it is only derived from the analysis of international standards and definitely needs verification by other stable isotope laboratories.

#### *Automation of $^{14}\text{C}$ sample preparation*

Automation of sample preparation techniques is a great advantage in terms of minimising the occurrence of errors. Furthermore automated methods ensure a similar pre-treatment of all samples enhancing their comparability. Chronology based on AMS  $^{14}\text{C}$  dated samples is essential to numerous studies and is always associated with carbon stable isotope analysis in order to correct for natural fractionation processes. Hence commonly a sample is handled for pre-treatment and analysis many times before the final result emerges as a  $^{14}\text{C}$  date associated with a  $\delta^{13}\text{C}$  value. The development of a combined  $\text{CO}_2$  trapping device with stable isotope analysis of  $\delta^{13}\text{C}$  and  $\delta^{15}\text{N}$  by the EA-CF method is therefore a simplifying step in the sample handling procedures of the radiocarbon dating laboratory. Furthermore, as has been demonstrated  $\delta^{15}\text{N}$  values are commonly of great importance to many studies and in the case of the  $^{14}\text{C}$  dated samples of the Bliden Lake this preparation device would have provided  $\delta^{15}\text{N}$  values of the dated sample material which may have turned out to provide invaluable information on the nitrogen isotopic composition of the dated macrofossils.

The designed AMS sample preparation device is fully integrated into mass spectrometer software through a user interface enabling the user to easily access method parameters. Furthermore the full mass spectrometer control over the trapping device system ensures a high safety level when handling the liquid nitrogen applied for cryogenic  $\text{CO}_2$  trapping. The system has successfully tested and the stable isotope analysis precision and accuracy is demonstrated to be in excellent agreement with the normal EA-CF isotope analysis and likewise that the  $^{14}\text{C}$  background level is demonstrated to be at an acceptable level with a PmC value of  $0.0029 \pm 0.0013$ . However, the existing prototype illustrated that further development of the trapping needle and needle holder is required to improve the method.

#### **Main conclusions on Bliden Lake climate history**

The multi-proxy geochemical data and sedimentological investigation of the Bliden Lake has been applied to construct a relative water level curve of the past 6700 years. The constructed water level curve is demonstrated to be decently well correlated with the observed lake level change of Lake Bysjön and Lake Igelsjön in southern Sweden (Digerfeldt 1988; Hammarlund *et al* 2003; Hammarlund *et al* 2005; Jessen *et al* 2005; Seppä *et al* 2005) as well as with the lake level changes of mid-European Lakes (Magny 2004). The observed lake level changes in Lake Bysjön and Lake Igelsjön may be employed as proxies of changes in effective humidity (Digerfeldt 1988; Hammarlund *et al* 2003; Jessen *et al* 2005; Seppä *et al* 2005), i.e. changes in net precipitation and evaporation. Hence, observed changes in the Bliden Lake water level uncorrelated to the mid-European and southern Swedish lakes may likely illustrated periods where regional or local factors played a decisive role. These local or regional factors may be of anthropogenic origin or induced by relative sea level changes, i.e. the so called Littorina transgressions (Iversen 1937; Christensen 1995; Christensen and Andreasen 1999; Christensen 2001; Hede 2003; Noe-Nygaard and Hede 2006).

The Holocene climate in the northern hemisphere has been illustrated to be highly variable and events influencing the northern hemisphere have been demonstrated by numerous studies (see e.g. reviews by Kaufman *et al* 2004; Mayewski *et al* 2004; Versteegh 2005). The northern hemisphere cold events occurring around 5200 cal BP and 2800 cal BP (see e.g. Geel *et al* 1996; Mauquoy *et al* 2004; Versteegh 2005) are both observed in the Bliden Lake and associated with decreasing solar activity suggesting a close link between solar activity and major climate

changes. This is further indicated by the wavelet analysis of the  $\delta^{18}\text{O}_{\text{carb}}$  values of the Bliden Lake revealing periodicities of *ca.* 210 and 425 years. However, these observed periodicities may be artificial due to the employment of bulk  $\text{CaCO}_3$  analysis and the lack of verification of the mineralogy in the Bliden Lake. Looking apart from this major weakness the observed periodicities are in accordance with solar cycles as inferred from counts of sunspot number and  $^{14}\text{C}$  and  $^{10}\text{Be}$  proxies of solar activity (Ogurtsov *et al* 2002; Vasiliev and Dergachev 2002; Dergachev 2004). Furthermore, the Bliden Lake record may show weak evidence of a prolonged seasonal ice cover during cold periods – this is revealed by increased anoxic conditions as indicated by elevated  $\delta^{15}\text{N}_{\text{ORG}}$  values and decreased  $\delta^{34}\text{S}_{\text{ORG}}$  values correlating with reduced NAWD formation (Bond *et al* 2001; Oppo *et al* 2003). The decreasing water level of the Bliden Lake during periods of reduced NAWD formation may further supply weak evidence of associating dryer conditions with reduced NAWD formation in some instances.

#### *The Littorina transgressions*

The Bliden Lake constructed water level curve do not correlate with the stable climate conditions in terms of effective humidity prior to 4600 cal BP and the pronounced warm and/or dry period around 4450 cal BP as inferred from Lake Igelsjön (Jessen *et al* 2005). Likewise the high lake levels of mid-European lake are not observed by the Bliden Lake around 4800 cal BP, from 4150 cal BP to 3950 cal BP and between 3500 cal BP and 3100 cal BP. These discrepancies may suggest periods where relative sea level changes contributed to the observed lake level changes of Bliden Lake. With the purpose of detecting possible water level changes induced by relative sea level change data from the adjacent Tissø Lake were applied. Mutual agreement of water level changes or periods with higher salinity between Tissø Lake and Bliden Lake are likely resulting from relative sea level changes.

Tissø Lake revealed higher salinity in the period from 4900 cal BP to 2600 cal BP as observed from the high TOC and TS values with C:S values approaching the value of marine algae. Likewise brackish diatom species have been identified in Tissø Lake during this period (Hansen 2003). Hence, the higher salinity and increasing lake water of Tissø Lake in the period between 4900 cal BP and 4000 cal BP combined with a simultaneous lake level rise in Bliden Lake is most likely induced by a relative sea level change. A high relative sea level period is further observed to occur between 4700 cal BP and 4000 cal BP from the adequately dated lake core from Tengslemark (*pers. com.* Noe-Nygaard). The succeeding high salinity period in Tissø Lake between 3600 cal BP and 2600 cal BP is however only weakly correlated with lake level changes in the Bliden Lake. Hence the high water level at 3500 cal BP to 3400 cal BP in Bliden Lake may likely be induced by a high relative sea level as well as other factors. Furthermore the high relative sea level observed in Tengslemark between 6500 cal BP and 6300 cal BP (*pers. com.* Noe-Nygaard) is concurrent with higher TS and TOC values in Tissø Lake and increasing water level in Bliden Lake thus further indicating lake level changes induced by relative sea level changes.

#### *The climate during the Mesolithic to Neolithic transition*

The adoption of agriculture appears to have occurred during a period of decreasing water level in the Bliden Lake terminating around 5300 cal BP. This may suggest that not only did the decreasing rate of the eustatic sea level rise result in a rapid progradation of the coastline into shallow coastal waters creating new unforested land (Noe-Nygaard *et al* 2005) so did likely the decreasing lake levels. This new unforested land provided areas ready for cattle grazing and cultivation which may have enhanced the potential for adopting the Neolithic culture. Drier climate conditions are clearly observed from 5700 cal BP and this seems to support the thesis of Bonsall *et al* (2002) that spreading of agriculture from Ireland to Sweden was caused or at

least partly caused by climatic changes towards a drier climate. However, a causal link between cultural changes and climatic events is hard to prove. That a climatic change enhanced the possibility of land cultivation and grass eating cattle does not imply that the Neolithic culture was actually adopted by human beings.



Appendix

---

**A**

**Age-to-depth model of Tissø Lake**

## The Site

The Tissø Lake (*see Figure 4-1*) is the second largest lake on Sjælland with an area of 12 km<sup>2</sup> and a hydrological catchments area of 418 km<sup>2</sup>. It has a total water volume of 100 km<sup>3</sup> (Høy and Dahl 1993). Tissø is an open lake basin with a main inlet in the north draining the Lille Åmose and Store Åmose areas. The main outlet of Tissø is placed to the south west the main outlet which transports water 5 km down to the sea shore in Jammerland Bugt. The lake water level is 1 metre above normal sea level and the lake depth reaches 13.5 metres (Høy and Dahl 1993). The Tissø Lake has very steep slopes and the water depths reach approximately 10 meters within the first 100 to 300 meters from the shoreline (Høy and Dahl 1993). Three cores B3, B5 and B6 have been drilled from the Tissø Lake and data from these cores has previously been presented by Hansen (2003) and Noe-Nygaard *et al* (2003). The core B3 is the most extensively studied and therefore this core is chosen for a comparison with the Bliden Lake record. The lithological log of core B3 is presented in Figure 9-4.

## Age-depth-model

The radiocarbon content of 4 terrestrial samples from the Tissø Lake core B3 and B5 have been measured (*see Table A.1*) and used to construct an age to depth model of the Tissø Lake core B3. The depth-to-age relation for the Tissø Lake is obtained by employing the Bpeat program (*see chapter 8, Blaauw and Christen 2005*) and applying the IntCal04 calibration curve (Reimer *et al* 2004b) and resulted in a fit with 1 section and a fit adequacy probability of 94.8% (*see Table A.1*). The resulting depth-to-age relation is shown in Figure A-1 together with the calibrated age distribution of each sample.

**Table A.1: Tissø Lake radiocarbon samples**

AAR	Core	Depth interval cm	material	$\delta^{13}\text{C}$ ‰ VPDB	<sup>14</sup> C Age	Fit I Outlier prob.
10052	B3K3	1417	Plant	@-27	2800 ± 70	5.0%
10053	B3K3	1426	Plant	@-27	2655 ± 50	14.0%
10055	B3K5	1555 - 1660	Plant	-28.91	3621 ± 45	0.8%
10056	B3K5	1611 - 1616	Plant	-27.79	3980 ± 50	1.1%

@: estimated  $\delta^{13}\text{C}$  by dating laboratory

## Discussion

The depth-to-age relationship presented here deviates significantly from depth-to-age models previously published (Hansen 2003; Noe-Nygaard *et al* 2003). For example, the presented age model yields an age of 2600 cal BP at 1400 cm in contrast to 4000 cal BP (Noe-Nygaard *et al* 2003) and 4300 cal BP at 1600 cm in contrast to 6000 cal BP (Noe-Nygaard *et al* 2003). The presented age model uses 4 new samples collected by Anthony Ruter from the Tissø Lake core B3, in contrast the previously studies which relied on correlated samples from the Tissø Lake core B5 and B6. The geochemistry of core B6 has not yet been analysed and the correlation between core B3 and B6 is performed solely on the basis of lithological similarities and by applying SUS values, and may thus be dubious (Hansen 2003). The elm decline has been identified in core B6 and associated with a radiocarbon dated sample found at a similar depth interval to 5070 ± 65 <sup>14</sup>C years (*approximately 3840 cal BC*). Hansen (2003) claims on the basis pollen counts that the elm decline to occur in core B3 at 1602 cm (Løvbjerg report 1995, pers. com. Nanna Noe-

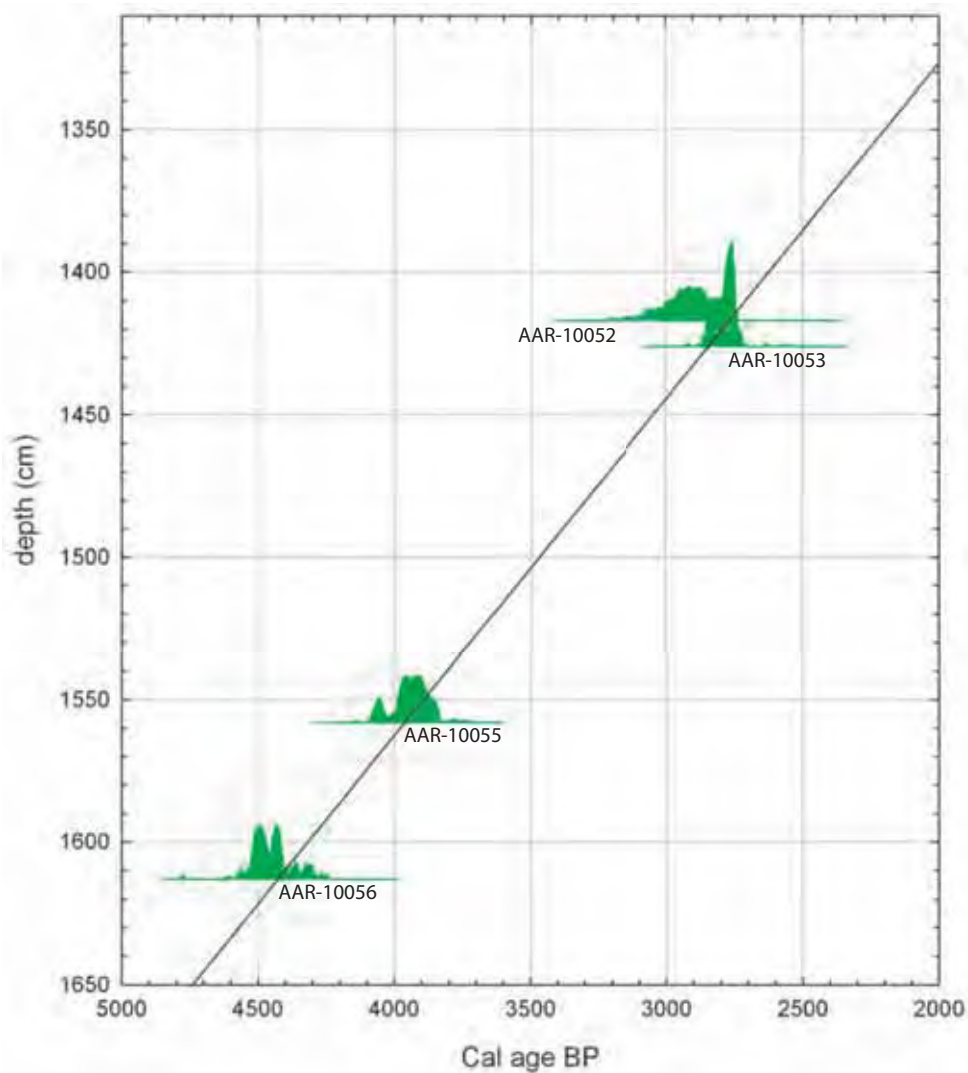


**Figure A-1.** Depth-to-age model of Tissø Lake constructed by employing the Bpeat program (Blaauw and Christen 2005). The illustrated sample age distributions are calculated by using OxCal 3.10 (Ramsey 2001, 1995). All presented samples were collected by Anthony Ruter, Geological Institute, University of Copenhagen.

Nygaard), and therefore substitutes the  $^{14}\text{C}$  age of  $5070 \pm 65$   $^{14}\text{C}$  years to this depth. However, the pollen diagram by Anthony Ruter (*work in progress*) does not reveal the elm decline at 1602 cm in the Tissø Lake core B3 (pers. com. Anthony Ruter) and hence the date of  $5070 \pm 65$   $^{14}\text{C}$  years associated with the depth 1602 cm in the Tissø Lake core B3 may also be cast into doubt. The cores B3 and B5 are closely connected and their geochemical parameters nicely correlate (Hansen 2003). One  $^{14}\text{C}$  sample has been obtained from core B5 and is dated to  $3440 \pm 40$   $^{14}\text{C}$  years. It is associated with the depth 1369 cm in the Tissø Lake core B3. This date disagrees with the newly dates obtained from the Tissø Lake core B3 which may then suggest a poor correlation at this depth interval between core B5 and B3. Hence in order to make an as solid founded age-to-depth model as possible and to avoid the complications of dubious correlations the presented depth-to-age model is based solely on material from the Tissø Lake core B3 which resulted in a single straight line fit to the four  $^{14}\text{C}$  samples originating from this core. However, even though this age-to-depth model produced a good fit adequacy more dates are highly needed to provide an adequate and well founded age-to-depth model of the Tissø Lake core B3.

## References

- Abrahamsen, S. E. (1994). *Biologiske ferskvandsundersøgelser*. Viby, Teknisk Forlag.
- Aerts-Bijma, A. T., J. van der Plicht and H. A. J. Meijer (2001). "Automatic AMS sample combustion and CO<sub>2</sub> collection." *Radiocarbon* **43**: 293-298.
- Alley, R. B., J. Marotzke, W. D. Nordhaus, J. T. Overpeck, D. M. Peteet, R. A. Pielke, R. T. Pierrehumbert, P. B. Rhines, T. F. Stocker, L. D. Talley and J. M. Wallace (2003). "Abrupt Climate Change." *Science* **299**: 2005-2010.
- Allison, C. E., R. J. Francey and H. A. J. Meijer (1993). Recommendations for the Reporting of Stable Isotope Measurements of Carbon and Oxygen in CO<sub>2</sub> Gas. *Reference and Intercomparison Materials for Stable Isotopes of Light Elements*. Vienna, IAEA-TECDOC-825: 155-162.
- Ambrose, S. H. and J. Krigbaum (2003). "Bone chemistry and bioarchaeology." *Journal of Anthropological Archaeology* **22**: 193-199.
- Ambrose, S. H. and L. Norr (1993). Experimental Evidence for the relationship of the Carbon Isotope Ratios of Whole Diet and Dietary Protein to Those of Bone Collagen and Carbonates. *Prehistoric Human Bone. Archaeology at the Molecular Level*. J. B. Lambert and G. Grupe. Berlin, Springer-Verlag: 1-37.
- Andersen, E. S., P. Jespergaard and O. G. Østergaard (1995). *Databog Fysik/Kemi*, F & K Forlaget.
- Anderson, L., M. B. Abbott and B. P. Finney (2001). "Holocene Climate Inferred from Oxygen Isotopes Ratios in Lake Sediments, Central Brooks Range, Alaska." *Quaternary Research* **55**: 313-321.
- Andresen, C. S., S. Björck, O. Bennike and G. Bond (2004). "Holocene climate changes in southern Greenland: evidence from lake sediments." *Journal of Quaternary Science* **19**: 783-795.
- Arneborg, J., J. Heinemeier, N. Lynnerup, H. L. Nielsen, R. N. and A. E. Sveinbjörndóttir (2002). "C-14 dating and the disappearance of Norsemen from Greenland." *Europhysics News* **May/June**.
- Assonov, S. S. and C. A. M. Brenninkmeijer (2003). "On the <sup>17</sup>O correction for CO<sub>2</sub> mass spectrometric isotopic analysis." *Rapid Communications in Mass Spectrometry* **17**: 1007-1016.
- Barber, K. E., F. M. Chambers and D. Maddy (2004). "Late Holocene climatic history of northern Germany and Denmark: peat macrofossil investigations at Dosenmoor, Schleswig-Holstein, and Svanemose, Jutland." *Boreas* **33**(2): 132-144.
- Bard, E., B. Hamelin, M. Arnold, L. Montaggioni, G. Cabioch, G. Faure and Rougerie (1996). "Deglacial sea-level record from Tahiti corals and the timing of global meltwater discharge." *Nature* **382**: 241-244.
- Bard, E., G. Raisback, F. Yiou and J. Jouzel (2000). "Solar irradiance during the last 1200 years based on cosmogenic nuclides." *Tellus B* **52**(3): 985-992.
- Bard, E., G. M. Raisbeck, F. Yiou and J. Jouzel (1997). "Solar modulation of cosmogenic nuclide production over the last millennium: comparison between <sup>14</sup>C and <sup>10</sup>Be records." *Earth and Planetary Science Letters* **150**(3-4): 453-462.
- Bartlein, P. J., M. E. Edwards, S. L. Shafer and J. Barker, Edward D. (1995). "Calibration of Radiocarbon Ages and the Interpretation of Paleoenvironmental Records." *Quaternary Research* **44**(3): 417-424.
- Baublys, K. A., S. D. Golding, E. Young and B. S. Kamber (2004). "Simultaneous determination of δ<sup>33</sup>S (V-CDT) and δ<sup>34</sup>S (V-CDT) using masses 48, 49 and 50 on a continuous flow isotope ratio mass spectrometer." *Rapid Communications in Mass Spectrometry* **18**(22): 2765-2769.
- Berg, K. (1950). *De ferske vande. Vort lands dyreliv*. F. W. Brædstrup, G. Thorson and E. Wesenberg-Lund. København, Nordisk Forlag. **III**.
- Berger, A. and M. F. Loutre (1991). "Insolation Values for the Climate of the Last 1000000 Years." *Quaternary Science Reviews* **10**(4): 297-317.
- Berger, A. and C. P. Sonett (1990). "The Spectrum of Radiocarbon: Discussion." *Philosophical Transactions of the Royal Society of London. Series A, Mathematical and Physical Sciences* **330**: 425-426.
- Berner, R. A. (1984). "Sedimentary pyrite formation: An update." *Geochimica et Cosmochimica Acta* **48**(4): 605-615.
- Berner, R. A. and R. Raiswell (1984). "C/S method for distinguishing freshwater from marine sedimentary rocks." *Geology* **12**: 365-368.
- Björck, S. (1995a). Late Weichselian to early Holocene development of the Baltic Sea - with implications for coastal settlements in the southern Baltic region. *Man and sea*. A. Fischer. Oxford, Oxbow Books.
- Björck, S. (1995b). "A Review of the history of the Baltic Sea, 13.0-8.0 ka BP." *Quaternary International* **27**: 19-40.
- Björck, S., R. Muscheler, B. Kromer, C. S. Andresen, J. Heinemeier, S. Johnsen, D. Conley, N. Koc, M. Spurk and S. Veski (2001). "High-resolution analysis of an early Holocene climate event may imply decreased solar forcing as an important climate trigger." *Geology* **29**: 1107-1110.
- Blockley, S. P. E., J. J. Lowe, M. J. C. Walker, A. Asioli, F. Trincardi, G. R. Coope and R. E. Donahue (2004). "Bayesian analysis of radiocarbon chronologies: examples from the European Late-glacial." *Journal of Quaternary Science* **19**: 159-175.
- Bluemle, J. P., J. M. Sabel and K. Wibjörn (2001). Rate and Magnitude of Past Global Climate Changes. *Geological Perspectives of Global Climate*. L. C. Gerhard, W. E. Harrison and B. M. Hanson. Tulsa, The American Association of Petroleum Geologists. **47**: 193-211.
- Blaauw, M. and J. A. Christen (2005). "Radiocarbon peat chronologies and environmental change." *Applied Statistics* **54**(4): 805-816.
- Blaauw, M., v. B. Geel and H. van der Plicht (2004a). "Carbon-14 wiggle-match dating of peat deposits: advantages and limitations." *Journal of Quaternary Science* **19**: 177-181.
- Blaauw, M., B. van Geel and H. van der Plicht (2004b). "Solar forcing of the climatic change during the mid-Holocene: indications from raised bog in The Netherlands." *Holocene* **14**: 35.
- Bocherens, H. and D. Drucker (2003). "Trophic Level Isotopic Enrichment of Carbon and Nitrogen in Bone

- Collagen: Case Studies from Recent and Ancient Terrestrial Ecosystems." *International Journal of Osteoarchaeology* **13**: 46-53.
- Bond, G., B. Kromer, J. Beer, R. Muscheler, H. Evans, W. Showers, S. Hoffmann, R. Lotti-Bond, I. Hajdas and G. Bonani (2001). "Persistent Solar Influence on North Atlantic Climate During the Holocene." *Science* **294**: 2130-2136.
- Bond, G., W. Showers, M. Cheseby, R. Lotti, P. Almasi, P. deMenocal, P. Priore, H. Cullen, I. Hajdas and G. Bonani (1997). "A Pervasive Millennial-Scale Cycle in North Atlantic Holocene and Glacial Climates." *Science* **278**: 1257-1266.
- Bonsall, C., M. Macklin, D. E. Anderson and R. W. Payton (2002). "Climate change and the adoption of agriculture in north-west Europe." *European Journal of Archaeology* **5**(1): 9-23.
- Bottrell, S. H. and R. J. Newton (2006). "Reconstruction of changes in global sulfur cycling from marine sulfate isotopes." *Earth-Science Reviews* **75**(1-4): 59-83.
- Bowmann, S. (1990). *Radiocarbon Dating*. Berkeley and Los Angeles, The Trustees of the British Museum.
- Bradshaw, E. G., P. Rasmussen, H. Nielsen and N. John Anderson (2005a). "Mid- to late-Holocene land-use change and lake development at Dallund Sø, Denmark: trends in lake primary production as reflected by algal and macrophyte remains." *The Holocene* **15**(8): 1130-1142.
- Bradshaw, E. G., P. Rasmussen and B. V. Odgaard (2005b). "Mid- to late-Holocene land-use change and lake development at Dallund Sø, Denmark: synthesis of multiproxy data, linking land and lake." *Holocene* **15**(8): 1152-1162.
- Brandt, S. (1999). *Data Analysis*. New York, Springer-Verlag New York Inc.
- Bransden, J. (1996). *Physics Of Atoms And Molecules*. Harlow, Longman.
- Brauer, A., T. Litt, J. F. W. Negendank and B. Zolitschka (2001). "Lateglacial varve chronology and biostratigraphy of lakes Holzmaar and Meerfelder Maar, Germany." *Boreas* **30**(83-88).
- Braun, H., M. Christi, S. Rahmstorf, A. Ganopolski, A. Mangini, C. Kubatzki, K. Roth and B. Kromer (2005). "Possible solar origin of the 1,470-year glacial climate cycle demonstrated in a coupled model." *Nature* **436**: 208-211.
- Brazdil, R., C. Pfister, H. Wanner, H. Von Storch and J. Luterbacher (2005). "Historical climatology in Europe - The state of the art." *Climatic Change* **70**(3): 363-430.
- Bright, J., D. S. Kaufman, R. M. Forester and W. E. Dean (In Press, Corrected Proof). "A continuous 250,000 yr record of oxygen and carbon isotopes in ostracode and bulk-sediment carbonate from Bear Lake, Utah-Idaho." *Quaternary Science Reviews*.
- Broecker, W. S. (2006). "The Holocene CO<sub>2</sub> rise: Anthropogenic or Natural?" *Eos* **87**(3): 27-29.
- Bronk Ramsey, C. and M. J. Humm (2000). "On-line combustion of samples for AMS and ion source developments at ORAU." *Nuclear Instruments and Methods in Physics Research B* **172**: 242-246.
- Brown, S. B., P., A. Lini, P. Thompson Davis and S. J. (2002). "Reconstructing Lake and drainage basin history using terrestrial sediment layers: analysis of cores from a post-glacial lake in New England, USA." *Journal of Paleolimnology* **28**: 219-236.
- Brown, T. A., D. E. Nelson, J. S. Vogel and J. R. Southon (1988). "Improved Collagen Extraction by Modified Longin Method." *Radiocarbon* **30**(2): 171-177.
- Brunner, B. and S. M. Bernasconi (2005). "A revised isotope fractionation model for dissimilatory sulfate reduction in sulfate reducing bacteria." *Geochimica et Cosmochimica Acta* **69**(20): 4759-4771.
- Buck, C. E., W. G. Cavanagh and C. D. Litton (1996). *Bayesian Approach to Interpreting Archaeological Data*. Eastbourne, John Wiley & Sons.
- Buck, C. E., T. F. G. Higman and D. J. Lowe (2003). "Bayesian tools for tephrochronology." *Holocene* **13**(5): 639-647.
- Butler, I. B., M. E. Böttcher, D. Rickard and A. Oldroyd (2004). "Sulfur isotope partitioning during experimental formation of pyrite via the polysulfide and hydrogen sulfide pathways: Implications for the interpretation of sedimentary and hydrothermal pyrite isotope records." *Earth and Planetary Science Letters* **228**(3-4): 495-509.
- Canfield, D. E. (2000). "The Archean Sulfur Cycle and the Early History of Atmospheric Oxygen." *Science* **288**: 658-661.
- Canfield, D. E. (2001). *Biochemistry of Sulfur Isotopes. Stable Isotope Geochemistry*. J. W. Walley and D. R. Cole. Washington, Mineralogical Society of America. **43**.
- Caseldine, C., G. Thompson, C. Langdon and D. Hendon (2005). "Evidence for an extreme climatic event on Achill Island, Co. Mayo, Ireland around 5200-5100 cal. yr BP." *Journal of Quaternary Science* **20**(2): 169-178.
- Chambers, L. A. and P. A. Trudinger (1978). "Microbiological Fractionation of Stable Sulfur Isotopes: A Review and Critique." *Geomicrobiology Journal* **1**(3): 249-293.
- Chappell, J. and H. Polach (1991). "Post-glacial sea-level rise from a coral record at Huon Peninsula, Papua New Guinea." *Nature* **349**: 147-149.
- Chiu, T.-c., R. G. Fairbanks, R. A. Mortlock and A. L. Bloom (2005). "Extending the radiocarbon calibration beyond 26,000 years before present using fossil corals." *Quaternary Science Reviews* **24**(16-17): 1797-1808.
- Christen, J. A. (1994). "Summarizing a Set of Radiocarbon Determinations: A Robust Approach." *Applied Statistics* **43**(3): 489-503.
- Christensen, C. (1981). "Havniveauændringer 5500-250 f.Kr. i Vedbækområdet, NØ-Sjælland." *Dansk Geologisk Forening Årskrift for 1981*: 91-107.
- Christensen, C. (1995). *The littorina transgressions in Denmark. Man and sea*. A. Fischer. Oxford, Oxbow Books.
- Christensen, C. (2001). *Kystbosættelse og havniveauændringer i stenalderen. Danmarks jægerstenalder - status og perspektiver*. O. L. Jensen, S. A. Sørensen and K. M. Hansen, Hørsholm Egns Museum.
- Christensen, C. and E. R. Andreasen (1999). "Strandforskydning i Nordvestsjælland i atlantisk og subborial tid." *Nationalmuseets Naturvidenskabelige Undersøgelser* **2**: 2-19.
- Clark, I. D. and P. Fritz (1997). *Environmental Isotopes in Hydrogeology*. New York, Lewis Publishers.
- Clemmensen, L. B., K. Pye, A. Murray and J. Heinemeier (2001). "Sedimentology, stratigraphy and landscape

- evolution of a Holocene coastal dune system, Lodbjerg, NW Jutland, Denmark." *Sedimentology* **48**: 3-27.
- Coddéris, Y. (2001). "The Early Paleozoic carbon cycle." *Earth and Planetary Letters* **190**: 181-196.
- Coe, A. L., Ed. (2003). *The Sedimentary Record of Sea-Level Change*. Glasgow, Cambridge University Press.
- Cohen, A. S. (2003). *Paleolimnology*. New York, Oxford University Press.
- Coleman, M. (2004). Data Corrections for Mass Spectrometer Analysis of SO<sub>2</sub>. *Handbook of Stable Isotope Analytical Techniques*. P. A. de Groot. Amsterdam, Elsevier: 957-970.
- Confiantini, R., W. Stichler and R. Rozanski (1993). Standards and Intercomparison Materials Distributed by the International Atomic Energy Agency for Stable Isotope Measurements. *Reference and Intercomparison Materials for Stable Isotopes of Light Elements*. Vienna, IAEA-TECDOC-825: 13-31.
- Cook, G. T., C. Bonsall, R. E. M. Hedges, K. McSweeney, V. Boronean and P. B. Pettitt (2001). "A freshwater diet-derived <sup>14</sup>C Reservoir effect at the stone age sites in the Iron Gates Gorge." *Radiocarbon* **43**: 453-460.
- Coombes, P. and K. Barber (2005). "Environmental determinism in Holocene research: causality or coincidence?" *Area* **37**(3): 303-311.
- Coplen, T. B. (1996). "New Guidelines for Reporting Stable Hydrogen, Carbon and Oxygen Isotope-Ratio Data." *Geochimica et Cosmochimica Acta* **60**: 3359-4460.
- Coplen, T. B., J. A. Hopple, J. K. Böhlke, H. S. Peiser, S. E. Rieder, H. R. Krouse, K. J. R. Rasman, T. Ding, R. D. Vocke, K. M. Révész, A. Lamberty, P. Taylor and P. De Bièvre (2002). *Compilation of Minimum and Maximum Isotope Ratios of Selected Elements in Naturally Occurring Terrestrial Materials and Reagents*. Reston, Virginia, USGS.
- Coplen, T. B. and H. R. Krouse (1998). "Sulphur isotope data consistency improved." *Nature* **392**(6671): 32-32.
- Craig, H. (1954). "Carbon 13 in Plants and the Relationship between Carbon 13 and Carbon 14 Variations in Nature." *The Journal of Geology* **62**(2): 115.
- Craig, H. (1957). "Isotopic standards for carbon and oxygen and correction factors for mass spectrometry analysis of carbon dioxide." *Geochimica et Cosmochimica Acta* **12**: 133-149.
- Craig, H. (1965). The measurement of oxygen isotope palaeotemperatures. *Stable isotopes in oceanographic studies and palaeotemperatures*. E. Tongiorgi. Pisa, Consiglio Nazionale delle Ricerche: 161-182.
- Criss, R. E. (1999). *Principles of Stable Isotope Distribution*, Oxford University Press.
- Crowley, T. J. and T. S. Lowery (2000). "How Warm Was the Medieval Warm Period?" *Ambio* **29**: 51-55.
- Dahl-Jensen, D. (1998). "Past Temperatures Directly from the Greenland Ice Sheet." *Science* **282**: 268-271.
- Danny Harvey, L. D. (2000). *Climate and Global Environmental Change*. Singapore, Pearson Education Limited.
- Dansgaard, W. (1961). "The isotopic Composition of Natural Waters." *Meddelelser om Grønland* **165**(2).
- Dansgaard, W. (1964). "Stable isotopes in precipitation." *Tellus* **16**/4: 436-468.
- Davidson, G. R., M. Carnley, T. Lange, S. J. Galicki and A. Douglas (2004). "Changes in sediment accumulation rate in an oxbow lake following late 19th century clearing of land for agricultural use: A <sup>210</sup>Pb, <sup>137</sup>Cs and <sup>14</sup>C study in Mississippi, USA." *Radiocarbon* **46**: 755-764.
- Davis, B. A. S., S. Brewer, A. C. Stevenson and J. Guiot (2003). "The temperature of Europe during the Holocene reconstructed from pollen data." *Quaternary Science Reviews* **22**(15-17): 1701-1716.
- Dean, W. E. (1981). "Carbonate Minerals and organic matter in sediments of modern north temperate hard-water lakes." *The Society of Economic Palaeontologists and Mineralogists* **31**: 213-231.
- Dean, W. E. (1999). "The carbon cycle and biogeochemical dynamics in lake sediments." *Journal of Paleolimnology* **21**: 375-393.
- Dean, W. E. (2002). "A 1500-year record of climatic and environmental changes in Elk Lake, Clearwater County, Minnesota II: geochemistry, mineralogy, and stable isotopes." *Journal of Paleolimnology* **27**: 301-319.
- Dean, W. E. and A. Schwab (2000). "Holocene environmental and climatic changes in the Northern Great Plains as recorded in the geochemistry of sediments in the Pickrel Lake, South Dakota." *Quaternary International* **67**: 5-20.
- DeNiro, M. J. (1985). "Postmortem preservation and alteration of *in vivo* bone collagen isotope ratios in relation to paleodietary reconstruction." *Nature* **317**: 806-809.
- DeNiro, M. J. (1987). "Stable Isotope Archaeology." *American Scientist* **75**: 182-191.
- DeNiro, M. J. and S. Epstein (1978). "Influence of diet on the distribution of carbon isotopes in animal diet." *Geochimica et Cosmochimica Acta* **42**: 495-506.
- DeNiro, M. J. and S. Epstein (1981). "Influence of diet on the distribution of nitrogen isotopes in animals." *Geochimica et Cosmochimica Acta* **45**: 341-351.
- Dergachev, V. A. (2004). "Manifestation of the long-term solar cyclicity in climate archives over 10 millennia." *Multi-Wavelength Investigations of Solar Activity* **223**: 699-704.
- Dergachev, V. A., O. M. Raspopov, B. van Geel and G. I. Zaitseva (2004). "The 'Sterno-Etrussia' geomagnetic excursion around 2700 BP and changes of solar activity, cosmic ray intensity, and climate." *Radiocarbon* **46**: 661-681.
- Digerfeldt, G. (1988). "Reconstruction and Regional Correlation of Holocene Lake-Level Fluctuations in Lake Bysjön, South Sweden." *Boreas* **17**(2): 165-182.
- Ding, T., R. Bai, Y. Li, D. Wan, X. Zou and Q. Zhang (1999). "Determination of the Absolute <sup>32</sup>S/<sup>34</sup>S ratio of IAEA-S-1 Reference Material and V-CDT Sulfur Standard." *Science in China Series D* **42**: 45-51.
- Ding, T., H. C. Li, G. Zhang, Y. Li and J. Li (1989). *A Study on determining <sup>33</sup>S/<sup>32</sup>S, <sup>34</sup>S/<sup>32</sup>S and <sup>36</sup>S/<sup>32</sup>S ratios by using the SF<sub>6</sub> method*. ISCRM '89, Beijing, International Academic Publishers.
- Ding, T., S. Valkiers, H. Kipphardt, P. De Bievre, P. D. P. Taylor, R. Gonfiantini and R. Krouse (2001). "Calibrated sulfur isotope abundance ratios of three IAEA sulfur isotope reference materials and V-CDT with a reassessment of the atomic weight of sulfur." *Geochimica et Cosmochimica Acta* **65**(15): 2433-2437.
- Eddy, J. A. (1976). "The Maunder Minimum." *Science* **192**(4245): 1189-1202.

- Eddy, J. A., T. M. L. Wigley, A. Berger and A. C. Renfrew (1990). "Holocene Climate Change,  $^{14}\text{C}$  Wiggles and Variations in Solar Irradiance: Discussion." Philosophical Transactions of the Royal Society of London. Series A, Mathematical and Physical Sciences **330**: 559-560.
- Eicher, U. and U. Siegenthaler (1976). "Palynological and oxygen isotope investigations on Late-Glacial sediment cores from Swiss lakes." Boreas **5**: 109-117.
- Eimers, M. C., A. M. Paterson, P. J. Dillon, S. L. Schiff, B. F. Cumming and R. I. Hall (2006). "Lake sediment core records of sulphur accumulation and sulphur isotopic composition in central Ontario, Canada lakes." Journal of Paleolimnology **35**: 99-109.
- Einsle, G. (2000). Sedimentary Basins: evolution, facies, and sediment budget. Berlin, Springer-Verlag.
- Erikson, G. (2003). Norm and difference. Stone Age dietary practice in the Baltic region. Archaeological Research Laboratory. Stockholm, Stockholm University.
- Fairbanks, R. G. (1989). "A 17,000-year glacio-eustatic sea level record: influence of glacial melting rates on the Younger Dryas event and deep-ocean circulation." Nature **342**: 637-642.
- Fairbanks, R. G., R. A. Mortlock, T.-C. Chiu, L. Cao, A. Kaplan, T. P. Guilderson, T. W. Fairbanks, A. L. Bloom, P. M. Grootes and M.-J. Nadeau (2005). "Radiocarbon calibration curve spanning 0 to 50,000 years BP based on paired  $^{230}\text{Th}/^{234}\text{U}/^{238}\text{U}$  and  $^{14}\text{C}$  dates on pristine corals." Quaternary Science Reviews **24**(16-17): 1781-1796.
- Filippi, M. L. and M. R. Talbot (2005). "The palaeolimnology of northern Lake Malawi over the last 25 ka based upon the elemental and stable isotopic composition of sedimentary organic matter." Quaternary Science Reviews **24**(10-11): 1303-1328.
- Fischer, A. (2002). Food for Feasting? The Neolithisation of Denmark - 150 Years of Debate. A. Fischer and K. Kristiansen, Sheffield Archaeological Monographs.
- Fischer, A., J. Olsen, M. Richards, J. Heinemeier, Á. E. Sveinbjörnsdóttir and P. Bennike (submitted for publication-a). "Coast-inland mobility and food composition in the Danish Mesolithic and Early Neolithic - evidence from stable isotope values of humans and dogs." Journal of Archaeological Science.
- Fischer, A., M. Richards, J. Olsen, D. Robinson, P. Bennike, L. Kubiak-Martens and J. Heinemeier (submitted for publication-b). "Reconstructing the Mesolithic Menu - food remains versus stable isotopes in bones. A case study from the submerged settlement on the Argus Bank, Denmark." European Journal of Archaeology.
- Fischer, H. and B. Mieding (2005). "A 1,000-year ice core record of interannual to multidecadal variations in atmospheric circulation over the North Atlantic." Climate Dynamics **25**: 65-74.
- Frich, P., S. Rosenørn, H. Madsen and J. J. Jensen (1997). Observed Precipitation in Denmark, 1961-90. Copenhagen, Danish Meteorological Institute.
- Friedman, I. and J. R. O'Neil (1977). Compilation of stable isotope fractionation factors of geochemical interest. Data of geochemistry. K. K. Chapter. Washington DC, USGS.
- Friis-Christensen, E. and K. Lassen (1991). "Length of the Solar-Cycle - an Indicator of Solar-Activity Closely Associated with Climate." Science **254**(5032): 698-700.
- Fry, B., W. Brand, F. J. Mersch, K. Tholke and R. H. Garritt (1992). "Automated Analysis System for Coupled  $\delta^{13}\text{C}$  and  $\delta^{15}\text{N}$ ." Analytical Chemistry **64**: 288-291.
- Fry, B., S. R. Silva, C. Kendall and R. Anderson (2002). "Oxygen isotope corrections for online  $\delta^{34}\text{S}$  analysis." Rapid Communications in Mass Spectrometry **16**: 854-858.
- Geel, v. B., J. Buurman and H. T. Waterbolk (1996). "Archaeological and palaeoecological indications of an abrupt climate change in The Netherlands, and evidence for climatological teleconnections around 2650 BP." Journal of Quaternary Science **11**: 451-460.
- Geel, v. B., B. V. Odgaard and M. Ralska-Jasiewiczowa "Cyanobacteria as indicators of phosphate-eutrophication of lakes and pools in the past." Pact **50**: 399-415.
- Gehrels, R. W., J. R. Kirby, A. Prokoph, R. M. Newnham, E. P. Achterberg, H. Evans, S. Black and D. B. Scott (2005). "Onset of recent rapid sea-level rise in the western Atlantic Ocean." Quaternary Science Reviews **24**: 2083-2100.
- Gerhard, L. C., W. E. Harrison and B. M. Hanson, Eds. (2001). Geological Perspectives of Global Climate. AAPG Studies in Geology. Tulsa, The American Association of Petroleum Geologists.
- Geyh, M. A. and H. Schleicher (1990). Absolute Age Determination. Heidelberg, Springer Verlag.
- Geyh, M. A., U. Schotterer and M. Grosjean (1998). "Temporal changes of the  $^{14}\text{C}$  reservoir effect in lakes." Radiocarbon **40**(2): 921-931.
- Ghosh, P. and W. A. Brand (2003). "Stable isotope ratio mass spectrometry in global climate change research." International Journal of Mass Spectrometry **228**: 1-33.
- Gil, I. M., F. Abrantes and D. Hebbeln (2006). "The North Atlantic Oscillation forcing through the last 2000 years: Spatial variability as revealed by high-resolution marine diatom records from N and SW Europe." Marine Micropaleontology **60**(2): 113-129.
- Glesemann, A., H. J. Jäger, A. L. Norman, H. R. Krouse and W. Brand (1994). "On-Line Sulfur-Isotope Determination Using an Elemental Analyzer Coupled to a Mass Spectrometer." Analytical Chemistry **66**: 2816-2819.
- Goslar, T. and W. Madry (1998). "Using the Bayesian method to study the precision of dating by wiggle-matching." Radiocarbon **40**(1): 551-560.
- Grassineau, N. V., D. P. Matthey and D. Lowry (2001). "Sulfur Isotope Analysis of Sulfide and Sulfate minerals by Continuous Flow-Isotope Ratio Mass Spectrometry." Analytical Chemistry **73**: 220-225.
- Griffiths, D. J. (1989). Introduction to Electrodynamics. Upper Saddle River, Prentice Hall.
- Habicht, K. S. and D. E. Canfield (1997). "Sulfur isotope fractionation during bacterial sulfate reduction in organic-rich sediments." Geochimica et Cosmochimica Acta **61**(24): 5351-5361.
- Hall, R. I., G. G. Bianchi and J. R. Evans (2004). "Centennial to millennial scale Holocene climate-deep water linkage in the North Atlantic." Quaternary Science Reviews **23**: 1529-1536.
- Hammarlund, D. (1993). "A distinct  $\delta^{13}\text{C}$  decline in organic lake sediments at the Pleistocene - Holocene transition in southern Sweden." Boreas **22**: 236-243.
- Hammarlund, D., S. Björck, B. Buchardt, C. Israelson and

- C. T. Thomsen (2003). "Rapid hydrological changes during the Holocene revealed by stable isotope records of lacustrine carbonates from Lake Igelsjön, southern Sweden." *Quaternary Science Reviews* **22**(2-4): 353-370.
- Hammarlund, D., S. Björck, B. Buchardt and C. T. Thomsen (2005). "Limnic responses to increased effective humidity during 8200 cal. yr BP cooling event in southern Sweden." *Journal of Paleolimnology* **34**: 471-480.
- Hammarlund, D. and B. Buchardt (1996). "Composite stable isotope records from a Late Weichselian lacustrine sequence at Grønge, Lolland, Denmark: evidence of Allerød and Younger Dryas environments." *Boreas* **25**: 8-22.
- Hammarlund, D. and D. H. Keen (1994). "A Late Weichselian stable isotope and molluscan stratigraphy from southern Sweden." *GFF* **116**: 235-248.
- Hansen, A. K. (2003). En palæoökologisk undersøgelse af Senaltlantikum og Subborial i Tissø. *Department of Geology*. Unpublished master thesis, Copenhagen, University of Copenhagen.
- Harrison, R. G. and M. A. Katzenberg (2003). "Paleodiet studies using carbon isotopes from bone apatite and collagen: examples from southern Ontario and San Nicolas Island, California." *Journal of Anthropological Archaeology* **22**: 227-244.
- Hatte, C., J. J. Poupeau, J. F. Tatman and M. Paterne (2003). "Development of an automated system for preparation of organic samples." *Radiocarbon* **45**(3): 421-430.
- Hede, S. U. (2003). "Prehistoric settlements and Holocene relative sea-level changes in north-west Sjælland, Denmark." *Bulletin of the Geological Society of Denmark* **50**: 141-149.
- Hedges, R. E. M. (2003). "On bone collagen - Apatite-carbonate isotopic relationships." *International Journal of Osteoarchaeology* **13**(1-2): 66-79.
- Heegaard, E., H. J. B. Birks and R. J. Telford (2005). "Relationships between calibrated ages and depth in stratigraphical sequences: an estimation procedure by mixed-effect regression." *Holocene* **15**(4): 612-618.
- Heier-Nielsen, S., J. Heinemeier, H. L. Nielsen and R. N. (1995). "Recent Reservoir for Danish Fjords and Marine Waters." *Radiocarbon* **37**: 875-882.
- Hodgson, P. E., E. Gadioli and E. Gadioli Erba (1997). *Introductory Nuclear Physics*. Oxford, Clarendon Press.
- Houmark-Nielsen, M. and K. H. Kjær (2003). "South-west Scandinavia, 40-15kyr BP: palaeogeography and environmental change." *Journal of Quaternary Science* **18**: 769-786.
- Howarth, R. W., J. W. B. Steward and M. V. Ivanov (1992). *Sulphur Cycling on the Continents*. SCOPE. Chichester, Wiley. **48**.
- Hughen, K. A., M. G. L. Baillie, E. Bard, J. W. Beck, C. J. H. Bertrand, P. G. Blackwell, C. E. Buck, G. S. Burr, K. B. Cutler, P. E. Damon, R. L. Edwards, R. G. Fairbanks, M. Friedrich, T. P. Guilderson, B. Kromer, G. McCormac, S. Manning, C. B. Ramsey, P. J. Reimer, R. W. Reimer, S. Remmele, J. R. Southon, M. Stuiver, S. Talamo, F. W. Taylor, J. van der Plicht and C. E. Weyhenmeyer (2004). "Marine04 marine radiocarbon age calibration, 0-26 cal kyr BP." *Radiocarbon* **46**(3): 1059-1086.
- Høy, T. and J. Dahl (1993). *Danmarks Søer. Søerne i Vestsjællands Amt*. Strandberg Bogtryk/ Offset A/S.
- Håkansson, S. (1985). "A Review of various factors influencing the stable carbon isotope ratio of organic lake sediments by the change from glacial to post-glacial environmental conditions." *Quaternary Science Reviews* **4**: 135-146.
- Ito, E. (2001). Application of Stable Isotope Techniques to Inorganic and Biogenic Carbonates. *Tracking Environmental Change Using Lake Sediments*. W. M. Last and J. P. Smol. Dordrecht, Kluwer Academic Publishers. **2**.
- Iversen, J. (1937). "Undersøgelser over Littorina transgressioner i Danmark." *Meddelelser fra Dansk Geologisk Forening* **9**: 223-232.
- Iversen, J. (1967). Naturens udvikling siden sidste istid. *Danmarks Natur*. T. W. Böcher, A. Schou and H. Volssøe. København, Politikens Forlag. **1**.
- Jedrysek, M. and G. Skrzypek (2005). "Hydrogen, carbon and sulphur isotope ratios in peat: the role of diagenesis and water regimes in reconstruction of past climates." *Environmental chemical letters* **2Q**(179-183).
- Jensen, J. (2001). *Danmarks Oldtid - Stenalder 13.000 - 2.000 f.Kr.* København, Gyldendal.
- Jensen, M. L. and N. Nakai (1962). Sulfur Isotope Meteoritic Standards, results and recommendations. *Biochemistry of Sulfur Isotopes*, NFS Symposium: 30-35.
- Jessen, C. A., M. Rundgren, S. Björck and D. Hammarlund (2005). "Abrupt climatic changes and an unstable transition into a late Holocene Thermal Decline: a multiproxy lacustrine record from southern Sweden." *Journal of Quaternary Science* **20**(4): 349-362.
- Johnsen, S., H. B. Clausen, J. Jouzel, J. Schwander, A. E. Sveinbjörndóttir and J. White (1999). Stable Isotope Records from Greenland Deep Ice Cores: The Climate Signal and the Role of Diffusion. *Ice Physics and the Natural Environment*. J. S. Wettlaufer, J. G. Dash and N. Untersteiner. Berlin Heidelberg, Springer-Verlag. **I 56**.
- Johnsen, S. J., D. Dahl-Jensen, N. Gundestrup, J. P. Steffensen, H. B. Clausen, H. Miller, V. Masson-Delmotte, A. E. Sveinbjörnsdóttir and J. White (2001). "Oxygen isotope and palaeotemperature records from six Greenland ice-core stations: Camp Century, Dye-3, GRIP, GISP2, Renland and NorthGRIP." *Journal of Quaternary Science* **16**(4): 299-307.
- Jørgensen, B. B. (1977). "The Sulfur Cycle of a Coastal Marine Sediment (Limfjorden, Denmark)." *Limnology and Oceanography* **22**: 814-832.
- Jørgensen, B. B. (1983). *The Microbial Sulphur Cycle*. *Microbial Geochemistry*. W. E. Krumbein. Oxford, Blackwell Scientific Publications.
- Jørgensen, B. B. (1990). "A Thiosulfate Shunt in the Sulfur Cycle of Marine Sediments." *Science* **249**: 152-154.
- Jørgensen, L., J. F. Bican, L. G. Thomsen and X. P. Jensen (2003). *Stormænd, købmænd og håndværkere ved Tissø i det 6.-11 århundrede. Tissø og Åmoserne - kulturhistorie og natur*. L. Pedersen. Kalundborg, Holbæk Amt: 50-65.
- Kaufman, D. S., T. A. Ager, N. J. Anderson, P. M. Anderson, J. T. Andrews, P. J. Bartlein, L. B. Brubaker, L. L. Coats, L. C. Cwynar, M. L. Duvall, A. S. Dyke, M. E. Edwards, W. R. Eisner, K. Gajewski, A. Geirsdóttir, F. S. Hu, A. E. Jennings, M. R. Kaplan, M. N. Kerwin, A. V. Lozhkin, G. M. MacDonald, G. H. Miller, C. J. Mock, W. W. Oswald, B. L. Otto-Bliesner, D. F. Porin-

- chu, K. Ruhland, J. P. Smol, E. J. Steig and B. B. Wolfe (2004). "Holocene thermal maximum in the western Arctic (0-180 degrees W)." *Quaternary Science Reviews* **23**(5-6): 529-560.
- Keller, C. F. (2004). 1000 years of climate change. *Solar Variability and Climate Change*. **34**: 315-322.
- Kester, C. L., R. O. Rye, C. A. Johnson, C. Schwartz and C. Holmes (2001). "On-line Sulfur Isotope Analysis of Organic Material by direct Combustion: Preliminary Results and Potential Applications." *Isotopes Environmental and Health Studies* **37**: 53-65.
- Kilian, M. R., B. van Geel and J. van der Plicht (2000). "C-14 AMS wiggle matching of raised bog deposits and models of peat accumulation." *Quaternary Science Reviews* **19**(10): 1011-1033.
- Kirby, M. E., C. J. Poulsen, S. P. Lund, W. P. Patterson, L. Reidy and D. E. Hammond (2004). "Late Holocene lake level dynamics inferred from magnetic susceptibility and stable oxygen isotope data: Lake Elsinore, southern California (USA)." *Journal of Paleolimnology* **31**(3): 275-293.
- Kjær, K. H., M. Houmark-Nielsen and N. Richardts (2003). "Ice-flow patterns and dispersal of erratics at the southwestern margin of the last Scandinavian Ice Sheet: Signature of palaeo-ice streams." *Boreas* **32**: 130-148.
- Kohn, M. J. and J. M. Law (2006). "Stable isotope chemistry of fossil bone as a new paleoclimate indicator." *Geochimica Et Cosmochimica Acta* **70**(4): 931-946.
- Kolstrup, E. and B. Buchardt (1982). "A Pollen Analytical Investigation Supported by an <sup>18</sup>O-Record of a Late Glacial Lake Deposit at Graenge (Denmark)." *Review of Palaeobotany and Palynology* **36**(3-4): 205-230.
- Kristjansson, J. E., J. Kristiansen and E. Kaas (2004). "Solar activity, cosmic rays, clouds and climate - an update." *Advances in Space Research, Solar Variability and Climate Change* **34**(2): 407-415.
- Krouse, H. R. and T. B. Coplen (1997). "Reporting of Relative Sulfur Isotope-Ratio Data." *Pure & Applied Chemistry* **69**(2): 293-295.
- Krumbein, W. E. and P. K. Swart (1983). *The Microbial Carbon Cycle. Microbial geochemistry*. W. E. Krumbein. Oxford, Blackwell Scientific Publications: 5-62.
- Kuznetsova, T. V. and L. B. Tsirulnik (2004). "Climate oscillations and abrupt changes in C14 data." *Advances in Space Research, Solar Variability and Climate Change* **34**(2): 426-431.
- Lamb, A. L., M. J. Leng, M. U. Mohammed and H. F. Lamb (2004). "Holocene climate and vegetation change in the Main Ethiopian Rift Valley, inferred from the composition (C/N and  $\delta^{13}\text{C}$ ) of lacustrine organic matter." *Quaternary Science Reviews* **23**: 881-891.
- Lamb, A. L., G. P. Wilson and M. J. Leng (2006). "A review of coastal palaeoclimate and relative sea-level reconstruction using  $\delta^{13}\text{C}$  and C/N ratios in organic material." *Earth-Science Reviews* **75**: 29-57.
- Lambeck, K. (1999). "Shoreline displacements in southern-central Sweden and the evolution of the Baltic Sea since the last glaciation." *Journal of the Geological Society, London* **156**(3): 465-486.
- Lanting, J. N., A. Aerts-Bijma and H. van der Plicht (2001). "Dating of Cremated Bones." *Radiocarbon* **43**(2): 1.
- Lanting, J. N. P. J. v. d. (1998). "Reservoir Effects and Apparent C-14 -Ages." *The Journal of Irish Archaeology* **IX**: 151-164.
- Larsen, G., J. Eirikson, K. L. Knudsen and J. Heinemeier (2002). "Correlation of late Holocene terrestrial and marine tephre markers, north Iceland: implications for reservoir age changes." *Polar Research* **21**(2): 283-290.
- Lassen, K. and E. Friis-Christensen (1995). "Variability of the Solar-Cycle Length During the Past 5 Centuries and the Apparent Association with Terrestrial Climate." *Journal of Atmospheric and Terrestrial Physics* **57**(8): 835-845.
- Last, W. M. and J. P. Smol, Eds. (2001). *Tracking Environmental Change Using Lake Sediments*. Dordrecht, Kluwer Academic Publishers.
- Laursen, E. V., R. S. Thomsen and J. Cappelen (1999). *Observed Air Temperature, Humidity, Pressure, Cloud Cover and Weather in Denmark - with Climatological Standard Normals, 1961-90*. Copenhagen, Danish Meteorological Institute.
- Laws, E. A., B. N. Popp, R. R. Bidigare, M. C. Kennicutt and S. A. Macko (1995). "Dependence of phytoplankton carbon isotope composition on growth rate and  $[\text{CO}_2]_{\text{atm}}$ : Theoretical considerations and experimental results." *Geochimica et Cosmochimica Acta* **59**: 1131-1138.
- Leach, F., C. J. Quinn, J. Morrison and G. Lyon (2001). "The use of Multiple Isotope Signatures in Reconstructing Prehistoric Human Diet from Archaeological Bone from the Pacific and New Zealand." *New Zealand Journal of Archaeology* **23**: 31-98.
- Leng, M. J. and J. D. Marshall (2004). "Palaeoclimate interpretation of stable isotope data from lake sediment archives." *Quaternary Science Reviews* **23**(7-8): 811-831.
- Li, H. C. and T. L. Ku (1997). " $\delta^{13}\text{C}$ - $\delta^{18}\text{O}$  covariance as a paleohydrological indicator for closed-basin lakes." *Palaeogeography Palaeoclimatology Palaeoecology* **133**: 69-80.
- Libby, W. F. (1946). "Atmospheric Helium Three and Radiocarbon from Cosmic Radiation." *Physical Review* **69**: 671.
- Lidén, K. (1995). *Prehistoric Diet Transitions. The Archaeological Research Laboratory*, Stockholm University.
- Little, J. D. C. and E. A. Little (1997). "Analysing prehistoric diets by linear programming." *Journal of Archaeological Science* **24**: 741-747.
- Loizeau, J. L., S. Rozé, C. Peytremann, F. Monna and J. Dominik (2003). "Mapping Sediment accumulation Rate by using volume magnetic susceptibility core correlation in a contaminated Bay (Lake Geneva, Switzerland)." *Eclogae Geologicae Helvetiae* **96**: 73-79.
- Lomborg, B. (2003). *Verdens sande tilstand*. Esbjerg, Satellit.
- Loshner, A. (1989). *The Sulfur Cycle in Freshwater Lake Sediments and Implications for the use of C/S Ratios as Indicators of Past Environmental Changes*. *Swiss Federal Institute of Technology*. Zürich.
- Loshner, A. and K. Kelts (1989). "Organic Sulphur fixation in freshwater lake sediments and the implication for C/S ratios." *Terra Nova* **1**: 253-261.
- Lowe, J. J. and M. J. C. Walker (1997). *Reconstructing Quaternary Environments*. Hong Kong, Addison Wesley Longman Limited.

- Magny, M. (2004). "Holocene climate variability as reflected by mid-European lake-level fluctuations and its probable impact on prehistoric human settlements." Quaternary International, The record of Human /Climate interaction in Lake Sediments **113**(1): 65-79.
- Magny, M. and J. N. Haas (2004). "A major widespread climatic change around 5300 cal. yr BP at the time of the Alpine Iceman." Journal of Quaternary Science **19**(5): 423-430.
- Mallat, S. (1999). A wavelet tour of signal processing. Cambridge, Academic Press.
- Manabe, S. and R. J. Stouffer (1999). "The rôle of thermohaline circulation in climate." Tellus **51A-B**: 91-109.
- Marchitto, T. M., W. B. Curry and D. W. Oppo (1998). "Millennial-scale changes in North Atlantic circulation since the last glaciation." Nature **393**(6685): 557-561.
- Marsh, N. and H. Svensmark (2000a). "Cosmic rays, clouds, and climate." Space Science Reviews **94**(1-2): 215-230.
- Marsh, N. D. and H. Svensmark (2000b). "Low cloud properties influenced by cosmic rays." Physical Review Letters **85**(23): 5004-5007.
- Matthews, J. A. and K. R. Briffa (2005). "The 'Little Ice Age': Re-evaluation of an evolving concept." Geografiska Annaler Series a-Physical Geography **87A**(1): 17-36.
- Mauquoy, D., B. van Geel, M. Blaauw, A. Speranza and J. van der Plicht (2004). "Changes in solar activity and Holocene climatic shifts derived from C-14 wiggle-match dated peat deposits." Holocene **14**(1): 45-52.
- Mayer, B. and L. Schwark (1999). "A 15,000-year stable isotope record from sediments of Lake Steisslingen, Southwest Germany." Chemical Geology **161**(1-3): 315-337.
- Mayewski, P. A., E. E. Rohling, J. C. Stager, W. Karlen, K. A. Maasch, L. D. Meeker, E. A. Meyerson, F. Gasse, S. van Kreveld, K. Holmgren, J. Lee-Thorp, G. Rosqvist, F. Rack, M. Staubwasser, R. R. Schneider and E. J. Steig (2004). "Holocene climate variability." Quaternary Research **62**(3): 243-255.
- McFadden, M. A., W. P. Patterson, H. T. Mullins and W. T. Anderson (2005). "Multi-proxy approach to long- and short-term Holocene climate-change: evidence from eastern Lake Ontario." Journal of Paleolimnology **33**: 371-391.
- McNamara, J. and H. G. Thode (1950). "Comparison of the Isotope Constitution of Terrestrial and Meteoritic Sulfur." Physical Review **78**: 307-308.
- McNichol, A. P., A. J. T. Jull and G. S. Burr (2001). "Converting AMS data to radiocarbon values: considerations and conventions." Radiocarbon **43**: 313-320.
- Meijer, H. A. J. and W. J. Li (1998). "The use of electrolysis for accurate delta O-17 and delta O-18 isotope measurements in water." Isotopes in Environmental and Health Studies **34**(4): 349-369.
- Mendoza, B., J. Ramirez and G. Cordero (2004). "Cosmic rays and terrestrial temperature: is there a direct longterm relation?" Advances in Space Research, Solar Variability and Climate Change **34**(2): 416-419.
- Merren, T. (2000). Application of an Electrostatic Filter for the Measurement of Hydrogen Isotopes in Continuous Flow Mode IRMS. Manchester, Micromass UK.
- Mertz, E. L. (1924). "De sen- og postglaciale Niveauforandringer i Danmark." Danmarks Geologiske Undersøgelse III Række **41**: 39pp.
- Meyers, P. A. (1997). "Organic geochemical proxies of paleoceanographic, paleolimnologic, and paleoclimatic processes." Organic Geochemistry **27**(5-6): 213-250.
- Meyers, P. A. (2006). "Paleoceanographic and paleoclimatic similarities between Mediterranean sapropels and Cretaceous black shales." Palaeogeography Palaeoclimatology Palaeoecology **235**: 305-320.
- Meyers, P. A. and E. Lallier-Vergés (1999). "Lacustrine sedimentary organic matter records of Late Quaternary paleoclimates." Journal of Paleolimnology **21**: 345-372.
- Meyers, P. A. and J. L. Teranes (2001). Sediment organic matter. Tracking Environmental Change Using Lake Sediments. W. M. Last and J. P. Smol. Dordrecht, Kluwer Academic Publishers. 2.
- Michelutti, N., M. S. V. Douglas, A. P. Wolfe and J. P. Smol (2006). "Heightened sensitivity of a poorly buffered high arctic lake to late-Holocene climatic change." Quaternary Research **65**: 421-430.
- Milner, N., O. E. Craig, G. N. Bailey, K. Pedersen and S. H. Andersen (2003). "Something fishy in the Neolithic? A re-evaluation of stable isotope analysis of Mesolithic and Neolithic coastal populations." Antiquity: 9-22.
- Minagawa, M. and E. Wada (1984). "Stepwise enrichment of  $\delta^{15}\text{N}$  along food chains: Further evidence and the relation between  $\delta^{15}\text{N}$  and animal age." Geochimica et Cosmochimica Acta **48**(5): 1135-1140.
- Misiti, M., Y. Misiti, G. Oppenheim and J. M. Poggi (2004). Wavelet Toolbox User's Guide Version 3 - For Use with MATLAB, MathWorks, Inc.
- Moberg, A., D. M. Sonechkin, K. Holgren, N. M. Datsenko and W. Karlén (2005). "Highly variable Northern Hemisphere temperatures reconstructed from low- and high-resolution proxy data." Nature **433**: 613-617.
- Morrison, J. (1996). A Discussion on the Causes of Memory using Continuous Flow-IRMS. Manchester, Micromass.
- Morrison, J., T. Brockwell, T. Merren, F. Fourel and A. M. Phillips (2001). "Online High-Precision Stable Hydrogen Isotopic Analysis on Nanoliter Samples." Analytical Chemistry **73**(15): 3570-3575.
- Morrison, J., F. Fourel and D. Churchman (1996). Isotopic Sulphur Analysis by Continuous Flow Isotope Ratio Mass Spectrometry (CF-IRMS). Manchester, Micromass.
- Morse, J. W. and R. A. Berner (1995). "What determines sedimentary C/S ratios?" Geochimica et Cosmochimica Acta **59**: 1073-1077.
- Muzuka, A. N. N., M. Ryner and K. Holmgren (2004). "12,000-Year, preliminary results of the stable nitrogen and carbon isotope record from the Empakai Crater lake sediments, Northern Tanzania." Journal of African Earth Sciences **40**(5): 293-303.
- Nederbragt, A. J. and J. Thurow (2005). "Geographic coherence of millennial-scale climate cycles during the Holocene." Palaeogeography Palaeoclimatology Palaeoecology **221**: 313-324.
- Newsome, S. D., D. L. Phillips, B. J. Culleton, T. P. Guilderson and P. L. Koch (2004). "Dietary reconstruction of an early to middle Holocene human population from the central California coast: insights from advanced stable isotope mixing models." Journal of Archaeological Science **31**(8): 1101-1115.

- Noe-Nygaard, N. (1988). " $\delta^{13}\text{C}$ -values of dog bones reveal the nature of changes in man's food resources at the mesolithic-neolithic transition, Denmark." Chemical Geology **73**: 87-96.
- Noe-Nygaard, N. (1995). Ecological, sedimentary, and geochemical evolution of the late-glacial to postglacial Åmose lacustrine, Denmark. Arlöf, Scandinavian University Press.
- Noe-Nygaard, N., C. H. Abildtrup, T. Albrechtsen, A. B. Gotfredsen and J. Ríchter (1998). "Palæobiologiske, sedimentologiske og geokemiske undersøgelser af Sen Weichsel og Holocæne aflejringer i Store Åmose, Danmark." Geologisk Tidsskrift **2**: 1-65.
- Noe-Nygaard, N. and M. U. Hede (2006). "The first appearance of cattle in Denmark occurred 6000 years ago: An effect of cultural or climate and environmental change." Geografiska Annaler **88**(2): 87-95.
- Noe-Nygaard, N., M. U. Hede, A. K. Hansen and C. H. Abildtrup (2003). Tissø, Lille Åmose og Store Åmoses dræningssystem gennem 18.000 år. Tissø og Åmoserne - kulturhistorie og natur. L. Pedersen. Kalundborg, Holbæk Amt: 127-154.
- Noe-Nygaard, N. and E. O. Heiberg (2001). "Lake-level changes in the late Weichselian Lake Tøvelde, Møn Denmark: induced by changes in climate and base level." Palaeogeography, Palaeoclimatology, Palaeoecology **174**: 351-382.
- Noe-Nygaard, N., T. D. Price and S. U. Hede (2005). "Diet of aurochs and early cattle in southern Scandinavia: evidence from N-15 and C-13 stable isotopes." Journal of Archaeological Science **32**(6): 855-871.
- Northrop, D. A. and R. N. Clayton (1966). "Oxygen-Isotope Fractionations in Systems Containing Dolomite." Journal of Geology **74**(2): 174-8.
- Nriagu, J. O. and Y. K. Soon (1985). "Distribution and isotopic composition of sulfur in lake sediments of northern Ontario." Geochimica et Cosmochimica Acta **49**: 823-834.
- O'Brian, S. R., P. A. Mayewski, L. D. Meeker, D. A. Meese, M. S. Twickler and S. I. Whitlow (1995). "Complexity of Holocene Climate as Reconstructed from Greenland Ice Core." Science **270**: 1962-1964.
- Oeschger, H. and J. Beer (1990). "The past 5000 Years History of Solar Modulation of Cosmic Radiation from  $^{10}\text{Be}$  and  $^{14}\text{C}$  Studies." Philosophical Transactions of the Royal Society of London. Series A, Mathematical and Physical Sciences **330**: 471-480.
- Ogrinc, N., G. Fontolan, J. Faganeli and S. Covelli (2005). "Carbon and nitrogen isotope compositions of organic matter in coastal marine sediments (the Gulf of Trieste, N Adriatic Sea): indicators of sources and preservation." Marine Chemistry **95**(3-4): 163-181.
- Ogurtsov, M. G., G. E. Kocharov, M. Lindholm, M. Eronen and Y. A. Nagovitsyn (2001). "Solar activity and regional climate." Radiocarbon **43**(2A): 439-447.
- Ogurtsov, M. G., Y. A. Nagovitsyn, G. E. Kocharov and H. Jungner (2002). "Long-period cycles of the Sun's activity recorded in direct solar data and proxies." Solar Physics **211**(1-2): 371-394.
- O'Leary, M. H. (1988). "Carbon Isotope in Photosynthesis." Bioscience **38**.
- Olsen, J., J. Heinemeier, K. G. Bahner, B. Graney and A. Pililps (submitted for publication). "Integrating Continuous Flow Mass Spectrometry with Automated  $\text{CO}_2$  collection for AMS." Radiocarbon.
- Olsen, J., J. Heinemeier, P. Bennike, K. M. Hornstrup and H. Thrane (in preparation). "Characterisation and Blind Testing of the Method for Radiocarbon Dating of Cremated Bone." Radiocarbon.
- Olsen, J., I. Seierstad, B. Vinther, S. Johnsen and J. Heinemeier (2006). "Memory effect in deuterium analysis by continuous flow isotope ratio measurement." International Journal of Mass Spectrometry **254**(1-2): 44-52.
- O'Neil, J. R., R. N. Clayton and T. K. Mayeda (1969). "Oxygen isotope fractionation in divalent metal carbonates." Journal of Chemical Physics **51**: 5547-5558.
- Oppo, D. W., J. F. McManus and J. L. Cullen (2003). "Palaeo-oceanography: Deepwater variability in the Holocene epoch." Nature **422**(6929): 277-278.
- O'Reilly, C. M., R. E. Hecky, A. S. Cohen and P. D. Plisnier (2002). "Interpreting stable isotopes in food webs: Recognizing the role of time averaging at different trophic levels." Limnology and Oceanography **47**: 306-309.
- O'Sullivan, P. (2004). Paleolimnology. The Lakes Handbook. P. E. O'Sullivan and C. S. Reynolds. Oxford, Blackwell Science. **1**: 609-666.
- O'Sullivan, P. E. and C. S. Reynolds, Eds. (2004). Limnology and Limnetic Ecology. The Lakes Handbook. Oxford, Blackwell Science.
- Padisák, J. (2004). Phytoplankton. The Lakes Handbook. P. E. O'Sullivan and C. S. Reynolds. Oxford, Blackwell Science. **1**: 251-308.
- Palmer, M. A., L. J. Gray, M. R. Allen and W. A. Norton (2004). "Solar forcing of climate: model results." Advances in Space Research, Solar Variability and Climate Change **34**(2): 343-348.
- Pardue, J. W. (1976). "Maximum carbon isotope fractionation in photosynthesis by blue-green algae and a green algae." Geochimica et Cosmochimica Acta **40**: 309-312.
- Pederson, D. C., D. M. Peteet, D. Kurdyla and T. Guilderson (2005). "Medieval Warming, Little Ice Age, and European impact on the environment during the last millennium in the lower Hudson Valley, New York, USA." Quaternary Research **63**(3): 238-249.
- Pekarek, A. H. (2001). Solar Forcing of Earth's Climate. Geological Perspectives of Global Climate. L. C. Gerhard, W. E. Harrison and B. M. Hanson. Tulsa, The American Association of Petroleum Geologists. **47**: 19-34.
- Peltier, W. R. (2002). "On eustatic sea level history: Last Glacial Maximum to Holocene." Quaternary Science Reviews **21**: 377-396.
- Peltier, W. R. and R. G. Fairbanks (In Press, Corrected Proof). "Global glacial ice volume and Last Glacial Maximum duration from an extended Barbados sea level record." Quaternary Science Reviews In Press, Corrected Proof.
- Petersen, B. J. and R. W. Howarth (1987). "Sulfur, Carbon, and Nitrogen Isotopes Used to Trace Organic Matter Flow in the Salt-Marsh Estuaries of Sapelo Island, Georgia." Limnology and Oceanography **32**: 1195-1213.
- Petersen, K. (2003). "Milankovitch-teorien - istidernes astronomiske forklaring." Geologisk Nyt **2**: 26-29.
- Platt, N. H. and V. P. Wright (1991). "Lacustrine carbonates: facies models, facies distributions and hydro-

- carbon aspects." *Special Publication International Association of Sedimentologists* **13**: 57-74.
- Platzner, I. T., K. Habfast, A. J. Walder and A. Goetz (1997). *Modern Isotope Ratio Mass Spectrometry*, John Wiley & Sons.
- Pokorný, J. and J. Kvet (2004). Aquatic plants and lake ecosystems. *The Lakes Handbook*. P. E. O'Sullivan and C. S. Reynolds. Oxford, Blackwell Science. **1**: 309-340.
- Poulson, S. R. (2005). "The effect of sulfate- $\delta^{18}\text{O}$  upon on-line sulfate- $\delta^{34}\text{S}$  analysis, and implications for measurements of  $\delta^{34}\text{S}$  and  $\Delta^{34}\text{S}$ ." *Rapid Communications in Mass Spectrometry* **19**(2): 105-107.
- Proctor, C. J., A. Baker and W. L. Barnes (2002). "A three thousand year record of North Atlantic climate." *Climate Dynamics* **19**(5-6): 449-454.
- Rahmstorf, S. (2000). "The thermohaline ocean circulation: A system with dangerous thresholds? An editorial comment." *Climatic Change* **46**(3): 247-256.
- Ramsey, C. B. (1995). "Radiocarbon Calibration and Analysis of Stratigraphy: The OxCal Program." *Radiocarbon* **37**(2): 425-430.
- Ramsey, C. B. (1998). "The role of statistical methods in the interpretation of radiocarbon dates." *Actes du colloque "C14 Archéologie"*: 83-86.
- Ramsey, C. B. (2001). "Development of the Radiocarbon Program OxCal." *Radiocarbon* **43**(2A): 355-363.
- Ramsey, C. B., J. van der Plicht and B. Weninger (2001). "Wiggle matching' radiocarbon dates." *Radiocarbon* **43**(2A): 381-389.
- Rasmussen, P. (2005). "Mid- to late-Holocene land-use change and lake development at Dallund Sø, Denmark: vegetation and land-use history inferred from pollen data." *Holocene* **15**(8): 1116-1129.
- Rasmussen, P. and N. J. Anderson (2005). "Natural and anthropogenic forcing of aquatic macrophyte development in a shallow Danish lake during the last 7000 years." *Journal of Biogeography* **32**(11): 1993-2005.
- Rasmussen, P. and E. G. Bradshaw (2005). "Mid- to late-Holocene land-use change and lake development at Dallund Sø, Denmark: study aims, natural and cultural setting, chronology and soil erosion history." *Holocene* **15**(8): 1105-1115.
- Rasmussen, P., K. Christensen and J. D. Møller (2002). "Elmesyge i geologisk perspektiv." *Naturens Verden* **1**: 36-40.
- Reading, H. G. (1989). *Facies. Sedimentary Environments and Facies*. H. G. Reading. Oxford, Blackwell Scientific Publications.
- Reading, H. G. (1996). *Sedimentary Environments: Processes, Facies and Stratigraphy*. Oxford, Blackwell Science Ltd.
- Rees, C. E., W. J. Jenkins and J. Monster (1978). "The sulphur isotopic composition of ocean water sulphate." *Geochimica et Cosmochimica Acta* **42**: 377-381.
- Reid, G. C. (2000). "Solar variability and the Earth's climate: Introduction and overview." *Space Science Reviews* **94**(1-2): 1-11.
- Reimer, P. J., M. G. L. Baillie, E. Bard, A. Bayliss, J. W. Beck, C. J. H. Bertrand, P. G. Blackwell, C. E. Buck, G. S. Burr, K. B. Cutler, P. E. Damon, R. L. Edwards, R. G. Fairbanks, M. Friedrich, T. P. Guilderson, A. G. Hogg, K. A. Hughen, B. Kromer, G. McCormac, S. Manning, C. B. Ramsey, R. W. Reimer, S. Remmele, J. R. Southon, M. Stuiver, S. Talamo, F. W. Taylor, J. van der Plicht and C. E. Weyhenmeyer (2004a). IntCal04 files, <http://www.radiocarbon.org/IntCal04%20files/>. 2006.
- Reimer, P. J., M. G. L. Baillie, E. Bard, A. Bayliss, J. W. Beck, C. J. H. Bertrand, P. G. Blackwell, C. E. Buck, G. S. Burr, K. B. Cutler, P. E. Damon, R. L. Edwards, R. G. Fairbanks, M. Friedrich, T. P. Guilderson, A. G. Hogg, K. A. Hughen, B. Kromer, G. McCormac, S. Manning, C. B. Ramsey, R. W. Reimer, S. Remmele, J. R. Southon, M. Stuiver, S. Talamo, F. W. Taylor, J. van der Plicht and C. E. Weyhenmeyer (2004b). "IntCal04 terrestrial radiocarbon age calibration, 0-26 cal kyr BP." *Radiocarbon* **46**(3): 1029-1058.
- Richards, M. P. and E. Kock (2001). Analyser af kvælstofisotopen  $^{15}\text{N}$  i menneskeskeletter fra yngre stenalder. *Aarbøger for Nordisk Oldkyndighed og Historie* 1999. København, Det Kongelige Nordiske Oldskriftselskab.
- Richards, M. P., T. D. Price and E. Koch (2003). "Mesolithic and Neolithic Subsistence in Denmark: New Stable Isotope Data." *Current Anthropology* **44**(2): 288-295.
- Richter, J. and N. Noe-Nygaard (2003). "A Late Mesolithic Hunting Station at Agernæs, Fyn, Denmark." *Acta Archaeologica* **74**: 1-64.
- Roberts, N. (2004). *The Holocene - An Environmental History*. Hong Kong, Blackwell Publishing.
- Rom, W. (2000). C-14 AMS - applications in Archaeology, Biomedicine and in the Atmospheric Sciences, Universität Wien.
- Routh, J., P. A. Meyers, Ö. Gustafsson, M. Baskaran, R. Hallberg and A. Schöldström (2004). "Sedimentary geochemical record of human-induced environmental changes in the Lake Brunnsviken watershed, Sweden." *Limnology and Oceanography* **49**(5): 1560-1569.
- Rowley-Conwy, P. (2004). "How the West Was Lost." *Current Anthropology* **45**: S83-S113.
- Rozanski, R., L. Araguas-Araguas and R. Gonfiantini (1992). "Relation between long-term trends of oxygen-18 isotope composition of precipitation and climate." *Science* **258**: 981-985.
- Ruddiman, W. F. (2001). *Earth's Climate. Past and future*. New York, W.H. Freeman and Company.
- Ruddiman, W. F. (2005). "How did humans first alter global climate." *Scientific American March*: 46-53.
- Ruzmaikin, A., J. K. Lawrence and A. C. Cadavid (2004). "A simple model of solar variability influence on climate." *Advances in Space Research, Solar Variability and Climate Change* **34**(2): 349-354.
- Sandgren, P., J. Risberg and R. Thomsen (1990). "Magnetic susceptibility in sediment records of Lake Ådran, eastern Sweden: correlation among cores and interpretation." *Journal of Paleolimnology* **3**: 129-141.
- Santrock, J., A. Studley and J. M. Hayes (1985). "Isotopic Analysis Based on the Mass Spectro of Carbon Dioxide." *Analytical Chemistry* **57**: 1444-1448.
- Schippers, A. and B. B. Jørgensen (2002). "Biochemistry of pyrite and iron sulfide oxidation in marine sediments." *Geochimica et Cosmochimica Acta* **66**: 86-92.
- Schlesinger, M. E. and N. Ramankutty (1994). "An Oscillation in the Global Climate System of Period 65-70 Years." *Nature* **367**(6465): 723-726.
- Schlesinger, W. H. (1997). *Biochemistry. An analysis of global change*, Academic Press.
- Schoeninger, M. (1989). Reconstructing prehistoric human diet. *The chemistry of prehistoric human bone*. T. D. Price, Cambridge University Press.

- Schoeninger, M. J. and M. J. DeNiro (1984). "Nitrogen and Carbon composition of bone collagen from marine and terrestrial animals." *Geochimica et Cosmochimica Acta* **48**: 625-639.
- Schulting, R. J. and M. P. Richards (2002a). "Finding the coastal Mesolithic in southwest Britain: AMS dates and stable isotopes results on human remains from Caldey Island, south Wales." *Antiquity* **76**: 1011-1025.
- Schulting, R. J. and M. P. Richards (2002b). "The Wet, The Wild and The Domesticated: The Mesolithic-Neolithic Transition on the West Coast of Scotland." *European Journal of Archeology* **5**: 147-189.
- Schwab, A. (2002). "Lacustrine ostracodes as stable isotope recorders of late-glacial and Holocene environmental dynamics and climate." *Journal of Paleolimnology* **29**: 267-351.
- Schwab, A. and W. E. Dean (1998). "Stable isotopes and sediments from Pickerel Lake, South Dakota, USA: a 12ky record of environmental changes." *Journal of Paleolimnology* **20**: 15-30.
- Schwab, A. and W. E. Dean (2002). "Reconstruction of hydrological changes and response to effective moisture variations from North-Central USA lake sediments." *Quaternary Science Reviews* **21**: 1541-1554.
- Schwarcz, H. P. (2000). Some Biochemical Aspects of Carbon Isotopic Paleodiet Studies. *Biogeochemical Approaches to Paleodietary Analysis*. S. H. Ambrose and M. A. Katzenberg, Kluwer Academic/ Plenum Publishers: 189-209.
- Seierstad, I. K., S. J. Johnsen, B. M. Vinther and J. Olsen (in press). "The duration of the Bølling-Allerød (Greenland Interstadial 1) period in the GRIP ice core." *Annals of Glaciology* **42**.
- Seppä, H., D. Hammarlund and K. Antonsson (2005). "Low-frequency and high-frequency changes in temperature and effective humidity during the Holocene in south-central Sweden: implications for atmospheric and oceanic forcings of climate." *Climate Dynamics* **25**: 285-297.
- Skak-Nielsen, N. V. (2003). "Hvordan kom bondebruget til Sydskandinavien?" *Fornvännen* **98**.
- Skak-Nielsen, N. V. (2004). "The neolithisation of Scandinavia." *Adoranten*: 89-102.
- Smith, F. A. and N. A. Walker (1980). "Photosynthesis by Aquatic Plants: Effects of unstirred layers in relation to assimilation of CO<sub>2</sub> and HCO<sub>3</sub> and Carbon isotope discrimination." *New Phytologist* **86**: 245-259.
- Solanki, S., M. Schüssler and M. Fligge (2000). "Evolution of the Sun's large-scale magnetic field since the Maunder minimum." *Nature* **408**: 445-447.
- Sonnett, C. P. and S. A. Finney (1990). "The Spectrum of Radiocarbon." *Philosophical Transactions of the Royal Society of London. Series A, Mathematical and Physical Sciences* **330**: 413-425.
- Southon, J. (2004). "A radiocarbon perspective on Greenland ice-core chronologies: Can we use ice cores for C-14 calibration?" *Radiocarbon* **46**(3): 1239-1259.
- Speranza, A., J. van der Plicht and B. van Geel (2000). "Improving the time control of the Subboreal/Subatlantic transition in a Czech peat sequence by C-14 wiggle-matching." *Quaternary Science Reviews* **19**(16): 1589-1604.
- Stichler, W. (1993). Interlaboratory Comparison of New Materials for Carbon and Oxygen Isotope Measurements. *Reference and Intercomparison Materials for Stable Isotopes of Light Elements*. Vienna, IAEA-TEC-DOC-825: 67-74.
- Stoddard, J. L. (1994). Long-Term Changes in Watershed Retention of Nitrogen. *Environmental chemistry of lakes and reservoirs*. L. A. Baker. Atlanta, American Chemical Society.
- Strauss, H. (1999). "Geological evolution from isotope proxy signals - sulfur." *Chemical Geology* **161**(1-3): 89-101.
- Strauss, H. (2003). "Sulphur isotopes and the early Archaean sulphur cycle." *Precambrian Research* **126**(3-4): 349-361.
- Stuiver, M., P. M. Grootes and T. F. Braziunas (1995). "The GISP2 δ<sup>18</sup>O Climate Record of the Past 16,500 Years and the Role of the Sun, Ocean, and Volcanoes." *Quaternary Research* **44**: 341-354.
- Stuiver, M. and H. A. Polach (1977). "Discussion Reporting of C-14." *Radiocarbon* **19**(3): 355.
- Svensmark, H. (1998). "Influence of cosmic rays on Earth's climate." *Physical Review Letters* **81**(22): 5027-5030.
- Talbot, M. R. (1990). "A review of the palaeohydrological interpretation of carbon and oxygen isotopic ratios in primary lacustrine carbonates." *Chemical Geology: Isotope Geoscience section* **80**(4): 261-279.
- Talbot, M. R., Ed. (2001). *Nitrogen isotopes in palaeolimnology*. Tracking Environmental Change Using Lake Sediments. Dordrecht, Kluwer Academic Publishers.
- Talbot, M. R. and P. A. Allen (1996). Lakes. *Sedimentary Environments: Processes, Facies and Stratigraphy*. H. G. Reading. Oxford, Blackwell Science Ltd.
- Talbot, M. R., N. B. Jensen, T. Lærdal and M. L. Filippi (2006). "Geochemical responses to a major transgression in giant African lakes." *Journal of Paleolimnology* **35**: 467-489.
- Talbot, M. R. and T. Johannessen (1992). "A high resolution palaeoclimatic record for the last 27,500 years in tropical West Africa from the carbon and nitrogen isotopic composition of lacustrine organic matter." *Earth and Planetary Science Letters* **110**(1-4): 23-37.
- Talbot, M. R. and D. A. Livingstone (1989). "Hydrogen index and carbon isotopes of lacustrine organic matter as lake level indicators." *Palaeogeography Palaeoclimatology Palaeoecology* **70**: 121-137.
- Tauber, H. (1981). "<sup>13</sup>C Evidence for Dietary Habits of Prehistoric Man in Denmark." *Nature* **292**: 332-334.
- Telford, R. J., E. Heegaard and H. J. B. Birks (2004a). "All age-depth models are wrong: but how badly?" *Quaternary Science Reviews* **23**: 1-5.
- Telford, R. J., E. Heegaard and H. J. B. Birks (2004b). "The intercept is a poor estimate of a calibrated radiocarbon date." *The Holocene* **14**(2): 296-298.
- Teranes, J. L. and S. M. Bernasconi (2005). "Factors controlling delta C-13 values of sedimentary carbon in hypertrophic Baldeggersee, Switzerland, and implications for interpreting isotope excursions in lake sedimentary records." *Limnology and Oceanography* **50**(3): 914-922.
- Thejll, P. and K. Lassen (2000). "Solar forcing of the Northern hemisphere land air temperature: New data." *Journal of Atmospheric and Solar-Terrestrial Physics* **62**(13): 1207-1213.
- Thode, H. G., J. Monster and H. B. Dunford (1961). "Sulphur Isotope Geochemistry." *Geochimica Et Cosmo-*

- chimica Acta* **25**(3): 159-174.
- Thompson, J. B. and F. G. Ferris (1990). "Cyanobacterial precipitation of gypsum, calcite, and magnesite from natural alkaline lake water." *Geology* **18**: 995-998.
- Thomsen, M. S. (1990). AMS spectrometry. *Institut for fysik*, Aarhus Universitet.
- Trust, B. A. and B. Fry (1992). "Stable sulphur isotopes in plants: a review." *Plant, Cell and Environment* **15**: 1105-1110.
- Tuniz, C., J. R. Bird, D. Fink and G. F. Herzog (1998). *Accelerator Mass Spectrometry. Ultrasensitive Analysis for Global Science*. Boca Raton, CRC Press.
- Turcq, B., A. L. S. Albuquerque, R. C. Cordeiro, A. Sifedine, F. E. L. Simoes, A. G. Souza, J. J. Abrão, F. B. L. Oliveira, A. O. Silva and J. Capitâneo (2002). "Accumulation of organic carbon in five Brazilian lakes during the Holocene." *Sedimentary Geology* **148**: 319-342.
- Turney, C., M. Baillie, S. Clemens, D. Brown, J. Palmer, J. Pilcher, P. J. Reimer and H. H. Leuschner (2005). "Testing solar forcing of pervasive Holocene climate cycles." *Journal of Quaternary Science* **20**: 511-518.
- Urban, N. R. (1994). Retention of Sulfur in Lake Sediments. *Environmental chemistry of lakes and reservoirs*. L. A. Baker. Atlanta, American Chemical Society.
- Urban, N. R., K. Ernst and S. Bernasconi (1999). "Addition of sulfur to organic matter during early diagenesis of lake sediments." *Geochimica et Cosmochimica Acta* **63**: 837-853.
- Usoskin, I. G. and B. Kromer (2005). "Reconstruction of the <sup>14</sup>C production rate from measured relative abundance." *Radiocarbon* **47**: 31-37.
- van der Plicht, H. (1998). "radiocarbon calibration: Towards the complete dating range." *Actes du colloque "C14 Archéologie"*: 73-77.
- van Strydonck, M., D. E. Nelson, P. Crombé, C. B. Ramsey, E. M. Scott, J. van der Plicht and R. E. M. Hedges (1998). "Rapport du groupe de travail: Les limites de méthode du carbone 14 appliquée à l'archéologie." *Actes du colloque "C14 Archéologie"*: 433-448.
- Vasiliev, S. S. and V. A. Dergachev (2002). "The ~2400-year cycle in the atmospheric radiocarbon concentration: bispectrum of <sup>14</sup>C data over the last 8000 years." *Annales Geophysicae* **20**: 115-120.
- Verkouteren, R. M. L. J. N. (2001). "WEB -based Interactive Data Processing: Application to Stable Isotope Metrology." *Fresenius' journal of analytical chemistry* **370**: 803-810.
- Versteegh, G. J. M. (2005). "Solar forcing of climate. 2: Evidence from the past." *Space Science Reviews* **120**(3-4): 243-286.
- Veski, S., H. Seppa and A. E. K. Ojala (2004). "Cold event at 8200 yr BP recorded in annually laminated lake sediments in eastern Europe." *Geology* **32**(8): 681-684.
- Vinther, B. M., H. B. Clausen, S. J. Johnsen, S. O. Rasmussen, K. K. Andersen, S. L. Buchardt, I. K. Seierstad, M.-L. Siggaard-Andersen, J. P. Steffensen, A. M. Svensson, J. Olsen and J. Heinemeier (2006). "A synchronized dating of three Greenland ice cores throughout the Holocene." *Journal of Geophysical Research*.
- Vinther, B. M., S. Johnsen, K. K. Andersen, H. B. Clausen and A. W. Hansen (2003). "NAO signal recorded in the stable isotopes of Greenland ice cores." *Geophysical Research Letters* **30**(7): 1-4.
- Visbeck, M. H., J. W. Hurrell, L. Plolvani and H. M. Cullen (2001). "The North Atlantic Oscillation: Past, present, and future." *PNAS* **98**(23): 12876-12877.
- von Grafenstein, U. (1998). "The cold event 8200 years ago documented in oxygen isotopes records of precipitation in Europe and Greenland." *Climate Dynamics* **14**: 73-81.
- Vos, H., A. Sanchez, B. Zolitschka, A. Brauer and J. F. W. Negendank (1997). "Solar Activity Variations Recorded in Varved Sediments from the Crater Lake of Holzmaar - A Maar Lake in the Westeifel Volcanic Field, Germany." *Surveys in Geophysics* **18**(2 - 3): 163-182.
- Wanner, H., S. Bronnimann, C. Casty, D. Gyalistras, J. Luterbacher, C. Schmutz, D. B. Stephenson and E. Xoplaki (2001). "North Atlantic Oscillation - Concepts and studies." *Surveys in Geophysics* **22**(4): 321-382.
- Watanabe, T., H. Naraoka, M. Nishimura and T. Kawai (2004). "Biological and environmental changes in Lake Baikal during the late Quaternary inferred from carbon, nitrogen and sulfur isotopes." *Earth and Planetary Science Letters* **222**(1): 285-299.
- Werner, R. A. and W. A. Brand (2001). "Referencing Strategies and Techniques in Stable Isotope Ratio Analysis." *Rapid Communications in Mass Spectrometry* **15**: 501-519.
- Werner, R. A., B. A. Bruch and W. A. Brand (1999). "ConFlo III - An interface for High Precision  $\delta^{13}\text{C}$  and  $\delta^{15}\text{N}$  Analysis with an Extended Dynamic Range." *Rapid Communications in Mass Spectrometry* **13**: 1237-1241.
- Wohlfarth, B., P. Tarasov, O. Bennike, T. Lacourse, D. Subetto, P. Torssander and F. Romanenko (2006). "Late glacial and Holocene palaeoenvironmental changes in the Tostov-Yaroslavl' area, West Central Russia." *Journal of Paleolimnology* **35**: 543-569.
- Wolfe, B. B., T. W. D. Edwards and R. Aravena (1999). "Changes in carbon and nitrogen cycling during tree-line retreat recorded in the isotopic content of lacustrine organic matter, western Taimyr Peninsula, Russia." *Holocene* **9**: 215-222.
- Wong, W. W. (1978). "Fractionation of stable carbon isotopes by marine phytoplankton." *Geochimica et Cosmochimica Acta* **42**: 1809-1815.
- Wortmann, U. G., S. Bernasconi and M. E. Böttcher (2001). "Hypersulfidic deep biosphere indicates extreme sulfur isotope fractionation during single-step microbial sulfate reduction." *Geological Society of America* **29**: 647-650.
- Yde, J. C., N. T. Knudsen, N. K. Larsen, C. Kornborg, O. Bjørslev-Nielsen, J. Heinemeier and J. Olsen (in press). "The presence of thrust-block naled after a major surge event." *Annals of Glaciology* **42**.
- Yun, M., B. Mayer and S. W. Taylor (2005). "delta S-34 measurements on organic materials by continuous flow isotope ratio mass spectrometry." *Rapid Communications in Mass Spectrometry* **19**(11): 1429-1436.
- Yun, M., M. A. Wadleigh and A. Pye (2004). "Direct measurement of sulphur isotopic composition in lichens by continuous flow-isotope ratio mass spectrometry." *Chemical Geology* **204**(3-4): 369-376.
- Zaitseva, G. I., v. B. Geel, N. A. Bokovenko, K. V. Chugunov, V. A. Dergachev, V. G. Dirksen, M. A. Koulkova, A. Nagler, G. Parzinger, H. van der Plicht, N. D. Bourova and L. M. Lebedeva (2004). "Chronology and

possible links between climatic and cultural change during the first millennium BC southern Siberia and Central Asia." Radiocarbon **46**: 259-276.

Aaby, B. (1976). "Cyclic Climatic Variations in Climate over Past 5,500 Yr Reflected in Raised Bogs." Nature **263**(5575): 281-284.